

Satellite Image Atlas
of Glaciers of the World

ANTARCTICA



United States Geological Survey
Professional Paper 1386-B

Cover: Landsat 1 MSS digitally enhanced false-color composite image of the Sentinel Range, Ellsworth Mountains, and Rutford Ice Stream. See page B 122.

ANTARCTICA

By CHARLES SWITHINBANK

With sections on

THE 'DRY VALLEYS' OF VICTORIA LAND

By TREVOR J. CHINN

LANDSAT IMAGES OF ANTARCTICA

By RICHARD S. WILLIAMS, JR., and JANE G. FERRIGNO

SATELLITE IMAGE ATLAS OF GLACIERS OF THE WORLD

Edited by RICHARD S. WILLIAMS, JR., and JANE G. FERRIGNO

U. S. GEOLOGICAL SURVEY PROFESSIONAL PAPER 1386 – B

Landsat images of Antarctica, from the coast to 81° south latitude, provide new glaciological information about the inland ice sheet, ice shelves, outlet glaciers, ice streams, and "blue ice" areas of our planet's largest present-day concentration of glacier ice



UNITED STATES GOVERNMENT PRINTING OFFICE, WASHINGTON: 1988

U.S. DEPARTMENT OF THE INTERIOR

BRUCE BABBITT, *Secretary*

U.S. GEOLOGICAL SURVEY

Dallas L. Peck, *Director*

The editors regret that the scanning software used to produce this Web version of the published document introduced several irregularities in the spacing and appearance of text and tables that could not be removed.

First printing 1988
Second printing 1993

Library of Congress Cataloging in Publication Data

Satellite image atlas of glaciers of the world.

(U.S. Geological Survey professional paper ; 1386)

Bibliography: p.

Supt. of Docs. no.: I 19.16:1386-B

Contents: B. Antarctica / by Charles Swithinbank ; with sections on the "dry valleys" of Victoria Land, by Trevor J. Chinn, and Landsat images of Antarctica, by Richard S. Williams, Jr., and Jane G. Ferrigno.

1. Glaciers—Remote sensing. I. Williams, Richard S. II Ferrigno, Jane G. III Series: Geological Survey professional paper ; 1386.

GB2401.72.R42S28 1988 551.3'12 87-600497

For sale by the U.S. Geological Survey, Map Distribution,
Box 25425, Bldg. 810, Federal Center, Denver, CO 80225

Foreword

On 23 July 1972, the first Earth Resources Technology Satellite (ERTS 1 or Landsat 1) was successfully placed in orbit. The success of Landsat inaugurated a new era in satisfying mankind's desire to better understand the dynamic world upon which we live. Space-based observations have now become an essential means for monitoring global changes.

The short- or long-term cumulative effects of processes that cause significant changes on the Earth's surface can be documented and studied by repetitive Landsat images. Such images provide a permanent historical record of the surface of our planet; they also make possible comparative two-dimensional measurements of change over time. This Professional Paper demonstrates the importance of the application of Landsat images to global studies by using them to determine the current areal distribution of glaciers on our planet. As images become available from future satellites, the new data will be used to document global changes in glacier extent by reference to the image record of the 1970's.

Although many geological processes take centuries or even millenia to produce obvious changes on the Earth's surface, other geological phenomena, such as glaciers and volcanoes, cause noticeable changes over shorter periods. Some of these phenomena can have a worldwide impact and often are interrelated. Explosive volcanic eruptions can produce dramatic effects on the global climate. Natural or culturally induced processes can cause global climatic cooling or warming. Glaciers respond to such warming or cooling periods by decreasing or increasing in size, thereby causing sea level to rise or fall.

As our understanding of the interrelationship of global processes improves and our ability to assess changes caused by these processes develops further; we will learn how to use indicators of global change, such as glacier variation, to more wisely manage the use of our finite land and water resources. This Professional Paper is an excellent example of the way in which we can use technology to provide needed earth-science information about our planet. The international collaboration represented by this report is also an excellent model for the kind of cooperation that scientists will increasingly find necessary in the future in order to solve important earth-science problems on a global basis.

[Signature]

Dallas L. Peck
Director,
U.S. Geological Survey

Preface

This chapter is one in a series of eleven that comprise U.S. Geological Survey Professional Paper 1386, *Satellite Image Atlas of Glaciers of the World*, which is directed at the use of remotely sensed images, primarily from the Landsat 1, 2, and 3 series of spacecraft, to document, monitor, and study the glacierized regions of our planet. The significance of the Landsat coverage of Antarctica lies in the wide-area coverage made possible, mostly at medium spatial resolution (79-m picture element), with individual images, covering an area 186 by 183 km, or mosaics of images. The configuration of and surface features on ice shelves, outlet glaciers, ice streams, large crevasse fields, areas of 'blue ice,' isolated or grouped nunataks, morainic debris, irregularities in the ice sheet surface caused by underlying mountain ranges, glacier flow lines, and the inland ice sheet can be mapped and delineated on Landsat images in their correct geometric relationship. With accurate knowledge of the geographic position of selected surface features, a Landsat image or image mosaic can be converted to a true map. Future satellite images of Antarctica will permit an accurate assessment of some glaciological changes over time, including the fluctuation of the dynamic ice sheet margin and the average velocity of outlet glaciers, of which only a few selected examples are included in the chapter.

Antarctica contains an estimated $13.9 \times 10^6 \text{ km}^2$ or $30.1 \times 10^6 \text{ km}^3$ of ice, 91 percent of the glacier ice on our planet. This enormous volume of ice influences the temperature, wind, and weather patterns over the entire Earth. Changes in the volume and dynamics of the ice sheet may cause global climate changes. In turn, changes in the temperature of the planet (for example, elevated temperatures caused by an increase in CO_2 and other "greenhouse" gases in the atmosphere), can affect the volume and dynamics of the Antarctic ice sheet.

To fully understand the effect of this ice-bound continent on the rest of the planet, it is necessary to measure and monitor as many of its physical characteristics as possible. Scientific research in the Antarctic, however, is limited by the severe weather conditions, the distance from the rest of the inhabited world, and the huge logistical expense of conducting scientific research throughout, and in the seas around, the continent. For these reasons, satellite images and other types of satellite data become important research tools for expanding our knowledge of this continent.

Some satellite images have already been used by several countries to create planimetric maps of the continent and its surficial glaciological features, monitor and study weather patterns, identify favorable sites for biological communities, and document the dynamics of outlet glaciers and ice streams. The increase in picture element resolution from the 79 m of the multispectral scanner (MSS) to the 30 m of the Landsat 3 return beam vidicon (RBV) and thematic mapper (TM) images makes it possible to map and delineate surface features more accurately and to monitor changes more closely. The continuing improvement in the methodology of digital image processing has also produced specially enhanced Landsat images of Antarctica, several of which are included in this chapter. The chapter contains numerous annotated Landsat 1, 2, and 3 images, oblique aerial photographs, maps, and other information to provide a comprehensive review of the diversity of glaciological features and vastness of the Antarctic ice sheet. This chapter will function as a standard reference of the Antarctic ice sheet's areal extent during the mid-1970's that can be compared with future satellite image data and maps of Antarctica.

Richard S. Williams, Jr.
Jane G. Ferrigno
Editors

About this Volume

U.S. Geological Survey Professional Paper 1386, *Satellite Image Atlas of Glaciers of the World*, contains eleven chapters designated by the letters A through K. Chapter A is a general chapter containing introductory material and a discussion of the physical characteristics, classification, and global distribution of glaciers. The next nine chapters, B through J, are arranged geographically and present glaciological information from Landsat and other sources of data on each of the geographic areas. Chapter B covers Antarctica; Chapter C, Greenland; Chapter D, Iceland; Chapter E, Continental Europe (except for the European part of the Soviet Union), including the Alps, the Pyrenees, Norway, Sweden, Svalbard (Norway), and Jan Mayen (Norway); Chapter F, Asia, including the European part of the Soviet Union, China (P.R.C.), India, Nepal, Afghanistan, and Pakistan; Chapter G, Turkey, Iran, and Africa; Chapter H, Irian Jaya (Indonesia) and New Zealand; Chapter I, South America; and Chapter J, North America. The final chapter, K, is a topically oriented chapter that presents related glaciological topics.

The realization that one element of the Earth's cryosphere, its glaciers, was amenable to global inventorying and monitoring with Landsat images led to the decision, in late 1979, to prepare this Professional Paper, in which Landsat 1, 2, and 3 multispectral scanner (MSS) and Landsat 2 and 3 return beam vidicon (RBV) images would be used to inventory the areal occurrence of glacier ice on our planet within the boundaries of the spacecraft's coverage (between about 81° north and south latitudes). Through identification and analysis of optimum Landsat images of the glacierized areas of the Earth during the first decade of the Landsat era, a global benchmark could be established for determining the areal extent of glaciers during a relatively narrow time interval (1972 to 1982). This global "snapshot" of glacier extent could then be used for comparative analysis with previously published maps and aerial photographs and with new maps, satellite images, and aerial photographs to determine the areal fluctuation of glaciers in response to natural or culturally induced changes in the Earth's climate.

To accomplish this objective, the editors selected optimum Landsat images of each of the glacierized regions of our planet from the Landsat image data base at the EROS Data Center in Sioux Falls, South Dakota, although some images were also obtained from the Landsat image archives maintained by the Canada Centre for Remote Sensing, Ottawa; Ontario, Canada, and by the European Space Agency in Kiruna, Sweden, and Fucino, Italy. Between 1979 and 1981, these optimum images were distributed to an international team of more than 50 scientists who agreed to author a section of the Professional Paper concerning either a geographic area or a glaciological topic. In addition to analyzing images of a specific geographic area, each author was also asked to summarize up-to-date information about the glaciers within the area and to compare their present areal distribution with historical information (for example, from published maps, reports, photographs, etc.) about their past extent. Because of the limitations of Landsat images for delineating or monitoring small glaciers in some geographic areas, either on the basis of inadequate spatial resolution, lack of suitable seasonal coverage, or absence of coverage, information on areal distribution is necessarily derived from ancillary sources. Completion of this atlas will provide an accurate regional inventory of the areal extent of glaciers on our planet during the 1970's.

Richard S. Williams, Jr.
Jane G. Ferrigno
Editors

CONTENTS

	Page
Foreword -----	III
Preface -----	V
About this volume -----	VI
Abstract -----	B1
Introduction -----	3
Geographic place-names -----	3
Definitions -----	4
Dimensions -----	12
FIGURE	
1. Map showing extent of 1:250,000-scale and larger scale mapping in Antarctica produced by aerial photogrammetric and satellite-image map techniques ----	2
2. Apollo 17 photograph of the Earth and part of Antarctica -----	2
3. Oblique aerial photograph of the ice front in Okuma Bay Ross Ice Shelf -----	5
4-5. Photograph of:	
4. An ice front on the Brunt Ice Shelf, Coats Land ----	6
5. An ice wall, Dorian Bay, Graham Land -----	6
6-10. Oblique aerial photograph of:	
6. An ice wall, Cape Norvegia, Princess Martha Coast -----	7
7. Gipps Ice Rise, Larsen Ice Shelf, Graham Land -----	8
8. Ice rises and ice rumples, Wordie Ice Shelf, Graham Land -----	9
9. McDonald Ice Rumples, Brunt Ice Shelf, Coats Land -----	10
10. An ice doline, Princess Astrid Coast-----	11
TABLE	
1. Frequency of coastal types around Antarctica -----	4
2. Morphometric data for Antarctica -----	12
3. Regional ice data -----	12
The Transantarctic Mountains -----	13
Western margin of Ross Ice Shelf -----	13
McMurdo Sound area -----	32
The 'dry valleys' of Victoria Land, by Trevor J Chinn -----	39
Northern Victoria Land -----	41
FIGURE	
11-12. Annotated NOAA 6 advanced very high resolution radiometer image of:	
11. The McMurdo Sound area and environs -----	14
12. A part of the Transantarctic Mountains -----	15
13-22. Oblique aerial photograph of:	
13. Reedy Glacier at the eastern extremity of the Queen Maud Mountains -----	16
14. Scott Glacier, Queen Maud Mountains -----	17
15. Amundsen Glacier, Queen Maud Mountains -----	18
16. Axel Heiberg Glacier, Queen Maud Mountains ----	19
17. The upper part of Liv Glacier, Queen Maud Mountains -----	20
18. Shackleton Glacier, Queen Maud Mountains -----	21
19. The northwestern end of the Queen Maud Mountains bordering on Beardmore Glacier -----	22
20. The mouth of Beardmore Glacier -----	23
21. Nimrod Glacier -----	24
22. Byrd Glacier -----	25

	Page
23. Annotated Landsat 1 MSS digitally enhanced false-color composite image of a part of the Byrd Glacier, the Ross Ice Shelf, and environs -----	B27
24. Landsat 1 MSS digitally enhanced false-color composite image showing (A) bare glacier ice on Byrd and Hatherton Glaciers and meltwater lakes on the lower part of Darwin Glacier and (B) bedrock areas of the surrounding mountains -----	28
25. Annotated Landsat 4 MSS image mosaic of a part of the Byrd Glacier, the Ross Ice Shelf, and environs -----	30
26. Oblique aerial photograph of Mulock Glacier -----	31
27. Annotated Landsat 1 MSS image mosaic of Ross Island and part of the Ross Ice Shelf and environs -----	33
28. Oblique aerial photograph of Koettlitz Glacier flowing into McMurdo Ice Shelf -----	34
29. Annotated Landsat 1 MSS image of Minna Bluff and environs -----	35
30–31. Oblique aerial photograph of:	
30. The ablation area of McMurdo Ice Shelf -----	36
31. Ross Island -----	37
32. Annotated Landsat 1 MSS digitally enhanced false-color composite image of the 'dry valleys' of Victoria Land -----	38
33. Oblique aerial photograph of Taylor Glacier and Lake Bonney -----	40
34–35. Annotated Landsat 1 MSS digitally enhanced false-color composite image of the Scott Coast of Victoria Land	
34. Southern section -----	43
35. Northern section -----	44
36. Oblique aerial photograph of David Glacier -----	45
37. Annotated Landsat 1 MSS digitally enhanced false-color composite image of the Borchgrevink Coast and Mount Melbourne -----	46
38. Annotated Landsat 1 MSS image of Cape Adare and Cape Hallett -----	48
39–40. Annotated Landsat 3 RBV image of:	
39. The Lillie Glacier and the Pennell Coast -----	49
40. The Rennick Glacier and the Oates Coast -----	50
41. Landsat 1 MSS digitally enhanced false-color composite image of the terminus of the Rennick Glacier and the Oates Coast -----	51
42. Annotated Landsat 1 MSS image mosaic of the Rennick Glacier and the Usarp Mountains -----	53
43. Annotated Landsat 3 RBV image of the Suvorov Glacier and the Oates Coast -----	54
The Indian Ocean sector -----	55
Wilkes Land, Bunger Hills, and Shackleton Ice Shelf -----	55
Queen Mary Coast and Amery Ice Shelf -----	62
Mawson Coast and Enderby Land -----	75
FIGURE 44–45. Annotated Landsat 1 MSS image of:	
44. The home of the blizzard Commonwealth Bay, George V Coast -----	56
45. Snow megadunes on the high plateau of East Antarctica -----	58
46. Annotated Landsat 1 MSS digitally enhanced image mosaic of Totten Glacier, Wilkes Land -----	60
47. Annotated Landsat 1 MSS false-color composite image of Denman Glacier and Bunger Hills -----	61
48–50. Annotated Landsat 1 MSS image of:	
48. Queen Mary Coast -----	63
49. The Gamburtsev Subglacial Mountains -----	64
50. Sørsdal Glacier and the Vestfold Hills -----	66
51. Landsat 1 MSS image of snow textures on the high plateau of East Antarctica -----	67

	Page
52. Annotated Landsat 1 MSS image of the source of Lambert Glacier	B 69
53. Annotated Landsat 1 MSS digitally enhanced false-color composite image mosaic of Lambert Glacier and Amery Ice Shelf	70
54. Annotated Landsat 1 MSS image of the left bank of Amery Ice Shelf	73
55. Uncontrolled Landsat MSS image mosaic of the Amery Ice Shelf and the terminus of the Lambert Glacier, East Antarctica	47
56. Annotated Landsat 1 MSS image of Mac. Robertson Land at Mawson Station	76
57. Annotated Landsat 1 and 2 MSS image mosaic of Enderby Land	78
58–59. Annotated Landsat 1 MSS image of:	
58. Alasheyev Bight at Molodezhnaya Station	80
59. Lützw-Holm Bay at Shōwa Station	81
60. Annotated Landsat 1 MSS digitally enhanced false-color composite image of ablation areas of the Queen Fabiola Mountains	82
The Atlantic Ocean sector	83
Princess Ragnhild Coast, Princess Astrid Coast, Borg Massif, and Fimbul Ice Shelf, Queen Maud Land	83
Riiser-Larsen Ice Shelf and Shackleton Range	97
Filchner and Ronne Ice Shelves	101
FIGURE 61. Annotated Landsat 1 MSS image of the Sør-Rondane Mountains	84
62. Annotated Landsat 1 MSS false-color composite image of the Orvin and Wohlthat Mountains	85
63. Annotated Landsat 2 MSS image of Lazarev Ice Shelf at Novolmarevskaya	87
64–67. Oblique aerial photograph of:	
64. The ablation area surrounding Schirmacher Hills	88
65. The tidal sea lake at the western end of Schirmacher Hills	89
66. Nunataks in Queen Maud Land	90
67. The Heimefront Range in Queen Maud Land	91
68. Annotated NOAA 7 advanced very high resolution radiometer three-image mosaic of New Schwabensland, Queen Maud Land	93
69. Annotated Landsat 1 and 2 MSS image mosaic of Jutulstraumen Glacier and environs, Princess Martha Coast	94
70. Landsat 2 MSS digitally enhanced false-color composite image of the Jutulstraumen Glacier and environs	95
71–72. Oblique aerial photograph of:	
71. The Berg Massif	96
72. Neumayer Cliffs, in the northeastern part of Kirwan Escarpment	96
73–77. Annotated Landsat 1 MSS image of:	
73. Stancomb-Wills Glacier	98
74. The upper Slessor Glacier, Queen Maud Land	99
75. Slessor Glacier and the Shackleton Range	100
76. Filchner Ice Shelf and the Grand Chasms	102
77. Ronne Ice Shelf and Korff Rise	104
The Antarctic Peninsula	105
FIGURE 78. Annotated Landsat 2 MSS image of the northern extremity of the Antarctic Peninsula	106
79. Annotated Landsat 3 MSS image of Graham Land plateau and the Larsen Ice Shelf	108
80. Oblique aerial photograph of Doumer, Wiencke, and Anvers Islands	109

	Page
81–82. Annotated Landsat 3 MSS image of:	
81. Marguerite Bay and the west coast of Graham Land -----	B110
82. Northern Palmer Land and Wordie Ice Shelf -----	112
83–85. Oblique aerial photograph of:	
83. Buffer Ice Rise and the mouth of Fleming Glacier, Graham Land -----	113
84. Tidal sea lakes, George VI Ice Shelf -----	114
85. Spartan Glacier, Alexander Island -----	115
86. Annotated Landsat 1 MSS image of Palmer Land and George VI Ice Shelf -----	116
87. Annotated Landsat 3 MSS image of Alexander Island -----	118
The Pacific Ocean sector-----	119
Ellsworth Land and Ellsworth Mountains-----	119
Marie Byrd Land -----	124
Eastern Margin of Ross Ice Shelf -----	135
 FIGURE	
88. Annotated Landsat 1 MSS digitally enhanced false-color composite image of the English Coast of Palmer Land -----	120
89. Annotated Landsat 1 MSS image of Fowler Ice Rise and Carlson Inlet -----	121
90. Annotated Landsat 1 MSS digitally enhanced false- color composite image of the Sentinel Range, Ellsworth Mountains, and Rutford Ice Stream -----	122
91. Oblique aerial photograph of the Sentinel Range, Ellsworth Mountains -----	123
92. Annotated Landsat 1 MSS image of Pine Island Glacier and the Walgreen Coast -----	125
93. Annotated Landsat 1 MSS image mosaic of Thwaites Glacier and Thwaites Iceberg Tongue, 1972–73 -----	126
94. Annotated Landsat 2 MSS images of selected volcanoes in Marie Byrd Land -----	128
95. Annotated Landsat 1 MSS image of Mount Takahe -----	130
96–97. Oblique aerial photograph of:	
96. Mount Takahe volcano -----	131
97. Mount Hampton volcano -----	131

	Page
98. Annotated Landsat 1 MSS image of Ruppert Coast---	B132
99-100. Oblique aerial photograph of:	
99. White Glacier, Marie Byrd Land -----	133
100. Fosdick Mountains, Ford Ranges, Marie Byrd Land --	134
101. Annotated Landsat 1 MSS image of 'Ice Stream E' flowing west from Marie Byrd Land-----	136
102. Annotated Landsat 1 MSS digitally enhanced false-color composite image of Shirase Coast and the Ross Ice Shelf at the mouth of 'Ice Stream E' -----	137
103. Oblique aerial photograph of the northern edge of 'Ice Stream B' -----	138
 Acknowledgments-----	 139
 Landsat images of Antarctica, by Richard S. Williams, Jr., and Jane G. Ferrigno -----	 139
Introduction -----	139
Index map to optimum Landsat 1, 2, and 3 images of Antarctica -----	141
Tables of optimum Landsat 1, 2, and 3 images of Antarctica -----	143
TABLE 4. Evaluation of optimum Landsat 1, 2, and 3 MSS images of Antarctica -----	143
5. Code used to classify each of the 2,514 Landsat nominal scene centers in Antarctica -----	143
 References cited -----	 146
TABLE 6. Optimum Landsat 1, 2, and 3 MSS and Landsat 2 RBV images of Antarctica -----	154
7. Usable and marginally usable Landsat 3 RBV images of glaciers of Antarctica -----	261
 [Plates in pocket]	
PLATE 1. Index map to principal geographic features and locations discussed in Chapter B, Antarctica	
2. Index map showing optimum Landsat 1, 2, and 3 images of glaciers of Antarctica	

ANTARCTICA

By CHARLES SWITHINBANK¹

Abstract

Of all the world's continents Antarctica is the coldest, the highest, and the least known. It is one and a half times the size of the United States, and on it lies 91 percent (30,109,800 km³) of the estimated volume of all the ice on Earth. Because so little is known about Antarctic glaciers compared with what is known about glaciers in populated countries, satellite imagery represents a great leap forward in the provision of basic data. From the coast of Antarctica to about 81° south latitude, there are 2,514 Landsat nominal scene centers (the fixed geographic position of the intersection of orbital paths and latitudinal rows). If there were cloud-free images for all these geographic centers, only about 520 Landsat images would be needed to provide complete coverage. Because of cloud cover, however, only about 70 percent of the Landsat imaging area, or 55 percent of the continent, is covered by good quality Landsat images. To date, only about 20 percent of Antarctica has been mapped at scales of 1:250,000 or larger, but these maps do include about half of the coastline. The area of Antarctica that could be planimetrically mapped at a scale of 1:250,000 would be tripled if the available Landsat images were used in image map production.

This chapter contains brief descriptions and interpretations of features seen in 62 carefully selected Landsat images or image mosaics. Images were chosen on the basis of quality and interest; for this reason they are far from evenly spaced around the continent. Space limitations allow less than 15 percent of the Landsat imaging area of Antarctica to be shown in the illustrations reproduced in this chapter. Unfortunately, a wealth of glaciological and other features of compelling interest is present in the many hundreds of images that could not be included. To help show some important features beyond the limit of Landsat coverage, and as an aid to the interpretation of certain features seen in the images, 38 oblique aerial photographs have been included. Again, these represent only a small fraction of the large number of aerial photographs now available in various national collections.

The chapter is divided into five geographic sections. The first is the Transantarctic Mountains in the Ross Sea area. Some very large outlet glaciers flow from the East Antarctic ice sheet through the Transantarctic Mountains to the Ross Ice Shelf. Byrd Glacier, one of the largest in the world, drains an area of more than 1,000,000 km². Next, images from the Indian Ocean sector are discussed. These include the Lambert Glacier–Amery Ice Shelf system, so large that about 25 images must be mosaicked to cover its complex system of tributary glaciers. Shirase Glacier, a tidal outlet glacier in the sector, flows at a speed of 2.5 km a⁻¹. About 200 km inland and 200 km west of Shirase Glacier lie the Queen Fabiola (“Yamato”) Mountains, whose extensive exposures of ‘blue ice’ lay claim to being the world’s most important meteorite-collecting locality, with more than 4,700 meteorite fragments discovered since 1969.

The Atlantic Ocean sector is fringed by ice shelves into which flow large ice streams like Jutulstraumen, Stancomb-Wills, Slessor, and Recovery Glaciers. Filchner and Ronne Ice Shelves together cover an area two-thirds the size of Texas. From the western margin of the Ronne Ice Shelf, the north-trending arc of the Antarctic Peninsula, with its fjord and alpine landscape and fringing ice shelves, stretches towards South America. The Pacific Ocean sector begins with the Ellsworth Mountains, which include the highest peaks (Vinson Massif at 4,897 m) in Antarctica. The area between the Ellsworth Mountains and the eastern margin of the Ross Ice Shelf is fringed with small ice shelves and some major outlet glaciers. One of these, Pine Island Glacier, was found from comparing 1973 and 1975 images to have an average ice-front velocity of 2.4 km a⁻¹. This part of Antarctica contains many dormant volcanoes; the summits of several, such as Mount Takahe with its 8-km-wide summit caldera, protrude through the West Antarctic ice sheet. Five major ice streams, ‘A’ through ‘E,’ drain into the eastern margin of the Ross Ice Shelf. The orbital range of Landsat allows only the northernmost of these, Ice Stream ‘E,’ to be imaged. A final section of the chapter lists optimum Landsat images for each of the 2,514 nominal scene centers.

¹British Antarctic Survey.

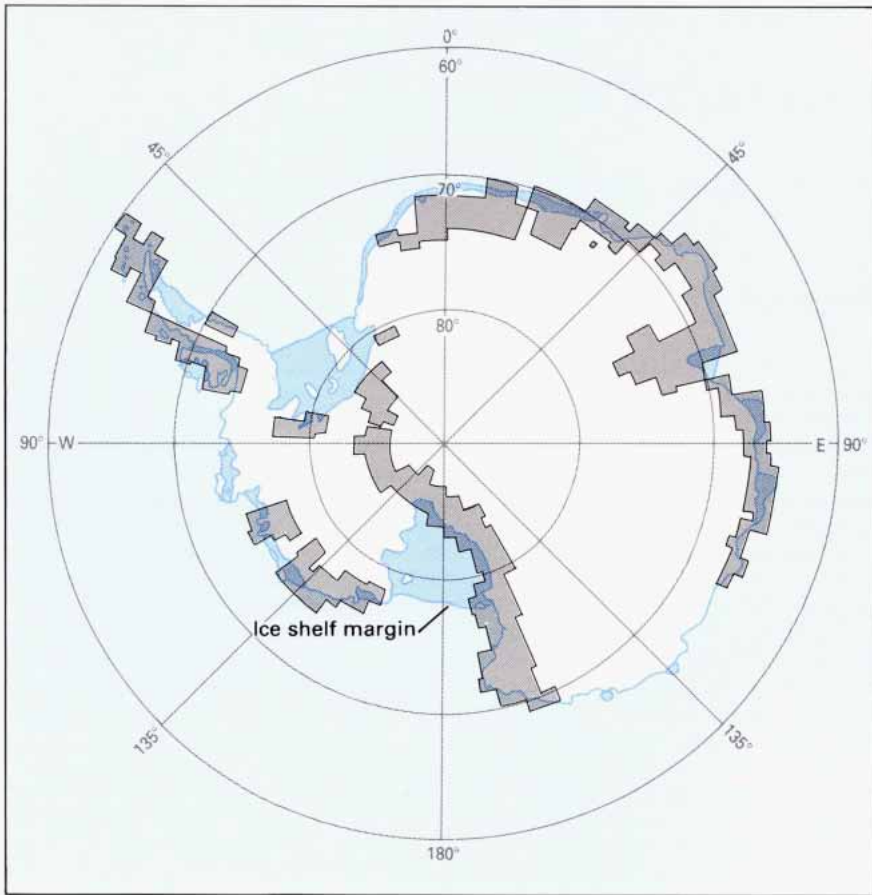


Figure 1.—Extent of 1:250,000-scale and larger scale mapping in Antarctica (shaded areas) produced by aerial photogrammetric and satellite-image map techniques.



Figure 2.—Apollo 17 color photograph of the Earth showing most of the continent of Antarctica. NASA photograph no. 72-HC-928, courtesy of the NASA Public Information Office, Washington, D.C.

INTRODUCTION

Satellite imagery has made a much greater contribution to polar glaciology than it has to the study of glaciers in temperate latitudes. This is because, at the dawn of the satellite era, little was known about the vast polar ice sheets compared with what was known about many of the small glaciers in populated countries. The first step in studying any glacier is to consider its location, shape, and size: in other words, we need a map. There are very good maps of the glaciers of the Alps and the Rocky Mountains, but much of the Antarctic is still unmapped today (figs. 1 and 2). Strange as it may seem, the far side of the Moon is better mapped than parts of our own planet. Position errors of more than 100 km were found in 1975 on the most up-to-date maps published of one part of the Antarctic. Over much of the continent we still lack maps even to minimum standards for air navigation, let alone for any scientific purpose. Conventional maps at a scale of 1:250,000 or larger—the minimum scale usable for glaciological purposes—presently cover (1986) only about 20 percent of the area of Antarctica (fig. 1). The cost of conventional mapping under polar conditions is so high that it will probably not proceed much faster in the future than it has done in the past.

While a conventional map is no more than a symbolic representation of features on the Earth's surface in their correct relative positions, the satellite image or photograph goes one better: it is an *image* of features on the Earth's surface in their correct relative positions. It is true that ground control is necessary in order to scale and orient the image as in conventional mapping. But unlike conventional mapping, a great wealth of detail is recorded in the image instantaneously. Although all good topographic maps should have contours (and satellite images have none), satellite images have redeeming virtues that make them infinitely preferable to no maps at all. In some areas, such as Greenland, it is practicable to use contemporary satellite images to measure changes that have taken place in the position of glacier margins since the area was first mapped half a century ago. In Antarctica, satellite images generally yield the first-ever reliable data not only on many glacier margins but also on the very existence of a great variety of features never seen before (plate 1) (Swithinbank, 1973a, 1973b; Southard and MacDonald, 1974; Swithinbank and Lucchitta, 1986). Glaciologists now have a baseline 'against which to observe glacier fluctuations, but new imagery will be needed after an interval of several years in order to measure any changes (Swithinbank and Lane, 1977).

Geographic Place-names

Most geographic place-names used in this chapter follow the gazetteer *Geographic Names of the Antarctic* (Alberts, 1981) and official supplements approved by the United States Board on Geographic Names and Secretary of the Interior for use by U.S. Government agencies. Names not listed in the gazetteer or supplements fall into two categories: (1) those used by other Antarctic Treaty nations whose respective languages have no equivalent in the gazetteer or supplements and (2) those used in the vernacular. Names in the first category will be shown in double quotation marks, and names in the second category will be shown in single quotation marks.

Definitions

In contrast to other continents, there are few independent (separate) local glaciers in Antarctica, that is to say glaciers having well-defined boundaries. Thus it is important to bear in mind that the definition of *glacier* used in this chapter includes ice sheets, ice shelves, ice rises, ice caps, ice piedmonts, outlet glaciers, and valley glaciers (Armstrong and others, 1973). In simple terms it can almost be said that there is only one glacier in Antarctica, although it is ten times the area of all the rest of the world's glaciers put together. Glacier units are therefore much harder to define here than in lower latitudes. It is for this reason and also because of the lack of maps at a suitable scale that no glacier inventory of Antarctica has yet been attempted (Swithinbank, 1980), except for an inventory of glaciers on James Ross Island and Vega Island, which lie to the east of the Trinity Peninsula in the northern part of the Antarctic Peninsula (Rabassa and others, 1982).

There are similar unusual circumstances when discussing the Antarctic coastline. In other continents, except where glaciers extend into the ocean (for example, northeastern Canada, northwestern Greenland, or Svalbard) everyone knows what we mean by the term coastline. But in Antarctica there is more than one coastline (table 1).

TABLE 1.—Frequency of coastal types around Antarctica
(from Drewry, 1983)

Type	Percent
Ice shelf (ice front) -----	44
Ice walls - - - - -	38
Ice stream/outlet glacier (ice front or ice wall) - -	13
Rock - - - - -	5
Total - - - - -	100

In the absence of sea ice, mariners would hold that the coastline is an immovable barrier at the limit of navigation. There are, however, several interpretations of this definition:

1. Almost half of the Antarctic coastline consists of *ice front* (ice barrier), a vertical cliff from 2 to 50 m above sea level (figs. 3 and 4). But the mariner will be surprised to find that at this coastline his echosounder may show the depth of water to be between 100 m and 600 m. Here the ice sheet is afloat.

2. Approaching an *ice wall*, the mariner will see a vertical cliff resembling an *ice front*. Here the ice sheet is aground. At this coastline the echosounder may show the depth of water to be between 0 and 500 m. If the rock basement is at sea level the ice cliff is called a *strand ice wall* (fig. 5); if below sea level it is called a *neritic ice wall* (fig. 6) (Roberts and others, 1955).

3. Our mariner will have no difficulty in recognizing the coastline where waves lap against a rocky shore. Only about 5 percent of the Antarctic coast is like this.

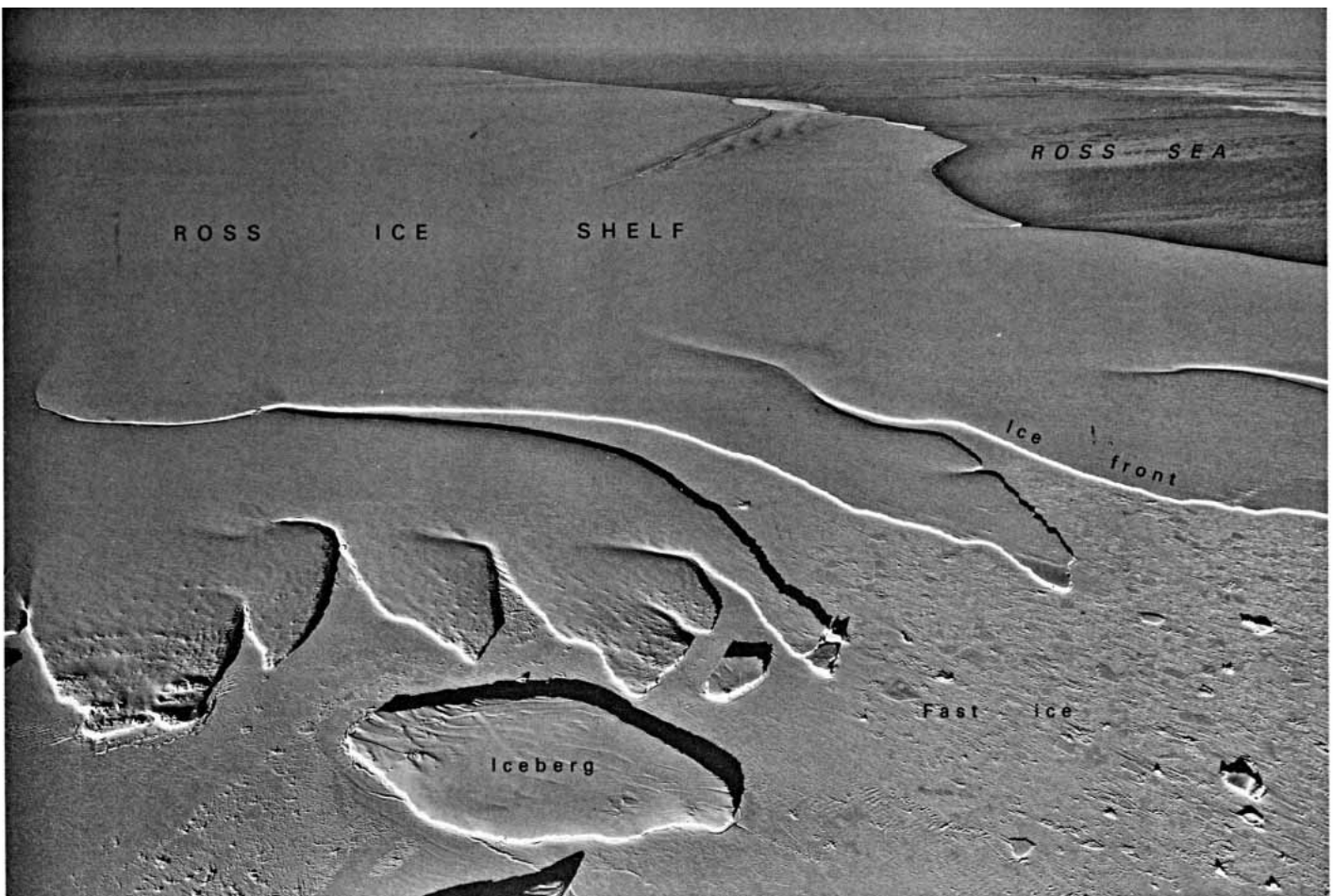
4. When told that an ice-front coastline can retreat by 50 km in a day by the calving of an iceberg, a lawyer might say that a floating coastline is tantamount to a contradiction in terms. For legal purposes, a coastline must be permanent; it is only permanent where the ice sheet is grounded. Apart from definitions 2 and 3 above, the permanent coastline is represented by the inland boundary of ice shelves and glacier tongues. It may be from 50 km to 800 km from the ice front, and the lawyer will be disconcerted to learn that the depth of ice below sea level there may be from 100 m to 2,000 m. But this coastline, like the

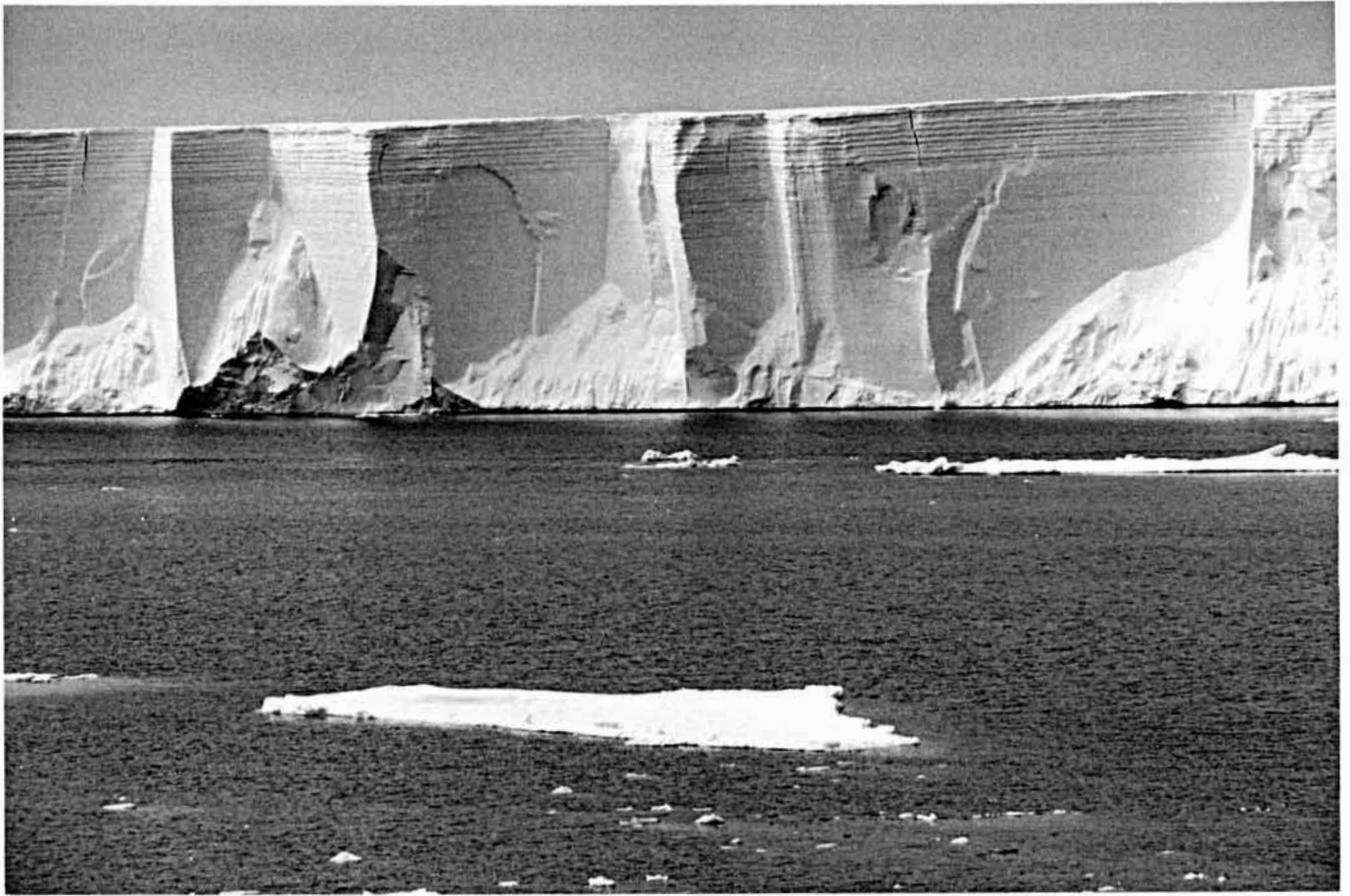
others, can generally be interpreted from Landsat images. On selected images (see figs. 47 and 63, for example) we have indicated with a dotted line the assumed position of the sub-ice coastline in order to draw attention to visible features we believe to be diagnostic. This coastline is referred to as the *inland boundary* of the ice shelves, or the *grounding line*, but it could with equal justification be called the *floatation line*. Some authors have called it the *hinge line* because tidal bending is taken up there.

5. If we find definitions 1, 2, and 4 unsatisfactory on the ground that their coasts are ephemeral, we may favor the concept of a sub-ice coastline at which the rock rises up to sea level. But this coastline cannot be identified from satellite images, can only be found by radio-echosounding, and is unknown over 90 percent of its length.

Figure 3.—Oblique aerial photograph of the ice front in Okuma Bay, eastern edge of the Ross Ice Shelf and Shirase Coast, taken from an altitude of 1,500 m on 22 October 1961, looking west. The ice shelf flows from left to right at a speed of 350 m a⁻¹ (Personal commun. from Andre Flotron). The ice front is approximately 20 m high. U.S. Navy trimetrogon aerial photograph no. 14 (TMA 822 F33)² from the Antarctic Map and photograph Library, U.S. Geological Survey.

²TMA is an abbreviation for Trimetrogon Antarctica. The number following TMA refers to the mission or sortie. A trimetrogon camera configuration includes three mapping cameras, a left oblique (F31), a vertical (F32), and a right oblique (F33), with reference to the flight path of the survey aircraft. Major post-World War II trimetrogon aerial survey operations in the Antarctic included U.S. Navy Operation Highjump (HJ), which used L, V, and R, and U.S. Navy Operation Deep Freeze (DF), which used 1, 2, and 3, for left oblique, vertical, and right oblique, respectively. Oblique aerial photographs have also been acquired during radio-echosounding surveys and are identified as RES (see figure 9, for example). In recent years, overlapping vertical aerial photographs have been acquired of specific field areas to support the preparation of conventional maps of such areas by stereophotogrammetric techniques. The U.S. Geological Survey's 1:50,000-scale topographic maps of the 'dry valleys' area are a good example of such modern maps.





◁ **Figure 4.**—An ice front on the Brunt Ice Shelf as seen from a ship, Coats Land, on 5 January 1977. The cliff is generally 20 to 30 m high. Photograph by Charles Swithinbank, British Antarctic Survey.

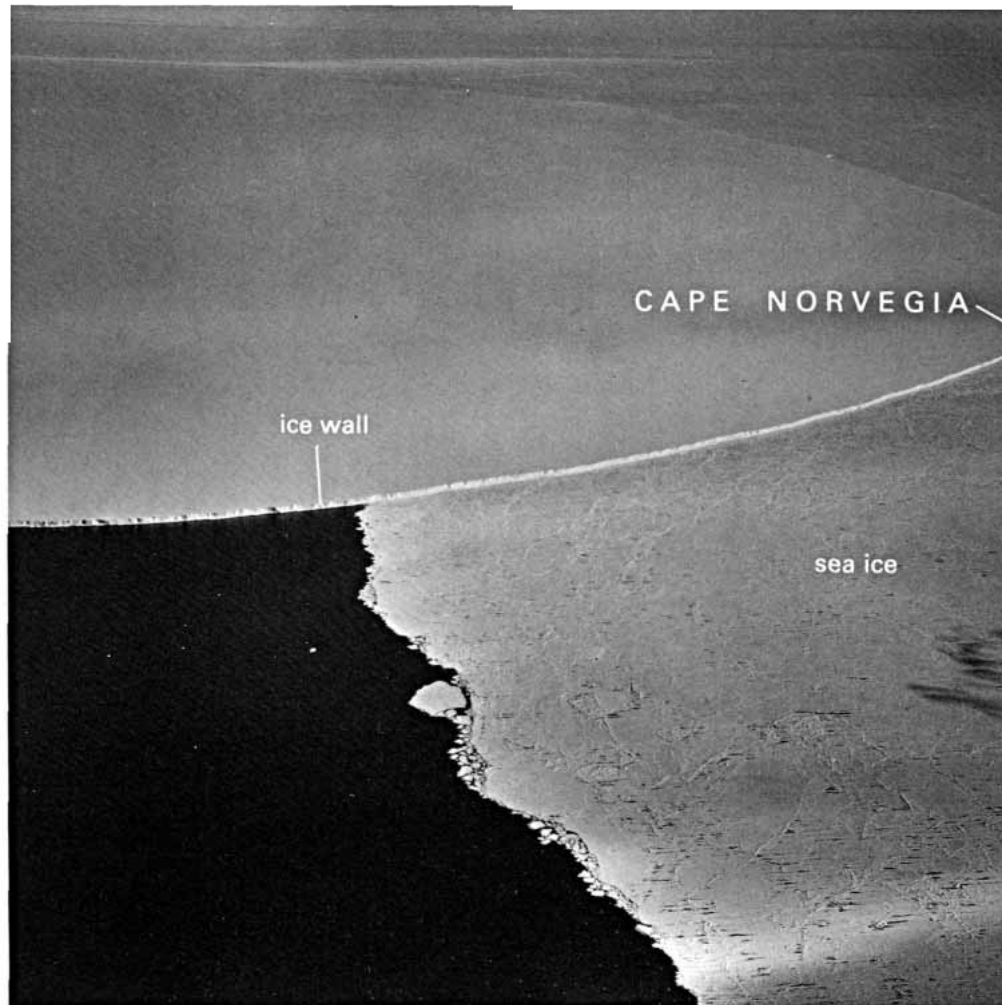
The best pre-satellite description of the glaciers of Antarctica and the sub-Antarctic islands is that of Mercer (1967), who also reported on glacier variations (Mercer, 1962). Such is the size of Antarctica that the satellite imagery selected for reproduction in this chapter can only cover a very small proportion of the coastline and a few places of special interest inland. No usable scenes were found of the sub-Antarctic islands. By contrast, it was very difficult to select the best scenes of Antarctica from the hundreds available. A typical scene shows a featureless expanse of snowy whiteness covering the whole frame. Bare rock, after all, covers a very small proportion of the surface area of the continent. However, many of the scenes contain a wealth of detail showing glaciological features that were unknown and unsuspected before the satellite images were studied.

Certain glacier features are unique to the Antarctic and for this reason are inadequately treated in the “Illustrated Glossary of Snow and Ice” (Armstrong and others, 1973). Here we shall discuss in greater detail ice shelves, ice rises, ice rumples, and ice dolines. Nearly half of the coastline of Antarctica is fringed by *ice shelves* (see figs. 3 and 54). Ice shelves are floating ice sheets that rise and fall with the tide. Their thicknesses range from a minimum of about 10 m to a maximum of about 2,000 m, though most are in the 100 to 500 m range. They are nourished partly by the seaward extension of land glaciers, partly by the accumulation of snow on their upper surface, and partly by bottom freezing. They are dissipated mainly by the calving of icebergs from their seaward edges and by melting from their lower and, exceptionally, from their upper surfaces. Forward movement consists of one

◁ **Figure 5.**—An ice wall, Dorian Bay, Graham Land, as seen from a ship on 13 December 1979. The ice wall is approximately 20 m high. Photograph by Charles Swithinbank, British Antarctic Survey.

Figure 6.—Annotated oblique aerial photograph of an ice wall, Cape Norvegia, Princess Martha Coast, taken from an altitude of 2,500 m on 25 January 1951, looking south. The ice wall is approximately 30 m high. Photograph no. DML³ 51–522323 by Sigvard Kjellberg, Norsk Polarinstitutt, Oslo.

³DML is an abbreviation for Dronning Maud Land (Queen Maud Land), the region of Antarctica most intensively studied by scientists of the Norsk Polarinstitutt.

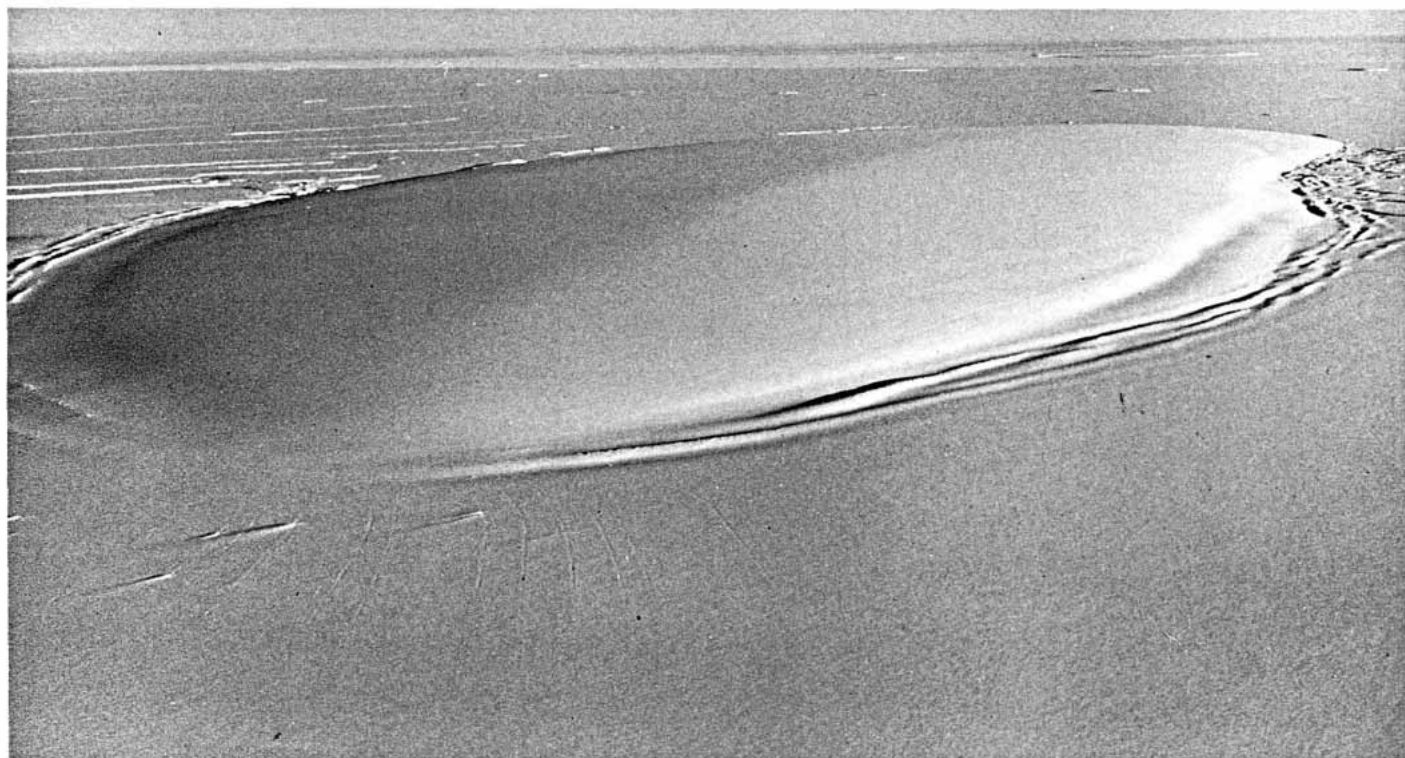


component contributed by the seaward flow of land glaciers and another, increasing towards the ice front, provided by spreading in response to the local accumulation of snow (Swithinbank, 1955). An Antarctic ice shelf may carry no ice of land origin by the time it reaches the ice front; bottom melting has removed both it and the debris of glacial erosion. As the ice shelf moves forward, a thinning wedge of ice of land origin is progressively displaced by a thickening wedge of ice formed from locally accumulated snow. In some cases the land ice may be underlain in places by a variable thickness of sea ice (Morgan, 1972; Zotikov and others, 1979; Neal, 1979). In contrast to an ice shelf representing the seaward extension of an inland ice sheet or a number of land glaciers, a *glacier tongue* represents the extension of a single land glacier. Most glacier tongues are composed of ice mainly of land origin; few are long enough to be substantially nourished by locally accumulated snow.

We become progressively less certain of the principal component of ice shelves as we approach their northern (climatic) limit. In the Antarctic Peninsula, for example, Wilkins Ice Shelf (fig. 87), at latitude 70°S. is the northernmost on the Pacific coast that is nourished principally by local snow. Wordie Ice Shelf, at latitude 69°S., consists essentially of coalescent glacier tongues. Two small ice shelves, Muller and Jones Ice Shelves, the northernmost on the west coast of the Antarctic Peninsula, are found in the fjord region between latitudes 67° and 68°S. (fig. 81). On the east coast of the peninsula, the thin but permanent floating ice in Prince Gustav Channel (latitude 64° 15' S.) is nourished not by snowfall but instead by the freezing of seawater (Reece, 1950). Other parts of the Antarctic have their share of ice shelves of uncertain composition.

Ice rises are dome-shaped ice caps grounded on shoals within or at the seaward edge of ice shelves (figs. 7 and 77). It is probable that most of them originate from localized grounding of areas of ice shelf. But being grounded, they are, by definition, not part of the ice shelf. Although nourished almost exclusively by local accumulation, many are to some

Figure 7.—Oblique aerial photograph of Gipps Ice Rise, Larsen Ice Shelf, Graham Land, taken from an altitude of 7,000 m on 1 January 1972, looking east. The ice rise has dimensions of 9 x 18 km and is 300 m high. Photograph by Charles Swithinbank, British Antarctic Survey.



extent dependent on the mechanical constraint provided by the surrounding ice shelf. Ice rises are bounded by the grounding line or, if they face the sea, by an ice wall. Because many of them rest on platforms of rock well below sea level, their horizontal dimensions are probably highly sensitive to isostatic or eustatic changes in relative sea level. Many unmapped ice rises have been seen for the first time on Landsat images. Orheim (1978) found several in Queen Maud Land, noting that they were generally ellipsoidal in shape, with the short axis about two thirds of the long axis. Ice rises of nearly circular shape are unusual.

Some locally grounded areas within ice shelves are overridden by the ice shelf, and for these the term *ice rumples* was proposed by Armstrong and others (1977). Ice rumples are distinguished by a characteristic crevasse pattern and a rise in the surface (figs. 8, 9, and 82). The criterion for distinguishing between ice rumples and an ice rise is the direction of ice movement, as shown by the crevasse pattern. Ice may be deflected or even halted by ice rumples, but in an ice rise movement

Figure 8.—Annotated oblique aerial photograph of ice rises and ice rumples, Wordie Ice Shelf, Graham Land, taken from an altitude of 6,000 m on 28 November 1966, looking southeast. The ice rise in the center is approximately 2 km in diameter. The camera position is marked on figure 82. U.S. Navy trimetrogon aerial photograph no. 78 (TMA 7835 F33) from the Antarctic Map and Photograph Library, U.S. Geological Survey.

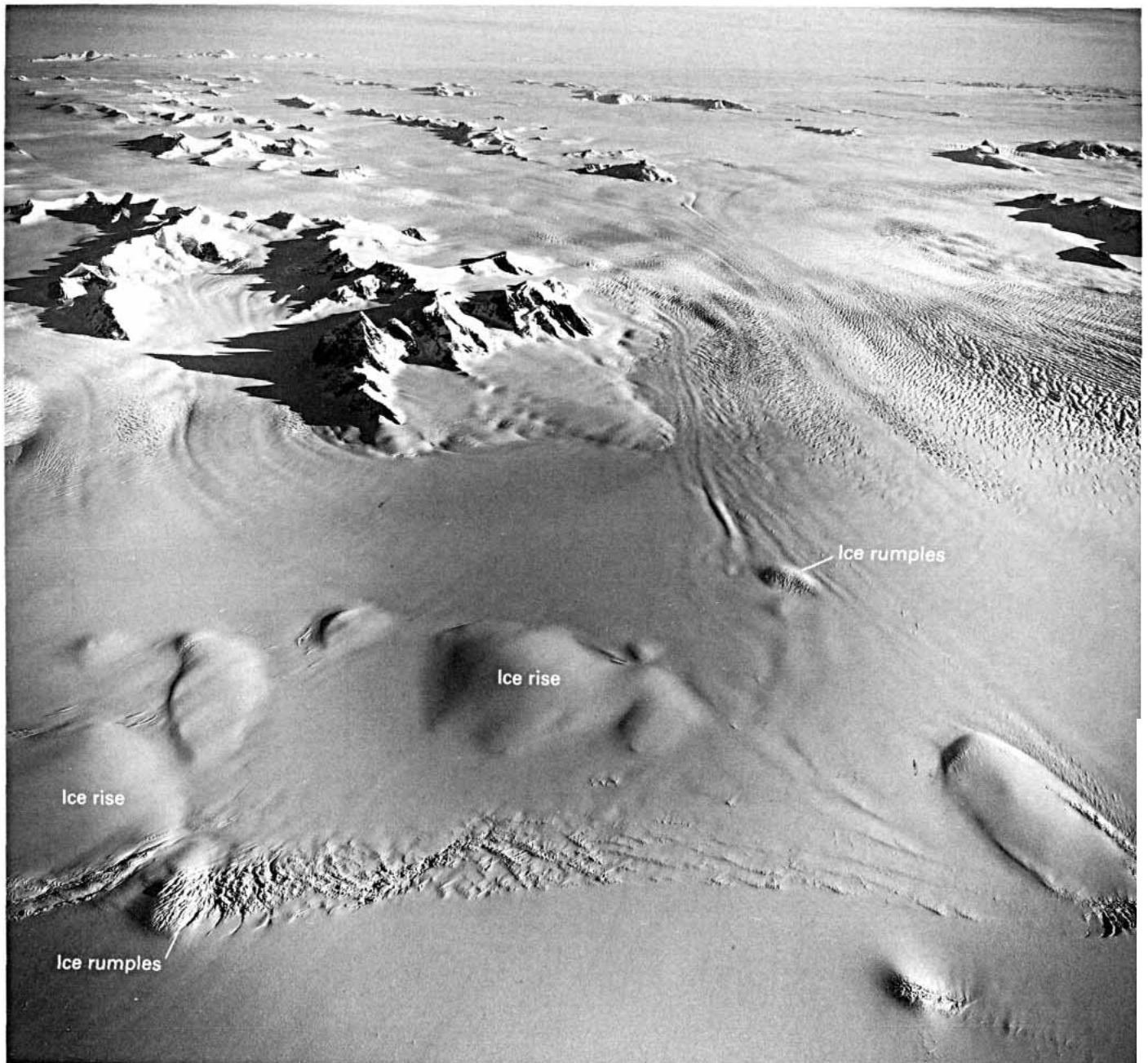




Figure 9.—Oblique aerial photograph of McDonald Ice Rumples, Brunt Ice Shelf, Coats Land, taken from an altitude of 2,400 m on 25 January 1970 looking southwest. The grounded area is very nearly an ice rise, but it falls within the definition of ice rumples because some ice flows across it. The ice rumples cover an area about 1.8 x 1.2 km. U. S. Navy trimetrogon aerial photograph no. 240 (RES 179 F31) from the Antarctic Map and Photograph Library, U.S. Geological Survey,

is independent of that of the ice shelf and, being in the main radial, will in places oppose it. No known ice rumples rise more than 50 m above ice shelf surface level, whereas ice rises may be up to 1,000 m high.

A number of large oval-shaped depressions have been found in ice shelves (fig. 10). Various descriptions in the literature as ice calderas, craters, or ice volcanoes, we use the term *ice doline* proposed by Mellor and McKinnon (1960). Ice dolines can be seen in figures 53, 63, and 79.

We have drawn contours at 500-m intervals on selected images in order to give the reader some idea of the general surface gradient of the ice sheet, particularly in featureless areas. However, contours have been broken or omitted in most mountain areas in order to avoid loss of image detail. Although taken or modified from published and unpublished maps, some contours may be substantially in error. Owing to the reconnaissance nature of most Antarctic mapping, it has been difficult to reconcile features seen on the images with those portrayed on the map. In some cases the maps are obviously wrong, and here we have sketched form lines or probable contours. Other contours have been interpreted from unpublished radio altimetry transmitted from constant density balloons of the Tropical Wind, Energy Conversion and

Reference Level Experiment (TWERLE) (Levanon and others, 1977; Levanon, 1982). This source is acknowledged in the figure captions as TWERLE data (unpublished). The most accurate one-sheet contour map of Antarctica is figure 2.1 in Drewry (1983).

We will refer to East Antarctica and West Antarctica. It has been found expedient to distinguish between the two parts of the continent that lie on either side of the constriction formed by the massive indentations of the Ross Sea and Weddell Sea. West Antarctica is the smaller part lying on the Pacific Ocean side of the Transantarctic Mountains, including the Ross Ice Shelf, Filchner Ice Shelf, Ronne Ice Shelf, and the Antarctic Peninsula. Some people consider the names 'Greater Antarctica' and 'Lesser Antarctica' to be more appropriate in that a sizeable part of East Antarctica lies west of the Greenwich meridian (Roberts, 1981). Indeed Hayes (1975) summarized the realm of confusion in these words: "In parts of East Antarctica West Antarctica is east, in others west. This of course depends on if you are in east East Antarctica or west. However, if you are in west West Antarctica, East Antarctica is west unless you want to go to west East Antarctica in which case it is east. The same holds for east West Antarctica only in the reverse except that if you want to go to West East Antarctica, you still go east." In spite of these problems, the names East and West Antarctica have come into general use in North America.

Figure 10.—Oblique aerial photograph of an ice doline, Princess Astrid Coast, taken from an altitude of 300 m on 25 January 1959, looking north. The ice doline is approximately 1 km in diameter. The camera position is marked on figure 63. Photograph no. DML 58-59 4116 by Sigurd Svindland, Norsk Polarinstitut, Oslo.



Dimensions

Glacier ice in Antarctica covers about 86 percent of the total glacierized area on Earth and contains about 91 percent of the total volume of freshwater ice. The glacier ice in Greenland represents about 8 percent of the volume and all other glaciers together make up the last 1 percent (Swithinbank, 1985). Thus, Antarctica must dominate any discussion of contemporary glacierization. Remote though it is from other continents, it influences weather and climate in both hemispheres. Owing to the incomplete large-scale map coverage (see fig. 1), there can be no precise data on the dimensions of Antarctica. The dimensions in tables 1, 2, and 3 are based on data reported by Drewry and others (1982) and Drewry (1983). Note that the total area of rock outcrop reported in table 2 more correctly describes the area taken up by mountain ranges, most of which are ice-covered (or at least snow-covered) even in the height of summer. The true area of rock outcrop as revealed by Landsat imagery represents less than 1 percent of the whole area of Antarctica.

TABLE 2.— *Morphometric data for Antarctica (from Drewry, 1983)*

Surface	Area (km ²)	Percent	Mean ice thickness (m)	Volume (km ³)	Percent
Inland ice sheet -----	11,965,700	85.97	2,450	29,324,700	97.39
Ice shelves -----	1,541,710	11.08	475	731,900	2.43
Ice rises -----	78,970	.57	670	53,100	.18
Glacier ice (total) ----	13,586,380		2,160	30,109,800¹	
Rock outcrop -----	331,690	2.38			
Antarctica (total) ----	13,918,070	100.00	2,160	30,109,800¹	100.00

¹The total ice volume is different from the sum of the component parts because individual figures have been rounded.

TABLE 3.— *Regional ice data (from Drewry and others, 1982; Drewry, 1983)*

Region	Area (km ²)	Mean ice thickness (m)	Volume (km ³)
East Antarctica:			
Inland ice sheet -----	9,855,570	2,630	25,920,100
Ice shelves -----	293,510	400	117,400
Ice rises -----	4,090	400	1,600
West Antarctica (excluding Antarctic Peninsula):			
Inland ice sheet -----	1,809,760	1,780	3,221,400
Ice shelves -----	104,860	375	39,300
Ice rises -----	3,550	375	1,300
Antarctic Peninsula:			
Inland ice sheet -----	300,380	610	183,200
Ice shelves -----	144,750	300	43,400
Ice rises -----	1,570	300	500
Ross Ice Shelf:			
Ice shelf -----	525,840	427	224,500
Ice rises -----	10,320	500	5,100
Ronne and Filchner Ice Shelves:			
Ice shelf -----	472,760	650	307,300
Ice rises -----	59,440	750	44,600

THE TRANSANTARCTIC MOUNTAINS

Western Margin of Ross Ice Shelf

The Transantarctic Mountains separate the high plateau of East Antarctica from the lower-lying ice sheet and the great ice shelves of West Antarctica. This 3,000-km-long chain of mountains contains more than half of the visible rock in the whole of Antarctica and some of the most spectacular glacier scenery to be found anywhere on Earth. Unfortunately nearly two-thirds of the whole range lies poleward of the orbital limit of Landsat (the circular area south of about latitude 81°S.). Weather satellites can image the South Pole, but they have a resolution of only about 1 km in comparison with the Landsat multispectral scanner's (MSS's) 79 m. Figures 11 and 12 show clearly many of the giant outlet glaciers that transect the mountain range on the Ross Sea side of the Antarctic. In many areas the level of detail revealed is quite remarkable. It is instructive to compare satellite imagery at different scales with aerial photographs of the same features taken from much lower altitudes. For this reason we have included a selection of oblique aerial photographs of glaciologically significant features. But the bulk of the aerial photographs in this section depict major glaciers that are beyond the range of Landsat. Figures 21 to 37 all fall within the area covered by figure 11, and figures 14 to 33 fall within the area of figure 12. The conspicuous gray-scale stairstep patterns in the bottom left corner of figure 11 are artifacts of image processing of the NOAA satellite images and do not represent real topographic or snow surface features; similarly the rippled appearance of the Ross Ice Shelf in figure 12 is considered to be an artifact.

Reedy Glacier (fig. 13) drains the polar plateau from an area just beyond the southeastern edge of figure 12. Its surface falls steadily over a length of 200 km from an altitude of 2,200 m at its head to 600 m at the foot of the range. This gentle gradient (1 in 125) produces an unusually crevasse-free surface, most of it also snow free. The climate is so cold (latitude 86°S.) that there are extensive ablation areas which are permanently dry: the ablation is solely by sublimation, except perhaps for a small amount of mechanical deflation. Mercer (1971) measured sublimation averaging 7.5 mm of ice per week over a 2-month period in summer. The glacial geology, of the area was described by Mercer (1968).

Scott Glacier (fig. 14) is the southernmost outlet glacier that flows from the polar plateau directly into the floating Ross Ice Shelf. According to McIntyre (in press) it drains an area of 85,000 km². Its surface falls steadily over a length of 240 km from an altitude of 2,800 m at its head to 120 m at the grounding line, an average gradient of 1 in 90. Its threshold on the polar plateau is the highest of any glacier in the Transantarctic Mountains. Mount Howe, at its head, is the southernmost nunatak in Antarctica and is only 285 km from the South Pole.

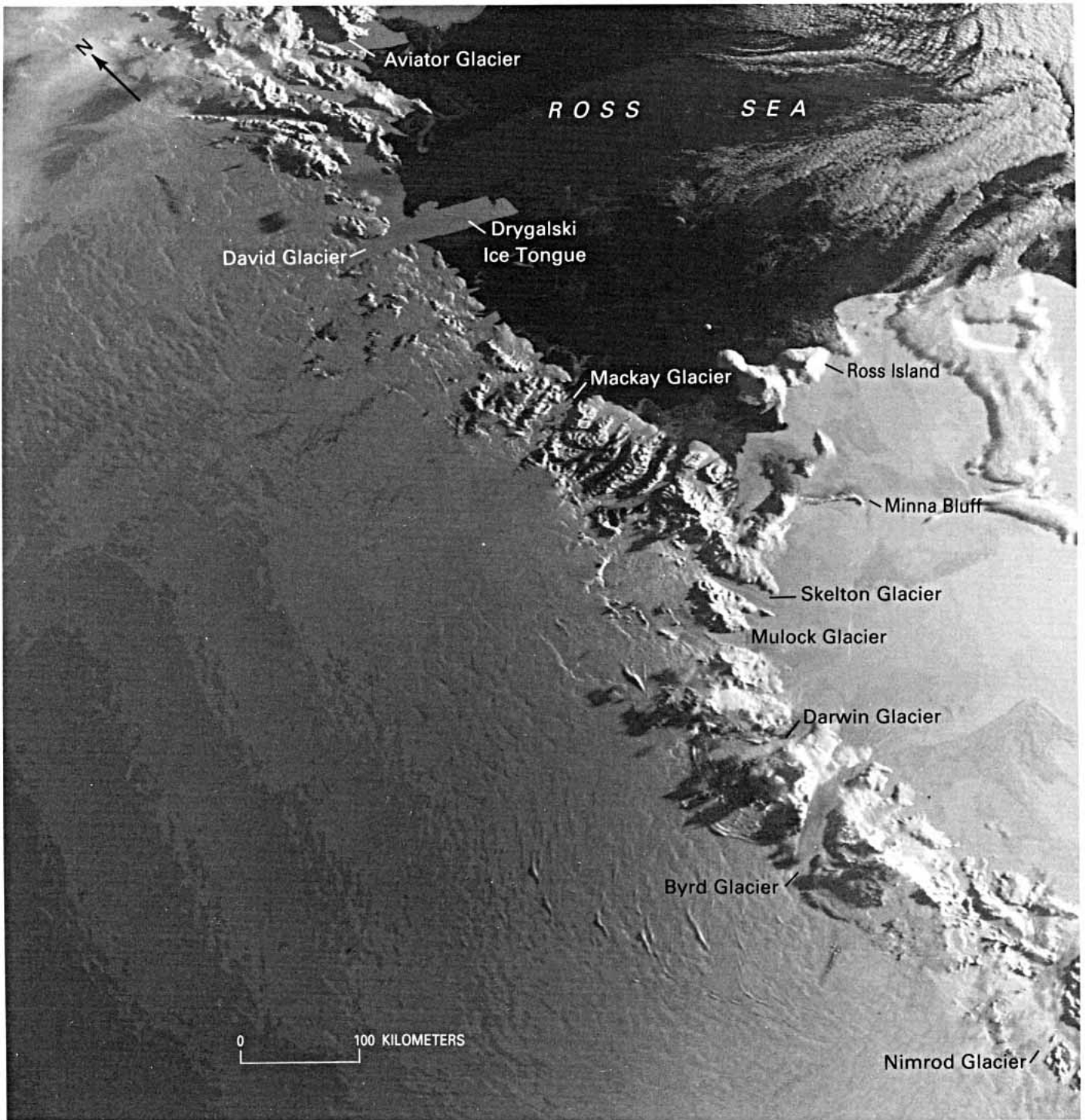


Figure 11.—Annotated NOAA 6 advanced very high resolution radiometer (AVHRR) image (0.8–1.1 μm) of the McMurdo Sound area and environs, acquired on 27 February 1980, at 1812 UT (Universal Time). NOAA 6 AVHRR images have a pixel resolution of about 1.1 km and can be used to monitor dynamic changes along the coast if the changes are sufficiently large (>3 km). NOAA image courtesy of Donald R. Wiesnet, National Oceanic and Atmospheric Administration. See also figures 22, 23, and 25 for an oblique aerial photograph, a Landsat 1 MSS image, and Landsat 4 MSS images, respectively, of the Byrd Glacier, and figure 21 for an oblique aerial photograph of the Nimrod Glacier.

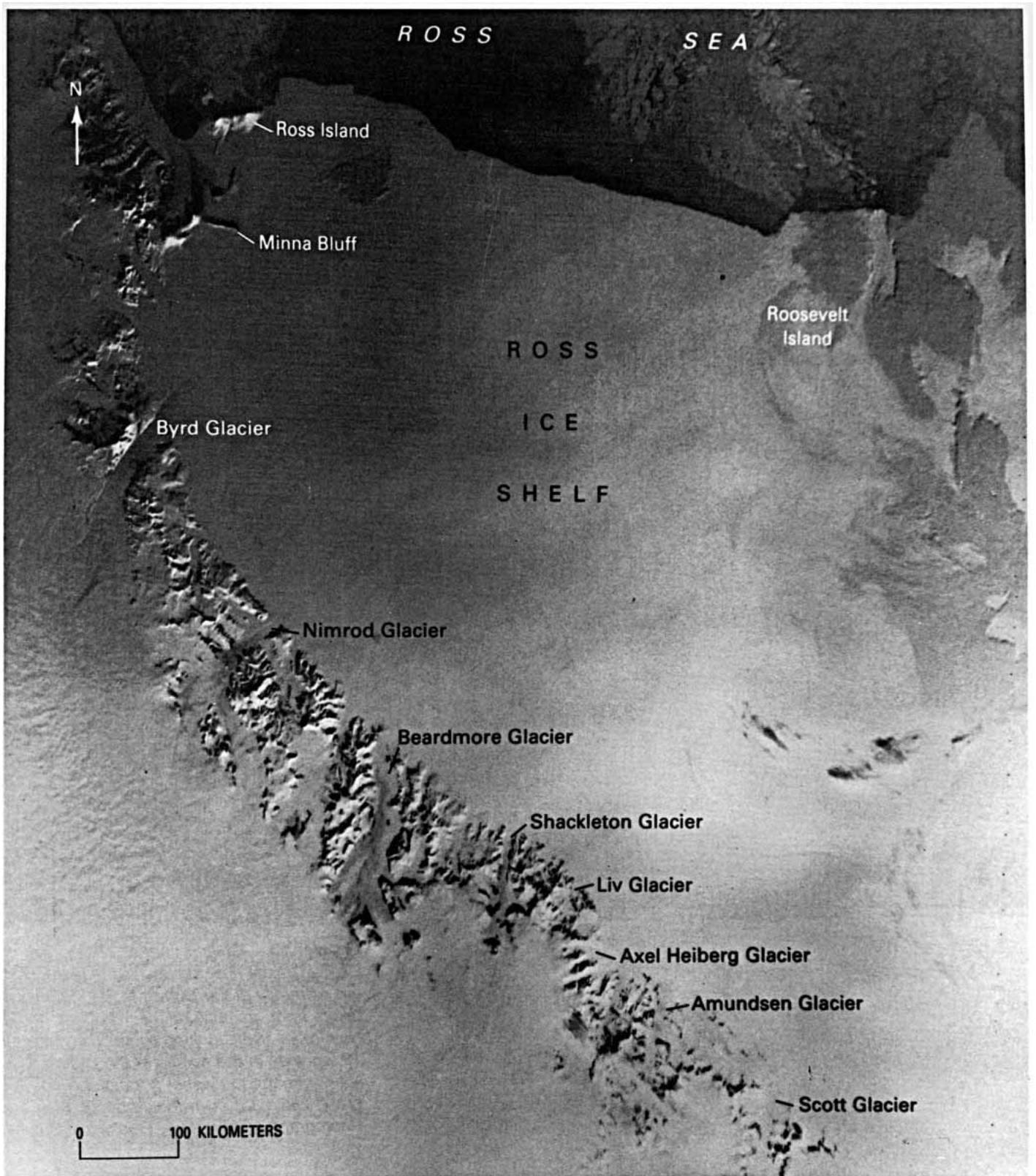


Figure 12. — Annotated NOAA 6 advanced very high resolution radiometer (AVHRR) image (0.8–1.1 μm) of a part of the Transantarctic Mountains acquired on 12 November 1980, at 1342 UT. NOAA meteorological satellite images record information not covered by the Landsat series of spacecraft (poleward of about 81°S. latitude). NOAA image courtesy of Donald R. Wiesnet, National Oceanic and Atmospheric Administration. See also figures 11, 21, 22, 23, 24, and 25.



Figure 13. — Oblique aerial photograph of Reedy Glacier (looking upstream) at the eastern extremity of the Queen Maud Mountains, taken from an altitude of 7,200 m on 25 November 1960, looking south. The glacier is 12 km wide in the middle of the picture. U.S. Navy trimetrogon aerial photograph no. 200 (TMA 780 F33) from the Antarctic Map and Photograph Library, U.S. Geological Survey.



Figure 14. — Oblique aerial photograph of Scott Glacier, Queen Maud Mountains, taken from an altitude of 7,200 m on 25 November 1960, looking south. The glacier is moving toward the foreground and is 12 km wide in the middle of the picture. U.S. Navy trimetrogon aerial photograph no. 144 (TMA 780 F33) from the Antarctic Map and Photograph Library, U.S. Geological Survey.

The grounding line is a few kilometers from the foot of the mountains. Ice surface velocity is 226 m a^{-1} in the middle of the photograph, and total ice output⁴ is about $2.0 \text{ km}^3 \text{ a}^{-1}$ (Giovinetto and others, 1966). The glacier has been traversed from end to end (Blackburn, 1937).

Amundsen Glacier (fig. 15) flows in such a deeply incised channel that parts of the glacier may be afloat even before reaching the foot of the mountains. The surface falls over a length of 200 km from an altitude of 2,600 m at its head to 120 m at the grounding line, an average gradient of 1 in 80. The ice is 1,300 m thick near the grounding line. Ice surface velocity is 240 m a^{-1} in the middle of the photograph, and total ice output is about $2.2 \text{ km}^3 \text{ a}^{-1}$.

⁴Because the overall specific gravity of a glacier is generally unknown, ice output is commonly reported in terms of volume per unit of time. In this chapter we use cubic kilometers per annum ($\text{km}^3 \text{ a}^{-1}$). Some authors, however, report in units of mass flux such as gigatons per annum (Gt a^{-1}). In these cases we have put the ice volume equivalent in parentheses, assuming an overall specific gravity of 910 kilograms per cubic meter.

Figure 15. — Oblique aerial photograph of Amundsen Glacier, Queen Maud Mountains, taken from an altitude of 7,200 m on 25 November 1960, looking south. The glacier is moving toward the foreground and is 10 km wide in the middle of the picture. U.S. Navy trimetrogon aerial photograph no. 125 (TMA 780 F33) from the Antarctic Map and Photograph Library, U.S. Geological Survey.



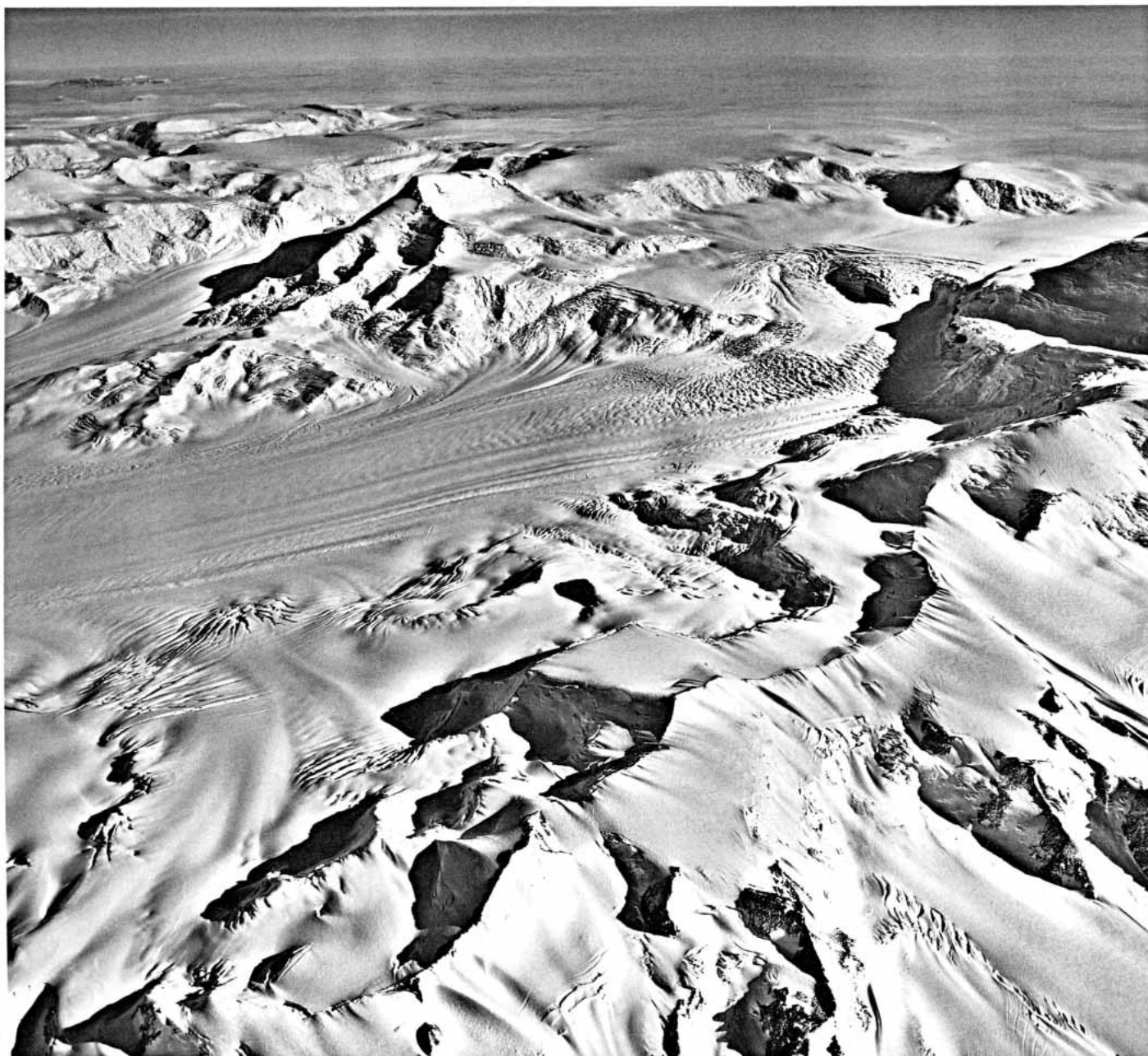


Figure 16.—Oblique aerial photograph of Axel Heiberg Glacier, Queen Maud Mountains, taken from an altitude of 7,200 m on 25 November 1960, looking south. The glacier is flowing from right to left and is 7 km wide at the icefall. Beyond (far left) is Cooper Glacier. U.S. Navy trimetrogon aerial photograph no. 108 (TMA 780 F33) from the Antarctic Map and Photograph Library, U.S. Geological Survey.

Axel Heiberg Glacier (fig. 16) looks uninviting to the surface traveler, but it was the path chosen by the Norwegian explorer Roald Amundsen and his four companions to reach the South Pole in 1911 (Amundsen, 1912). The surface falls in two great steps over a length of 65 km from an altitude of 2,800 m at its head to 120 m at the grounding line, an average gradient of 1 in 24. The glacier carries no ice from the polar plateau, being fed only by snow falling in the mountains. Amundsen Icefall in the middle of the photograph drops 800 m in 3 km. It was not until 50 years after the Norwegian party that another attempt was made to descend the icefall, this time by a New Zealand survey party using dog sledges (Herbert, 1962, 1963).

Liv Glacier (fig. 17) was the route chosen by R.E. Byrd to fly to the South Pole in 1929 (Byrd, 1930). It descends over a length of 100 km from an altitude of 2,600 m at its head to 100 m at the grounding line, which here is some 10 km beyond the foot of the mountains and separated from it by a gently sloping ice piedmont. The glacier probably drains no ice from the polar plateau. Surface velocity is 112 m a⁻¹ in



the middle of the glacier just above the lower icefall at the foot of the range, and total ice output is only about $0.5 \text{ km}^3 \text{ a}^{-1}$ (Giovinetto and others, 1966).

Shackleton Glacier (fig. 18) boasts a fine medial moraine and some large meltwater lakes on its surface. Like Reedy Glacier, it is an ablation area almost throughout its length. The surface falls gently over a length of 150 km from 2,400 m at its head to 90 m at the foot of the mountains, an average gradient of 1 in 65. The ice is 750 m thick near the grounding line. Surface velocity is 81 m a^{-1} in the middle of the glacier (R.H. Thomas, personal commun.), and total ice output is about $0.5 \text{ km}^3 \text{ a}^{-1}$.

Figure 17. —Oblique aerial photograph of the upper part of Liv Glacier, Queen Maud Mountains (looking upstream) taken from an altitude of 7,200 m on 25 November 1960, looking south-southwest. The glacier is 4 km wide in the middle of the picture. The large tributary entering from the right is La Vergne Glacier. U.S. Navy trimetrogon aerial photograph no. 95(TMA780 F33) from the Antarctic map and Photograph Library, U.S. Geological Survey.



Figure 18.—Oblique aerial photograph of Shackleton Glacier, Queen Maud Mountains, taken from an altitude of 7,200 m on 25 November 1960, looking southwest. The glacier is flowing toward the foreground and is 8 km wide in the middle of the picture. U.S. Navy trimetrogon aerial photograph no. 59 (TMA 780 F33) from the Antarctic Map and Photograph Library, U.S. Geological Survey.

Beardmore Glacier (figs. 19 and 20) was the path chosen by the British explorer E.H. Shackleton to reach the polar plateau in 1908 (Shackleton, 1909). He was followed by R.F. Scott, who reached the South Pole in 1912 but died with his four companions on the Ross Ice Shelf after descending the glacier (Scott, 1913). According to McIntyre (in press) the glacier drains an area of 121,000 km². The surface falls gently over a length of 210 km from 2,400 m at the plateau threshold to 100 m at the grounding line. The ice is about 800 m thick near the grounding line. Surface velocity is 372 m a⁻¹ in the middle of the glacier just below the grounding line, and total ice output is about 4.6 km³ a⁻¹. The physiography of the area has been described by Wright (1923), Oliver (1964), and Mercer (1972).

Figure 20 looks across the mouth of Beardmore Glacier. Mount Hope (836 m) is the nearest nunatak, and behind it on the horizon is Mount Miller (4,160 m). The ice is flowing from the Beardmore Glacier (left) into the Ross Ice Shelf (right). Sea water could be found in the giant rifts at the grounding line (Barrett, 1975).

Figure 19. —Annotated oblique aerial photograph of the northwestern end of the Queen Maud Mountains bordering on Beardmore Glacier (right background), taken from an altitude of 7,200 m over Good Glacier on 25 November 1960, looking southwest. The small plateau (center) is 3,100 m above sea level; Mount Kaplan (left middle distance) rises to 4,230 m. U.S. Navy trimetrogon aerial photograph no 26 (TMA 780 F33) from the Antarctic Map and Photograph Library, U.S. Geological Survey.

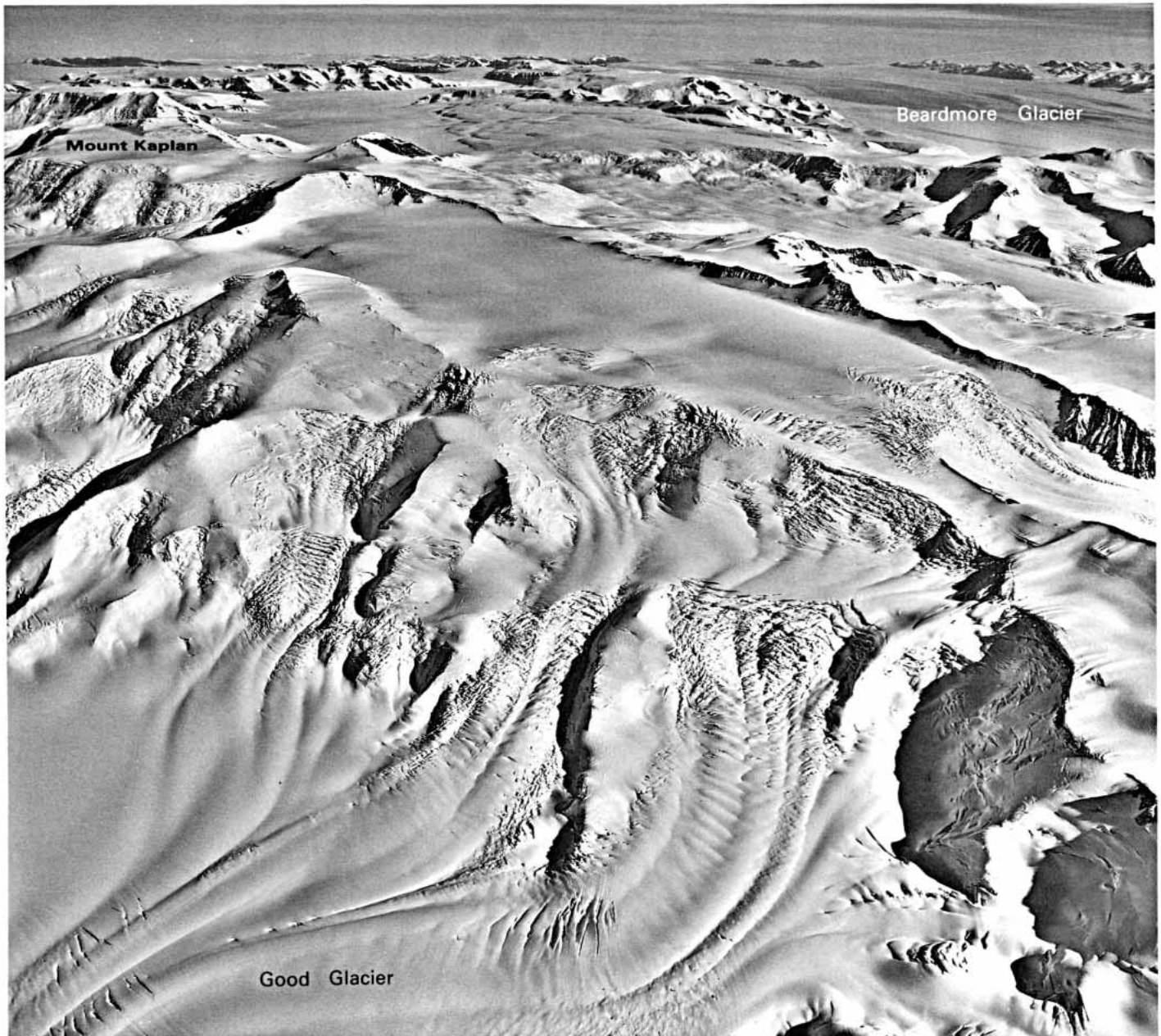


Figure 20. — Oblique aerial photograph of the mouth of Beardmore Glacier, taken from an altitude of 3,000 m on 13 January 1956, looking west. The glacier is flowing from the inland part of the Beardmore Glacier (left) into the Ross Ice Shelf (right). The leftmost giant rift in the middle of the picture marks the grounding line, where the glacier is 20 km wide. U.S. Navy trimetrogon aerial photograph no. 19 (TMA 406 F33) from the Antarctic Map and Photograph Library, U.S. Geological Survey.



Nimrod Glacier (fig. 21) drains an area of 152,000 km² (McIntyre, in press). Its surface falls over a length of 200 km from its plateau threshold at an elevation of 2,200 m to 100 m where it joins the Ross Ice Shelf. The medial nunatak is an unusual feature. Comparing the surface velocity profile with those of Scott, Amundsen, Liv, Beardmore, Byrd, and Mulock Glaciers, Swithinbank (1963) found a reduced rate of movement on the medial flowline, although his measurements were made 60 km downstream from the nunatak. Velocity was 278 m a⁻¹ in the middle of the glacier at a point where it is 18.3 km wide. A cross section that was measured at the same place by airborne radio-echosounding (Harrison, 1970, p. 1113) showed maximum ice depths of 960 m. The deconvoluted cross-sectional area of the glacier is 14.4 km², and total ice output is about 2.2 km³ a⁻¹. Swithinbank (1964) described traveling and working on this and six other giant glaciers flowing through the Transantarctic Mountains. He was surprised to find running water at the side of Nimrod Glacier.

At the southern extremity of Landsat coverage of the Transantarctic Mountains lies Byrd Glacier (figs. 11, 12, 22, 23, 24, and 25) one of the largest valley glaciers in the world and possibly the most active glacier

Figure 21. —Annotated oblique aerial photograph of Nimrod Glacier (looking upstream) showing the conspicuous medial flowline emanating from Kon-Tiki Nunatak, from an altitude of 5,800 m taken on 10 November 1960, looking west-southwest. The glacier is 13 km wide at its narrowest point. U.S. Navy trimetron aerial photograph no 215 (TMA 768 F33) from the Antarctic Map and Photograph Library, U.S. Geological Survey. See also figures 11 and 12.



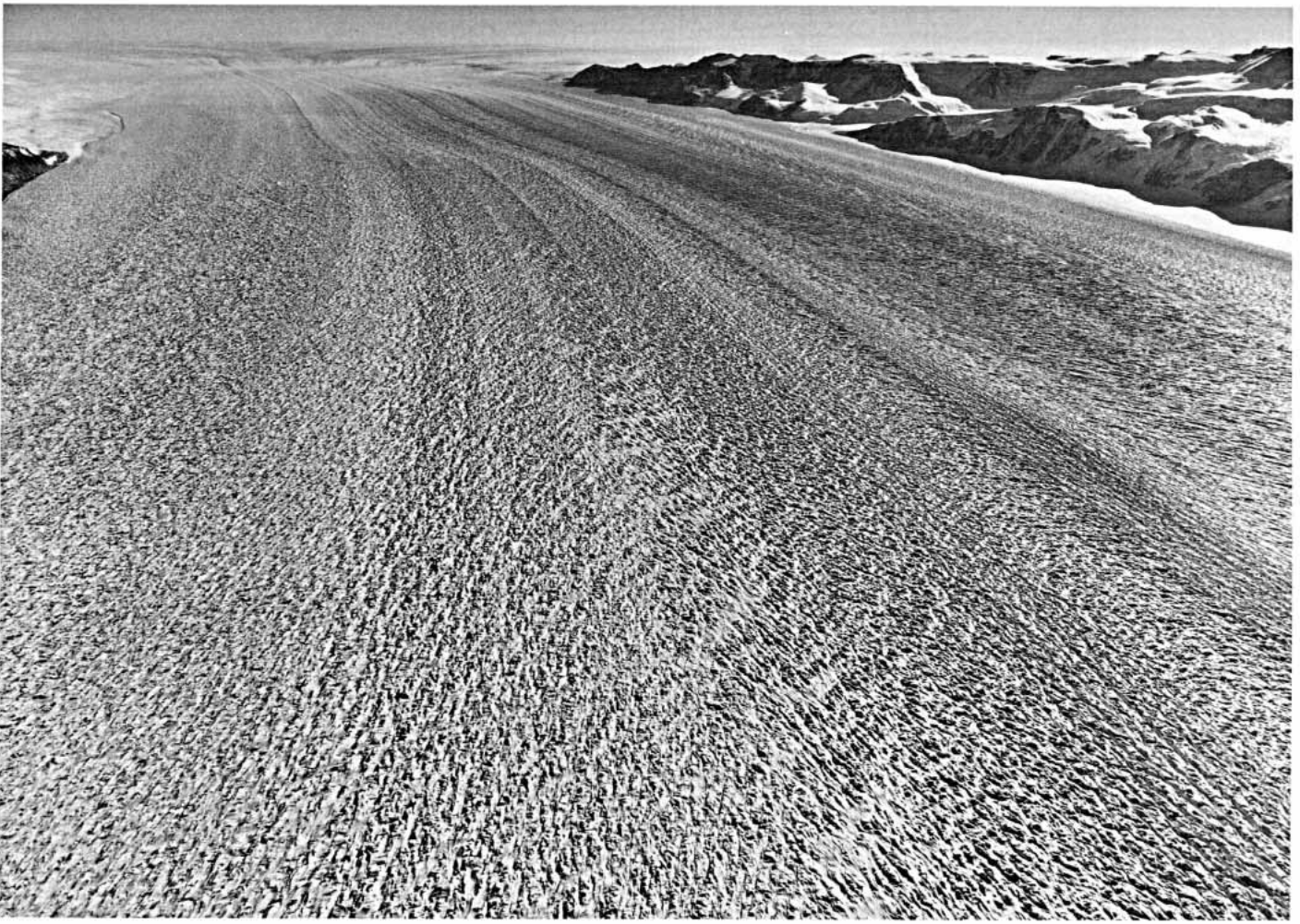


Figure 22. — Oblique aerial photograph of Byrd Glacier (looking upstream), the biggest outlet glacier crossing the Transantarctic Mountains, taken from an altitude of 2,800 m on 14 November 1956, looking west-southwest. The width of the glacier is approximately 23 km. The camera position is marked on figure 23. U.S. Navy trimetrogon aerial photograph no. 134 (TMA 341 F31) from the Antarctic Map and Photograph Library, U.S. Geological Survey. See also figures 11, 12, 23, and 24.

draining any part of the East Antarctic plateau. According to McIntyre (in press) it drains an area of 1,017,000 km², greater than any other glacier in the world. Byrd Glacier occupies a gently curving fiord trough in part of which the vertical (peak-to-trough) relief exceeds 5,000 m. Its surface falls over a length of 180 km from a plateau threshold at an elevation of 1,400 m to 70 m where it joins the Ross Ice Shelf. Its valley through the Transantarctic Mountains is 100 km long, but as a distinct ice stream it has been traced by radio-echo strength measurements the whole way to the ice front, 430 km from the foot of the mountains (Shabtaie and Bentley, 1982). At its narrowest point the glacier is 22 km wide. The ice is afloat everywhere downstream of the narrowest part of the valley. The actual grounding line is considered to lie between the 1,300 m and 1,500 m spot soundings (fig. 22). The bare ice is an ablation area evidently kept bare of snow by sublimation caused by adiabatic warming of downslope (katabatic) winds (fig. 24A). Crevasses 20 m deep near the grounding line largely ablate away by the time they reach the mouth of the valley. This corresponds with an ablation rate⁵ of about 400 kg m⁻² a⁻¹ (personal commun. from T.J. Hughes). There is an equilibrium line (or zone) near the mouth of the valley, beyond which there is net accumulation on the surface of the Ross Ice Shelf.

⁵Because glaciologists routinely determine the specific gravity of fallen snow, it is customary to report accumulation and ablation in terms not of snow depth but of mass per unit area. In this chapter we describe rate of accumulation and ablation in terms of kilograms per square meter per annum (kg m⁻² a⁻¹).

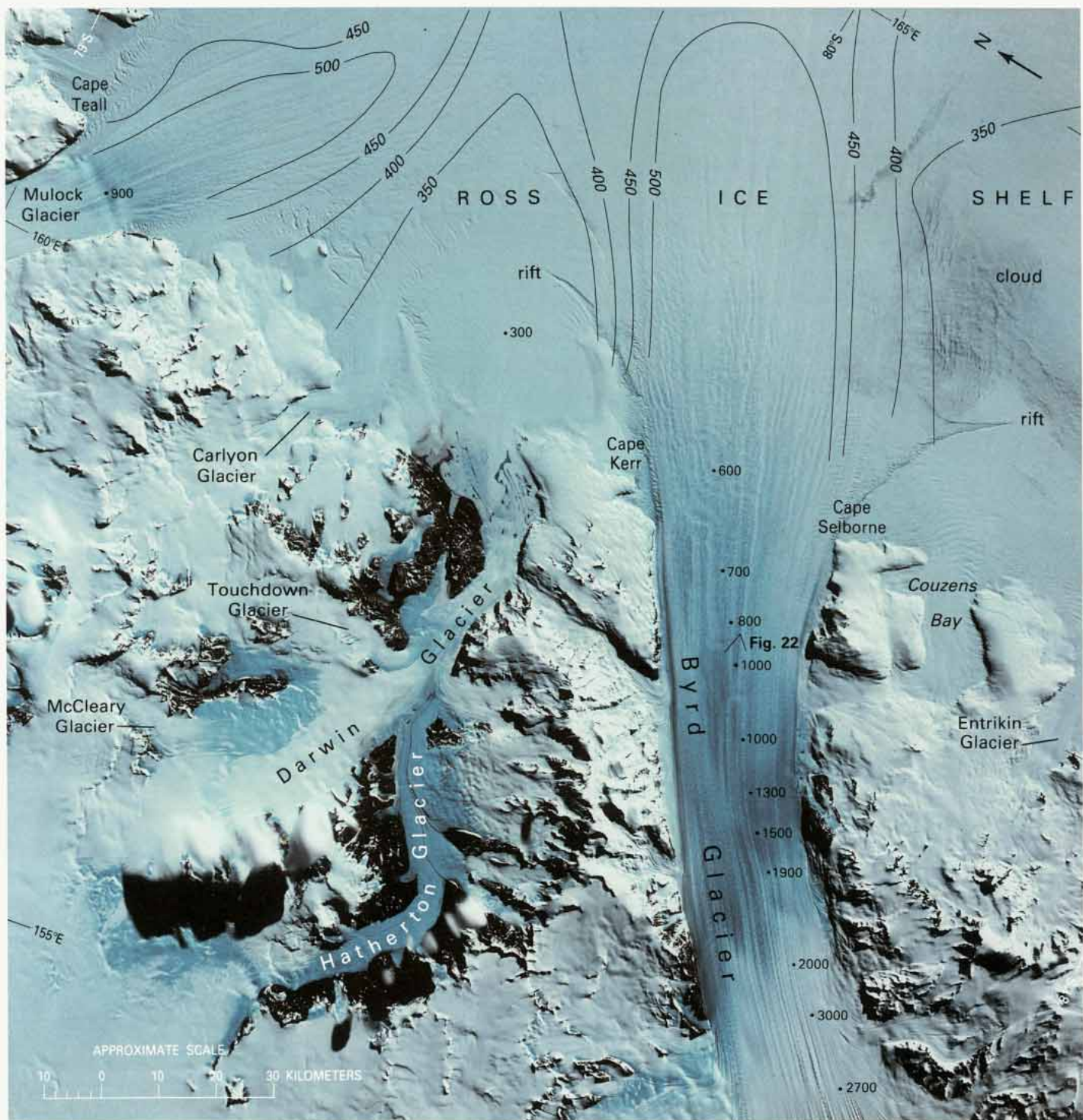
Several features in figure 23 are characteristic of the disturbance caused by a fast-moving glacier as it punches its way into an ice shelf. Off Cape Selborne and Cape Kerr giant rifts reveal that the shearing between faster and slower moving ice is so great that the 500-m-thick floating ice sheet has not only been crevassed but literally torn apart from top to bottom. Within the rifts, a mixture of calved but captive icebergs is ground into a tortuous mass of jumbled ice blocks that thinly mask the sea beneath. Byrd Glacier flows seaward at the rate of 840 m a⁻¹ in the vicinity of the 1,000-m spot thickness (Swithinbank, 1963) and discharges about 18 km³ a⁻¹ into the Ross Ice Shelf. This is as fast as some surging glaciers; indeed throughout its passage between the mountains the surface bears every resemblance to a typical surging glacier: it is chaotically broken. Serrate ridges and giant furrows are aligned parallel with the abrupt rock walls (fig. 24B) of the valley, but there are crevasses in every direction. Velocity vectors and velocity isopleths have been reported by Brecher (1986): the maximum observed velocity was 875 m a⁻¹. The grounding line along the margin of the Ross Ice Shelf can be plotted more reliably from this image than from any other source. Neither the 25-km-long land-ice peninsula jutting into the ice shelf from Cape Kerr nor the similar peninsula to the left of the mouth of Darwin Glacier was known or mapped before Landsat.

Landsats 1, 2 and 3 acquired several useful images of part of Byrd Glacier (figs. 23 and 24), but they were only able to image the northerly half of the glacier because of the orbital limitations. When Landsat 4 was put into a new orbit in 1982, which extended a little farther to the south, it became possible to image the entire extent of Byrd Glacier for the first time (fig. 25).

By comparison with its giant neighbor, Darwin Glacier is a quiet backwater. Both Darwin and its sluggish tributary, Hatherton Glacier, are starved of ice from the plateau by reason of high rock thresholds at the head of each valley. The surface of Hatherton Glacier is probably kept bare of snow more by the sublimation resulting from adiabatic warming of downslope winds than by the sweeping away of snow by the winds themselves (see fig. 24A). Both medial and lateral moraines can be seen on the glacier. An extensive network of meltwater lakes has formed on the surface of Darwin Glacier immediately seaward of the grounding line (figs. 23 and 24A); whether or not there is a direct outlet to the sea beneath the ice shelf is unknown.

Mulock Glacier (figs. 23 and 26) is half the width of Byrd but nevertheless is an important outlet glacier. Its surface falls over a length of 80 km from an elevation of 1,400 m at the plateau threshold to 100 m where it joins the Ross Ice Shelf. The grounding line probably coincides with the visible surface inflection that crosses the glacier at the 900-m depth sounding. Mulock Glacier moves 390 m a⁻¹ near its mouth (Swithinbank, 1963) and discharges about 5.6 km³ a⁻¹ into the Ross Ice Shelf.

Figure 23. — Annotated Landsat 1 MSS digitally enhanced false-color composite image of a part of the Byrd Glacier, the Ross Ice Shelf, and environs. Spot soundings (in meters) from airborne radio-echosounding surveys (Scott Polar Research Institute, unpublished). Ice thickness isopleths (in meters) from airborne radio-echosounding (Ross Ice Shelf Map Sheet; scale, 1:1,000,000, U.S. Geological Survey, 1972). All isopleths are on the floating ice shelf. NASA image (1542–18435, bands 4, 5, and 7, 16 January 1974, Path 46, Row 119) courtesy of Baerbel K. Lucchitta and the Flagstaff (Arizona) Image Processing Facility, U.S. Geological Survey. See also figures 11, 12, 24, and 25.



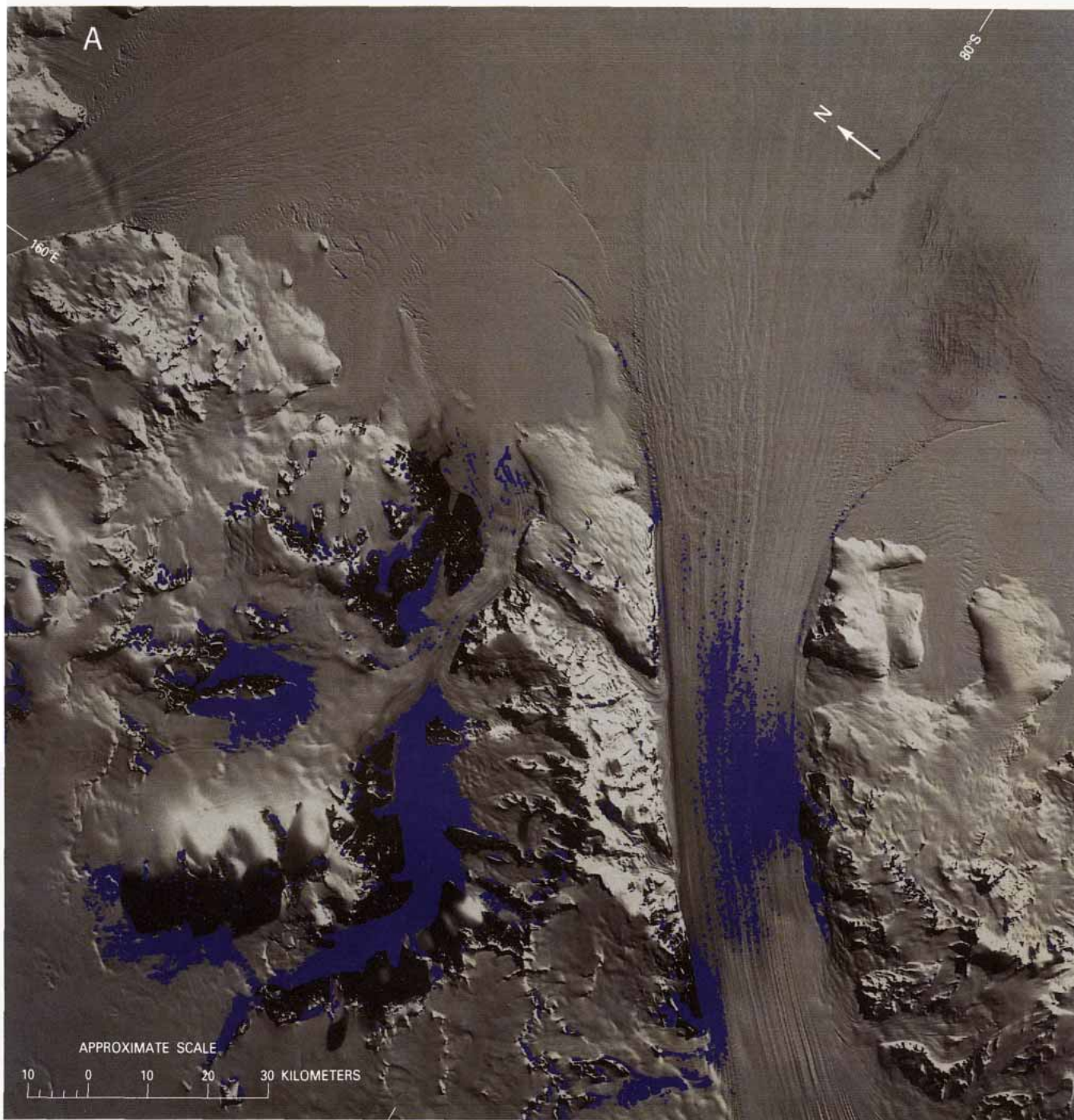
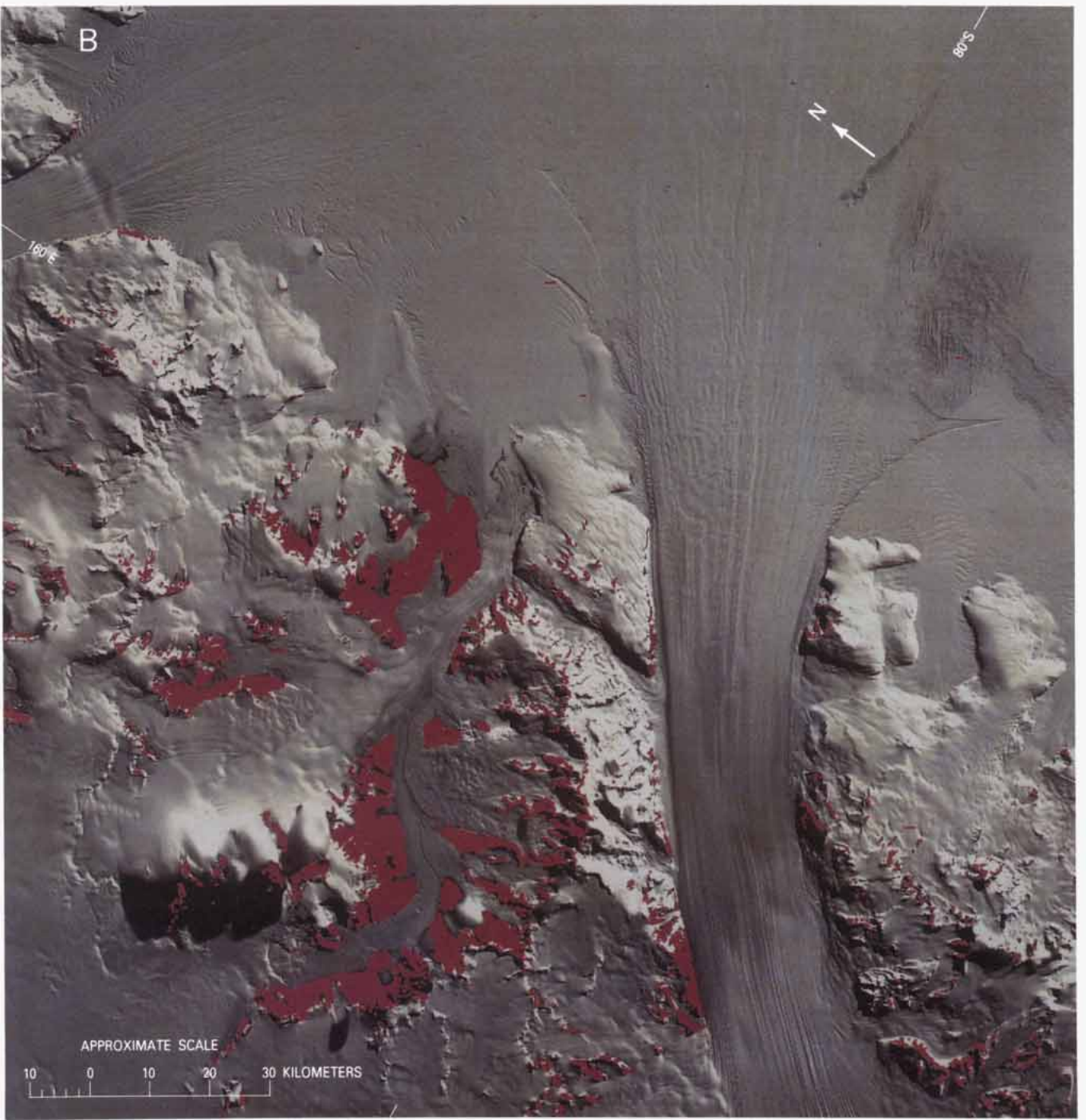
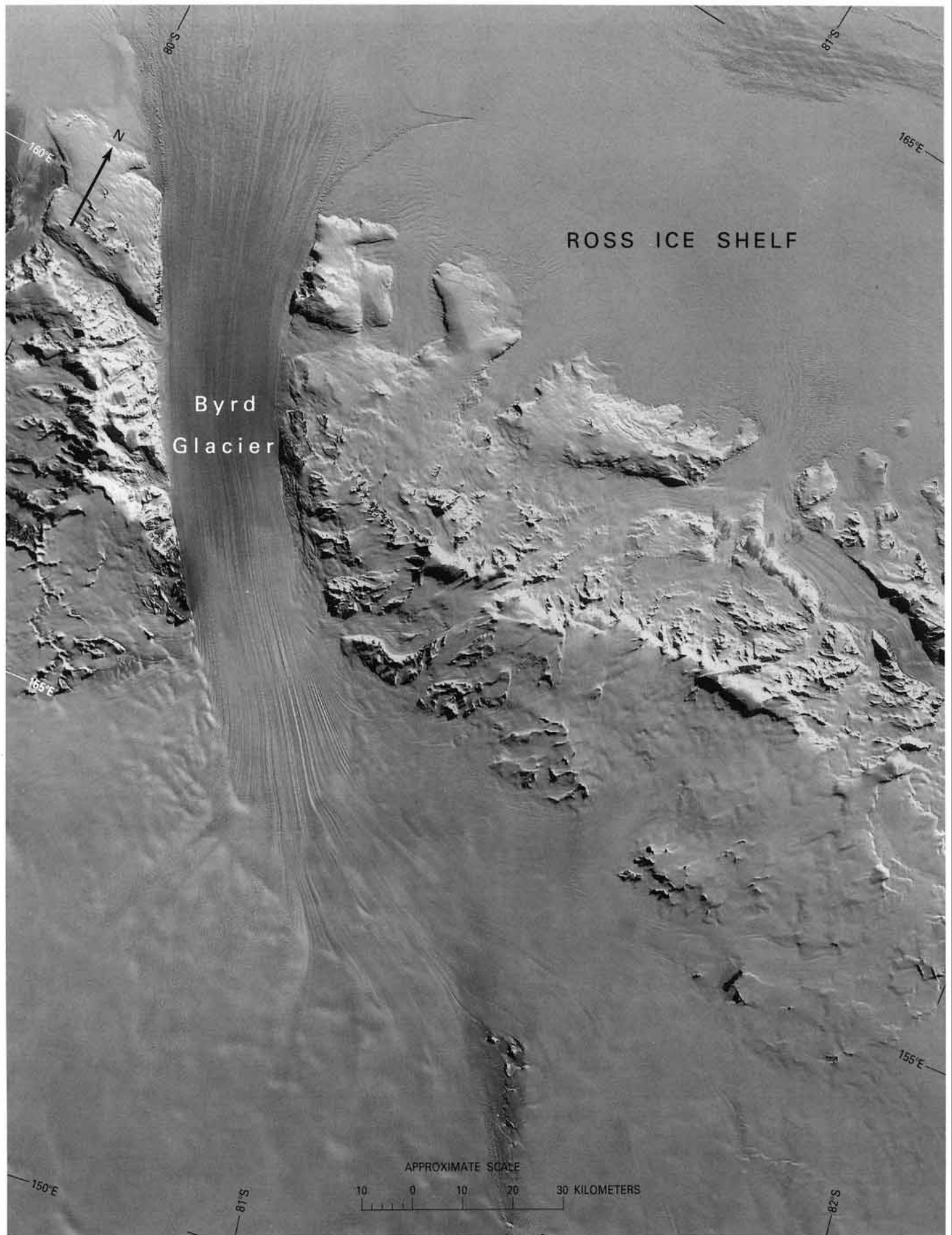


Figure 24. — Landsat 1 MSS digitally enhanced false-color composite image showing (A) bare glacier ice ('blue ice') on Byrd and Hatherton Glaciers and meltwater lakes on the lower part of the Darwin Glacier and (B) bedrock areas (red) of the surrounding mountains. Digital-image processing using a DeAnza color monitor and PDP 1144 computer permitted the classification and delineation of all picture elements (pixels) identified as bare ice or water in A and bedrock in B on the basis of spectral reflectance. The bare-ice and water classes (shown in royal blue on A) and the bedrock class (shown in red on B) were digitally merged with the basic image data and printed out by using an Optronics film writer in the U.S. Geological Survey's Flagstaff (Arizona) Image Processing Facility. NASA image (1542–18435, bands 4, 5, and 7; 16 January 1974; Path 46, Row 119) courtesy of Baerbel K. Lucchitta, U.S. Geological Survey. See also figures 23 and 25.







◁ **Figure 25.**—Annotated Landsat 4 MSS image mosaic of a part of the Byrd Glacier, the Ross Ice Shelf, and environs. NOAA images (40495–18544, band 4 (0.80–1.1 μm); 23 November 1983; Path 45, Row 119; and 40495–18551, band 4; 23 November 1983; Path 45, Row 120) from the EROS Data Center, National Oceanic and Atmospheric Administration. See also figures 11, 12, 23, and 24.

△ **Figure 26.**—Oblique aerial photograph of Mulock Glacier (looking upstream) taken from an altitude of 2,800 m on 14 November 1956, looking northwest. The glacier is 12 km wide in the center. U.S. Navy trimetrogon aerial photograph no. 274 (TMA 341 F31) from the Antarctic Map and Photograph Library, U.S. Geological Survey.

McMurdo Sound Area

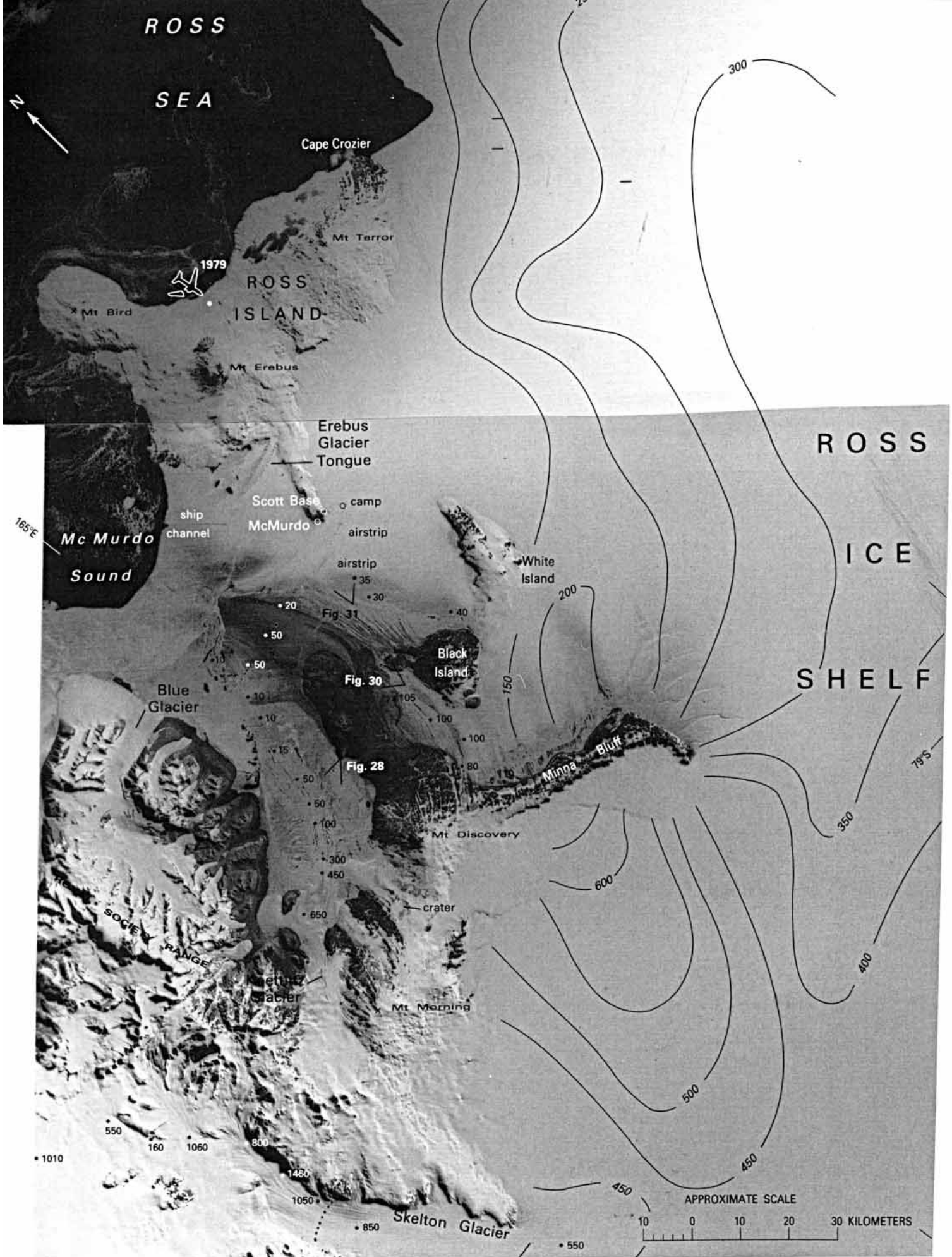
The area of figure 27 almost adjoins that of figure 23 and shows something quite rare in Antarctica—an extensive ablation area and several volcanoes. At the bottom of the image, Skelton Glacier flows southeastward to join the Ross Ice Shelf. Its surface falls over a length of 130 km from the plateau at an elevation of 2,200 m to 100 m at the grounding line, which, as determined by Crary (1966), is shown as a dotted line. Unlike Byrd and Mulock Glaciers, Skelton is nourished by local snow accumulation from the mountain areas and carries no ice from the plateau. For this reason it is slow-moving (90 m a^{-1}) and discharges only $0.8 \text{ km}^3 \text{ a}^{-1}$ at its mouth (Wilson and Crary, 1961). A radio-echosounding cross section of the glacier at its mouth was published by Swithinbank (1969b). According to Robin (1975, fig. 2) the ice tongues from Mulock and Skelton Glaciers are laterally confined on the Ross Ice Shelf to such an extent that at the ice front both are contained within a 10-km band flowing past Cape Crozier. Beyond this, the northward bulge in the ice front, together with the northward bulge in the 150 to 300 m isopleths, bears witness to the overwhelmingly greater contribution to the ice shelf of a band of ice from Byrd Glacier.

Mount Morning (2,725 m) and Mount Discovery (2,680 m) are both conical extinct volcanoes; halfway between them is a circular feature 3 km in diameter that could be another caldera filled with ice. Minna Bluff is a 45-km-long, rather level-topped ridge projecting into the Ross Ice Shelf. At the eastern end of it, rifts show where the 200- to 300-m-thick floating ice is rapidly deformed and even torn apart as it is dragged past the land at a speed of 450 m a^{-1} (Wright and Priestley, 1922). The interpretation of these tapering rifts as fractures that reach from top to bottom of the ice sheet is borne out by Bruchhausen and others (1979, p. 449), who not only found 500-m-deep sea water in one of the rifts but even caught a fish in it.

The surface ablation area of the McMurdo Ice Shelf (shown on figs. 27, 29, and 30) is one of the most extensive in Antarctica. The McMurdo Ice Shelf is the small part of the Ross Ice Shelf that lies between Minna Bluff and Ross Island. Beginning with a 6-km-wide strip along the north side of Minna Bluff, there are two sets of linear features. Broad bands of differing morphology are aligned parallel with the bluff. Each band consists of narrow ridges and troughs trending at right angles to the major pattern. The bands are perhaps caused by standing waves in strong winds that spill over the ridge from the south. Ablation under these conditions would be due largely to sublimation. The ice shelf does not ablate entirely under this onslaught because of a unique characteristic of the area—nourishment of the floating ice shelf by the freezing of sea water from below. First proposed by Debenham (1920), who could offer no better explanation for faunal remains that he found on the ice surface off Koettlitz Glacier, the idea was developed by Swithinbank (1970), Gow and Epstein (1972), and Kellogg and others (1977) to explain vast areas of marine deposits found in ablation areas as far inland as this one near Minna Bluff. Ridges and troughs perpendicular to the bands are ablation phenomena related to ice movement away from the bluff and to the direction of the prevailing wind. Most of the many aligned ablation features that curve smoothly from a northeasterly direction off Minna Bluff to a northerly direction in McMurdo Sound are due to wind.

The 25-km-long floating tongue of Koettlitz Glacier (fig. 28) wastes away by melting from the upper surface. It is 300 m thick at the point

Figure 27. — Annotated Landsat 1 MSS image mosaic of Ross Island and part of the Ross Ice Shelf and environs. Spot soundings and ice thickness isopleths (in meters) from seismic (Crary, 1966) and airborne radio-echosounding (Ross Ice Shelf Map Sheet, scale, 1:1,000,000, U.S. Geological Survey, 1972; Swithinbank, 1970). Image center at $78^{\circ}04'S.$, $167^{\circ}06'E.$ All isopleths are on floating ice shelf areas. The 1979 crash site of a New Zealand DC-10 aircraft is marked on the north-central part of Ross Island. NASA images (1530–19173, band 7; 4 January 1974; Path 52, Row 116; and 1529–19121, band 7; 3 January 1974; Path 51, Row 117) from the EROS Data Center, U.S. Geological Survey. See also figures 28, 30, and 31.



where it leaves the land; the tongue thins to 100 m during the first 8 km of its journey. It is a wafer-thin 15 m at the point where the land ice is replaced by a wedge of locally-grown sea ice (Gow, 1973). Ablation rates of $40 \text{ kg m}^{-2} \text{ a}^{-1}$ have been observed, and all indications are that a comparable thickness of ice is accreting annually onto the bottom of the ice tongue, which is only moving 5 to 10 m a^{-1} . At these rates of accretion, ablation, and forward movement, Gow estimates that the bottom ice should reconstitute itself between 50 and 100 times as it traverses the final 26 km to its terminus. This sequence leads to a progressive increase in the quantity of surficial debris in the downglacier direction.

The limits of the ablation area more or less coincide with the limits of dark-colored ice in figure 27. Rates of movement from 1 m a^{-1} to 18 m a^{-1} have been measured (Swithinbank, 1970); these are exceptionally slow speeds for an Antarctic ice shelf. It takes the ice so long to travel from Minna Bluff to the ice front that moraines exposed on the surface (figs. 29 and 30) could span more than 10,000 years of the glacier's history. However, Stuiver and others (1981) believe that the area shown here formed part of a grounded ice sheet less than 10,000 years ago and that the direction of ice movement changed from west to north as the ice began to float. Taken together with the possible age of the moraine, perhaps this explains the confused indications of flow direction in the foreground of figure 28. In contrast to other glaciers, mass flux across the equilibrium line here plays a very small part in the total regime of the ice shelf.

So sparse is the human population of Antarctica that very few artifacts have been seen in satellite pictures. But the McMurdo Sound area (fig. 27) is an exception. Two airstrips and a large field camp can be seen near McMurdo Station, the main base of operations for United States scientific activities in Antarctica. The black line to the left of McMurdo Station (fig. 27) that might be mistaken for a partially lost scan line of the MSS is in fact a 200-m-wide channel being broken through fast ice by the icebreaker U.S. Coast Guard Cutter (USCGC)

Figure 28.— Oblique aerial photograph of Koettlitz Glacier flowing into McMurdo Ice Shelf (foreground), taken from an altitude of 4,400 m on 19 December 1957, looking west-southwest. The camera position is marked on figure 27. The floating ice shelf in the foreground is little more than 10 m in thickness. The grounding line is shown by the conspicuous break in slope at the landward extremity of the rifts and meltwater lakes. The glacier is approximately 4 km wide at its narrowest point. U.S. Navy trimetrogon aerial photograph no. 159 (TMA 348 F33) from the Antarctic Map and Photograph Library, U.S. Geological Survey.



Figure 29. — Annotated Landsat 1 MSS image of Minna Bluff and environs. The ablation area of McMurdo Ice Shelf is better displayed on this MSS band 6 image than on the MSS band 7 image of the area shown in figure 27. NASA image (1529–19121, band 6; 3 January 1974; Path 51, Row 117) from the EROS Data Center, U.S. Geological Survey. See also figure 30.

Glacier to allow access by supply ships. The progress of the icebreaking can be followed in successive Landsat images taken on 3, 4, 5, 7, and 8 January 1974 (1529–19121, band 7; 3 January 1974; Path 51, Row 117; 1530–19173, band 7; 4 January 1974; Path 52, Row 116; 1531–19231, band 7; 5 January 1974; Path 53, Row 116; 1533–19343, band 7; 7 January 1974; Path 55, Row 116; and 1534–19402, band 7; 8 January 1974; Path 56, Row 116). This unique series brings home one of the special advantages of Landsats 1, 2, and 3 for studying transient phenomena in high latitudes: the coverage of the orbital paths overlaps enough that although the satellite only repeats the same track once every 18 days, any given point on the ground could be monitored (if the weather were clear and the MSS were recording) for several successive days; the number of actual days varies with latitude. From 1 to 3 January, Glacier cut 13 km of ice, and by the following day she had cut

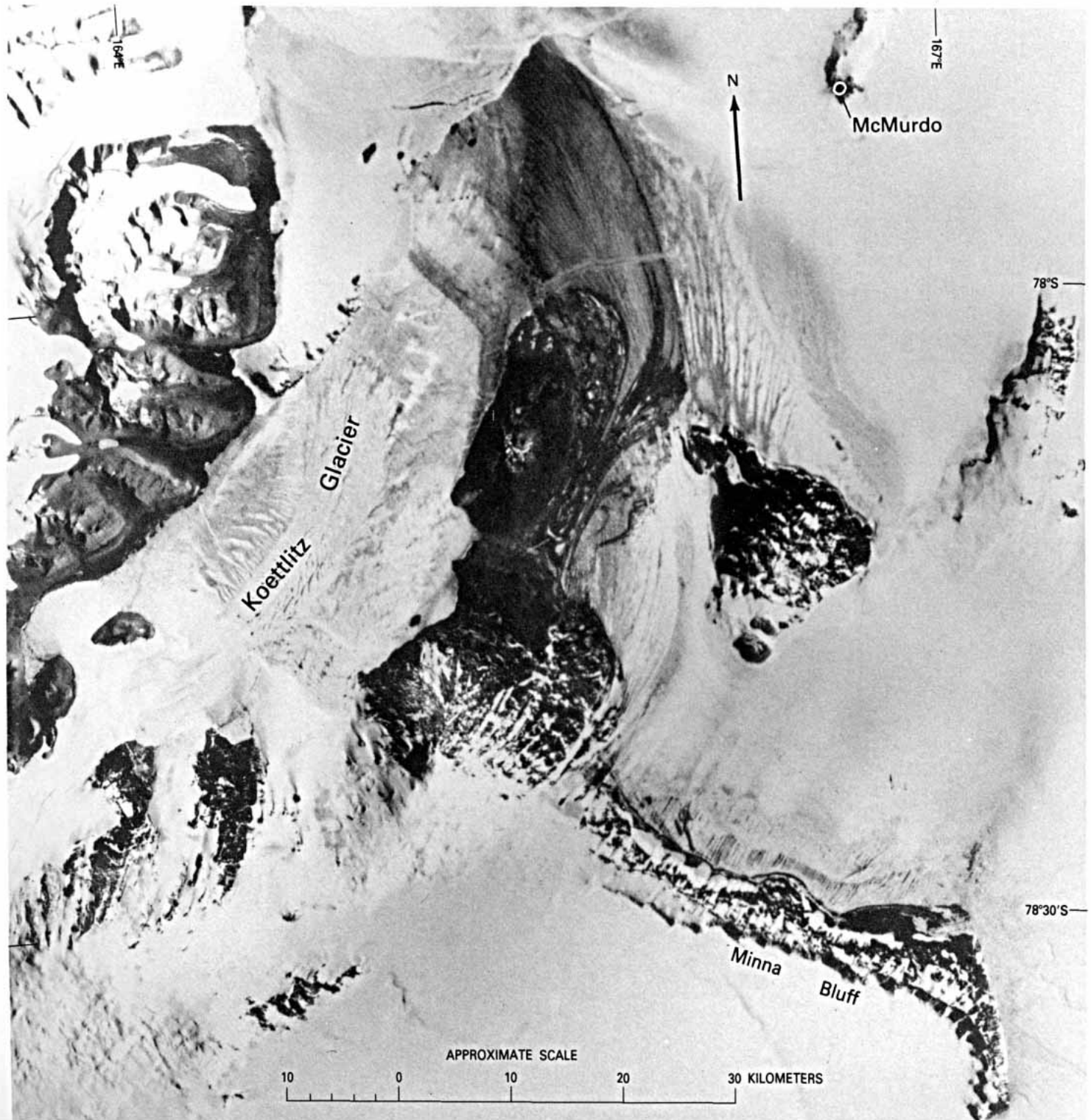




Figure 30. — Oblique aerial photograph of the ablation area of McMurdo Ice Shelf taken from an altitude of 4,200 m on 5 December 1956, looking north-northwest. The camera position is marked on figure 27. Cape Hodgson on Black Island is in the right foreground. From Cape Hodgson to the open water of McMurdo Sound is approximately 55 km. U.S. Navy trimetrogon aerial photograph no. 232 (TMA 335 F31) from the Antarctic Map and Photograph Library, U.S. Geological Survey. See also figure 29.

a further 4 km. At this point she was joined by USCGC *Staten Island* (Antarctic Journal of the United States, 1974), and Landsat recorded them making fast progress by cutting parallel tracks 200 m apart on 5 January. They broke the last 8 km into McMurdo Station between 5 and 7 January.

There are four volcanoes on the mainland of Antarctica that are considered to be active on the basis of observed fumarolic activity or "recent" tephra deposits: Mount Melbourne (2,730 m) ($74^{\circ}21'S.$, $164^{\circ}42'E.$), a stratovolcano (fig. 37); Mount Berlin (3,500 m) ($76^{\circ}03'S.$, $135^{\circ}52'W.$), a stratovolcano (fig. 98); Mount Kauffman (2,365 m) ($75^{\circ}37'S.$, $132^{\circ}25'W.$), a stratovolcano (fig. 94); and Mount Hampton (3,325 m) ($76^{\circ}29'S.$, $125^{\circ}48'W.$), a volcanic caldera (fig. 97). Several volcanoes on offshore islands do have records of historic activity, however (Simkin and others, 1981). Mount Erebus (3,795 m), a stratovolcano on Ross Island with 10 known eruptions and 1 suspected eruption (see figs. 27 and 31), and, on the opposite side of the continent, Deception Island ($62^{\circ}57'S.$, $60^{\circ}38'W.$) (Orheim, 1972), a volcanic caldera with 10 known and 4 suspected eruptions, have been the most active (Simkin and others, 1981). Buckle Island in the Balleny Islands ($66^{\circ}50'S.$, $163^{\circ}12'E.$), Penguin Island ($62^{\circ}06'S.$, $57^{\circ}54'W.$), Paulet Island ($63^{\circ}35'S.$, $55^{\circ}47'W.$), and Lindenberg Island ($64^{\circ}55'S.$, $59^{\circ}40'W.$) are also considered to be active, on the basis of field studies (Simkin and others, 1981).

A plume of steam emanates from the summit crater of Erebus (fig. 31). The cone of Erebus rising from the sea has beckoned many explorers to the Antarctic since it was first seen from the decks of its namesake sailing ship, *Erebus*, by Captain James Clark Ross on 28 January 1841. The physiography of the area has been described by Debenham (1923) and McCrae (1984a). The mountain hit the headlines of the world's press when a DC-10 airliner carrying 257 people crashed into its northern slopes on 28 November 1979, killing all on board (see fig. 27) (Mahon, 1981).

Figure 31.—Oblique aerial photograph of Ross Island taken from an altitude of 4,700 m on 14 November 1959, looking north-northeast. The camera position is marked on figure 27. Hut Point Peninsula stretches towards the camera from the venting Mount Erebus (3,794 m) volcano in the background. McMurdo Station is at the landward end of the tractor tracks (left) and Scott Base is on the opposite (east) side of Hut Point Peninsula in the middle of the picture. The Erebus Glacier Tongue, with its distinctive serrated edges, is in the left-middle background. U.S. Navy trimetrogon aerial photograph no. 217 (TMA 550 F33) from the Antarctic Map and Photograph Library, U.S. Geological Survey.



Figure 31 also shows Mount Terror (3,230 m) on the right and Mount Bird (1,765 m) on the left beyond Mount Erebus. Erebus Glacier Tongue is in the left-middle distance. The inconspicuous jagged line in the foreground is the ice front. The level ice between it and Hut Point Peninsula is first-year sea ice (Heine, 1963), as is everything to the left of the peninsula. Everything to the right of the ice front and Hut Point Peninsula is part of the McMurdo Ice Shelf (Stuart and Bull, 1963). The surface waves in the ice shelf represent buckling caused by horizontal compressive stresses in the direction of ice movement (Collins and McCrae, 1985; McCrae, 1984b).

A well-documented climatic warming in McMurdo Sound over the years 1960 to 1970 (Budd, 1975, p. 422) was followed by a conspicuous retreat of the ice front in the ablation area. Between 24 December 1972 (image 1154–19322; Path 54, Row 116) and 6 January 1976 (image 2349–19240; Path 54, Row 116) parts of the ice front retreated up to 2.4 km.

Erebus Glacier Tongue is 13 km in length and has a 10-m temperature of -20°C (Holdsworth and Holdsworth, 1978). It is 350 m thick at the grounding line but thins to 120 m at the distal end, where the velocity is 165 m a^{-1} (Holdsworth, 1974, 1982). At the opposite end of Ross Island, a velocity of the ice shelf of 690 m a^{-1} was measured at a point 11 km east of Cape Crozier (Swithinbank, 1970, p. 473). A velocity of 748 m a^{-1} was measured at a point due east of Minna Bluff (fig. 27) (Dorrer and others, 1969, p. 86).



160° E

Webb Glacier

Frazier Glacier

Packard Glacier

Cotton Glacier

Miller Glacier

Debenham Glacier

Packard Glacier

Wright Upper Glacier

Victoria Valley

Victoria Lower Glacier

Lake Vanda

Bull Pass

Sykes Glacier

Heimdall Glacier

Wright Valley

Meserve Glacier

Wright Lower Glacier

Taylor Glacier

Fig. 33

Rhone Glacier

Matterhorn Glacier

Suess Glacier

Canada Glacier

Commonwealth Glacier

Windy Gully

fast ice

Lacroix Glacier

Taylor Valley

Ferrari Glacier

Emmanuel Glacier

Condit Glacier

Glacier

MC MURDO SOUND

ROSS SEA ASSOCIATION

Blue Glacier

pack ice

Radian Glacier

Salmon Glacier

fast ice

Walcott Glacier

Hobbs Glacier

Dailey Islands

APPROXIMATE SCALE

ice shelf

Walcott Bay



The 'Dry Valleys' of Victoria Land

By TREVOR J. CHINN^a

The 'dry valley' region in figure 32 is a cold desert of about 2000 km² that is essentially snow free. Three major valleys—the Taylor, Wright, and Victoria Valleys—separate east-west-trending mountain ranges rising to 2,400 m. Three main types of glaciers occur within the region. Outlet glaciers from the inland ice sheet enter the western valley heads, while higher coastal precipitation feeds broad low ice piedmonts. The mountain ranges between these two areas support individual alpine-type glaciers.

The glaciers of the 'dry valleys' are generally clean of surface moraine and have a variety of marginal forms ranging from actively calving ice cliffs, normally about 20 m in height, to convex ice ramps, to low-angled margins infilled with snow wedges. That the glaciers are discordant with their valleys is suggested by partially ice-filled valleys (fig. 33), overflowing cirques, and by transverse and even upvalley flow directions. Because of the very cold and arid climate, they show a degree of activity 1 to 2 orders of magnitude less than comparable temperate glaciers. Summer precipitation rates are higher than those of winter, which is to be expected, because higher summer temperatures and the open sea in McMurdo Sound allow the atmosphere to carry more moisture to the area. The very cold climate, with mean annual temperatures below -20°C , causes the usual glacier-climate relationship to be reversed, so that a glacier advance would indicate a warming climate.

Mean elevations of the alpine glaciers increase inland towards the west, along with a general decrease in glacier size and frequency. All of the alpine glaciers are dry based, producing negligible basal erosion. No movement occurs at the bed, and basal shear strain takes place in a zone of salt-rich, amber-colored ice approximately 1 m thick (Holdsworth and Bull, 1970). The trunks of the larger alpine glaciers are not incised but stand above the wind-deflated valley sides. This low erosional activity suggests that such glaciers may flow over a surface for long periods yet leave the surface essentially unchanged.

Extremely light snowfalls and low temperatures permit strong winds to dictate the location of accumulation areas. Without wind redeposition of snow into drifts it is unlikely that many glaciers would exist, because overall ablation losses exceed precipitation at all altitudes. Accumulation areas commonly occur on one glacier at different locations and elevations separated by ablation zones. This phenomenon prevents the glaciers from having a definable equilibrium line altitude (Chinn, 1980). Results of 6 years of mass-balance studies indicate that the alpine glaciers are approximately in equilibrium (Anderton and Fenwick, 1976; Chinn, 1971; Chinn, unpublished; Fenwick and Anderton, 1975; Hawes, 1972). The measured balance changes of about $\pm 20 \text{ kg m}^{-2} \text{ a}^{-1}$ are very small, an order of magnitude less than comparable changes on a temperate glacier. Such small yearly balance changes indicate that most snowfalls are well under $20 \text{ kg m}^{-2} \text{ a}^{-1}$.

Ablation from the glaciers is predominantly by sublimation, and

Figure 32. — Annotated Landsat 1 MSS digitally enhanced false-color composite image of the 'dry valleys' of Victoria Land. NASA image (1174-19433, bands 4, 5, and 7; 13 January 1973; Path 56, Row 116) courtesy of the Physics and Engineering Laboratory, Department of Scientific and Industrial Research, New Zealand. See also figure 33.

^aMinistry of Works and Development, New Zealand.



Figure 33. — Oblique aerial photograph of Taylor Glacier (right foreground) and Lake Bonney (center) taken from an altitude of 5,900 m on 7 November 1959, looking east-northeast. The camera position is marked on figure 32. Ross Island and Mount Erebus volcano are in the distance beyond the fast ice in McMurdo Sound. Ferrar Glacier parallels Taylor Glacier beyond the Kukri Hills (right center). Both flow toward the background. U.S. Navy trimetrogon aerial photograph no. 250 (TMA 540 F31) from the Antarctic Map and Photograph Library, U.S. Geological Survey.

meltwater is rarely seen above 1,500 m altitude even on the warmest summer days. Below 1,500 m meltwater channels run intermittently beside the lower tongues of the glaciers for approximately 2 months each year, but the proportion of the total losses from the glaciers by melt is minimal. Ice and snow ablation rates increase directly with both temperature (altitude and seasonal changes) and exposure to wind. Measured ablation values show highest losses on convex slopes exposed to the wind where the surfaces are deflated to bare ice. Measured ablation rates vary from 46 to 209 kg m⁻² a⁻¹.

The glaciers carry very small volumes of debris that consists mainly of material derived from rockfalls off the headwalls and sand of aeolian origin. Wind-blown sand constitutes a major fraction of surface moraines, particularly on the lower glaciers. Beside these glaciers, interbedded sand and snow layers are common. One small glacier above Bull Pass is said to consist of up to 50 percent by volume of sand of aeolian origin (Dort, 1967). Well-developed barchan sand dunes occur adjacent to the snout of Packard Glacier in Victoria Valley.

Flow rates have been measured on a number of the glaciers with results showing typically low rates of movement. The fastest recorded are those of the steep trunk of Meserve Glacier, Wright Valley, where movement reaches 3 m a⁻¹ (Bull and Carnein, 1970). Surveys from near the lower margin of Sykes Glacier near Lake Vanda indicate movement rates varying from 0.1 m a⁻¹ to 0.5 m a⁻¹. A cross section of stakes near the center of Heimdall Glacier, Wright Valley, gave a maximum flow of 1.23 m a⁻¹ and a mean velocity of 1.02 m a⁻¹. Ice passing through this cross section travels 5 km from the headwall to the glacier snout. The observed mean flow rate shows that the time taken for ice to travel the full length of the glacier is at least 5,000 years.

The identification of individual glacier boundaries on satellite images is difficult in the shadow areas cast by the low sun angle on high relief: Glacier margins can rarely be interpreted correctly in shadow, while on sunlit faces, snow and light-colored rock frequently have similar tonal characteristics on Landsat images. In this region the distinction between glaciers and permanent snow patches is very subjective, because low-gradient snow patches may be some kilometers in areal extent. Where movement is significant, an ice bulge is apparent at the lower margin of a snow area, enabling it to be classified as a glacier. Higher ice velocities produce readily recognizable ice cliffs (fig. 33).

Northern Victoria Land

Figure 34 shows the coast of Victoria Land 250 km north of the area of figure 27. The last giant ice floes can be seen departing from the coast off Drygalski Ice Tongue. This is the optimum season for ships to approach the coast, although fast ice still fills Granite Harbor. The most conspicuous feature in the belts of pack ice lingering off the coast is their vortex pattern. Because vortices 20 to 30 km in diameter are uncommon in wind systems, we presume that the pack ice is reflecting circulation patterns in the coastal currents. Similar vortices have been seen in Arctic pack ice (Solomon and Ahlnäs, 1980). The coastal region is one of small glaciers draining local nunatak areas, each glacier ending in an ice tongue projecting seaward. Drygalski Ice Tongue is the only one large enough to indicate that it must drain a substantial area of the plateau west of the Transantarctic Mountains; indeed contour maps confirm this. The rest draw their nourishment locally from snows

that fall among the mountains. Between each ice tongue is a low ice piedmont. Coastal ice piedmonts of this kind generally hold ice of no more than about 500 m in thickness.

Inland, analysis of the Landsat image (fig. 34) is complicated by thin clouds and plumes of drifting snow wafted into the air from the top of every escarpment. The prevailing southwest wind has caused extensive areas of snow-free ice ('blue ice') on the downwind side of the major escarpments. Such areas are common throughout the Antarctic in similar topographic situations. Mountain or ridge vortices evidently combine with sublimation to keep the surface net balance close to zero. Around Reckling Peak and on the 'blue-ice' patch to the west of it (bottomleft corner of image), an interesting mechanism has been found to bring rare meteorites to the surface (Cassidy, 1980). In this area it is likely that sublimation has combined with an upward component of ice movement caused by rising subglacial terrain to concentrate and expose, over a very long period of time, meteorites that fell on the ice sheet some distance upglacier (Nagata, 1979a, b, 1980).

The area of figure 35 overlaps that of figure 34 but was recorded three months earlier. The 'blue-ice' areas are more conspicuous in this digitally enhanced image, and in a few places, narrow strings of medial moraines are visible.

Despite the use of two different names, we must note that David Glacier and Drygalski Ice Tongue are the same feature. David Glacier is probably the first major outlet glacier north of Mulock Glacier to drain a significant amount of ice from the main Antarctic plateau (Drewry, 1980). According to McIntyre (in press) it drains an area of 224000 km² and should have a balance discharge of 14 km³ a⁻¹. Steed and Drewry (1982) found that it coincides with a subglacial trench that transects the whole mountain range and extends inland for more than 300 km. That it is deep is shown by spot soundings of up to 2530 m. Equally clear is the rapid thinning that is characteristic of floating glacier tongues once they extend beyond the confining walls of a valley. While one reason for the observed thinning from 1,190 m to 500 m over a distance of 40 km is probably an acceleration in longitudinal strain rate as the ice leaves the valley, this image shows that much of the thinning can be accounted for by lateral spreading of the ice tongue, from 12 km wide at the glacier mouth to 22 km wide at the 500-m sounding. The pattern of transverse depressions is characteristic of rapidly diverging flow in glacier tongues and ice shelves. Comparison of identifiable features in Landsat multispectral scanner (MSS) images separated by an interval of 14 months indicates that the landward end of the glacier tongue is moving at about 580 m a⁻¹. Holdsworth (1985) reports a speed of 730 ± 36 m a⁻¹ at about 50 km from the coast.

The ice-surface elevation at the 2,530-m sounding just above the main icefall of David Glacier is 900 m above sea level (fig. 35). In other words, the bed of the glacier on the inland side of the icefall is 1,630 m below sea level, so that the icefall itself is due to a subglacial ridge cutting across the glacier rather than to an elevated rock plateau whose edge coincides with the icefall. Figure 36 is an oblique aerial photograph of the icefall, looking upsteam. The convergence of flowlines below the icefall suggests that the stream is entering a deep fiord-like valley at this point. The longitudinal flowline ridges and chaotic crevassing are typical of fast-moving Antarctic ice streams. By noting their appearance in figure 35, one can identify ice streams in other Landsat images.

The area of figure 37 overlaps that of figure 35 on the north and was recorded on the same day. Nansen Ice Sheet, which appears on both images, is a floating ice sheet formed by the confluence of Reeves and

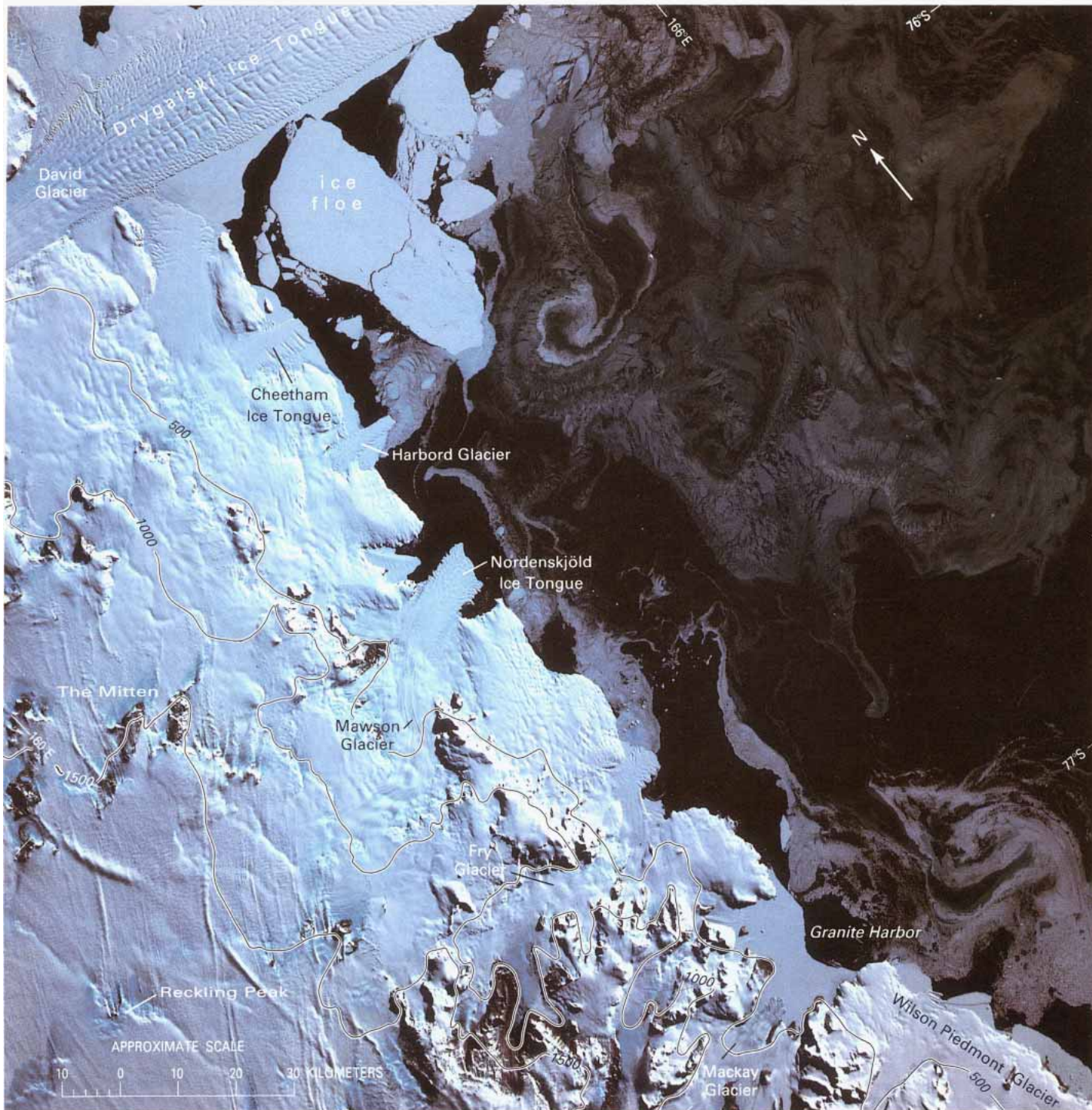


Figure 34. — Annotated Landsat 1 MSS digitally enhanced false-color composite image of the Scott Coast of Victoria Land (southern section). Surface contours (in meters) modified from Antarctica 1:250,000-scale Reconnaissance Series, map sheets SS55–57/16 (1968), ST57–60/1 (1965), and ST57–60/2 (1965), U.S. Geological Survey. NASA image (1214–20064, bands 4, 5, and 7; 22 February 1973; Path 60, Row 115) courtesy of Baerbel K. Lucchitta and the Flagstaff (Arizona) Image Processing Facility, U.S. Geological Survey.

Priestley Glaciers. Its very dark tone indicates that it is an ablation area. Melt lakes, some of them 1 to 2 km in length, occupy many surface hollows formed by longitudinal and transverse flow features. The name Inexpressible Island commemorates one of the most celebrated stories of survival in the history of Antarctic exploration. In 1912, six men unintentionally spent a winter on the island in an unheated snow cave. Despite extreme privation, all of them survived (Priestley, 1914). The physiography of the area was described by Priestley (1923).

Nathan and Schulte (1968) reported abundant evidence of recent volcanism throughout the area between Aviator and Campbell

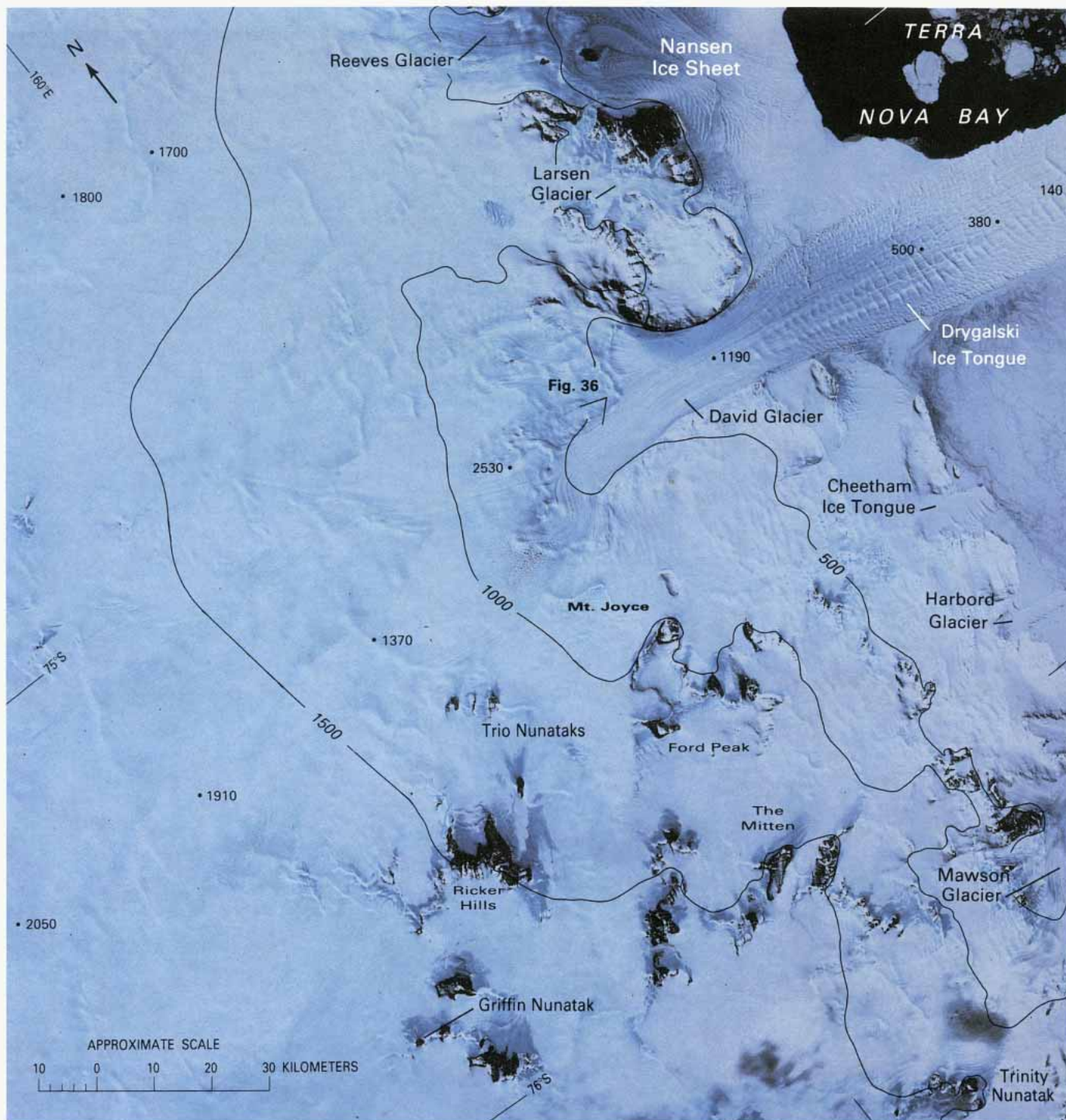


Figure 35. — Annotated Landsat 1 MSS digitally enhanced false-color composite image of the Scott Coast of Victoria Land (northern section). Surface contours (in meters) modified from Antarctica 1:250,000-scale Reconnaissance Series, map sheets SS55–57/12 (1968), SS55–57/16 (1968), SS58–60/9 (1963), and ST57–60/1 (1965), U.S. Geological Survey. Spot soundings (in meters) from airborne radio-echosounding (Scott Polar Research Institute, unpublished). NASA image (1128–20290, bands 5, 6, and 7; 28 November 1972; Path 64, Row 114) courtesy of Baerbel K. Lucchitta and the Flagstaff (Arizona) Image Processing Facility, U.S. Geological Survey. See also figure 36.

Glaciers. Mount Melbourne (2,730 m) is an almost perfect low-angle stratovolcano, showing little dissection and almost no glacial erosion. Probable ash layers exposed in the nearby floating glacier tongues suggest that the volcano has erupted in historic times. There are many small areas of hot steaming ground near the summit, one of them too hot to be touched (Nathan and Schulte, 1967).

The Landsat image (fig. 37) is remarkable in that every glacier that reaches the coast extends into the sea as a glacier tongue. The floating tongues tend to hold the fast ice in place until late in the summer; sometimes it stays in place from one summer to the next. Priestley Glacier falls steadily over a length of 200 km from the plateau threshold at 2,000 m above sea level to its terminus at Inexpressible Island. Campbell and Aviator Glaciers are each about 140 km long and 5 to 10 km wide. Priestley and Reeves Glaciers both drain ice from the East Antarctic plateau; the rest draw their sustenance from locally accumulated snow. Sublimation due to dry, "warmer" winds coming from the plateau may explain why the extensive ablation areas are confined to the two outlet glaciers. Kurtz and Bromwich (1985) noted

Figure 36. — Oblique aerial photograph of David Glacier (looking upstream) taken from an altitude of 4,600 m on 19 December 1957, looking west. The camera position is marked on figure 35. U.S. Navy trimetrogon aerial photograph no. 20 (TMA 348 F33) from the Antarctic Map and Photograph Library, U.S. Geological Survey.



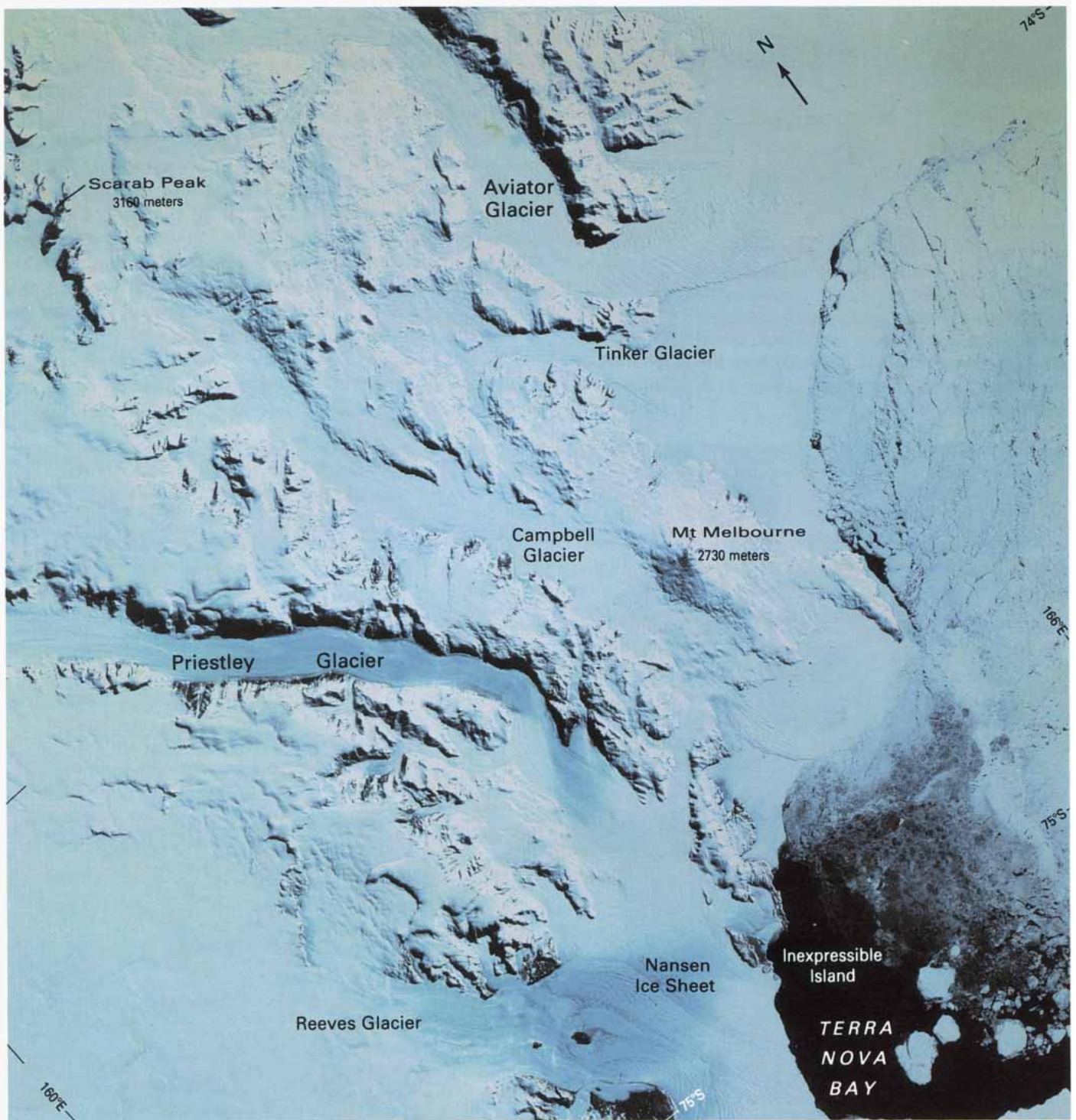


Figure 37. — Annotated Landsat 1 MSS digitally enhanced false-color composite image of the Borchgrevink Coast and Mount Melbourne. NASA image (1128-20284, bands 4, 5, and 7; 28 November 1972; Path 64, Row 113) courtesy of Baerbel K. Lucchitta and the Flagstaff (Arizona) Image Processing Facility, U.S. Geological Survey.

that the Terra Nova Bay polynya is a large, stable, annually recurring feature that markedly influences sea ice dynamics in the region; they ascribe its persistence to katabatic winds from Reeves Glacier that prevent new sea ice from consolidating in situ (Bromwich and Kurtz, 1984).

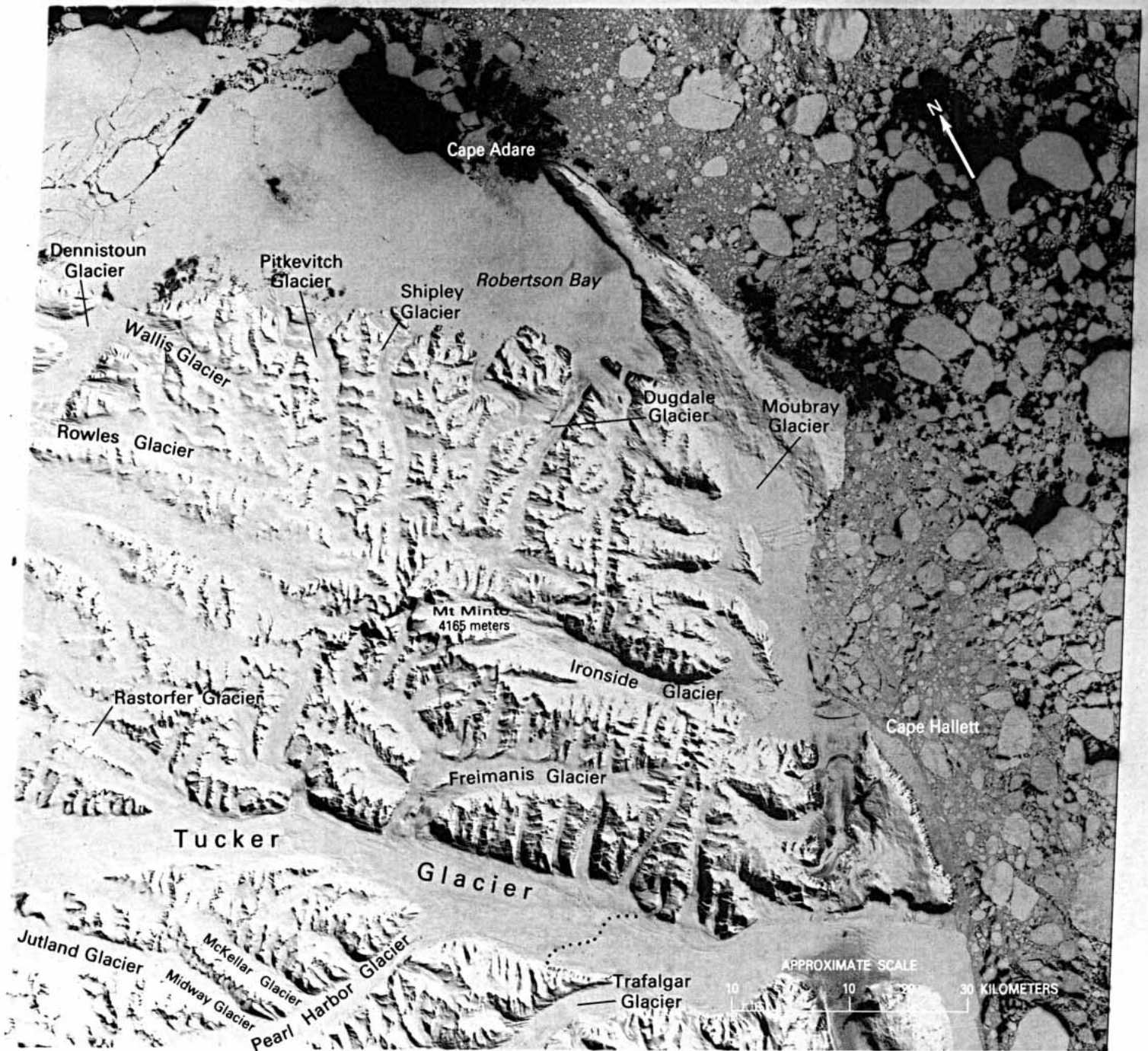
Figure 38 was recorded on the same orbit and just to the north of the area of figure 37. Fast ice fills every embayment in the coastline and pack ice, while a mixture of floe sizes, from small (20–100m across) to giant (more than 10 km across), can be seen at sea. The physiography of the coastal area was described by Priestley (1923). The most remarkable feature inland is the structurally controlled perpendicular pattern of trunk and tributary glaciers. Tucker Glacier dominates the scene: it is 170 km long and 6 to 11 km wide. In spite of its size, the source of the glacier is within the mountains, and it drains no ice from the inland plateau. The glacier evidently occupies a mature valley, because the ice appears to be afloat for a distance of more than 60 km upstream from its terminus.

Cape Adare was the site of the first recorded landing from a ship on the Antarctic mainland (in 1895) and later was the home of the first expedition ever to winter in Antarctica. An international team spent the winter of 1899 in a hut built in an Adelie penguin (*Pygoscelis adeliae*) rookery on a raised beach at the foot of the cape (Borchgrevink, 1901). Although they were lured by the spectacular peak of Mount Minto (4,165 m), the expedition was ill-equipped and thus unable to travel inland. Fifty-seven years passed before a modern research station was established in another Adelie penguin rookery at Cape Hallett. A joint United States/New Zealand station was set up for the International Geophysical Year in 1957–58, and it remained manned year round until 1964; after that, it continued to be used during the austral summer each season until 1972–73.

Figure 39 is the best of the very small number of correctly exposed Landsat 3 return beam vidicon (RBV) images yet obtained from any part of the Antarctic. The resolution is quite remarkable, revealing intimate details of glacier flowlines, surface expressions of subglacial features, and areas of crevassing. Whereas MSS imagery can reveal crevassed areas by surface textural and tonal differences, RBV images can resolve even individual large crevasses, for example those over the subglacial escarpment marking the confluence of Graveson Glacier with Lillie Glacier. Lillie Glacier is 220 km long but it drains no ice from the plateau west of the Transantarctic Mountains. As such it may be the longest local glacier in the world. It is 19 km wide just below the confluence of Ebbe Glacier. There are no clear indications of the position of the grounding line, but it probably lies at the upstream end of the giant transverse waves a few kilometers above the confluence of George Glacier.

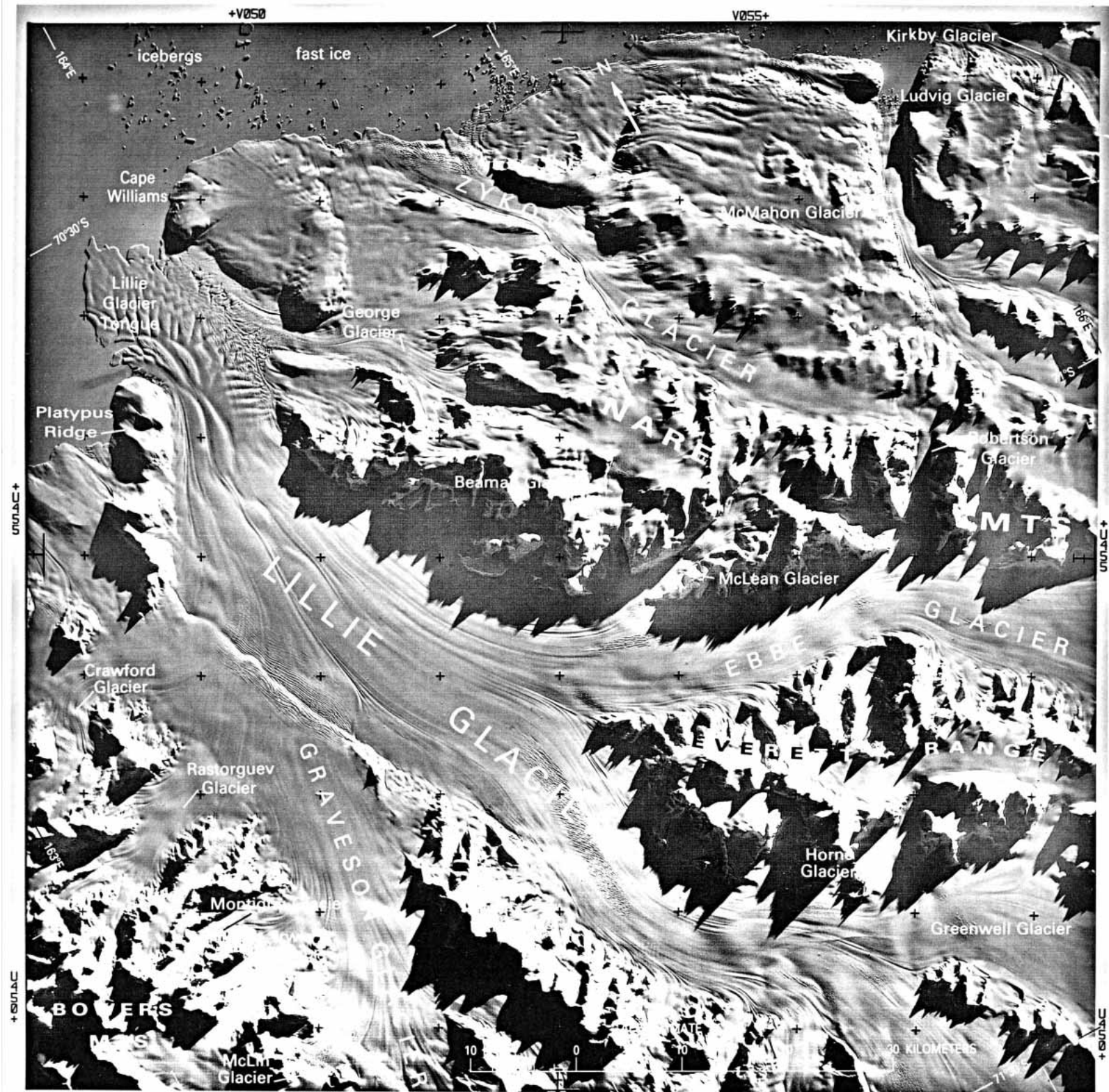
The areas of coverage in figures 40, 41, and 42 overlap that of figure 39 on the west and show Rennick Glacier, the only major northward-flowing glacier in the Transantarctic Mountains north of Beardmore Glacier and, by any standard, one of the largest glaciers in the world. Occupying an almost straight fault-controlled trench (Dow and Neall, 1974) that can be followed over a distance of 370 km, the glacier is 20 to 30 km wide throughout most of its length.

The shear stress at the glacier bed causes glaciers on land to develop a significant surface slope, whereas floating glaciers are almost level; consequently, our first step in finding the probable position of the grounding line is to search for a break in slope (fig. 42). There must be a finite surface slope on a floating glacier in order to overcome the



1E166-00 28NOV72 C S71-45/E169-23 N S71-52/E169-44 MSS 1E167-00 7 R SUN EL29 AZ068 209-1786-R-1-N-D-IL NASA ERTS E-1128-20275-7 01 1E168-00 1E169-00

Figure 38.— Annotated Landsat 1 MSS image of Cape Adare and Cape Hallett. The dotted line on Tucker Glacier represents the inferred position of the grounding line. NASA image (1 128-20275, band 7; 28 November 1972; Path 64, Row 111) from the EROS Data Center, U. S. Geological Survey.



17SEP80 C 570-50/E164-36 USGS-EDC N 570-31/E163-37 R DXBOR SUN EL06 A065 S2H-CP-N NASA LANDSAT E-30927-20382-D

Figure 39.—Annotated Landsat 3 RBV image of the Lillie Glacier and the Pennell Coast. NASA image (30927-20382-0; 17 September 1980; Path 70, Row 110) from the EROS Data Center, U.S. Geological Survey.

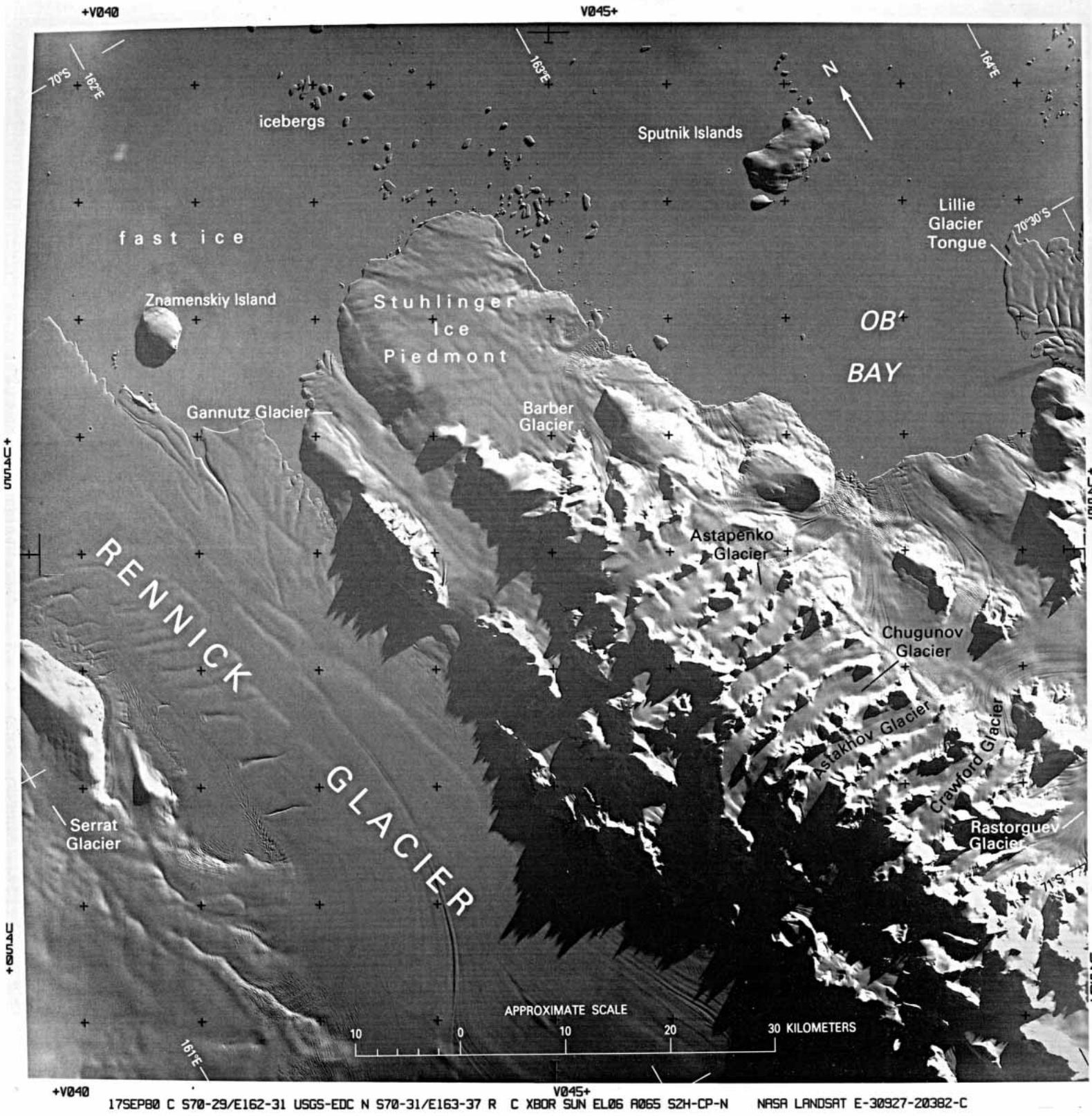


Figure 40. — Annotated Landsat 3 RBV image of the Rennick Glacier and the Oates Coast. NASA image (30927-20382-C; 17 September 1980; Path 70, Row 110) from the EROS Data Center, U.S. Geological Survey. See also figure 41.

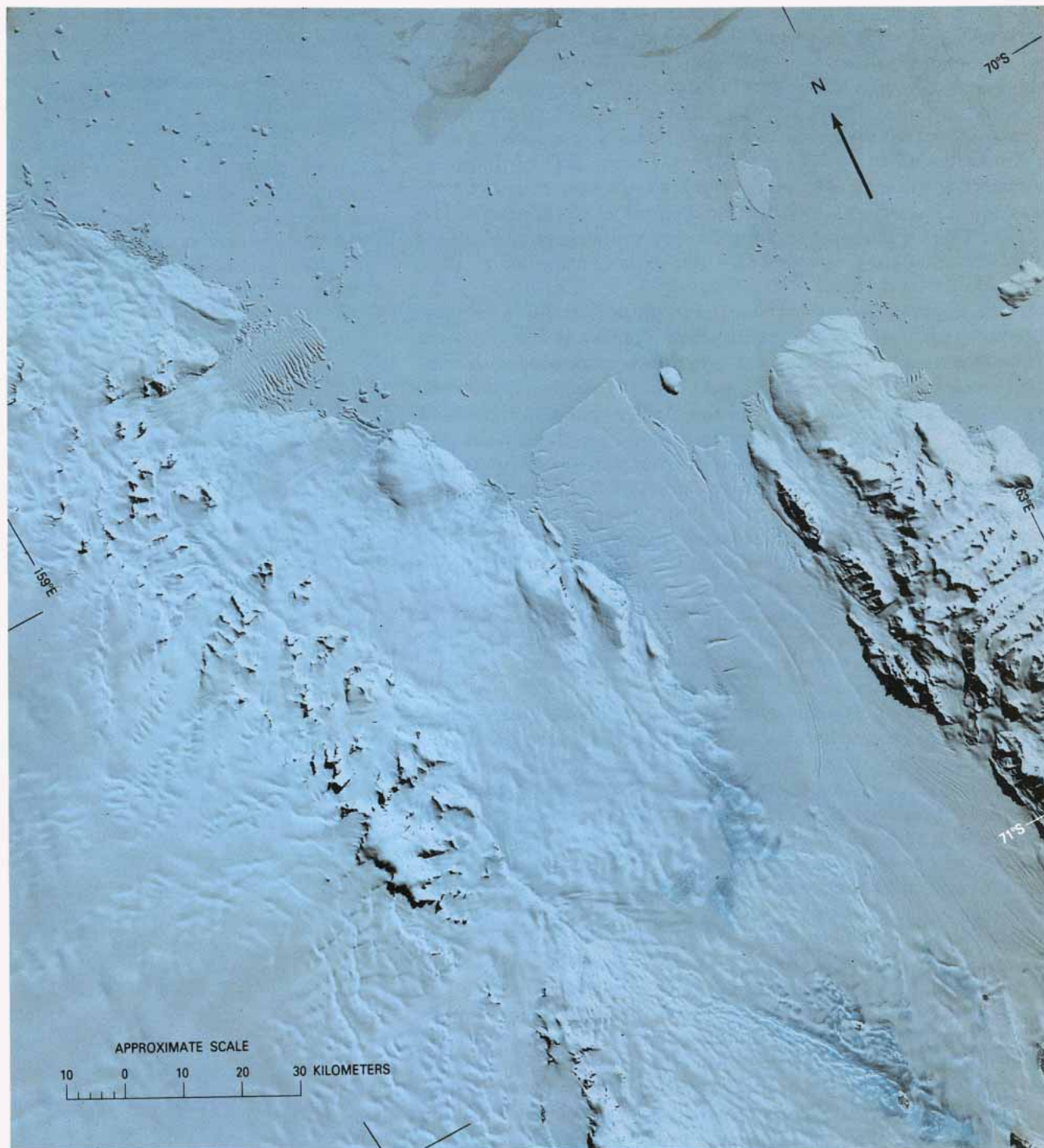


Figure 41. — Landsat 1 MSS digitally enhanced false-color composite image of the terminus of the Rennick Glacier and the Oates Coast. Compare glaciologic details visible with figure 40, a Landsat 3 RBV image of the northeast quadrant of the area. NASA image (1460–21103, bands 4, 5, and 7; 26 October 1973; Path 72, Row 110) courtesy of Baerbel K. Lucchitta and the Flagstaff (Arizona) Image Processing Facility, U.S. Geological Survey.

shear stress acting on the sides of the glacier, but it is much less than on grounded ice. Meltwater, where there is any, will tend to collect at the grounding line, where the slope changes. When the capacity of hollows close to the grounding line is exceeded, the meltwater flows gently down glacier to fill new hollows. Thus on morphological grounds alone we would expect the grounding line of Rennick Glacier to be close to the dotted line off the mouth of Sledgers Glacier. If our interpretation is correct, the glacier is afloat for 140 km upstream from its terminus. Mayewski and others (1979) studied the area on the ground and by means of airborne radio-echosounding. Their conclusion on the basis of radio-echosounding data was that the glacier is floating for at least 130 km.

Other imagery recorded a month earlier in the season shows very few melt lakes on the glacier. The accumulation of meltwater at any time of the season is generally, though not invariably, associated with comparatively slow-moving glaciers. Figure 40 (RBV) makes an interesting comparison with the same part of the glacier shown in figures 41 and 42 (MSS). The RBV shows far more detail on the glacier and shadows are less harsh. The conspicuous medial flowline shows rather convincingly that at its distal end, more than half of the total width of Rennick Glacier consists of ice from tributary ice streams entering from the west, rather than from the trunk glacier. The implication is that Rennick Glacier itself must be sluggish. Recent mapping of the ice sheet surface inland (Steed and Drewry, 1982) suggests that Rennick Glacier has a small drainage basin and receives little, if any, of its ice from interior sectors of the East Antarctic ice sheet. The average surface gradient from source to grounding line is 1 in 85, midway between those of Scott and Amundsen Glaciers.

Using evidence from flowlines, supraglacial meltwater lakes (melt lakes), and surface gradient, we have now found three independent and purely morphological grounds for expecting a slow rate of ice movement. Can a sequence of Landsat images support this deduction? Comparison of front positions in MSS images separated by an interval of 8 years indicates a rate of movement of around 190 m a⁻¹. This makes Rennick Glacier one of the slowest moving of the major glaciers in the region. Total output at the ice front must be only about 0.6 km³ a⁻¹, very small for a glacier of this size.

The Rennick Glacier has two major tributaries: Canham and Gressitt Glaciers. The visible ice-surface topography suggests a deep subglacial trench trending southwest from the head of Gressitt Glacier at least to the edge of the image (fig. 42). Extensive moraines are on the left-bank nunataks in the bottom half of the image and on the 'blue-ice' areas surrounding them. Mayewski and others (1979) present evidence that a larger Rennick Glacier once covered all but the highest peaks in the Morozumi Range area. However, the glacier is now believed to be in a phase of retreat, with the grounding line migrating upstream.

Figure 43 is an RBV image recorded with a lower sun elevation angle (2° above the horizon) than any other RBV or MSS image in this chapter. The very dark area at the bottom of the image and in patches on the sea ice is an artifact caused by vidicon shading (*Landsat Data Users Notes*, No. 20, 1981, p. 6-7) and is not related to the low sun angle. By measuring the length of real shadows, we can use the known sun elevation to calculate the freeboard of icebergs. Many of those shown here stand 30 m above the surrounding fast ice. Suvorov Glacier is the largest glacier in this area, but it is of no regional significance. Leningradskaya is a Soviet research station manned by 12 men; it has been continuously occupied since 1971.

Figure 42. —Annotated Landsat 1 MSS image mosaic of the Rennick Glacier and the Usarp Mountains. Image center is at 71°10'S., 162°E. Ice-surface contours (in meters) modified from Antarctica 1:250,000 Reconnaissance Series, map sheets SR57-58/10 (1970), SR57-58/14(1970), SR57-58/15 (1970), SS55-57/4 (1970), and SS58-60/1 (1969), U.S. Geological Survey. The dotted line represents the inferred position of the grounding line. Spot soundings (in meters) from airborne radio-echosounding (Scott Polar Research Institute, unpublished). NASA images (1551-21144, band 7; 25 January 1974; Path 73, Row 110; 1117-21075, band 7; 17 November 1972, Path 71, Row 111; 1169-20554, band 7; 8 January 1973; Path 69, Row 110; and 1169-20561, band 7; 8 January 1973; Path 69, Row 111) from the EROS Data Center, U.S. Geological Survey. See also figures 40 and 41.



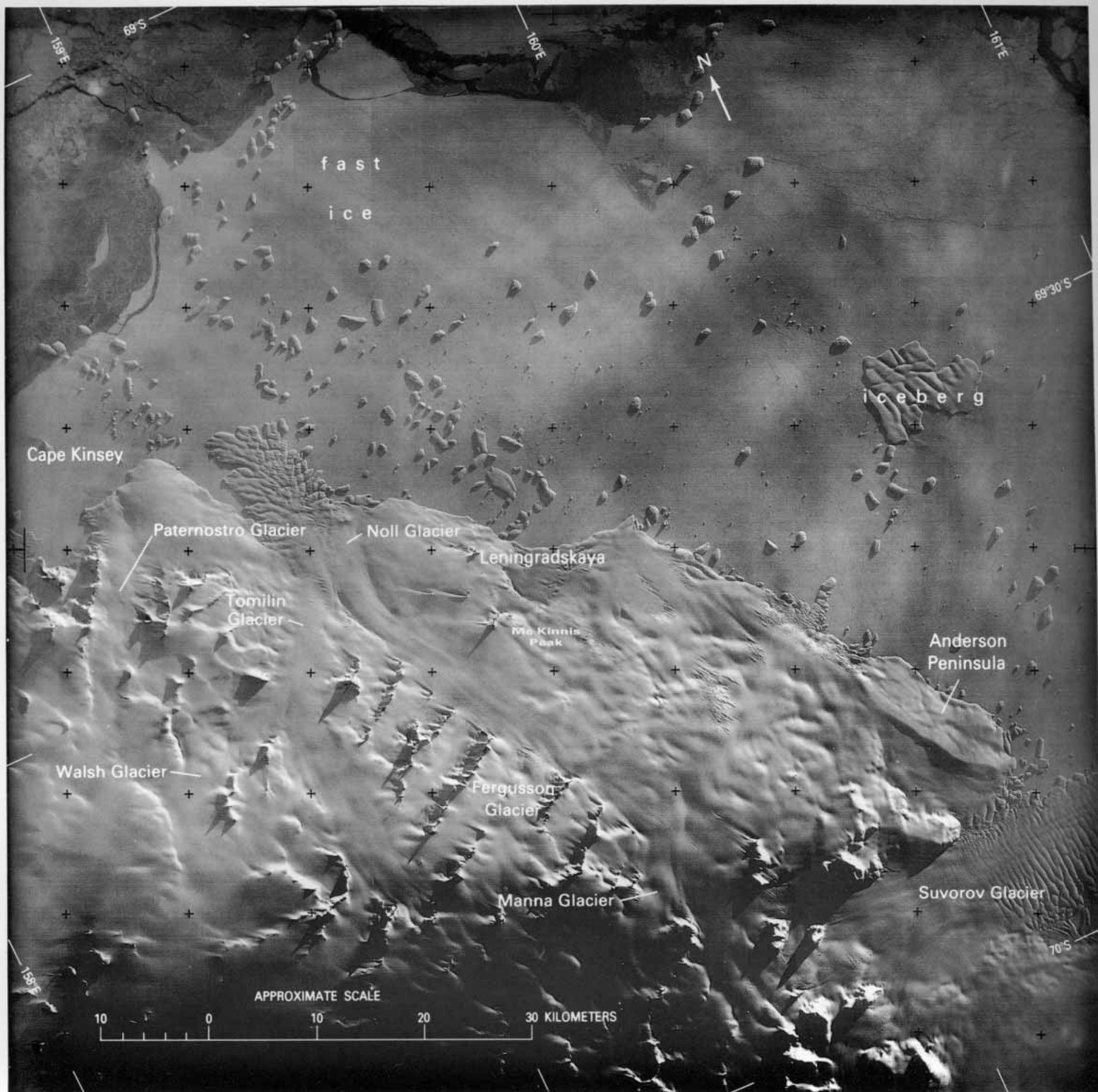


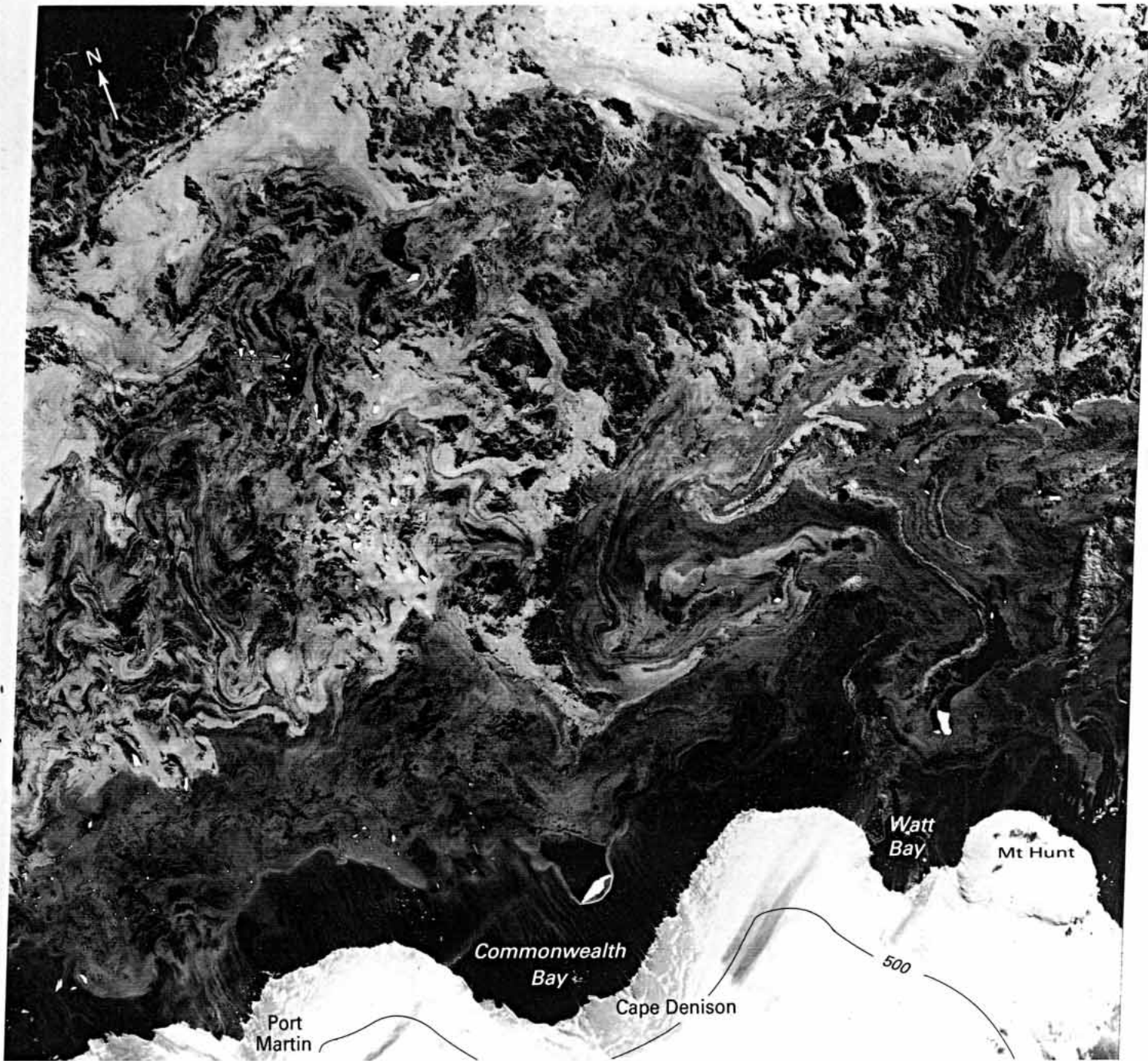
Figure 43.—Annotated Landsat 3 RBV image of the Suvorov Glacier and the Oates Coast. NASA image (30914-21070-D; 4 September 1980; Path 75, Row 109) from the EROS Data Center, U.S. Geological Survey.

THE INDIAN OCEAN SECTOR

Wilkes Land, Bunger Hills, and Shackleton Ice Shelf

Figure 44 depicts, if not the windiest place on Earth, certainly the windiest place at which meteorological records have ever been kept. The mean wind speed measured at Cape Denison over 22 months in 1912-13 was 19 m s^{-1} . The highest monthly mean was 25 m s^{-1} for July 1913. The highest daily mean was 43 m s^{-1} . Maximum gust speeds were much higher, but they were not measured. Madigan (1929), who made the observations, wrote: "For nine months of the year an almost continuous blizzard rages, and for weeks on end one can only crawl about outside the shelter of the hut, unable to see an arm's length owing to the blinding drift snow." Evidence of the wind can be found in all parts of this image. The lower slopes of the ice sheet are swept bare of snow in places. Note the fine plumes of snow being carried across the ice-wall coast of Commonwealth Bay to the east of Cape Denison. Note that similar plumes of snow in Watt Bay are directed at an angle of 50° to the right of those in Commonwealth Bay. In each case the wind is roughly perpendicular to the contours on the lower slopes of the ice sheet. This important clue shows that we are dealing not with geostrophic or normal cyclonic winds but with katabatic winds caused by gravity drainage of a rather thin surface layer of radiatively cooled air from inland. The broad pattern is part of a topographically controlled confluence zone extending several hundred kilometers into the interior (Parish, 1981). In a theoretical paper, Ball (1960) discussed gravity and Coriolis effects to explain why in this region movement of a low-pressure storm system along the coast causes temporal variations in wind strength but not in wind direction. The glaciological significance of katabatic winds is that they carry phenomenal amounts of snow out to sea. Loewe (1956), who wintered at the French station of Port Martin in 1951, calculated that on each blizzard day 240,000 tons of drifting snow crossed each kilometer of the coast. Extrapolation to an annual total gave 18 million tons per kilometer, a figure Loewe believed to be a minimum. Extrapolating further to the width of this scene yields a staggering total of 34 billion tons of snow wafted out to sea each year. This transport removes one half of an assumed accumulation of $200 \text{ kg m}^{-2} \text{ a}^{-1}$ over an areal strip that extends from the coast to about 200 km inland. The loss of snow by drift is more important in the mass balance of the ice sheet in this area than evaporation, melting, or iceberg formation.

It is known that katabatic winds do not extend far out to sea (Davis, 1919). By keeping his vessel *Aurora* about 6 km from the shore, Captain Davis found that he was beyond the reach of the more violent gusts. At anchor in Commonwealth Bay, he noted that to the north, gusts appeared to be traveling in various directions. The satellite image tells the same story. Off Port Martin and Commonwealth Bay the steady wind direction persists only to a distance of 10 to 20 km from the shore. Slowing of the wind speed over this distance causes snow to precipitate onto the sea. Combining with ice crystals formed from rapid freezing of the sea surface, the snow yields shuga, an accumulation of spongy white lumps. Shuga is invisible in satellite pictures, thus the



IE141-00 S067-001 IE142-00 E143-001 E144-001
 04MAR73 C S66-19/E143-16 N S66-24/E143-25 MSS 7 R SUN EL17 AZ062 202-3126-A-1-N-D-1L NASA ERTS E-1224-22440-7 01

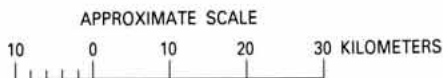


Figure 44. — Annotated Landsat 1 MSS image of the home of the blizzard: Commonwealth Bay, George V Coast. Ice-surface contour (in meters) from Australian Antarctic Territory 1:1,000,000, sheet SQ53-54 (1971), Canberra, Division of National Mapping. NASA image (1224–22440, band 7; 4 March 1973; Path 88, Row 107) from the EROS Data Center, U.S. Geological Survey.

shore lead appears ice free. Loewe (1956) observed that if all the snow drifting from the continent in this area were precipitated within a 20 km strip along the coast, the water level would be raised 3 mm per day, a rather important addition. Melting of this drift snow would require $350 \text{ MJ m}^{-2} \text{ a}^{-1}$. This loss of heat from the sea water is of the same order of magnitude as the loss by outgoing radiation. While the loss of heat caused by the continual freezing of sea water in the shore lead is probably the principal factor, in this particular sector drift snow carried across the coast contributes appreciably to the formation of cold Antarctic ocean-bottom water.

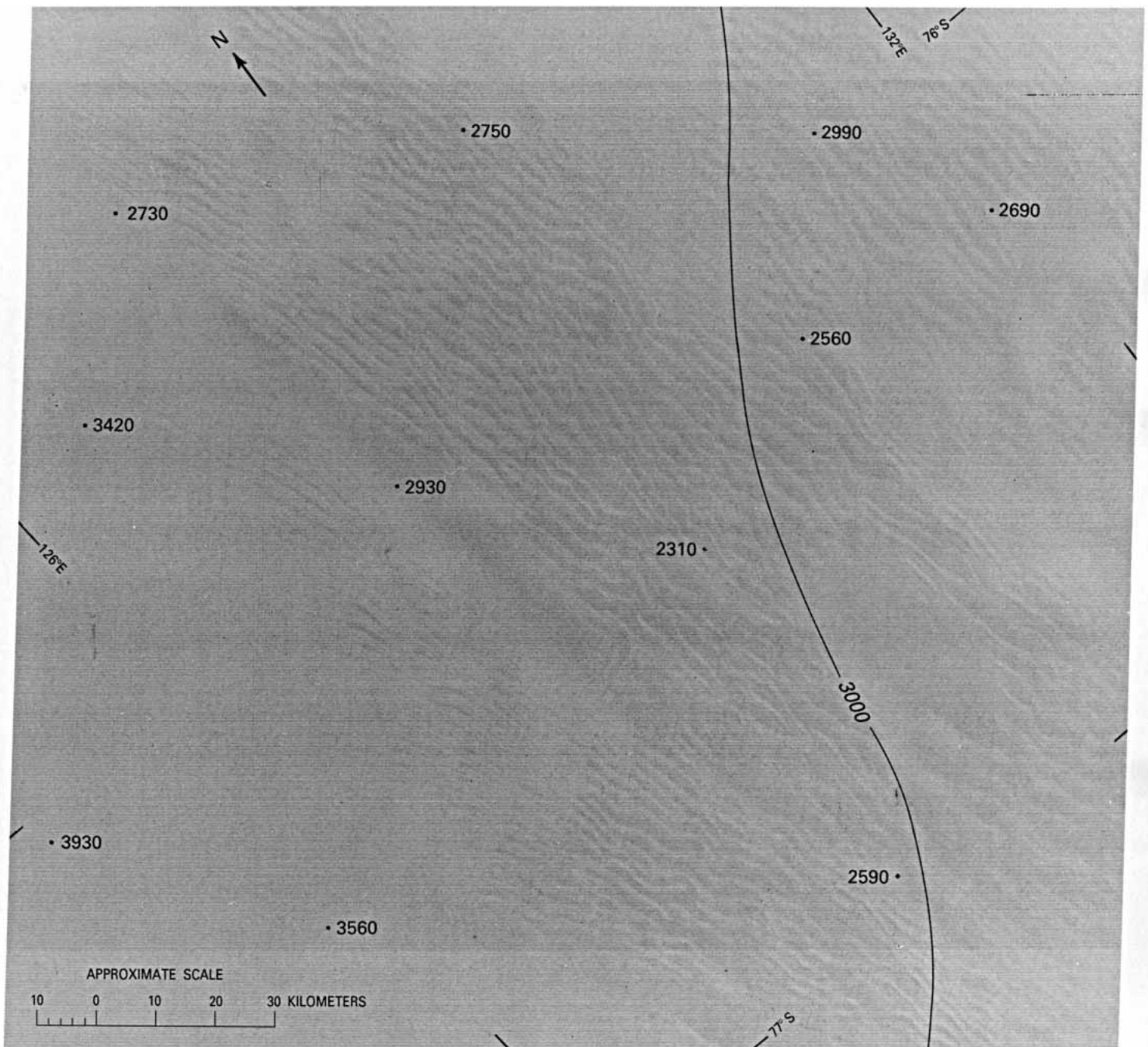
Everything seen in the fascinating complex of ice patterns to seaward of the shore lead illustrates variable winds and sea current vortices. The steady katabatic flow has been replaced by a maze of eddies made visible by the new ice that is being swept out to sea from the shore lead where it formed. We say new ice here because the sea ice is in the first stage of formation. In contrast to the pack ice in figure 38, there is no single ice floe large enough to be resolved by the Landsat MSS image. What may appear to be ice floes are most probably all icebergs. Note how the sea ice is being moved past the icebergs, leaving an ice-free “plume,” or shadow, on the downwind side. The new ice thickens with time: despite the complexity caused by mixing, in the image it changes from dark gray in the first 30 km outside the shore lead to light gray in the middle of the scene and to white at the top. The 7-km-long iceberg in Commonwealth Bay substantiates the conclusion that new ice forms in the shore lead. Only where the iceberg blocks its path does the ice become visible; it can be seen concentrating behind and then streaming northward from both ends of the obstruction.

Figure 45 shows an unusual area of snow “megadunes” 1,000 km inland from the Indian Ocean coast. Because cloud patterns on Landsat images of Antarctica sometimes resemble megadunes, we would be cautious about describing these as megadunes were it not for the persistence of the same pattern over a period of weeks. The patterns can also be seen on image 1489–22154, band 7, Path 83, Row 115, recorded 17 days later on 24 November 1973. What we see in figure 45 is a pattern probably caused by the redistribution by wind of newly fallen snow. The lighter bands apparently represent newer snow than the darker bands. The MSS is evidently responding to differences in albedo caused by differing degrees of metamorphosis of the constituent snow grains (Zwally and Gloersen, 1977). Another explanation for the change in reflectivity may be morphologic. Slight changes in slope may produce the observed albedo differences. The general surface slope is downwards from left to right but the prevailing wind is probably from the west, perpendicular to the dune lines. Snow accumulation may be so low in this area (Bull, 1971) that the darker bands could be months or even a year or more old (compare fig. 51). The physics of desert sand dunes, which were described in classic works by Cornish (1914) and Bagnold (1941), and the physics of snow dunes have a great deal in common. Sand megadunes with a wave length and pattern generally similar to Antarctic snow megadunes are known from eastern Iran and from the Namib Desert (McKee, 1979; Short and others, 1976, plates 285 and 348). While sand megadunes are known in places to rise tens of meters above the general surface level, snow megadunes are likely to be so low (estimated at 1–2m) that they may be imperceptible to the surface traveler.

Figure 46 shows Totten Glacier, the first major ice stream to be discussed. According to McIntyre (in press) it drains an area of 150,000 km^2 and should have a balance discharge of $43 \text{ km}^3 \text{ a}^{-1}$. Dolgushin (1966) measured ice-front velocities in the range 850 to 1,200 m a^{-1} .

Although most ice streams flow in a subglacial valley, the essential contrast with a valley or outlet glacier is that there are no rock exposures. Thus, although we infer the presence of a valley here on the basis of surface indications of the subglacial relief, we can only prove it by radio-echosounding of the ice depth. Two soundings on this image prove the existence of a subglacial valley, though neither is close to where maximum depths are to be expected. The 1,000-m spot sounding occurs well below the 500-m surface contour, and the 2,000-m sounding is below the 1,000-m contour. The direction of surface ice movement is, as usual, essentially perpendicular to the surface contours, and in uncounted areas, it can be inferred from many faint but unmistakable flowline features. The rifts north of latitude 67°S. are destined one day to control the calving of icebergs. The origin of similar rifts on Beardmore Glacier was discussed by Collins and Swithinbank (1968). The grounding line is clearly defined along the margins of the glacier. On the centerline, all that we can say is that it probably lies a short way

Figure 45. — Annotated Landsat 1 MSS image of snow megadunes on the high plateau of East Antarctica. Surface contour (in meters) from Antarctica 1 :3,000,000 (Scott Polar Research Institute, unpublished). Spot soundings (in meters) from airborne radio-echosounding (Scott Polar Research Institute, unpublished). NASA image (1472-22213, band 7; 7 November 1973; Path 84, Row 115) from the EROS Data Center, U.S. Geological Survey.



upglacier from the single line of smooth depressions indicated. There are no rock outcrops or nunataks within the whole area of this image mosaic.

The Bunger Hills (fig. 47) were discovered in February 1947 by the pilot of an aircraft involved in US. Navy Operation Highjump. At the time, the discovery of about 1,000 km² of snow- and ice-free terrain was considered sensational, and it was described as an “oasis.” Other snow- and ice-free areas were known in Antarctica, including the larger ‘dry-valley’ area in southern Victoria Land (figs. 32 and 33) that was discovered during the British National Antarctic Expedition of 1901–04. Byrd (1947, p. 498) described the Bunger Hills as “a land of blue and green lakes and brown hills in an otherwise limitless expanse of ice.” There were “three open-water lakes—each large enough to provide a smooth three-mile take-off for a flying boat—and about 20 smaller water bodies.” A flying boat did in fact land on one of the lakes: “An island suitable for life had been found in a universe of death.”

In 1956, the Soviet Antarctic Expedition set up a research station, Oasis, on Bunger Hills. It was handed over to Polish scientists in 1959, who renamed it Dobrowolski. The area has been described in a book by Simonov (1971). Most of the lake area, which runs to several hundred square kilometers, consists of tidal sea lakes. These are simply localized exposures of the sea that underlies all ice shelves. However, 50 km of Shackleton Ice Shelf, hundreds of meters in thickness, separate the lake area from what people generally regard as the coast, in this case an ice front. Although a surface vessel approaching the ice shelf from the north would find her passage barred by the normal 20 to 30 m high ice cliff, it might be physically possible (but perhaps inadvisable) for a submarine to continue southwards to surface in a sea lake at Bunger Hills.

The subglacial coastline can readily be identified where it trends diagonally across the image from Bunger Hills, roughly paralleling the 500-m ice-surface contour. Denman Glacier cuts a conspicuous 10- to 20-km swath as it sweeps 200 km across the scene from Mount Strathcona. According to McIntyre (in press) it drains an area of 199,000 km² and should have a balance discharge of 29 km³ a⁻¹. The probable position of the grounding line has been marked with dots, with the boundary between smooth and wavy surfaces being used as evidence. Wavy or rifted surfaces are characteristic of floating glacier tongues, particularly where they are no longer confined within a valley. The rifts, as on Totten Glacier (fig. 461), represent lines of weakness that, at the time of calving, will localize fractures. The ice stream punches its way across Shackleton Ice Shelf without losing its identity. According to a 1:1,000,000-scale map of the Australian Division of National Mapping (1969), in 1956 the glacier front was only 14 km from Chugunov Island, whereas in this image (fig. 47) it is off the frame. A Landsat image of 29 November 1972 (1129–01353, band 7; Path 118, Row 106) shows the ice front 22 km beyond its 1956 position, indicating a minimum rate of advance of 1,370 m a⁻¹, and more if any calving took place during the 16-year period. The Soviet Atlas Antarktiki (Tolstikov, 1966, p. 162) gives a maximum rate of movement for Denman Glacier of 1,500 m a⁻¹ and for Scott Glacier, 1,300 m a⁻¹.

There are some exceptionally large areas of bare ice in this image and a number of surface meltwater lakes, south of the southern tip of Bunger Hills. Other imagery shows that both the bare ice and melt lakes vary greatly in size at different seasons of the year. An MSS band 4, band 5, or false-color composite (bands 4, 5, and 7) image is generally needed to distinguish bare ice from bare rock because the two have different spectral characteristics in these bands.



Figure 46. — Annotated Landsat 1 MSS digitally enhanced image mosaic of Totten Glacier, Wilkes Land. Ice-surface contour (in meters) modified from Australian Antarctic Territory 1:1,000,000 sheets SR49–50(1969) and SQ49–50(1975), Canberra, Division of National Mapping. Spot soundings (in meters) south of latitude 67°30'S., surface velocity vectors, and elevation data after D. Sheehy (unpublished M.Sc. thesis, University of Melbourne). Spot soundings and elevation data on Law Dome from N.W. Young (personal commun., 4 January 1982). NASA images (1460–00300, band 7; 26 October 1973; Path 107, Row 107; 1460–00303, band 7, 26 October 1973; Path 107, Row 108) courtesy of N.W. Young, Antarctic Division, and CSIRO Division of Computing Research, Australia.

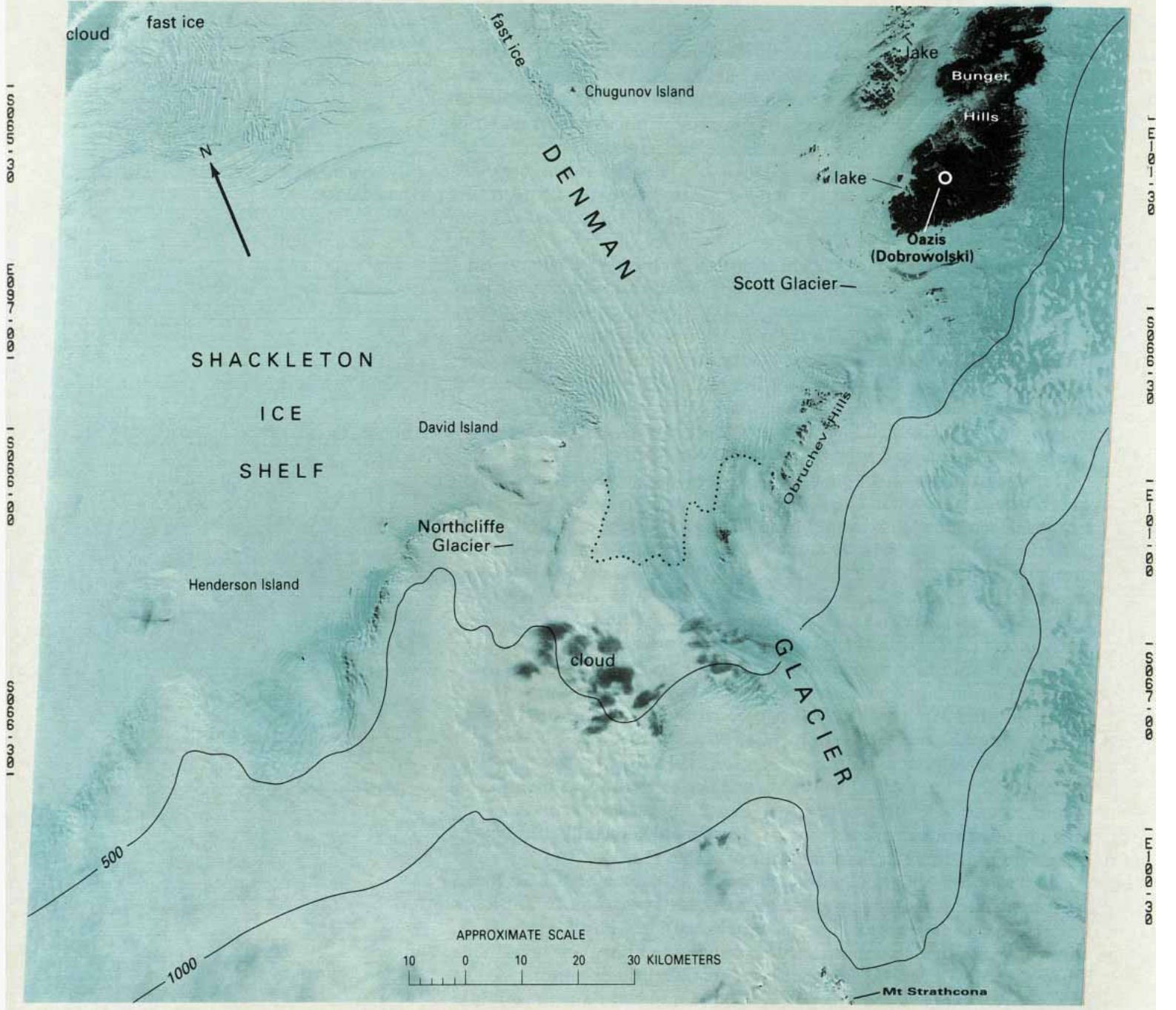
1E098-00

1S065-30

1E099-00

E100-001

E101-001



E097-001 E098-001 E099-001
 23FEB74 C S66-28/E098-50 N S66-35/E099-02 MSS 45 7 R SUN EL20 AZ065 202-8078-N-1-N-D-2L NASA ERTS E-1580-01364-3 02

Figure 47. — Annotated Landsat 1 MSS false-color composite image of Denman Glacier and Bunger Hills. Ice-surface contours (in meters) modified from Australian Antarctic Territory 1:1,000,000 sheet SQ47-48 (1969), Canberra, Division of National Mapping. The dotted line represents the inferred position of the grounding line. NASA image (1580-01364, bands 4, 5, and 7; 23 February 1974; Path 119, Row 107) from the EROS Data Center, U.S. Geological Survey.

Queen Mary Coast and Amery Ice Shelf

Figure 48 shows a typical ice-wall coastline, though the termini of Helen Glacier and “Annenkov Glacier” are afloat. The diagnostic indication of an ice-wall coastline is the small-scale visible topography of the ice surface extending right up to the coast. Note the contrast with Shackleton Ice Shelf, an almost featureless, flat, floating ice shelf. The probable grounding line of Helen Glacier is where the severe crevassing on its grounded ice stream gives way to the water-filled rifts of the floating glacier tongue. The clusters of icebergs off Helen Glacier have been in the same place at least since 1956, from which we infer that they are grounded on shoals. This coastline is the site of Mirnyy Station, which served as the main base of the Soviet Antarctic Expeditions from 1956 to 1965 and is still manned today. Buildings were erected on two small nunataks, which are the only ice-free outcrops on the mainland within the area of this scene. The larger nunatak was 400 m long in 1956, but snowdrifts created by the buildings had so reduced the area of bare rock that it was too small to be seen on the Landsat imagery in 1974. Haswell Island, where there is a penguin rookery, can just be distinguished, 3 km off the coast near Mirnyy.

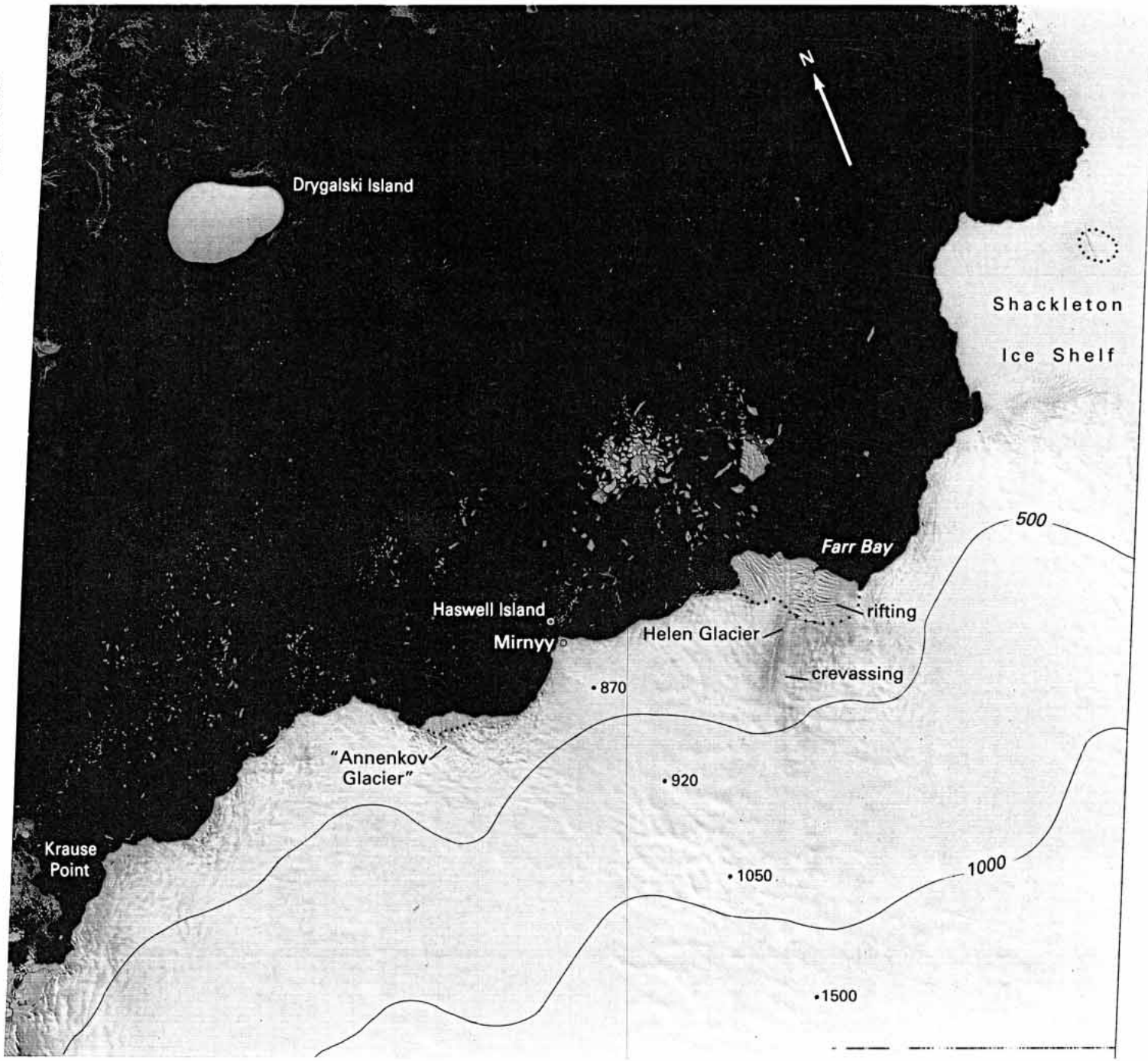
The topography seen on the inland ice sheet suggests that it is everywhere less than 2,000 m thick. Bogorodskiy and Fedorov (1968) ran a radio-echosounding line inland from Mirnyy and reported that, apart from the Mirnyy outcrops, bedrock is generally below sea level for the first 30 km inland. Beyond this it rises but then drops back to below sea level at the 1,500-m spot sounding. The bare floating tongues of “Annenkov Glacier” and Helen Glacier are certainly ablation areas. Kotlyakov (1963) reported that, in general, net snow accumulation increases inland to a maximum at 15 to 30 km, beyond which it decreases. The average for the first 50 km was found to be $421 \text{ kg m}^{-2} \text{ a}^{-1}$.

Schmidt and Mellinger (1966) measured the rate of ice movement, finding velocities typically around 60 to 80 m a^{-1} near the 1,500-m spot sounding. Equally typical, however, were velocities of 300 m a^{-1} at points 30 to 35 km inland, where their track crossed what must be an inland extension of Helen Glacier. These figures are typical of the range to be expected near an ice-wall coastline. Dolgushin (1966) measured 600 m a^{-1} at the floating front of Helen Glacier.

The flat expanse of Shackleton Ice Shelf (30 to 40 m above sea level) is interrupted by a single grounded area that has produced a rift 5 km long and 200 to 400 m wide. The upward bulge of the surface is conspicuous although the summit reaches to only 50 m above sea level. This contrasts with Drygalski Island, an independent dome-shaped ice cap rising to 326 m above sea level. Drygalski Island is unique in that it is an ice cap built on a shoal, no part of which rises higher than 60 m below sea level. The ice cap could have originated as a grounded ice-berg, its surface progressively rising as snow accumulated upon it. Shumskiy and others (1961) reported an annual accumulation of 830 $\text{kg m}^{-2} \text{ a}^{-1}$ on the summit. No part of the ice cap is afloat; the ice-wall coastline appears to maintain a constant position, because the ice velocity, here measured at 27 m a^{-1} , is in dynamic equilibrium with the rate of calving. The snow temperature at 10 m depth on the summit was found to be -12°C .

The central plateau of East Antarctica is often held to be a featureless snow plain. If by “features” we mean mountain ranges, valley glaciers, icefalls, and crevasses, then featureless it is. But there are features to be seen, although some of them may be hard to distinguish.

Figure 48.—Annotated Landsat 1 MSS image of Queen Mary Coast. Ice-surface contours (in meters) modified from Mirnyy, *Antarktida*, 1:1,000,000, Moskva, Ministerstvo Morskogo Flota SSSR, 1959. Spot soundings (in meters) from surface radio-echosounding by Bogorodskiy and Fedorov (1968). Dotted line represents the inferred position of the grounding line. NASA image (1584–01593, band 7; 27 February 1974; Path 123, Row 107) from the EROS Data Center, U.S. Geological Survey.



27FEB74 C S66-22/E093-09 N S66-29/E093-24 MSS | E091-00 | S067-00 | E092-00 | E093-001 | E094-001
 7 R SUN ELI9 AZ065 201-8134-N-1-N-D-IL NASA ERTS E-1584-01593-7 02

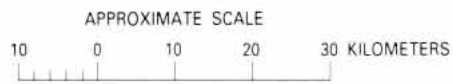
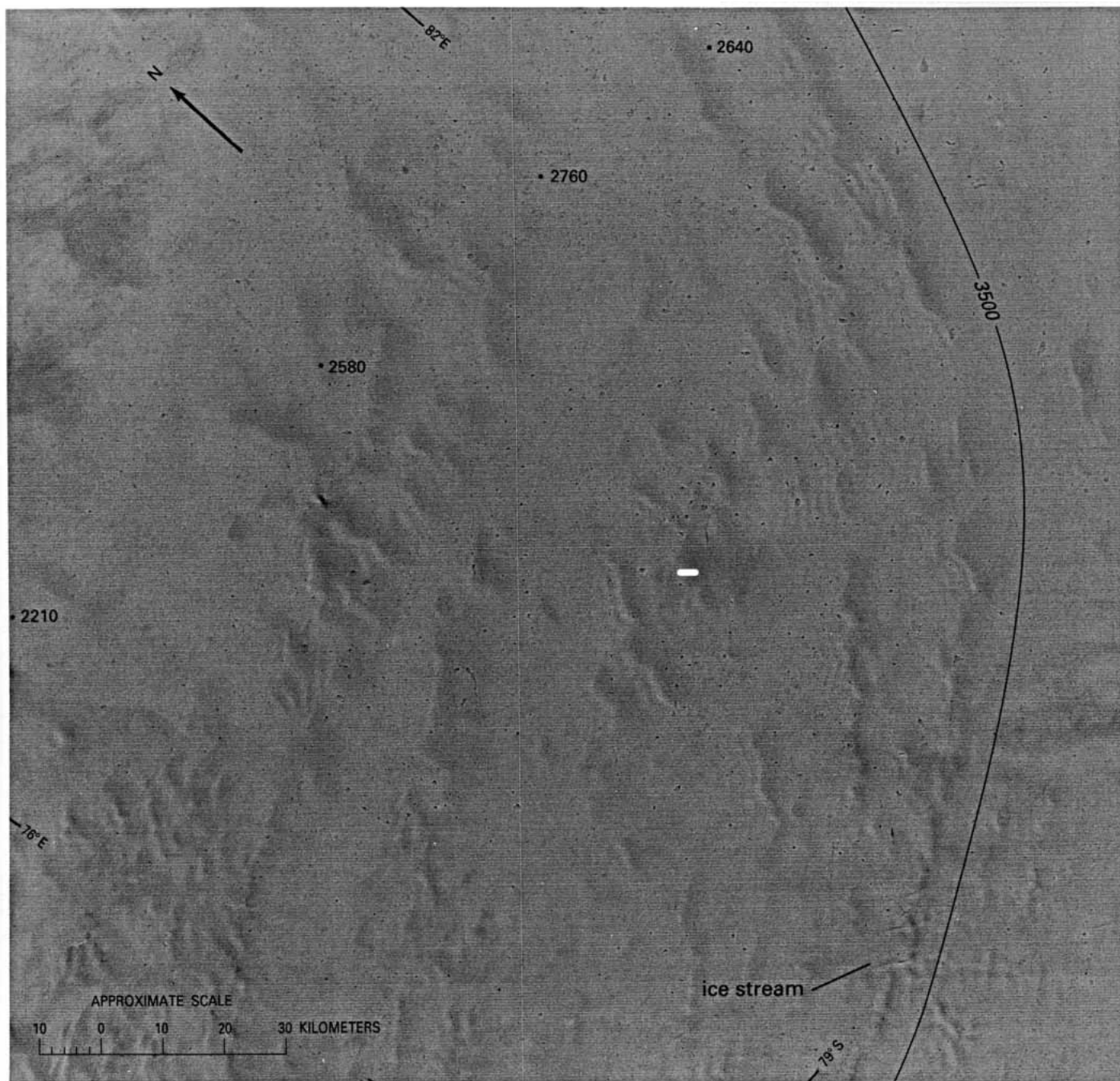


Figure 49 shows the plateau in an area where the surface is 3,500 m above sea level, and the ice sheet is flowing towards the head of Lambert Glacier, 500 km to the northwest. The linear features (emphasized by shadows) indicate a steplike surface topography falling away towards the west. The general direction of ice flow is from right to left, but locally it is most likely to be perpendicular to the trend of the surface steps. The subdued escarpment slopes that cause the shadows probably indicate the presence of subglacial ridges. The steepest surface slopes have been found to lie over the ridges themselves. The slope of the surface at any point is related not only to the thickness of the ice but also to changes in longitudinal stress resulting from flow of the ice over varying bottom slopes (Robin, 1967).

All of the features in this image, including the subregular snow dunes at the foot of many of the escarpments, can be identified in other images, so that we are convinced they are not ephemeral, like cloud

Figure 49. — Annotated Landsat 1 MSS image of the Gamburtsev Subglacial Mountains. Surface contour (in meters) from Antarctica 1:3,000,000 (Scott Polar Research Institute, unpublished); spot soundings (in meters) from airborne radio-echosounding (Scott Polar Research Institute, unpublished). NASA image (1482-00571, band 7; 17 November 1973; Path 111, Row 117) from the EROS Data Center, U. S. Geological Survey.



shadows for example. Two faint longitudinal features (bottom right) reveal the presence of a small ice stream, a rarity so far from the edge of the ice sheet.

Seismic soundings made in this area by the Soviet Antarctic Expedition of 1958–59 showed that the ice sheet hides an elevated and rugged subglacial mountain range, the Gamburtsev Subglacial Mountains. Ice thicknesses as low as 600 to 800 m have been reported. We can speculate that ice thicknesses much smaller than this may one day be found close to the steep slope (black shadow) in the left center of the picture.

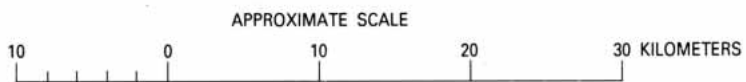
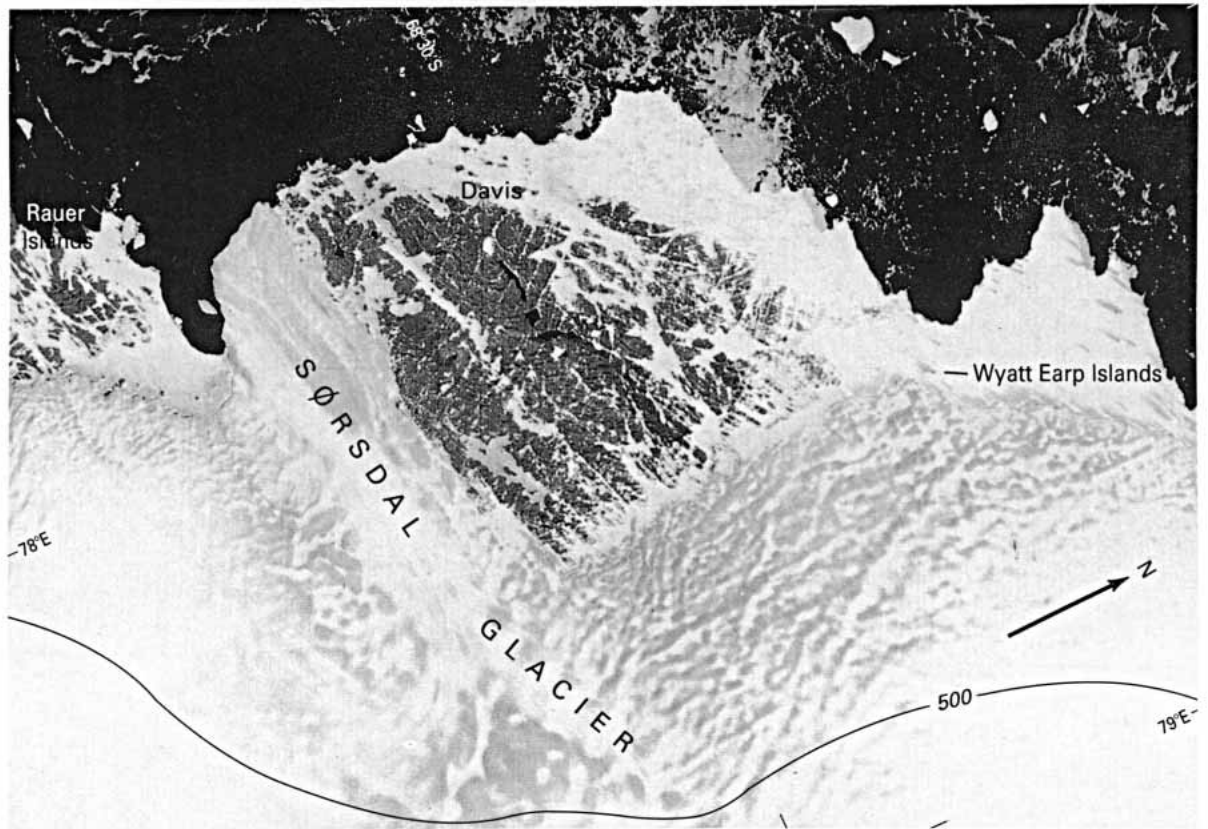
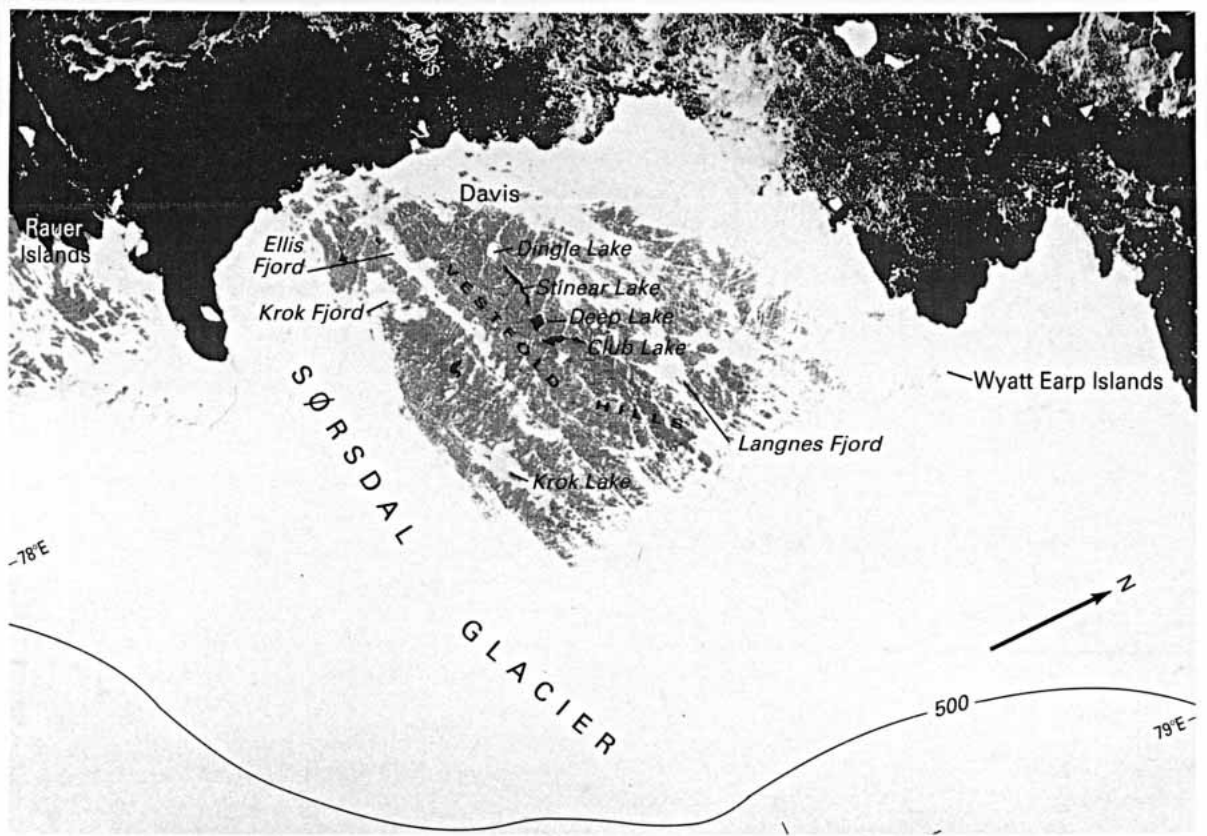
The presence of subglacial lakes has been suggested to explain anomalously strong bottom reflections found by airborne radio-echosounding surveys not far from here (Robin and others, 1970). More lakes have been reported elsewhere (Oswald, 1975), and Robin and others (1977) reported seeing surface expressions of subglacial lakes in the form of very shallow depressions. The long dimension of one apparently continuous lake was about 180 km.

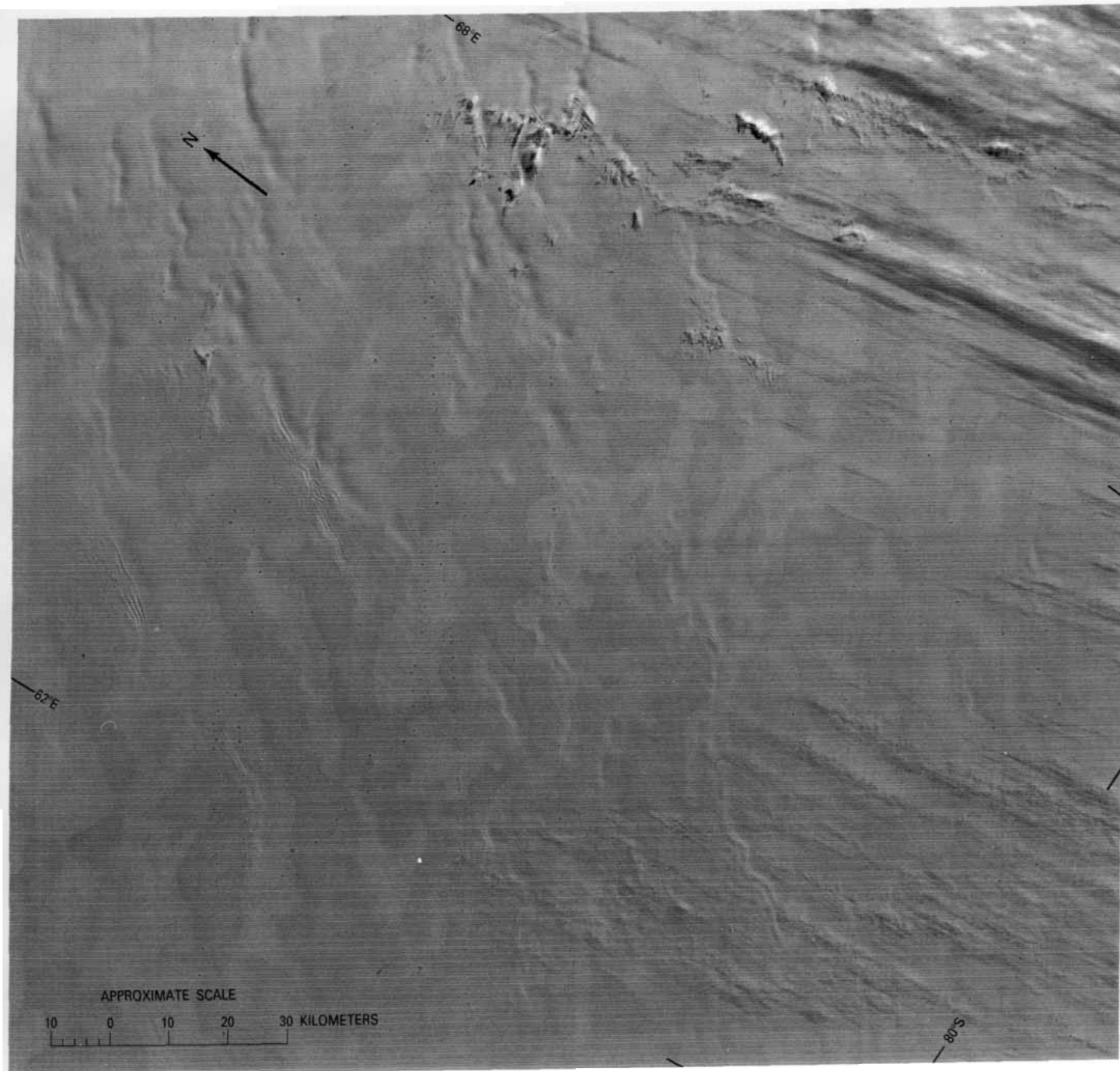
Figure 50 shows another so-called oasis like Bunger Hills (fig. 47). Sørsdal Glacier has captured the ice drainage from an area of the ice sheet to the east of Vestfold Hills and, in consequence, ablation near the edge of the ice sheet can now keep pace with the reduced rate of flow. The hills cover an area of about 400 km². Their physiography is one of low, hummocky hills up to 160 m high, with moraine- and lake-filled valleys, offshore islands, and fjord-like inlets (Tierney, 1975). Precambrian gneisses are exposed on most hilltops and ridges. There are numerous freshwater and some saline lakes (Law, 1959; Burton, 1981). Three large fjord systems break the ice-free area into three peninsulas. Krok Fjord and Langnes Fjord extend as far as the inland ice sheet. Ellis Fjord receives fresh water draining from a series of meltwater lakes, including Krok Lake, which is the largest lake in the Vestfold Hills, nearly 6 km long and 162 m deep. Dingle Lake, Stinear Lake, Deep Lake, and Club Lake are all below sea level, the surface of Deep Lake being at an elevation of -56m (Qingsong and others, 1983). It follows that evaporation must, on average, equal the inflow from all sources. Salinities as high as 275‰ have been measured in Club Lake which, like Deep Lake, never freezes at any time of the year. McLeod (1964) and Kerry and others (1977) concluded that the valley in which the lakes occur was once a long narrow arm of the sea, similar to the present-day sea fjords, and that the lakes were isolated by isostatic uplift and subsequently concentrated by evaporation.

The MSS band 5 image (fig. 50, top) shows that on 12 December 1972, most of the lakes and all of the fjords were still ice covered. However the highly saline Stinear, Deep, and Club Lakes were ice free. The ice-sheet ablation areas and the flow features of Sørsdal Glacier are evident only in the band 7 image (fig. 50, bottom), which also shows much of the detailed step structure of the ice sheet, but with this band it is hard to distinguish the ice-free lakes from the very dark tones of the bare rock.

Davis is an Australian research station that has been continuously occupied since 1969. Prior to that it was in use from 1954–65. A number of icebergs can be seen (in MSS band 7) frozen into a large area of fast ice northeast of Davis Station and north of the Wyatt Earp Islands. Each iceberg has a “tail” extending about 1 km to the southwest. The tail indicates that the prevailing wind is northeasterly, which is parallel with the general trend of the coast in the area. The tail consists of sea ice that has been swept bare by wind turbulence caused by the iceberg. In summer the tail area becomes weaker by preferential melting, owing to the lower albedo of the snow-free sea ice.

Figure 51 shows the plateau in an area where the surface is 3,500 m





◁ **Figure 50.**—Annotated Landsat 1 MSS image of Sørsdal Glacier and the Vestfold Hills. Ice-surface contour (in meters) modified from Australian Antarctic Territory 1 :1,000,000 sheet SR 43-44 (1971), Canberra, Division of National Mapping. Image center at 68°33'S., 78°23'E. NASA image (1 142-02510, band 5 (top), band 7 (bottom); 12 December 1972; Path 132, Row 108) from the EROS Data Center, U.S. Geological Survey.

△ **Figure 51.**—Landsat 1 MSS image of snow textures on the high plateau of East Antarctica. NASA image (1578-01295, band 7; 21 February 1974; Path 117, Row 118) from the EROS Data Center, U.S. Geological Survey.

above sea level, and the ice sheet is flowing towards the head of Lambert Glacier 500 km to the north. Despite the fact that we are looking at part of the greatest store of freshwater substance on Earth, in climatological terms the whole area is a desert. Whereas the average annual precipitation over most of the world's deserts is 50 to 100 mm, Bull (1971) estimated the surface net balance in this region of the 'Antarctic plateau' to be at the lower end of this range ($50 \text{ kg m}^{-2} \text{ a}^{-1}$). Wind sweeps new snow from the surface in some areas and deposits it in hollows so subdued that they may be imperceptible even to the surface traveler. As a result, large areas remain uncovered by new snow for periods of more than a year. Soviet pilots flying the direct route from Mirnyy Station on the coast (66°33'S., 93°01'E.) to Vostok Station in the interior (78°28'S., 106°48'E.) consistently follow the 10- to 12-month-old tracks left by tractor trains that once each year carry supplies to Vostok. But the tracks are intermittent, a few kilometers of

visible trail being followed by a few kilometers over which the tracks are buried. We can therefore hypothesize that the darker patches on this image consist of old snow in which recrystallization has lowered the surface albedo. The whiter patches must then be newer snow containing more interstitial air. An alternative hypothesis is that the different reflectivities of the surface, caused by subtle slope variations, produce a different albedo in response to solar illumination.

Gow and Rowland (1965) measured the rate of snow accumulation near Byrd Station (80°01'S., 119°31'W.) over an area that in Landsat imagery would appear to be as featureless as this one (fig. 51). They found a gently undulating surface over which accumulation was 50 percent higher in troughs than on ridges. Although this would tend to eliminate the undulations by filling in the hollows, the topography persisted. Black and Budd (1964) found that for undulations of 5 to 15 km in wave length, like those in this image, the net accumulation maxima occurred slightly downwind of the bottoms of the troughs, with minimum deposits occurring downwind of the tops of the crests. Rather than filling in the waves, this should perpetuate them and move the waves into the wind at a rate of about 25 m a⁻¹.

Note that there are cloud patches throughout the image (fig. 51) that may be confused with surface features; the main pattern trends at an angle of 110° to the frame of the image. The linear shadows in the top left quadrant indicate a step-like surface topography falling away towards the left; ice flow is therefore from right to left. The subdued escarpment slopes causing the shadows suggest the presence of subglacial ridges.

Figure 52 shows the eastern half of the confluent ice streams that feed Lambert Glacier. The image was taken 500 km downglacier from the area of figure 49 and probably depicts ice draining from the Gamburtsev Subglacial Mountains area. Allison (1979) described Lambert Glacier as the largest ice stream in the world, noting that for a distance of 400 km upglacier from its grounding line it is possible to follow surface flowlines on Landsat imagery. According to McIntyre (1985a) the glacier drains an area of 902,000 km², second only to that of Byrd Glacier. Allison (1979, p. 229) calculated the total mass influx into this part of the glacier system to be 11.5 Gt a⁻¹ (12.6 km³ a⁻¹), equivalent to about two-thirds of the mass flux down Byrd Glacier. The main ice stream entering Lambert Glacier can be identified from the flowlines as that coming from the lower right side of the image. A surface velocity of 231 m a⁻¹ was measured at the 1,950-m sounding. Note that even at this point, which is 600 km from the Amery Ice Shelf front, bedrock elevation was found to be 840 m below sea level. Although there are extensive ablation areas downglacier, surface annual net balance at the same point was measured at +80 kg m⁻² a⁻¹. The 800-m sounding is typical of those expected in an area with such visible surface topography; here ice movement is only 25 m a⁻¹. The 430-m sounding is evidently on a subglacial ridge between two ice streams; ice movement is only 7 m a⁻¹. In reporting the results of a network of airborne radio-echosounding profiles, Morgan and Budd (1975) plotted bedrock elevation contours in this area. Their 1,000-m bedrock contour follows the conspicuous wavy line that can be traced in the image from Mount Twigg to Mawson Escarpment. Their deepest sounding showed 2,500 m of ice in the middle of Lambert Glacier some distance below the 500-m contour, showing that the true peak to trough relief of Mawson Escarpment is about 3,000 m.

Meltwater in the form of lakes and rivers stands at and below the 500-m ice-surface contour, and there are scattered lakes in places upglacier. An isolated line of clouds nearly parallel with the pattern of flowlines confuses the picture downglacier from Cumpston Massif.

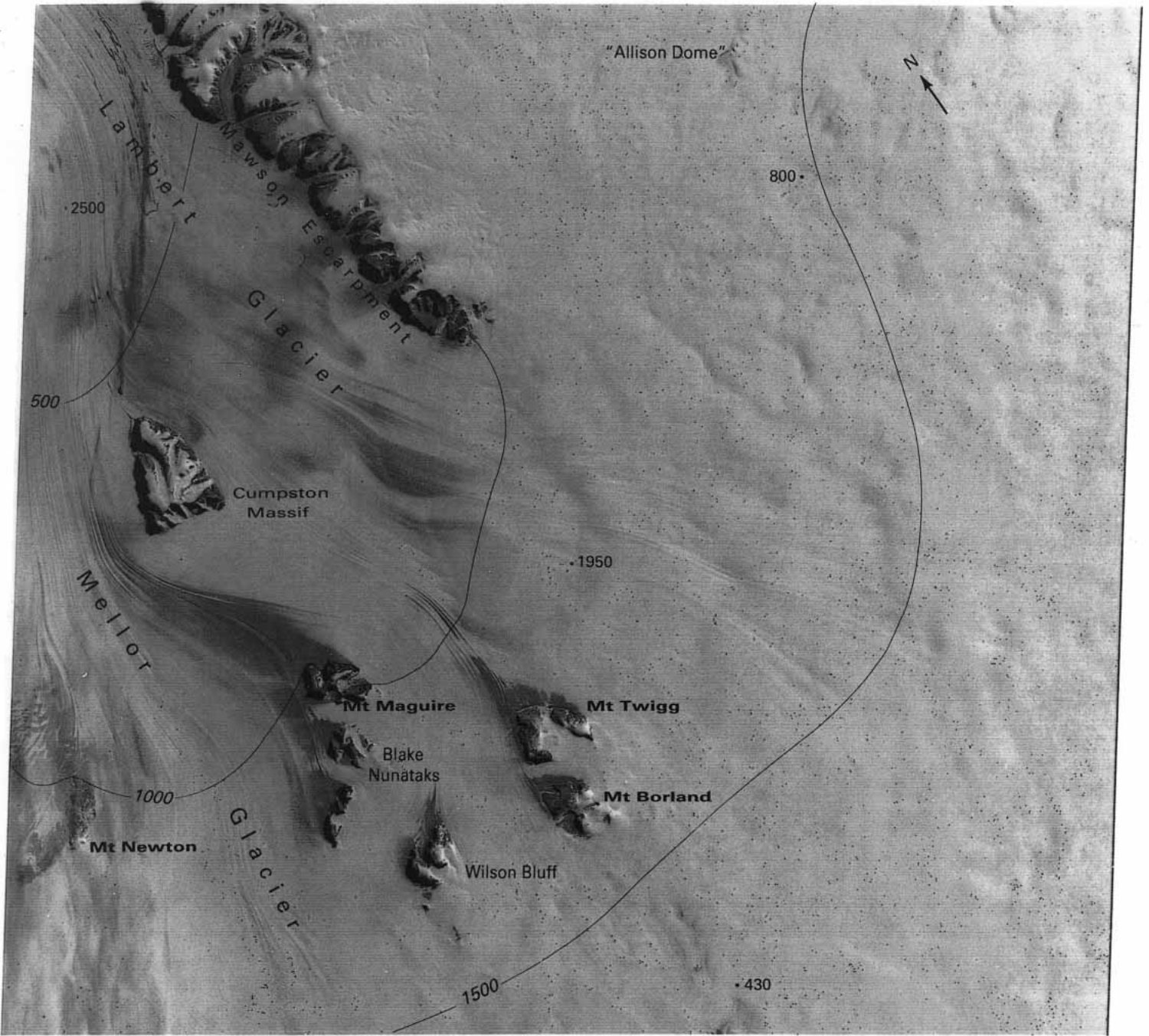
Figure 52.—Annotated Landsat 1 MSS image of the source of Lambert Glacier. Ice-surface contour (in meters) modified from Australian Antarctic Territory 1:1,000,000 sheet SS40-42 (1973), Canberra, Division of National Mapping. Spot soundings (in meters) from Morgan and Budd (1975) and from N.W. Young (personal commun.). NASA image (1196-02530, band 6; 4 February 1973; Path 131, Row 113) from the EROS Data Center, U.S. Geological Survey.

1E068-00

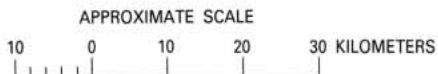
1E069-00

1E070-00

1E071-00



04FEB73 C S73-57/E068-17 N S74-05/E068-38 MSS ^{E068-001} 7 R SUN EL20 AZ076 213-2724-A-1-N-D-IL ^{E068-001} NASA ERTS E-1196-02530-7 01



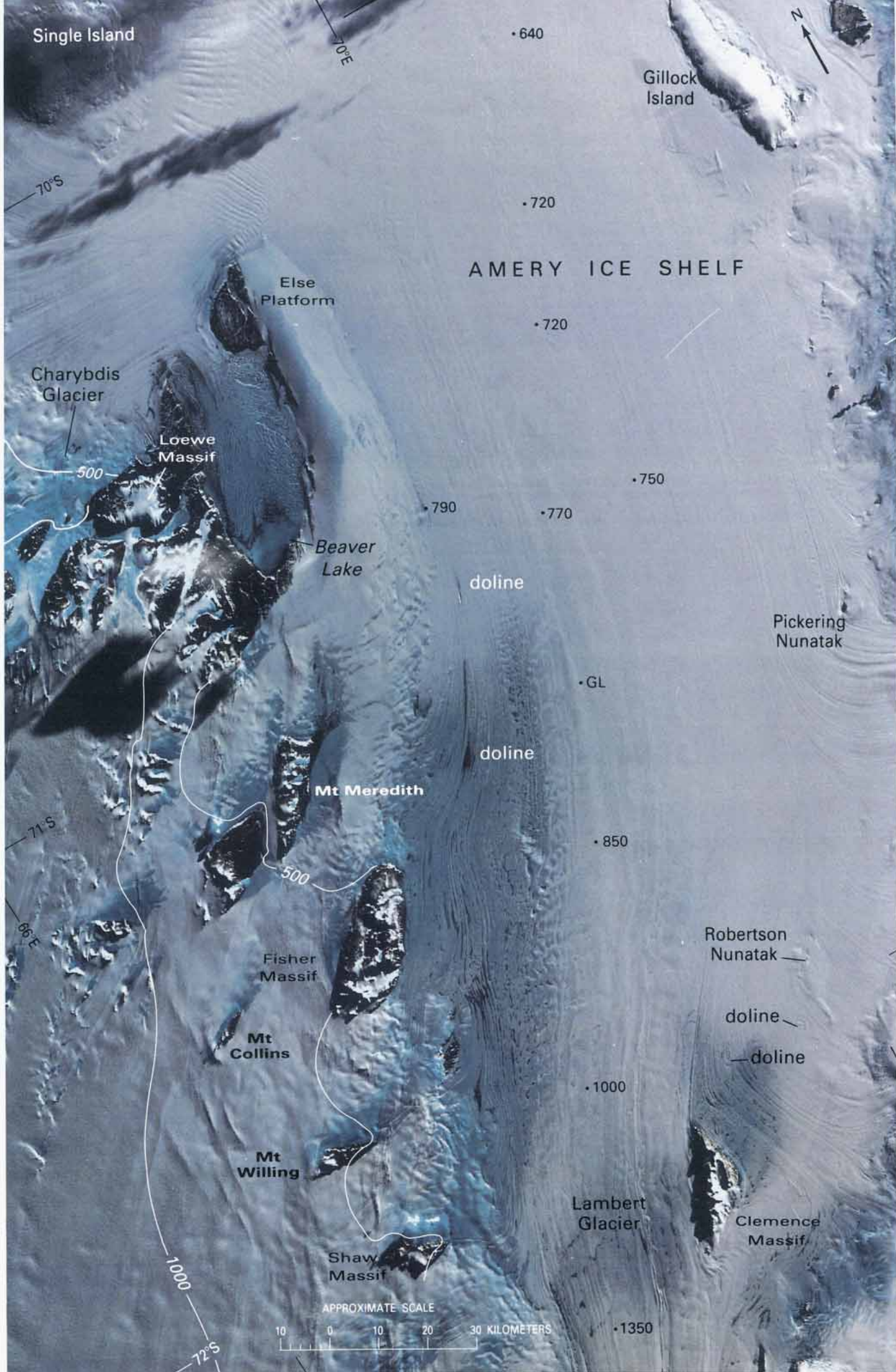


Figure 53. — Annotated Landsat 1 MSS digitally enhanced false-color composite image mosaic of Lambert Glacier and Amery Ice Shelf. Ice-surface contours (in meters) modified from Australian Antarctic Territory 1:1,000,000 sheet SR41–42 (1971), Canberra, Division of National Mapping. Spot soundings (in meters) from surface radio-echosounding (personal commun. from N.W. Young, 28 February 1980). The letters GL represent the grounding line as determined by Morgan and Budd (1975) on the basis of a break in slope detected by optical leveling (Budd and others, 1982). NASA images (1236–03150, bands 5, 6, and 7; 16 March 1973; Path 135, Row 110; 1236–03153, bands 5, 6, and 7; 16 March 1973; Path 135, Row 111) courtesy of N. W. Young, Antarctic Division, and CSIRO Division of Computing Research, Australia. See also figure 55.

Figure 53 is a Landsat image mosaic of the area located to the north of that in figure 52. It shows Lambert Glacier at its junction with Amery Ice Shelf. Allison (1979, p. 231) believes that the lower Lambert Glacier, having a very low surface slope but high velocity, is moving almost completely by basal sliding. Although the sliding area is bordered on one side by the left bank of the glacier with its extensive mountain massifs, the other side (to the right of a line joining the points marked GL–850–1000) appears to include large areas of freely floating ice shelf. If we could stretch the definition of ice rumpled to include zones of sliding that are only partially bordered by ice shelf, the extensive wavy area seen on this image would represent the largest known ice rumpled on any ice shelf. The letters GL mark the grounding line as determined by Morgan and Budd (1975, figure 4) on the basis of a break in slope detected by optical leveling (Budd and others, 1982). Significantly, it coincides exactly with the visible boundary of the markedly rumpled area to the left of it. The very small average thickness gradient of 1.7 m km^{-1} over the 215 km interval between the 1,000-m and 640-m soundings is unusually low, even for a floating ice shelf. Evidently it is related to the very small angular divergence of the flowlines allowed by the essentially parallel-sided trench. A velocity of 347 m a^{-1} was measured at the 770-m sounding and 462 m a^{-1} at the 640-m sounding (personal commun. from W.F. Budd). So many tributary ice streams have joined the trunk glacier by the time it reaches the section opposite Beaver Lake that Allison (1979, p. 229) calculates a possible mass flux of 30 Gt a^{-1} ($33 \text{ km}^3 \text{ a}^{-1}$), equivalent to nearly twice the mass flux down Byrd Glacier. However, actual measurements through the 770-m spot sounding gave a total mass flux of only 11 Gt a^{-1} ($12 \text{ km}^3 \text{ a}^{-1}$). The discrepancy argues strongly for a contemporary build-up of the ice sheet inland, or alternatively for intermittent surging (Wellman, 1982).

Some 35 km east of Mount Meredith is a meltwater lake 5 km long and up to 1.3 km wide. Mellor and McKinnon (1960) reported an “oval-shaped depression, 3 km long by 1.3 km wide” in the same position, and Mellor (1960) proposed the term “ice doline” to describe this and similar large depressions in ice shelves (see figs. 10, 53, 63, and 79). Although in the 1973 image (fig. 53), the feature appears as a lake whose surface level was close to that of the surrounding ice shelf, the earlier report stated that the bottom of the depression was 80 m below the surrounding ice. If the ice is 800 m thick and is floating in equilibrium in sea water, the bottom of the doline could consist of thin ice afloat on water at sea level. Thus, we may be dealing with two different stages in the life cycle of a melt lake that intermittently drains through fractures to the sea beneath. Floating ice at this point would imply a southward embayment in the grounding line to the left of the central belt of ice rumpled. Two unfilled or frozen-over features similar to ice dolines can be seen near Robertson Nunatak.

An arm of the ice shelf fed by Charybdis Glacier turns sharp right (southeast) to flow between Else Platform and Loewe Massif into a mountain-rimmed valley. The glacier tongue terminates in Beaver Lake, an ice-covered freshwater sea lake into which icebergs calve (Mellor and McKinnon, 1960). While a freshwater sea lake may sound like a contradiction in terms, such features have been reported elsewhere (Simonov, 1964; Korotkevich, 1965; Solopov, 1969; Heywood and Light, 1975; Keys, 1978). Beaver Lake is a 10-by-10 km stably stratified tidal lake in which the halocline is depressed by the addition of meltwater to the surface. The halocline in such lakes most probably lies at a depth equivalent to that of the draft of the ice tongue blocking

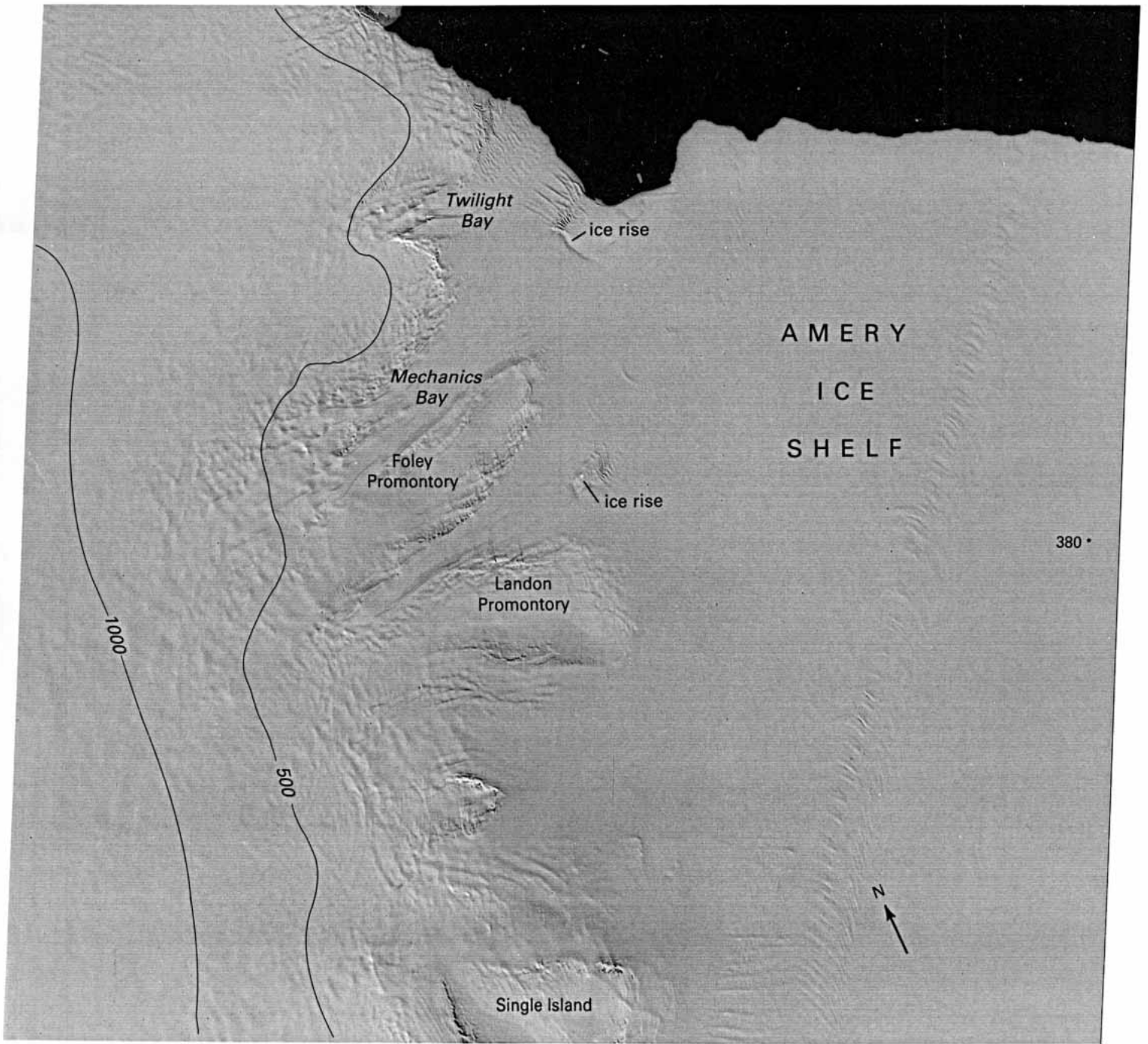
the outlet to the sea; hence it may be under the ice tongue and thus inaccessible to investigation by sounding through the lake ice.

The area shown in figure 54 overlaps the area of figure 53 at Single Island and shows the final stage in the mighty Lambert Glacier–Amery Ice Shelf system. A conspicuous line of disturbed ice towards the right of the picture can be traced back to Else Platform in figure 53. It represents the left bank of the main ice stream derived from Lambert Glacier and bears witness to intense shearing between this and the slower-moving streams feeding into the ice shelf from the west. Another line of disturbed ice on the east side of Amery Ice Shelf originates at the northern tip of Gillock Island and marks the eastern boundary of the main ice stream as can be seen on Landsat image 1236–03150, band 7; 16 March 1973; Path 135, Row 110 (not included here). A wealth of morphologic features along the western margin of the ice shelf indicates the position of the grounding line more accurately than can be achieved on conventional line maps, although the ease with which the line can be followed is inversely proportional to the ice thickness. While the grounding line in Mechanics Bay and on the ice stream between Foley and Landon Promontories is clearly indicated by a single break in slope, it is not possible on morphological grounds to be certain of its position on the two broad ice streams between Landon Promontory and Single Island. Two ice rises can be seen, one off Foley Promontory and the other off Twilight Bay.

A velocity of 787 m a^{-1} was measured at the 380-m spot sounding (Budd and others, 1982). The product of these figures gives a seaward flow of $0.30 \text{ km}^3 \text{ km}^{-1} \text{ a}^{-1}$. This is identical with the product of the measured velocity and the ice thickness 84 km upglacier between Single and Gillock Islands (fig. 53). In another image (1506–03112; 11 December 1973; Path 135, Row 109) (not included here) we note that the width of the Lambert ‘ice stream’ between its marginal shear zones does not change over the distance between the two measurement sites. The implication is that the sum of the top and bottom surface mass fluxes over the interval must be close to zero. The surface net balance is known (Budd and others, 1982); the bottom mass flux can therefore be deduced. This is a good example of the usefulness of Landsat imagery for critical data on the width of the ice stream. A Landsat image mosaic can also be prepared to serve as a map base for analysis of regional glaciological features, too large to be seen on a single image, and for the plotting of other types of geological (Wolmarans and Kry-nauw, 1981; Tingey and Convine, 1982) and geophysical (Brooks and others, 1983) data. Figure 55 shows a Landsat MSS image mosaic of the Amery Ice Shelf and the lower part of the Lambert Glacier, on which 1- and 5-m contours derived from Seasat radar altimeter data have been plotted.

Sooner or later, all this ice must reach the sea. Centerline velocities exceed $1,200 \text{ m a}^{-1}$ near the ice front, and Ledenev and Yevdokimov (1965, p. 16) report a single iceberg calving event that yielded $11,000 \text{ km}^2$ from Amery Ice Shelf. This probably occurred in late 1963 (Swith-inbank, 1969a). Budd (1966, p. 356) has documented the changing position of Amery Ice Shelf front over the period 1936–65.

Figure 54.—Annotated Landsat 1 MSS image of the left bank of Amery Ice Shelf. Ice-surface contours (in meters) modified from Australian Antarctic Territory 1:1,000,000 sheet SR41–42(1971), Canberra, Division of National Mapping. Spot soundings (in meters) from surface radio-echosounding (personal commun. from N.W. Young, 28 February 1980). NASA image (1580–03205, band 7; 23 February 1974; Path 137, Row 109) from the EROS Data Center, U.S. Geological Survey. See also figure 55.



IE067-00 E068-001 E069-001 S070-001 IE070-00
 23FEB74 C S69-04/E069-35 N S69-12/E069-50 MSS 7 R SUN EL18 AZ068 204-0079-G-1-N-D-IL NASA ERTS E-1580-03205-7 02

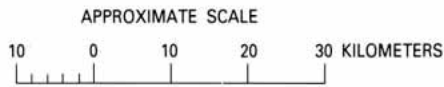


Figure 55.—Uncontrolled Landsat MSS image mosaic of the Amery Ice Shelf and the terminus of Lambert Glacier, East Antarctica, with the 1- and 5-m contours determined from numerous Seasat radar altimeter traverses across the area. Contours courtesy of Geo-Science Research Corporation (Brooks and others, 1983). Landsat images can be used as planimetric base maps, where adequate geodetic control is present, for the plotting of geological (Wolmarans and Krynauw, 1981; Tingey and Convine, 1982) and geophysical (Drewry, 1983) data. Image mosaic compiled by J.G. Ferrigno, U.S. Geological Survey. NASA images from the EROS Data Center, U.S. Geological Survey. See also figures 53 and 54.

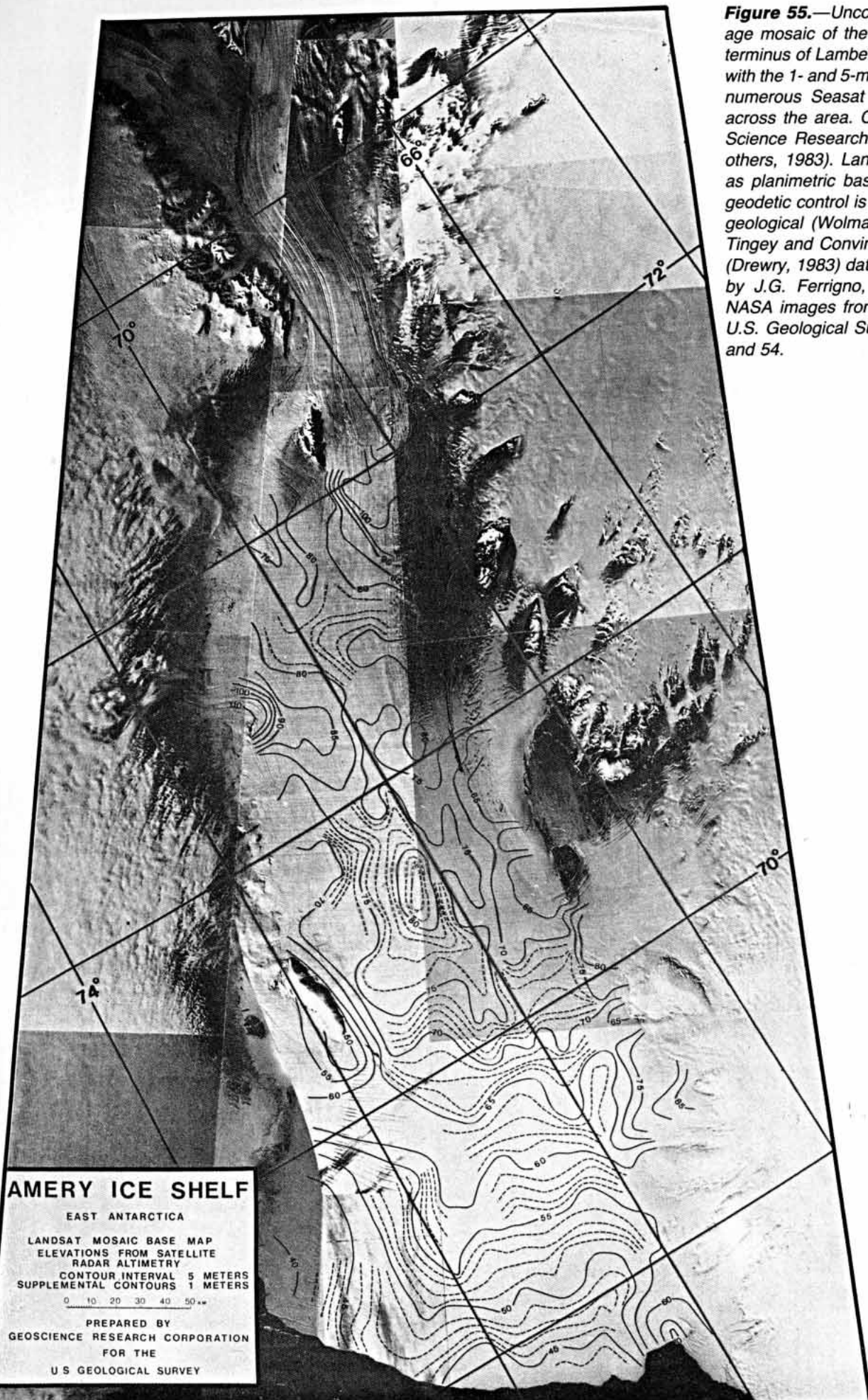
AMERY ICE SHELF

EAST ANTARCTICA

LANDSAT MOSAIC BASE MAP
 ELEVATIONS FROM SATELLITE
 RADAR ALTIMETRY
 CONTOUR INTERVAL 5 METERS
 SUPPLEMENTAL CONTOURS 1 METERS

0 10 20 30 40 50**

PREPARED BY
 GEOSCIENCE RESEARCH CORPORATION
 FOR THE
 U.S. GEOLOGICAL SURVEY



Mawson Coast and Enderby

Land

Figure 56 shows a typical ice-wall coastline crossing an island archipelago. At this latitude (68°S.) on the Mawson Coast, a narrow band of rock is commonly visible at low tide at the foot of the ice cliff, except in places where an ice stream discharges into the sea. Further advance of the ice wall is prevented by a comparatively high rate of marine melting. Under these conditions, an ice-wall coastline is likely to remain in a stable position that is chiefly controlled by sea level (Hollin, 1962).

It was necessary to use both Landsat MSS bands 5 and 7 in order to distinguish between mountain ranges, nunataks, and the extensive bare-ice ablation areas. Band 5 effectively isolates the exposed rock areas; the only ice feature that it shows is a coastal zone of wet fast ice. Band 7, on the other hand, reveals bare-ice areas throughout the scene. The tendency for ablation areas to form downwind of obstacles that serve to break up the ice flow reveals a southeasterly prevailing surface-wind pattern. Where winds originating inland encounter winds moving over the sea ice, they often intersect at a small angle, because those on the ice sheet have an added gravity (downslope) component.

A number of surface meltwater lakes can be seen in hollows north of Casey and David Ranges. "Henderson Lake," between the northward-trending arms of Mount Henderson, contains $80 \times 10^6 \text{ m}^3$ of water (Pickard and Adamson, 1983). Seismic soundings in the 400- to 500-m range close to the 500-m ice-surface contour suggest that, if the ice sheet disappeared, the area would appear as a low-lying island archipelago of the strandflat type (Reusch, 1894; Nansen, 1922; Høltedahl, 1929).

Mellor (1959a, 1967) studied the mass economy of the area and found from surface ablation measurements that the annual loss of ice varied from about $500 \text{ kg m}^{-2} \text{ a}^{-1}$ at the coast to $100 \text{ kg m}^{-2} \text{ a}^{-1}$ 20 km inland. Summer melting accounted for most of the ablation, but there was loss by sublimation throughout the year. Surface velocities between Casey Range and Mount Henderson were 20 to 40 m a^{-1} and at the ice wall 10 to 20 m a^{-1} . Utstikker Glacier and "Forbes Glacier" each feed a double-pronged glacier tongue. The east tongue of Utstikker Glacier was found to move at a rate of 321 m a^{-1} . Morgan and others (1982) calculated a mass flux of 0.49 Gt a^{-1} ($0.54 \text{ km}^3 \text{ a}^{-1}$) for the whole of Utstikker Glacier. Mellor (1959b) found no significant changes in the position of glacier tongues between 1936 and 1958. Other characteristics of the ice sheet of Mac. Robertson Land have been described by McLeod (1967).

Mawson is one of three scientific stations maintained by the Australian government in Antarctica; it was established in 1954 and is permanently manned.

The ragged coastline in figure 56 suggests a strand (or shallow water) ice wall; the smoother outline in parts of figure 57 suggests a neritic (or submerged) ice wall. The distinction was proposed by Roberts and others (1955). Neritic ice walls are known to rest on rock that is in places hundreds of meters below sea level (Robin, 1979, p. 266; Klepšvik and Fossum, 1980). Inland, the area is one of small mountain groups separated by glacier-filled valleys draining the ice sheet. Some of the outlet glaciers were unknown before Landsat and even today have no names. The smoothly curving glacier feeding into Adams Fjord can readily be traced back into the heart of Enderby Land

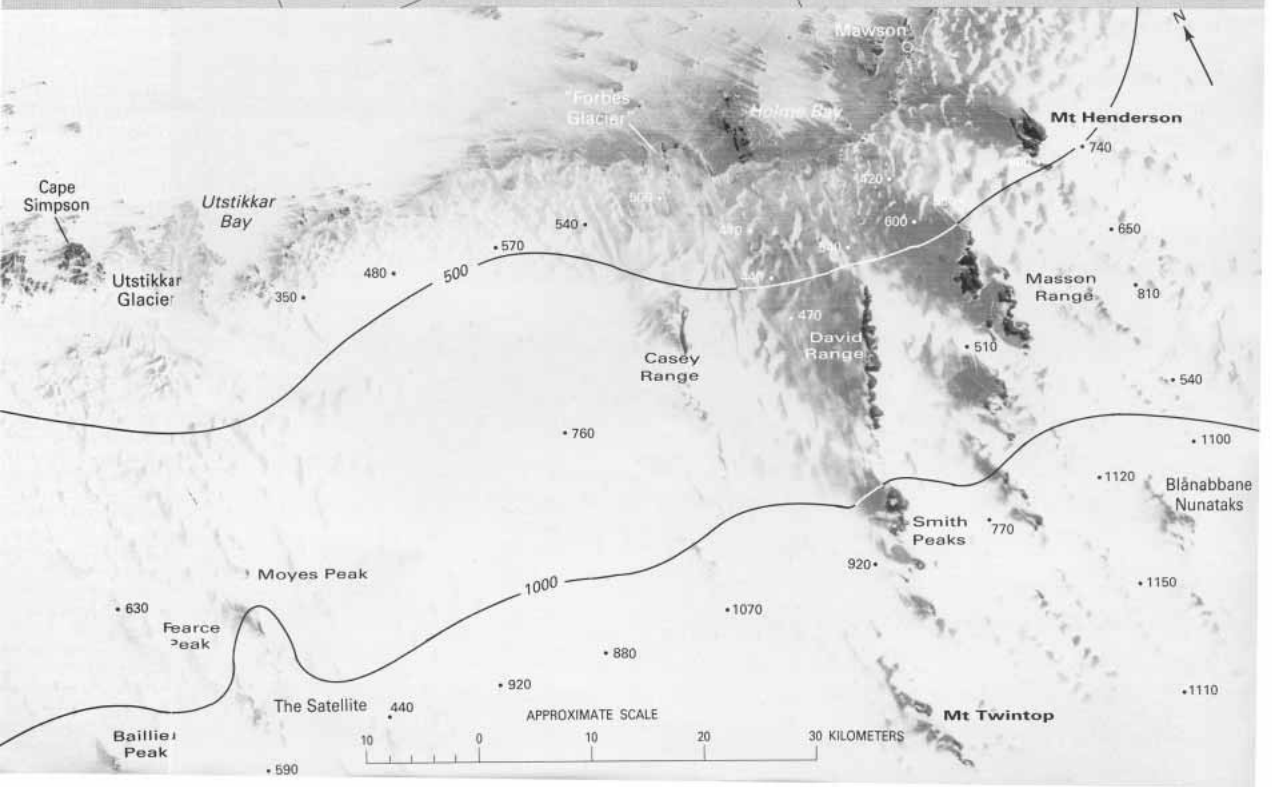
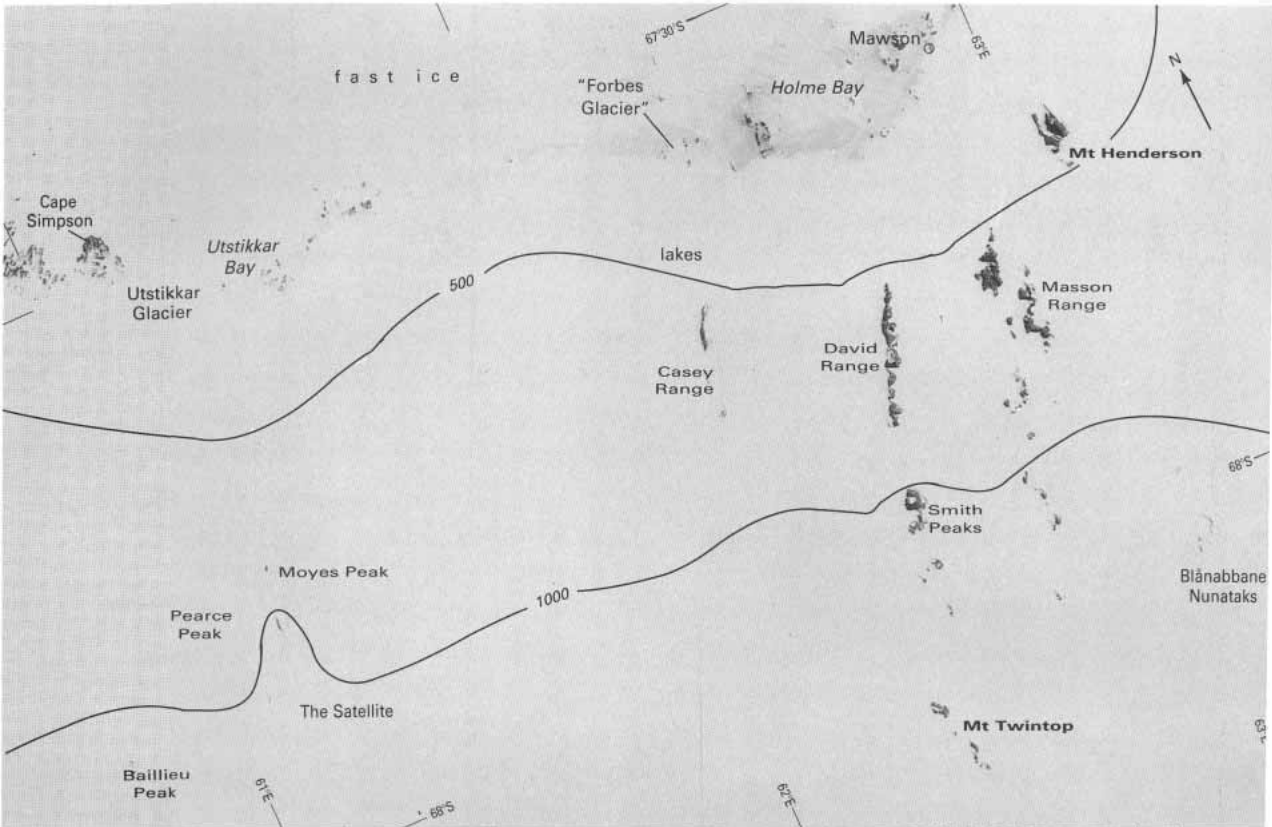


Figure 56.—Annotated Landsat 1 MSS image of Mac. Robertson Land at Mawson Station. Ice-surface contours (in meters) modified from *International Map of the World 1:1,000,000, Mawson, sheet SQ41-42 (1978), Canberra, Division of National Mapping*. Spot soundings (in meters) from airborne radio-echosounding by Australian National Antarctic Research Expeditions (unpublished) and seismic measurements reported in *Australian Antarctic Territory 1:1,000,000, Framnes Mountains, Canberra, Division of National Mapping, 1963*. Image center at 67°47'S., 62°05'E. NASA image (1137-04053, band 5 (top) and band 7 (bottom)); 7 December 1972; Path 144, Row 108) from the EROS Data Center, U.S. Geological Survey.

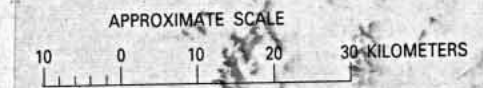
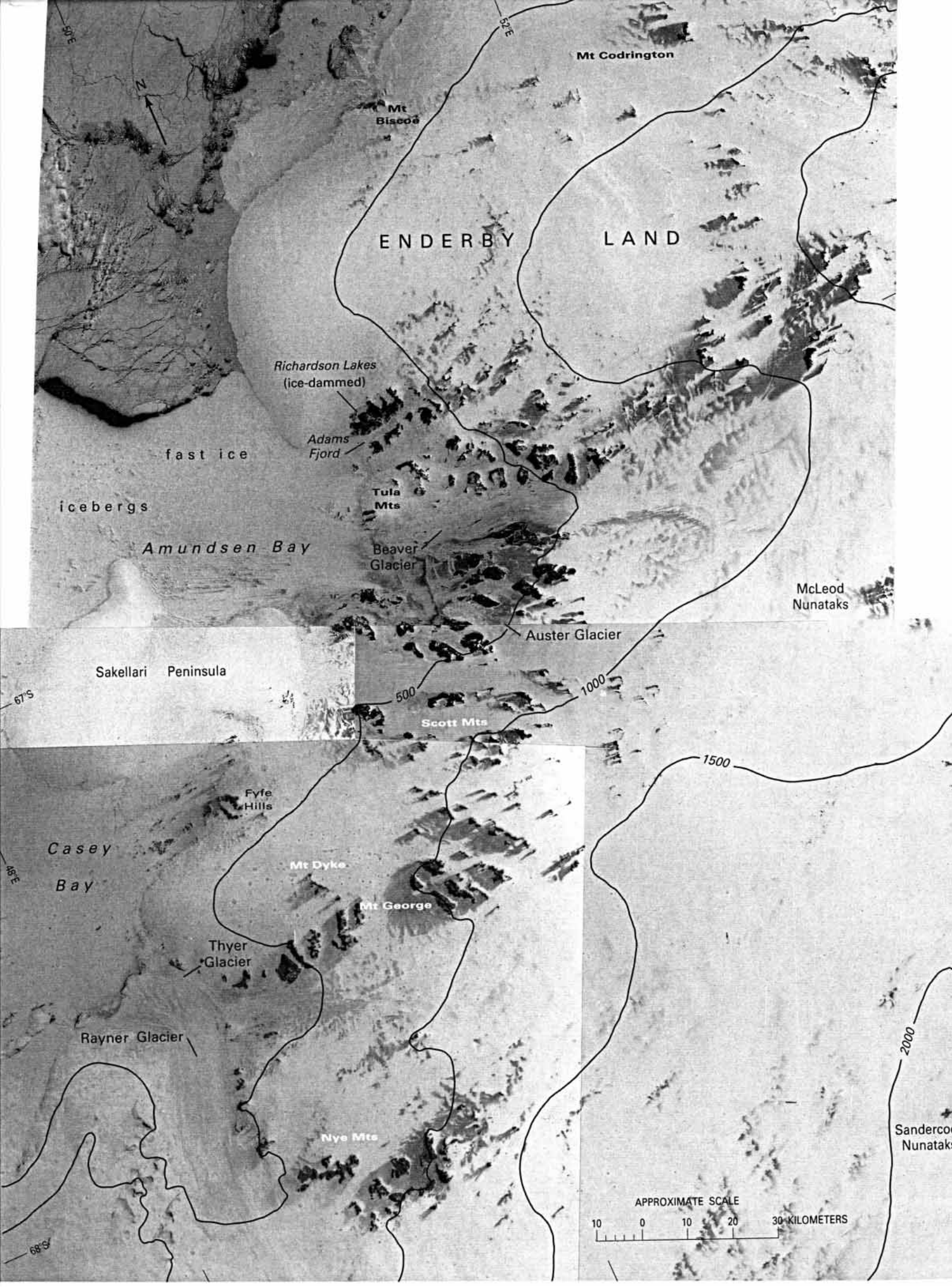
for a distance of 50 km. Between this and the Tula Mountains a 5-km-wide glacier follows a clear and roughly parallel path through the mountains. The rifts and ponds on Beaver Glacier suggest that at least the last 10 km are afloat. The largest glacier in the region is Rayner Glacier, with its minor tributary from the east, Thyer Glacier. Rayner can be traced far inland in other imagery and is 11 km wide at its confluence with Thyer Glacier.

We have no spot soundings for the area, but Korotkevich and others (1977) have prepared maps of the ice surface and bedrock relief with a contour interval of 200 m. The subglacial topography is based on Soviet airborne radio-echosounding surveys. Their maps show a deep depression extending up Beaver Glacier for a distance of 40 km from the terminus. The grounding line may therefore coincide (as it does on Byrd Glacier in figure 23) with the boundary between white snow and gray ice. The subglacial depression continues eastward, bedrock remaining below sea level to the Wilma Glacier (approximately 150 km to the east, beyond the area covered by the image), which flows to the east into Edward VIII Bay. If the ice sheet were removed, the peninsula of Enderby Land would become an island. Later radio-echosoundings reported by Allison and others (1982) support the generalized results of Korotkevich and others (1977) but differ in detail where they have new data. Rayner Glacier occupies a deep depression extending more than 200 km inland. According to McIntyre (in press) the glacier drains an area of 118,000 km². The curving snow-filled rifts near its snout suggest that at least the last 20 km are afloat. Morgan and others (1982) measured a velocity of 861 m a⁻¹ a short distance downstream from the 500-m contour. The ice thickness decreased from a maximum of 2,300 m on the centerline, 30 km upglacier from this point, to 500 m at the floating ice front. Mass flux down Rayner Glacier is 10.4 Gt a⁻¹ (11.4 km³ a⁻¹). Beaver Glacier was found to move 353 m a⁻¹; ice thicknesses decreased from 1,340 m at the observation point to 300 m at the floating ice front. Mass flux down Beaver Glacier is 1.66 Gt a⁻¹ (1.83 km³ a⁻¹).

Broad rivers of meltwater can be seen flowing over the ice surface from a number of massifs in the Scott and Nye Mountains. Other imagery shows that there are major differences from month to month and from year to year, not only in the various manifestations of meltwater but also in the extent of ablation areas. Richardson Lakes are a group of ice-dammed freshwater lakes, the largest of which measures 1 by 3 km. Descriptions of travel in the area are given by Crohn (1959) and McLeod (1967).

The area shown in figure 58 slightly overlaps that of figure 57 in Casey Bay on the west and shows another ice wall with coastal nunataks and offshore islands. Recorded early in the austral summer, the image shows that a 60-km stretch of iceberg-studded fast ice still separates the coast from the open sea. There are many small ablation areas near the edge of the ice sheet, but most of them are confined to convex patches that are particularly exposed to downslope winds. Note how close to the coast is the 500-m contour; the ice sheet rises steeply from the sea. A number of calving glaciers can be seen and, on the right, the small Hannan Ice Shelf owes its existence to a coalescence of outlet glaciers in a sheltered environment.

Hays Glacier is the largest shown on this image (fig. 58). According to Meier (1977, 1983) it has a relatively small catchment area of 10,000 km². However, the area is one of high snow accumulation and in consequence, the rate of movement is high. A speed of 1,400 m a⁻¹, measured at the grounding line, which is some way up the valley, corresponds to an annual discharge from the glacier of 3 km³ a⁻¹. The bedrock contour



map of Korotkevich and others (1977) shows that the valley occupied by Hays Glacier extends inland at elevations of 200 to 400 m below sea level for more than 100 km, where it joins the valley occupied by Rayner Glacier (see fig. 57). There is a similar connection well below sea level between Assender and Molle Glaciers that makes Tange Promontory in effect an island. Another depression at elevations of 200 to 400 m below sea level connects the valley of the "Campbell Glacier" with that of Hays Glacier; thus the land between them from latitude 68°S. to the coast is also an island.

Molodezhnaya is the principal Soviet research station in the Antarctic. Built in 1962 on a series of gently undulating nunataks on the coast, it has been permanently occupied since 1963. Fresh water for station use is pumped throughout the year from meltwater lakes, the largest of which can be identified on this image. Multi-engine, long-range transport aircraft have landed on wheels on patches of bare ice between the station and Hays Glacier.

Figure 59 shows Shirase Glacier, the largest ice stream west of Rayner Glacier. According to McIntyre (in press) it drains an area of 165,000 km²; mapped ice-surface contours show a distinct drainage basin extending 500 km inland from the coast. There is little doubt that the whole of the glacier tongue shown in this image is afloat; other Landsat images (for example, 1528–05170, band 7; 2 January 1974; Path 157, Row 109; 1528–05173, band 7; 2 January 1974; Path 157, Row 110) show a probable grounding line 65 km upglacier from the 2 January 1974 position of the terminus. Shirase Glacier sweeps down from the inland plateau in a 9-km-wide valley, forcing its way between Padda Island and a tiny island to the east of it that has split some elongate icebergs from the main stream. Nakawo and others (1978) report a glacier-front velocity of 2,500 m a⁻¹, the fastest surveyed rate of flow of any ice stream in Antarctica. Fujii (1981) reports some points moving at 2,900 m a⁻¹. Comparing figure 59 with the map of Hansen (1946) based on 1936–37 aerial photography, the glacier front would appear to have advanced 86 km in 37 years. Averaged over the interval, this would correspond with a minimum rate of movement of 2,324 m a⁻¹. However, an examination of the 1936–37 mapping photographs in the archives of Norsk Polarinstittutt suggests that Hansen's map is incorrect and that Shirase Glacier, then as now, extended well into Lützw-Holm Bay. The ice front itself is not visible in the photographs. Nakawo and others (1978) calculate that the glacier yields 7.4 Gt a⁻¹ (8.1 km³ a⁻¹), but Fujii (1981), using greater ice thickness values, arrives at a figure of 14 Gt a⁻¹ (15.4 km³ a⁻¹). The uncertainty of early maps and the uncertainty of ice thickness values together provide dramatic evidence of the pitfalls inherent in quantitative estimates based on inadequate data.

The rough agreement between ice-surface contours and the spot soundings suggests that the bed of the ice sheet remains close to sea level for some distance inland. Korotkevich and others (1977) show Shirase Glacier occupying a deep subglacial trench that remains below sea level for a distance of 200 km inland from the coast. Of equal interest, submarine contours trace a canyon extending seaward from the mouth of the glacier as far as the 1,000-m isobath. Wada and Mae (1981) report the results of airborne radio-echosounding inland.

Kusunoki and Ono (1964) have described the region. Extensive ablation areas close to the coast give way to large patches of superimposed ice inland. The different ice surface zones may correspond with the two contrasting gray shades seen on the bare-ice slopes below the snow in the top right corner of the image (fig. 59). Rivers emanate from melt lakes on the ice sheet, and there are large land-locked lakes on many

Figure 57.—Annotated Landsat 1 and 2 MSS image mosaic of Enderby Land. Ice-surface contours (in meters) modified from Australian Antarctic Territory 1:1,000,000, sheets SQ39–40 (1969) and SR39–40 (1973), Canberra, Division of National Mapping. Image center at 67°15'S., 50°45'E. NASA images (2339–04365, band 7: 27 December 1975; Path 152, Row 107: 1540–04415, band 7: 14 January 1974; Path 151, Row 108; 1525–04590, band 7; 30 December 1973; Path 154, Row 107; 1506–04541, band 7: 11 December 1973; Path 153, Row 108) from the EROS Data Center, U.S. Geological Survey.

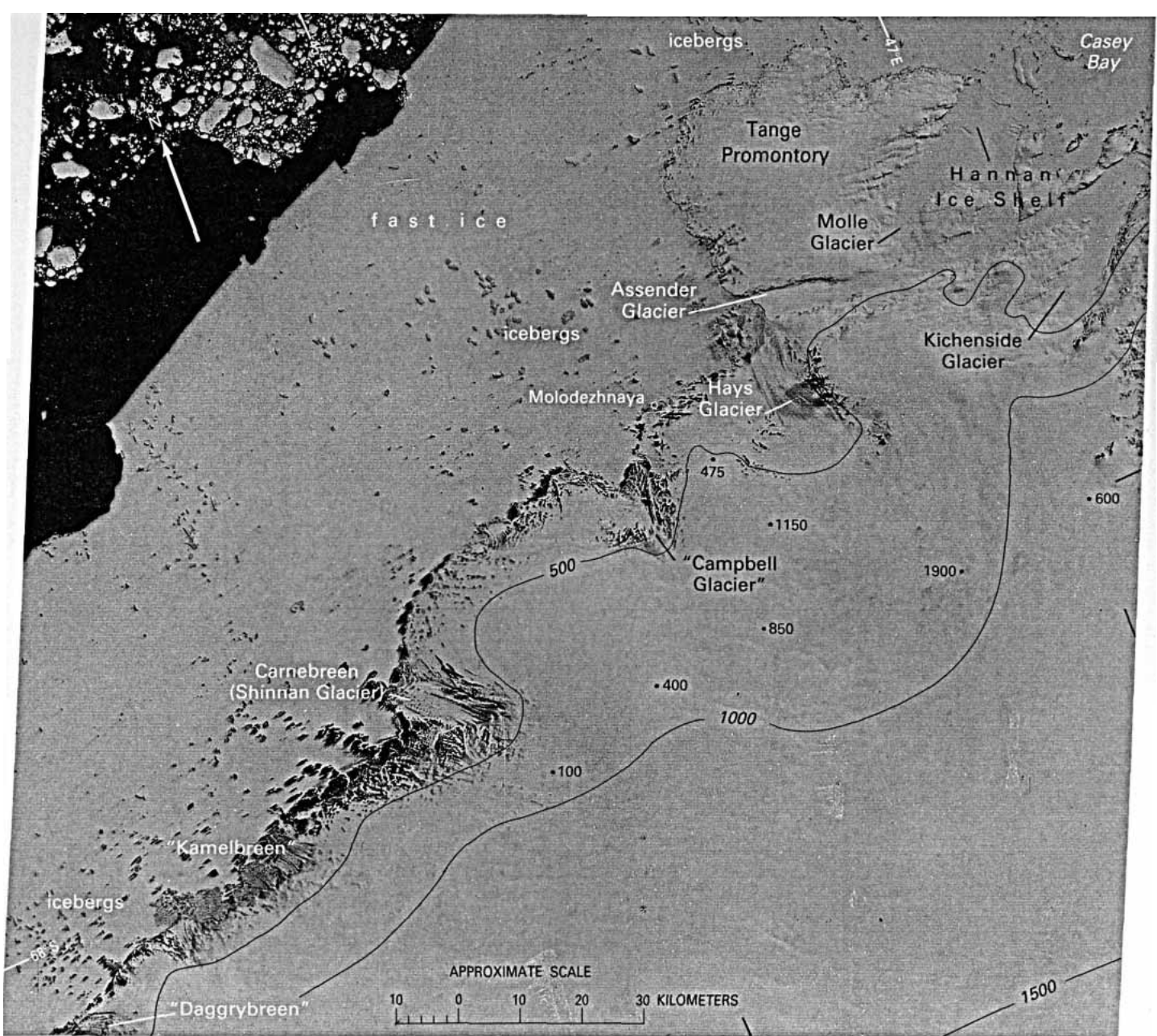


Figure 58.—Annotated Landsat 1 MSS image of Alasheyev Bight at Molodezhnaya Station. Ice contours (in meters) modified from *Dronning Maud land—Australian Antarctic Territory 1:1,000,000, sheets SR37–38 and SQ37–38, Canberra, Division of National Mapping, 1974*. Spot soundings (in meters) from surface radio-echosounding by Trepov and others (1979). NASA image (1490–05055, band 7; 25 November 1973; Path 155, Row 108) from the EROS Data Center, U.S. Geological Survey.

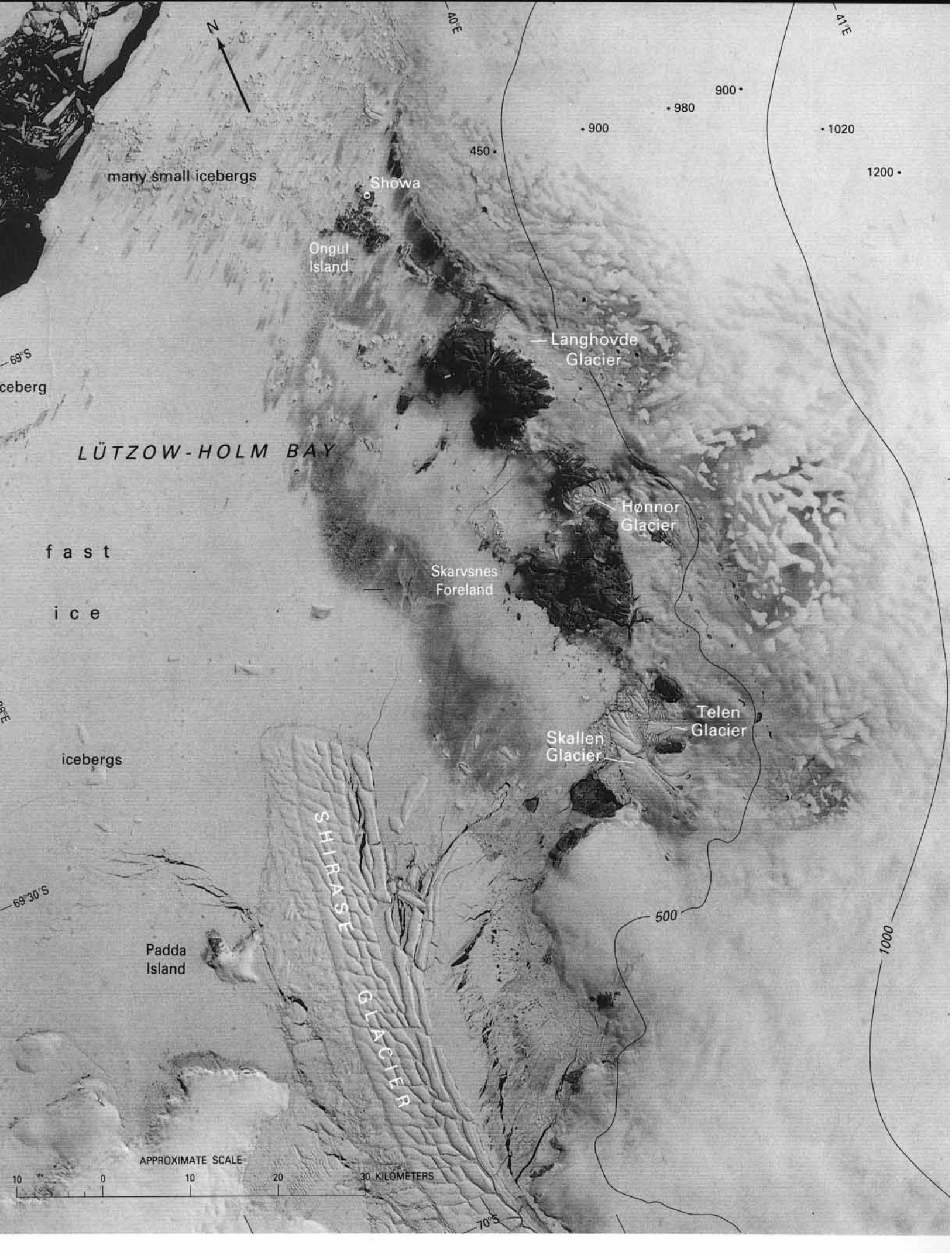
Figure 59.—Annotated Landsat 1 MSS image of Lützow-Holm Bay at Shōwa Station. Ice-surface contours (in meters) modified from *Lützow-Holm Bay 1:250,000, Tokyo, Geographical Survey Institute, 1981, and Naruse (1979)*. Spot soundings (in meters) from surface radio-echosounding (personal commun. from Kou Kusunoki). Image center at 69°25'S., 39°25'E. NASA image (1547–05221, band 7; 21 January 1974; Path 157, Row 109) from the EROS Data Center, U.S. Geological Survey.

of the nunataks. Measured rates of sheet-flow 1 km inland were found to be less than 10 m a^{-1} (Fujiwara and Yoshida, 1972; Langhovde Glacier moved at only 86 m a^{-1}).

On figure 59 Lützow-Holm Bay is entirely filled with fast ice, at the time of the Landsat image (21 January 1974) held in place by a 20-km-long iceberg perhaps grounded on a shoal. Hundreds of trapped icebergs at the top of the picture have visible tails caused by turbulence that extends downwind for a distance of 3 to 4 km. The tails reliably indicate that the prevailing wind in the area is northeasterly.

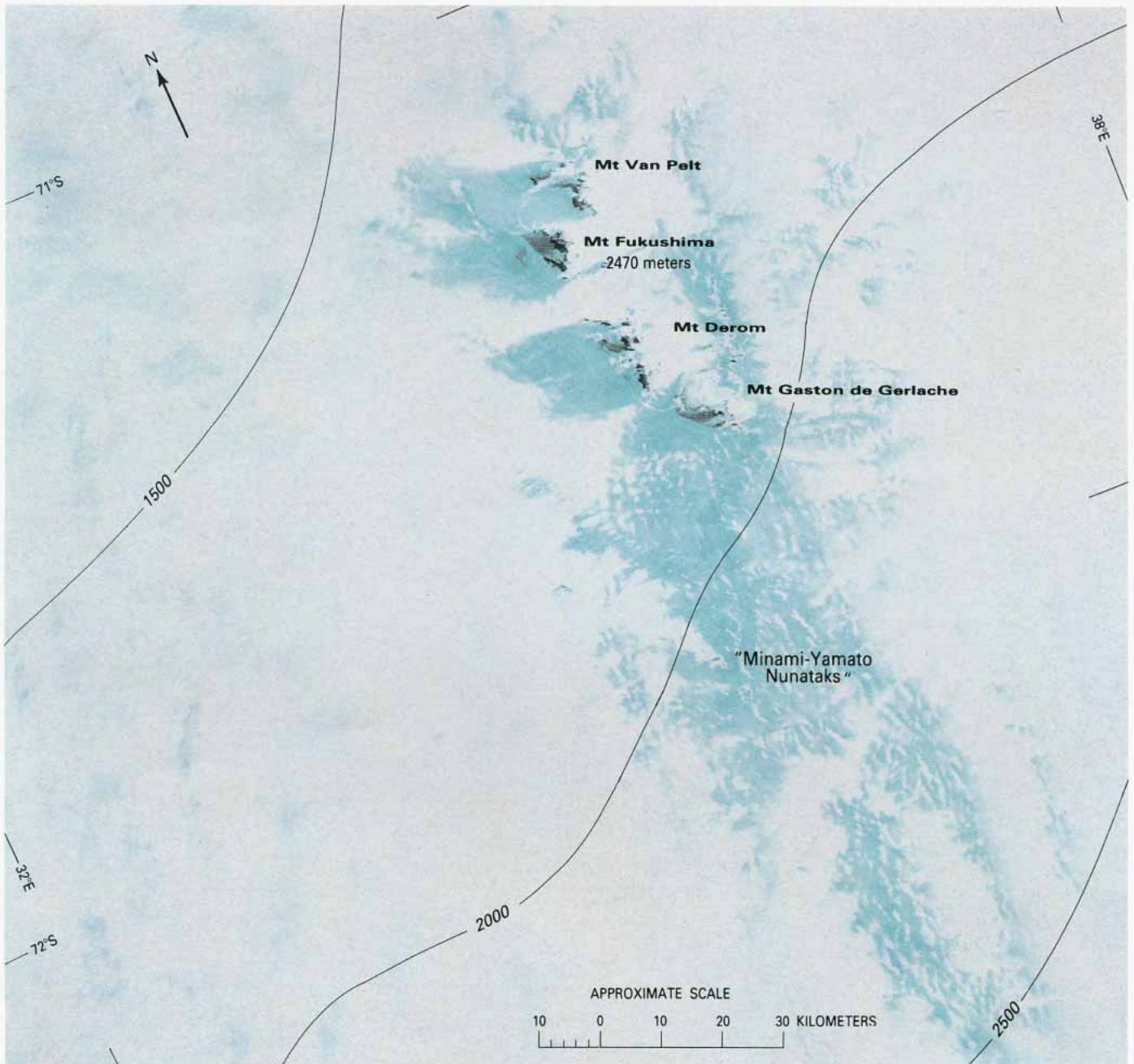
Syowa Station (Shōwa Station) on Ongul Island is the principal Japanese research station in the Antarctic. It was built in 1957 and has been permanently occupied since 1965.

Figure 60 shows some extensive ablation areas on the ice sheet 200 km inland from the coast and 200 km west of Shirase Glacier. The small group of nunataks was named Queen Fabiola Mountains in 1960 and “Yamato Mountains” in 1961. It has come to prominence since the discovery of more than 4,700 meteorite fragments (representing about 500 different meteorites) lying on the surface of many of the neighboring bare-ice areas (Yoshida and others, 1971; Nagata, 1975, 1978,



1979a, b, 1980; Nagata and Yanai, 1982). Before this local concentration was found, fragments from only about 2,100 different meteorites had ever been recovered from the rest of the world. A substantially larger number of meteorite fragments has been collected since 1969 from this one small area of Antarctica (Antarctic Meteorite Working Group, 1981). This is not the only concentration of meteorites in Antarctica, but it is the largest so far discovered. Up to March 1983, more than 1,500 fragments have been recovered from other inland ablation areas in Victoria Land (see for example, Reckling Peak area on fig. 34). It is likely that, in both areas, sublimation has combined with an upward component of ice movement caused by rising subglacial terrain to concentrate and expose, over a very long period of time, meteorites that fell on the ice sheet some distance upstream (Bull and Lipschutz, 1982). Wada and others (1982) discuss a network of airborne radio-echosounding profiles crossing the Queen Fabiola Mountains and ice-particle trajectories deduced from them. The general direction of ice flow can be seen both from visible flowline features on the ice and from lateral moraines on the west side of the main massifs.

Figure 60. — Annotated Landsat 1 MSS digitally enhanced false-color composite image of ablation areas of the Queen Fabiola Mountains, showing extensive areas of 'blue ice' (bare glacier ice) around nunataks and associated morainal debris. Ice-surface contours from Antarctica 1:3,000,000 (Scott Polar Research Institute, unpublished). Some areas of 'blue ice' in Antarctica have proven to contain extraordinary accumulations of meteorites. Since 1969, Japanese scientists have collected 4,813 meteorites within the 'blue-ice' areas shown on this image, or about 25 percent of the extant worldwide collection of meteorites (Williams and others, 1983). NASA image (151 1-05240, bands 4, 5, and 7; 16 December 1973; Path 158, Row 111) courtesy of Baerbel K. Lucchitta and the Flagstaff (Arizona) Image Processing Facility, U.S. Geological Survey.



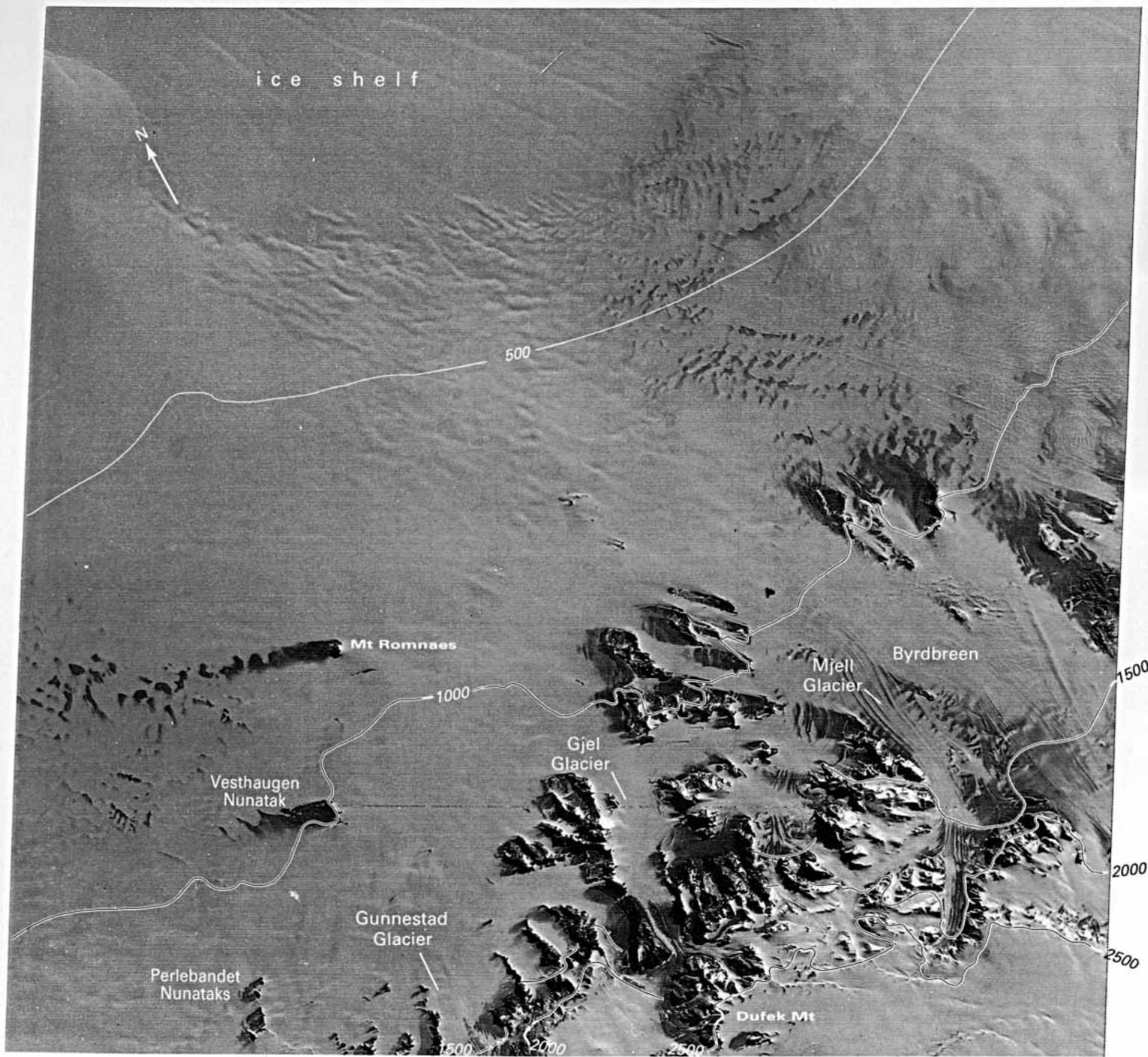
THE ATLANTIC OCEAN SECTOR

Princess Ragnhild Coast, Princess Astrid Coast, Berg Massif, and Fimbul Ice Shelf, Queen Maud Land

Figure 61 shows part of the Sør Rondane Mountains 300 km west of the area of figure 60 and 200 km inland from an ice-front coastline. The inland boundary of the ice shelf (the grounding line) can be seen near the top of the image; it was first mapped in this area from NOAA-2 satellite imagery (Swithinbank, 1973a). Flowline features in the form of shallow grooves 1 to 2 km wide show the direction of flow of the ice shelf. The inland ice sheet is dammed up by the mountain range, leading to an unusually steep overall surface gradient from elevations of nearly 3,000 m in the bottom right corner to only 100 m at the grounding line. The mountain range serves to deflect the main drainage of the inland ice sheet into broad ice streams to the east and to the west. Van Autenboer and Declair (1978) found that the combined total discharge of Byrdreen, Mjell Glacier, Gjøl Glacier, and Gunnesstad Glacier was only $0.65 \text{ km}^3 \text{ a}^{-1}$. Surface velocities were everywhere sluggish ($<40 \text{ m a}^{-1}$), and maximum ice thicknesses calculated for the outlet glacier valleys were between 1,000 and 1,500 m.

Close examination of this scene reveals small local glaciers and moraine-strewn dry (snow- and ice-free) valleys that were formerly ice-filled. A conspicuous series of arcuate moraines in the valleys on the west side of Gjøl Glacier indicate such extensive downwasting that, over large areas, the basal layers of the ice sheet are now exposed on the surface. Van Autenboer (1964) studied the Sør Rondane Mountains on the ground, finding all the classic signs of former glaciation at levels hundreds of meters above the contemporary ice level. Vast areas of bare ice indicate substantial sublimation from the surface, the climate here being too cold for significant melting. The patchiness of the bare ice suggests considerable redistribution of accumulated snow by strong winds. A later Landsat 2 MSS image recorded at the same time of year in 1976 (2386-05405, band 7; 12 February 1976; Path 163, Row 111) shows about four times as much bare ice. Evidently, only a thin layer of snow hides a great deal of bare ice; its actual distribution at any given time is ephemeral. The nearly 50-km-long tail of bare ice downwind of Mount Romnaes speaks of the extraordinary persistence of the turbulence caused by isolated nunataks in a smooth snowfield. A Japanese summer research station at Mount Romnaes was formally opened on 1 January 1985. Finally, we note the gently curving, north-south ice ridge in the upper left part of the image. The lack of any surface expression of subglacial topography near the ridge contrasts with the rest of the scene and indicates that we are looking at the ice divide of an essentially independent ice cap nourished by locally accumulated snow.

Figure 62 shows the Orvin and Wohlthat Mountains that, although breached in many places by outlet glaciers, serve to deflect the main



20FEB73 C S71-26/E025-05 N S71-34/E025-27 MSS 7 R SUN EL17 AZ070 208-2949-A-1-N-D-IL NASA ERTS E-1212-06072-7 01

APPROXIMATE SCALE

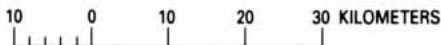
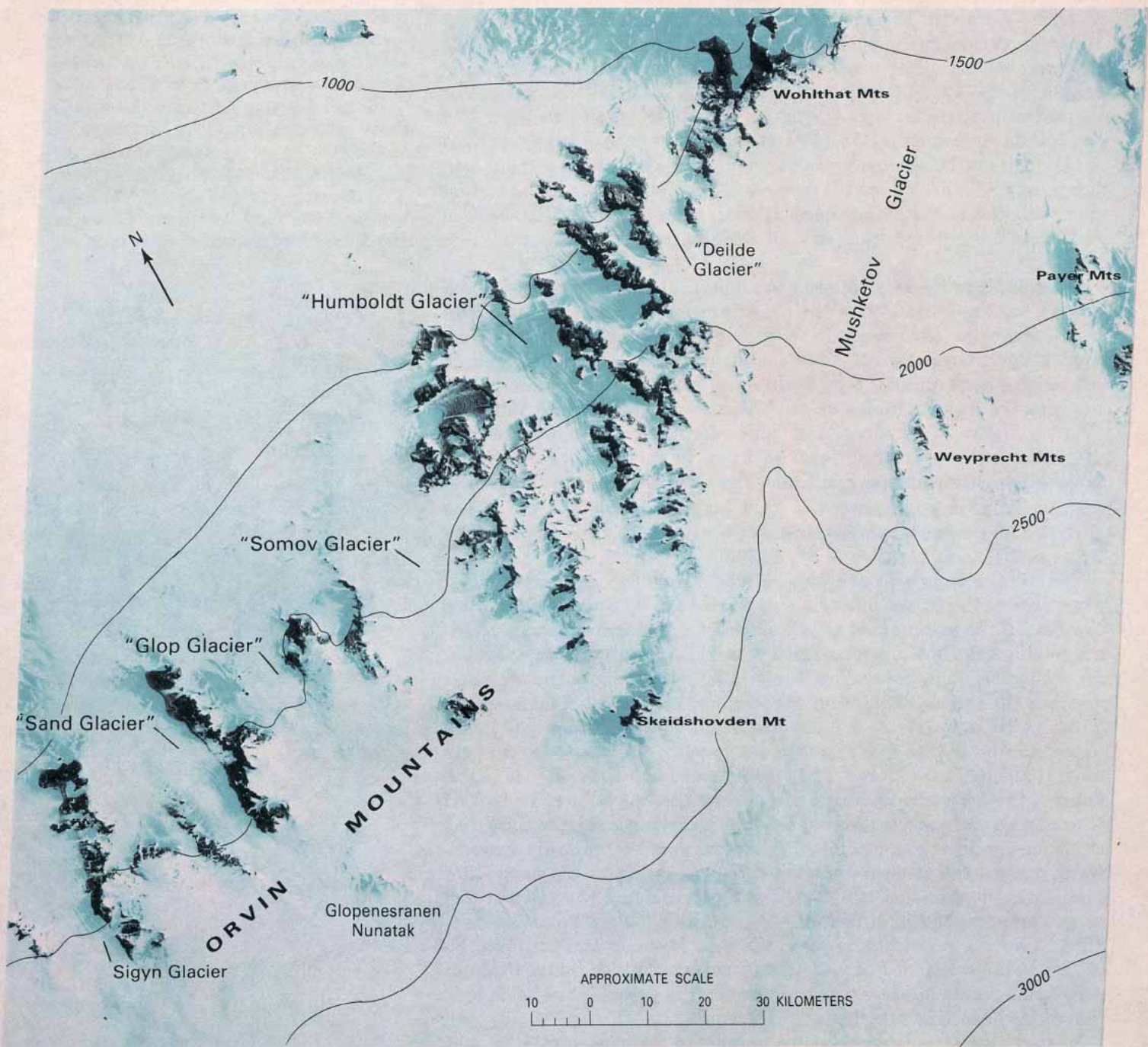


Figure 61.—Annotated Landsat 1 MSS image of the Sør-Rondane Mountains. Ice-surface contours (in meters) modified from unpublished data supplied by Norsk Polarinstitt. NASA image (1212-06072, band 7, 20 February 1973; Path 165, Row 111) from the EROS Data Center, U.S. Geological Survey.



1E008-00 1E009-00 1E010-00 1E011-00
 06JAN73 C S71-53/E012-03 N S71-53/E012-03 MSS 5 7 R SUN EL29 AZ073 208-2322-A-1-N-D-2L NASA ERTS E-1167-06583-3 69

Figure 62. — Annotated Landsat 1 MSS false-color composite image of the Orvin and Wohlthat Mountains. Ice-surface contours (in meters) modified from Novolazarevskaya 1:1,000,000 and Shelf. Ledn. Lazareva 1:1,000,000, Moskva, Ministerstvo Morskogo Flota SSSR, 1976. NASA image (1167-06583, bands 4, 5, and 7; 6 January 1973; Path 174, Row 111) from the EROS Data Center, U.S. Geological Survey.

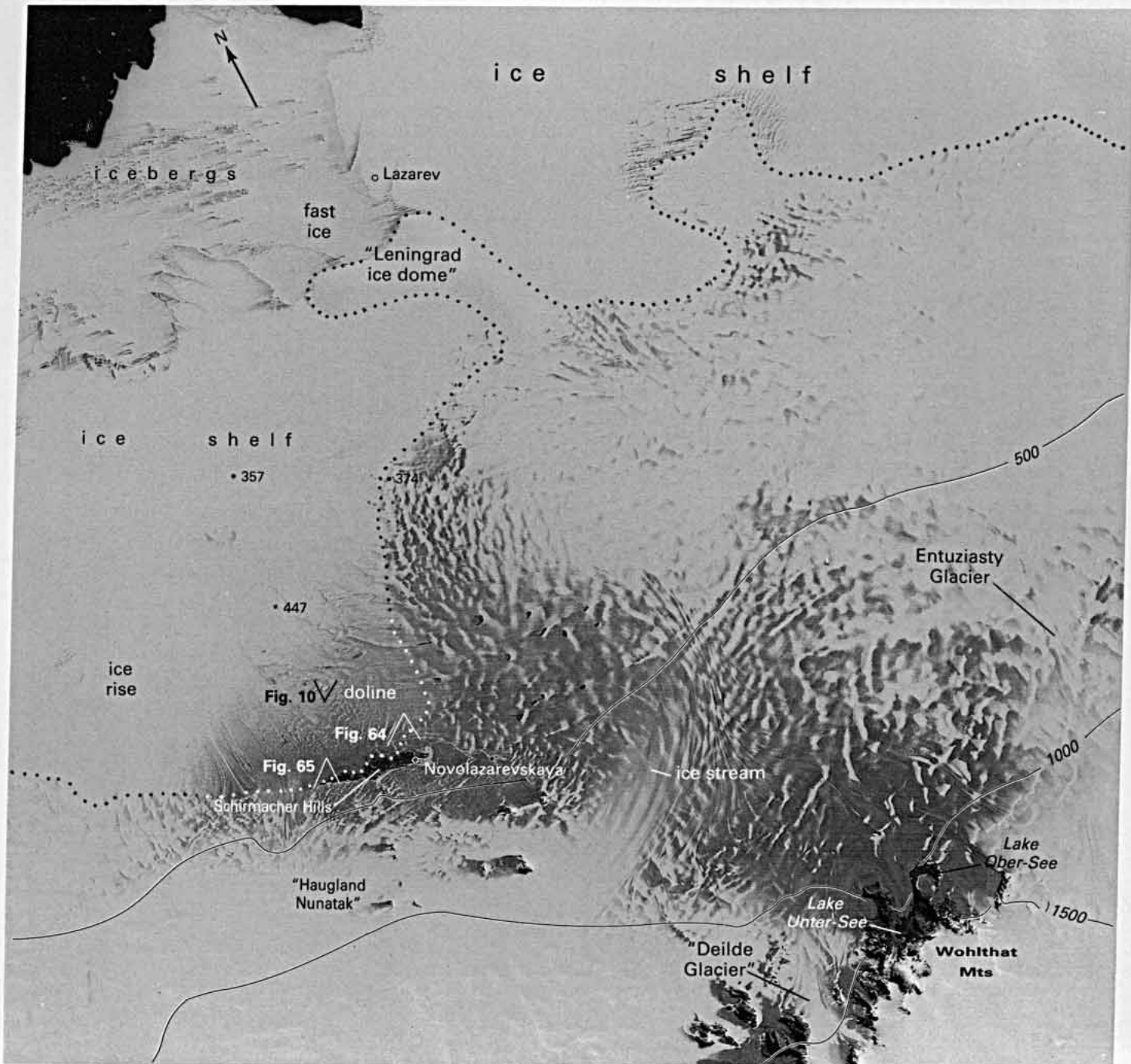
drainage of the inland ice sheet to one side or the other. This is the mountain area discovered in 1939 by what was at the time a secret German Antarctic Expedition dispatched by Adolf Hitler to claim sovereignty over an unexplored sector of the Antarctic (Ritscher, 1942). The extensive ice-free areas subsequently seen in the aerial photographs of the expedition led to speculation that the then prevalent retreat of glaciers in the Northern Hemisphere might be part of a worldwide phenomenon. We now understand that the existence of local ablation areas, lakes, and dry valleys in itself says nothing about contemporary advance or retreat of the ice sheet and may well be consistent with steady-state conditions. It does, however, generally speak of relatively low precipitation, dry air leading to sublimation, and high winds.

Several large glaciers transect the mountain range, but the lack of any ice surface indication of their continuity with subglacial trenches above and below the mountain range suggests that the outlet glaciers are, in geomorphological terms, immature. A desert of arcuate moraines covers an area 5 by 7 km in an extensive dry-valley region between the lower “Humboldt” and “Somov Glaciers.” Here, in figure 62, as in figure 61, downwasting from a former ice level deprived the dry valley of ice overflowing a ridge from “Humboldt Glacier.” Sublimation has subsequently continued the downwasting until now the moraine-filled basal layers of the stagnant ice mass are exposed on the surface. Oblique aerial photographs of the same area were published by Ritscher (1942, v. 1, plates 8, 38, and 40).

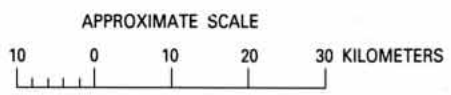
The area of figure 63 overlaps that of figure 62 on the north and shows one of the larger inland ablation areas in Antarctica. Note that the bare ice is surrounded on all sides by snow accumulation areas, suggesting that low precipitation by itself is an unlikely explanation for the lack of snow cover. Kruchinin (1965) wrote about the area and ascribed the extensive ablation phenomena to the effect of föhn (foehn) winds. Although extensive lakes are about the last thing one would expect to find 600 to 800 m above sea level at this latitude, there is more than one in this scene. The conspicuous Lake Unter-See is in the heart of the northern Wohlthat Mountains and has an area of 10 km² (Hermichen and others, 1985). It is fed by a calving glacier tongue that curves around the mountains at an elevation of 800 m to flow southward, against the general direction of ice movement, to discharge into the lake at an elevation of 620 m. The less conspicuous Lake Ober-See at an elevation of 795 m has an area of 3 km² (Norsk Polarinstitut, 1968). Lacking an outlet, similar lakes in lower latitudes would be subject to intermittent and occasionally catastrophic drainage through subglacial channels. Here this is unlikely; it is probable that evaporation alone keeps the lake from overflowing.

Solopov (1969) has described the climate of Schirmacher Hills, and Simonov (1971) discussed the abundant and highly developed ablation features of the area. Hundreds of melt lakes appear on the surface in summer, and raging torrents of water flow in shallow ravines over the ice shelf, making travel quite hazardous and in places almost impossible. Tidal freshwater sea lakes fill the rocky bays along the north coast of the nunatak (Simonov, 1964; Korotkevich, 1965). Swithinbank (1966) and Kruchinin and others (1967) measured surface velocities in the area where the conspicuous ice stream can be seen to curve sharply to the left to pass in front of Schirmacher Hills. The maximum speed measured was 324 m a⁻¹. Kruchinin (1965) described the ice shelves in this area and, in 1959, photographed the ice doline seen both in this Landsat image (fig. 63) and in figure 10. It was then estimated as being 300 m in diameter, with steep sides representing a drop of about 20 m.

Figure 63. — Annotated Landsat 2 MSS image of Lazarev Ice Shelf at Novolazarevskaya. Ice-surface contours (in meters) modified from Novolazarevskaya 1:1,000,000 and Shelf. Ledn. Lazareva 1:1,000,000, Moskva, Ministerstvo Morskogo Flota SSSR, 1976. The dotted line shows the estimated position of the grounding line. Spot soundings are derived from ice drilling (Korotkevich and others, 1978). NASA image (2308-06502, band 7; 26 November 1975; Path 175, Row 110) from the EROS Data Center, U.S. Geological Survey. See also figures 10, 64, and 65.



IS071-00 E011-001 E012-001 S071-301 IE013-00
 26NOV75 C S70-34/E012-53 N S70-35/E013-04 MSS 7 R SUN EL29 AZ069 207-4288-A-1-N-D-IL NASA ERTS E-2308-06502-7 01



The image suggests that by 1975 it may have grown bigger. There is no generally agreed explanation for the origin of ice dolines. One theory is that they are ephemeral meltwater lakes that intermittently drain through fractures to the sea beneath. The possibility of an alternative and very different explanation is suggested by a striking resemblance with some impact craters on the moon (see for example Briggs and Taylor, 1982, p. 116).

Korotkevich and others (1978) drilled three holes to study the ice sheet. The locations of these three drillholes are indicated on figure 63. The easternmost hole struck rock at 374 m depth, where the basal temperature was at the pressure melting point (-1.7°C). This suggests that bottom sliding may account for the low surface gradient of the ice sheet in the vicinity. The northern hole found 203 m of water beneath 357 m of ice, and the southern hole found 40 m of water beneath 447 m of ice. Lazarev was a small Soviet research station built on the ice shelf and occupied from 1959 to 1961. In 1961 it was replaced by Novolazarevskaya, which was built on rock on Schirmacher Hills at an elevation of 100 m above sea level and is still occupied today.

Figure 64 shows the smooth glaciated surface of Schirmacher Hills and also streams of meltwater flowing from left to right. All the streams flow into one or other of the tidal sea lakes fronting the long

Figure 64. —Oblique aerial photograph of the ablation area surrounding Schirmacher Hills taken from an altitude of 1,950 m on 19 January 1959, looking south-southwest. The camera position is marked on figure 63. The Orvin Mountains fill the horizon in the middle of the picture. Photograph no. DML 58-592416 by Bernhard Luncke, Norsk Polarinstitut, Oslo.



nunatak. The Soviet station, Novolazarevskaya, is situated among the snow patches close to the left-hand end of the nunatak, and Soviet aircraft land on the rising surface of the inland ice sheet behind. The ice shelf at the opposite end of the nunatak (fig. 65) is reminiscent of some landscapes on the moon. The surface is pitted with craterlike melt lakes and canyons. Note that the ice shelf is flowing away from the camera and towards the nunatak, whereas the inland ice sheet behind is flowing towards the camera. Thus the lake is supplied with meltwater and with calving icebergs from a floating ice shelf and a grounded ice sheet flowing in the opposite direction. The tidal nature of the lake is shown by the conspicuous tidal cracks fronting the nunatak; there are, of course, no tidal cracks between the wasting icebergs calving into the lake (left center) and the lake ice. The lake ice melts out completely in very warm summers and it would be possible to land a flying boat here. Note the narrow shore lead (left) and the inland (nontidal) melt lake behind, which is 93 m above sea level.

Figure 66 shows a typical scene from the inland nunatak area of Queen Maud Land 600 km to the west of the area of figure 65. The higher nunataks rise about 400 m above the surrounding snow, but ice thicknesses between the nunataks are such that the peak-to-trough relief exceeds 2,000 m in places (Robin, 1958). The Heimefront Range

Figure 65. — Oblique aerial photograph of the tidal sea lake at the western end of the Schirmacher Hills taken from an altitude of 270 m on 25 January 1959, looking south-south west. The camera position is marked on figure 63. The foreground consists of floating ice shelf. Photograph no. DML 58-594 134 by Sigurd Svindland, Norsk Polarinstittutt, Oslo.





(fig. 67) marks the sinuous escarpment, here exposed, but in places hidden beneath the ice sheet, that roughly parallels the Queen Maud Land coast all the way from the Queen Fabiola Mountains at longitude 35°E . to the mountains in this picture situated 45° farther to the west at 10°W . longitude. To the left lies the polar plateau, unbroken by nunataks between here and the South Pole. To the right lies 150 km of ice sheet leading by gentle gradients to Riiser-Larsen Ice Shelf. The height of the exposed cliffs in the center is on the order of 400 m. Swithinbank (1958, p. 108-109) characterized the area as one of active scarp recession accentuated by the channeling of ice drainage from the plateau. The flat, mesalike summit of the nunatak in the center shows a clear angular unconformity between banded gneisses dipping sharply in towards the plateau and flatlying sediments that rest upon them. Worsfold (1967) discussed the glacial geomorphology of the area, and Juckes (1972) concluded that the degree of dissection of the different mountain blocks is, in part, controlled by the height of a pre-Permian erosion surface.

Figure 66. — Oblique aerial photograph of nunataks in Queen Maud Land taken from an altitude of 4,800 m on 28 December 1951, looking south-southeast. The camera position is marked on figure 69. Photograph no. DML 51-52784 by Helge Skappel, Norsk Polarinstittutt, Oslo.



Figure 67. — Oblique aerial photograph of the Heimfront Range in Queen Maud Land taken from an altitude of 4,050 m on 2 January 1952, looking southwest. Photograph no. DML 51-52 1180 by Helge Skappel, Norsk Polarinstittutt, Oslo.

Figures 68, 69, and 70 represent a nested set of satellite images, each encompassing a different part of Queen Maud Land, and each providing different types of data used in the analysis of glaciological features. Figure 68 is a digital-image mosaic, prepared from parts of three NOAA 7 AVHRR images of New Schwabenland, Queen Maud Land, by the Institut für Angewandte Geodäsie (1982). The image mosaic includes the coast from the Riiser-Larsen Ice Shelf to Breid Bay, north of the Sør Rondane Mountains. Large areas of 'blue ice' can be delineated on the mosaic. Note especially the flowlines of the large outlet glacier, Jutulstraumen, as it extends through the gap between Neumayer Cliffs and the 0° meridian before flowing down a deep trough onto the Fimbul Ice Shelf. Figure 69 is a mosaic of a number of Landsat scenes. Figure 70 is a Landsat 2 MSS digitally enhanced false-color composite image of the Jutulstraumen Glacier where it meets the Fimbul Ice Shelf. Areas of disturbed ice (heavily crevassed) are apparent on the ice shelf. Jutulstraumen is the largest outlet glacier between longitudes 15°E. and 20°W. According to McIntyre (in press) it drains an area of 124,000 km². The morphology of the ice sheet and mountain areas bordering the ice stream was described by Swithinbank (1958). Wolmarans and Kent (1982) have produced a synthesis of the geology of the area. The lower portion of Jutulstraumen Glacier flows in a major trough believed to be of structural origin (Decleir and Van Autenboer, 1982). Although the glacier is fed by an ice stream that joins it from the east side of Neumayer Cliffs, the main subglacial valley can be traced to the southwest through Penck Trough as far as longitude 6°W. The upper part of this valley appears to have captured the drainage that formerly reached the coast via Schytt Glacier. Figure 71 is an oblique aerial photograph of the Borg Massif area in longitude 3°30'W., where peaks rise to 2,717 m above sea level; figure 72 shows Neumayer Cliffs with the Borg Massif in the background.

Many ice-thickness measurements have been made within the area of the Landsat image mosaic (fig. 69) (Robin, 1958; Neethling, 1972; Van Autenboer and Decleir, 1972; Schaefer, 1973; van Zyl, 1973; Schonfeld and van Zyl, 1974; Barnard, 1975; Decleir and Van Autenboer, 1982; Wolmarans, 1982), but at this small scale it is not practicable to indicate more than a few of them. Note that the 2,340-m sounding in Penck Trough and the similar ice depths in two narrow parallel valleys to the north are all between the 1,500-m and 2,000-m surface contours, indicating that the valley bottoms are far below sea level.

Decleir and Van Autenboer (1982) used surface velocity measurements by Gjessing (1972) and gravity profiles across Jutulstraumen Glacier to calculate an ice discharge of 12.5 km³ a⁻¹ at latitude 72°15'S., although the fastest observed rate of flow was only about 390 m a⁻¹. The sudden development of giant rifts at the left bank of the glacier 17 km below Utkikken Hill shows that at this point the ice is afloat. Orheim (1979) observed a velocity of 1 km a⁻¹ at the ice front north of here. A large glacier tongue calved from the seaward extension of Jutulstraumen Glacier in 1967, yielding a single iceberg called 'Trolltunga' with dimensions of 53 by 104 km. Swithinbank and others (1977) surmised that the immediate cause of calving was impact by another giant drifting iceberg. Robin (1979, p. 267) called this glaciology's "big bang" theory. Decleir and Van Autenboer (1982) calculated

Neuschwabenland 1982

1:6 000 000

Bilder:

NOAA-7 AVHRR, Kanal 2 (0.73...1.10 Mikrometer)

Weitere Daten in der Bildübersicht

Digitale Bildverarbeitung:

- geometrische Entzerrung auf ein 1 km-Raster; 10 Pulzpunkte (siehe Bildübersicht)
- radiometrischer Ausgleich der Bänder
- Kontrastverstärkung

Abbildung:

Polare Azimutal-Abbildung, Schrittbreitenkonk 75° S (Stereographische Abb.)

Höhenlinien der Eisoberfläche:

Entnommen aus GEBCO 1:6 000 000 (B.18) vom August 1980

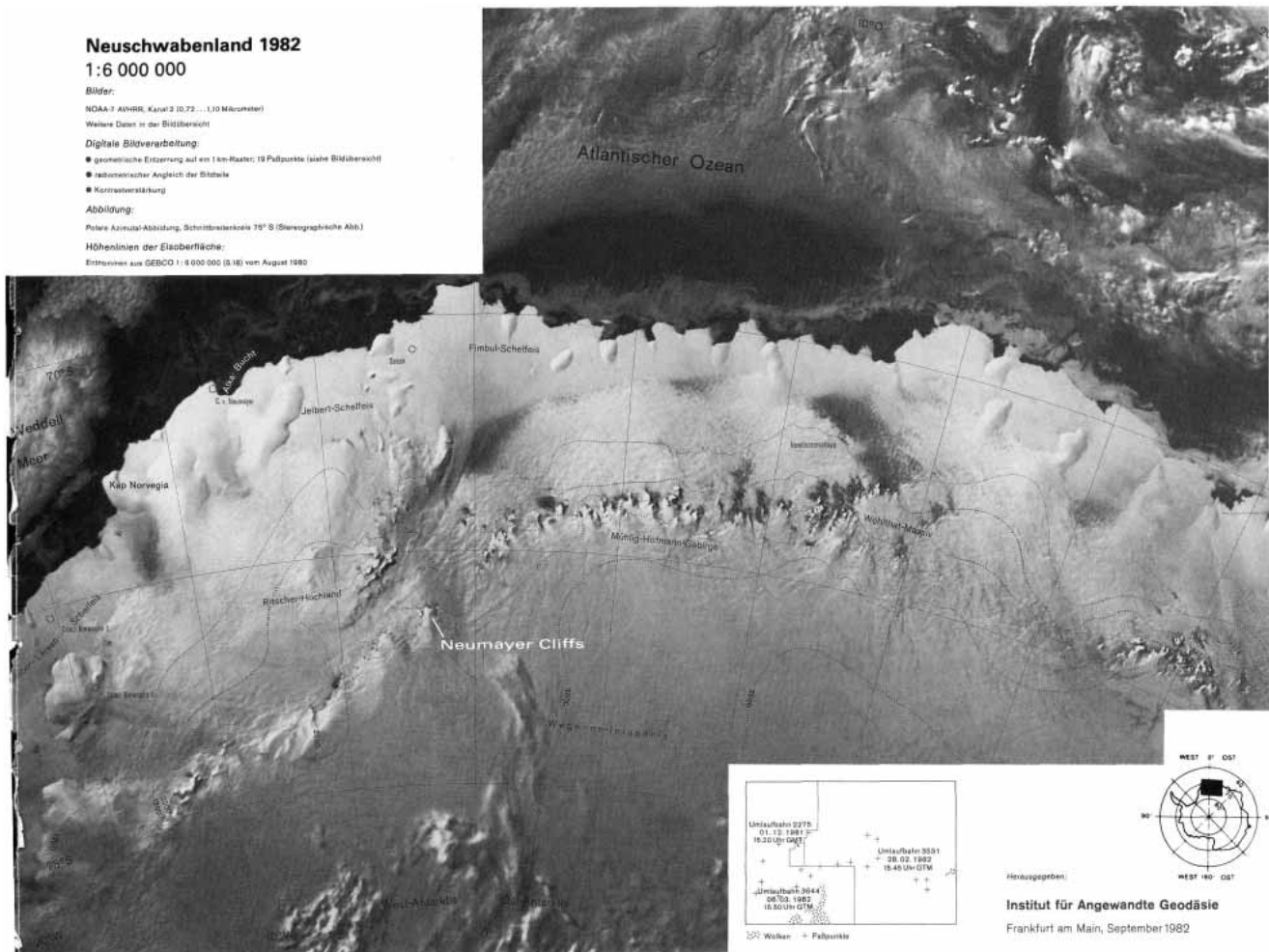
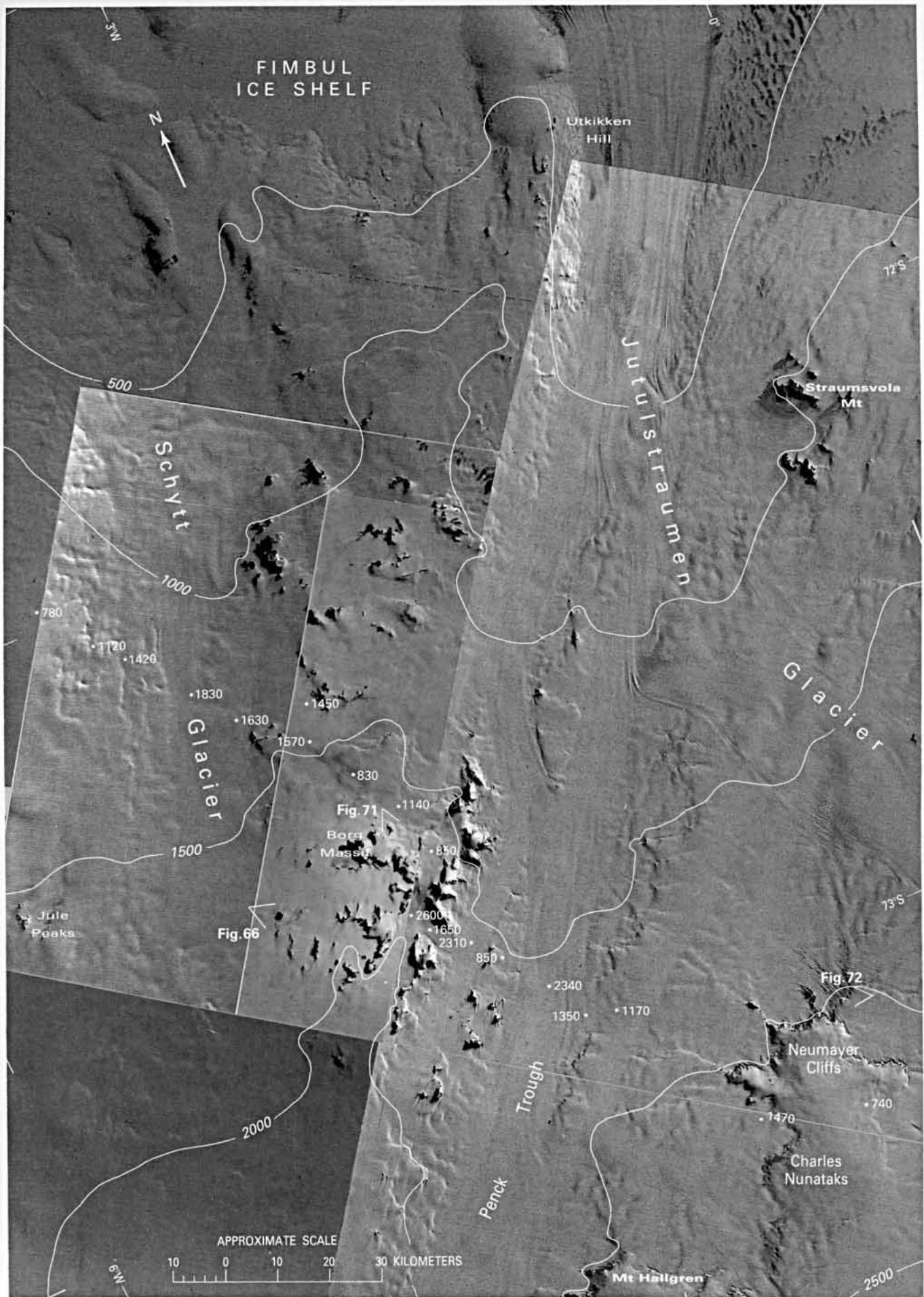


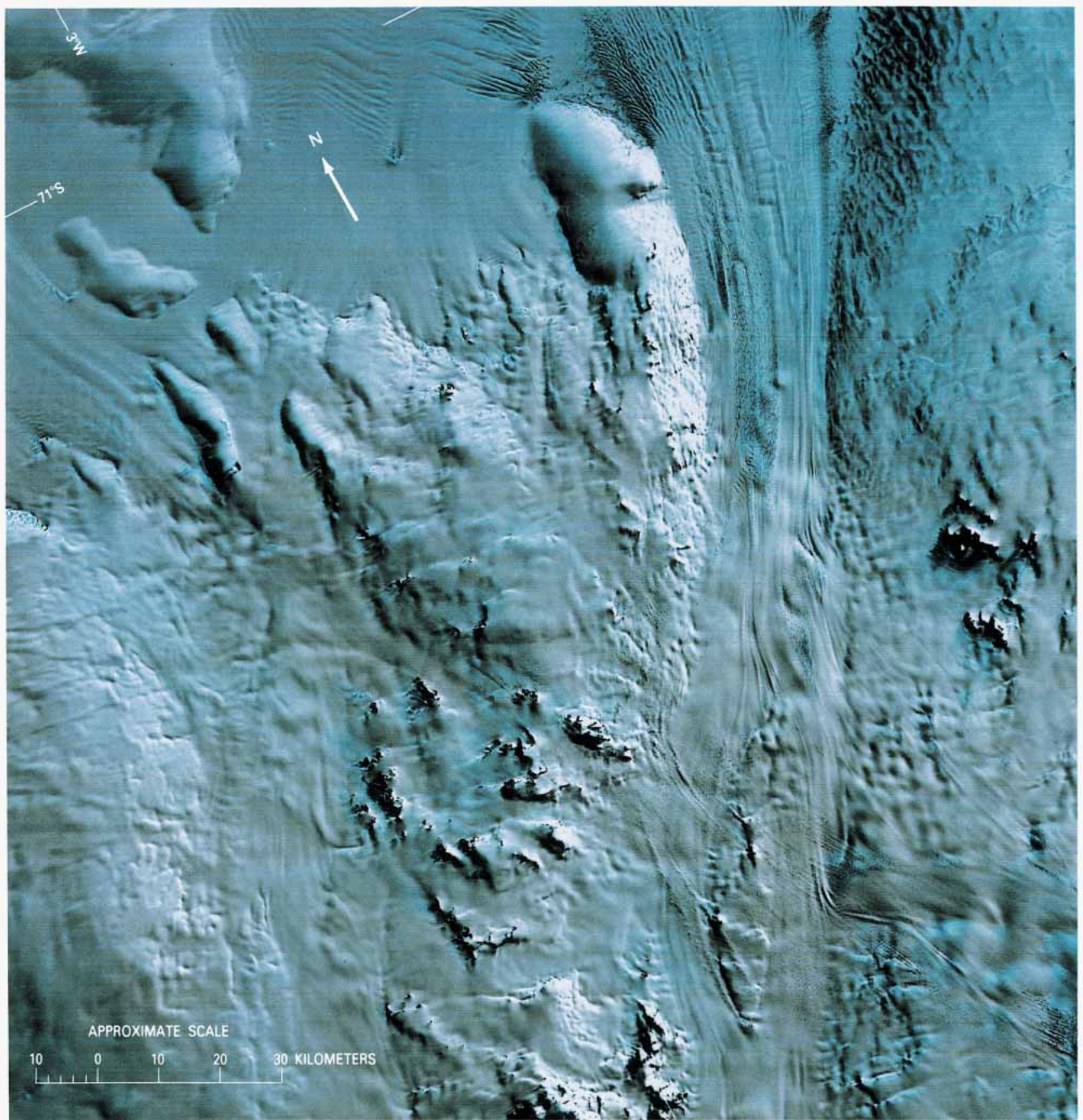
Figure 68.—Annotated NOAA 7 advanced very high resolution radiometer (AVHRR) three-image mosaic of New Schwabenland, Queen Maud Land. Original map scale is 1:3,000,000. Courtesy of Institut für Angewandte Geodäsie Frankfurt am Main, September 1982.

that the minimum time necessary for the formation of a glacier tongue of this size is in the order of 100 years. Thus, giant icebergs will continue to be rare.

Surface velocities away from the major ice streams are sluggish. L.E. Kent (personal commun.) reported a maximum velocity of 25 m a⁻¹ in Penck Trough, and Swithinbank (1960) found some mountain glaciers flowing even slower. An icefield adjacent to the Borg Massif was found to be moving 0.1 m a⁻¹. The characteristics of this and other icefields have been described by Schytt (1961, p. 183-189). A more extensive icefield can be seen on the west side of Straumsvola Mountain.

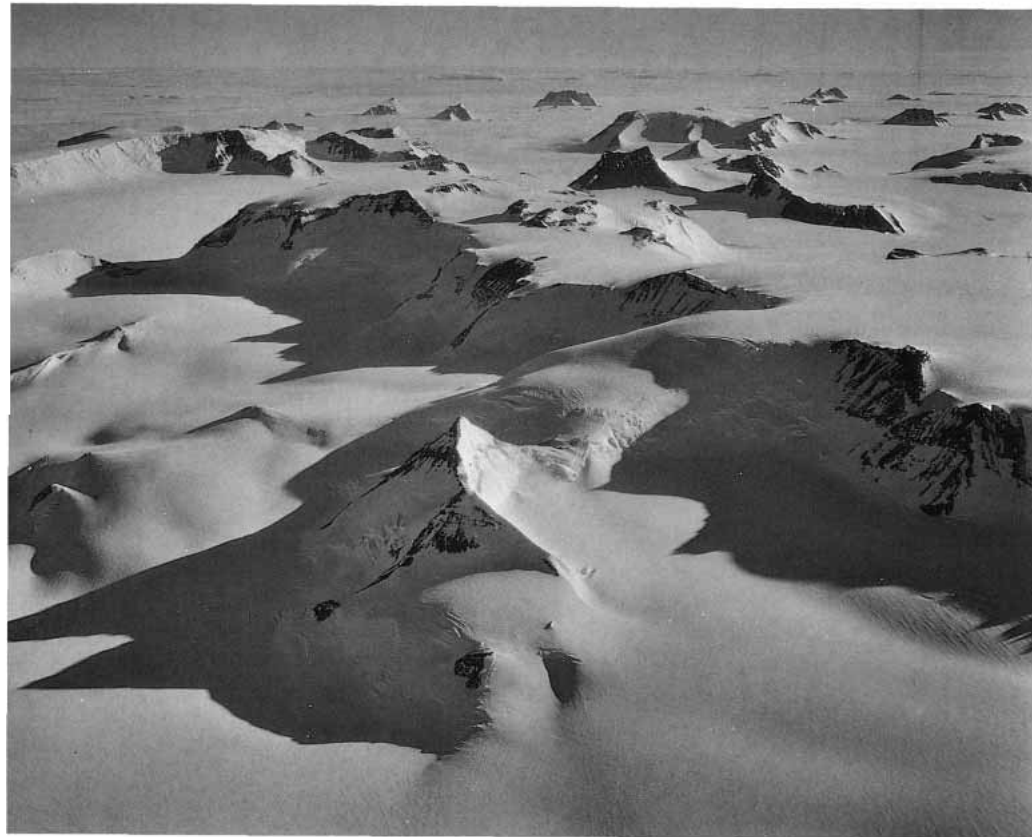


B94 SATELLITE IMAGE ATLAS OF GLACIERS OF THE WORLD



◁ **Figure 69.**—Annotated Landsat 1 and 2 MSS image mosaic of Jutulstraumen Glacier and environs, Princess Martha Coast. Ice-surface contours (in meters) modified from Dronning Maud Land Vest 1:3,000,000, Oslo, Norsk Polarinstitutt, 1972. Spot soundings (in meters) from seismic sounding by Robin (1958). NASA images (12 10–07393, band 7; 18 February 1973; Path 181, Row 112; 1230–07511, band 7; 10 March 1973; Path 183, Row 112; 1553–07405, band 7; 27 January 1974; Path 182, Row 112; 2281–07424, band 7; 30 October 1975; Path 184, Row 111) from the EROS Data Center, U. S. Geological Survey. See also figures 66, 71, and 72.

Figure 70.—Landsat 2 MSS digitally enhanced false-color composite image of the Jutulstraumen Glacier and environs. Jutulstraumen Glacier flows in a northerly direction from the bottom right corner to the top of the image. NASA image (2281–07424, bands 4, 5, and 7; 30 October 1975; Path 184, Row 111) courtesy of Baerbel K. Lucchitta and the Flagstaff (Arizona) Image Processing Facility, U.S. Geological Survey.



◁ **Figure 71.**—Oblique aerial photograph of the Borg Massif taken from an altitude of 4,650 m on 28 December 1951, facing south. The camera position is marked on figure 69. Photograph no. DML 51-52 901 by Helge Skappell, Norsk Polarinstitut, Oslo.

Figure 72.—Oblique aerial photograph of Neumayer Cliffs, in the northeastern part of Kirwan Escarpment, taken from an altitude of 4,600 m on 28 December 1951, facing west-northwest. The camera position is marked on figure 69. Photograph no. DML 51-52 0854 by Helge Skappell, Norsk Polarinstitut, Oslo.

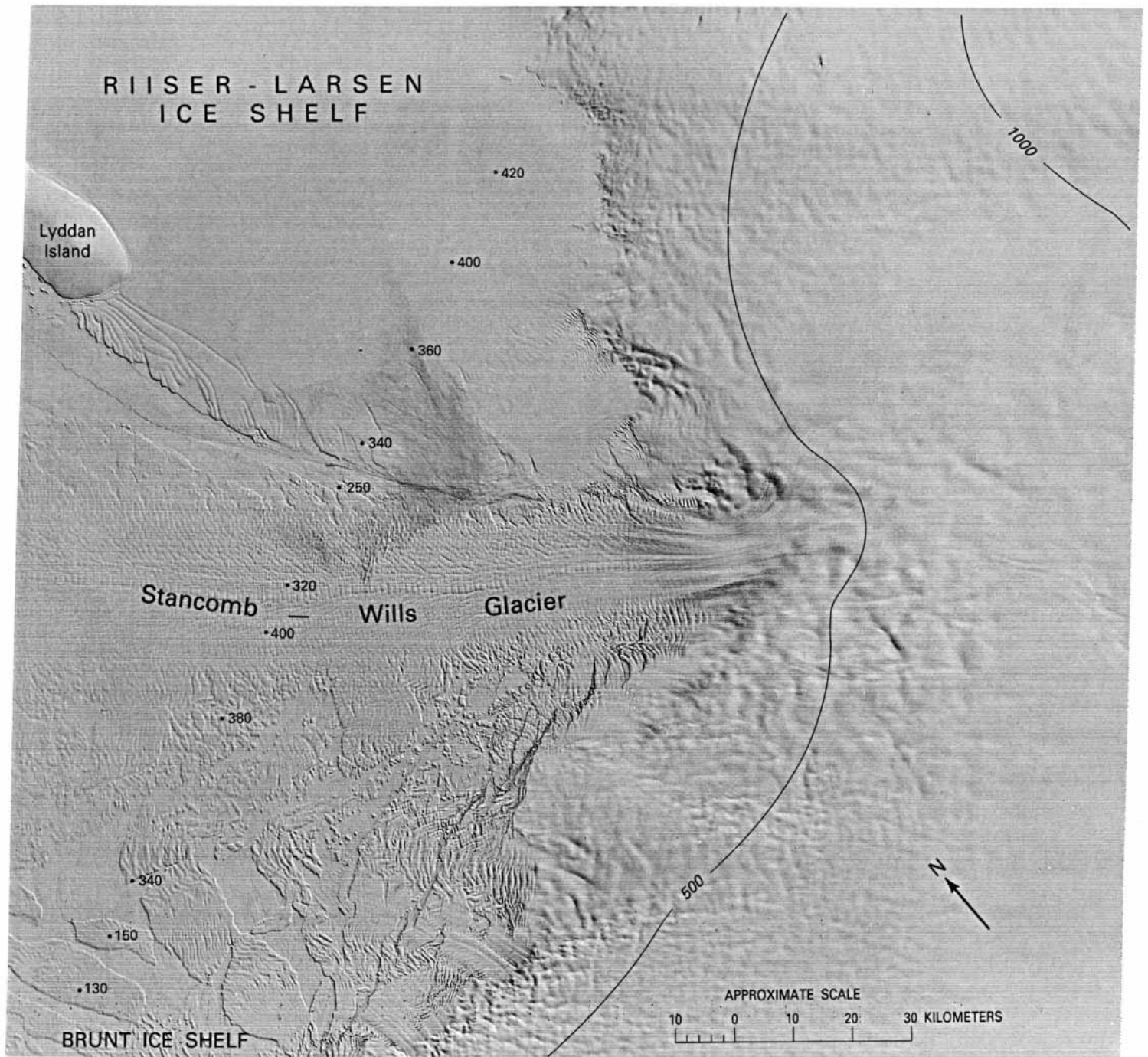


Riiser-Larsen Ice Shelf and Shackleton Range

Figure 73 depicts the largest ice stream between Jutulstraumen (fig. 69) and Slessor Glacier (fig. 74), the Stancomb-Wills Glacier Tongue, discovered in January 1915 by Shackleton (1919, p. 251, who saw its seaward terminus as an ice shelf promontory ('Stancomb-Wills Promontory') of unexplained provenance. The great ice stream (Stancomb-Wills Glacier) tumbling from the inland ice sheet was first seen only in 1957 (personal commun. from Sir Vivian Fuchs). The Stancomb-Wills Glacier was photographed on 5 November 1967 during a U.S. Navy LC-130 Hercules survey flight over the area and subsequently mapped by the U.S. Geological Survey from these U.S. Navy trimetrogon aerial photographs (Alberts, 1981). According to McIntyre (in press) it drains an area of 35,000 km². The full extent of the Stancomb-Wills Glacier was unknown before Landsat. A tortuous grounding line bisects the image from top to bottom. Lyddan Island is an ice rise that obstructs the westward flow of Riiser-Larsen Ice Shelf, causing, in conjunction with the flow of the Stancomb-Wills Glacier, an unusual pattern of rifts and depressions that form once the floating ice sheet is no longer confined within the strait between the ice rise and the mainland.

Thomas (1973) described the area and reported a northwestward movement of 1,300 m a⁻¹ near the right bank of the ice stream close to the left-hand margin of this scene. Orheim (1982) reported velocities of about 4 km a⁻¹ at the ice front. The product of this velocity and an estimated ice thickness of 200 m where the floating ice stream is 50 km wide yields an ice discharge of about 40 km³ a⁻¹. The bottom left corner of the image (fig. 73) offers a rare example of the way in which an ice shelf responds to strain rates too extreme to be accommodated by deformation. Icebergs calving from the ice sheet at or near the grounding line are pulled along by the fast-moving ice stream to the north and forced to rotate in a counterclockwise direction. One iceberg 50 km long is being slowly broken into three pieces. The spaces between the icebergs are filled with incipient, or 'low', ice shelf consisting essentially of a sea ice base on which snow has accumulated to a considerable thickness. Low ice shelves become progressively thicker with age and in places can become indistinguishable from areas of an ice shelf derived from the inland ice sheet. Whereas most ice shelves consist of a thinning wedge of ice of land origin overlain by a thickening wedge of locally accumulated snow, the components of this particular ice shelf are in horizontally separate blocks.

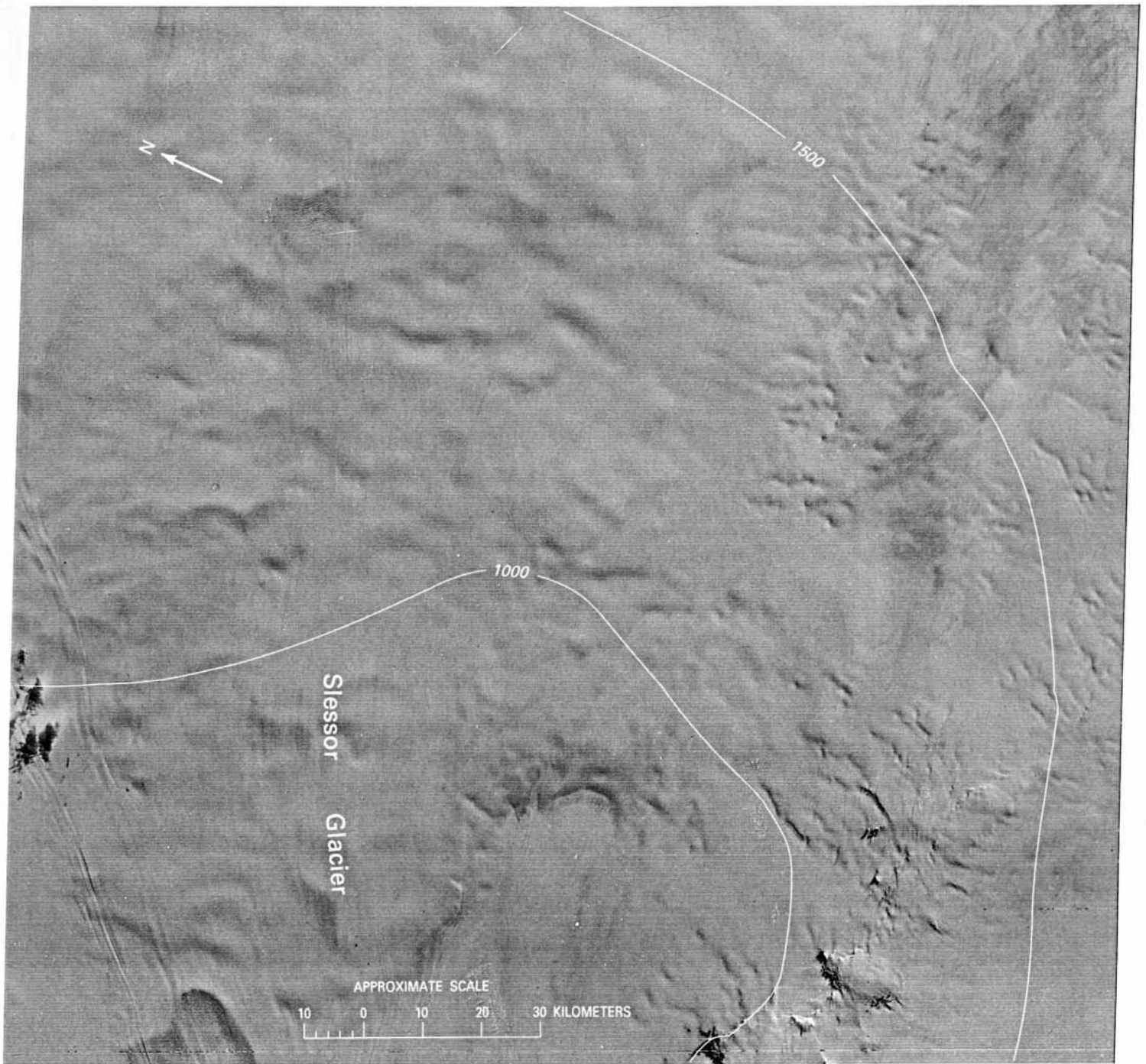
The area in figure 74 adjoins but does not overlap that of figure 75 on the north. Together, they show Slessor Glacier, one of the longest coherent ice streams known. Its upstream length, as defined by flow features visible in satellite imagery, is around 500 km from Parry Point. Downstream, distinct flowlines can be traced from Parry Point through a further 350 km to the ice front (Crabtree and Doake, 1980). According to McIntyre (in press) the glacier drains an area of 575,000 km² and should have a balance discharge of 34 km³ a⁻¹. No velocity or ice-thickness measurements have been made on the glacier itself, but we may infer by following Slessor Glacier flowlines to the ice front and using ice thicknesses (fig. 76) and velocity measurements summarized by Crabtree and Doake (1980) that the ice discharge must approach 30



W022-001 S076-001 W020-001
 22FEB74 C S75-11/W019-28 N S75-19/W019-13 MSS 7 R SUN EL13 AZ078 216-8068-A-1-N-D-IL NASA ERTS E-1579-08270-7 01

$\text{km}^3 \text{a}^{-1}$. The ice surface topography seen in figure 74 is typical of that found in the upper reaches of a major ice stream. Characterized by a series of escarpments trending generally across the flowlines, we speculate that each west-facing slope indicates a subglacial ridge or peak over which the ice is attenuated by faster flow. The long-wavelength topography is commonly diagnostic of the presence of an ice stream, but it must not be confused with the short-wavelength, ice-surface topography seen towards the right-hand side of the image. The short-wavelength topography reveals an eastward-trending subglacial extension of the Shackleton Range over which ice thicknesses are

Figure 73. — Annotated Landsat 1 MSS image of Stancomb-Wills Glacier. Ice-surface contours from British Antarctic Territory 1:3,000,000, sheet BAS Misc. 2, Tolworth, Directorate of Overseas Surveys, 1981. Spot soundings (in meters) from airborne radio-echosounding (Scott Polar Research Institute, unpublished). NASA image (1579-08270, band 7; 22 February 1974; Path 190, Row 114) from the EROS Data Center, U.S. Geological Survey.

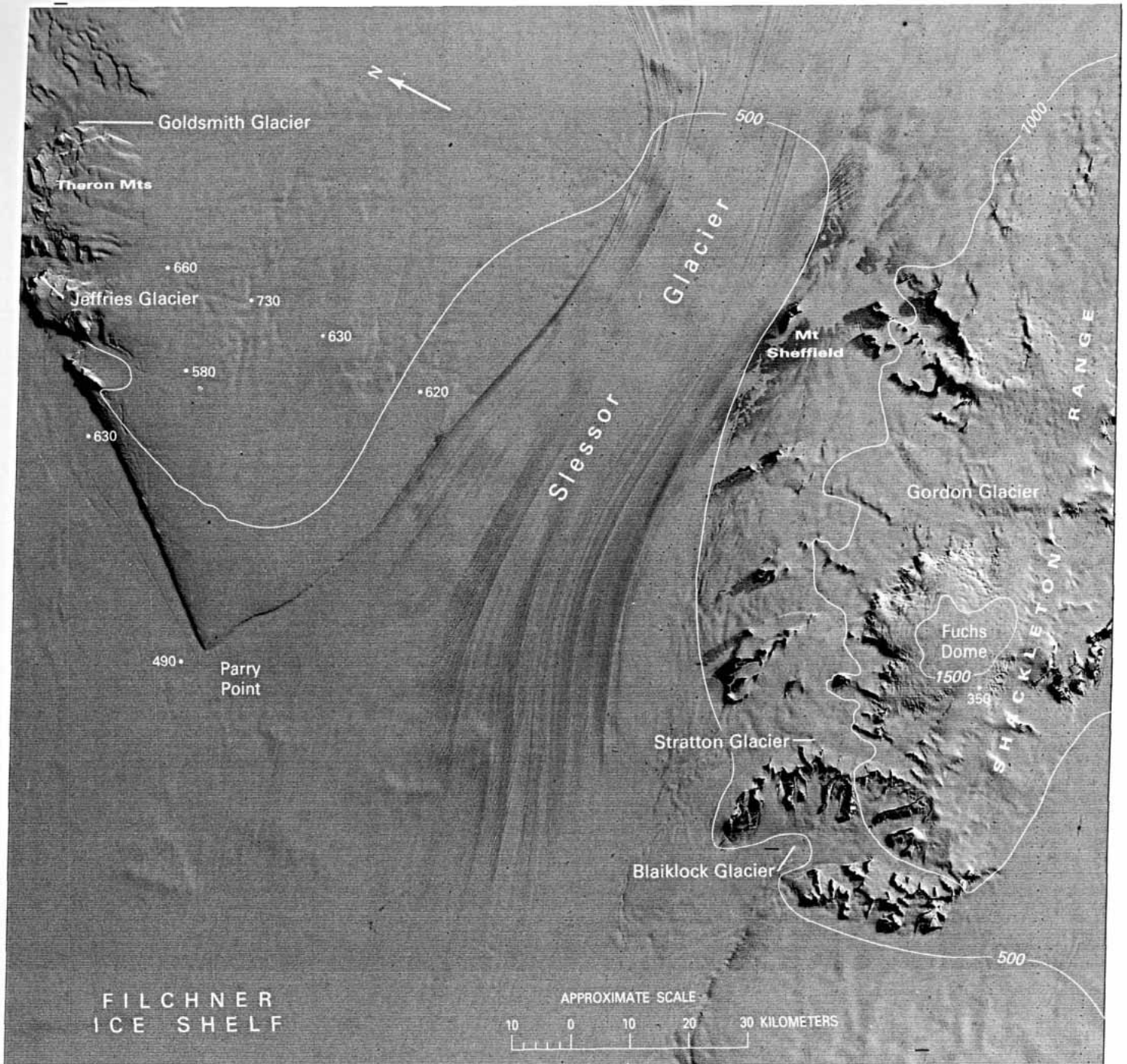


22NOV73 C S79-50/W018-15 N S79-59/W017-42 MSS 7 R SUN EL18 AZ098 242-6784-A-1-N-D-IL NASA ERTS E-1487-06363-7 01

Figure 74. — Annotated Landsat 1 MSS image of the upper Slessor Glacier, Queen Maud Land. The easternmost nunataks of Shackleton Range can be seen. Ice-surface contours (in meters) modified from British Antarctic Territory 1:3,000,000, sheet BAS Misc. 2, Tolworth, Directorate of Overseas Surveys, 1981 NASA image (1487-06363, band 7; 22 November 1973; Path 170, Row 119) from the EROS Data Center, U. S. Geological Survey.

probably much less than they are on Slessor Glacier. The sinuous escarpment that crosses the glacier near the bottom of the image evidently reflects a major structural feature of the subglacial landscape (Marsh, 1985).

McIntyre (1985b) has suggested a physical explanation for ice-stream features similar to those seen in figure 74 (upper Slessor Glacier). Here it is worth noting the contrast with figure 49 (Gamburtsev Subglacial Mountains). No velocity measurements have been made within the area of either image, but steady-state velocities over the Gamburtsev Subglacial Mountains are calculated to be only 3 to 5 m



1W034-00 22JAN74 C S79-52/W028-17 N S80-02/W028-16 MSS 7 R SUN EL17 AZ105 243-7635-A-1-N-D-IL NASA ERTS E-1548-07151-7 01

a⁻¹ (Budd and others, 1971, map 22). In spite of the low snow accumulation rate that is to be expected so far inland (Bull, 1971), the extremely slow movement allows some of the ice-surface topography to be buried and concealed by new snow. Although snow accumulation may be somewhat greater within the area of figure 74, surface velocities would be expected to be two orders of magnitude greater than in the interior. Thus the typical ice stream topography of upper Slessor Glacier may be preserved essentially because it is being renewed by flow over the subglacial landscape faster than snow accumulation can serve to soften or conceal it.

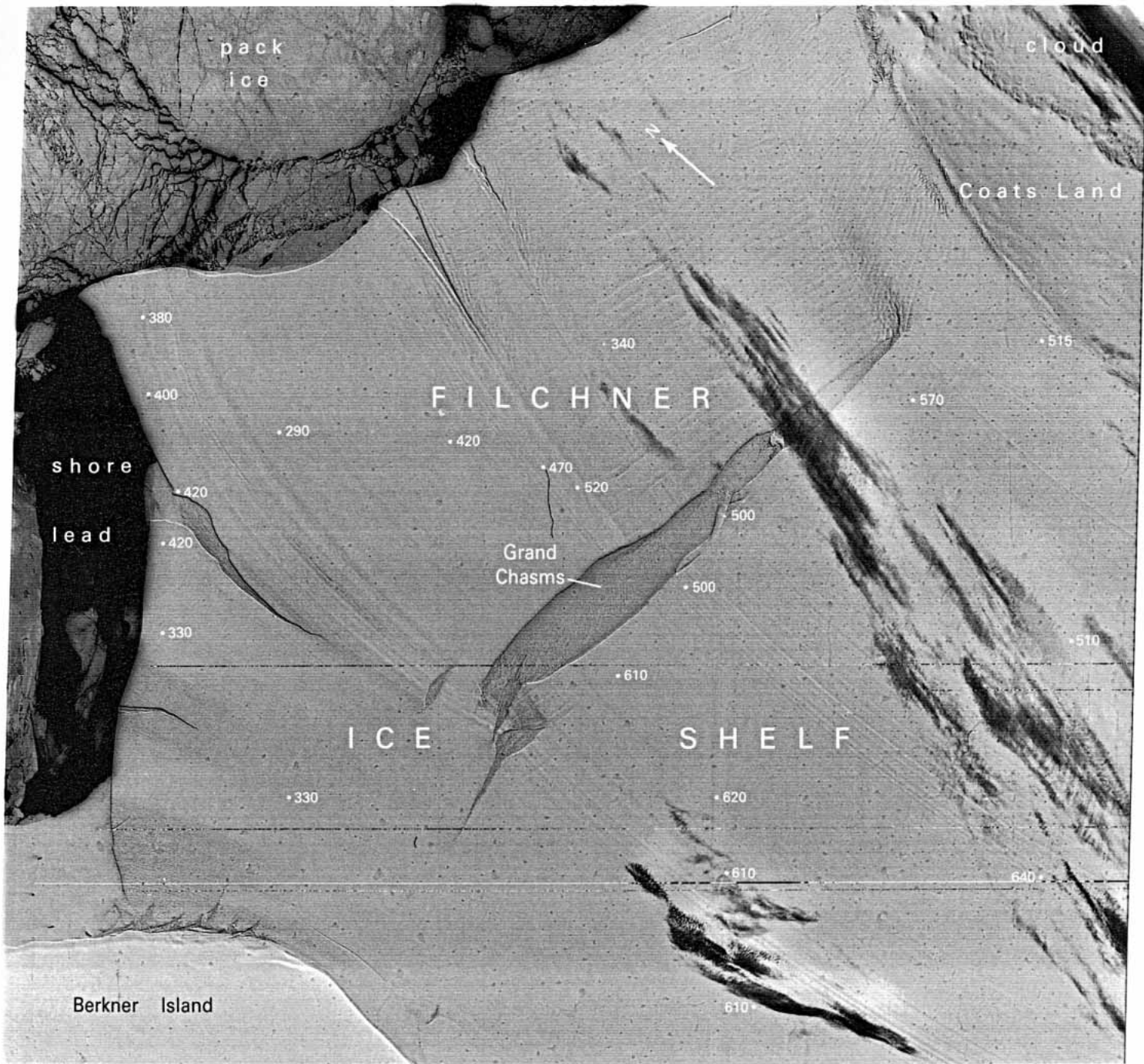
Figure 75. — Annotated Landsat 1 MSS image of Slessor Glacier and the Shackleton Range. Ice-surface contours (in meters) modified from British Antarctic Territory 1:3,000,000, sheet BAS Misc. 2, Tolworth, Directorate of Overseas Surveys, 1981. Spot soundings (in meters) from airborne radio-echosounding (Scott Polar Research Institute, unpublished). NASA image (1548–07151, band 7; 22 January 1974; Path 177, Row 119) from the EROS Data Center, U.S. Geological Survey.

Slessor Glacier is 30 km wide at its narrowest point, which is opposite Mount Sheffield (fig. 75). The position of the grounding line is unknown. However, the isolated smooth surface undulations down-glacier from Parry Point and towards Blaiklock Glacier from Parry Point seem to be characteristic of glaciers sliding on their beds close to the grounding line (see also fig. 102). Perhaps the undulations represent isolated patches of grounding on an ice sheet that is otherwise essentially floating. None of the tributary glaciers flowing through the Theron Mountains and from the Shackleton Range is significant in terms of ice discharge, all of them having very small and local catchments.

Filchner and Ronne Ice Shelves

Figure 76 shows the Filchner Ice Shelf, a fast-moving ice shelf that has conspicuous evidence of diverging flow. The diverging flow regime dominates the flowline pattern as soon as the ice sheet passes beyond the narrowest point of its constriction between Berkner Island and Coats Land. The area has been described by Fuchs and Hillary (1958) and Behrendt (1962). Neuburg and others (1959) described the Grand Chasms as “a gigantic rupture” that in 1957 was 100 km long and 400 m to 5 km wide. By 1973, the time of this image, the rupture had grown to 115 km in length and was 11 km wide at its widest point. The maximum width in 1985 was 19 km (Landsat 5 MSS image 50364–09084, band 4; 28 February 1985; Path 183, Row 117). In 1957 the measured depth was 53 m to a bottom consisting of a chaotic confusion of ice blocks floating on the sea. In July 1986, it was reported that most of the ice shelf on the seaward side of Grand Chasms had separated to form icebergs. Similar rifts have been noted on Ross Ice Shelf (Swithinbank and Zumberge, 1965). Some of them appear to be simple fractures caused by lateral compressive stresses in areas of converging flow. Once carried forward into a region of diverging flow, as in the case of Grand Chasms, the rift may be widened by a hinging of parts of the ice shelf with respect to flanking arms of land ice. The rifts perpendicular to the ice front are solely due to this kind of hinging. North of the eastern half of Grand Chasms is a transverse pattern of undulations with a wavelength of 2 to 3 km and an amplitude of about 10 m (Blaiklock and others, 1966). Swithinbank (1957b, p. 54) observed the progress of deepening in one such depression, and Robin (1958, p. 120) concluded that depressions form when diverging flow is too great to be accommodated by spreading of the ice in the normal course of thinning. That the depressions do not visibly become deeper is due to the compensating effect of snow accumulation, which tends to smooth all surface features. Indeed, their amplitude has been seen to decrease towards the ice front (personal commun. from P.D. Clarkson).

Note the sharp change in direction of the western group of flowlines as they cross the chasms. The change is paralleled by and must be related to the angle in the adjacent coastline of Berkner Island. Note also the 5-km westward displacement of the middle group of flowlines as they cross the central section of the long chasm. Crabtree and Doake (1980) analyzed the flow pattern and reported considerable scatter in velocity data at the ice front which, however, averaged out at about 1,240 m a⁻¹. Orheim (1979) reported a maximum velocity of 2 km a⁻¹ at the ice front due north of the widest part of the Grand Chasms.



W044-001 S079-001 W042-00
 11NOV73 C S78-14/W040-10 N S78-21/W039-50 MSS 7 R SUN EL18 AZ084 229-6632-N-I-N-D-IL NASA ERTS E-1476-08591-7 01

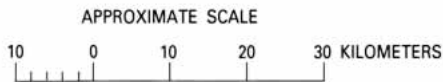


Figure 76. — Annotated Landsat 1 MSS image of Filchner Ice Shelf and the Grand Chasms. Spot soundings (in meters) from seismic sounding reported by Behrendt (1962) and airborne radio-echosounding (ScottPolarResearchInstitute, unpublished). NASA image (1476-08591, band 7; 11 November 1973; Path 194, Row 117) from the EROS Data Center, U. S. Geological Survey.

Berkner Island is the world's largest ice rise. It is 378 km long, 150 km wide, and rises to about 1,000 m above sea level. Like most ice rises, it is an independent ice cap built on a shoal on the continental shelf. The highest bedrock elevation found by Behrendt (1962) was 80 m below sea level.

Figure 77 shows the largest known area of ice rumpled (1,700 km²). The ice shelf is being forced over an extensive shoal on the sea bed. In adjusting to the underlying topography, the ice surface over the grounded area acquires a characteristic waviness, which, although subtle, is at the same time so conspicuous that it can be seen even in the infrared band of weather satellite pictures. A typical radio-echosounding profile over ice rumpled shows a thickening of the ice shelf where it is dammed against the upglacier side of a grounded area (Swithinbank, 1977, figure 8b). Smith (1986) found ice thicknesses of 1,000 m on the upglacier side of the obstruction, attenuating to 700 m as the ice slides over the grounded area. One controlling factor in this case is the diverging flow regime once the ice has moved through the constriction between Korff Ice Rise and Henry Ice Rise (Crabtree and Doake, 1980, 1986). Note from the 440-m and 430-m soundings that there is no significant change in thickness once the ice has ridden over the shoal. It looks as though a tongue of floating ice bypasses the grounded area on both sides close to the ice rises and a channel separates the northern portion of the ice rumpled from the main part to the south of it.

Recent data both from seismic sounding (personal commun. from L.D.B. Herrod) and radio-echosounding (personal commun. from F. Thyssen) suggest that the shallower depths indicated towards the top of the image may represent depths to a reflecting horizon below which lies a significant thickness of sea ice frozen onto the base of the freshwater ice.

Korff Ice Rise is 160 km long, 40 km wide, and about 500 m high. Ice thicknesses of up to 980 m have been measured by airborne radio-echosounding. The highest calculated or observed bedrock elevation is 115 m below sea level (Behrendt, 1962). Note the trail of crevasses downglacier (along the edge of the scene) from the northern tip of the ice rise. As yet we have no explanation for the several terraces along the east side of the ice rise; most ice rises show only a single break in slope at the grounding line. Note also the well-marked ice divide along the summit. Martin (1976) attempted to explain ice-rise ridges seen on Landsat images, and Martin and Sanderson (1980) suggested that their clarity could be due to differing reflective properties of the superficial snow on either side of the ridge line.

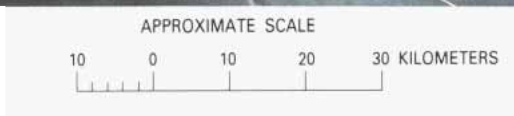
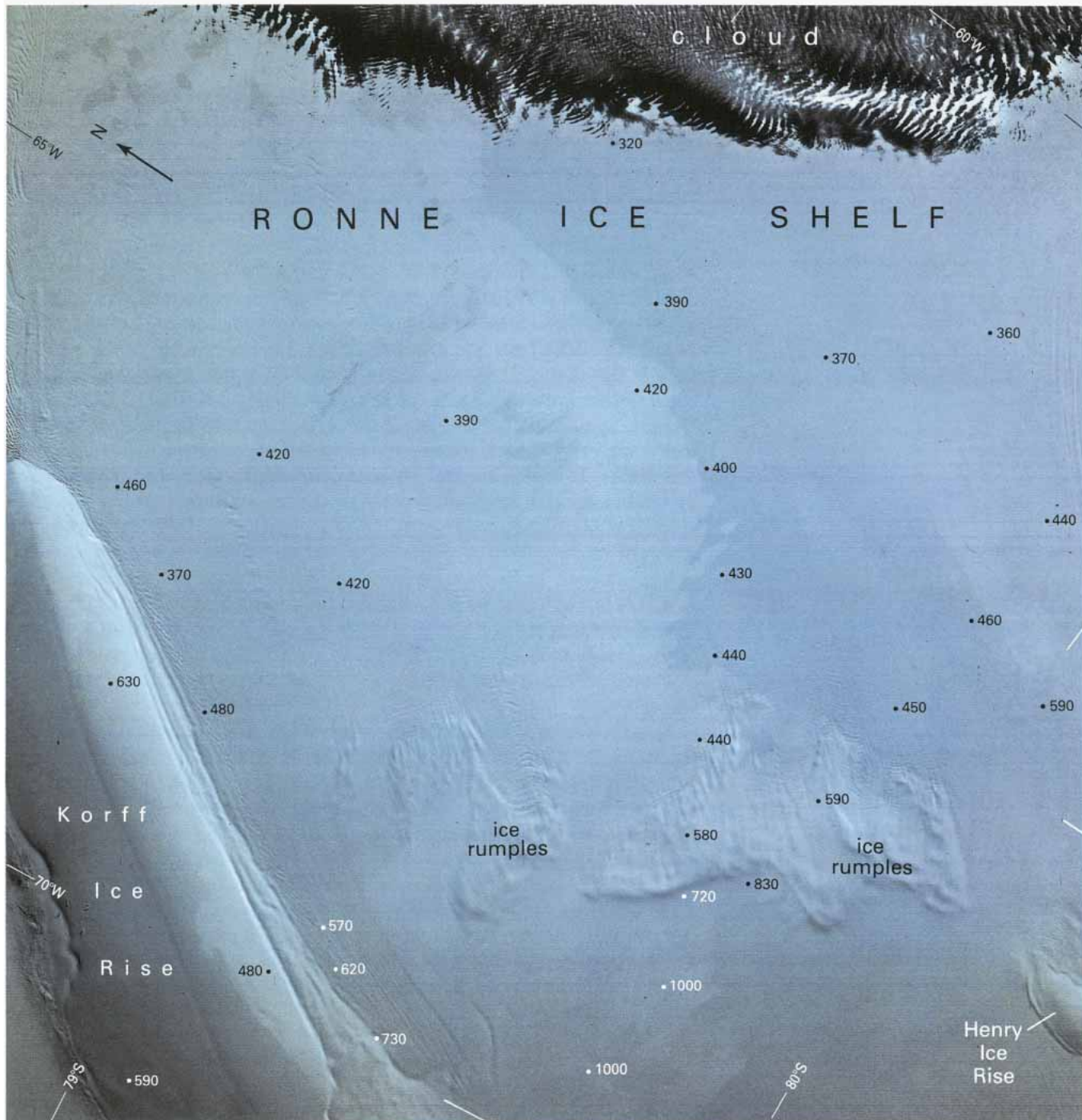


Figure 77. — Annotated Landsat 1 MSS digitally enhanced false-color composite image of Ronne Ice Shelf and Korff Ice Rise. Spot soundings (in meters) from seismic sounding reported by Behrendt (1962), airborne radio-echosounding (Scott Polar Research Institute, unpublished), and airborne radio-echosounding by British Antarctic Survey (unpublished). NASA image (1561–10121, Row 118) Courtesy of Baerbel K. Lucchitta and the Flagstaff (Arizona) Image Processing Facility, U.S. Geological Survey.

THE ANTARCTIC PENINSULA

Figure 78 is the northernmost of all the images selected for this chapter. It includes some of the largest areas of bare ground to be found anywhere in West Antarctica. Glaciologically it is an area of variable snow accumulation and prodigious summer melting at lower elevations. Mount Haddington, the summit of James Ross Island, rises to 1,628 m but is completely hidden beneath an ice cap that radio-echosounding has shown to be generally 200 to 300 m thick. A snow temperature of -13°C was measured at 10-m depth on the summit (Martin and Peel, 1978). Rabassa and others (1982) compiled a glacier inventory of James Ross and Vega Islands.

Apart from the ubiquitous highland and island ice caps, there are no glaciers of special significance in this scene. Esperanza is the principal Argentine station in Antarctica; it has been permanently manned since 1952. Vicecomodoro Marambio, a station on Seymour Island manned since 1969 by the Argentine Air Force, boasts one of only two bare-ground runways in the Antarctic capable of handling large transport aircraft; the other is at the Chilean Air Force Rodolfo Marsh station on King George Island in the South Shetland Islands. Seymour Island, because of its latitude and rich harvest of diverse fossils, is considered to be geologically unique and of great importance to paleontologists. In fact, the nearly ice-free island has been called “a ‘Rosetta Stone’ for paleontological study of the Southern Hemisphere” (Feldmann, 1984).

Figure 79 shows the southward continuation of the Trinity Peninsula plateau depicted in figure 78. At this latitude, the west coast of Graham Land is outside the climatic limit for ice shelves but the east coast is just within it. The small section of permanent ice in Prince Gustav Channel is the most northerly floating ice shelf in the Southern Hemisphere. The climatic limit for ice shelves coincides, on both sides of the peninsula, with the -5°C mean annual isotherm at sea level (Reynolds, 1981a).

It is impracticable to show surface contours on this image, because most of the relief throughout the area is contained within a single tortuous escarpment. The spine of Detroit Plateau maintains elevations of 1,500 to 2,000 m above sea level. From it, icefalls tumble into short, steep valley glaciers. Short, perhaps we should add, by Antarctic standards: Sjögren Glacier is substantially longer than the longest glacier in the European Alps.

The grounding line of Larsen Ice Shelf is fairly easy to pick out as a break in slope at the foot of the glaciers. In general, the ice shelf is around 400 m thick at the grounding line, tapering to 200 m or less at the ice front. The summer of 1978–79 was rather cool, and, in consequence, there are few signs of melting in this image (fig. 79). In warm summers, the ice shelf becomes covered with such a well-developed pattern of melt streams and lakes aligned along flowlines that it is impassable for surface travel. On the date of this image (February 1979) all that remains of the melt features is a curious group of five apparently dry ice dolines spaced around a central depression at the bottom of the image.



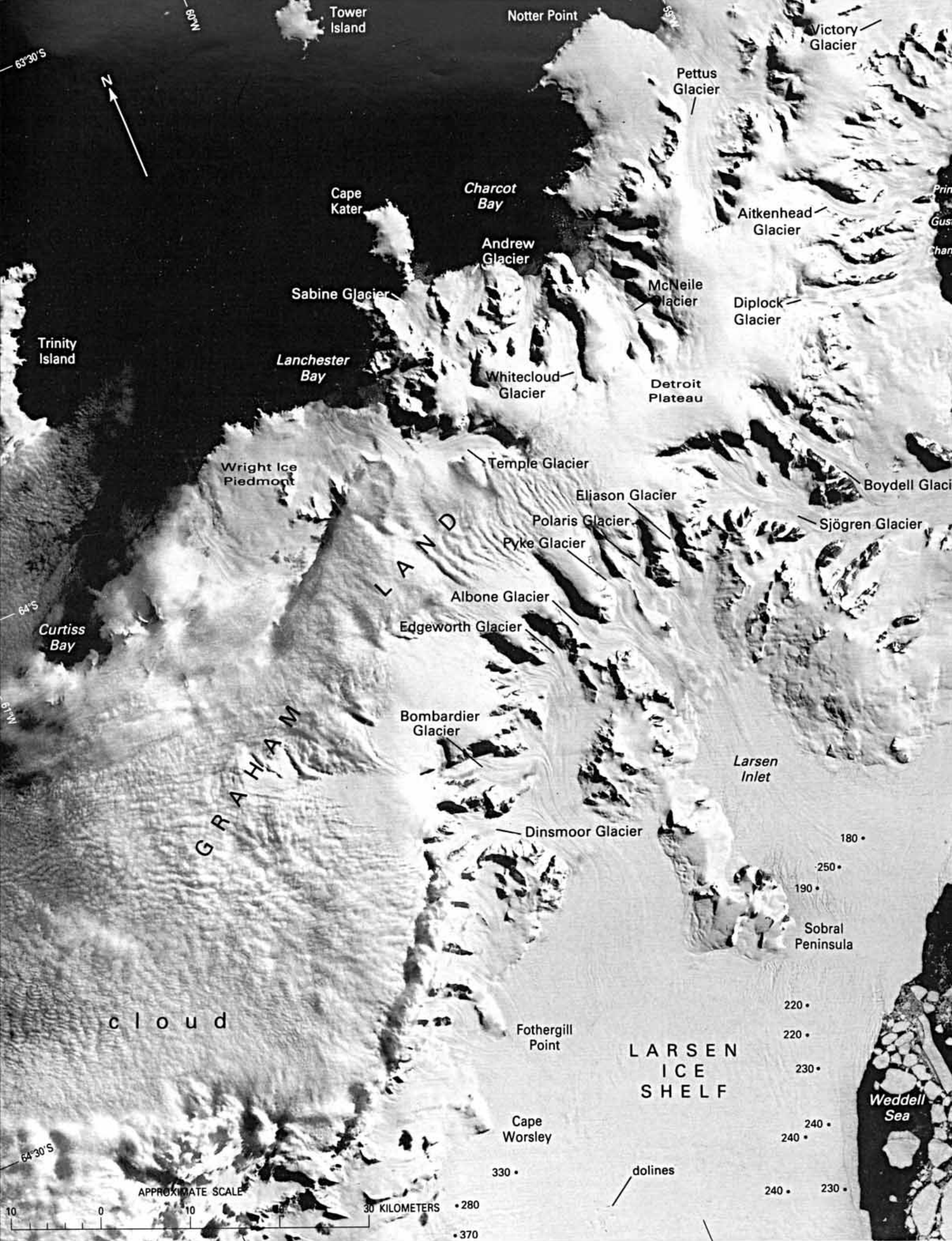
Figure 78. —Annotated Landsat 2 MSS image of the northern extremity of the Antarctic Peninsula. Surface contours (in meters) from British Antarctic Territory Geological Map, 1:500,000, sheet 2, Cambridge, British Antarctic Survey, 1979. Spot soundings (in meters) from airborne radio-echosounding by British Antarctic Survey (unpublished). Image center is at 63°51'S., 57°03' W. NASA image (2740-11454, band 7; 31 January 1977; Path 229, Row 105) from the EROS Data Center, U.S. Geological Survey.

Figure 80 represents a typical summer scene between latitudes 64° and 65°S. off the west coast of the Antarctic Peninsula in the vicinity of Anvers Island of Palmer Archipelago, Graham Land. There are a few small buildings on an island in the small cove that is filled with fast ice in the right center of the photograph. Known as Port Lockroy, the buildings date from the British Royal Navy Operation "Tabarin" of 1943–44, forerunner of the present British Antarctic Survey. They were occupied from 1944 to 1961.

Although it was discovered as long ago as 1909 by the French Antarctic Expedition (Charcot, 1911), the Marguerite Bay area of Graham Land remains comparatively unexplored in glaciological terms. The reasons should be evident from figure 81, a Landsat image acquired on 29 December 1978. Much of the terrain consists of precipitous mountain glaciers plunging from alpine peaks or plateaus into an ice-choked sea, of calving ice cliffs and hanging glaciers, of steep ice piedmonts furrowed by crevasses, of rugged massifs fringed by icefalls, and of an archipelago of ice-capped islands. In this scene, Marguerite Bay and the many fjord-like inlets are filled with level first-year fast ice in an advanced stage of deterioration. Only The Gullet is ice-free. The fast ice broke up two months after the scene was recorded; in some summers the sea becomes almost ice-free in March. An important characteristic of the area is that it contains two floating ice masses that could be the northernmost true ice shelves on the Pacific Ocean side of the Antarctic Peninsula. Muller Ice Shelf flows into Lallemand Fjord and extends a few kilometers on either side of the 125-m spot sounding; it was first recognized as an ice shelf during airborne radio-echosounding in 1975. Jones Ice Shelf extends for a few kilometers on either side of the 170-m spot sounding. Both ice masses are thin because they are at the extreme climatic limit for ice shelves; none would survive in the area but for the sheltered fjord environment. The mean annual temperature at sea level in the fjords is around -5°C (Reynolds, 1981a).

Clouds on the right-hand corner of figure 81 hide the ice-covered Graham Land plateau lying at elevations of 1,500 to 1,700 m. The spot soundings suggest that beneath the ice cap lies a true rock plateau at an elevation of about 1,000 m; its dissected western escarpment is exposed in the outlet-glacier valleys and on the massifs that separate them. Rothera on Adelaide Island is the principal British base of operations for ski-equipped aircraft used in support of research in the earth sciences; it was established in 1976. General San Martin is a weather station operated by the Argentine army; it, too, was established in 1976.

Figure 82 covers the northwest corner of Palmer Land, the northern entrance to George VI Sound, and a corner of Alexander Island (bottom left). At the top, Wordie Ice Shelf can be seen to be punctuated by ice rises and ice rumples, some of them better shown in figures 8 and 83. Although the area has been much traveled by topographic surveyors and geologists, a number of the ice rises and ice rumples were unknown and unsuspected before the advent of Landsat. An almost catastrophic disintegration of the ice shelf is shown by two former positions of the ice front. Swithinbank (1968) obtained radio-echosounding cross sections over Wordie Ice Shelf in 1966 but was unable to get results over most of the area lying between the 1966 and 1974 ice fronts. He attributed the difficulty to horizontal brine penetration from fractures extending from top to bottom of the ice shelf; evidently the seeds of destruction had already been sown in 1966, although the actual retreat did not take place until 1972 or 1973. Colvill (1977) found that 585 km² had calved at that time. This image of 3 February 1979 shows that a further 250 km² calved between 1974 and 1979 (Doake, 1982). The rifts



63°30' S
 N

64° S
 64°30' S

APPROXIMATE SCALE
 10 0 10 20 30 KILOMETERS
 • 280
 • 370

180 •
 250 •
 190 •
 220 •
 220 •
 230 •
 240 •
 240 •
 240 • 230 •

cloud

LARSEN
 ICE
 SHELF

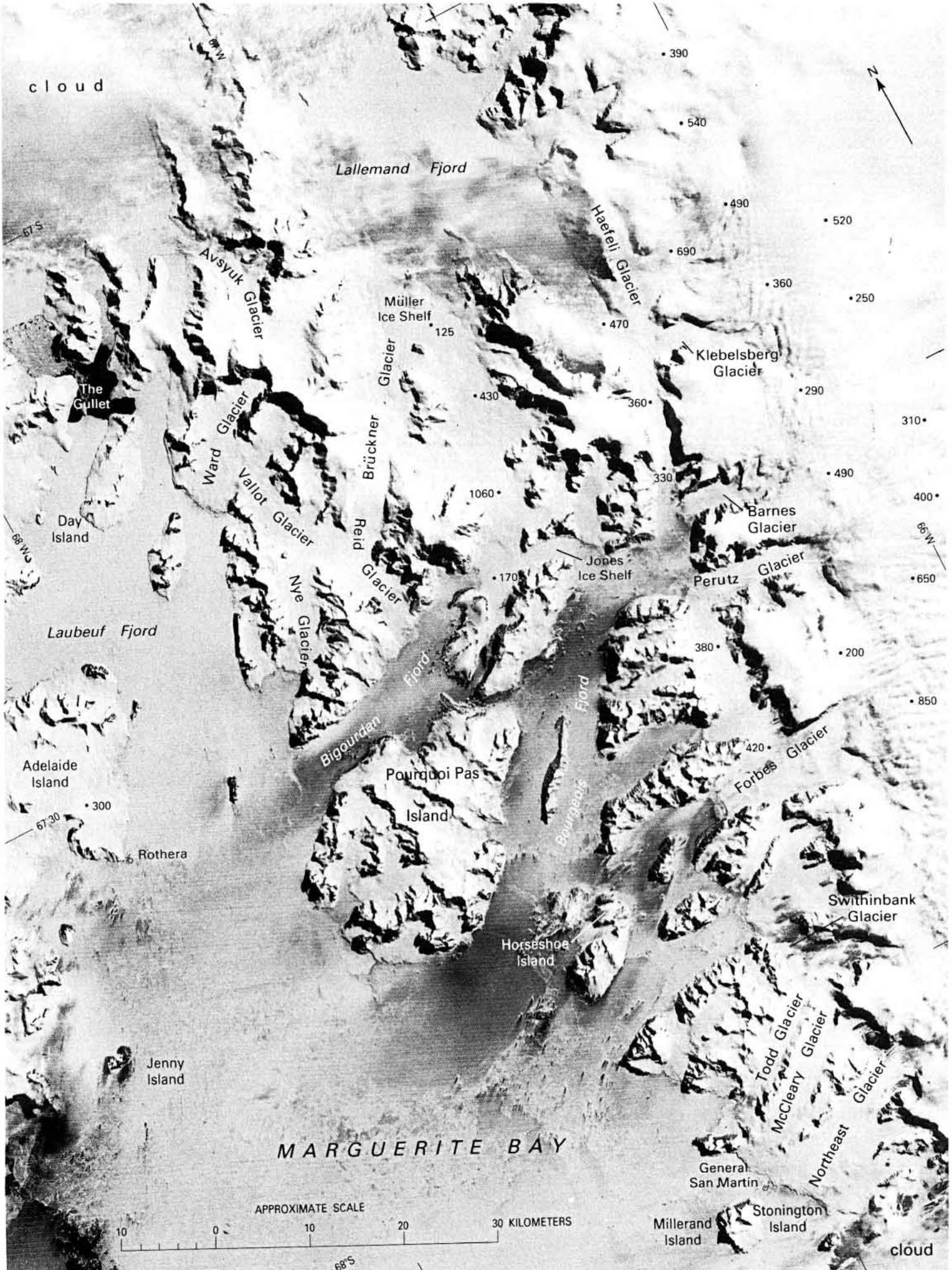
dolines

Weddell
 Sea

◁ **Figure 79.**—Annotated Landsat 3 MSS image of Graham Land plateau and the Larsen Ice Shelf. Spot soundings (in meters) from airborne radio-echosounding by British Antarctic Survey (unpublished). Image center is at 64°10'S., 60°W. NASA image (30352–12180, band 7; 20 February 1979; Path 232, Row 105) from the EROS Data Center, U.S. Geological Survey.

Figure 80.—Oblique aerial photograph of Doumer Island (foreground), Wiencke Island (right), and Anvers Island (left), taken from an altitude of 5,800 m on 16 November 1966, facing northeast. Mount Français, the highest peak on Anvers Island, rises to 2,822 m. U.S. Navy trimetrogon aerial photograph no. 15 (TMA 1819 F33) from the Antarctic Map and Photograph Library, U.S. Geological Survey.





cloud



Lallemand Fjord

• 390
• 540
• 490
• 520
• 690
• 360
• 250
• 910

Avsyuk Glacier

Müller Ice Shelf
125

Haefeli Glacier

Klebelsberg Glacier

The Gullet

Ward Glacier

Brückner Glacier

• 470

• 290

• 920

Day Island

Vallot Glacier

Reid Glacier

• 360

• 490

• 310

68°W

Laubeuf Fjord

Nve Glacier

1060

Barnes Glacier

• 400

Perutz Glacier

66°W

• 650

• 170

Jones Ice Shelf

• 380

• 200

• 850

Adelaide Island

Bigoundan Fjord

Pourquoi Pas Island

Forbes Glacier

• 420

67°30'

Rothera

Bourgeois Fjord

Swithinbank Glacier

Horseshoe Island

General San Martin

Jenny Island

MARGUERITE BAY

Todd Glacier

McCleary Glacier

Northeast Glacier

APPROXIMATE SCALE
0 10 20 30 KILOMETERS

Millerand Island

Stonington Island

cloud

68°S

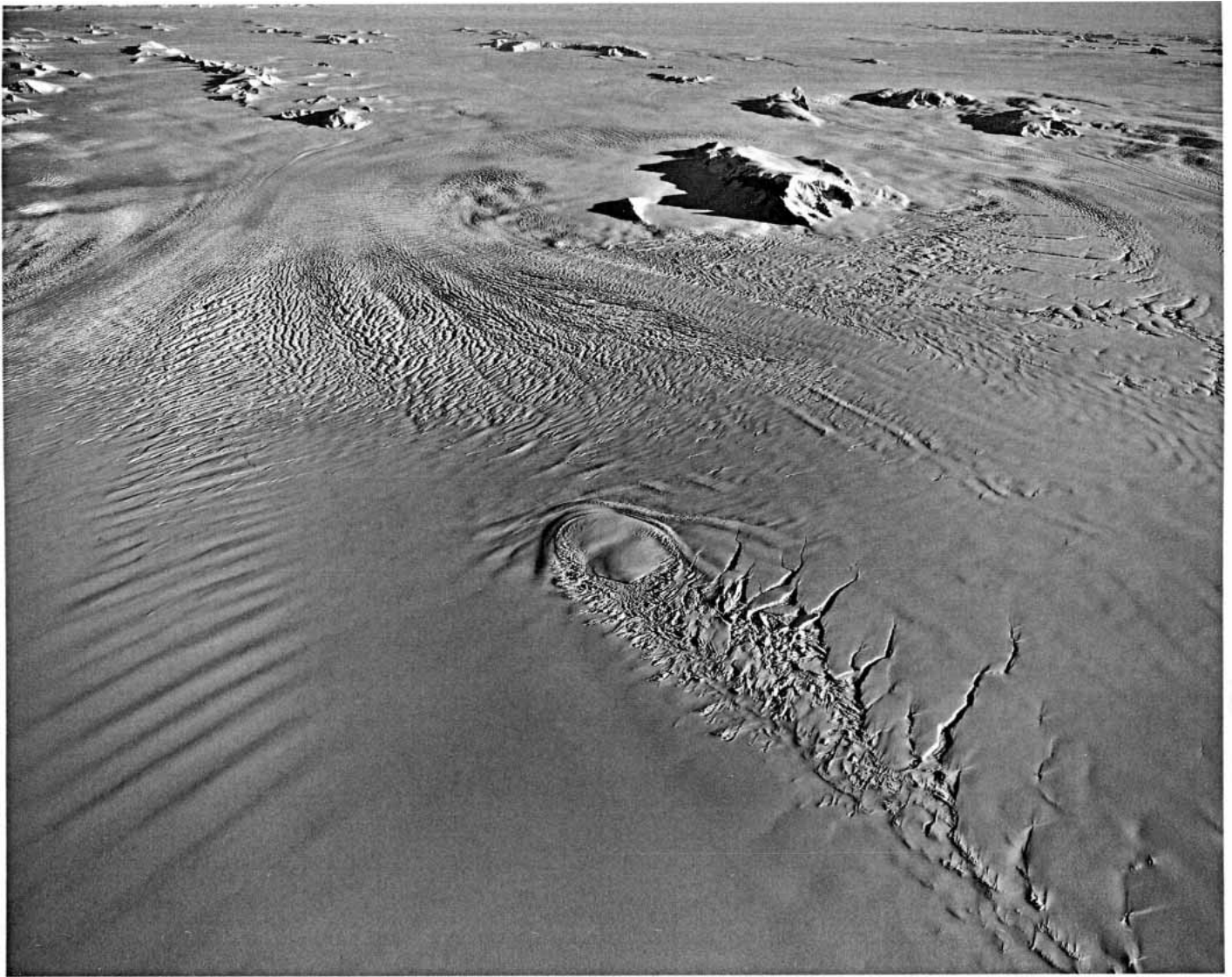
Figure 81.—Annotated Landsat 3 MSS image of Marguerite Bay and the west coast of Graham Land. Spot soundings (in meters) from airborne radio-echosounding by British Antarctic Survey (unpublished). Image center is at 67°35'S., 67°05'W. NASA image (30299-J12250, band 7; 29 December 1978; Path 233, Row 108) from the EROS Data Center, U.S. Geological Survey.

upstream of Buffer Ice Rise are particularly significant in that it is generally believed that longitudinal stresses in this region must be compressive, so that disintegration is unlikely before the ice rise has disappeared (Thomas and others, 1979, p. 355). Wordie Ice Shelf, however, has already retreated past a number of ice rises and looks set to retreat further. Perhaps accelerated bottom melting (Robin, 1979) or even surface meltwater penetration (Hughes, 1982) has led to significant thinning. Mercer (1978) suggested that the breakup of ice shelves in the Antarctic Peninsula was a warning sign of what might become a CO₂-induced atmospheric warming leading to disintegration of the West Antarctic ice sheet. The image also reveals a recession of the front of the George VI Ice Shelf between 1974 and 1979 that appears to continue a trend dating from the 1930's (Doake, 1982).

Figure 83 shows Wordie Ice Shelf with Buffer Ice Rise (fig. 82) in the foreground. Being only 3 km across, Buffer Ice Rise is on the conceptual borderline between an ice rise and ice rumpled. As with McDonald Ice Rumples (fig. 91), it is possible that while most of the ice is deflected to flow around the grounded area, some ice flows across it. A series of splayed anticlines on the upstream side of the feature closely resembles, in plan view, the shock waves revealed by schlieren photographs of a projectile in flight. The two situations are analogous although the velocities differ by 7 orders of magnitude. Note that 'while there is a field of giant crevasses upstream of the grounded feature, there are no rifts such as on the downstream side of it. Now contrast this 1966 picture with the 1979 satellite image (fig. 82) in which there are a whole series of new rifts superimposed on the field of giant crevasses upstream of the grounded feature. Evidently the breakup of Wordie Ice Shelf is likely to continue. That we can readily perceive glacier changes by comparing an oblique aerial photograph taken from an altitude of 6 km with a satellite image taken from an altitude of 915 km offers eloquent testimony to the glaciological importance of Landsat. Whereas the potential value of Landsat for time-series studies of glacier fluctuations became evident after the launch of Landsat 1 (Swithinbank, 1973b), we can now see the value of comparing even the earliest aerial photographs of glaciers with later satellite imagery. Thus we already have the means, for some parts of the world at least, to study glacier fluctuations during the last half century without setting foot near any glacier.

Figure 84 shows two tidal sea lakes on the east coast of Alexander Island in a situation comparable with that of the Schirmacher Hills area shown in figure 65. George VI Ice Shelf in the foreground flows away from the camera towards Ablation Lake (center) and Moutonnee Lake (left). The ice shelf dissipates from a thickness of 150 m directly beneath the aircraft to nothing where it melts into the lake. Both longitudinal and transverse flow features can be seen on the glacier tongue. The tidal nature of the lakes is revealed by tidal cracks paralleling the shore. Heywood and Light (1975) studied Ablation Lake (named after Ablation Point, nearby), finding it to be more than 117 m deep and covered with freshwater ice 3 m thick. Salinity measurements revealed that the top 55 m of water in the lake was fresh (0.1–1.0‰). The halocline was very steep, so that between 66.00 m and 66.25 m the salinity rose from 18 to 31.5‰. Stable density stratification is a characteristic feature not only of Antarctic sea lakes (Simonov, 1971) but also of Arctic sea lakes (Hattersley-Smith and others, 1970). The geomorphology of the Ablation Point massif (center) was described by Clapperton and Sugden (1983).

Figure 85, which is located on the east coast of Alexander Island south of figure 84, shows Spartan Glacier (center foreground), a 6.3-km² local glacier flowing into George VI Ice Shelf. It ranges in altitude



◁ **Figure 82.**—Annotated Landsat 3 MSS image of northern Palmer Land and Wordie Ice Shelf. Ice-surface contours (in meters) modified from British Antarctic Territory Geological Map 1:500,000, sheets 4 (1981) and 5 (1982), Cambridge, British Antarctic Survey. Spot soundings (in meters) from airborne radio-echosounding by British Antarctic Survey (Smith, 1972, supplemented by unpublished data). The 1966 ice front is from Antarctica Sketch Map 1:500,000, Palmer Land, North Part, U.S. Geological Survey, 1979. The 1974 ice front is from Landsat MSS image 1532-12325, band 7 (6 January 1974; Path 233, Row 109). Image center is at 69°30'S., 67°35'W. NASA image (30335-12253, band 7; 3 February 1979; Path 233, Row 109) from the EROS Data Center, U.S. Geological Survey. See also figures 8 and 83.

△ **Figure 83.**—Oblique aerial photograph of Buffer Ice Rise and the mouth of Fleming Glacier, Graham Land, taken from an altitude of 6,000 m on 28 November 1966, facing southeast. The camera position is marked on figure 82. U.S. Navy trimetrogon aerial photograph no. 73 (TMA 1835 F33) from the Antarctic Map and Photograph Library, U.S. Geological Survey.

from 450 m to 40 m above sea level, has an average surface slope of 5.1° , and an average surface velocity of 6.3 m a^{-1} (Wager and Jamieson, 1983). When ice depths were measured in 1972 (Wager, 1982), no other glacier in the world had been subjected to such thorough sounding by means of a radio-echosurvey. The ice, water, and energy balances of the glacier were determined on the basis of a variety of observations made over a period of 2 years (Jamieson and Wager, 1983).

George VI Sound (fig. 86) is a 500-km-long trench that separates Alexander Island from Palmer Land. It is filled almost throughout its length by George VI Ice Shelf. Unlike most ice shelves, this one flows in two directions from an ice divide. Radio-echosounding (Switbank, 1968) has established that it is afloat and that it varies in thickness from 100 m at the northern ice front to about 500 m at the ice divide (lying south of the area shown on the image). In normal circumstances an ice shelf can be expected to flow from thicker to thinner ice in the direction of the thickness gradient. Here, however, the ice-thickness isopleths trace a strangely contorted pattern far removed from a straightforward south to north thinning. Stranger still, the pattern of flow features that is made conspicuous by surface meltwater indicates that the ice is moving not along the sound but across it. That the predominantly east-west alignment of melt features does coincide with the direction of ice movement has been proven by classical survey methods (Bishop and Walton, 1981; Pearson and Rose, 1983). While the principal sources of this part of George VI Ice Shelf are Millett, Bertram, and Ryder Glaciers flowing from Palmer Land, significant contributions from Grotto and Uranus Glaciers on the Alexander Island side can be seen to oppose the general direction of flow.



Figure 84.— Annotated oblique aerial photograph of tidal sea lakes, George VI Ice Shelf, taken from an altitude of 5,800 m on 4 November 1966, facing west. The camera position is marked on figure 86. U.S. Navy trimetrogon aerial photograph no. 53 (TMA 1800 F31) from the Antarctic Map and Photograph Library, U.S. Geological Survey.



Figure 85.—Annotated oblique aerial photograph of Spartan Glacier, Alexander Island, taken from an altitude of 5,800 m on 4 November 1966, facing west. The camera position is marked on figure 86. U.S. Navy trimetrogon aerial photograph no. 44 (TMA 1800 F31) from the Antarctic Map and Photograph Library, U.S. Geological Survey.

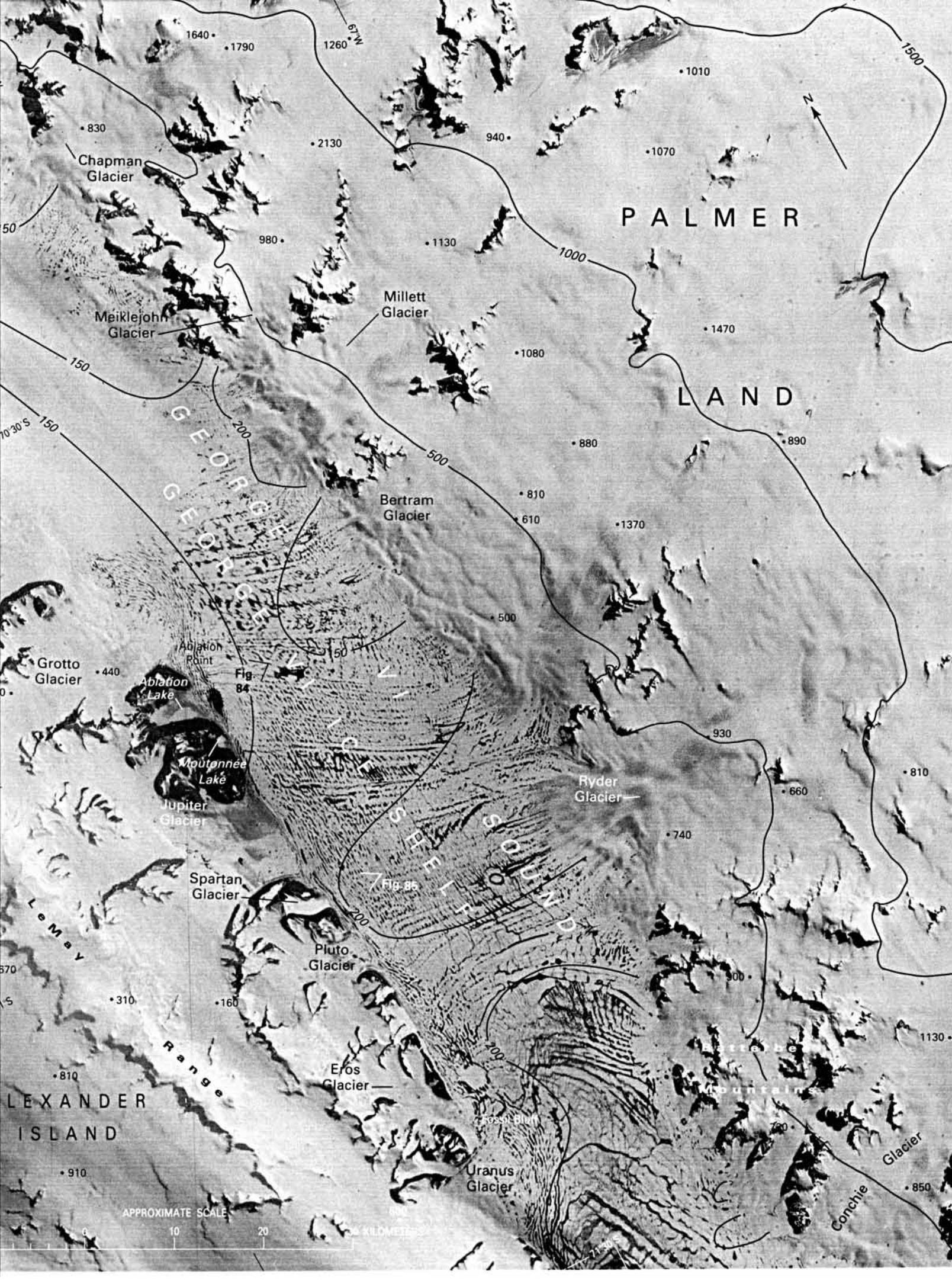


Figure 86.—Annotated Landsat 1 MSS image of Palmer Land and George VI Ice Shelf. Ice-surface contours (in meters) from British Antarctic Survey (unpublished). Ice-thickness isopleths (in meters) on George VI Ice Shelf from British Antarctic Territory Ice Thickness Map 1:500,000, Alexander Island, Cambridge, British Antarctic Survey, 1983. Image center is at 70°08'S., 67°30' W. NASA image (1170-12251, band 7; 9 January 1973; Path 231, Row 110) from the EROS Data Center, U.S. Geological Survey. See also figures 84, 85, and 87.

No ice can cross a flowline, and because it does not flow on to Alexander Island, the ice must discharge either through the top or the bottom surfaces of the ice shelf. Bishop and Walton (1981) report that in spite of the melt pools, the top surface net mass balance is positive, while Reynolds (1981b) considers it possible that parts of the ice shelf have a marginally negative balance. All investigators agree, however, that the principal losses are through bottom melting. Bishop and Walton (1981) deduced bottom melt rates of up to $4,500 \text{ kg m}^{-2} \text{ a}^{-1}$, while Potter and others (1984) calculated that the average equilibrium bottom melt rate is $2 \text{ m}^3 \text{ m}^{-2} \text{ a}^{-1}$ ($1,800 \text{ kg m}^{-2} \text{ a}^{-1}$). If it is in mass balance, this small ice shelf alone provides $53 \text{ km}^3 \text{ a}^{-1}$ melt from its base compared with a total for Antarctica of only $320 \text{ km}^3 \text{ a}^{-1}$.

Stephenson and Fleming (1940) and Wager (1972) ascribed the exceptional amount of surface meltwater to a local decrease in albedo caused by wind-blown rock dust, while Pearson and Rose (1983) noted that it is evidently also due to meltwater flowing from nunataks onto the ice shelf. Reynolds (1981b), however, attributed the lakes to the saturation of snow overlying the impermeable ice that is known to occur here at an unusually shallow depth. Because the area of melt lakes coincides with the area in which flowlines are directed predominantly towards Alexander Island instead of along George VI Sound, the impermeability could be due to densification of the ice shelf through abnormal compressive strains in the manner proposed by Crary and Wilson (1961). Reynolds (1981b) calculated that about 0.4 km^3 of water drains into the sea through moulins and tidal cracks each summer.

The area of figure 87 overlaps that of figure 86 on the west but shows a degree of fine detail that is almost without equal in Landsat MSS images of Antarctica. Unfortunately, interpretation is complicated in places by thin clouds and cloud shadows. Central Alexander Island is characterized by a series of parallel north-south-trending mountain ranges. Summit levels reach about 3,000 m above sea level in the Douglas Range at the top of the image. Glacier-filled trenches between the main ridges extend to depths of 500 to 800 m below sea level. George VI Ice Shelf separates Alexander Island from Palmer Land, and Wilkins Ice Shelf marks the topographic western boundary of this part of Alexander Island. The extensive ice piedmonts in this scene are easily distinguished from ice shelves by their hummocky surface topography. The ice-shelf grounding line coincides with the break in slope at the foot of the ice piedmonts. The front of the George VI Ice Shelf can be seen trending 60° east of north from the southern extremity of the 4-by-11-km recurring polynya at the top of the picture; beyond the ice front is multi-year fast ice. Although there are a great many meltwater lakes on low-lying tracts of ice piedmont and on the adjacent ice shelf, there are only two places where the sea shows through. The 2-by-2-km lake at the northeast end of Dorsey Island is one of them; the other can be seen 25 km west of Dorsey Island. Sea lakes at the inland boundary of an ice shelf are uncommon (figs. 65 and 84), but sea lakes surrounded by ice shelf are very rare. This is a reminder that here, too, we are at the climatic limit of ice shelves. Although Wilkins Ice Shelf is 350 km southwest of the ice shelves in figure 81, the trend of the isotherms is such that the mean annual temperature at sea level is little different (-8°C). A hole drilled with a hand auger in January 1972 penetrated soaked snow and found a water table at a depth of 5.5 m. The presence of a number of ice rises with dimensions on the order of 1 km indicates that much of the ice is unusually thin. The failure of several attempts at radio-echosounding could indicate that parts of the ice shelf are brine-soaked to sea level.

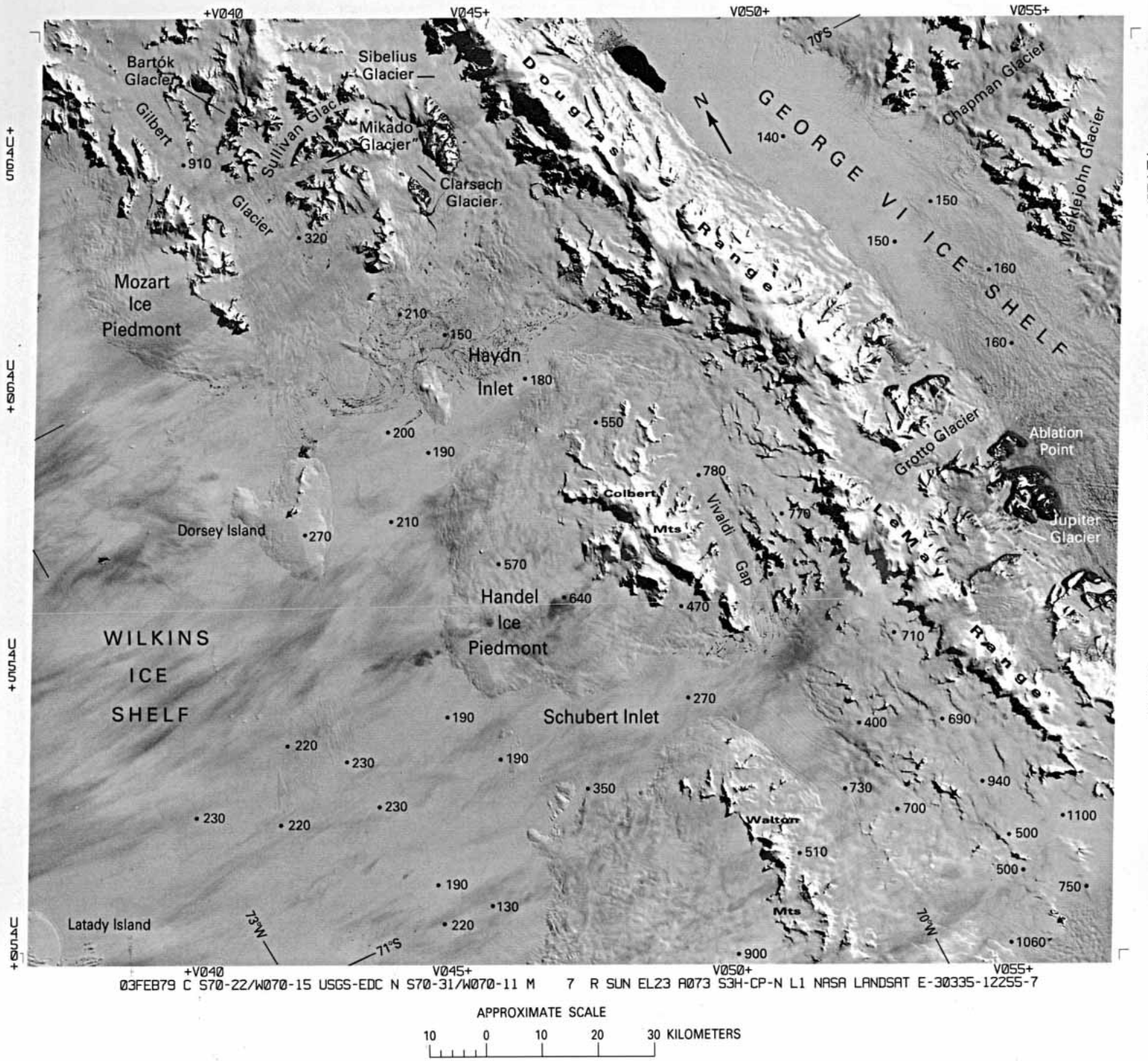


Figure 87.—Annotated Landsat 3MSS image of Alexander Island. Spot soundings (in meters) from airborne radio-echosounding by British Antarctic Survey (unpublished). NASA image (30335-12255, band 7, 3 February 1979; Path 233, Row 110) from the EROS Data Center, U. S. Geological Survey.

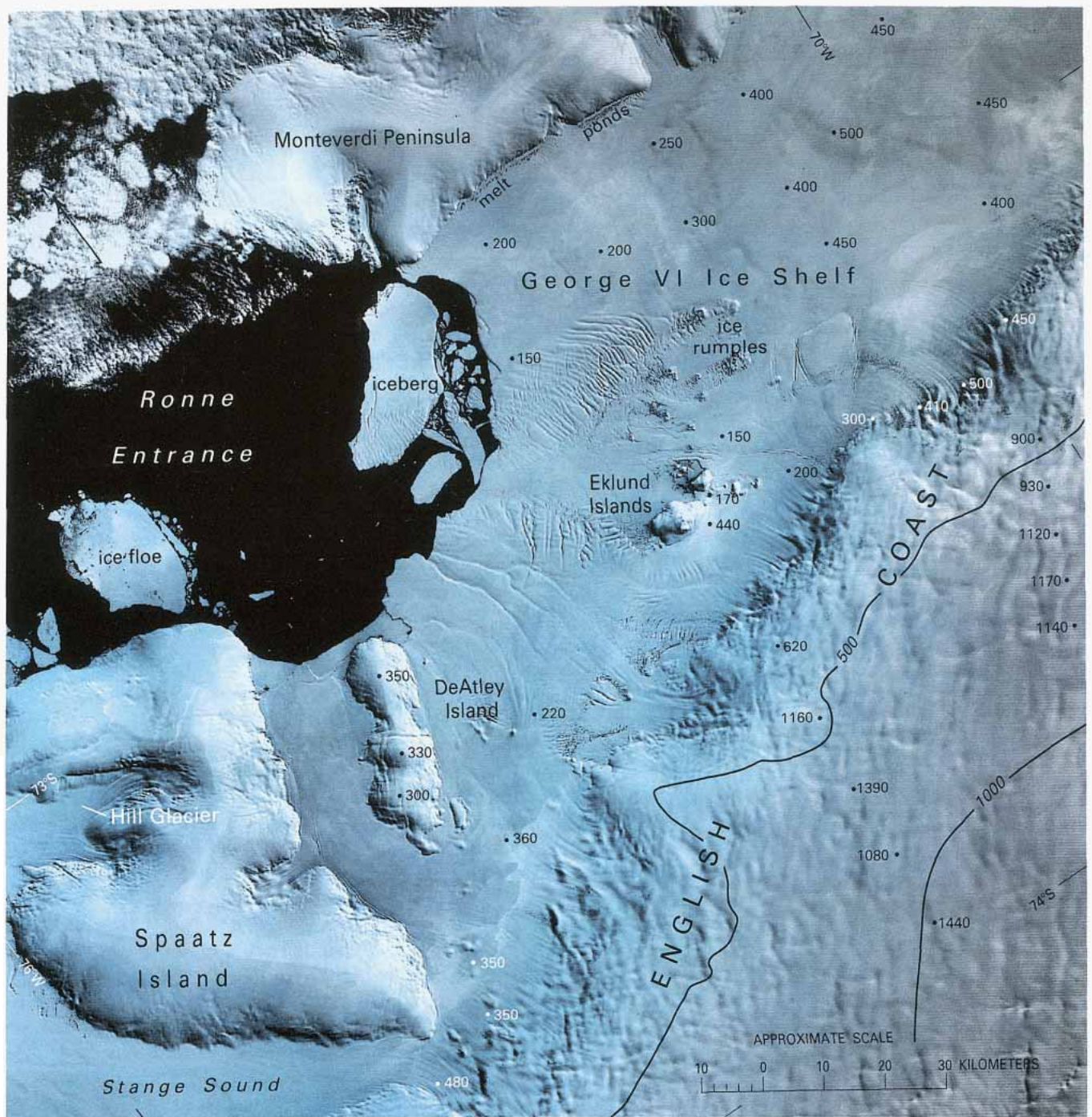
THE PACIFIC OCEAN SECTOR

Ellsworth Land and Ellsworth Mountains

Figure 88 is centered about 300 km south of figure 87 and shows evidence of the higher latitude climatic conditions. Although the color-composite image was recorded at the height of summer, the only melt-water visible is confined to a line of small ponds in the marginal depression where George VI Ice Shelf meets the Monteverdi Peninsula of Alexander Island. A group of icebergs newly calved from the southwestern edge of the George VI Ice Shelf show an almost jigsaw-puzzle fit with the remaining ice front. The southern half of the ice shelf near Eklund Islands is disturbed by the presence of ice rumples. Spaatz and DeAtley Islands are ice rises, and like most ice rises, they are independent ice caps built on shoals. In contrast, Eklund Islands are true islands with bedrock showing at and above sea level. They block the general northwesterly flow of ice from English Coast, so that there is an extensive sea lake on the downstream (northwestern) side. In this scene the lake is concealed by ice probably only about 1 m thick, but in some summers it is ice-free (Fuchs, 1951). Ronne Entrance is a recurring polynya; weather satellite pictures indicate that offshore winds keep it ice-free throughout the winter.

More than any other image we have seen, figure 89 shows what a wealth of information can reside in the ice-surface topography revealed by Landsat if radio-echosoundings are available to interpret it. Moreover, there are general relationships between ice thickness and the wavelength of surface undulations which allow rough estimates of ice thickness to be made at a glance (Budd, 1970; Budd and Carter, 1971). Swithinbank (1977) published an observed cross section of the ice sheet adjacent to Haag Nunataks and mapped ice thickness and bedrock contours for the area. In general, the amount of surface topography varies inversely with ice thickness. Each of the conspicuous ice escarpments was shown to overlie a bedrock escarpment. The shallowest ice was found under the steepest slopes. The narrow linear feature 15 km west of Haag Nunataks coincides with a subglacial trench, presumably of structural origin. Note the curving flowlines that trace the path of the ice stream draining south from Fowler Ice Rise. The right-lateral flowline reaches three quarters of the way across Carlson Inlet towards Fletcher Ice Rise, a clear indication that very little ice flows from the left side of the picture into Carlson Inlet.

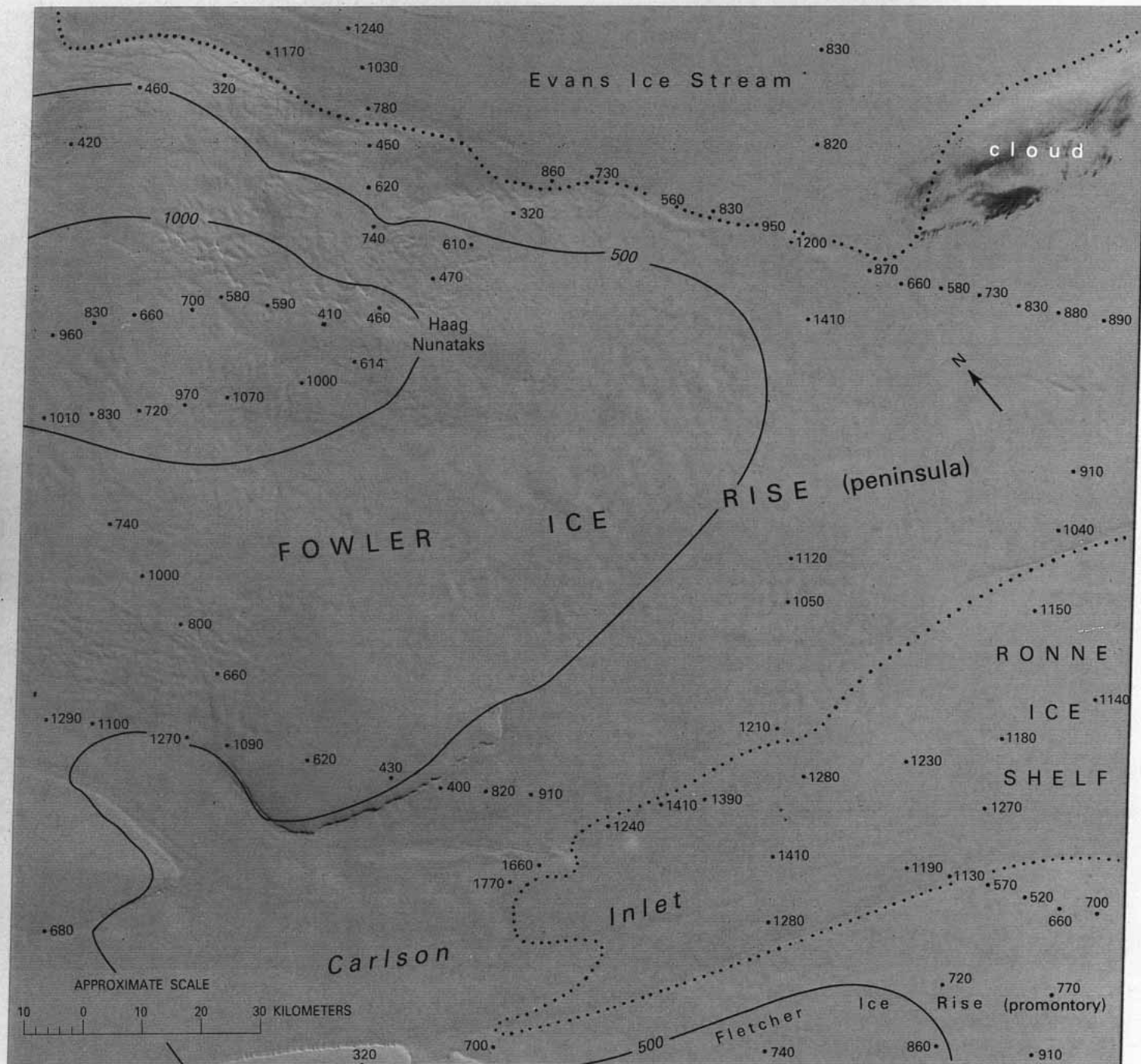
Figure 90 shows the Sentinel Range, Ellsworth Mountains, which includes the Vinson Massif (4,897 m), the highest mountain in Antarctica, and, only 60 km to the east, the thickest floating ice sheet in the world (2,000 m). This adds up to a peak to trough relief of 7 km, a scale unparalleled on any other continent. Only a few oceanic trenches have greater relief. The ice plateau on the west side of the mountain range lies at 1,500 to 2,000 m above sea level. Thus, like most mountain ranges in Antarctica, the Ellsworth Mountains dam the natural drainage of the ice sheet, sending it both northward and southward



from an ice divide located close to the bottom left-hand corner of this image. Rutford Ice Stream drains all the ice diverted round the north end of the mountains.

In contrast to grounding lines indicated on other images in this chapter, the positions of which are speculative and generally based on morphological indications alone, the central portion of Rutford Ice Stream has been extensively researched on the ground (Stephenson, 1984). Stephenson and Doake (1982) found that the grounding line of the Rutford Ice Stream was not a simple hinge across the ice stream but instead curved sinuously around what may be local pinning points. The velocity measured over a longitudinal stake network near the center of the glacier was, however, fairly uniform, decreasing from 400 m a⁻¹ to 380 m a⁻¹ over a distance of 40 km. It now seems highly likely that

Figure 88.—Annotated Landsat 1 MSS digitally enhanced false-color composite image of the English Coast of Palmer Land. Ice-surface contours (in meters) from British Antarctic Survey (unpublished). Spot soundings (in meters) from airborne radio-echosounding by British Antarctic Survey (unpublished). NASA image (1170–12260, bands 4, 5, and 7; 9 January 1973; Path 231, Row 112) courtesy of Baerbel K. Lucchitta and the Flagstaff (Arizona) Image Processing Facility, U.S. Geological Survey.



03FEB74 C S77-34/4078-22 N S77-34/4078-22 MSS 4082-001 5078-001 4089-001
7 R SUN ELI7 RZ088 225-7805-A-I-N-D-IL NASA ERTS E-1560-11485-7 01

Figure 89.—Annotated Landsat 1 MSS image of Fowler Ice Rise and Carlson Inlet. Surface contours (in meters) and probable grounding line (dotted line) from Swithinbank (1977). Spot soundings (in meters) from airborne radio-echosounding by British Antarctic Survey (unpublished). NASA image (1560-11485, band 7; 3 February 1974; Path 226, Row 116) from the EROS Data Center, U.S. Geological Survey.

most ice-stream and calving-glacier grounding lines will be found, on close investigation, to be sinuous rather than straight. It is significant that the thinnest spot sounding on the grounded part of Rutford Ice Stream (1,670 m) coincides with a topographic rise visible on the image. It may also be significant that after some 50 years afloat and 20 km of cumulative movement, the ice stream appears to have adjusted itself to a uniform cross-sectional thickness of around 1,650 m. Crabtree and Doake (1982) calculated the area of the drainage basin of Rutford Ice Stream to be $40,500 \pm 4,000 \text{ km}^2$ and mass flux at the grounding line to be $18.5 \pm 2.0 \text{ Gt a}^{-1}$ ($20.3 \text{ km}^3 \text{ a}^{-1}$).

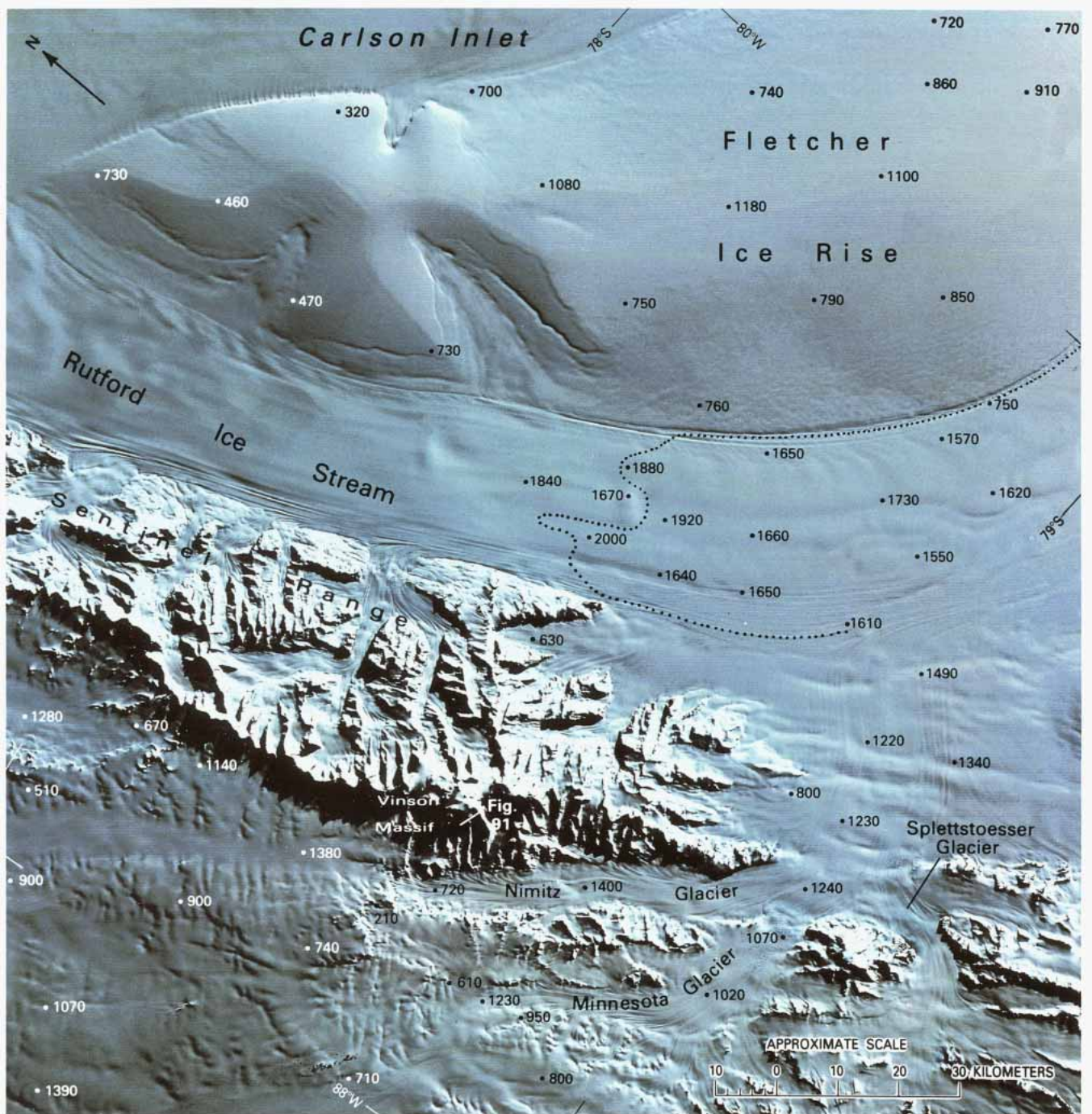


Figure 90.—Annotated Landsat 1 MSS digitally enhanced false-color composite image of the Sentinel Range, Ellsworth Mountains, and Rutford Ice Stream. Spot soundings (in meters) from airborne and surface radio-echosounding by British Antarctic Survey (unpublished). The dotted line represents the inferred position of the grounding line extrapolated from Stephenson and Doake (1982). NASA image (1560–11492, bands 4, 5, and 7; 3 February 1974; Path 225, Row 117) courtesy of Baerbel K. Lucchitta and the Flagstaff (Arizona) Image Processing Facility, U.S. Geological Survey. See also figure 91.



Figure 91.—Annotated oblique aerial photograph of the Sentinel Range, Ellsworth Mountains, taken from an altitude of 5,600 m on 15 December 1959, facing north-northwest. The camera position is marked on figure 90. The view is across Vinson Massif, which includes the highest point in Antarctica (4,897 m), to Mount Tyree in the background. U. S. Navy trimetrogon aerial photograph no. 263 (TMA 570 F33) from the Antarctic Map and Photograph Library, U.S. Geological Survey.

Nimitz and Minnesota Glaciers drain ice from the plateau to the west of the mountains. The 1,380-m sounding at the head of Nimitz Glacier coincides with surface indications of a subglacial trench that can be followed in Landsat imagery for a further 100 km north-northwest to an area that is well beyond the present ice divide. The 1,230-m sounding on Minnesota Glacier likewise indicates the depth of a trench that can be followed upstream for a further 150 km. Splettstoesser Glacier, in contrast, is almost starved of ice from inland.

Figure 91 is a view northward along the trend of the Sentinel Range. The ice divide runs along the western (left side) ridge from which the highest peaks in Antarctica look down on a generally eastward-flowing network of valley glaciers tributary to Rutford Ice Stream, which can be seen in the right background. Webers and Splettstoesser (1982) have compiled a geological bibliography of the Ellsworth Mountains.

Marie Byrd Land

Figure 92 shows one of the principal ice streams of West Antarctica. Whereas a majority of the ice streams of West Antarctica discharge into Ross or Ronne Ice Shelves and thereafter lose their identity, Pine Island Glacier is afloat for only about 80 km before it calves into Pine Island Bay. The grounding line passes close to the 1,400-m sounding (Crabtree and Doake, 1982). A comparison of ice-front positions between this image and a sketch map based on 1966 aerial photographs shows a retreat or calving of about 10 km between 1966 and 1973. Comparison with a 13 February 1975 MSS image (2022-13582, band 7; Path 249, Row 113) indicates an ice-front velocity averaging 2.4 km a^{-1} (Lindstrom and Tyler, 1985). Crabtree and Doake (1982) calculated the drainage basin of Pine Island Glacier to be $214,000 \pm 20,000 \text{ km}^2$ and mass flux at the ice front to be $25 \pm 6 \text{ Gt a}^{-1}$ ($28 \text{ km}^3 \text{ a}^{-1}$).

Referring to this area as “the weak underbelly of the West Antarctic ice sheet,” Hughes (1973, 1975, 1977) has drawn attention to the potential instability of the ice sheet arising from the presence of major ice streams largely unprotected from the sea by ice shelves. Pine Island Glacier and the Thwaites Glacier, 200 km further west, are the two biggest ice streams draining any part of the northern margin of the ice sheet between longitudes 90° and 160°W . In contrast to the East Antarctic ice sheet, much of West Antarctica is covered by what is called a marine ice sheet, that is to say an ice sheet resting on a rock basement that is well below sea level. T.J. Hughes’ ice sheet-disintegration model (Stuiver and others, 1981) indicates that this may be the area most likely to control any collapse of the West Antarctic ice sheet. Surging could produce a basal water layer that would uncouple the ice from its bed and thus draw down the surface level of the ice sheet. In the absence of a high bedrock sill to prevent it, the grounding line could migrate inland until ultimately the whole marine portion of the ice sheet is converted into an ice shelf. Hughes (1973) and Thomas and others (1979) go so far as to suggest that today the northern part of the ice sheet could already be collapsing. The exceptionally low ice-surface gradient implied by the presence of only one surface contour within the area of this scene could lend support to their hypothesis. Crabtree and Doake (1982), however, were able to model the longitudinal profile of Pine Island Glacier by using steady-state assumptions and found no evidence to suggest instability.

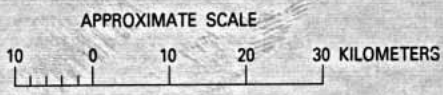
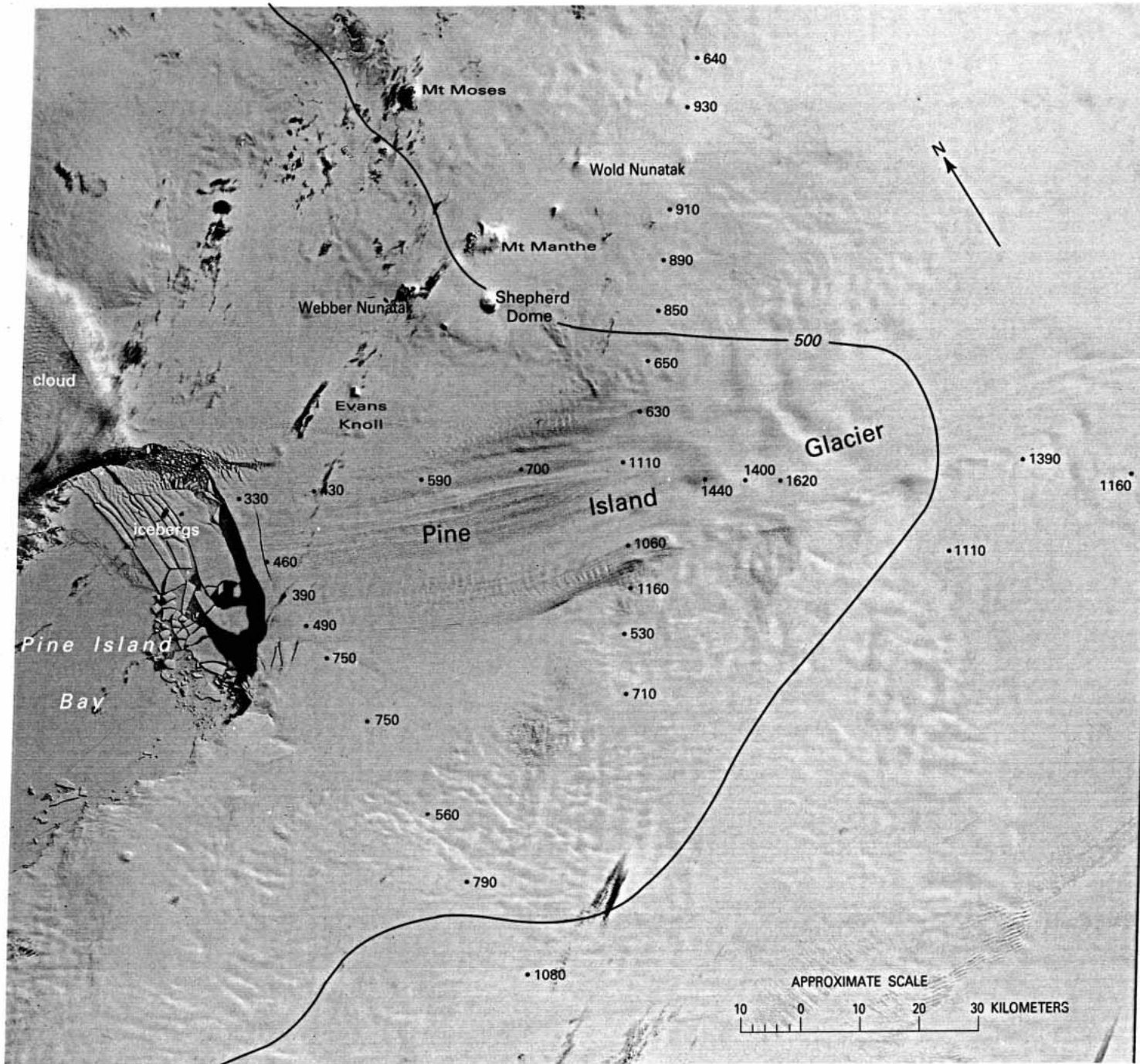
Figure 93 is a Landsat image mosaic that almost overlaps the area shown in figure 92, being only 200 km to the west of Pine Island Glacier. Thwaites Glacier projects farther out to sea than any other single glacier on Earth. Discovered by U.S. Navy Operation Highjump in 1946–47 (Byrd, 1947), it has remained in place ever since although clearly broken in two places. The iceberg tongue at some time rotated 40° to the west before grounding on shoals (Holdsworth, 1985). The spot soundings beside the 500-m surface contour indicate that the main part of the glacier occupies a deep trench that extends inland well below sea level. Southard and MacDonald (1974) and MacDonald (1976) noted a 60 percent increase in the area of Thwaites Iceberg Tongue between 1965 and 1974. Hughes (1977) has drawn attention to the possible surge history of the glacier, and the exceptionally long glacier tongue could indeed be the product of a recent surge. Thomas and others (1979) quote photogrammetric estimates by R.J. Allen of velocities greater than 2 km a^{-1} that, in their view, would be “approximately the velocity

Figure 92.—Annotated Landsat 1 MSS image of Pine Island Glacier and the Walgreen Coast. Ice-surface contour (in meters) modified from Karta Antarktidy 1:3,000,000, sheet 4, Moskva, Ministerstvo Morskogo Flota SSSR, 1975. Spot soundings (in meters) from airborne radio-echosounding by British Antarctic Survey (unpublished). NASA image (1185–13530, band 7; 24 January 1973; Path 246, Row 114) from EROS Data Center, U.S. Geological Survey.

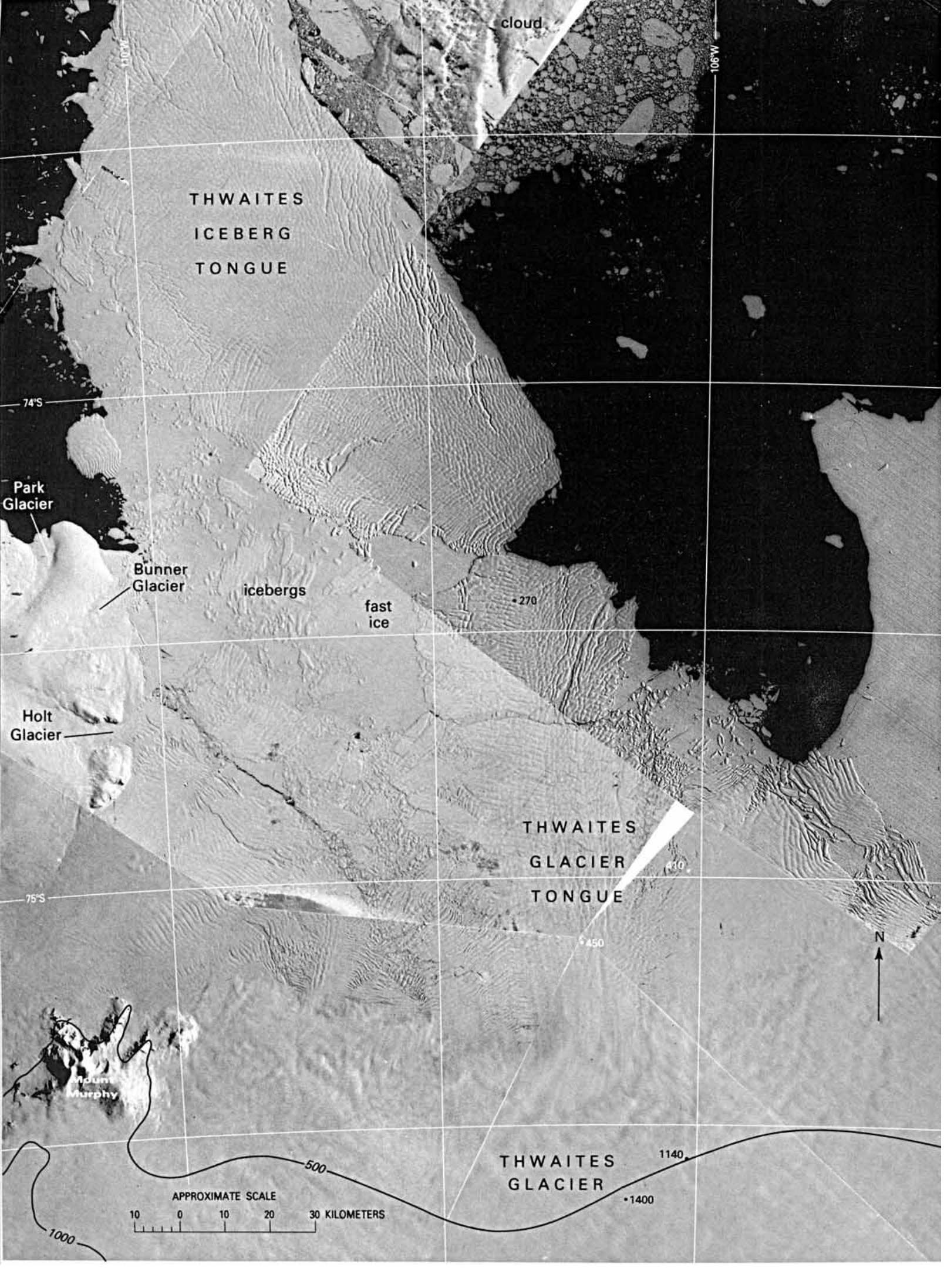
I 0 0 1 0 0 1

I 0 0 1 0 0 1

I 0 0 1 0 0 1



IW104-00 IW103-00 IW102-00 IW101-00
 24JAN73 C S75-10/W100-03 N S75-18/W099-48 MSS 7 R SUN EL22 AZ000 217-2577-G-1-N-D-IL NASA ERTS E-1185-13530-7 01



appropriate to equilibrium." Thwaites Glacier Tongue moves 3.5 km a^{-1} (Lindstrom and Tyler, 1985). According to McIntyre (in press) the glacier drains an area of $121,000 \text{ km}^2$ and should have a balance discharge of $47 \text{ km}^3 \text{ a}^{-1}$.

A chain of volcanoes parallels the coast of West Antarctica from the Jones Mountains in longitude 94°W . to the Fosdick Mountains in longitude 145°W . (fig. 100). Figure 94 shows six of the biggest. LeMasurier (1972a) has concluded on the basis of volcanic evidence that glaciation began in Marie Byrd Land as early as the Eocene, but the evidence is insufficient to prove uninterrupted glaciation of the region throughout the last 40 million years. LeMasurier and Rex (1982a) believe that both volcanism and the formation of deep subglacial grabens postdate the formation of the ice sheet. Mount Siple (fig. 94A) appears to have no major crater but a large number of small vents scattered over the cone. It has the greatest exposed height (3,110 m) and the greatest exposed diameter (50 km) of any volcano in West Antarctica. Toney Mountain (fig. 94B) blocks a northward-flowing ice sheet; its exposed height is 2,000 m on the south side and 2,400 m to the north. Its conspicuously breached summit crater beside Richmond Peak is 3 km in diameter. The Ames Range and Mount Bursey (fig. 94C) rise above a generally northward-flowing ice sheet: Mount Boennighausen stands 1,400 m above the ice sheet; Mount Bursey rises 700 m on the southeast side and 1,000 m on the northwest side. While Mount Bursey has a number of smaller craters, Mount Boennighausen appears to have glaciers flowing both northwest and northeast from a breached summit crater 4 km in diameter. LeMasurier and Rex (1982b) report actively steaming fumaroles on the north flank of Mount Kauffman. Mount Takahe (figs. 94D, 95, and 96) interrupts a northeastward-flowing ice sheet, standing 2,200 m above its surface. Its ice-filled caldera is 8 km in diameter, one of the largest in Antarctica (fig. 96). The Executive Committee Range (fig. 94E) blocks a southward-flowing ice sheet that drains into the Ross Ice Shelf. The north face of Mount Sidley rises 2,000 m above the ice sheet, the south face of Mount Waesche, 2,200 m. Doumani (1964) has described the major volcanoes of the range that extend a further 70 km beyond this image and north of Mount Sidley. The summit crater of Mount Waesche is 1,500 m in diameter and is situated at the southern edge of an older caldera about 10 km in diameter and filled with ice. Mount Sidley has a 5-km-diameter caldera open to the south. The northern rim of the caldera (4,181 m) is the highest peak in the range. Contemporary fumarolic activity has been observed on Mount Hampton (fig. 97), 70 km north of Mount Sidley (LeMasurier and Wade, 1968). The Crary Mountains (fig. 94F and background of fig. 97) stem an eastward-flowing ice sheet, the west face of the range standing 1,750 m above the ice surface and the east face rising 2,050 m above it. Mount Frakes is the highest peak (3,654 m), being topped by a nearly circular ice-filled caldera 2.5 km in diameter. Craterlike forms can also be seen on Mount Rees and Mount Steere, and on Boyd Ridge.

Figure 98 represents a typical scene from the Marie Byrd Land volcanic province. Mount Berlin (3,478 m) interrupts a northward-flowing ice sheet, having an exposed height of 1,300 m on the south side and 2,100 m on the north side. The mountain is a late Cenozoic stratovolcano composed of subaerially erupted felsic rock superimposed on basaltic hyaloclastites (LeMasurier, 1972b; LeMasurier and Wade, 1976). Its conspicuous summit crater is 1,500 m in diameter.

The visible small-scale ice-surface topography throughout the area suggests that ice thicknesses are generally less than 1,500 m. The deepest radio-echosounding is 1,790 m. Except at the northern end of

Figure 93.—Annotated Landsat 1 MSS image mosaic of Thwaites Glacier and Thwaites Iceberg Tongue, 1972–73. Ice-surface contours from Antarctica 1:3,000,000 (Scott Polar Research Institute, unpublished). Spot soundings (in meters) from airborne radio-echosounding (Scott Polar Research Institute, unpublished). NASA images (1191–14270, band 7; 30 January 1973; Path 1, Row 113; 1205–14044, band 7; 13 February 1973; Path 248, Row 114; 1205–14051, band 7; 13 February 1973; Path 248, Row 115; 1160–14551, band 7; 30 December 1972; Path 6, Row 112; 1157–14383, band 7; 27 December 1972; Path 3, Row 113; 1174–14325, band 7; 13 January 1973; Path 2, Row 114) from the EROS Data Center, U.S. Geological Survey.

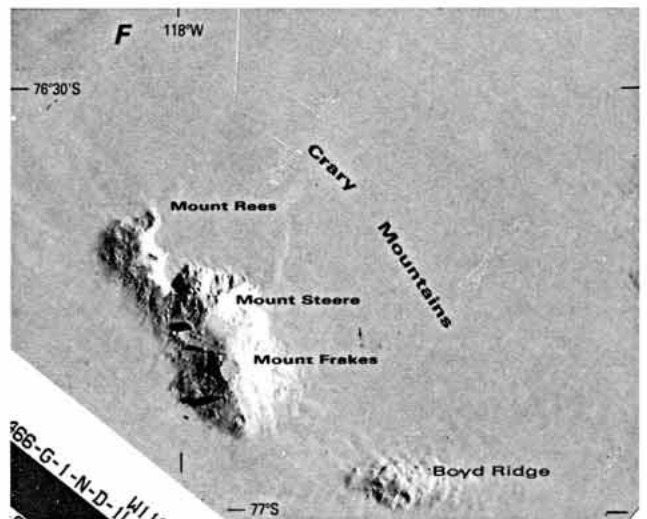
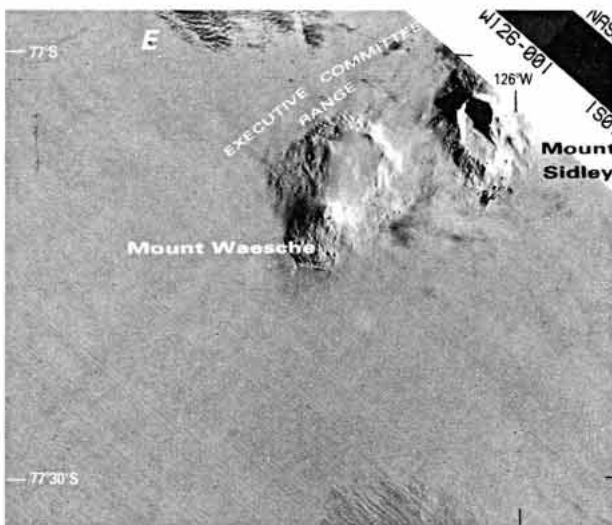
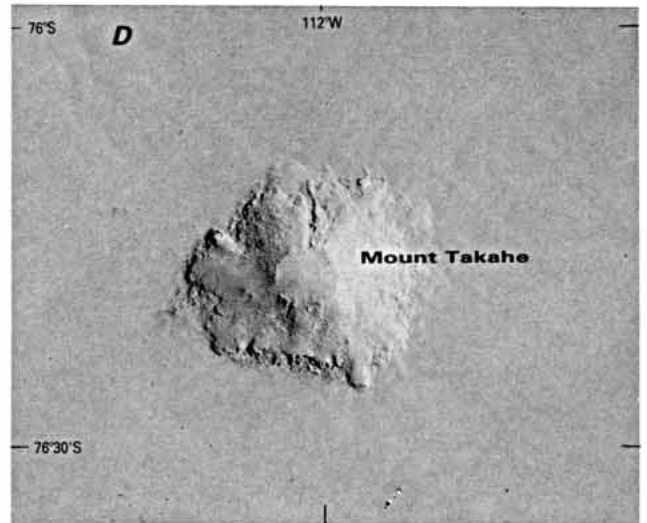
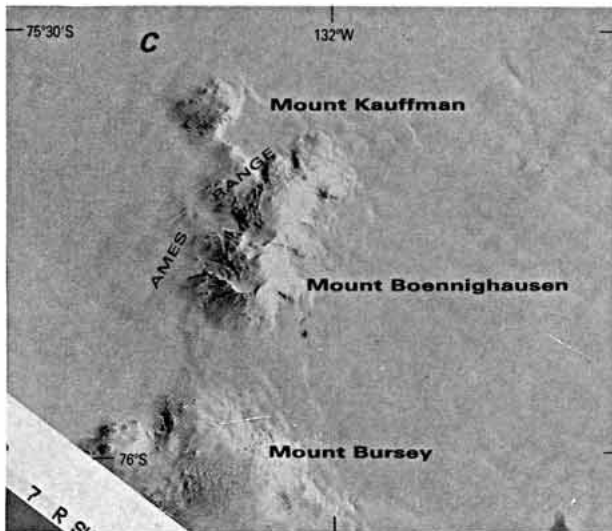
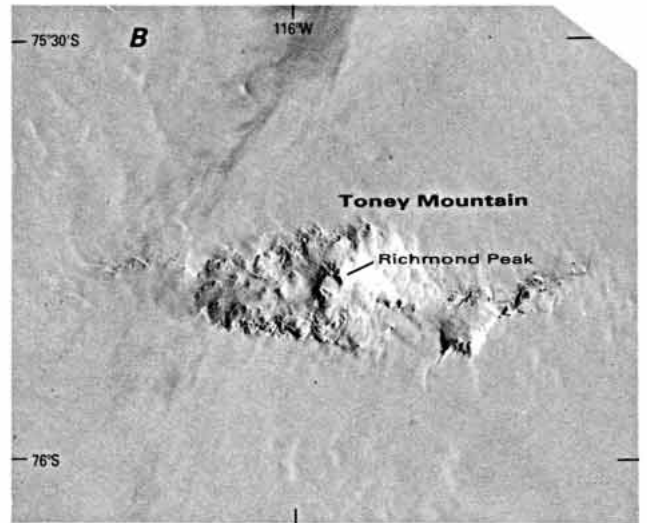
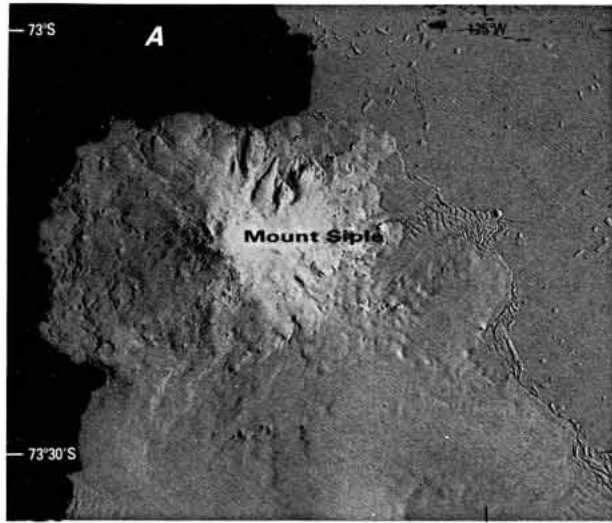


Figure 94.— Annotated Landsat 2 MSS images of selected volcanoes in Marie Byrd Land. A, Mount Siple, 3,110 m (1172–16035, band 7; 11 January 1973; Path 18, Row 112); B, Toney Mountain, 3,565 m (1177–14503, band 7; 16 January 1973; Path 4, Row 115); C, The Ames Range, 2,971 m, and Mount Bursey, 2,780 m (1152–15533, band 7; 22 December 1972; Path 16, Row 114); D, Mount Takahe, 3,400 m (1119–14280, band 7; 19 November 1972; Path 1, Row 115) (see also figures 95 and 96); E, Executive Committee Range: Mount Sidley, 4,285 m, and Mount Waesche, 3,290 m (1200–15201, band 6; 8 February 1973; Path 10, Row 116); and F, Crary Mountains: Mount Frakes, 3,675 m (1177–14503, band 7; 16 January 1973; Path 4, Row 115) (see also figure 97). NASA images from the EROS Data Center, U.S. Geological Survey.

the scene, there is little apparent channeling of the prevailing sheet flow into ice streams, a feature that suggests an immature landscape consistent with the known Pleistocene age of some of the volcanoes (Andrews and LeMasurier, 1973; LeMasurier and Wade, 1976). Instead of significant ice streams we see a very active ice-wall coastline discharging icebergs into the sea. In a few places, a break in slope gives way to signs of rifts developing on a flat surface; here we conclude that the last few kilometers of the ice sheet are afloat.

The very large number of icebergs off the coast is explained by the persistence of fast ice from one year to the next. In fact the area is well known, on the basis of weather satellite images, for having some of the oldest areas of sea ice of any Antarctic coast. Although the icebergs progressively move apart, the pattern of their calving is preserved as they drift northward. It is of interest to speculate on the nature of the forces that serve to separate one iceberg from the next at the point of calving and then to increase this separation as the train of icebergs leaves the coast. Debenham (1948, p. 210) and Swithinbank (1957a, p. 27) invoked the freezing of sea water in tidal cracks to explain the initial separation, and Nichols (1960) suggested that continued minor calving from each iceberg subsequently forced them apart.

Russkaya on Cape Burks is the smallest of six Soviet research stations on mainland Antarctica. First occupied for two weeks in 1973, it was then abandoned for 7 years because of resupply problems posed by the persistent belt of fast ice. It was reopened for a nine-man wintering party in March 1980, the fast-ice problem then being overcome by the use of large helicopters over a ship-to-shore distance of 24 km.

Figure 99 shows the White Glacier, a typical fast-flowing West Antarctic ice stream, flowing onto the sea. The shallow, snow-filled synclines that separate the heavily crevassed anticlines already reveal the lines along which calving of the glacier tongue will later take place. The right lateral margin of the ice stream in the background has already separated into icebergs. Giant rifts in the cloud shadow are filled with debris floating close to sea level.

Figure 100 shows a thin ice cap covering a highland area of volcanic origin 80 km from the Ruppert Coast of Marie Byrd Land. Warm summer weather has resulted in a stream of meltwater flowing down the middle of Ragle Glacier (left foreground). An ice-covered lake can be seen at the foot of the ridge in the center foreground, and there are other lakes associated with lateral moraines on both sides. The surface of most of the outlet glaciers from the ice cap seems to be snow-free at this time of the year.

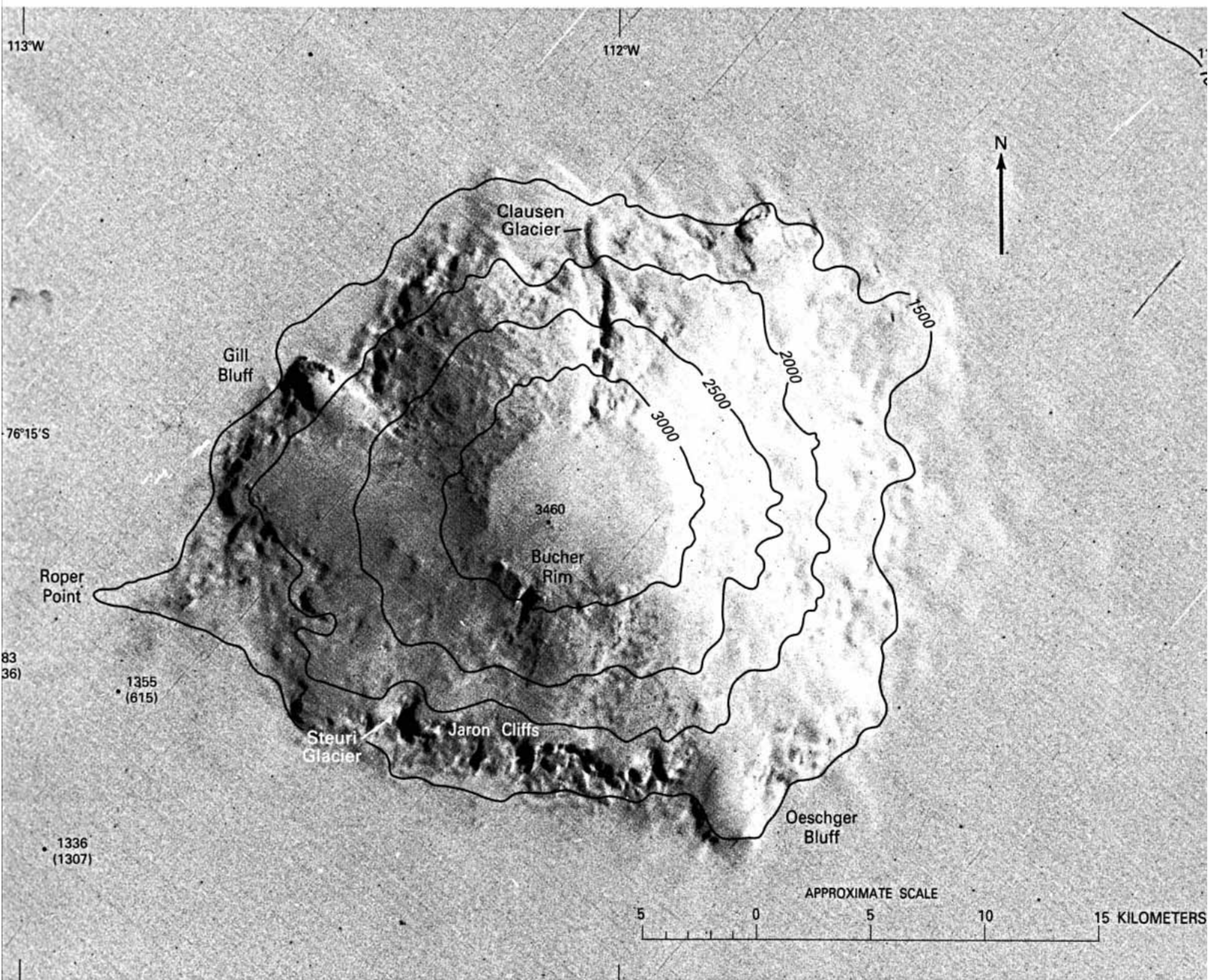
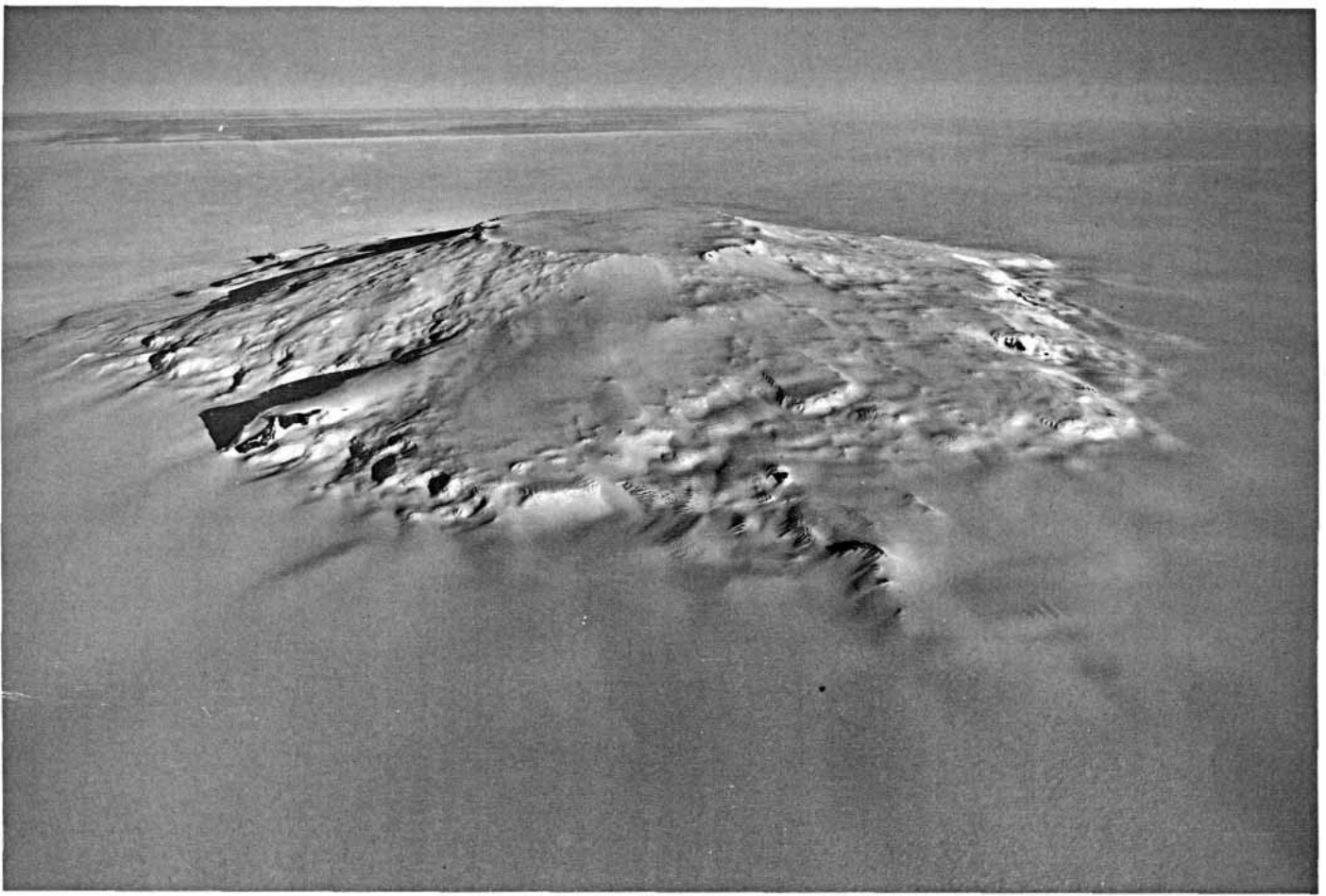


Figure 95.—Annotated Landsat 1 MSS image of Mount Takahe, a partially buried shield volcano, approximately 30 km in diameter and topped by an 8-km-wide quasi-circular caldera. Ice-surface contours (in meters) modified from Antarctic 1:250,000 Reconnaissance Series, sheet ST 9–12/4, U.S. Geological Survey, 1976. Spot soundings (in meters) of ice thickness given in parentheses following the spot elevations from data obtained during Marie Byrd Land Traverse, 1957–58. NASA image (1119–14280, band 7; 19 November 1972; Path 1, Row 115) from the EROS Data Center, U.S. Geological Survey.

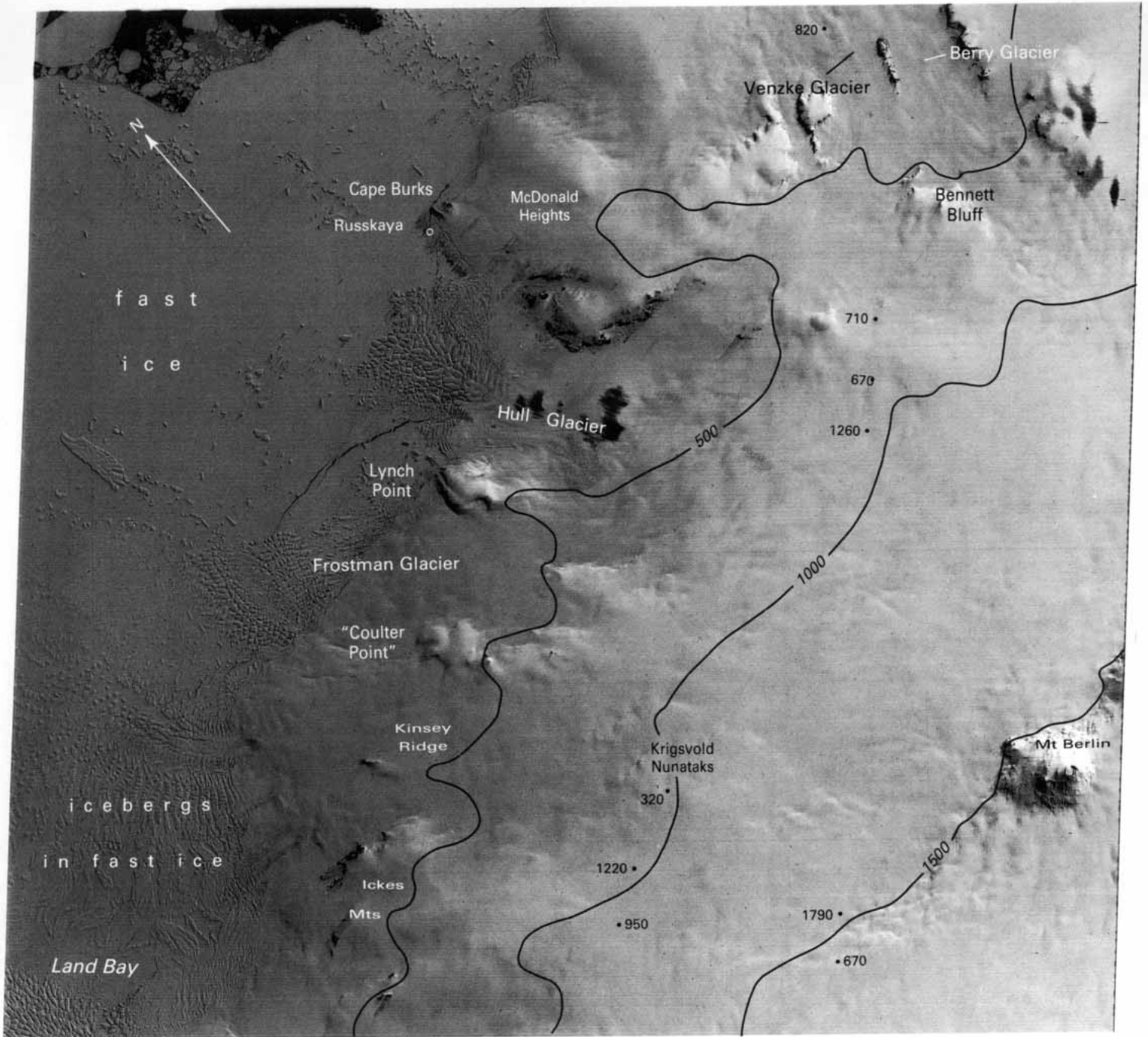


△ **Figure 96.**—Oblique aerial photograph of Mount Takahe volcano ($76^{\circ}17'S.$, $112^{\circ}05'W.$), Marie Byrd Land, taken from an altitude of 7,400m on 5 January 1956, looking east. U.S. Navy trimetrogon aerial photograph no. 22 (TMA 1718 F33) from the Antarctic Map and Photograph Library, U.S. Geological Survey. See also figures 94, 95, and 97.

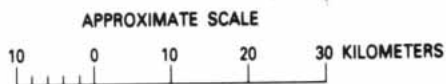
Figure 97.— Oblique aerial photograph of Mount Hampton volcano ($76^{\circ}29'S.$, $125^{\circ}48'W.$), Executive Committee Range, Marie Byrd Land, taken from an altitude of 7,400 m on 6 January 1960, looking east across the 3,325-m-high summit towards the three peaks of Mount Rees, Mount Steere, and Mount Frakes in the Crary Mountains (see figure 94F) in the distant background. U.S. Navy trimetrogon aerial photograph no. 199 (TMA 573 F33) from the Antarctic Map and Photograph library, U.S. Geological Survey.



W-001.001
W-001.001
W-001.001
W-001.001
W-001.001



W140-001 S076-001 W138-001
14JAN73 C S75-12/W137-31 N S75-20/W137-08 MSS 7 R SUN EL24 AZ080 217-2439-G-I-N-D-IL NASA ERTS E-1175-16215-7 02



◁ **Figure 98.**—Annotated Landsat 1 MSS image of Ruppert Coast. Ice-surface contours (in meters) modified from Antarctica 1:250,000 Reconnaissance Series, sheets SS7-9/10 (1974), SS7-9/11 (1974), SS7-9/13 (1973), SS7-9/14 (1975), SS7-9/15 (1976), and ST5-84 (1974), U.S. Geological Survey. Spot soundings (in meters) from airborne radio-echosounding (Scott Polar Research Institute, unpublished). NASA image (1175-16215, band 7; 14 January 1973; Path 21, Row 114) from the EROS Data Center, U.S. Geological Survey.

Figure 99.—Oblique aerial photograph of White Glacier, Marie Byrd Land, taken from an altitude of 1,800 m on 22 December 1969, facing east. The glacier is flowing from right to left. The right-hand rift in the cloud shadow marks a possible position of the grounding line. U.S. Navy trimetrogon aerial photograph no. 215 (RES 0073 F33) from the Antarctic Map and Photograph Library, U.S. Geological Survey.

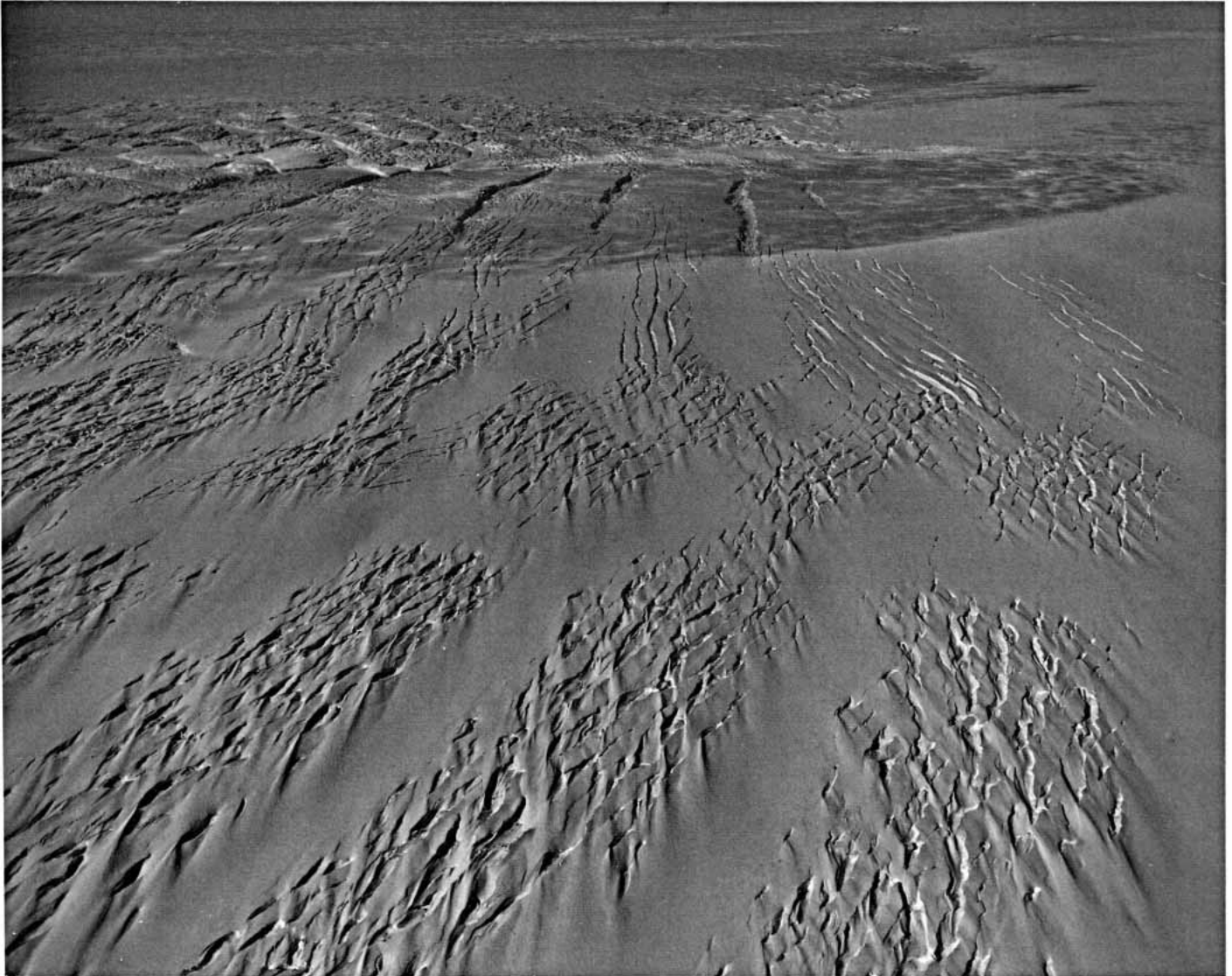




Figure 100.—Oblique aerial photograph of Fosdick Mountains, Ford Ranges, Marie Byrd Land, taken from an altitude of 2,200 m on 22 December 1969, facing east. Ragle Glacier flows towards the camera (center). U. S. Navy trimetrogon aerial photograph no. 243 (RES 0075 F31) from the Antarctic Map and Photograph Library, U.S. Geological Survey.

Eastern Margin of Ross Ice Shelf

Figure 101 shows 'Ice Stream E' flowing from Marie Byrd Land toward the Ross Ice Shelf. The flow is from top to bottom of the scene, and a short length of the right bank of 'Ice Stream D' can be seen in the bottom right corner. According to McIntyre (in press) 'Ice Stream D' drains an area of 170,000 km² and should have a balance discharge of 27 km³ a⁻¹, while 'Ice Stream E' drains an area of 154,000 km² and should have a balance discharge of 22 km³ a⁻¹. The margins of 'Ice Stream E' are exceptionally well defined (as in fig. 103), showing conspicuous flowlines funneling towards a minimum width of 69 km near the bottom of the picture. According to Rose (1979), Jankowski and Drewry (1981), and Rose (1982), the whole area is inland of the grounding line. Bedrock throughout is hundreds of meters below sea level. Rose (1979) calculated that there is bottom melting under the ice stream but that the bed of the ice sheet on either side must be below the pressure melting point; hence the sharp boundary between the two regimes. He estimates a balance velocity of 100 m a⁻¹ at the 600-m surface contour. Robin and others (1970) found surface slopes so low on comparable parts of 'Ice Stream C' (plate 1) that they suggested the possibility of "pseudo ice shelves" afloat on trapped water bodies. The ice-surface topography on 'Ice Stream E' makes an interesting comparison with that of another major ice stream, Slessor Glacier (fig. 74).

Figure 102 overlaps figure 101 on the south and shows the mouth of the same 'Ice Stream E' where it joins the Ross Ice Shelf. Flowlines from the confluent 'Ice Stream D' can be seen entering the scene halfway down the right-hand margin; they make a sharp angle with those of 'Ice Stream E' and are quickly deflected by them to the west. The presence 70 km downstream from the bottom of this scene of Roosevelt Island, the largest ice rise on the Ross Ice Shelf, bifurcates the flow from 'Ice Stream E' in such a way that less than half of it discharges to the east of the ice rise. The remainder of 'Ice Stream E' and the total output of 'Ice Stream D' discharge to the west of Roosevelt Island. This can best be seen by superimposing the scene on the Ross Ice Shelf map (US. Geological Survey, 1972).

Rose (1982) plots the grounding line here as crossing the ice streams from a point halfway down the right-hand side of the scene to the nearest point on the curving Shirase Coast opposite. This would make it wrong (by definition) to describe as ice rumpled the features so described on the overprint just above the 930-m spot sounding. But Rose makes it clear that his grounding line was determined only by comparing measured ice-surface elevations (230 m) with the values predicted for a free-floating ice shelf of the observed thickness. With the low ice-surface gradients hereabouts (perhaps 1 in 1000), the line could be misplaced by tens of kilometers. In any case, we should think in terms of a grounding zone rather than a grounding line in areas where it is so indeterminate. The spatial frequency of grounded areas must progressively increase as we move from freely floating ice shelf onto the grounded ice stream in the top right corner of the scene.

All the ice rumpled so labeled on this picture have been identified without difficulty in other Landsat images. What could easily be misinterpreted as cloud shadows are in reality fields of giant crevasses extending 10 to 20 km downstream from the ice rumpled. Surface velocities measured at points on 'Ice Stream E' in the bottom half of this

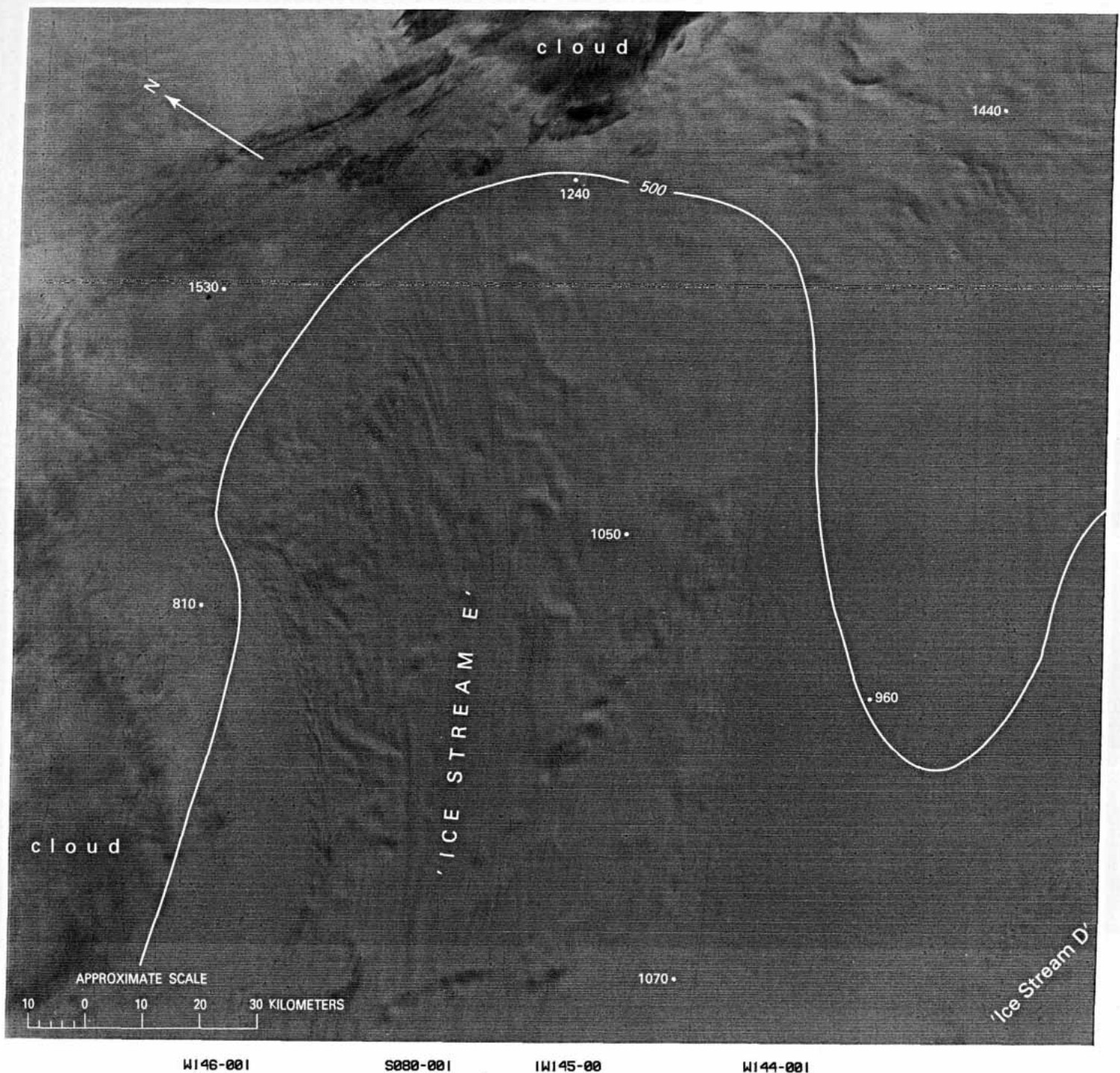


Figure 101.—Annotated Landsat 1 MSS image of 'Ice Stream E' flowing west from Marie Byrd Land (flow direction is from top to bottom of the scene). Ice-surface contour modified from Antarctica 1:3,000,000 (Scott Polar Research Institute, unpublished). Spot soundings (in meters) from airborne radio-echosounding (Scott Polar Research Institute, unpublished). NASA image (1465-1450, band 7; 31 October 1973; Path 4, Row 119) from the EROS Data Center, U.S. Geological Survey.

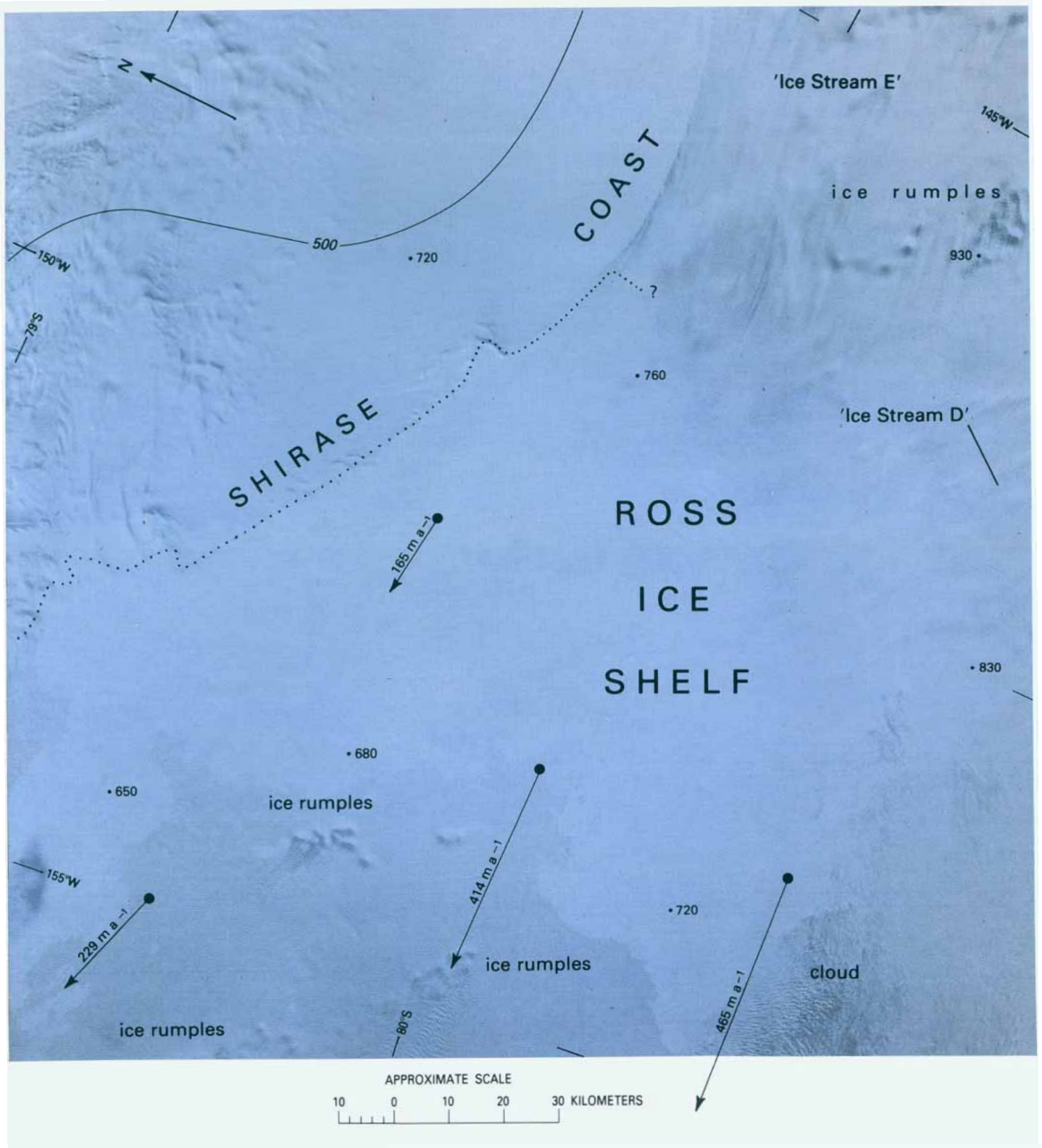


Figure 102. —Annotated Landsat 1 MSS digitally enhanced false-color composite image of Shirase Coast and the Ross Ice Shelf at the mouth of 'Ice Stream E.' Ice-surface contour interpolated from Tropical Wind Energy Conversion and Reference Level Experiment (TWERLE) data (unpublished). The dotted line represents the inferred position of the grounding line. Spot soundings (in meters) from airborne radio-echosounding (Scott Polar Research Institute, unpublished). Velocity vectors from Thomas and others (1984). NASA image (1472–15300, bands 4, 5, and 7; 7 November 1973; Path 11, Row 119) courtesy of Baerbel K. Lucchitta and the Flagstaff (Arizona) Image Processing Facility, U.S. Geological Survey.

scene are in the range 400 to 500 m a⁻¹ (Thomas and others, 1984), more than twice the balance velocities calculated by Robin (1975) but close to those of Rose (1979). Note the elegant unnamed ice stream flowing down the inland ice sheet on the left of the picture and the change in the crevasse pattern at the point where we suggest the grounding zone may strike across 'Ice Stream E' from Shirase Coast.

Few ice streams in any part of Antarctica show quite such a well-defined margin as 'Ice Stream B' (fig. 103). A chaotically crevassed surface gives way to a smooth and undisturbed ice sheet within a horizontal distance of little more than 100 m. Apart from the unyielding rock walls of a valley glacier, what physical characteristics can give rise to such an abrupt change of flow regime? Swithinbank (1977, p. 173) speculated that we must be looking either at the boundary between a sliding glacier (right) and an ice sheet frozen to its bed (left) or alternatively the line between floating ice (right) and grounded ice (left). Although radio-echosounding by Jankowski and Drewry (1981) shows that the area is close to the eastern margin of the Ross Ice Shelf, it also suggests that the ice stream is grounded here, thus favoring the sliding explanation.

Figure 103. — Oblique aerial photograph of the northern edge of 'Ice Stream B' (83°50'S., 150°W.) taken from an altitude of 3,000 m on 14 February 1947, facing northeast (up-stream). The transition from the crevassed surface of the ice stream to the undisturbed ice sheet covers a distance of a little more than 100 m. U.S. Navy trimetrogon aerial photograph no. 10 (Can no. 4145) from the Antarctic Map and Photograph Library, U.S. Geological Survey.



ACKNOWLEDGMENTS

The author is particularly grateful to all those who kindly provided unpublished ice thickness, surface elevation, or velocity data: D.J. Drewry, A.P.R. Cooper, and S.R. Jordan of the Scott Polar Research Institute; Ian Allison, N.W. Young, and D. Sheehy of the Australian Antarctic Division; K. Kusunoki of the Japanese National Institute of Polar Research; and C.S.M. Doake, R.D. Crabtree, and S.N. Stephenson of the British Antarctic Survey.

LANDSAT IMAGES OF ANTARCTICA

By RICHARD S. WILLIAMS, JR., *and* JANE G. FERRIGNO
U.S. GEOLOGICAL SURVEY

Introduction

There are 2,514 Landsat 1, 2, and 3 nominal scene centers within the part of Antarctica that extends from the coastline to about 81° south latitude (the southern limit of the Landsat orbit) (plate 2). This annular area is covered by all 251 Landsat orbits (paths) and all or parts of 17 rows from Row 103 (about 61°s. latitude) to Row 119 (about 81° S. latitude). Because Landsat orbits converge at high latitudes, sidelap of adjacent Landsat scenes increases towards the poles. Complete coverage of the part of Antarctica covered by Landsat could therefore be accomplished with only about 520 Landsat images by using every other Landsat scene at Row 103, with a gradual reduction to every ninth scene at Row 118. At Row 119, however, because of the east to west (rather than the usual northeast to southwest) travel of the satellite, every sixth scene is required.

For the majority of the 2,514 nominal Landsat scene centers in Antarctica, one or more images is available (tables 6 and 7). A serious problem for the casual user in the evaluation of Landsat images of Antarctica is that the cloud-cover assessment appearing on either the computer or the microfiche summaries of each image archived at the EROS Data Center is quite often unreliable; snow, for example, is often mistaken for clouds. In addition, the 1972 to 1980 16-mm microfilm cassettes contain only Landsat multispectral scanner (MSS) band 5 images, which are often overexposed and make it almost impossible to distinguish clouds from snow. Landsat MSS band 7 images on the 70-mm archival film rolls stored at the NASA Goddard Space Flight Center, Greenbelt, Md., had to be used to make a definitive determination of cloud cover.

More than 10,000 individual Landsat images were evaluated by direct inspection of MSS band 7 images on 70-mm archival rolls or paper prints in the search for the best available Landsat image of Antarctica for each nominal scene center. Each optimum image was classified into one of the following four categories: excellent, good, fair to poor, and unusable. A fifth category was used to indicate no available image. Table 4 provides criteria for the classification and the number and percentage of nominal scenes that fall into each category.

The first two categories, comprising 44.6 percent of the nominal scene centers, have little or no cloud cover, minimum snow cover in

areas of exposed rock, or were acquired during times of low solar elevation angle (above the horizon) to maximize morphologic details in the inland areas of the ice-sheet surface. Taking into account both image sidelap and suitability, about 70 percent of the Antarctic continent, from the coast to about 81°S. latitude, has high quality Landsat MSS images available.

Landsat has the potential for imaging about 1.1×10^7 km², or 79 percent of the area of Antarctica. The region around the geographic South Pole cannot be imaged because it is beyond the Landsat orbit. About 70 percent of the Landsat imaging area (about 7.7×10^6 km²), or about 55 percent of the continent, now has excellent or good coverage provided by Landsat MSS images. According to Swithinbank (1980), less than 20 percent of Antarctica, including about 50 percent of the coastal regions, has been mapped at scales of 1:250,000 or larger (see fig. 1). Consequently, the area of Antarctica planimetrically mapped at a 1:250,000 scale could be tripled if available Landsat images were effectively used.

Many countries, including Australia, Japan, New Zealand, the Republic of South Africa, the United Kingdom, and the United States, have already utilized these image data to prepare Landsat image maps of Antarctica, either as single Landsat scenes or as mosaics of two or more images (Williams and others, 1982).

Nearly all the Landsat coverage of Antarctica was acquired during the austral summers of 1972–73 and 1973–74, the direct result of W.R. MacDonald's ERTS-1 (Landsat 1) experiment (SR-194) requirements. Subsequent to 1974, the available Landsat spacecraft had tape recorders that were either inoperative or were assigned to higher priority needs for Landsat data. Therefore, only a few Landsat MSS images of Antarctica were acquired between 1974 and 1981.

With the launch of Landsat 3 on 5 March 1978, a considerable number of higher resolution return beam vidicon (RBV) images (30-m pixel for Landsat 3 RBV images versus 79-m pixel for MSS images) have been acquired. Unfortunately, most Landsat 3 RBV images of Antarctica are overexposed and not generally useful (Ferrigno and others, 1983; Ferrigno and Williams, 1983). Of the 3,771 Landsat 3 RBV subscenes (4 overlapping subscenes encompass one standard MSS image) acquired, only about 400 subscenes can be classified (by direct inspection) as good or marginal (some usability). Of these only about 100 fall into the good category. A few properly processed and exposed Landsat 3 RBV images are superb, however (see fig. 40). Figures 40, a Landsat 3 RBV image of part of the Rennick Glacier, and 41, a Landsat 1 MSS image of the Rennick Glacier and environs, provide an excellent comparison and show the significant improvement in glaciological features that can be discerned with a 30-m pixel size versus 79-m.

Although the overexposure problem with Landsat 3 RBV images of Antarctica is readily apparent, what is not so obvious is a related problem with MSS images of Antarctica. Research carried out in conjunction with the preparation of digital image mosaics of Antarctica with Landsat 1, 2, and 3 MSS images by Baerbel K. Lucchitta and her colleagues (written commun., 11 and 30 March 1983) at the U.S. Geological Survey's Branch of Astrogeology reveals a serious problem for those planning digital processing of the Landsat images. Bands 4, 5, and 6, and to some extent MSS band 7, show detector saturation caused by high solar elevation angles from November through January. In many cases, more than 50 percent of the area imaged by MSS bands 4, 5, or 6 is unusable because of loss of surface information. It seems probable that detectors for those MSS bands are not designed to record the high reflectivity in the snow-covered terrain, resulting in detector

saturation and information loss. An identical problem had been previously discovered when analyzing a Landsat image of Vatnajökull, Iceland (Ferrigno and Williams, 1983).

The Landsat 4 and 5 spacecraft, launched on 16 July 1982, and 1 March 1984, respectively have acquired approximately 2,000 MSS images of Antarctica, including 2 of the Byrd Glacier area on 23 November 1983 (fig. 25). These images, like all Landsat 4 images, are centered on a different path-row system than used with previous Landsats, providing coverage a little farther south than possible with Landsats 1, 2, and 3. This is the result of a slightly different orbital inclination and altitude, 99.09° and 919 km for Landsats 1, 2, and 3 and 98.2° and 705 km for Landsats 4 and 5. The repeat cycle is also different, 18 days for Landsats 1, 2, and 3, and 16 days for Landsats 4 and 5. A few Landsat 4 and 5 images of Antarctica have also been acquired during the ascending part of the orbital track over the continent. These images also have a variation in solar azimuth compared with images acquired on the descending part of the orbital track. Approximately 1,000 Landsat 4 and 5 thematic mapper (TM) images have been acquired of Antarctica. All Landsat 4 and 5 image data outside the range of ground stations must be transmitted through a tracking and data relay satellite system (TDRSS) that is not yet fully operational; neither satellite has on-board tape recorders.

Although Landsat images of Antarctica can be used to triple the area planimetrically mapped at present, Landsat MSS image maps can also be used, with adequate geodetic control, to satisfy the need for 1:250,000-scale base maps for already acquired geological and geophysical data (either from ground traverses or from airborne instrumentation). If usable Landsat 3 RBV or Landsat 4 or 5 TM images exist of an area, then 1:100,000-scale image maps could be prepared if adequate geodetic control exists.

The Australian Bureau of Mineral Resources, Geology and Geophysics has already published a 1:500,000-scale color geologic map of the southern part of the Prince Charles Mountains, East Antarctica, in which a Landsat image mosaic is used as the base map (Tingey and Convine, 1982). The South African Committee for Antarctic Research has also published a set of three 1:250,000-scale color geologic maps of part of western Dronning (Queen) Maud Land (Wolmarans and Krynauw, 1981). Landsat images were also used by the Scott Polar Research Institute in the preparation of a more accurate 1:6,000,000-scale base map of Antarctica for their folio of glaciological and geophysical maps of Antarctica (Drewry, 1983).

Index Map to Optimum Landsat 1, 2, and 3 Images of Antarctica

Plate 2 is a 1:10,000,000-scale index map of Antarctica. On this map are plotted the 2,514 nominal scene centers (path-row pairs) of all Landsat images that cover any part of the continent of Antarctica. Each of the nominal scene centers is coded with one of the codes shown in table 5. The corresponding code is also used in the table of optimum Landsat 1, 2, and 3 MSS images of Antarctica (table 6). The availability of usable Landsat 3 RBV subscenes is indicated by the printing of one or more of the four subscenes (A, B, C, or D) around the periphery of the coded circles.

The path and row numbers for Landsat 1, 2, and 3 nominal scene centers follow the "Extended Canadian or Worldwide Reference System (WRS)" used by the U.S. Geological Survey's EROS Data Center, Sioux Falls, SD 57198, where all Landsat multispectral scanner (MSS) and return beam vidicon (RBV) images of Antarctica are archived. Complete imaging of the Earth's surface between about 81° north and south latitudes is achieved with Landsat 1, 2, and 3 MSS and RBV sensors in 251 orbits. These 251 orbits are divided into 119 rows of overlapping (15 percent), successive Landsat images acquired along the orbital path. The points of intersection of the orbital paths and the rows are known as nominal scene centers. This index map includes all nominal scene centers that give coverage of Antarctica beginning at the coast (defined as the boundary between the ocean and either bedrock or glacial ice) or all or parts of 17 rows from Row 103 (tip of Antarctic Peninsula) to Row 119 (about 81°S. latitude) and all 251 paths (orbits).

More than 10,000 Landsat MSS band 7 images were evaluated by direct inspection of 70-mm archival roll positive transparencies at NASA's Goddard Space Flight Center. The optimum Landsat 1, 2, and 3 MSS and Landsat 2 RBV images of Antarctica were then classified on the basis of cloud cover (table 6). In the inland-ice regions the optimum image was selected both on the basis of minimum cloud cover and low solar elevation angle to enhance subtle morphologic details on the ice-sheet surface. Landsat 3 RBV images were evaluated (see table 7) on the basis of the amount of distinguishable ground features on the image. Only usable (classified in table 7 as G for good or M for marginally usable) Landsat 3 RBV subscenes (A, B, C, D) are included. Landsat 3 RBV subscenes encompass slightly more than one overlapping quadrant (A, NW.; B, NE.; C, SW.; D, SE.) of an MSS nominal scene. At a scale of 1:10,000,000 a Landsat image encompasses a parallelogram-shaped area that has sides about 19 mm long.

It should be realized that for many nominal scene centers in Antarctica more than one Landsat image may have been acquired. Only the code for the optimum image is given on this index map. There may also exist more than one image in the optimum category, although only one has been listed. For those involved in time-lapse studies of glaciological phenomena in Antarctica, it will be necessary to request the EROS Data Center to do a computer search for all Landsat images of a particular nominal scene center. Because of the general inaccuracy of the cloud-cover rating on the computer printout, however, it will probably be necessary to inspect an MSS band 7 image to ascertain the overall usefulness of a particular scene.

All of the figures discussed in the chapter are keyed to plate 1 on the basis of their geographic positions. The actual latitude and longitude of the nominal scene center is provided in the tables (tables 6 and 7). It should be recognized, however, that the actual Landsat 1, 2, and 3 scene centers can vary up to 40 km from the latitude and longitude coordinates of the nominal scene center depending upon specific orbital path and framing; therefore, the precise area of coverage of each image can also vary. For those figures in which the full Landsat image is printed, a data-annotation block is printed on the bottom of the image. Tick marks indicating the approximate latitude and longitude grid are plotted around all four edges of the image. The actual, rather than the nominal, scene center of the image is noted in the left-hand part of the bottom annotation.

Plate 2 represents the best index map to optimum usable Landsat 1, 2, and 3 images of Antarctica and replaces the two previous Landsat index maps to Antarctica published by the U.S. Geological Survey in

1975 (Index to Landsat Coverage, Antarctica—WPS—Edition 1, August 1972–July 1974, scale 1:18,000,000), and by the National Oceanic and Atmospheric Administration in 1982 (Index to Landsat Worldwide Reference Systems (WRS), Landsats 1, 2, 3, and 4, sheet 26, scale 1:10,000,000), both of which have serious shortcomings because of errors in cloud-cover assessment. A combined “Index Map to and Table of Optimum Landsat 1, 2, and 3 Images of Antarctica” was previously released by the US. Geological Survey as an open-file report (Williams and others, 1984).

Tables of Optimum Landsat 1, 2, and 3 Images of Antarctica

Table 6 provides information about the optimum Landsat 1, 2, and 3 MSS and Landsat 2 RBV images of Antarctica, and table 7 provides information about optimum Landsat 3 RBV images of Antarctica in concise form. A more abbreviated version of these tables was published by the U.S. Geological Survey as an open-file report (Williams and others, 1984). For a discussion of Landsat nominal scene centers and the codes, refer to the previous section and tables 4 and 5.

TABLE 4.—*Evaluation of optimum Landsat 1, 2, and 3 MSS images of Antarctica*

Assessment category	Number of nominal scenes	Percentage of total
Excellent image (0 to ≤5 percent cloud cover) -----	753	30.0
Good image (>5 to ≤10 percent cloud cover) -----	367	14.6
Fair to poor image (>10 to ≤100 percent cloud cover) -----	937	37.3
Unusable image (100 percent cloud cover) -----	153	6.0
No image available (no image ever acquired) -----	304	12.1
Total -----	2,514	100

TABLE 5.—*Code used to classify each of the 2,514 Landsat nominal scene centers in Antarctica*

Code	Evaluation of image usability for glaciologic, geologic, and cartographic applications. Symbols defined as follows:
	Excellent image (0 to ≤5 percent cloud cover)
	Good image (>5 to ≤10 percent cloud cover)
	Fair to poor image (>10 to ≤100 percent cloud cover)
	Unusable image (100 percent cloud cover)
	No image available
	Nominal scene center for a Landsat image that lies beyond the coast of Antarctica
	Usable Landsat 3 return beam vidicon (RBV) scenes (A, B, C, D refer to usable RBV subscenes)

The following explanation provides information about the optimum Landsat image for each of the 2,514 path-row pairs that encompass Antarctica. For most path-row pairs, only one optimum image is given.

In a few cases, however, two scenes were needed to provide coverage of the nominal image area. The code column carries the same symbol that appears on plate 2.

An explanation of the column headings for tables 6 and 7 is as follows:

**PATH-ROW AND NOMINAL
SCENE CENTER**

Complete imaging of the Earth's surface between about 81° north and south latitudes with Landsat 1, 2, and 3 MSS and RBV sensors is achieved in 251 orbits. These 251 orbits are divided into 119 rows of overlapping (15 percent), successive Landsat images acquired along the orbital path. The points of intersection of the orbital paths and the rows are known as nominal scene centers. These tables include all nominal scene centers that give coverage of Antarctica beginning at the coast (defined as the boundary between the ocean and either bedrock or glacial ice), which, in the case of Antarctica, includes all or parts of 17 rows from Row 103 (tip of Antarctica Peninsula) to Row 119 (about 81°S. latitude) and all 251 paths (orbits).

**LANDSAT IDENTIFICATION
NUMBER**

Each landsat image acquired of the Earth's surface has a unique identification number. The first (left-hand) digit refers to the numbered Landsat series (i.e., 1, 2, or 3). The other digits to the left of the hyphen record the number of days since launch of the spacecraft. The 5 numbers to the right of the hyphen record the time of acquisition of the image to the nearest 10 seconds in Greenwich Mean Time (GMT). For example, Landsat image 1191-14264(Path 001-Row112) of the King Peninsula, West Antarctica, was acquired by Landsat 1, 191 days after the 23 July 1972 launch (30 January 1973) at 14 hr, 26 min, 40 s GMT.

SUBSCENE (Table 7)

Landsat 3 RBV subscenes are indicated as A, B, C, or D and encompass slightly more than one overlapping quadrant (A, NW.; B, NE.; C, SW.; D, SE.) of an MSS nominal scene.

DATE

Date of acquisition of the Landsat image.

SOLAR ELEVATION ANGLE

Angle of the height of the Sun above the horizon. In Antarctica this can vary from 0 to about 40 degrees, depending on latitude and time of year.

CODE (Table 6)



Evaluation of image usability for glaciologic, geologic, and cartographic applications. Symbols defined as follows:

- Excellent image (0 to ≤5 percent cloud cover)
- Good image (>5 to ≤10 percent cloud cover)
- Fair to poor image (>10 to ≤100 percent cloud cover)
- Unusable image (100 percent cloud cover)
- No image available

CODE (Table 7)

- G Good image (Ground features clearly visible and identifiable)
- M Marginally usable image (Ground features difficult to see and identify, but some information is present).

25, 50, 75, 100

The percentage of image with either good (G) or marginally usable (M) ground features visible. Obscuration of surface features can be caused by one or more of the following factors: clouds, overexposure of image, electronic-processing artifacts, etc. Direct evaluation of usable percentage of Landsat 3 RBV subscene from either 1:500,000-scale paper prints or positive or negative film transparencies or 1:3,369,000-scale 70-mm positive or negative film transparencies (archival rolls) located at the U.S. Geological Survey's EROS Data Center, Sioux Falls, SD 57198.

CLOUD COVER PERCENT (Table 6)

Direct evaluation of cloud-cover percentage from either Landsat 1, 2, and 3 MSS band 7 or Landsat 2 RBV band 3 70-mm positive or negative film (1:3,369,000-scale) transparencies (archival rolls) located at NASA's Goddard Space Flight Center, Greenbelt, MD 20771, and from MSS band 7 or RBV band 3 (1:1,000,000-scale) paper prints from the U.S. Geological Survey's EROS Data Center. Landsat MSS band 7 or RBV band 3 images were used for cloud-cover evaluation because of maximum discrimination between clouds and snow. If an MSS band 7 image was unavailable, then an MSS band 6 image was used, and so forth.

REMARKS

The place-name of prominent geographic features (Alberts, 1981) is given where applicable. Mention of noteworthy glaciological phenomena may also be given.

REFERENCES CITED

- Alberts, F.G., ed., 1981, Geographic names of the Antarctic: Washington, D.C., US. Board on Geographic Names, National Science Foundation, Report No. 81-5,959 p.
- Allison, Ian, 1979, The mass budget of the Lambert Glacier drainage basin, *Antarctica: Journal of Glaciology*, v. 22, no. 87, p. 223-235.
- Allison, Ian, Frew, Rowan, and Knight, Ian, 1982, Bedrock and ice surface topography of the coastal regions of Antarctica between 48°E and 64°E: *Polar Record*, v. 21, no. 132, p. 241-252.
- Amundsen, Roald, 1912, *The South Pole: an account of the Norwegian Antarctic Expedition in the "Fram" 1910-1912*: London, John Murray, 2 v., 841 p.
- Anderton, P.W., and Fenwick, J.K., 1976, Dry valleys, Antarctica 1973-74, *in* Hydrological Research Annual Report No. 37: Wellington, Ministry of Works and Development, 42 p.
- Andrews, J.T., and LeMasurier, W.E., 1973, Rates of Quaternary glacial erosion and corrie formation, Marie Byrd Land, Antarctica: *Geology*, v. 1, no. 2, p. 75-80.
- Antarctic Journal of the United States, 1974, Ship operations: v. 9, no. 2, p. 59-60.
- Antarctic Meteorite Working Group, 1981, Antarctic meteorites. An international resource for scientific research Houston, Lunar and Planetary Institute, 9 p.
- Armstrong, Terence, Roberts, Brian, and Swithinbank, Charles, 1973, Illustrated glossary of snow and ice: Cambridge, Scott Polar Research Institute, Special Publication Number 4, 60 p.
- 1977, Proposed new terms and definitions for ice features: *Polar Record*, v. 18, no. 116, p. 501-502.
- Australia Division of National Mapping, 1969, Australian Antarctic Territory, Sheet SQ 47-48: Canberra, 1:1,000,000 scale.
- Bagnold, R.A., 1941, *The physics of blown sand and desert dunes*: London, Methuen, 265 p.
- Ball, F.K., 1960, Winds on the ice slopes of Antarctica, *in* Antarctic meteorology, Proceedings of the symposium held in Melbourne, February 1959: London, Pergamon, p. 9-16.
- Barnard, H.P., 1975, Radio-echosounding in western Dronning Maud Land, 1974: *South African Journal of Antarctic Research*, no. 5, p. 37-41.
- Barrett, P.J., 1975, Seawater near the head of the Ross Ice Shelf: *Nature*, v. 256, no. 5516, p. 390-392.
- Behrendt, J.C., 1962, Summary and discussion of the geophysical and glaciological work in the Filchner Ice Shelf area of Antarctica: University of Wisconsin Geophysical and Polar Research Center, Research Report Series, no. 62-3, 66 p.
- Bishop, J.F., and Walton, J.L.W., 1981, Bottom melting under George VI Ice Shelf, Antarctica: *Journal of Glaciology*, v. 27, no. 97, p. 429-447.
- Black, H.P., and Budd, W.F., 1964, Accumulation in the region of Wilkes, Wilkes Land, Antarctica: *Journal of Glaciology*, v. 5, no. 37, p. 3-15.
- Blackburn, Q.A., 1937, The Thorne Glacier [Editor's note: Officially named Scott Glacier] section of the Queen Maud Mountains: *Geographical Review*, v. 27, no. 4, p. 598-614.
- Blaiklock, K.V., Stratton, D.G., and Miller, J.H., 1966, Survey: Trans-Antarctic Expedition 1955-58: Scientific Reports, no. 15, 28 p.
- Bogorodskiy, V.V., and Fedorov, B.A., 1968, Radar soundings of glaciers: Soviet Antarctic Expedition Information Bulletin (translation): Washington, D.C., American Geophysical Union, v. 6, no. 6, p. 511-518.
- Borchgrevink, C.E., 1901, *First on the Antarctic continent; being an account of the British Antarctic expedition, 1898-1900*: London, George Newnes, 333 p.
- Brecher, H.H., 1986, Surface velocity determinations on large polar glaciers by aerial photogrammetry: *Annals of Glaciology*, v. 8, p. 22-26.
- Briggs, Geoffrey, and Taylor, Fredric, 1982, *The Cambridge photographic atlas of the planets*: Cambridge University Press, 255 p.
- Bromwich, D.H., and Kurtz, D.D., 1984, Katabatic wind forcing of the Terra Nova Bay polynya: *Journal of Geophysical Research*, v. 89, no. C3, p. 3561-3572.
- Brooks, R.L., Williams, R.S., Jr., Ferrigno, J.G., and Krabill, W.B., 1983, Amery Ice Shelf topography from satellite radar altimetry, *in* Oliver, R.L., James, P.R., and Jago, J.B., eds., *Antarctic earth science*: Canberra, Australian Academy of Science, p. 441-445.
- Bruchhausen, P.M., Raymond, J.A., Jacobs, S.S., DeVries, A.L., Thorndike, E.M., and DeWitt, H.H., 1979, Fish, crustaceans, and the sea floor under the Ross Ice Shelf: *Science*, v. 203, no. 4379, p. 449-451.
- Budd, W.F., 1966, The dynamics of the Amery Ice Shelf: *Journal of Glaciology*, v. 6, no. 45, p. 335-358.
- 1970, Ice flow over bedrock perturbations: *Journal of Glaciology*, v. 9, no. 55, p. 29-48.
- 1975, Antarctic sea-ice variations from satellite sensing in relation to climate: *Journal of Glaciology*, v. 15, no. 73, p. 417-427.
- Budd, W.F., and Carter, D.B., 1971, An analysis of the relation between the surface and bedrock profiles of ice caps: *Journal of Glaciology*, v. 10, no. 59, p. 197-209.
- Budd, W.F., Corry, M.J., and Jacka, T.H., 1982, Results from the Amery Ice Shelf project: *Annals of Glaciology*, v. 3, p. 36-41.
- Budd, W.F., Janssen, D., and Radok, Uwe, 1971, Derived physical characteristics of the Antarctic ice sheet: Australian National Antarctic Research Expeditions, Reports, Melbourne, Antarctic Division, Publication No. 120, Series A, *Glaciology*, v. 4, 178 p.
- Bull, Colin, 1971, Snow accumulation in Antarctica, *in* Quam, L.O., ed., *Research in the Antarctic: American Association for the Advancement of Science*, Publication No. 93, p. 367-421.
- Bull, Colin, and Carnein, C.R., 1970, The mass balance of a cold glacier: Meserve Glacier, south Victoria Land, Antarctica, *in* Gow, A.J., Keeler, C., Langway, C.C., and Weeks, W.F., eds., *International Symposium on Antarctic Glaciological Exploration (ISAGE)*, Hanover, New Hampshire, USA, 3-7 September 1968, International Association of Scientific Hydrology Publication No. 86, p. 429-446.
- Bull, Colin, and Lipschutz, M.E., eds., 1982, Workshop on Antarctic glaciology and meteorites: LPI Technical Report no. 82-03, Lunar and Planetary Institute, Houston, Texas, 57 p.
- Burton, H.R., 1981, Chemistry, physics and evolution of Antarctic saline lakes—review: *Hydrobiologia*, v. 82, p. 339-362.
- Byrd, R.E., 1930, *Little America, aerial exploration in the Antarctic, the flight to the South Pole*: New York, G.P. Putnam's Sons, 422 p.
- 1947, Our navy explores Antarctica: *National Geographic Magazine*, v. 92, no. 4, p. 429-522.
- Cassidy, W.A., 1980, Antarctic search for meteorites, 1979-80: *Antarctic Journal of the United States*, v. 15, no. 5, p. 49-50.
- Charcot, Jean [1911], *The voyage of the "Why Not?" in the Antarctic; the journal of the second French south polar expedition, 1908-1910*: New York, Hodder and Stoughton, 315 p.
- Chinn, T.J., 1971, Report on hydrological programme, Lake Vanda 1970-71: Wellington, Ross Dependency Research Committee, Report No. 639.
- 1980, Glacier balances in the dry valleys area, Victoria Land, Antarctica, *in* World glacier inventory, Proceedings of the workshop at Riederalp, Switzerland, 17-22 September 1978: International Association of Hydrological Sciences Publication No. 126, p. 237-247.
- Unpublished, Hydrological research report, Dry valleys, Antarctica 1974-75: Christchurch, Ministry of Works and Development, Water and Soil Division, 57 p.
- Clapperton, C.M., and Sugden, D.E., 1983, Geomorphology of the Ablation Point Massif, Alexander Island, Antarctica: *Boreas*, v. 12, p. 125-135.
- Collins, I.F., and McCrae, I.R., 1985, Creep buckling of ice shelves and the formation of pressure rollers: *Journal of Glaciology*, v. 31, no. 109, p. 242-252.

- Collins, Ian, and Swithinbank, Charles, 1968, Rifts at the foot of Beardmore Glacier, Antarctica: International Association of Scientific Hydrology Publication No. 79, p. 109–114.
- Colvill, A.J., 1977, Movement of Antarctic ice fronts measured from satellite imagery: *Polar Record*, v. 18, no. 115, p. 390–394.
- Cornish, Vaughan, 1914, Waves of sand and snow and the eddies which make them: London, T. Fisher Unwin, 383 p.
- Crabtree, R.D., and Doake, C.S.M., 1980, Flow lines on Antarctic ice shelves: *Polar Record*, v. 20, no. 124, p. 31–37.
- 1982, Pine Island Glacier and its drainage basin: Results from radio echo-sounding: *Annals of Glaciology*, v. 3, p. 65–70.
- 1986, Radio-echo investigations of Ronne Ice Shelf: *Annals of Glaciology*, v. 8, p. 37–41.
- Crary, A.P., 1966, Mechanism for fiord formation indicated by studies of an ice-covered inlet: *Geological Society of America Bulletin*, v. 77, no. 9, p. 911–929.
- Crary, A.P., and Wilson, C.R., 1961, Formation of “blue” glacier ice by horizontal compressive forces: *Journal of Glaciology*, v. 3, no. 30, p. 1045–1050.
- Crohn, P.W., 1959, A contribution to the geology and glaciology of the western part of Australian Antarctic Territory: Australian National Antarctic Research Expeditions (ANARE) Reports, Melbourne, Antarctic Division, Series A, Geology, v. 3, 103 p.
- Davis, J.K., 1919, With the “Aurora” in the Antarctic, 1911–1914: London, Andrew Melrose, 183 p.
- Debenham, Frank, 1920, A new mode of transportation by ice: The raised marine muds of South Victoria Land (Antarctica): *Quarterly Journal of the Geological Society*, London, v. 75, part 2, p. 51–76.
- 1923, The physiography of the Ross archipelago: British (Terra Nova) Antarctic Expedition 1910–1913: London, Harrison and Sons, 40 p.
- 1948, The problem of the Great Ross Barrier: *Geographical Journal*, v. 112, nos. 4–6, October–December 1948, p. 196–218.
- Declair, H., and Van Autenboer, T., 1982, Gravity and magnetic anomalies across Jutulstraumen, a major geologic feature in western Dronning Maud Land, *in* Craddock, Campbell, ed., *Antarctic geoscience*: Madison, University of Wisconsin Press, p. 941–948.
- Doake, C.S.M., 1982, State of balance of the ice sheet in the Antarctic Peninsula: *Annals of Glaciology*, v. 3, p. 77–82.
- Dolgushin, L.D., 1966, Noviyе danniyе o skorostyakh dvizheniya lednikov Antarktity [New data on the rates of movement of Antarctic glaciers]: *Informatsionnyy Byulleten’ Sovetskoy Antarkticheskoy Ekspeditsii* [Information Bulletin of the Soviet Antarctic Expedition], no. 56, p. 17–20.
- Dorrer, Egon, Hofmann, Walther, and Seufert, Wilfried, 1969, Geodetic results of the Ross Ice Shelf Survey Expeditions, 1962–63 and 1965–66: *Journal of Glaciology*, v. 8, no. 52, p. 67–90.
- Dort, Wakefield, Jr., 1967, Internal structure of Sandy Glacier, southern Victoria Land, Antarctica: *Journal of Glaciology*, v. 6, no. 46, p. 529–540.
- Doumani, G.A., 1964, Volcanoes of the Executive Committee Range, Byrd Land, *in* Adie, R.J., ed., *Antarctic geology*: Amsterdam, North-Holland, p. 666–675.
- Dow, J.A.S., and Neall, V.E., 1974, Geology of the lower Rennick Glacier, northern Victoria Land, Antarctica: *New Zealand Journal of Geology and Geophysics*, v. 17, no. 3, p. 659–714.
- Drewry, D.J., 1980, Pleistocene bimodal response of Antarctic ice: *Nature*, v. 287, no. 5779, p. 214–216.
- ed., 1983, *Antarctica: Glaciological and geophysical folio*: Cambridge, England, Scott Polar Research Institute, University of Cambridge, sheets 2–9.
- Drewry, D.J., Jordan, S.R., and Jankowski, E., 1982, Measured properties of the Antarctic ice sheet Surface configuration, ice thickness, volume and bedrock characteristics: *Annals of Glaciology*, v. 3, p. 83–91.
- Feldmann, R.M., 1984, Antarctic treasures found Earth Science, v. 37, no. 2, p. 22–24.
- Fenwick, J.K., and Anderton, P.W., 1975, Dry valleys, Antarctica 1972–73: Hydrological Research Annual Report, Wellington, Ministry of Works and Development, No. 34, 37 p.
- Ferrigno, J.G., and Williams, R.S., Jr., 1983, Limitations in the use of Landsat images for mapping and other purposes in snow- and ice-covered regions: Antarctica, Iceland, and Cape Cod, Massachusetts, *in* Proceedings of the Seventeenth International Symposium on Remote Sensing of Environment: Ann Arbor, Environmental Research Institute of Michigan, v. 1, p. 335–355.
- Ferrigno, J.G., Williams, R.S., Jr., and Kent, T.M., 1983, Evaluation of Landsat 3 RBV images, *in* Oliver, R.L., James, P.R., and Jago, J.B., eds., *Antarctic Earth Science, Proceedings of the Fourth International Symposium on Antarctic Earth Sciences (16–20 August 1982)*, University of Adelaide, South Australia: Canberra, Australian Academy of Science, p. 446–449.
- Fuchs, V.E., 1951, Exploration in British Antarctica: *Geographical Journal*, v. 117, part 4, p. 399–421.
- Fuchs, Vivian, and Hillary, Edmund, 1958, The crossing of Antarctica: The Commonwealth Trans-Antarctic Expedition 1955–58 London, Cassell, 338 p.
- Fujii, Yoshiyuki, 1981, Aerial photographic interpretation of surface features and an estimation of ice discharge at the outlet of the Shirase drainage basin, Antarctica: *Nankyoku Shiryo* [Antarctic Record], no. 72, p. 1–15.
- Fujiwara, Kenzo, and Yoshida, Yoshio, 1972, Ice flow measurements on the east coast of Lützow-Holm Bay, Antarctica: *Nankyoku Shiryo* [Antarctic Record], no. 44, p. 79–92.
- Giovinetto, M.B., Robinson, E.S., and Swithinbank, C.W.M., 1966, The regime of the western part of the Ross Ice Shelf drainage system: *Journal of Glaciology*, v. 6, no. 43, p. 55–68.
- Gjessing, Y.T., 1972, Mass transport of Jutulstraymen ice stream in Dronning Maud Land Norsk Polarinstittut Arbok 1970, p. 227–232.
- Gow, A.J., 1973, The hydrology and compositional structure of the Koettlitz Glacier tongue, McMurdo Sound, Antarctica (abs.), *in* Symposium on the hydrology of glaciers, Cambridge, 7–13 September 1969: International Association of Scientific Hydrology Publication No. 95, p. 256.
- Gow, A.J., and Epstein, Samuel, 1972, On the use of stable isotopes to trace the origins of ice in a floating ice tongue: *Journal of Geophysical Research*, v. 77, no. 33, p. 6552–6557.
- Gow, A.J., and Rowland, Robert, 1965, On the relationship of snow accumulation to surface topography at Byrd Station, Antarctica: *Journal of Glaciology*, v. 5, no. 42, p. 843–847.
- Hansen, H.E., 1946, Antarctica from latitude 68°40’ to 70°20’ s. and from longitude 36°50’ to 40°20’ E.: Oslo, Norges Geografiske Oppmåling, scale 1:250,000.
- Harrison, C.H., 1970, Reconstruction of subglacial relief from radio-echosounding records: *Geophysics*, v. 35, no. 6, p. 1099–1115.
- Hattersley-Smith, G., Keys, J.E., Serson, H., and Mielke, J.E., 1970, Density stratified lakes in northern Ellesmere Island: *Nature*, v. 225, no. 5227, p. 55–56.
- Hawes, J., 1972, Report on the 1971–72 hydrological-glaciological programme, southern Victoria Land dry valleys region: Wellington, New Zealand, Antarctic Research Programme (event 1), 53 p.
- Hayes, D.E., *in* Initial reports of the deep sea drilling project, v. 28: Washington, D.C., National Science Foundation, p. 1.
- Heine, A.J., 1963, Ice breakout around the southern end of Ross Island, Antarctica: *New Zealand Journal of Geology and Geophysics*, v. 6, no. 3, p. 395–401.
- Herbert, W.W., 1962, The Axel Heiberg Glacier: *New Zealand Journal of Geology and Geophysics*, v. 5, no. 5, p. 681–706.
- 1963, *In* Amundsen’s tracks on the Axel Heiberg Glacier: *Geographical Journal*, v. 129, part 4, p. 397–411.
- Hermichen, W.D., Kowski, P., and Wand, U., 1985, Lake Untersee, a first isotope study of the largest freshwater lake in the interior of East Antarctica: *Nature*, v. 315, no. 6015, p. 131–133.
- Heywood, R.B., and Light, J.J., 1975, First direct evidence of life under Antarctic shelf ice: *Nature*, v. 254, no. 5501, p. 591–592.
- Holdsworth, G., 1974, Erebus Glacier Tongue, McMurdo Sound,

- Antarctica: *Journal of Glaciology*, v. 13, no. 67, p. 27–35.
- 1982, Dynamics of Erebus Glacier Tongue: *Annals of Glaciology*, 3, p. 131–137.
- 1985, Some effects of ocean currents and wave motion on the dynamics of floating glacier tongues, *in* Jacobs, S., ed., *Oceanology of the Antarctic Continental Shelf*, Antarctic Research Series, American Geophysical Union, v. 43, p. 253–271.
- Holdsworth, G., and Bull, Colin, 1970, The flow law of cold ice; investigations on Meserve Glacier, Antarctica, *in* Gow, A.J., Keeler, C., Langway, C.C., and Weeks, W.F., eds., *International Symposium on Antarctic Glaciological Exploration (ISAGE)*, Hanover, New Hampshire, U.S.A., 3–7 September 1968: International Association of Scientific Hydrology Publication No. 86, p. 204–216.
- Holdsworth, G., and Holdsworth, R., 1978, Erebus Glacier Tongue movement *Antarctic Journal of the United States*, v. 13, no. 4, p. 61–63.
- Hollin, J.T., 1962, On the glacial history of Antarctica: *Journal of Glaciology*, v. 4, no. 32, p. 173–195.
- Holtedahl, O., 1929, On the geology and physiography of some Antarctic and sub-Antarctic islands: Oslo, Det Norske Videnskaps-Akademi, 172 p.
- Hughes, T., 1973, Is the West Antarctic ice sheet disintegrating?: *Journal of Geophysical Research*, v. 78, no. 33, p. 7884–7910.
- 1975, The West Antarctic ice sheet: Instability, disintegration, and initiation of ice ages: *Reviews of Geophysics and Space Physics*, v. 13, no. 4, p. 502–526.
- 1977, West Antarctic ice streams: *Reviews of Geophysics and Space Physics*, v. 15, no. 1, p. 1–46.
- 1982, On the disintegration of ice shelves: The role of thinning: *Annals of Glaciology*, v. 3, p. 146–151.
- Institut für Angewandte Geodäsie, 1982, Neuschwabenland; Frankfurt am Main, 1:3,000,000 scale.
- Jamieson, A.W., and Wager, A.C., 1983, The ice, water, and energy balances of Spartan Glacier, Antarctica: *British Antarctic Survey Bulletin*, no. 52, p. 155–186.
- Jankowski, E.J., and Drewry, D.J., 1981, The structure of West Antarctica from geophysical studies: *Nature*, v. 291, no. 5810, p. 17–21.
- Jukes, L.M., 1972, The geology of north-eastern Heimefrontfjella, Dronning Maud Land *British Antarctic Survey Scientific Reports*, no. 65, 44 p.
- Kellogg, T.B., Stuiver, Minze, Kellogg, D.E., and Denton, G.H., 1977, Marine microfossils on the McMurdo Ice Shelf: *Antarctic Journal of the United States*, v. 12, no. 4, p. 82–83.
- Kerry, K.R., Grace, D.R., Williams, R., and Burton, H.R., 1977, Studies on some saline lakes of the Vestfold Hills, Antarctica, *in* Llano, G.A., ed., *Adaptations within Antarctic ecosystems*, Proceedings of the 3rd SCAR Symposium on Antarctic Biology: Houston, Gulf Publishing Company, p. 839–858.
- Keys, J.E., 1978, Water regime of Disraeli Fiord, Ellesmere Island: Ottawa, Defence Research Establishment Ottawa, DREO Report No. 792.
- Klepvik, J.O., and Fossum, B.A., 1980, Studies of icebergs, ice fronts and ice walls using side-scanning sonar: *Annals of Glaciology*, v. 1, p. 31–36.
- Korotkevich, E.S., 1965, Ocean bays in the Schirmacher Hills in Queen Maud Land, *in* *Soviet Antarctic Expedition*, v. 3: Amsterdam, Elsevier Publishing Company, p. 3–4.
- Korotkevich, E.S., Koblents, Ya. P., and Kosenko, N.G., 1977, Antarktida. Karta koren'nogo rel'efa Zemli Enderby [Antarctica. Map of the bedrock relief of Enderby Land]: Leningrad, Arctic and Antarctic Research Institute, scale 1:2,500,000.
- Korotkevich, E.S., Savatyugin, L.M., and Morev, V.A., 1978, Skvoznoe burenie shel'fovogo lednika v rayone stantsii Novolazarevskoy [Drilling through the ice shelf in the vicinity of Novolazarevskaya Station]: *Informatsionnyy Byulleten' Sovetskoy Antarkicheskoy Ekspeditsii* [Information Bulletin of the Soviet Antarctic Expedition], no. 98, p. 49–52.
- Kotlyakov, V.M., 1963, Snegonakopleniye v beregovoy polose Vostochnoy Antarktity v 1957–1961 gg [Snow accumulation in the coastal belt of East Antarctica 1957–1961]: *Informatsionnyy Byulleten' Sovetskoy Antarkicheskoy Ekspeditsii* [Information Bulletin of the Soviet Antarctic Expedition], no. 44, p. 59–62.
- Kruchinin, Y.A., 1965, Shel'fovye ledniki Zemli Korolevy Mod [The ice shelves of Queen Maud Land]: Leningrad, Gidrometeorologicheskoe Izdatel'stvo, 180 p.
- Kruchinin, Y.A., Pinter, S., and Simonov, I.M., 1967, Opreделение skorosti i napravleniya dvizheniya lednikov v rayone stantsii Novolazarevskoy [Determination of the speed and direction of glacier movements in the area of Novolazarevskaya Station]: *Informatsionnyy Byulleten' Sovetskoy Antarkicheskoy Ekspeditsii* [Information Bulletin of the Soviet Antarctic Expedition], no. 61, p. 26–31.
- Kurtz, D.D., and Bromwich, D.H., 1985, A recurring, atmospherically forced polynya in Terra Nova Bay, *in* Jacobs, S., ed., *Oceanology of the Antarctic Continental Shelf*, Antarctic Research Series, American Geophysical Union, v. 43, p. 177–201.
- Kusunoki, K., and Ono, N., 1964, Ice conditions in Lützow-Holm Bay, Antarctica, 1956–59, presented on the basis of photo-interpretation: *Contributions from the Institute of Low Temperature Science, Hokkaido University Series A*, no. 19, p. 1–21.
- Law, P.G., 1959, The Vestfold Hills: Australian National Antarctic Research Expeditions (ANARE) Reports, Melbourne, Antarctic Division, Publication No. 47, Series A, Narrative, v. 1, 50 p.
- Ledenev, V.G., and Yevdokimov, A.P., 1965, Izmeneniya shel'fovyykh lednikov Zapadnogo i Eymeri [Changes in the West and Amery Ice shelves]: *Informatsionnyy Byulleten' Sovetskoy Antarkicheskoy Ekspeditsii* [Information Bulletin of the Soviet Antarctic Expedition], no. 55, p. 12–18.
- LeMasurier, W.E., 1972a, Volcanic record of Antarctic glacial history: Implications with regard to Cenozoic sea levels, *in* Price, R.J., and Sugden, D.E., eds., *Polar geomorphology*: London, Institute of British Geographers Special Publication, no. 4, p. 59–74.
- 1972b, Volcanic record of Cenozoic glacial history of Marie Byrd Land, *in* Adie, R.J., ed., *Antarctic geology and geophysics*: Oslo, Universitetsforlaget, p. 251–259.
- LeMasurier, W.E., and Rex, D.C., 1982a, Volcanic record of Cenozoic glacial history in Marie Byrd Land and western Ellsworth Land: Revised chronology and evaluation of tectonic factors, *in* Craddock, Campbell, ed., *Antarctic geoscience*: Madison, University of Wisconsin Press, p. 725–734.
- 1982b, Eruptive potential of volcanoes in Marie Byrd Land: *Antarctic Journal of the United States*, v. 17, no. 5, p. 34–36.
- LeMasurier, W.E., and Wade, F.A., 1968, Fumarolic activity in Marie Byrd Land, *Antarctica: Science*, v. 162, no. 3851, p. 352.
- 1976, Volcanic history in Marie Byrd Land: Implications with regard to southern hemisphere tectonic reconstructions: International Association of Volcanology and Chemistry of the Earth's Interior, Proceedings of the Symposium on Andean and Antarctic Volcanology Problems, Santiago, Chile, September 1974, p. 398–424.
- Levanon, Nadav, 1982, Antarctic ice elevation maps from balloon altimetry: *Annals of Glaciology*, v. 3, p. 184–188.
- Levanon, Nadav, Julian, P.R., and Suomi, V.E., 1977, Antarctic topography from balloons: *Nature*, v. 268, no. 5620, p. 514–516.
- Lindstrom, D., and Tyler, D., 1985, Preliminary results of Pine Island and Thwaites Glaciers study: *Antarctic Journal of the United States*, v. 19, no. 5, p. 53–55.
- Loewe, F., 1956, Contributions to the glaciology of the Antarctic: *Journal of Glaciology*, v. 2, no. 19, p. 657–665.
- MacDonald, W.R., 1976, Antarctic cartography, *in* Williams, R.S., Jr., and Carter, W.D., eds., *ERTS-1, A new window on our planet*: U.S. Geological Survey Professional Paper 929, p. 37–43.
- Madigan, C.T., 1929, Meteorology. Tabulated and reduced records of the Cape Denison station, Adelie Land Australasian Antarctic Expedition 1911–14, Scientific Reports, Sydney, Government Printer, Series B, v. 4, 286 p.
- Mahon, P.T., 1981, Report of the royal commission to inquire into the crash on Mount Erebus, Antarctica, of a DC-10 aircraft operated by Air New Zealand Limited Wellington, Government Printer, 167 p.

- Marsh, P.D., 1985, Ice surface and bedrock topography in Coats Land and part of Dronning Maud Land, Antarctica: British Antarctic Survey Bulletin, no. 68, p. 19–36.
- Martin, P.J., 1976, Ridges on Antarctic ice rises: *Journal of Glaciology*, v. 17, no. 75, p. 141–144.
- Martin, P.J., and Peel, D.A., 1978, The spatial distribution of 10 m temperatures in the Antarctic Peninsula: *Journal of Glaciology*, v. 20, no. 83, p. 311–317.
- Martin, P.J., and Sanderson, T.J.O., 1980, Morphology and dynamics of ice rises: *Journal of Glaciology*, v. 25, no. 91, p. 33–45.
- Mayewski, P.A., Attig, J.W., Jr., and Drewry, D.J., 1979, Pattern of ice surface lowering for Rennick Glacier, northern Victoria Land, Antarctica: *Journal of Glaciology*, v. 22, no. 86, p. 53–65.
- McCrae, I.R., 1984a, A summary of glaciological measurements made between 1960 and 1984 on the McMurdo Ice Shelf, Antarctica: Auckland, New Zealand, Department of Theoretical and Applied Mechanics, School of Engineering, University of Auckland, Report No. 360.
- 1984b, A summary and analysis of glaciological measurements made between 1960 and 1984 on the Pram Point pressure rollers, Antarctica: Auckland, New Zealand, Department of Theoretical and Applied Mechanics, School of Engineering, University of Auckland, Report No. 362.
- McIntyre, N.F., 1985a, A re-assessment of the mass balance of the Lambert Glacier drainage basin, Antarctica: *Journal of Glaciology*, v. 31, no. 107, p. 34–38.
- 1985b, The dynamics of ice-sheet outlets: *Journal of Glaciology*, v. 31, no. 108, p. 99–107.
- in press, Ice sheet drainage basins, balance and measured ice velocities and sub-glacial water, in Drewry, D.J., ed., Antarctica: Glaciological and geophysical folio: Cambridge, Scott Polar Research Institute, University of Cambridge, sheet 12.
- McKee, E.D., ed., 1979, A study of global sand seas: U.S. Geological Survey Professional Paper 1052, 429 p.
- McLeod, I.R., 1964, The saline lakes of the Vestfold Hills, Princess Elizabeth Land, in Adie, R.J., ed., Antarctica geology: Amsterdam, North-Holland, p. 65–72.
- 1967, Glaciological observations in Enderby, Kemp, and Mac. Robertson Lands, Antarctica: Australian National Antarctic Research Expeditions (ANARE) Interim Reports, Melbourne, Antarctic Division, Publication No. 90, Series A, *Glaciology*, v. 4, 48 p.
- Meier, S., 1977, Die kustennahe Eisdecke des westlichen Enderby-Landes, Antarktis; Beiträge zu Relief, Bewegung und Massenhaushalt [The near coastal ice sheet of western Enderby Land, Antarctica; observations on topography, movement, and mass balance]: Gotha/Lipzig, VEB Hermann Haack, 104 p.
- 1983, Portrait of an Antarctic outlet glacier: *Hydrological Sciences Journal*, v. 28, no. 3, p. 403–416.
- Mellor, Malcolm, 1959a, Ice flow in Antarctica: *Journal of Glaciology*, v. 3, no. 25, p. 377–385.
- 1959b, Variations of the ice margins in East Antarctica: *Geographical Journal*, v. 125, part 2, p. 230–235.
- 1960, Antarctic ice terminology: Ice dolines: *Polar Record*, v. 10, no. 64, p. 92.
- 1967, Mass economy of Antarctica: Measurements at Mawson: Australian National Antarctic Research Expeditions (ANARE) Scientific Reports, Melbourne, Antarctic Division, Publication No. 97, Series A, *Glaciology*, v. 4, 110 p.
- Mellor, Malcolm, and McKinnon, Graeme, 1960, The Amery Ice Shelf and its hinterland: *Polar Record*, v. 10, no. 64, p. 30–34.
- Mercer, J.H., 1962, Glacier variations in the Antarctic: *Glaciological Notes*, New York, American Geographical Society, no. 11, p. 5–25.
- 1967, *Glaciers of the Antarctic*: Antarctic Map Folio Series, New York, American Geographical Society, Folio 7, 10 p.
- 1968, Glacial geology of the Reedy Glacier area, Antarctica: *Geological Society of America Bulletin*, v. 79, no. 4, p. 471–486.
- 1971, Cold glaciers in the Transantarctic Mountains, Antarctica: Dry ablation areas and subglacial erosion: *Journal of Glaciology*, v. 10, no. 59, p. 319–321.
- 1972, Some observations on the glacial geology of the Beardmore Glacier area, in Adie, R.J., ed., Antarctica geology and geophysics: Oslo, Universitetsforlaget, p. 427–433.
- 1978, West Antarctic ice sheet and CO₂ greenhouse effect: A threat of disaster: *Nature*, v. 271, no. 5643, p. 321–325.
- Morgan, V.I., 1972, Oxygen isotope evidence for bottom freezing on the Amery Ice Shelf: *Nature*, v. 238, no. 5364, p. 393–394.
- Morgan, V.I., and Budd, W.F., 1975, Radio-echosounding of the Lambert Glacier basin: *Journal of Glaciology*, v. 15, no. 73, p. 103–112.
- Morgan, V.I., Jacka, T.H., Akerman, G.J., and Clarke, A.L., 1982, Outlet glacier and mass-budget studies in Enderby, Kemp and Mac. Robertson Lands, Antarctica: *Annals of Glaciology*, v. 3, p. 204–210.
- Nagata, Takeshi, ed., 1975, Yamato meteorites collected in Antarctica in 1969: *Memoirs of National Institute of Polar Research*, Special Issue No. 5, 110 p.
- ed., 1978, Proceedings of the Second Symposium on Yamato Meteorites: *Memoirs of National Institute of Polar Research*, Tokyo, Special Issue No. 8, 267 p.
- ed., 1979a, Proceedings of the Third Symposium on Antarctic Meteorites: *Memoirs of National Institute of Polar Research*, Tokyo, Special Issue No. 12, 282 p.
- ed., 1979b, Proceedings of the Fourth Symposium on Antarctic Meteorites: *Memoirs of National Institute of Polar Research*, Tokyo, Special Issue No. 15, 293 p.
- ed., 1980, Proceedings of the Fifth Symposium on Antarctic Meteorites: *Memoirs of National Institute of Polar Research*, Tokyo, Special Issue No. 17, 317 p.
- Nagata, Takeshi, and Yanai, Keizo, 1982, The Japanese Antarctic meteorite program-collection and curation (abs.), in Bull, Colin, and Lipschutz, M.E., eds., Workshop on Antarctic glaciology and meteorites: LPI Technical Report No. 82-03, Lunar and Planetary Institute, Houston, Texas, p. 33.
- Nakawo, Masayoshi, Ageta, Yutaka, and Yoshimura, Aiichiro, 1978, Discharge of ice across the Soya Coast, in Ishada, Tamotsu, ed., *Glaciological studies in Mizuho Plateau, East Antarctica, 1969–1975*: Tokyo, *Memoirs of National Institute of Polar Research*, Special Issue No. 7, p. 235–244.
- Nansen, Fridtjof, 1922, The strandflat and isostasy: *Videnskapselskabet Skrifter. I. Matematisk-Naturvidenskabelig Klasse*, v. 2, no. 11, 313 p.
- Naruse, Renji, 1979, Thinning of the ice sheet in Mizuho plateau, East Antarctica: *Journal of Glaciology*, v. 24, no. 90, p. 45–52.
- Nathan, Simon, and Schulte, F.J., 1967, Recent thermal and volcanic activity on Mount Melbourne, northern Victoria Land, Antarctica: *New Zealand Journal of Geology and Geophysics*, v. 10, no. 2, p. 422–430.
- 1968, Geology and petrology of the Campbell-Aviator divide, northern Victoria Land, Antarctica. Part I, Post Paleozoic rocks: *New Zealand Journal of Geology and Geophysics*, v. 11, no. 4, p. 940–975.
- Neal, C.S., 1979, The dynamics of the Ross Ice Shelf revealed by radio echo-sounding: *Journal of Glaciology*, v. 24, no. 90, p. 295–307.
- Neethling, D.C., 1972, South African Antarctic earth science programme 1959–1969: Solid earth geophysics, oceanography and glaciology: *South African Journal of Antarctic Research*, no. 2, p. 2–15.
- Neuburg, H.A.C., Thiel, E., Walker, P.T., Behrendt, J.C., and Aughenbaugh, N.B., 1959, The Filchner Ice Shelf: *Annals of the Association of American Geographers*, v. 49, no. 2, p. 110–119.
- Nichols, R.L., 1960, Geomorphology of Marguerite Bay area, Palmer Peninsula, Antarctica: *Bulletin of the Geological Society of America*, v. 71, no. 10, p. 1421–1450.
- Norsk Polarinstitutt, 1968, Dronning Maud Land, Wohlthatmassivet, sheet M5: Oslo, 1:250,000 scale.
- Oliver, R.L., 1964, The level of former glaciation near the mouth of Beardmore Glacier, in Adie, R.J., ed., Antarctica geology: Amsterdam, North-Holland, p. 138–142.
- Orheim, Olav, 1972, Volcanic activity on Deception Island, South Shetland Islands, in Adie, R.J., ed., Antarctica geology and

- geophysics: Oslo, Universitetsforlaget, p. 117–120.
- 1978, Glaciological studies by Landsat imagery of perimeter of Dronning Maud Land, Antarctica: Norsk Polarinstitutt Skrifter, no. 169, p. 69–80.
- 1979, Flow of Antarctic ice shelves between longitudes 29°E and 44°W (abs.): *Journal of Glaciology*, v. 24, no. 90, p. 484–485.
- 1982, Radio echo-sounding of Riiser-Larsenisen (abs.): *Annals of Glaciology*, v. 3, p. 355.
- Oswald, G.K.A., 1975, Investigation of sub-ice bedrock characteristics by radio-echo sounding: *Journal of Glaciology*, v. 15, no. 73, p. 75–87.
- Parish, T.R., 1981, The katabatic winds of Cape Denison and Port Martin: *Polar Record*, v. 20, no. 129, p. 525–532.
- Pearson, M.R., and Rose, I.H., 1983, The dynamics of George VI Ice Shelf: *British Antarctic Survey Bulletin*, no. 52, p. 205–220.
- Pickard, J., and Adamson, D.A., 1983, Perennially frozen lakes at glacierhock margins, East Antarctica, in Oliver, R.L., James, P.R., and Jago, J.B., eds., *Antarctic earth science*: Canberra, Australian Academy of Science, p. 470–472.
- Potter, J.R., Paren, J.G., and Loynes, J., 1984, Glaciological and oceanographic calculations of the mass balance and oxygen isotope ratio of a melting ice shelf: *Journal of Glaciology*, v. 30, no. 105, p. 161–170.
- Priestley, R.E., 1914, *Antarctic adventure: Scott's northern party*: London, T. Fisher Unwin, 382 p.
- 1923, *Physiography (Robertson Bay and Terra Nova Bay region)*: *British (Terra Nova) Antarctic Expedition 1910–1913*: London, Harrison and Sons, 87 p.
- Qingsong, Zhang, Youyu, Xie, and Yuanfang, Li, 1983, A preliminary study of the evolution of the post late Pleistocene Vestfold Hills environment, East Antarctica, in Oliver, R.L., James, P.R., and Jago, J.B., eds., *Antarctic earth science*: Canberra, Australian Academy of Science, p. 473–477.
- Rabassa, Jorge, Skvarca, Pedro, Bertani, Luis, and Mazzoni, Elizabeth, 1982, Glacier inventory of James Ross and Vega Islands, Antarctic Peninsula: *Annals of Glaciology*, v. 3, p. 260–264.
- Reece, Alan, 1950, The ice of Crown Prince Gustav Channel, Graham Land, Antarctica: *Journal of Glaciology*, v. 1, no. 8, p. 404–409.
- Reusch, Hans, 1894, The Norwegian coast plain: *Journal of Geology*, v. 2, p. 347–349.
- Reynolds, J.M., 1981a, The distribution of mean annual temperatures in the Antarctic Peninsula: *British Antarctic Survey Bulletin*, no. 54, p. 123–133.
- 1981b, Lakes on George VI Ice Shelf, Antarctica: *Polar Record*, v. 20, no. 128, p. 425–432.
- Ritscher, A., 1942, *Deutsche Antarktische Expedition 1938–39, Wissenschaftliche und fliegerische Ergebnisse [German Antarctic Expedition 1938–39, scientific and aerial photographic results]*: Leipzig, Koehler and Amelang, 2 v., 304 p.
- Roberts, Brian, 1981, The place names 'Greater Antarctica' and 'Lesser Antarctica' versus 'East Antarctica' and 'West Antarctica': *British Antarctic Survey Bulletin*, no. 53, p. 257–259.
- Roberts, Brian, Roots, E.F., and Swithinbank, C.W.M., 1955, Suggested terms for ice features: *Polar Record*, v. 7, no. 49, p. 331–332.
- Robin, G. de Q., 1958, Seismic shooting and related investigations; Norwegian-British-Swedish Antarctic Expedition 1949–52, *Scientific Results*, v. 5 Oslo, Norsk Polarinstitutt, 134 p.
- 1967, Surface topography of ice sheets: *Nature*, v. 215, no. 5105, p. 1029–1032.
- 1975, Ice shelves and ice flow: *Nature*, v. 253, no. 5488, p. 168–172.
- 1979, Formation, flow and disintegration of ice shelves: *Journal of Glaciology*, v. 24, no. 90, p. 259–271.
- Robin, G. de Q., Drewry, D.J., and Meldrum, D.T., 1977, International studies of ice sheet and bedrock: *Philosophical Transactions of the Royal Society of London, Series B*, v. 279, no. 963, p. 185–196.
- Robin, G. de Q., Swithinbank, C.W.M., and Smith, B.M.E., 1970, Radio echo exploration of the Antarctic ice sheet, in Gow, A.J., Keeler, C., Langway, C.C., and Weeks, W.F., eds., *International Symposium of Antarctic Glaciological Exploration (ISAGE)*, Hanover, New Hampshire, U.S.A., 3–7 September 1968 International Association of Scientific Hydrology Publication No. 86, p. 97–115.
- Rose, K.E., 1979, Characteristics of ice flow in Marie Byrd Land, Antarctica: *Journal of Glaciology*, v. 24, no. 90, p. 63–75.
- 1982, Radio-echo studies of bedrock in southern Marie Byrd Land, West Antarctica, in Craddock, Campbell, ed., *Antarctic geoscience*: Madison, University of Wisconsin Press, p. 985–992.
- Schaefer, T.G., 1973, Radio-echosounding in western Dronning Maud Land, 1971: *South African Journal of Antarctic Research*, no. 3, p. 45–52.
- Schmidt, T., and Mellinger, G., 1966, Bestimmungen von Eisbewegungen am Rand des antarktischen Inlandeises [Determination of ice movement on the margin of the inland ice sheet of Antarctica]: *Nationalkomitee für Geodäsie und Geophysik der Deutschen Demokratischen Republik, Reihe III, Heft 4*, 32 p.
- Schonfeld, S.G., and van Zyl, C.Z., 1974, Geophysical traverses in the Ahlmannryggen, western Dronning Maud Land, 1973: *South African Journal of Antarctic Research*, no. 4, p. 50–57.
- Schytt, Valter, 1961, Blue ice-fields, moraine features, and glacier fluctuations: Norwegian-British-Swedish Antarctic Expedition 1949–52, *Scientific Results*, v. 4E: Oslo, Norsk Polarinstitutt, p. 181–204.
- Scott, R.F., 1913, *Scott's last expedition*: London, Smith Elder and Co., 2 v., 1167 p.
- Shabtaie, Sion, and Bentley, C.R., 1982, Tabular icebergs: Implications from geophysical studies of ice shelves: *Journal of Glaciology*, v. 28, no. 100, p. 413–430.
- Shackleton, E.H., 1909, *The heart of the Antarctic; being the story of the British Antarctic expedition 1907–1909*: London, William Heinemann, 2 v., 791 p.
- 1919, *South, the story of Shackleton's last expedition 1914–1917*: London, Heinemann, 376 p.
- Short, N.M., Lowman, P.D., Jr., Freden, S.C., and Finch, W.A., Jr., 1976, *Mission to Earth: Landsat views the world* Washington, D.C., National Aeronautics and Space Administration, NASA SP-360,460 p.
- Shumskiy, P.A., Kotlyakov, V.M., and Yevteyev, S.A., 1961, Lednikovyi kupol ostrova Drigal'skogo [The Drygalski Island ice cap]: *Glytzyologicheskoye Issledovaniya, Sbornik Statey, IX Razdel Programmy MGG (Glytzyologiya)*, no. 6, Moscow, U.S.S.R, Academy of Sciences, p. 45–69.
- Simkin, Tom, Siebert, Lee, McClelland, Lindsay, Bridge, David, Newhall, Christopher, and Latter, J.H., 1981, *Volcanoes of the world*: New York, Van Nostrand Reinhold, 232 p.
- Simonov, I.M., 1964, Tidal phenomena in the sea inlets of the Schirmacher Ponds: *Soviet Antarctic Expedition Information Bulletin*, no. 41, (Translated into English by American Geophysical Union, Washington, D.C.), p. 328–329.
- 1971, *Oazisy Vostochnoy Antarktity [Oases of eastern Antarctica]*: Leningrad, Gidrometeorologicheskoye Izdatel'stvo, 176 p.
- Smith, A.M., 1986, Ice rumples on Ronne Ice Shelf, Antarctica: *British Antarctic Survey Bulletin*, no. 72, p. 47–52.
- Smith, B.M.E., 1972, Airborne radio echo sounding of glaciers in the Antarctic Peninsula: *British Antarctic Survey Scientific Reports*, no. 72, 11 p.
- Solomon, Harold, and Ahlnäs, Kristina, 1980, Ice spirals off Barrow as seen by satellite: *Arctic*, v. 33, no. 1, p. 184–188.
- Solopov, A.V., 1969, *Oases in Antarctica: Meteorology*, Jerusalem, Israel Program for Scientific Translations, no. 14, 146 p.
- Southard, R.B., and MacDonald, W.R., 1974, The cartographic and scientific application of ERTS—Imagery in polar regions: *Journal of Research, U.S. Geological Survey*, v. 2, no. 4, p. 385–394.
- Steed, R.H.N., and Drewry, D.J., 1982, Radio-echosounding investigations of Wilkes Land, Antarctica, in Craddock, Campbell, ed., *Antarctic geoscience*: Madison, University of Wisconsin Press, p. 969–975.
- Stephenson, Alfred, and Fleming, W.L.S., 1940, King George the Sixth Sound: *Geographical Journal*, v. 96, no. 3, p. 153–166.

- Stephenson, S.N., 1984, Glacier flexure and the position of grounding lines: Measurements on Rutford Ice Stream, Antarctica: *Annals of Glaciology*, v. 5, p. 165-169.
- Stephenson, S.N., and Doake, C.S.M., 1982, Dynamic behaviour of Rutford Ice Stream: *Annals of Glaciology*, v. 3, p. 295-299.
- Stuart, A.W., and Bull, Colin, 1963, Glaciological observations on the Ross Ice Shelf near Scott Base, Antarctica: *Journal of Glaciology*, v. 4, no. 34, p. 399-414.
- Stuiver, Minze, Denton, G.H., Hughes, T.J., and Fastook, J.L., 1981, History of the marine ice sheet in West Antarctica during the last glaciation: A working hypothesis, *in* Denton, G.H., and Hughes, T.J., eds., *The last great ice sheets*: New York, Wiley-Interscience, p. 319-436.
- Swithinbank, Charles, 1955, Ice shelves: *Geographical Journal*, v. 121, part 1, p. 64-76
- 1957a, The morphology of the ice shelves of western Dronning Maud Land; Norwegian-British-Swedish Antarctic Expedition 1949-52, *Scientific Results*, v. 3A Oslo, Norsk Polarinstittutt, 37 p.
- 1957b, The regime of the ice shelf at Maudheim as shown by stake measurements: Norwegian-British-Swedish Antarctic Expedition 1949-52, *Scientific Results*, v. 3B: Oslo, Norsk Polarinstittutt, p. 43-75.
- 1958, The morphology of the inland ice sheet and nunatak areas of western Dronning Maud Land; Norwegian-British-Swedish Antarctic Expedition 1949-52, *Scientific Results*, v. 3D: Oslo, Norsk Polarinstittutt, p. 99-117.
- 1960, Ice movement inland; Norwegian-British-Swedish Antarctic Expedition 1949-52, *Scientific Results*, v. 3F Oslo, Norsk Polarinstittutt, p. 147-158.
- 1963, Ice movement of valley glaciers flowing into the Ross Ice Shelf, Antarctica: *Science*, v. 141, no. 3580, p. 523-524.
- 1964, To the valley glaciers that feed the Ross Ice Shelf: *Geographical Journal*, v. 130, part 1, p. 32-48
- 1966, A year with the Russians in Antarctica: *Geographical Journal*, v. 132, part 4, p. 463-475.
- 1968, Radio echo sounding of Antarctic glaciers from light aircraft, *in* Ward, W., ed., *General Assembly of Bern, Commission of Snow and Ice, Reports and discussions*: International Association of Scientific Hydrology, Publication No. 79, p. 405-414.
- 1969a, Giant icebergs in the Weddell Sea, 1967-68: *Polar Record*, v. 14, no. 91, p. 477-478.
- 1969b, Airborne radio echo sounding by the British Antarctic Survey: *Geographical Journal*, v. 135, part 4, p. 551-553.
- 1970, Ice movement in the McMurdo Sound area of Antarctica, *in* Gow, A.J., Keeler, C., Langway, C.C., and Weeks, W.F., eds., *International Symposium on Antarctic Glaciological Exploration (ISAGE)*, Hanover, New Hampshire, U.S.A., 3-7 September 1968: International Association of Scientific Hydrology Publication No. 86, p. 472-487.
- 1973a, Higher resolution satellite pictures: *Polar Record*, v. 16, no. 104, p. 739-741.
- 1973b, Satellite view of McMurdo Sound, Antarctica: *Polar Record*, v. 16, no. 105, p. 851-854.
- 1977, Glaciological research in the Antarctic Peninsula: *Philosophical Transactions of the Royal Society of London*, Series B, 'v. 279, no. 941, p. 141-183.
- 1980, The problem of a glacier inventory of Antarctica, *in* World glacier inventory, Proceedings of the workshop at Riederalp, Switzerland, 17-22 September 1978: International Association of Hydrological Sciences, Publication No. 126, p. 229-236.
- 1985, A distant look at the cryosphere: *Advances in Space Research*, v. 5, no. 6, p. 263-274.
- Swithinbank, Charles, and Lane, Charles, 1977, Antarctic mapping from satellite imagery, *in* Peel, R.F., Curtis, L.F., and Barrett, E.C., eds., *Remote sensing of the terrestrial environment: Proceedings of the Twenty-eighth Symposium of the Colston Research Society*, held in the University of Bristol, April 5th to 9th, 1976 London, Butterworths, p. 212-221.
- Swithinbank, Charles, and Lucchitta, B.K., 1986, Multispectral digital image mapping of Antarctic ice features: *Annals of Glaciology*, v. 8, p. 159-163.
- Swithinbank, Charles, McClain, Paul, and Little, Patricia, 1977, Drift tracks of Antarctic icebergs: *Polar Record*, v. 18, no. 116, p. 495-501.
- Swithinbank, Charles, and Zumbege, J.H., 1965, The ice shelves, *in* Hatherton, Trevor, ed., *Antarctica: A New Zealand Antarctic Society Survey*: London, Methuen, p. 199-220.
- Thomas, R.H., 1973, The dynamics of the Brunt Ice Shelf, Coats Land, Antarctica: *British Antarctic Survey Scientific Reports*, no. 79, 45 p.
- Thomas, R.H., MacAyeal, D.R., Eilers, D.R., and Gaylord, D.R., 1984, Glaciological studies on the Ross Ice Shelf, Antarctica, 1973-1978, *in* Bentley, C.R., and Hayes, D.E., eds., *Antarctic Research Series*, v. 42 Washington, D.C., American Geophysical Union, p. 21-53.
- Thomas, R.H., Sanderson, TJO, and Rose, K.E., 1979, Effect of climatic warming on the West Antarctic ice sheet: *Nature*, v. 277, no. 5695, p. 355-358.
- Tierney, T.J., 1975, An externally draining freshwater system in the Vestfold Hills, Antarctica: *Polar Record*, v. 17, no. 111, p. 684-686.
- Tingey, R.J., and Convine, J.W., compilers, 1982, *Geology of the southern Prince Charles Mountains, Australian Antarctic Territory*: Canberra, Bureau of Mineral Resources, Geology and Geophysics, Department of National Development and Energy; scale, 1:500,000.
- Tolstikov, E.I., chief editor, 1966, *Atlas Antarktiki*: Moskva, Glavnoe upravlenie geodezii i kartografii, v. 1, 236 p.
- Trepov, G.V., Sheremet'ev, A.N., and Stepanov, V.K., 1979, Raboty po radiolokatsionnomu zondirovaniyu lednikov v rayone Molodezhnoy [Radio-echosounding of glaciers in the region of Molodezhnaya]: *Informatsionnyy Byulleten' Sovetskoy Antarkicheskoy Ekspeditsii* [Information Bulletin of the Soviet Antarctic Expedition], no. 99, p. 35-38.
- U.S. Geological Survey, 1972, *Ross Ice Shelf*: Washington, D.C. 1:1,000,000 scale.
- Van Autenboer, T., 1964, The geomorphology and glacial geology of the *Sar* Rondane, Dronning Maud Land, *in* Adie, R.J., ed., *Antarctic geology*: Amsterdam, North-Holland, p. 81-103.
- Van Autenboer, T., and Declair, H., 1972, Ice thickness and subglacial relief of the Jelbartisen-Trolltunga area, Dronning Maud Land, *in* Adie, R.J., ed., *Antarctic geology and geophysics*: Oslo, Universitetsforlaget, p. 713-722.
- 1978, Glacier discharge in the *Sar* Rondane, a contribution to the mass balance of Dronning Maud Land, Antarctica: *Zeitschrift für Gletscherkunde und Glazialgeologie*, v. 14, part 1, p. 1-16.
- van Zyl, R.B., 1973, Radio-echosounding in western Dronning Maud Land, 1972: *South African Journal of Antarctic Research*, No. 3, p. 53-59.
- Wada, Makoto, and Mae, Shinji, 1981, Airborne radio-echosounding on the Shirase Glacier and its drainage basin, East Antarctica: *Nankyoku Shiryo* [Antarctic Record], no. 72, p. 16-25.
- Wada, Makoto, Yamanouchi, Takashi, and Mae, Shinji, 1982, Radio echo-sounding of Shirase Glacier and the Yamato Mountains area: *Annals of Glaciology*, v. 3, p. 312-315.
- Wager, A.C., 1972, Flooding of the ice shelf in George VI Sound: *British Antarctic Survey Bulletin*, no. 28, p. 71-74.
- 1982, Mapping the depth of a valley glacier by radio echo sounding: *British Antarctic Survey Bulletin*, no. 51, p. 111-123.
- Wager, A.C., and Jamieson, A.W., 1983, Glaciological characteristics of Spartan Glacier, Alexander Island, Antarctica: *British Antarctic Survey Bulletin*, no. 52, p. 221-228.
- Webers, G.F., and Spletstoesser, J.F., 1982, *Geology, paleontology, and bibliography of the Ellsworth Mountains*: *Antarctic Journal of the United States*, v. 17, no. 5, p. 36-38.
- Wellman, Peter, 1982, Surging of Fisher Glacier, eastern Antarctica: Evidence from geomorphology: *Journal of Glaciology*, v. 28, no. 98, p. 23-28.
- Williams, R.S., Jr., Ferrigno, J.G., and Kent, T.M., 1984, Index map

- and table of optimum Landsat 1 2, and 3 images of Antarctica: U.S. Geological Survey Open-File Report 84-573 2 p. (includes 1:5,000,000-scale map).
- Williams, R.S., Jr., Ferrigno, J.G., Kent, T.M., and Schoonmaker, J.W., Jr., 1982, Landsat images and mosaics of Antarctica for mapping and glaciological studies: *Annals of Glaciology*, v. 3 p. 321-326
- Williams, R.S., Jr., Meunier, T.K., and Ferrigno, J.G., 1983, Blue ice, meteorites, and satellite imagery in Antarctica: *Polar Record*, v. 21, no. 134, p. 493-496
- Wilson, C.R., and Crary, A.P., 1961, Ice movement studies on the Skelton Glacier: *Journal of Glaciology*, v. 3, no. 29, p. 873-878.
- Wolmarans, L.G., 1982, Subglacial morphology of the Ahlmannryggen and Borgmassivet, western Dronning Maud Land, *in* Craddock, Campbell, ed., *Antarctic geoscience*: University of Wisconsin Press, Madison, p. 963-968
- Wolmarans, L.G., and Kent, L.E., 1982, Geological investigations in western Dronning Maud Land—a synthesis: *South African Journal of Antarctic Research*, Supplement 2 p. 1-93.
- Wolmarans, L.G., and Krynauw, J.R., compilers, 1981, Reconnaissance geological maps of the Ahlmannryggen (sheet 1), Borgmassivet (sheet 2), and Kirwanveggen (sheet 3) areas, western Dronning Maud Land, Antarctica: Pretoria, South African Committee for Antarctic Research, series of 3 satellite image map sheets; scale, 1:250,000
- Worsfold, R.J., 1967, Physiography and glacial geomorphology of Heimefrontfjella, Dronning Maud Land *British Antarctic Survey Bulletin*, no. 11, p. 49-57.
- Wright, C.S., 1923, Physiography of the Beardmore Glacier region; *British (Terra Nova) Antarctic Expedition 1910-1913*: London, Harrison and Sons, 25 p.
- Wright, C.S., and Priestley, R.E., 1922, *Glaciology*; *British (Terra Nova) Antarctic Expedition 1910-1913*: London, Harrison and Sons, 581 p.
- Yoshida, Masaru, Ando, Hisao, Omoto, Kunio, Naruse, Renji, and Ageta, Yutaka, 1971, Discovery of meteorites near Yamato Mountains, East Antarctica: *Nankyoku Shiryo [Antarctic Record]*, no. 39, p. 62-65.
- Zotikov, I.A., Zagorodnov, V.S., and Raikovsky, J.V., 1979, Sea ice on bottom of Ross Ice Shelf: *Antarctic Journal of the United States*, v. 14, no. 5, p. 65-66
- Zwally, H.J., and Gloersen, Per, 1977, Passive microwave images of the polar regions and research applications: *Polar Record*, v. 18, no. 116, p. 431-450.

TABLES 6 AND 7

TABLE 6.—Optimum Landsat 1,2, and 3 MSS and Landsat 2 RBV images of glaciers of Antarctica

[See table 5 for explanation of code]

Path-Row	Nominal scene center (lat.-long.)	Landsat identification number	Date	Solar elev. angle (degrees)	Code	Cloud cover (percent)	Remarks
001-111	071°50'S. 099°47'W.	1137-14262	07 Dec 72	30		90	Ice front
001-112	073°04'S. 102°23'W.	1191-14264	30 Jan 73	22		0	King Peninsula, Burke Island
001-113	074°16'S. 105°22'W.	1191-14270	30 Jan 73	21		0	Pine Island Bay
001-114	075°25'S. 108°47'W.	1119-14273	19 Nov 72	24		15	Mount Murphy
001-115	076°31'S. 112°46'W.	1119-14280	19 Nov 72	23		0	Mount Takahe (volcano with caldera)
001-116	077°33'S. 117°23'W.	1191-14282	30 Jan 73	18		50	
001-117	078°29'S. 122°46'W.	1191-14284	30 Jan 73	17		50	
001-118	079°19'S. 129°01'W.						
001-119	080°01'S. 136°11'W.						
002-111	071°50'S. 101°13'W.	1174-14314	13 Jan 73	27		20	Thurston Island
002-112	073°04'S. 103°49'W.	1174-14320	13 Jan 73	26		10	King Peninsula, Burke Island
002-113	074°16'S. 106°48'W.	1174-14323	13 Jan 73	25		30	Pine Island Bay
002-114	075°25'S. 110°13'W.	1174-14325	13 Jan 73	24		5	Mount Murphy
002-115	076°31'S. 114°12'W.						
002-116	077°33'S. 118°49'W.	1588-14290	03 Mar 74	8		80	
002-117	078°29'S. 124°12'W.						
002-118	079°19'S. 130°27'W.						
002-119	080°01'S. 137°37'W.						
003-111	071°50'S. 102°39'W.	1157-14374	27 Dec 72	30		50	
003-112	073°04'S. 105°15'W.	1157-14380	27 Dec 72	29		0	Burke Island
003-113	074°16'S. 108°14'W.	1157-14383	27 Dec 72	28		10	Thwaites Iceberg Tongue
003-114	075°25'S. 111°40'W.	1157-14385	27 Dec 72	26		50	
003-115	076°31'S. 115°38'W.	1157-14392	27 Dec 72	25		20	Toney Mountain, Crary Mountains (volcanoes with craters)

TABLE 6.—Optimum Landsat 1, 2, and 3 MSS and Landsat 2 RBV images of glaciers of Antarctica—Continued

Path-Row	Nominal scene center (lat.-long.)	Landsat identification number	Date	Solar elev. angle (degrees)	Code	Cloud cover (percent)	Remarks
003-116	077°33'S. 120°15'W.	1157-14394	27 Dec 72	24		65	
003-117	078°29'S. 125°38'W.						
003-118	079°19'S. 131°53'W.						
003-119	080°01'S. 139°03'W.						
004-111	071°50'S. 104°05'W.					100	
004-112	073°04'S. 106°41'W.					100	
004-113	074°16'S. 109°40'W.	1177-14494	16 Jan 73	25		20	Thwaites Iceberg Tongue, Bear Island
004-114	075°25'S. 113°06'W.	1177-14500	16 Jan 73	24		10	Kohler Range
004-115	076°31'S. 117°04'W.	1177-14503	16 Jan 73	23		20	Toney Mountain, Crary Mountains (volcanoes with craters)
004-116	077°33'S. 121°41'W.						
004-117	078°29'S. 127°04'W.						
004-118	079°19'S. 133°19'W.	1518-14431	23 Dec 73	22		10	
004-119	080°01'S. 140°29'W.	1465-14500	31 Oct 73	13		20	Ice Stream E
005-112	073°04'S. 108°07'W.	1140-14440	10 Dec 72	29		0	Tip of Thwaites Iceberg Tongue
005-113	074°16'S. 111°06'W.	1140-14442	10 Dec 72	28		5	Thwaites Iceberg Tongue, Bear Island
005-114	075°25'S. 114°32'W.						
005-115	076°31'S. 118°30'W.	1140-14451	10 Dec 72	25		80	
005-116	077°33'S. 123°07'W.					100	
005-117	078°29'S. 128°30'W.						
005-118	079°19'S. 134°45'W.						
005-119	080°01'S. 141°55'W.						
006-112	073°04'S. 109°33'W.	1160-14551	30 Dec 72	28		10	Tip of Thwaites Iceberg Tongue'
006-113	074°16'S. 112°32'W.	1160-14554	30 Dec 72	27		15	Bear Island, Martin Peninsula
006-114	075°25'S. 115°58'W.	1160-14560	30 Dec 72	26		60	Kohler Range, Toney Mountain

TABLE 6.—*Optimum Landsat 1, 2, and 3 MSS and Landsat 2 RBV images of glaciers of Antarctica—Continued*

Path-Row	Nominal scene center (lat.—long.)	Landsat identification number	Date	Solar elev. angle (degrees)	Code	Cloud cover (percent)	Remarks
006-115	076°31'S. 119°56'W.	2337-14481	25 Dec 75	25		10	Crary Mountains (volcanoes with craters)
006-116	077°33'S. 124°33'W.						
006-117	078°29'S. 129°56'W.						
006-118	079°19'S. 136°11'W.	1538-14541	12 Jan 74	20		50	
006-119	080°01'S. 143°21'W.					100	
007-112	073°04'S. 110°59'W.	1179-15005	18 Jan 73	25		100	Ice front visible through clouds
007-113	074°16'S. 113°58'W.	1179-15011	18 Jan 73	24		90	Kohler Range
007-114	075°25'S. 117°24'W.	1179-15014	18 Jan 73	23		60	Toney Mountain
007-115	076°31'S. 121°22'W.	1177-14505	16 Jan 73	22		10	
007-116	077°33'S. 125°59'W.					100	
007-117	078°29'S. 131°22'W.	1179-15025	18 Jan 73	20		60	
007-118	079°19'S. 137°37'W.	1521-15002	26 Dec 73	22		70	
007-119	080°01'S. 144°47'W.	1521-15005	26 Dec 73	21		70	
008-112	073°04'S. 112°25'W.	1540-15030	14 Jan 74	26		80	
008-113	074°16'S. 115°24'W.						
008-114	075°25'S. 118°50'W.						
008-115	076°31'S. 122°48'W.						
008-116	077°33'S. 127°25'W.						
008-117	078°29'S. 132°48'W.					100	
008-118	079°19'S. 139°03'W.						
008-119	080°01'S. 146°03'W.						
009-112	073°04'S. 113°51'W.					100	
009-113	074°16'S. 116°50'W.	1217-15132	25 Feb 73	13		90	Ice front visible through clouds
009-114	075°25'S. 120°16'W.	1217-15134	25 Feb 73	12		65	

TABLE 6.—Optimum Landsat 1, 2, and 3 MSS and Landsat 2 RBV images of glaciers of Antarctica—Continued

Path-Row	Nominal scene center (lat.—long.)	Landsat identification number	Date	Solar elev. angle (degrees)	Code	Cloud cover (percent)	Remarks
009-115	076°31'S. 124°14'W.	1217-15141	25 Feb 73	11		85	
009-116	077°33'S. 128°51'W.	1217-15143	25 Feb 73	10		80	
009-117	078°29'S. 134°14'W.						
009-118	079°19'S. 140°29'W.	1505-15121	10 Dec 73	22		90	
009-119	080°01'S. 147°39'W.	1505-15124	10 Dec 73	21		70	
010-112	073°04'S. 115°17'W.	2016-15064	07 Feb 75	19		0	
010-113	074°16'S. 118°16'W.	1488-15160	23 Nov 73	26		0	Wright Island, Scott Peninsula
010-114	075°25'S. 121°42'W.	1488-15163	23 Nov 73	25		25	Bakutis Coast, Getz Ice Shelf
010-115	076°31'S. 125°40'W.	1200-15194	08 Feb 73	17		60	Volcanoes in Executive Committee Range
010-115	076°31'S. 125°40'W.	1488-15165	23 Nov 73	23		50	
010-116	077°33'S. 130°17'W.	1200-15201	08 Feb 73	16		15	Band 6, volcanoes in Executive Committee Range
010-117	078°29'S. 135°40'W.	1200-15203	08 Feb 73	14		70	
010-118	079°19'S. 141°55'W.						
010-119	080°01'S. 149°05'W.						
011-112	073°04'S. 116°43'W.						
011-113	074°16'S. 119°42'W.	1146-15185	16 Dec 72	28		0	Bakutis Coast, Getz Ice Shelf
011-114	075°25'S. 123°08'W.	1146-15191	16 Dec 72	27		5	
011-115	076°31'S. 127°06'W.	1146-15194	16 Dec 72	26		55	Mount Hampton (volcano with caldera)
011-116	077°33'S. 131°43'W.	1146-15200	16 Dec 72	24		70	
011-117	078°29'S. 137°06'W.	1472-15291	07 Nov 73	17		25	
011-118	079°19'S. 143°21'W.	1472-15294	07 Nov 73	16		25	'Ice Stream E'
011-119	080°01'S. 150°31'W.	1472-15300	07 Nov 73	15		5	'Ice Stream E'
012-112	073°04'S. 118°09'W.	1166-15293	05 Jan 73	28		40	
012-113	074°16'S. 121°08'W.	1166-15300	05 Jan 73	26		90	

TABLE 6.—*Optimum Landsat 1, 2, and 3 MSS and Landsat 2 RBV images of glaciers of Antarctica—Continued*

Path-Row	Nominal scene center (lat.—long.)	Landsat identification number	Date	Solar elev. angle (degrees)	Code	Cloud cover (percent)	Remarks
012-114	075°25'S. 124°34'W.						
012-115	076°31'S. 128°32'W.	1472-15282	07 Nov 73	20		90	Mount Sidley (volcano with caldera), Mount Waesche (volcano)
012-116	077°33'S. 133°09'W.						
012-117	078°29'S. 138°32'W.						
012-118	079°19'S. 144°47'W.	1491-15352	26 Nov 73	20		10	'Ice Stream E'
012-119	080°01'S. 151°57'W.	1491-15354	26 Nov 73	19		10	'Ice Stream E'
013-112	073°04'S. 119°36'W.					100	
013-113	074°16'S. 122°34'W.	1131-15360	01 Dec 72	27		95	
013-114	075°25'S. 126°00'W.	1491-15334	26 Nov 73	25		30	USAS Escarpment
013-115	076°31'S. 129°58'W.	1491-15340	26 Nov 73	24		40	Mount Hampton (volcano with caldera), Mount Flint, Mount Petros
013-116	077°33'S. 134°36'W.	1491-15343	26 Nov 73	23		80	
013-117	078°29'S. 139°58'W.	1131-15374	01 Dec 72	22		10	
013-118	079°19'S. 146°13'W.	1492-15410	27 Nov 73	21		50	'Ice Stream E
013-119	080°01'S. 153°24'W.	1492-15413	27 Nov 73	19		5	Ice rumples
014-112	073°04'S. 121°02'W.	1132-15412	02 Dec 72	28		90	
014-113	074°16'S. 124°00'W.	1492-15390	27 Nov 73	26		80	
014-114	075°25'S. 127°26'W.	1492-15392	27 Nov 73	25		50	Mount Flint, Mount Petros
014-114	075°25'S. 127°26'W.	1186-15420	25 Jan 73	22		90	Mount Flint, Mount Petros
014-115	076°31'S. 131°24'W.	1492-15394	27 Nov 73	24		50	Ames Range, eastern portion Flood Range, Mount Flint, Mount Petros
014-116	077°33'S. 136°02'W.	1186-15425	25 Jan 73	19		70	
014-117	078°29'S. 141°24'W.	1186-15431	25 Jan 73	18		90	
014-118	079°19'S. 147°39'W.						
014-119	080°01'S. 154°50'W.						

TABLE 6. — *Optimum Landsat 1, 2, and 3 MSS and Landsat 2 RBV images of glaciers of Antarctica — Continued*

Path-Row	Nominal scene center (lat.—long.)	Landsat identification number	Date	Solar elev. angle (degrees)	Code	Cloud cover (percent)	Remarks
015-112	073°04'S. 122°28'W.					100	
015-113	074°16'S. 125°26'W.	1169-15471	08 Jan 73	26		95	
015-114	075°25'S. 132°50'W.					100	
015-115	076°31'S. 132°50'W.					100	
015-116	077°33'S. 137°28'W.					100	
015-117	078°29'S. 142°50'W.	1169-15485	08 Jan 73	22		90	
015-118	079°19'S. 149°05'W.						
015-119	080°01'S. 156°16'W.	2309-15361	27 Nov 75	19		20	
016-112	073°04'S. 123°53'W.	1206-15525	14 Feb 73	18		90	
016-113	074°16'S. 126°52'W.	1152-15531	22 Dec 72	28		40	Ice front visible through clouds
016-114	075°25'S. 130°18'W.	1152-15533	22 Dec 72	27		10	Ames Range, eastern portion Flood Range, Mount Flint, Mount Petros
016-115	076°31'S. 134°16'W.	1152-15540	22 Dec 72	26		60	Flood Range, Mount Berlin (volcano with crater)
016-116	077°33'S. 138°53'W.						
016-117	078°29'S. 144°16'W.						
016-118	079°19'S. 150°31'W.						
016-119	080°01'S. 157°42'W.	2310-15415	28 Nov 75	19		40	
017-112	073°04'S. 125°20'W.	1135-15583	05 Dec 72	28		70	Mount Siple
017-112	073°04'S. 125°20'W.	1152-15524	22 Dec 72	29		60	Mount Siple
017-113	074°16'S. 128°19'W.	1135-15590	05 Dec 72	27		90	
017-114	075°25'S. 131°44'W.	1117-15592	17 Nov 72	24		40	Ames Range, Mount Bursey
017-115	076°31'S. 135°43'W.	1117-15594	17 Nov 72	22		0	Flood Range, Mount Berlin (volcano with crater)
017-116	077°33'S. 140°20'W.	1117-16001	17 Nov 72	21		0	Clark Mountains
017-117	078°29'S. 145°43'W.	1135-16004	05 Dec 72	23		80	
017-118	079°19'S. 151°58'W.	2671-15374	23 Nov 76	19		10	RBV

TABLE 6.—*Optimum Landsat 1, 2, and 3 MSS and Landsat 2 RBV images of glaciers of Antarctica—Continued*

Path-Row	Nominal scene center (lat.—long.)	Landsat identification number	Date	Solar elev. angle (degrees)	Code	Cloud cover (percent)	Remarks
017–119	080°01'S. 159°08'W.	2671–15381	23 Nov 76	18	●	0	RBV
018–112	073°04'S. 126°46'W.	1172–16035	11 Jan 73	27	●	0	Best image of Mount Siple
018–113	074°16'S. 129°45'W.	1172–16042	11 Jan 73	26	●	0	Getz Ice Shelf , Dean Island, Grant Island
018–114	075°25'S. 133°10'W.	1172–16044	11 Jan 73	24	●	5	Ames Range, Mount Bursey , Flood Range, Bennett Bluff
018–115	076°31'S. 137°09'W.	1514–16022	19 Dec 73	26	◐	15	Flood Range , Mount Berlin, Mount Moulton
018–116	077°33'S. 141°46'W.	1514–16025	19 Dec 73	25	●	5	Ford Ranges, Boyd Glacier
018–117	078°29'S. 147°09'W.	1514–16031	19 Dec 73	23	◐	20	Ford Ranges, Hammond Glacier
018–118	079°19'S. 153°24'W.	1514–16034	19 Dec 73	22	◐	30	Shirase Coast
018–119	080°01'S. 160°34'W.	1514–16040	19 Dec 73	21	◐	50	South edge Roosevelt Island
019–112	073°04'S. 128°12'W.	1209–16101	17 Feb 73	17	◐	90	Mount Siple
019–113	074°16'S. 131°11'W.	1209–16103	17 Feb 73	16	◐	50	Getz Ice Shelf
019–114	075°25'S. 134°36'W.	1209–16110	17 Feb 73	15	◐	80	Hobbs Coast
019–115	076°31'S. 138°35'W.				◑	100	
019–116	077°33'S. 143°12'W.	1209–16115	17 Feb 73	13	◐	90	Ford Ranges
019–117	078°29'S. 148°35'W.	2673–15484	25 Nov 76	20	◐	20	RBV
019–118	079°19'S. 154°50'W.	2673–15490	25 Nov 76	19	◐	25	RBV
019–119	080°01'S. 162°00'W.	2313–15590	01 Dec 75	19	◑	25	South edge Roosevelt Island
020–113	074°16'S. 132°37'W.	1120–16161	20 Nov 72	25	◑	10	Grant Island
020–114	075°25'S. 136°03'W.	1120–16163	20 Nov 72	24	◐	40	McDonald Heights, Flood Range
020–115	076°31'S. 140°01'W.	2026–16052	17 Feb 75	13	◐	50	
020–116	077°33'S. 144°38'W.	2026–16055	17 Feb 75	12	◐	80	
020–116	077°33'S. 144°38'W.	1192–16172	31 Jan 73	18	◐	80	
020–117	078°29'S. 150°01'W.	1534–16141	08 Jan 74	22	◐	40	Shirase Coast
020–118	079°19'S. 156°16'W.	1534–16143	08 Jan 74	21	◐	50	South edge Roosevelt Island

TABLE 6.—*Optimum Landsat 1, 2, and 3 MSS and Landsat 2 RBV images of glaciers of Antarctica—Continued*

Path-Row	Nominal scene center (lat.—long.)	Landsat identification number	Date	Solar elev. angle (degrees)	Code	Cloud cover (percent)	Remarks
020-119	080°01'S. 163°26'W.					100	
021-113	074°16'S. 134°03'W.	1175-16213	14 Jan 73	25		0	Grant Island, Getz Ice Shelf
021-114	075°25'S. 137°29'W.	1175-16215	14 Jan 73	24		0	Hull Glacier, Ruppert Coast, Mount Berlin
021-115	076°31'S. 141°27'W.	1175-16222	14 Jan 73	23		20	Land Glacier, Ruppert Coast
021-116	077°33'S. 146°04'W.						
021-117	078°29'S. 151°27'W.					100	
021-118	079°19'S. 157°42'W.						
021-119	080°01'S. 164°52'W.					100	
022-113	074°16'S. 135°29'W.	1158-16273	28 Dec 72	27		80	Ice front
022-114	075°25'S. 138°55'W.	1158-16275	28 Dec 72	26		50	
022-115	076°31'S. 142°53'W.	1158-16282	28 Dec 72	25		10	Balchen Glacier, Fosdick Mountains
022-116	077°33'S. 147°30'W.	1158-16284	28 Dec 72	24		20	Sulzberger Shelf, Boyd Glacier
022-117	078°29'S. 152°53'W.						
022-118	079°19'S. 159°08'W.						
022-119	080°01'S. 166°18'W.	2316-16161	04 Dec 74	20		60	
023-113	074°16'S. 136°55'W.					100	
023-114	075°25'S. 140°21'W.	2317-16195	05 Dec 75	25		60	Ruppert Coast, Mount McCoy
023-115	076°31'S. 144°19'W.					100	
023-116	077°33'S. 148°56'W.						
023-117	078°29'S. 154°19'W.						
023-118	079°19'S.. 160°34'W.						
023-119	080°01'S. 167°44'W.					100	
024-114	075°25'S. 141°47'W.						
024-115	076°31'S. 145°45'W.						

TABLE 6.—*Optimum Landsat 1, 2, and 3 MSS and Landsat 2 RBV images of glaciers of Antarctica—Continued*

Path-Row	Nominal scene center (lat.—long.)	Landsat identification number	Date	Solar elev. angle (degrees)	Code	Cloud cover (percent)	Remarks
024–116	077°33'S. 150°22'W.				☉		
024–117	078°29'S. 155°45'W.				☉		
024–118	079°19's. 162°00'W.				☉		
024–119	080°01'S. 169°10'W.				☉		
025–114	075°25'S. 143°13'W.	1575–16402	18 Feb 74	14	☾	80	
025–115	076°31'S. 147°11'W.	2391–16304	17 Feb 76	13	☾	15	Guest Peninsula
025–116	077°33'S. 151°48'W.	2391–16311	17 Feb 76	12	☾	20	Kizer Island, Sulzberger Shelf
025–117	078°29'S. 157°11'W.				☾	100	
025–118	079°19'S. 163°26'W.	1575–16420	18 Feb 74	10	☾	70	
025–119	080°01'S. 170°36'W.	1575–16423	18 Feb 74	9	☾	70	
026–114	075°25'S. 144°39'W.	1126–16510	26 Nov 72	25	☾	80	
026–115	076°31'S. 148°37'W.	1126–16513	26 Nov 72	24	☾	60	Guest Peninsula
026–116	077°33'S. 153°14'W.	1126–16515	26 Nov 72	23	☾	80	Kizer Island
026–117	078°29'S. 158°37'W.	1126–16522	26 Nov 72	22	☾	40	Ross Ice Shelf, east edge Roosevelt Island, chasm
026–118	079°19'S. 164°52'W.	2320–16384	08 Dec 75	21	☾	60	Ross Ice Shelf, Roosevelt Island, crevasses
026–119	080°01'S. 172°02'W.				☉		
027–113	074°16'S. 142°39'W.	1144–16504	14 Dec 72	28	☾	40	Cruzen Island
027–114	075°25's. 146°05'W.	1144–16510	14 Dec 72	27	☾	60	Land Glacier tongue
027–115	076°31'S. 150°03'W.	1144–16513	14 Dec 72	26	☾	95	
027–116	077°33'S. 154°40'W.	1144–16515	14 Dec 72	24	☾	50	Rockefeller Mountains, Shirase Coast
027–117	078°29'S. 160°03'W.				☾	100	
027–118	079°19'S. 166°18'W.				☉		
027–119	080°01'S. 173°28'W.				☉		
028–114	075°25'S. 147°31'W.	1164–17021	03 Jan 73	26	☾	80	Ice front

TABLE 6.—*Optimum Landsat 1, 2, and 3 MSS and Landsat 2 RBV images of glaciers of Antarctica—Continued*

Path-Row	Nominal scene center (lat.—long.)	Landsat identification number	Date	Solar elev. angle (degrees)	Code	Cloud cover (percent)	Remarks
028-115	076°31'S. 151°29'W.						
028-116	077°33'S. 156°06'W.						
028-117	078°29'S. 161°29'W.						
028-118	079°19'S. 167°44'W.						
028-119	080°01'S. 174°54'W.						
029-114	075°25'S. 148°57'W.					100	
029-115	076°31'S. 152°55'W.	1129-17084	29 Nov 72	24		90	
029-116	077°33'S. 157°32'W.	1129-17090	29 Nov 72	23		60	Okuma Bay, Ross Ice Shelf
029-117	078°29'S. 162°55'W.	1129-17093	29 Nov 72	22		60	Roosevelt Island
029-118	079°19'S. 169°10'W.						
029-119	080°01'S. 176°20'W.						
030-115	076°31'S. 154°21'W.						
030-116	077°33'S. 158°58'W.						
030-117	078°29'S. 164°21'W.	1491-17181	26 Nov 73	22		15	Ross Ice Shelf, chasms
030-118	079°19'S. 170°36'W.						
030-119	080°01'S. 177°46'W.						
031-115	076°31'S. 155°47'W.						
031-116	077°33'S. 160°25'W.	1474-17233	09 Nov 73	19		90	Ice front
031-117	078°29'S. 165°47'W.	1474-17240	09 Nov 73	18		100	Ice front
031-118	079°19'S. 172°02'W.						
031-119	080°01'S. 179°13'W.						
032-115	076°31'S. 157°13'W.	1474-17231	09 Nov 73	20		10	Edward VII Peninsula
032-116	077°33'S. 161°51'W.					100	
032-117	078°29'S. 167°13'W.	1492-17235	27 Nov 73	22		0	Ross Ice Shelf, chasms

TABLE 6.—*Optimum Landsat 1, 2, and 3 MSS and Landsat 2 RBV images of glaciers of Antarctica—Continued*

Path-Row	Nominal scene center (lat.—long.)	Landsat identification number	Date	Solar elev. angle (degrees)	Code	Cloud cover (percent)	Remarks
032-118	079°19'S. 173°28'W.				☉		
032-119	080°01'S. 179°21'W.				☉		
033-115	076°31'S. 158°39'W.	1133-17314	03 Dec 72	25	●	0	Edward VII Peninsula
033-116	077°33'S. 163°17'W.	1133-17320	03 Dec 72	24	◐	25	Ice front
033-117	078°29'S. 168°39'W.	1187-17321	26 Jan 73	18	◐	90	Ice front
033-118	079°19'S. 174°54'W.				☉		
033-119	080°01'S. 177°55'W.				☉		
034-117	078°29'S. 170°06'W.	1207-17440	15 Feb 73	12	◐	90	Ice front
034-118	079°19'S. 176°21'W.				☉		
034-119	080°01'S. 176°29'E.				☉		
035-117	078°29'S. 171°32'W.				☉		
035-118	079°19'S. 177°47'W.				☉		
035-119	080°01'S. 175°03'E.				☉		
036-117	078°29'S. 172°58'W.				☉		
036-118	079°19'S. 179°73'W.				☉		
036-119	080°01'S. 173°37'E.				☉		
037-117	078°29'S. 174°24'W.				☉		
037-118	079°19'S. 179°21'E.				☉		
037-119	080°01'S. 172°11'E.				☉		
038-117	078°29'S. 175°50'W.				☉		
038-118	079°19'S. 177°55'E.				☉		
038-119	080°01'S. 170°45'E.				☉		
039-117	078°29'S. 177°16'W.	1121-18065	21 Nov 72	21	◐	50	Ross Ice Shelf
039-118	079°19'S. 176°29'E.				☉		

TABLE 6.—*Optimum Landsat 1, 2, and 3 MSS and Landsat 2 RBV images of glaciers of Antarctica—Continued*

Path-Row	Nominal scene center (lat.—long.)	Landsat identification number	Date	Solar elev. angle (degrees)	Code	Cloud cover (percent)	Remarks
039-119	080°01'S. 169°19'E.				☉		
040-117	078°29'S. 178°42'W.				☉		
040-118	079°19'S. 175°03'E.	2389-18035	15 Feb 76	11	☾	30	Ross Ice Shelf, chasm
040-119	080°01'S. 167°53'E.				☉		
041-117	078°29'S. 179°52'E.				☉		
041-118	079°19'S. 173°37'E.	2317-18044	05 Dec 75	21	●	5	Ross Ice Shelf, chasm
041-119	080°01'S. 166°27'E.				☉		
042-117	078°29'S. 178°26'E.	2318-18100	06 Dec 75	22	☾	10	Ice front, chasms
042-118	079°19'S. 172°11'E.				☉		
042-119	080°01'S. 165°01'E.	1502-18220	07 Dec 73	21	☾	40	Byrd Glacier/Ross Ice Shelf
043-116	077°33'S. 177°37'W.				☉		
043-117	078°29'S. 177°00'E.				☉		
043-118	079°19'S. 170°45'E.				☉		
043-119	080°01'S. 163°35'E.				☉		
044-116	077°33'S. 179°03'W.				☉		
044-117	078°29'S. 175°34'E.				☉		
044-118	079°19'S. 169°19'E.				☉		
044-1191	080°01'S. 162°09'E.				☉		
045-116	077°33'S. 179°31'E.				☉		
045-117	078°29'S. 174°08'E.				☉		
045-118	079°19'S. 167°53'E.				☾	100	
045-119	080°01'S. 160°43'E.				☉		
046-116	077°33'S. 178°05'E.				☉		
046-117	078°29'S. 172°42'E.				☉		

TABLE 6.—*Optimum Landsat 1, 2, and 3 MSS and Landsat 2 RBV images of glaciers of Antarctica- Continued*

Path-Row	Nominal scene center (lat.-long.)	Landsat identification number	Date	Solar elev. angle (degrees)	Code	Cloud cover (percent)	Remarks
046-118	079°19'S. 166°27'E.	1542-18433	16 Jan 74	19	●	0	Minna Bluff
046-119	080°01'S. 159°17'E.	1542-18435	16 Jan 74	18	●	5	Byrd Glacier, excellent image
047-116	077°33'S. 176°39'E.	1165-18520	04 Jan 73	23	◐	50	Ice front, chasm
047-117	078°29'S. 171°16'E.	1165-18523	04 Jan 73	22	◐	70	Minna Bluff
047-117	078°29'S. 171°16'E.	1202-18583	10 Feb 73	14	◐	95	
047-118	079°19'S. 165°01'E.				⊙		
047-119	080°01'S. 157°51'E.				⊙		
048-116	077°33'S. 175°12'E.	1130-18580	30 Nov 72	23	◐	70	Ice front
048-117	078°29'S. 169°50'E.	1526-18550	31 Dec 73	23	◐	20	Minna Bluff
048-118	079°19'S. 163°35'E.	1526-18553	31 Dec 73	22	◐	45	Skelton Glacier, Mulock Glacier
048-119	080°01'S. 156°24'E.	1526-18555	31 Dec 73	20	◐	30	Byrd Glacier, Darwin Glacier
049-116	077°33'S. 173°46'E.	2344-18552	01 Jan 76	23	◐	90	
049-117	078°29'S. 168°24'E.	1527-19005	01 Jan 74	22	●	0	Minna Bluff
049-118	079°19'S. 162°09'E.	1492-19073	27 Nov 73	21	●	0	Skelton Glacier, Mulock Glacier, excellent image
049-119	080°01'S. 154°58'E.	1492-19080	27 Nov 73	19	●	0	Darwin Glacier, Darwin Névé
050-116	077°33'S. 172°20'E.	2272-18560	21 Oct 75	12	◐	10	Unusual sea ice patterns, band 6
050-117	078°29'S. 166°58'E.	1528-19063	02 Jan 74	22	●	0	Minna Bluff, Koettlitz Glacier
050-118	079°19'S. 160°43'E.	1528-19065	02 Jan 74	21	●	0	Mulock Glacier, Cook Mountains
050-119	080°01'S. 153°32'E.				⊙		
051-116	077°33'S. 170°54'E.	1151-19151	21 Dec 72	24	●	5	Ross Island
051-117	078°29'S. 165°32'E.	1529-19121	03 Jan 74	22	●	0	Minna Bluff, Koettlitz Glacier, excellent image
051-118	079°19'S. 159°17'E.	1476-19191	11 Nov 73	17	●	0	Skelton Glacier, Mulock Glacier, Darwin Glacier
051-119	080°01'S. 152°06'E.	1476-19193	11 Nov 73	16	●	0	Darwin Mountains
052-116	077°33'S. 169°28'E.	1530-19173	04 Jan 74	23	●	5	Mount Erebus, Ross Island

TABLE 6.—Optimum Landsat 1, 2, and 3 MSS and Landsat 2 RBV images of glaciers of Antarctica—Continued

Path-Row	Nominal scene center (lat.—long.)	Landsat identification number	Date	Solar elev. angle (degrees)	Code	Cloud cover (percent)	Remarks
052-117	078°29's. 164°05'E.	1530-19175	04 Jan 74	22	●	0	Minna Bluff, Koettlitz Glacier
052-118	079°19'S. 157°50'E.				◐	100	
052-119	080°01'S. 150°40'E.				◑		
053-115	076°31'S. 172°39'E.	2653-19034	05 Nov 76	18	◑	80	RBV, ice front
053-116	077°33'S. 168°02'E.	1531-19231	05 Jan 74	23	●	0	Mount Erebus, Ross Island
053-117	078°29'S. 162°39'E.	1531-19233	05 Jan 74	22	●	0	Royal Society Range, Skelton Glacier
053-118	079°19'S. 156°24'E.	1478-19304	13 Nov 73	18	●	5	Cook Mountains, Darwin Névé
053-119	080°01'S. 149°14'E.	1478-19310	13 Nov 73	17	●	0	Nunataks, surface features, band 4
054-115	076°31'S. 171°13'E.	2654-19092	06 Nov 76	18	●	0	RBV, ice front
054-116	077°33'S. 166°36'E.	2637-19161	20 Oct 76	12	●	0	RBV, Ross Island
054-117	078°29'S. 161°13'E.	1532-19292	06 Jan 74	22	◑	75	
054-118	079°19'S. 154°58'E.	1532-19294	06 Jan 74	21	●	5	Cook Mountains, Darwin Névé
054-119	080°01'S. 147°48'E.	1532-19301	06 Jan 74	20	●	0	Nunataks
055-115	076°31'S. 169°47'E.	2655-19150	07 Nov 76	19	●	0	RBV, ice front
055-116	077°33'S. 165°10'E.	2638-19215	21 Oct 76	12	●	0	RBV, Ross Island, 'dry valleys'
055-117	078°29's. 159°47'E.	1191-19383	30 Jan 73	17	◑	25	Mulock Glacier, Skelton Névé, Skelton Glacier
055-118	079°19'S. 153°32'E.	1533-19352	07 Jan 74	21	◑	30	Westhaven Nunatak
055-119	080°01'S. 146°22'E.	1474-19083	09 Nov 73	14	●	0	Crevasses, surface features
056-115	076°31's. 168°21 'E.	1174-19431	13 Jan 73	23	●	0	Cape Bird
056-115	076°31'S. 168°21'E.	2639-19271	22 Oct 76	14	●	0	RBV, Franklin Island, Beaufort Island
056-116	077°33's. 163°44'E.	1174-19433	13 Jan 73	22	●	0	'Dry valleys'
056-116	077°33'S. 163°44'E.	2639-19273	22 Oct 76	12	●	0	RBV, 'dry valleys'
056-117	078°29's. 158°21'E.	1552-19400	26 Jan 74	18	●	0	Skelton Névé, Mulock Glacier, 'crevasses'
056-118	079°19'S. 152°06'E.	1552-19403	26 Jan 74	17	●	0	Darwin Névé

TABLE 6.—*Optimum Landsat 1, 2, and 3 MSS and Landsat 2 RBV images of glaciers of Antarctica—Continued*

Path-Row	Nominal scene center (lat.—long.)	Landsat identification number	Date	Solar elev. angle (degrees)	Code	Cloud cover (percent)	Remarks
056-119	080°01'S. 144°56'E.	1552-19405	26 Jan 74	16	●	0	Crevasses
057-115	076°31'S. 166°55'E.	2640-19325	23 Oct 76	14	●	0	RBV, Franklin Island, Beaufort Island
057-116	077°33'S. 162°18'E.	2279-19361	18 Oct 75	15	●	0	'Dry valleys'
057-117	078°29'S. 156°55'E.	1177-20010	16 Jan 73	21	●	0	Skelton Névé
057-117	078°29'S. 156°55'E.	1194-19555	02 Feb 73	16	◐	10	Skelton Névé
057-118	079°19'S. 150°40'E.	1499-19474	04 Dec 73	22	●	5	Darwin Névé, band 4
057-119	080°01'S. 143°30'E.	1499-19480	04 Dec 73	20	●	0	Band 4
058-115	076°31'S. 165°29'E.	1518-19515	23 Dec 73	25	◐	10	Oates Piedmont Glacier
058-115	076°31'S. 165°29'E.	1500-19521	05 Dec 73	25	◐	20	Oates Piedmont Glacier
058-116	077°33'S. 160°52'E.	1518-19521	23 Dec 73	24	◐	20	Wilson Piedmont Glacier, 'dry valleys'
058-117	078°29'S. 155°29'E.	1518-19524	23 Dec 73	23	◐	10	Skelton Névé, crevasses
058-118	079°19'S. 149°14'E.	1554-19515	28 Jan 74	16	●	0	Nunataks, band 6
058-119	080°01'S. 142°04'E.	1554-19522	28 Jan 74	15	●	0	Band 6
059-115	076°31'S. 164°03'E.	1519-19573	24 Dec 73	25	●	5	Mawson Glacier, band 6
059-116	077°33'S. 159°26'E.	1501-19581	06 Dec 73	24	●	0	'Dry valleys,' Allan Hills
059-117	078°29'S. 154°03'E.	1501-19584	06 Dec 73	23	●	0	Boomerang Range
059-118	079°19'S. 147°48'E.	1537-19581	11 Jan 74	20	●	0	Surface features
059-119	080°01'S. 140°38'E.	1478-19313	13 Nov 73	15	●	0	Surface features
060-113	074°16'S. 170°01'E.	1214-20055	22 Feb 73	14	●	0	Coulman Island, Borchgrevink Glacier
060-114	075°25'S. 166°35'E.	1214-20062	22 Feb 73	13	●	0	Drygalski Ice Tongue
060-115	076°31'S. 162°37'E.	1214-20064	22 Feb 73	12	◐	10	Mawson and Fry Glaciers
060-116	077°33'S. 158°00'E.	1520-20034	25 Dec 73	24	●	0	Wright Glacier, 'Elephant Moraine,' band 6
060-117	078°29'S. 152°37'E.	1520-20040	25 Dec 73	23	●	0	Crevasses, nunataks
060-118	079°19'S. 146°22'E.	1520-20043	25 Dec 73	22	●	5	

TABLE 6.—*Optimum Landsat 1, 2, and 3 MSS and Landsat 2 RBV images of glaciers of Antarctica — Continued*

Path-Row	Nominal scene center (lat.—long.)	Landsat identification number	Date	Solar elev. angle (degrees)	Code	Cloud cover (percent)	Remarks
060-119	080°01'S. 139°12'E.	1520-20045	25 Dec 73	21	●	0	
061-112	073°04'S. 171°34'E.				☉	100	
061-113	074°16'S. 168°35'E.	1197-20112	05 Feb 73	20	☉	50	Borchgrevink Coast
061-114	075°25'S. 165°09'E.	1177-20001	16 Jan 73	23	☉	10	Drygalski Ice Tongue
061-115	076°31'S. 161°11'E.	1177-20004	13 Jan 74	23	☉	10	'Dry valleys,' Evans Piedmont Glacier
061-116	077°33'S. 156°34'E.	1539-20085	13 Jan 74	22	●	5	'Elephant Moraine'
061-117	078°29'S. 151°11'E.	1539-20091	13 Jan 74	21	●	5	
061-118	079°19'S. 144°56'E.	1539-20094	13 Jan 74	20	●	0	
061-119	080°01'S. 137°46'E.	1539-20100	13 Jan 74	19	●	0	
062-111	071°50'S. 172°44'E.	1180-20160	19 Jan 73	26	☉	95	
062-112	073°04'S. 170°08'E.	1180-20162	19 Jan 73	25	☉	95	
062-112	073°04's. 170°08'E.	1143-20110	13 Dec 72	29	☉	95	
062-113	074°16's. 167°09'E.	1540-20132	14 Jan 74	25	☉	40	Mount Melbourne (volcano)
062-114	075°25'S. 163°43'E.	1540-21034	14 Jan 74	24	☉	10	Reeves Glacier, numerous melt ponds
062-115	076°31'S. 159°45'E.	1540-20141	14 Jan 74	23	●	0	Convoy Range, 'Elephant Moraine'
062-116	077°33'S. 155°08'E.	1540-20143	14 Jan 74	22	●	0	
062-117	078°29'S. 149°45'E.	1540-20150	14 Jan 74	20	●	0	
062-118	079°19'S. 143°30'E.	1540-20152	14 Jan 74	19	●	0	
062-119	080°01's. 136°20'E.	1540-20155	14 Jan 74	18	●	0	Snow dunes
062-119	080°01's. 136°20'E.	1504-20164	09 Dec 73	21	●	0	Snow dunes
063-111	071°50'S. 171°18'E.	1163-20215	02 Jan 73	29	☉	60	Admiralty Mountains
063-112	073°04'S. 168°42'E.				☉		
063-113	074°16'S. 165°43'E.	1217-20231	25 Feb 73	13	☉	50	Aviator Glacier, Campbell Glacier
063-114	075°25'S. 162°17'E.	1217-20233	25 Feb 73	12	☉	50	Reeves Glacier, Priestley Glacier

TABLE 6.—Optimum Landsat 1, 2, and 3 MSS and Landsat 2 RBV images of glaciers of Antarctica — Continued

Path-Row	Nominal scene center (lat.—long.)	Landsat identification number	Date	Solar elev. angle (degrees)	Code	Cloud cover (percent)	Remarks
063–114	075°25'S. 162°17'E.	1487–20203	22 Nov 73	24		40	David Glacier
063–115	076°31'S. 158°19'E.	1487–20210	22 Nov 73	23		25	Convoy Range, 'blue ice'
063–116	077°33'S. 153°42'E.	1541–20201	15 Jan 74	21		0	
063–117	078°29'S. 148°19'E.	1541–20204	15 Jan 74	20		0	
063–118	079°19'S. 142°04'E.	1541–20210	15 Jan 74	19		0	
063–119	080°01'S. 134°54'E.	1541–20213	15 Jan 74	18		0	
064–111	071°50'S. 169°52'E.	1128–20275	28 Nov 72	29		0	Cape Adare, Tucker Glacier, excellent image
064–112	073°04'S. 167°16'E.	1128–20281	28 Nov 72	28		0	Borchgrevink Glacier, Mariner Glacier Tongue
064–113	074°16'S. 164°17'E.	1128–20284	28 Nov 72	27		0	Aviator Glacier, Mount Melbourne, Priestley Glacier
064–114	075°25'S. 160°51'E.	1128–20290	28 Nov 72	25		0	David Glacier, crevasses; 'blue ice'
064–114	075°25'S. 160°51'E.	1200–20290	08 Feb 73	18		0	David Glacier, Reeves Glacier
064–114	075°25'S. 160°51'E.	1542–20250	16 Jan 74	23		5	David Glacier, Reeves Glacier, melt ponds
064–115	076°31'S. 156°53'E.	1128–20293	28 Nov 72	24		20	'Elephant Moraine,' 'blue ice'
064–115	076°31'S. 156°53'E.	1200–20293	08 Feb 73	17		10	'Elephant Moraine,' 'blue ice'
064–116	077°33'S. 152°16'E.	1489–20325	24 Nov 73	23		15	Subglacial relief
064–117	078°29'S. 146°53'E.	1489–20331	24 Nov 73	21		0	
064–118	079°19'S. 140°38'E.	1489–20334	24 Nov 73	20		0	
064–119	080°01'S. 133°28'E.	1471–20341	06 Nov 73	15		0	Snow dunes
065–111	071°50'S. 168°25'E.						
065–112	073°04'S. 165°49'E.						
065–113	074°16'S. 162°51'E.						
065–114	075°25'S. 159°25'E.	1543–20305	17 Jan 74	23		0	David Glacier, 'blue ice'
065–115	076°31'S. 155°27'E.	1489–20322	24 Nov 73	24		60	'Elephant Moraine'
065–116	077°33'S. 150°49'E.	1490–20383	25 Nov 73	23		30	

TABLE 6.—Optimum Landsat 1, 2, and 3 MSS and Landsat 2 RBV images of glaciers of Antarctica—Continued

Path-Row	Nominal scene center (lat.-long.)	Landsat identification number	Date	Solar elev. angle (degrees)	Code	Cloud cover (percent)	Remarks
065-117	078°29'S. 145°27'E.	1490-20390	25 Nov 73	22	●	5	
065-118	079°19'S. 139°12'E.	1490-20392	25 Nov 73	20	●	0	
065-119	080°01'S. 132°01'E.	1490-20395	25 Nov 73	19	●	0	Snow dunes
066-110	070°35'S. 169°17'E.				⊙		
066-111	071°50'S. 166°59'E.				⊙		
066-112	073°04'S. 164°23'E.	1220-20400	28 Feb 73	13	◐	25	Evans Névé, Aviator Glacier
066-113	074°16'S. 161°25'E.	1220-20402	28 Feb 73	12	◐	20	Campbell Glacier
066-114	075°25'S. 157°59'E.	1526-20370	31 Dec 73	26	●	0	Upper David Glacier
066-115	076°31'S. 154°01'E.	1544-20365	18 Jan 74	22	●	0	'Blue ice'
066-115	076°31'S. 154°01'E.	1526-20373	31 Dec 73	25	●	0	'Blue ice'
066-116	077°33'S. 149°23'E.	1544-20372	18 Jan 74	21	●	0	
066-117	078°29'S. 144°01'E.	1544-20374	18 Jan 74	20	●	0	
066-118	079°19'S. 137°46'E.	1544-20381	18 Jan 74	19	●	0	Snow dunes
066-119	080°01'S. 130°35'E.	1491-20453	26 Nov 73	19	◐	10	
067-110	070°35'S. 167°51'E.	1131-20444	01 Dec 72	30	●	0	Barnett Glacier, Cape Moore
067-111	071°50'S. 165°33'E.	1131-20450	01 Dec 72	29	●	0	Ebbe Glacier, Concord Mountains
067-112	073°04'S. 162°57'E.	1131-20453	01 Dec 72	28	●	0	Evans Névé, Monument Nunataks
067-113	074°16'S. 159°59'E.	1131-20455	01 Dec 72	27	◐	10	Priestley Glacier
067-114	075°25'S. 156°33'E.	1131-20462	01 Dec 72	26	●	0	'Blue ice'
067-115	076°31'S. 152°35'E.	1131-20464	01 Dec 72	25	◐	20	
067-116	077°33'S. 147°57'E.	1203-20471	11 Feb 73	15	●	5	Surface features, band 6
067-117	078°29'S. 142°35'E.	1203-20473	11 Feb 73	13	●	0	
067-118	079°19'S. 136°20'E.	1474-20510	09 Nov 73	17	●	5	Snow dunes
067-119	080°01'S. 129°09'E.	1474-20512	09 Nov 73	16	●	5	Surface features

TABLE 6.—Optimum Landsat 1,2, and 3 MSS and Landsat 2 RBV images of glaciers of Antarctica—Continued

Path-Row	Nominal scene center (lat.—long.)	Landsat identification number	Date	Solar elev. angle (degrees)	Code	Cloud cover (percent)	Remarks
067–119	080°01'S. 129°09'E.	1509–20452	14 Dec 73	21	●	0	Surface features
068–110	070°35'S. 166°25'E.	1186–20501	25 Jan 73	26	◐	10	Cape Hooker, band 6
068–111	071°50'S. 164°07'E.	1186–20503	25 Jan 73	25	◐	10	Rennick Glacier, melt ponds
068–111	071°50'S 164°07'E.	1132–20505	02 Dec 72	29	◐	10	Concord Mountains, 'blue ice'
068–112	073°04's. 161°31'E.	1132–20511	02 Dec 72	28	◐	40	Outback Nunataks
068–113	074°16'S. 158°33'E.	1186–20512	25 Jan 73	23	●	0	Priestley Glacier
068–113	074°16's. 158°33'E.	1149–20455	19 Dec 72	28	●	0	Priestley Glacier
068–114	075°25'S. 155°07'E.	1186–20515	25 Jan 73	22	●	5	Nunataks, 'blue ice'
068–114	075°25'S. 155°07'E.	1149–20461	19 Dec 72	27	●	0	Nunataks, 'blue ice'
068–115	076°31'S. 151°09'E.	1186–20521	25 Jan 73	21	◐	40	
068–116	077°33'S. 146°31'E.	1186–20524	25 Jan 73	19	◐	60	
068–117	078°29'S. 141°09'E.				⊙		
068–118	079°19'S. 134°54'E.	1546–20493	20 Jan 74	18	●	0	Snow dunes
068–119	080°01'S. 127°43'E.	1546–20500	20 Jan 74	17	●	0	Snow dunes
069–110	070°35'S. 164°59'E.	1169–20554	08 Jan 73	29	◐	50	Ob' Bay
069–111	071°50'S. 162°41'E.	1169–20561	08 Jan 73	28	●	5	Upper Rennick Glacier, melt ponds
069–112	073°04'S. 160°05'E.	1223–20571	03 Mar 73	12	◐	25	Roberts Butte, Frontier Mountain
069–113	074°16'S. 157°06'E.	1223–20573	03 Mar 73	11	◐	20	Nunataks
069–114	075°25'S. 153°41'E.	1223–20580	03 Mar 73	10	◐	25	Nunataks, crevasses
069–115	076°31'S. 149°42'E.	1223–20582	03 Mar 73	9	◐	60	
069–116	077°33'S. 145°05'E.	1206–21042	14 Feb 73	14	◐	70	
069–117	078°29's. 139°42'E.	1169–20584	08 Jan 73	22	◐	15	
069–118	079°19'S. 133°27'E.	1511–20562	16 Dec 73	22	◐	10	Snow dunes
069–119	080°01'S. 126°17'E.	1471–20343	06 Nov 73	14	◐	10	Snow dunes

TABLE 6.—*Optimum Landsat 1, 2, and 3 MSS and Landsat 2 RBV images of glaciers of Antarctica—Continued*

Path-Row	Nominal scene center (lat.-long.)	Landsat identification number	Date	Solar elev. angle (degrees)	Code	Cloud cover (percent)	Remarks
070-109	069°17'S. 165°34'E.					100	
070-110	070°35'S. 163°33'E.	1206-21015	14 Feb 73	20		80	Sputnik Island
070-111	071°50'S. 161°15'E.	1206-21022	14 Feb 73	19		50	Usarp Mountains
070-112	073°04'S. 158°39'E.	1206-21024	14 Feb 73	18		20	Roberts Butte, Frontier Mountain
070-112	073°04'S. 158°39'E.	1169-20563	08 Jan 73	27		50	Roberta Butte, Frontier Mountain
070-113	074°16'S. 155°40'E.	1206-21031	14 Feb 73	17		15	
070-114	075°25'S. 152°15'E.	1206-21033	14 Feb 73	16		60	
070-115	076°31'S. 148°16'E.	1206-21040	14 Feb 73	15		30	
070-116	077°33'S. 143°39'E.	1169-20581	08 Jan 73	23		20	
070-117	078°29'S. 138°16'E.	1189-21102	28 Jan 73	18		90	
070-118	079°19'S. 132°01'E.	1548-21010	22 Jan 74	18		5	Snow dunes
070-119	080°01'S. 124°51'E.	1548-21012	22 Jan 74	17		15	Snow dunes
071-108	067°59'S. 165°58'E.	1135-21064	05 Dec 72	33		0	Sturge Island (see Landsat 3 RBV 73/108 B)
071-109	069°17'S. 164°08'E.	1135-21071	05 Dec 72	32		95	Ice front
071-110	070°35'S. 162°07'E.	1135-21073	05 Dec 72	31		25	Bowers Mountains
071-110	070°35'S. 162°07'E.	1117-21073,	17 Nov 72	28		35	Bowers Mountains
071-111	071°50'S. 159°49'E.	1135-21080	05 Dec 72	30		5	Mount Southard
071-112	073°04'S. 157°13'E.	1531-21045	05 Jan 74	27		0	Frontier Mountain
071-113	074°16'S. 154°14'E.	1135-21085	05 Dec 72	27		10	
071-114	075°25'S. 150°49'E.	1135-21091	05 Dec 72	26		10	
071-115	076°31'S. 146°50'E.	1531-21060	05 Jan 74	24		0	
071-116	077°33'S. 142°13'E.	1531-21063	05 Jan 74	23		0	
071-117	078°29'S. 136°50'E.	1531-21065	05 Jan 74	22		0	Snow dunes
071-118	079°19'S. 130°35'E.	1531-21072	05 Jan 74	21		0	Snow dunes

TABLE 6.—Optimum Landsat 1, 2, and 3 MSS and Landsat 2 RBV images of glaciers of Antarctica—Continued

Path-Row	Nominal scene center (lat.-long.)	Landsat identification number	Date	Solar elev. angle (degrees)	Code	Cloud cover (percent)	Remarks
071-119	080°01'S. 123°25'E.	1531-21074	05 Jan 74	20	●	0	Snow dunes
072-108	067°59'S. 164°31'E.				◐	100	
072-109	069°17'S. 162°42'E.				◐	100	
072-110	070°35'S. 160°40'E.	1460-21103	26 Oct 73	22	●	0	Rennick Glacier, Suvorov Glacier, excellent image
072-111	071°50'S. 158°23'E.	1460-21110	26 Oct 73	21	◐	10	Usarp Mountains
072-112	073°04'S. 155°47'E.	1550-21095	24 Jan 74	24	◐	80	
072-113	074°16'S. 152°48'E.	1514-21112	19 Dec 73	28	◐	70	
072-114	075°25'S. 149°22'E.	1514-21115	19 Dec 73	27	◐	70	
072-115	076°31'S. 145°24'E.	1532-21114	06 Jan 74	24	●	0	
072-116	077°33'S. 140°47'E.	1532-21121	06 Jan 74	23	●	0	
072-117	078°29'S. 135°24'E.	1514-21130	19 Dec 73	23	●	0	Snow dunes
072-118	079°19'S. 129°09'E.	1514-21133	19 Dec 73	22	●	0	Snow dunes
072-119	080°01'S. 121°59'E.	1532-21132	06 Jan 74	20	●	0	Snow dunes
073-107	066°40'S. 164°44'E.				◐	100	See Landsat 3 RBV 73/107 C
073-108	067°59'S. 163°05'E.				◐	100	See Landsat 3 RBV 73/108 B
073-109	069°17'S. 161°16'E.				◐	100	
073-110	070°35'S. 159°14'E.	1551-21144	25 Jan 74	25	◐	10	Kooperatsiya Ice Piedmont
073-111	071°50'S. 156°57'E.	1551-21151	25 Jan 74	24	●	5	Usarp Mountains
073-112	073°04'S. 154°21'E.	1551-21153	25 Jan 74	23	●	0	
073-113	074°16'S. 151°22'E.	1209-21202	17 Feb 73	16	◐	55	
073-114	075°25'S. 147°56'E.	1515-21173	20 Dec 73	27	◐	15	
073-115	076°31'S. 143°58'E.	1515-21175	20 Dec 73	26	●	0	
073-116	077°33'S. 139°21'E.	1515-21182	20 Dec 73	24	●	0	
073-117	078°29'S. 133°58'E.	1515-21184	20 Dec 73	23	●	0	Snow dunes

TABLE 6.—Optimum Landsat 1, 2, and 3 MSS and Landsat 2 RBV images of glaciers of Antarctica—Continued

Path-Row	Nominal scene center (lat.-long.)	Landsat identification number	Date	Solar elev. angle (degrees)	Code	Cloud cover (percent)	Remarks
073-118	079°79'S. 127°43'E.	1515-21191	20 Dec 73	22		10	
073-119	080°01'S. 120°33'E.	1515-21193	20 Dec 73	21		0	Snow dunes
074-107	066°40'S. 163°18'E.					100	
074-109	069°17'S. 159°50'E.					100	
074-110	070°35'S. 157°48'E.	1534-21210	08 Jan 74	29		0	Pomerantz Tableland
074-111	071°50'S. 155°31'E.	1192-21250	31 Jan 73	23		0	
074-112	073°04'S. 152°55'E.	1192-21253	31 Jan 73	22		0	
074-113	074°76's. 149°56'E.	1192-21255	31 Jan 73	21		0	
074-114	075°25'S. 146°30'E.	1192-21262	31 Jan 73	20		0	
074-115	076°31'S. 142°32'E.	1192-21264	31 Jan 73	19		0	
074-116	077°33's. 137°55'E.	1192-21271	31 Jan 73	18		0	
074-117	078°29'S. 132°32'E.	1480-21250	15 Nov 73	19		60	Snow dunes
074-118	079°19'S. 126°17'E.	1516-21245	21 Dec 73	22		0	Snow dunes
074-119	080°01'S. 119°07'E.	1516-21252	21 Dec 73	21		0	Snow dunes
075-107	066°40'S. 161°52'E.	1175-21285	14 Jan 73	31		95	See Landsat 3 RBV 75/107 D
075-109	069°17'S. 158°24'E.	1463-21272	29 Oct 73	24		40	Matusевич Glacier
075-110	070°35'S. 156°22'E.	1463-21275	29 Oct 73	23		5	Nunataks
075-111	071°50'S. 154°05'E.	1499-21280	04 Dec 73	29		5	
075-112	073°04'S. 151°29'E.	1463-21284	29 Oct 73	21		0	
075-113	074°16'S. 148°30'E.	1499-21285	04 Dec 73	27		5	
075-114	075°25'S. 145°04'E.	1517-21285	22 Dec 73	27		0	
075-115	076°31'S. 141°06'E.	1517-21292	22 Dec 73	25		0	
075-116	077°33'S. 136°29'E.	1517-21294	22 Dec 73	24		0	Snow dunes
075-117	078°29'S. 131°06'E.	1517-21301	22 Dec 73	23		0	Snow dunes

TABLE 6.—*Optimum Landsat 1, 2, and 3 MSS and Landsat 2 RBV images of glaciers of Antarctica—Continued*

Path-Row	Nominal scene center (lat.—long.)	Landsat identification number	Date	Solar elec. angle (degrees)	Code	Cloud cover (percent)	Remarks
075-118	079°19'S. 124°51'E.	1517-21303	22 Dec 73	22	●	0	Snow dunes
075-119	080°01'S. 117°41'E.	1517-21310	22 Dec 73	21	●	0	Snow dunes
076-107	066°40'S. 160°26'E.	1212-21351	20 Feb 73	21	◐	50	Young and Row Islands (see Landsat 3 RBV 75/107 D)
076-109	069°17'S. 156°58'E.	1212-21360	20 Feb 73	19	●	5	Matusевич Glacier, Oates Coast
076-110	070°35'S. 154°56'E.	1212-21362	20 Feb 73	18	◐	10	Upper Matusевич Glacier
076-111	071°50'S. 152°39'E.	1212-21365	20 Feb 73	17	●	5	
076-112	073°04'S. 150°03'E.	1158-21365	28 Dec 72	28	●	5	
076-113	074°16'S. 147°04'E.	1158-21372	28 Dec 72	27	●	0	Band 6
076-114	075°25'S. 143°38'E.	1554-21333	28 Jan 74	20	●	0	
076-115	076°31'S. 139°40'E.	1554-21335	28 Jan 74	19	●	0	
076-116	077°33'S. 135°03'E.	1554-21342	28 Jan 74	18	●	0	Snow dunes
076-117	078°29'S. 129°40'E.	1554-21344	28 Jan 74	17	◐	10	Snow dunes
076-118	079°19'S. 123°25'E.	1518-21362	23 Dec 73	22	●	0	Snow dunes
076-119	080°01'S. 116°15'E.	1518-21364	23 Dec 73	21	●	0	Snow dunes
077-109	069°17'S. 155°32'E.	1483-21385	18 Nov 73	29	◐	50	Oates Coast
077-110	070°35'S. 153°30'E.	1195-21415	03 Feb 73	23	◐	20	
077-111	071°50'S. 151°13'E.	1195-21422	03 Feb 73	22	●	0	
077-112	073°04'S. 148°37'E.	1483-21400	18 Nov 73	26	◐	50	
077-113	074°16'S. 145°38'E.	1483-21403	18 Nov 73	25	◐	60	
077-114	075°25'S. 142°12'E.	1159-21433	29 Dec 72	26	●	0	
077-115	076°31'S. 138°14'E.	1159-21435	29 Dec 72	25	●	0	
077-116	077°33'S. 133°37'E.	1159-21442	29 Dec 72	24	●	0	Snow dunes
077-117	078°29'S. 128°14'E.	1466-21475	01 Nov 73	16	●	0	Snow dunes, band 6
077-118	079°19'S. 121°59'E.	1466-21482	01 Nov 73	14	●	0	Snow dunes, band 6

TABLE 6.—Optimum Landsat 1, 2, and 3 MSS and Landsat 2 RBV images of glaciers of Antarctica—Continued

Path-Row	Nominal scene center (lat.—long.)	Landsat identification number	Date	Solar elev. angle (degrees)	Code	Cloud cover (percent)	Remarks
077-119	080°01'S. 114°49'E.	1501-21425	06 Dec 73	21	●	0	Snow dunes
078-109	069°17'S. 154°06'E.	1466-21443	01 Nov 73	25	◐	25	Mawson Peninsula
078-110	070°35'S. 152°04'E.	1466-21450	01 Nov 73	24	●	0	
078-111	071°50'S. 149°47'E.	1466-21452	01 Nov 73	23	●	0	
078-112	073°04'S. 147°11'E.	1466-21455	01 Nov 73	22	●	0	Scan lines missing, band 6
078-113	074°16'S. 144°12'E.	1520-21454	25 Dec 73	27	◑	10	
078-114	075°25'S. 140°46'E.	1538-21453	12 Jan 74	24	●	0	
078-115	076°31'S. 136°48'E.	1538-21460	12 Jan 74	23	●	0	Snow dunes
078-116	077°33'S. 132°11'E.	1538-21462	12 Jan 74	22	●	0	Snow dunes
078-117	078°29'S. 126°48'E.	1467-21534	02 Nov 73	16	●	0	Snow dunes
078-118	079°19'S. 120°33'E.	1467-21540	02 Nov 73	15	●	0	Snow dunes
078-119	080°01'S. 113°23'E.	1467-21543	02 Nov 73	14	●	0	Snow dunes
079-108	067°59'S. 154°29'E.				⊙		
079-109	069°17'S. 152°40'E.				⊙		
079-110	070°35'S. 150°38'E.	1215-21534	23 Feb 73	17	◑	10	Surface features
079-111	071°50'S. 148°21'E.	1215-21540	23 Feb 73	16	●	0	
079-112	073°04'S. 145°45'E.	1215-21543	23 Feb 73	15	●	0	
079-113	074°16'S. 142°46'E.	1215-21545	23 Feb 73	14	●	0	
079-114	075°25'S. 139°20'E.	1215-21552	23 Feb 73	13	●	0	
079-115	076°31'S. 135°22'E.	1215-21554	23 Feb 73	12	◑	10	Snow dunes
079-116	077°33'S. 130°45'E.	1161-21554	31 Dec 72	24	●	0	Snow dunes
079-117	078°29'S. 125°22'E.	1539-21523	13 Jan 74	21	●	0	Snow dunes
079-118	079°19'S. 119°07'E.	1539-21525	13 Jan 74	20	●	0	Snow dunes
079-119	080°01'S. 111°57'E.	1575-21522	18 Feb 74	9	●	0	Snow dunes

TABLE 6.—*Optimum Landsat 1, 2, and 3 MSS and Landsat 2 RBV images of glaciers of Antarctica—Continued*

Path-Row	Nominal scene center (lat.-long.)	Landsat identification number	Date	Solar elev. angle (degrees)	Code	Cloud cover (percent)	Remarks
080-108	067°59'S. 153°03'E.					100	
080-109	069°17'S. 151°14'E.					100	
080-110	070°35'S. 149°12'E.					100	
080-111	071°50'S. 146°55'E.					100	
080-112	073°04'S. 144°19'E.					100	
080-113	074°16'S. 141°20'E.					100	
080-114	075°25'S. 137°54'E.	1198-22005	06 Feb 73	18		60	
080-115	076°31'S. 133°56'E.	1198-22011	06 Feb 73	17		5	Snow dunes
080-116	077°33'S. 129°19'E.	1198-22014	06 Feb 73	16		5	Snow dunes, band 6
080-117	078°29'S. 123°56'E.	1487-22050	22 Nov 73	21		10	Snow dunes
080-118	079°19'S. 117°41'E.	1469-22053	04 Nov 73	15		0	Snow dunes, band 6
080-119	080°01'S. 110°31'E.	1469-22060	04 Nov 73	14		0	Snow dunes
081-108	067°59'S. 152°04'E.					100	
081-109	069°17'S. 150°14'E.	1469-22015	04 Nov 73	26		0	Cape Freshfield, George V Coast
081-110	070°35'S. 148°13'E.	1469-22021	04 Nov 73	25		0	Surface features, Southern Cross Subglacial Highland
081-111	071°50'S. 145°55'E.	1469-22024	04 Nov 73	24		0	
081-112	073°04'S. 143°19'E.	1469-22030	04 Nov 73	22		0	
081-113	074°16'S. 140°20'E.	1469-22033	04 Nov 73	21		0	
081-114	075°25'S. 136°55'E.	1487-22035	22 Nov 73	24		0	
081-115	076°31'S. 132°56'E.	1541-22030	15 Jan 74	22		0	Snow dunes
081-116	077°33'S. 128°19'E.	1541-22033	15 Jan 74	21		0	Snow dunes
081-117	078°29'S. 122°56'E.	1181-22073	20 Jan 73	19		30	Snow dunes
081-118	079°19'S. 116°41'E.	1488-22111	23 Nov 73	20		80	Snow dunes
081-119	080°01'S. 109°31'E.	1488-22113	23 Nov 73	19		60	Snow dunes

TABLE 6.—*Optimum Landsat 1, 2, and 3 MSS and Landsat 2 RBV images of glaciers of Antarctica—Continued*

Path-Row	Nominal scene center (lat.—long.)	Landsat identification number	Date	Solar elev. angle (degrees)	Code	Cloud cover (percent)	Remarks
082-108	067°59'S. 150°11'E.	1542-22055	16 Jan 74	30		50	Cape Freshfield, George V Coast
082-109	069°17'S. 148°22'E.	1560-22053	03 Feb 74	24		60	Ninnis Glacier
082-110	070°35'S. 146°20'E.	1506-22074	11 Dec 73	31		0	
082-111	071°50'S. 144°03'E.	1506-22080	11 Dec 73	30		0	
082-112	073°04'S. 141°27'E.	1506-22083	11 Dec 73	29		0	
082-113	074°16'S. 138°28'E.	1506-22085	11 Dec 73	28		0	
082-114	075°28'S. 135°02'E.	1488-22093	23 Nov 73	25		0	
082-115	076°31'S. 131°04'E.	1506-22094	11 Dec 73	25		0	Snow dunes
082-116	077°33'S. 126°27'E.	1471-22161	06 Nov 73	18		0	Snow dunes
082-117	078°29'S. 121°04'E.	1506-22103	11 Dec 73	23		0	Snow dunes
082-118	079°19'S. 114°49'E.	1506-22110	11 Dec 73	22		0	Snow dunes
082-119	080°01'S. 107°39'E.	1506-22112	11 Dec 73	21		0	Snow dunes
083-108	067°59'S. 148°45'E.					100	
083-109	069°17'S. 146°56'E.					100	
083-110	070°35'S. 144°54'E.	1507-22132	12 Dec 73	31		0	Band 6
083-110	070°35'S. 144°54'E.	1471-22134	06 Nov 73	25		10	
083-111	071°50'S. 142°37'E.	1507-22134	12 Dec 73	30		0	Band 6
083-111	071°50'S. 142°37'E.	1471-22140	06 Nov 73	24		5	
083-112	073°04'S. 140°01'E.	1164-22111	03 Jan 73	28		0	
083-113	074°16'S. 137°02'E.	1164-22114	03 Jan 73	27		0	
083-114	075°25'S. 133°36'E.	1164-22120	03 Jan 73	26		0	
083-115	076°31'S. 129°38'E.	1489-22154	24 Nov 73	24		0	Snow dunes
083-116	077°33'S. 125°01'E.					100	
083-117	078°29'S. 119°38'E.	1472-22222	07 Nov 73	17		50	Snow dunes

TABLE 6.—*Optimum Landsat 1, 2, and 3 MSS and Landsat 2 RBV images of glaciers of Antarctica—Continued*

Path-Row	Nominal scene center (lat.—long.)	Landsat identification number	Date	Solar elev. angle (degrees)	Code	Cloud cover (percent)	Remarks
083-118	079°19'S. 113°23'E.	1490-22224	25 Nov 73	20	●	0	Snow dunes.
083-119	080°01'S. 106°13'E.	1490-22230	25 Nov 73	19	◐	15	Snow dunes
084-108	067°59'S. 147°19'E.	1544-22171	18 Jan 74	29	◐	40	Ninnis Glacier Tongue
084-109	069°17'S. 145°30'E.	1472-22190	07 Nov 73	27	●	0	Upper Mertz Glacier
084-110	070°35'S. 143°28'E.	1472-22192	07 Nov 73	26	●	0	
084-111	071°50'S. 141°11'E.	1472-22195	07 Nov 73	25	●	0	
084-112	073°04'S. 138°35'E.	1472-22201	07 Nov 73	23	●	0	
084-113	074°16'S. 135°36'E.	1472-22204	07 Nov 73	22	●	0	
084-114	075°25'S. 132°10'E.	1472-22210	07 Nov 73	21	●	0	Snow dunes
084-115	076°31'S. 128°12'E.	1472-22213	07 Nov 73	20	●	0	Snow dunes
084-116	077°33'S. 123°35'E.	1544-22203	18 Jan 74	21	◐	10	Snow dunes
084-117	078°29'S. 118°12'E.	1129-22192	29 Nov 72	22	◐	40	Snow dunes
084-118	079°19'S. 111°57'E.	1129-22194	29 Nov 72	21	◐	10	Snow dunes
084-119	080°01'S. 104°47'E.	1129-22201	29 Nov 72	20	●	5	
085-107	066°40'S. 147°32'E.	1509-22233	14 Dec 73	34	◐	90	Mertz Glacier Tongue
085-108	067°59'S. 145°53'E.	1509-22240	14 Dec 73	33	◐	90	Mertz Glacier Tongue
085-109	069°17'S. 144°04'E.	1167-22271	06 Jan 73	30	◐	80	
085-110	070°35'S. 142°02'E.	1509-22245	14 Dec 73	31	◐	10	
085-111	071°50'S. 139°45'E.	1509-22251	14 Dec 73	30	●	0	
085-112	073°04'S. 137°09'E.	1473-22260	08 Nov 73	24	●	5	
085-113	074°16'S. 134°10'E.	1473-22262	08 Nov 73	22	◐	30	
085-114	075°25'S. 130°44'E.	1473-22265	08 Nov 73	21	◐	15	Snow dunes
085-115	076°31'S. 126°46'E.	1221-22301	01 Mar 73	10	◐	15	Snow dunes
085-116	077°33'S. 122°09'E.				◉		

TABLE 6.—*Optimum Landsat 1,2, and 3 MSS and Landsat 2 RBV images of glaciers of Antarctica — Continued*

Path-Row	Nominal scene center (lat.-long.)	Landsat identification number	Date	Solar elev. angle (degrees)	Code	Cloud cover (percent)	Remarks
085-117	078°29'S. 116°46'E.	1204-22364	12 Feb 73	13	●	0	Snow dunes
085-118	079°19'S. 110°31'E.	1474-22341	09 Nov 73	17	◐	80	
085-119	080°01'S. 103°21'E.	1492-22343	27 Nov 73	19	◑	10	
086-107	066°40'S. 146°06'E.				◒	100	
086-108	067°59'S. 144°27'E.	1564-22280	07 Feb 74	24	◑	30	Mertz Glacier
086-108	067°59'S. 144°27'E.	1546-22284	20 Jan 74	29	◑	50	Coast visible
086-109	069°17'S. 142°38'E.	1546-22290	20 Jan 74	28	◑	10	
086-110	070°35'S. 140°36'E.	1546-22293	20 Jan 74	27	●	0	
086-111	071°50'S. 138°19'E.	1546-22295	20 Jan 74	26	●	0	
086-112	073°04'S. 135°43'E.	1546-22302	20 Jan 74	25	●	0	
086-113	074°16'S. 132°44'E.	1510-22314	15 Dec 73	28	●	0	
086-114	075°25'S. 129°18'E.	1510-22321	15 Dec 73	27	●	0	Snow dunes
086-115	076°31'S. 125°20'E.	1510-22323	15 Dec 73	26	●	0	Snow dunes
086-116	077°33'S. 120°43'E.	1510-22330	15 Dec 73	25	●	0	Snow dunes
086-117	078°29'S. 115°20'E.	1510-22332	15 Dec 73	23	●	0	Snow dunes
086-118	079°19'S. 109°05'E.	1510-22335	15 Dec 73	22	●	0	Snow dunes
086-119	080°01'S. 101°55'E.	1510-22341	15 Dec 73	21	●	0	
087-107	066°40'S. 144°40'E.				⊙		
087-108	067°59'S. 143°01'E.				⊙		
087-109	069°17'S. 141°12'E.				⊙		
087-110	070°35'S. 139°10'E.	1511-22361	16 Dec 73	31	◐	15	
087-111	071°50'S. 136°53'E.	1187-22393	26 Jan 73	24	●	0	
087-112	073°04'S. 134°17'E.	1187-22400	26 Jan 73	23	◑	15	
087-113	074°16'S. 131°18'E.	1187-22402	26 Jan 73	22	◑	70	

TABLE 6.—*Optimum Landsat 1, 2, and 3 MSS and Landsat 2 RBV images of glaciers of Antarctica—Continued*

Path-Row	Nominal scene center (lat.—long.)	Landsat identification number	Date	Solar elev. angle (degrees)	Code	Cloud cover (percent)	Remarks
087-114	075°25'S. 127°52'E.	1187-22405	26 Jan 73	21		60	Snow dunes
087-115	076°31'S. 123°54'E.	1187-22411	26 Jan 73	20		45	Snow dunes
087-116	077°33'S. 119°17'E.	1187-22414	26 Jan 73	19		20	Snow dunes
087-117	078°29'S. 113°54'E.	1187-22420	26 Jan 73	18		15	Snow dunes
087-118	079°19'S. 107°39'E.						
087-119	080°01's. 100°29'E.						
088-107	066°40'S. 143°13'E.	1224-22440	04 Mar 73	17		10	Commonwealth Bay
088-107	066°40'S. 143°13'E.	1170-22433	09 Jan 73	32		30	Commonwealth Bay, 'blue ice'
088-108	067°59'S. 141°35'E.	1170-22435	09 Jan 73	31		0	
088-109	069°17'S. 139°46'E.	1170-22442	09 Jan 73	30		0	
088-110	070°35'S. 137°44'E.	1224-22452	04 Mar 73	14		5	
088-111	071°50'S. 135°27'E.	1224-22454	04 Mar 73	13		10	
088-112	073°04'S. 132°51'E.	1224-22461	04 Mar 73	12		20	
088-113	074°16'S. 129°52'E.	1224-22463	04 Mar 73	11		10	
088-114	075°25'S. 126°26'E.	1224-22470	04 Mar 73	10		50	
088-115	076°31'S. 122°28'E.	1207-22530	15 Feb 73	14		0	
088-116	077°33'S. 117°51'E.	1207-22532	15 Feb 73	13		0	Snow dunes
088-117	078°29'S. 112°28'E.	1207-22535	15 Feb 73	12		0	Snow dunes
088-118	079°19'S. 106°13'E.	1189-22540	28 Jan 73	16		80	
088-119	080°01's. 099°03'E.	1189-22542	28 Jan 73	15		90	Band 6
089-107	066°40'S. 141°47'E.	1189-22492	28 Jan 73	28		25	Astrolabe Glacier Tongue
089-108	067°59'S. 140°09'E.	1549-22454	23 Jan 74	28		95	
089-109	069°17'S. 138°20'E.	1189-22501	28 Jan 73	26		75	
089-110	070°35'S. 136°18'E.	1170-22444	09 Jan 73	29		0	

TABLE 6.—Optimum Landsat 1, 2, and 3 MSS and Landsat 2 RBV images of glaciers of Antarctica — Continued

Path-Row	Nominal scene center (lat.—long.)	Landsat identification number	Date	Solar elev. angle (degrees)	Code	Cloud cover (percent)	Remarks
089-111	071°50'S. 134°01'E.	1170-22451	09 Jan 73	28	●	0	
089-112	073°04'S. 131°25'E.	1170-22453	09 Jan 73	27	●	0	
089-113	074°16'S. 128°26'E.	1207-22521	15 Feb 73	17	●	0	
089-114	075°25'S. 125°00'E.	1207-22523	15 Feb 73	15	●	0	Snow dunes
089-115	076°31'S. 121°02'E.	1170-22465	09 Jan 73	24	◐	20	
089-116	077°33'S. 116°25'E.	1170-22471	09 Jan 73	22	◐	45	Snow dunes
089-117	078°29'S. 111°02'E.	1189-22533	28 Jan 73	18	◐	60	Snow dunes
089-118	079°19'S. 104°47'E.	1478-22571	13 Nov 73	18	◐	70	
089-119	080°01'S. 097°37'E.	1129-22203	29 Nov 72	18	●	0	Surface features
090-107	066°40'S. 140°21'E.	1190-22551	29 Jan 73	28	●	5	Astrolabe Glacier Tongue, Français Glacier Tongue
090-108	067°59'S. 138°43'E.	1190-22553	29 Jan 73	27	●	0	
090-109	069°17'S. 136°54'E.	1190-22560	29 Jan 73	26	◐	50	
090-110	070°35'S. 134°52'E.	1190-22562	29 Jan 73	25	◐	60	
090-111	071°50'S. 132°35'E.	1190-22565	29 Jan 73	24	◐	55	
090-112	073°04'S. 129°59'E.	1190-22571	29 Jan 73	23	◐	40	
090-113	074°16'S. 127°00'E.	1190-22574,	29 Jan 73	22	◐	40	
090-114	075°25'S. 123°34'E.	1190-22580	29 Jan 73	21	◐	70	
090-115	076°31'S. 119°36'E.				◑	100	
090-116	077°33'S. 114°59'E.	1190-22585	29 Jan 73	18	◐	95	
090-117	078°29'S. 109°36'E.	1190-22592	29 Jan 73	17	◐	80	Snow dunes
090-118	079°19'S. 103°21'E.	1514-22564	19 Dec 73	22	●	0	
090-119	080°01'S. 096°11'E.	1514-22571	19 Dec 73	21	●	0	
091-107	066°40'S. 138°55'E.	1245-23012	25 Mar 73	10	◐	90	Coast visible
091-108	067°59'S. 137°17'E.				◑	100	

TABLE 6.—Optimum Landsat 1, 2, and 3 MSS and Landsat 2 RBV images of glaciers of Antarctica—Continued

Path-Row	Nominal scene center (lat.—long.)	Landsat identification number	Date	Solar elev. angle (degrees)	Code	Cloud cover (percent)	Remarks
091-109	069°17'S. 135°28'E.					100	
091-110	070°35'S. 133°26'E.	1173-23015	12 Jan 73	28		75	
091-111	071°50'S. 131°08'E.						
091-112	073°04'S. 128°32'E.	1136-22572	06 Dec 72	29		50	
091-113	074°16'S. 125°34'E.	1136-22575	06 Dec 72	27		5	Dome C
091-114	075°25'S. 122°08'E.	1136-22581	06 Dec 72	26		50	
091-115	076°31'S. 118°10'E.	1136-22584	06 Dec 72	25		50	
091-116	077°33'S. 113°32'E.	1210-23104	18 Feb 73	12		5	Snow dunes
091-117	078°29'S. 108°10'E.	1210-23110	18 Feb 73	11		40	Vostok, snow dunes
091-118	079°19'S. 101°55'E.	1551-23012	25 Jan 74	17		55	Surface features, 'Vostok Subglacial Highlands'
091-119	080°01'S. 094°44'E.	1551-23014	25 Jan 74	16		50	
092-107	066°40'S. 137°29'E.	1210-23065	18 Feb 73	22		0	Francais Glacier Tongue, Commandant Charcot Glacier
092-108	067°59'S. 135°51'E.	1210-23072	18 Feb 73	21		5	
092-108	067°59'S. 135°51'E.	1552-23025	26 Jan 74	27		5	
092-109	069°17'S. 134°02'E.	1210-23074	18 Feb 73	20		0	Surface features
092-110	070°35'S. 132°00'E.	1210-23081	18 Feb 73	19		0	
092-111	071°50'S. 129°42'E.	1210-23083	18 Feb 73	18		5	
092-112	073°04'S. 127°06'E.	1210-23090	18 Feb 73	17		5	
092-113	074°16'S. 124°08'E.	1210-23092	18 Feb 73	16		0	
092-114	075°25'S. 120°42'E.	1156-23093	26 Dec 72	26		0	
092-115	076°31'S. 116°44'E.	1210-23101	18 Feb 73	13		0	
092-116	077°33'S. 112°06'E.	1156-23102	26 Dec 72	24		5	Snow dunes
092-116	077°33'S. 112°06'E.	1173-23042	12 Jan 73	22		5	Snow dunes
092-117	078°29'S. 106°44'E.	1193-23163	01 Feb 73	16		50	

TABLE 6.—*Optimum Landsat 1, 2, and 3 MSS and Landsat 2 RBV images of glaciers of Antarctica—Continued*

Path-Row	Nominal scene center (lat.—long.)	Landsat identification number	Date	Solar elev. angle (degrees)	Code	Cloud cover (percent)	Remarks
092-118	079°19'S. 100°29'E.						
092-119	080°01'S. 093°18'E.						
093-107	066°40'S. 136°03'E.	1193-23122	01 Feb 73	27		60	Dibble Glacier
093-108	067°59'S. 134°25'E.	1193-23125	01 Feb 73	26		15	
093-109	069°17'S. 132°36'E.	1193-23131	01 Feb 73	25		50	
093-110	070°35'S. 130°34'E.					100	
093-111	071°50'S. 128°16'E.	1193-23140	01 Feb 73	23		85	
093-112	073°04'S. 125°40'E.	1193-23143	01 Feb 73	22		80	
093-113	074°16'S. 122°42'E.					100	
093-114	075°25'S. 119°16'E.					100	
093-115	076°31'S. 115°18'E.	1193-23154	01 Feb 73	19		70	
093-116	077°33'S. 110°40'E.	1193-23161	01 Feb 73	18		15	
093-117	078°29'S. 105°18'E.	1499-23135	04 Dec 73	23		10	
093-118	079°19'S. 099°03'E.	1499-23141	04 Dec 73	22		5	
093-119	080°01'S. 091°52'E.	1499-23144	04 Dec 73	20		0	
094-106	065°20'S. 136°06'E.					100	
094-107	066°40'S. 134°37'E.	1464-23153	30 Oct 73	27		25	Dibble Iceberg Tongue
094-108,	067°59'S. 132°59'E.	1464-23160	30 Oct 73	26		90	Surface features
094-109	069°17'S. 131°10'E.	1139-23132	09 Dec 72	32		75	
094-110	070°35'S. 129°08'E.	1158-23192	28 Dec 72	31		45	
094-111	071°50'S. 126°50'E.	1158-23194	28 Dec 72	30		25	
094-112	073°04'S. 124°14'E.	1572-23153	15 Feb 74	17		0	
094-113	074°76'S. 121°16'E.	1572-23160	15 Feb 74	16		0	
094-114	075°25'S. 117°50'E.	1572-23162	15 Feb 74	15		0	

TABLE 6.—*Optimum Landsat 1, 2, and 3 MSS and Landsat 2 RBV images of glaciers of Antarctica—Continued*

Path-Row	Nominal scene center (lat.—long.)	Landsat identification number	Date	Solar elev. angle (degrees)	Code	Cloud cover (percent)	Remarks
094-115	076°31'S. 113°52'E.	1572-23165	15 Feb 74	14	●	0	
094-116	077°33'S. 109°14'E.	1572-23171	15 Feb 74	13	◐	10	Snow dunes
094-117	078°29'S. 103°52'E.	1572-23174	15 Feb 74	12	◑	25	Snow dunes
094-118	079°19'S. 097°37'E.	1572-23180	15 Feb 74	11	◒	50	'Vostok Subglacial Highlands'
094-119	080°01'S. 090°26'E.	1572-23183	15 Feb 74	10	◓	40	
095-106	065°20'S. 134°40'E.	2353-23091	10 Jan 76	32	●	0	Dibble Iceberg Tongue, Freeman Glacier
095-107	066°40'S. 133°11'E.	1447-23214	13 Oct 73	21	●	0	
095-108	067°59'S. 131°33'E.	1447-23220	13 Oct 73	20	●	0	Surface features
095-109	069°17'S. 129°43'E.	1447-23223	13 Oct 73	19	●	0	Surface features
095-110	070°35'S. 127°42'E.	1447-23225	13 Oct 73	17	●	0	
095-111	071°50'S. 125°24'E.	1213-23255	21 Feb 73	17	◐	95	
095-112	073°04'S. 122°48'E.	1158-23201	28 Dec 72	28	●	0	
095-112	073°04'S. 122°48'E.	1213-23261	21 Feb 73	16	◐	10	Band 6
095-113	074°16'S. 119°49'E.	1213-23264	21 Feb 73	14	●	0	
095-114	075°25'S. 116°24'E.	1555-23222	29 Jan 74	20	●	0	
095-115	076°31'S. 112°25'E.	1501-23242	06 Dec 73	25	●	0	
095-116	077°33'S. 107°48'E.	1501-23245	06 Dec 73	24	◐	30	
095-117	078°29'S. 102°25'E.	1196-23335	04 Feb 73	16	◑	75	
095-118	079°19'S. 096°10'E.	1555-23240	29 Jan 74	16	◒	50	
095-119	080°01'S. 089°00'E.	1555-23243	29 Jan 74	15	◓	50	
096-106	065°20'S. 133°14'E.	1466-23263	01 Nov 73	29	●	0	Dibble Iceberg Tongue
096-107	066°40'S. 131°45'E.	1466-23270	01 Nov 73	27	●	0	Blodgett Iceberg Tongue
096-108	067°59'S. 130°07'E.	1466-23272	01 Nov 73	26	●	0	Frost Glacier
096-109	069°17'S. 128°17'E.	1466-23275	01 Nov 73	25	●	0	

TABLE 6.—Optimum Landsat 1, 2, and 3 MSS and Landsat 2 RBV images of glaciers of Antarctica— Continued

Path-Row	Nominal scene center (lat.—long.)	Landsat identification number	Date	Solar elev. angle (degrees)	Code	Cloud cover (percent)	Remarks
096-110	070°35'S. 126°16'E.	1466-23281	01 Nov 73	24		0	
096-111	071°50'S. 123°58'E.	1466-23284	01 Nov 73	23		10	
096-112	073°04'S. 121°22'E.	1484-23290	19 Nov 73	23		0	Band 6
096-113	074°16'S. 118°23'E.	1484-23293	19 Nov 73	25		20	Scan lines missing
096-114	075°25'S. 114°58'E.	1520-23292	25 Dec 73	26		0	
096-115	076°31'S. 110°59'E.	1520-23294	25 Dec 73	25		0	
096-116	077°33'S. 106°22'E.	1484-23304	19 Nov 73	22		0	Scan line missing
096-117	078°29'S. 100°59'E.	1467-23365	02 Nov 73	16		0	Band 6
096-118	079°19'S. 094°44'E.	1467-23372	02 Nov 73	15		40	Band 6
096-119	080°01'S. 087°34'E.	1124-23344	24 Nov 72	19		10	
097-106	065°20'S. 131°48'E.						
097-107	066°40'S. 130°19'E.						
097-108	067°59'S. 128°41'E.					100	
097-109	069°17'S. 126°51'E.					100	
097-110	070°35'S. 126°16'E.	1575-23315	18 Feb 74	18		15	
097-111	071°50'S. 123°58'E.	1521-23335	26 Dec 73	30		0	
097-112	073°04'S. 121°22'E.	1557-23330	31 Jan 74	22		0	
097-113	074°16's. 118°23'E.	1557-23332	31 Jan 74	21		0	
097-114	075°25'S. 114°58'E.	1179-23380	18 Jan 73	23		25	
097-115	076°31'S. 110°59'E.	1467-23360	02 Nov 73	18		0	
097-116	077°33'S. 106°22'E.	1539-23352	13 Jan 74	22		5	
097-117	078°29'S. 100°59'E.	1576-23403	19 Feb 74	11		25	Crevasses, 'Vostok Subglacial Highlands'
097-117	078°29'S. 100°59'E.	1521-23362	26 Dec 73	23		0	
097-118	079°19's. 094°44'E.	1521-23364	26 Dec 73	22		0	

TABLE 6.—Optimum Landsat 1, 2, and 3 MSS and Landsat 2 RBV images of glaciers of Antarctica—Continued

Path-Row	Nominal scene center (lat.—long.)	Landsat identification number	Date	Solar elev. angle (degrees)	Code	Cloud cover (percent)	Remarks
097–119	080°01'S. 087°34'E.	1521–23371	26 Dec 73	21	●	0	
098–106	065°20'S. 130°22'E.	1468–23380	03 Nov 73	29	●	0	Blodgett Iceberg Tongue
098–107	066°40'S. 128°53'E.	1468–23383	03 Nov 73	28	●	0	Frost Glacier, DeHaven Glacier
098–108	067°59'S. 127°14'E.	1468–23385	03 Nov 73	27	●	0	Upper Frost and DeHaven Glaciers
098–109	069°17'S. 125°25'E.	1468–23392	03 Nov 73	26	●	0	
098–110	070°35'S. 123°23'E.	1558–23375	01 Feb 74	24	●	0	
098–111	071°50'S. 121°06'E.	1558–23382	01 Feb 74	23	●	0	
098–112	073°04'S. 118°30'E.	1558–23384	01 Feb 74	21	●	0	
098–113	074°16'S. 115°31'E.	1558–23391	01 Feb 74	20	●	0	
098–114	075°25'S. 112°05'E.	1468–23412	03 Nov 73	20	●	0	
098–115	076°31'S. 108°07'E.	1486–23415	21 Nov 73	23	●	0	
098–116	077°33'S. 103°30'E.	1486–23421	21 Nov 73	22	●	0	
098–117	078°29'S. 098°07'E.	1486–23424	21 Nov 73	21	◐	10	Surface features
098–118	079°19'S. 091°52'E.	1522–23422	27 Dec 73	22	●	5	
098–119	080°01'S. 084°42'E.	1487–23491	22 Nov 73	19	◑	20	Gamburtsev Subglacial Mountains
099–107	066°40'S. 127°27'E.	1469–23441	04 Nov 73	28	●	5	DeHaven Glacier, Holmes Glacier
099–108	067°59'S. 125°48'E.	1469–23444	04 Nov 73	27	●	0	Upper DeHaven Glacier
099–109	069°17'S. 123°59'E.	1559–23431	02 Feb 74	24	●	0	
099–110	070°35'S. 121°57'E.	1559–23433	02 Feb 74	23	●	0	
099–111	071°50'S. 119°40'E.	1559–23440	02 Feb 74	22	●	0	
099–112	073°04'S. 117°04'E.	1559–23442	02 Feb 74	21	●	0	
099–113	074°16'S. 114°05'E.	1559–23445	02 Feb 74	20	●	0	
099–114	075°25'S. 110°39'E.	1469–23471	04 Nov 73	20	●	0	
099–115	076°31'S. 106°41'E.	1469–23473	04 Nov 73	19	●	0	

TABLE 6.—Optimum Landsat 1, 2, and 3 MSS and Landsat 2 RBV images of glaciers of Antarctica—Continued

Path-Row	Nominal scene center (lat.—long.)	Landsat identification number	Date	Solar elev. angle (degrees)	Code	Cloud cover (percent)	Remarks
099-116	077°33'S. 102°04'E.	1469-23480	04 Nov 73	18	●	5	
099-117	078°29'S. 096°41'E.	1505-23481	10 Dec 73	23	●	0	
099-118	079°19'S. 090°26'E.	1505-23483	10 Dec 73	22	●	0	
099-119	080°01'S. 083°16'E.	1505-23490	10 Dec 73	21	◐	10	Gamburtsev Subglacial Mountains
100-106	065°20'S. 127°30'E.				⊙		
100-107	066°40'S. 126°01'E.	1145-23465	15 Dec 72	34	●	5	Holmes Glacier
100-108	067°59'S. 124°22'E.	1145-23472	15 Dec 72	33	●	0	
100-109	069°17'S. 122°33'E.	1145-23474	15 Dec 72	32	●	0	
100-110	070°35'S. 120°31'E.	1560-23491	03 Feb 74	23	●	0	
100-111	071°50'S. 118°14'E.	1560-23494	03 Feb 74	22	●	0	
100-112	073°04'S. 115°38'E.	1560-23500	03 Feb 74	21	●	0	
100-113	074°16'S. 112°39'E.	1560-23503	03 Feb 74	20	●	0	
100-114	075°25'S. 109°13'E.	1182-23552	21 Jan 73	23	●	0	
100-115	076°31'S. 105°15'E.	1182-23554	21 Jan 73	21	●	0	
100-116	077°33'S. 100°38'E.	1182-23561	21 Jan 73	20	●	0	
100-117	078°29'S. 095°15'E.	1182-23563,	21 Jan 73	19	●	0	
100-118	079°19'S. 089°00'E.	1127-23513	27 Nov 72	21	●	5	
100-119	080°01'S. 081°50'E.	1524-23541	29 Dec 73	21	●	0	Surface features, partial scene follows, adding 4 percent more area
101-106	065°20'S. 126°04'E.	1543-23540	17 Jan 74	31	◐	85	Ice wall
101-107	066°40'S. 124°35'E.	1543-23542	17 Jan 74	30	◐	30	Hudson Glacier, melt ponds
101-108	067°59'S. 122°56'E.	1543-23545	17 Jan 74	29	◐	40	
101-109	069°17's. 121°07'E.	1579-23542	22 Feb 74	18	◐	80	Band 6
101-110	070°35'S. 119°05'E.	1579-23544	22 Feb 74	17	◐	30	
101-111	071°50'S. 116°48'E.	1579-23551	22 Feb 74	16	◐	10	

TABLE 6—Optimum Landsat 1, 2, and 3 MSS and Landsat 2 RBV images of glaciers of Antarctica—Continued

Path-Row	Nominal scene center (lat.—long.)	Landsat identification number	Date	Solar elev. angle (degrees)	Code	Cloud cover (percent)	Remarks
101-112	073°04'S. 114°12'E.	1471-23575	06 Nov 73	23		15	Scan lines missing
101-113	074°16'S. 111°13'E.	1507-23575	12 Dec 73	28		30	
101-114	075°25'S. 107°47'E.	1507-23582	12 Dec 73	27		0	
101-115	076°31'S. 103°49'E.	1507-23584	12 Dec 73	26		0	
101-116	077°33'S. 099°12'E.	1507-23591	12 Dec 73	24		5	
101-117	078°29'S. 093°49'E.	1473-00053	08 Nov 73	17		30	
101-118	079°19'S. 087°34'E.	1473-00060	08 Nov 73	16		0	Gamburtsev Subglacial Mountains, scan lines missing
101-119	080°01'S. 080°24'E.	1473-00062	08 Nov 73	15		5	Gamburtsev Subglacial Mountains
102-106	065°20'S. 124°37'E.						
102-107	066°40'S. 123°09'E.	1149-00041	19 Dec 72	34		50	Dalton Iceberg Tongue
102-108	067°59'S. 121°30'E.	1149-00043	19 Dec 72	33		5	
102-109	069°17'S. 119°41'E.	1203-00050	11 Feb 73	22		0	
102-110	070°35'S. 117°39'E.	1203-00053	11 Feb 73	21		10	
102-111	071°50'S. 115°22'E.	1203-00055	11 Feb 73	20		5	
102-112	073°04'S. 112°46'E.	1203-00062	11 Feb 73	19		0	
102-113	074°16'S. 109°47'E.	1203-00064	11 Feb 73	18		0	
102-114	075°25'S. 106°21'E.	1203-00071	11 Feb 73	17		5	
102-115	076°31'S. 102°23'E.	1166-00013	05 Jan 73	24		10	Defective negative
102-116	077°33'S. 097°46'E.	1166-00015	05 Jan 73	23		20	Defective negative
102-117	078°29'S. 092°23'E.	1474-00112	09 Nov 73	18		10	
102-118	079°19'S. 086°08'E.	1492-00114	27 Nov 73	21		10	Gamburtsev Subglacial Mountains
102-119	080°01'S. 078°58'E.	1492-00120	27 Nov 73	19		0	Gamburtsev Subglacial Mountains
103-106	065°20'S. 123°11'E.						
103-107	066°40'S. 121°43'E.						

TABLE 6.—Optimum Landsat 1, 2, and 3 MSS and Landsat 2 RBV images of glaciers of Antarctica—Continued

Path-Row	Nominal scene center (lat.—long.)	Landsat identification number	Date	Solar elev. angle (degrees)	Code	Cloud cover (percent)	Remarks
103-108	067°59'S. 120°04'E.	2415-23543	12 Mar 76	12	●	5	Sabrina Coast
103-109	069°17'S. 118°15'E.				◐	100	
103-110	070°35'S. 116°13'E.	1510-00080	15 Dec 73	31	●	0	
103-111	071°50'S. 113°56'E.	1510-00083	15 Dec 73	30	●	0	
103-112	073°04'S. 111°20'E.	1492-00091	27 Nov 73	27	●	0	
103-113	074°16'S. 108°21'E.	1492-00093	27 Nov 73	26	●	0	
103-114	075°25'S. 104°55'E.	1492-00100	27 Nov 73	25	●	0	
103-115	076°31'S. 100°57'E.	1492-00102	27 Nov 73	24	●	0	
103-116	077°33'S. 096°20'E.	1131-00075	01 Dec 72	23	●	0	
103-117	078°29'S. 090°57'E.	1492-00111	27 Nov 73	22	◐	15	
103-118	079°19'S. 084°42'E.	1475-00173	10 Nov 73	17	●	0	Gamburtsev Subglacial Mountains
103-119	080°01'S. 077°32'E.	1493-00175	28 Nov 73	19	●	0	Gamburtsev Subglacial Mountains
104-106	065°20'S. 121°45'E.				◉		
104-107	066°40'S. 120°17'E.				◉		
104-108	067°59'S. 118°38'E.				◉		
104-109	069°17'S. 116°49'E.	1493-00134	28 Nov 73	31	◐	40	
104-110	070°35'S. 114°47'E.	1475-00141	10 Nov 73	26	●	0	
104-111	071°50'S. 112°30'E.	1583-00122	26 Feb 74	15	●	0	
104-112	073°04'S. 109°54'E.	1475-00150	10 Nov 73	24	●	0	
104-113	074°16'S. 106°55'E.	1583-00131	26 Feb 74	13	●	0	
104-114	075°25'S. 103°29'E.	1493-00154	28 Nov 73	26	●	0	
104-115	076°31'S. 099°31'E.	1475-00161	10 Nov 73	20	◐	40	
104-116	077°33'S. 094°54'E.	1493-00163	28 Nov 73	23	◐	40	
104-117	078°29'S. 089°31'E.	1511-00164	16 Dec 73	23	●	5	

TABLE 6.—Optimum Landsat 1, 2, and 3 MSS and Landsat 2 RBV images of glaciers of Antarctica—Continued

Path-Row	Nominal scene center (lat.—long.)	Landsat identification number	Date	Solar elev. angle (degrees)	Code	Cloud cover (percent)	Remarks
104-118	079°19'S. 083°16'E.	1493-00172	28 Nov 73	21	●	0	Gamburtsev Subglacial Mountains
104-119	080°01'S. 076°06'E.	1476-00234	11 Nov 73	16	◐	30	Gamburtsev Subglacial Mountains
105-107	066°40'S. 118°50'E.				◑	100	
105-108	067°59'S. 117°12'E.	1566-00170	09 Feb 74	24	◐	95	
105-109	069°17'S. 115°23'E.	1512-00190	17 Dec 73	32	●	0	
105-110	070°35'S. 113°21'E.	1476-00195	11 Nov 73	26	●	0	
105-111	071°50'S. 111°04'E.	1206-00231	14 Feb 73	19	●	0	
105-112	073°04's. 108°28'E.	1206-00233	14 Feb 73	18	●	0	
105-113	074°16'S. 105°29'E.	1206-00240	14 Feb 73	17	●	0	
105-114	075°25'S. 102°03'E.	1476-00213	11 Nov 73	22	●	0	
105-115	076°31'S. 098°05'E.	1476-00220	11 Nov 73	21	◐	20	
105-116	077°33'S. 093°28'E.	1476-00222	11 Nov 73	19	◐	15	
105-117	078°29'S. 088°05'E.	1477-00283	12 Nov 73	19	◐	40	Gamburtsev Subglacial Mountains
105-118	079°19'S. 081°50'E.	1477-00290	12 Nov 73	17	◐	30	Gamburtsev Subglacial Mountains
105-119	080°01'S. 074°40'E.	1477-00292	12 Nov 73	16	◐	40	Gamburtsev Subglacial Mountains
106-107	066°40'S. 117°24'E.				⊙		
106-108	067°59'S. 115°46'E.	1549-00232	23 Jan 74	28	◐	60	
106-109	069°17'S. 113°57'E.	1189-00274	28 Jan 73	26	◐	20	
106-110	070°35'S. 111°55'E.	1189-00281	28 Jan 73	25	●	0	
106-111	071°50'S. 109°38'E.	1189-00283	28 Jan 73	24	●	0	
106-112	073°04'S. 107°02'E.	1189-00290	28 Jan 73	23	●	0	
106-113	074°16'S. 104°03'E.	1585-00243	28 Feb 74	12	●	0	
106-114	075°25's. 100°37'E.	1585-00250	28 Feb 74	11	●	0	
106-115	076°31'S. 096°39'E.	1585-00252	28 Feb 74	10	●	5	

TABLE 6.—*Optimum Landsat 1, 2, and 3 MSS and Landsat 2 RBV images of glaciers of Antarctica—Continued*

Path-Row	Nominal scene center (lat.-long.)	Landsat identification number	Date	Solar elev. angle (degrees)	Code	Cloud cover (percent)	Remarks
106-116	077°33'S. 092°02'E.	1585-00255	28 Feb 74	9	●	5	
106-117	078°29'S. 086°39'E.	1549-00270	23 Jan 74	19	◐	40	Gamburtsev Subglacial Mountains
106-118	079°19'S. 080°24'E.	1513-00283	18 Dec 73	22	◐	40	Gamburtsev Subglacial Mountains
106-119	080°01'S. 073°14'E.	1513-00290	18 Dec 73	21	●	0	Gamburtsev Subglacial Mountains
107-107	066°40'S. 115°58'E.	1460-00300	26 Oct 73	25	●	0	Totten Glacier Tongue, Williamson Glacier Tongue
107-108	067°59'S. 114°20'E.	1460-00303	26 Oct 73	24	●	0	Upper Totten Glacier
107-109	069°17'S. 112°31'E.	1172-00332	11 Jan 73	30	◐	90	
107-110	070°35'S. 110°29'E.	1226-00342	06 Mar 73	14	◐	25	
107-111	071°50'S. 108°12'E.	1226-00344	06 Mar 73	13	◐	25	
107-112	073°04'S. 105°36'E.	1226-00351	06 Mar 73	11	◐	40	
107-113	074°16'S. 102°37'E.	1226-00353	06 Mar 73	10	◐	60	
107-114	075°25'S. 099°11'E.	1226-00360	06 Mar 73	9	◐	90	
107-115	076°31'S. 095°13'E.	1209-00420	17 Feb 73	14	◐	50	
107-116	077°33'S. 090°36'E.	1135-00305	05 Dec 72	24	◐	80	Scan lines missing
107-117	078°29'S. 085°13'E.	1479-00400	14 Nov 73	19	◐	30	Gamburtsev Subglacial Mountains
107-117	078°29'S. 085°13'E.	1514-00335	19 Dec 73	23	◑	10	Gamburtsev Subglacial Mountains
107-118	079°19'S. 078°58'E.	1514-00341	19 Dec 73	22	●	0	Gamburtsev Subglacial Mountains
107-119	080°01'S. 071°48'E.	1514-00344	19 Dec 73	21	◐	20	Gamburtsev Subglacial Mountains
108-107	066°40'S. 114°32'E.	1209-00384	17 Feb 73	23	●	0	Totten Glacier Tongue, Williamson Glacier Tongue
108-108	067°59'S. 112°54'E.	1209-00390	17 Feb 73	22	◐	25	Upper Totten Glacier
108-109	069°17'S. 111°05'E.	1209-00393	17 Feb 73	21	◐	15	
108-110	070°35'S. 109°03'E.	1209-00395	17 Feb 73	19	●	0	
108-111	071°50'S. 106°46'E.	1209-00402	17 Feb 73	18	●	0	
108-112	073°04'S. 104°10'E.	1209-00404	17 Feb 73	17	●	0	Band 6

TABLE 6.—Optimum Landsat 1, 2, and 3 MSS and Landsat 2 RBV images of glaciers of Antarctica —Continued

Path-Row	Nominal scene center (lat.—long.)	Landsat identification number	Date	Solar elev. angle (degrees)	Code	Cloud cover (percent)	Remarks
108-113	074°16'S. 101°11'E.	1209-00411	17 Feb 73	16		0	Band 6
108-114	075°25'S. 097°45'E.	1209-00413	17 Feb 73	15		20	
108-115	076°31'S. 093°47'E.	1172-00355	11 Jan 73	23		50	
108-116	077°33'S. 089°10'E.	1172-00361	11 Jan 73	22		25	
108-117	078°29'S. 083°47'E.	1551-00383	25 Jan 74	18		50	Gamburtsev Subglacial Mountains
108-118	079°19'S. 077°32'E.	1551-00385	25 Jan 74	17		60	Gamburtsev Subglacial Mountains
108-119	080°01'S. 070°22'E.	1474-00123	09 Nov 73	14		50	Gamburtsev Subglacial Mountains
109-106	065°20'S. 114°35'E.	1192-00435	31 Jan 73	29		30	Budd Coast
109-107	066°40'S. 113°06'E.	1192-00441	31 Jan 73	28		50	Vanderford Glacier, Budd Coast
109-108	067°59'S. 111°28'E.	1192-00444	31 Jan 73	27		10	Upper Vanderford Glacier
109-109	069°17'S. 109°39'E.	1192-00450	31 Jan 73	25		50	
109-110	070°35'S. 107°37'E.	1192-00453	31 Jan 73	24		60	
109-111	071°50'S. 105°19'E.	1192-00455	31 Jan 73	23		0	
109-112	073°04'S. 102°43'E.	1192-00462	31 Jan 73	22		20	
109-113	074°16'S. 099°45'E.	1480-00440	15 Nov 73	24		20	
109-114	075°25'S. 096°19'E.	1480-00443	15 Nov 73	23		40	
109-115	076°31'S. 092°21'E.	1192-00473	31 Jan 73	19		10	
109-116	077°33'S. 087°43'E.	1192-00480	31 Jan 73	18		15	
109-117	078°29'S. 082°21'E.	1552-00441	26 Jan 74	18		20	Gamburtsev Subglacial Mountains
109-118	079°19'S. 076°06'E.	1552-00443	26 Jan 74	17		25	Gamburtsev Subglacial Mountains
109-119	080°01'S. 068°55'E.	1552-00450	26 Jan 74	16		40	
110-106	065°20'S. 113°09'E.					100	
110-107	066°40'S. 111°40'E.	1247-00502	27 Mar 73	10		90	Ice front
110-108	067°59'S. 110°02'E.	1247-00505	27 Mar 73	9		70	

TABLE 6.—Optimum Landsat 1, 2, and 3 MSS and Landsat 2 RBV images of glaciers of Antarctica—Continued

Path-Row	Nominal scene center (lat.—long.)	Landsat identification number	Date	Solar elev. angle (degrees)	Code	Cloud cover (percent)	Remarks
110-109	069°17'S. 108°13'E.	1175-00503	14 Jan 73	29		30	
110-110	070°35'S. 106°11'E.	1175-00505	14 Jan 73	28		50	
110-111	071°50'S. 103°53'E.	1229-00520	09 Mar 73	12		70	
110-112	073°04'S. 101°17'E.	1589-00470	04 Mar 73	12		60	
110-113	074°16's. 098°19'E.	1138-00465	08 Dec 72	27		70	Band 6
110-114	075°25'S. 094°53'E.	1589-00475	04 Mar 74	10		30	
110-115	076°31's. 090°55'E.	1589-00481	04 Mar 74	9		20	
110-116	077°33's. 086°17'E.	1553-00493	27 Jan 74	19		15	
110-117	078°29's. 080°55'E.	1553-00495	27 Jan 74	18		15	Gamburtsev Subglacial Mountains
110-118	079°19'S. 074°40'E.	1482-00574	17 Nov 73	19		0	Gamburtsev Subglacial Mountains
110-119	080°01's. 067°29'E.	1482-00580	17 Nov 73	17		5	Gamburtsev Subglacial Mountains
111-106	065°20'S. 111°43'E.					100	
111-107	066°40'S. 110°14'E.	1482-00530	17 Nov 73	31		30	Adams Glacier tongue, 'blue ice'
111-108	067°59'S. 108°36'E.	1482-00533	17 Nov 73	30		40	Surface features
111-109	069°17'S. 106°47'E.	1482-00535	17 Nov 73	29		15	
111-110	070°35'S. 104°45'E.	1482-00542,	17 Nov 73	28		5	
111-111	071°50'S. 102°27'E.	1212-00573	20 Feb 73	17		0	
111-112	073°04'S. 099°51'E.	1212-00580	20 Feb 73	16		0	
111-113	074°16'S. 096°53'E.	1212-00582	20 Feb 73	15		0	
111-114	075°25'S. 093°27'E.	1212-00585	20 Feb 73	14		20	
111-115	076°31'S. 089°29'E.	1482-00562	17 Nov 73	22		15	
111-116	077°33'S. 084°51'E.	1482-00565	17 Nov 73	21		5	Gamburtsev Subglacial Mountains
111-117	078°29'S. 079°29'E.	1482-00571	17 Nov 73	20		10	Gamburtsev Subglacial Mountains
111-118	079°19's. 073°14'E.	1483-01032	18 Nov 73	19		0	Gamburtsev Subglacial Mountains

TABLE 6.—*Optimum Landsat 1, 2, and 3 MSS and Landsat 2 RBV images of glaciers of Antarctica — Continued*

Path-Row	Nominal scene center (lat.-long.)	Landsat identification number	Date	Solar elev. angle (degrees)	Code	Cloud cover (percent)	Remarks
111-119	080°01'S. 066°03'E.						
112-106	065°20's. 110°17'E.						
112-107	066°40'S. 108°48'E.	1501-00583	06 Dec 73	34		60	Adams Glacier tongue
112-108	067°59'S. 107°10'E.	1483-00591	18 Nov 73	30		70	
112-109	069°17'S. 105°20'E.	1483-00594	18 Nov 73	29		60	
112-110	070°35'S. 103°19'E.	1555-00582	29 Jan 74	25		60	
112-111	071°50'S. 101°01'E.	1483-01003	18 Nov 73	27		25	
112-112	073°04's. 098°25'E.	1483-01005	18 Nov 73	26		0	
112-113	074°16's. 095°26'E.	1483-01012	18 Nov 73	25		0	
112-114	075°25'S. 092°01'E.	1501-01013	06 Dec 73	26		0	
112-115	076°31'S. 088°02'E.	1158-00590	28 Dec 72	25		5	
112-116	077°33'S. 083°25'E.	1195-01051	03 Feb 73	17		0	Gamburtsev Subglacial Mountains
112-117	078°29's. 078°02'E.	1483-01030	18 Nov 73	20		0	Gamburtsev Subglacial Mountains
112-118	079°19'S. 071°47'E.	1466-01091	01 Nov 73	14		0	Gamburtsev Subglacial Mountains
112-119	080°01'S. 064°37'E.	1478-00353	13 Nov 73	15		5	Band 6
113-107	066°40'S. 107°22'E.	1178-01064	17 Jan 73	31		60	Underwood Glacier tongue
113-107	066°40'S. 107°22'E.	1232-01073	12 Mar 73	15		40	Knox Coast
113-108	067°59'S. 105°44'E.	1232-01080	12 Mar 73	14		70	
113-109	069°17'S. 103°54'E.	1484-01052	19 Nov 73	29		30	
113-110	070°35'S. 101°53'E.	1232-01085	12 Mar 73	12		40	
113-111	071°50'S. 099°35'E.	1232-01091	12 Mar 73	10		5	
113-112	073°04'S. 096°59'E.	1232-01094	12 Mar 73	9		0	
113-113	074°16'S. 094°00'E.	1232-01100	12 Mar 73	8		10	
113-114	075°25'S. 090°35'E.	1232-01103	12 Mar 73	7		60	

TABLE 6. — *Optimum Landsat 1, 2, and 3 MSS and Landsat 2 RBV images of glaciers of Antarctica — Continued*

Path-Row	Nominal scene center (lat.-long.)	Landsat identification number	Date	Solar elev. angle (degrees)	Code	Cloud cover (percent)	Remarks
113-115	076°31'S. 086°36'E.					100	
113-116	077°33'S. 081°59'E.	1160-01105	30 Dec 72	24		40	Gamburtsev Subglacial Mountains
113-117	078°29'S. 076°36'E.	1574-01063	17 Feb 74	11		80	
113-118	079°19'S. 070°21'E.	1484-01090	19 Nov 73	19		20	Gamburtsev Subglacial Mountains
113-119	080°01'S. 063°11'E.	1485-01151	20 Nov 73	18		25	Gamburtsev Subglacial Mountains
114-107	066°40'S. 105°56'E.	1449-01103	15 Oct 73	21		0	Underwood Glacier tongue, Knox Coast
114-108	067°59'S. 104°18'E.	1449-01110	15 Oct 73	20		5	Surface features
114-109	069°17'S. 102°28'E.	1449-01112	15 Oct 73	19		0	
114-110	070°35'S. 100°27'E.	1449-01115	15 Oct 73	18		0	
114-111	071°50'S. 098°09'E.	1449-01121	15 Oct 73	17		0	
114-112	073°04'S. 095°33'E.	1449-01124	15 Oct 73	15		5	
114-112	073°04'S. 095°33'E.	1160-01091	30 Dec 72	28		0	
114-113	074°16'S. 092°34'E.	1160-01093	30 Dec 72	27		10	
114-114	075°25'S. 089°09'E.	1160-01100	30 Dec 72	26		30	
114-115	076°31'S. 085°10'E.	1160-01102	30 Dec 72	25		70	
114-116	077°33'S. 080°33'E.						
114-117	078°29'S. 075°10'E.	1198-01225	06 Feb 73	15		0	Gamburtsev Subglacial Mountains
114-118	079°19'S. 068°55'E.	1521-01142	26 Dec 73	22		5	Gamburtsev Subglacial Mountains
114-119	080°01'S. 061°45'E.	1521-01144	26 Dec 73	21		0	Gamburtsev Subglacial Mountains
115-106	065°20'S. 105°59'E.	1144-01182	14 Dec 72	35		90	Shackleton Ice Shelf
115-107	066°40'S. 104°30'E.	1144-01184	14 Dec 72	34		80	
115-108	067°59'S. 102°51'E.						
115-109	069°17'S. 101°02'E.						
115-110	070°35'S. 099°00'E.	1198-01200	06 Feb 73	23		10	

TABLE 6.—Optimum Landsat 1, 2, and 3 MSS and Landsat 2 RBV images of glaciers of Antarctica—Continued

Path-Row	Nominal scene center (lat.-long.)	Landsat identification number	Date	Solar elev. angle (degrees)	Code	Cloud cover (percent)	Remarks
115-111	071°50'S. 096°43'E.	1198-01202	06 Feb 73	22	●	0	
115-112	073°04'S. 094°07'E.	1198-01205	06 Feb 73	21	●	0	
115-113	074°16'S. 091°08'E.	1198-01211	06 Feb 73	20	●	0	
115-114	075°25'S. 087°42'E.	1198-01214	06 Feb 73	19	●	0	
115-115	076°31'S. 083°44'E.	1198-01220	06 Feb 73	17	◐	10	
115-116	077°33'S. 079°07'E.	1198-01223	06 Feb 73	16	◐	10	Gamburtsev Subglacial Mountains
115-117	078°29'S. 073°44'E.				◑		
115-118	079°19'S. 067°29'E.	1522-01200	27 Dec 73	22	●	0	Gamburtsev Subglacial Mountains
115-119	080°01'S. 060°19'E.	1522-01202	27 Dec 73	21	●	5	Surface features
116-106	065°20'S. 104°33'E.	1469-01212	04 Nov 73	29	●	0	Bowman Island
116-107	066°40'S. 103°04'E.	1469-01214	04 Nov 73	28	●	0	Shackleton Ice Shelf, 'blue ice'
116-108	067°59'S. 101°25'E.	1469-01221	04 Nov 73	27	●	0	'Blue ice'
116-109	069°17'S. 099°36'E.				◑	100	
116-110	070°35'S. 097°34'E.				◑	100	
116-111	071°50'S. 095°17'E.	1144-01202	14 Dec 72	30	◐	90	
116-112	073°04'S. 092°41'E.	1144-01205	14 Dec 72	29	◐	90	
116-113	074°16'S. 089°42'E.	1144-01211	14 Dec 72	28	●	5	
116-114	075°25'S. 086°16'E.	1144-01214	14 Dec 72	27	●	0	
116-115	076°31'S. 082°18'E.	1144-01220	14 Dec 72	25	●	0	Surface features
116-116	077°33'S. 077°41'E.	1144-01223	14 Dec 72	24	●	5	
116-117	078°29'S. 072°18'E.				◑		
116-118	079°19'S. 066°03'E.	1505-01260	10 Dec 73	22	●	0	Surface features
116-119	080°01'S. 058°53'E.	1523-01261	28 Dec 73	21	●	0	
117-106	065°20'S. 103°07'E.				◑		

TABLE 6.—Optimum Landsat 1, 2, and 3 MSS and Landsat 2 RBV images of glaciers of Antarctica — Continued

Path-Row	Nominal scene center (lat.—long.)	Landsat identification number	Date	Solar elev. angle (degrees)	Code	Cloud cover (percent)	Remarks
117-107	066°40'S. 101°38'E.						
117-108	067°59'S. 099°59'E.	1542-01264	16 Jan 74	30		90	
117-109	069°17'S. 098°10'E.	1181-01250	20 Jan 73	28		10	Surface features
117-110	070°35'S. 096°08'E.	1181-01253	20 Jan 73	27		0	
117-111	071°50'S. 093°51'E.	1181-01255	20 Jan 73	26		10	Surface features
117-112	073°04'S. 091°15'E.	1181-01262	20 Jan 73	25		80	Surface features
117-113	074°16'S. 088°16'E.	1164-01322	03 Jan 73	27		80	
117-114	075°25'S. 084°50'E.	1164-01325	03 Jan 73	26		50	
117-115	076°31'S. 080°52'E.	1164-01331	03 Jan 73	25		60	
117-116	077°33'S. 076°15'E.	1181-01280	20 Jan 73	20		70	Surface features
117-117	078°29'S. 070°52'E.	1578-01293	21 Feb 74	10		65	Surface features
117-118	079°19'S. 064°37'E.	1578-01295	21 Feb 74	9		40	Surface features
117-118	079°19'S. 064°37'E.	1524-01312	29 Dec 73	22		0	Surface features
117-119	080°01'S. 057°27'E.	1524-01315	29 Dec 73	21		0	
118-106	065°20'S. 101°41'E.	1129-01353	29 Nov 72	35		10	Mill Island, Shackleton Ice Shelf
118-107	066°40'S. 100°12'E.	1129-01360	29 Nov 72	33		0	Bunger Hills, Denman Glacier
118-108	067°59'S. 098°33'E.	1129-01362	29 Nov 72	32		0	Upper Denman Glacier
118-109	069°17'S. 096°44'E.	1129-01365	29 Nov 72	31		0	
118-110	070°35'S. 094°42'E.	1129-01371	29 Nov 72	30		0	Band 6
118-111	071°50'S. 092°25'E.	1129-01374	29 Nov 72	29		0	Surface features
118-112	073°04'S. 089°49'E.	1129-01380	29 Nov 72	28		0	
118-113	074°16'S. 086°50'E.	1129-01383	29 Nov 72	27		0	
118-114	075°25'S. 083°24'E.	1129-01385	29 Nov 72	25		0	Band 6
118-115	076°31'S. 079°26'E.	1129-01392	29 Nov 72	24		0	Band 6

TABLE 6.—*Optimum Landsat 1, 2, and 3 MSS and Landsat 2 RBV images of glaciers of Antarctica—Continued*

Path-Row	Nominal scene center (lat.—long.)	Landsat identification number	Date	Solar elev. angle (degrees)	Code	Cloud cover (percent)	Remarks
118-116	077°33'S. 074°49'E.	1472-01424	07 Nov 73	18	●	0	
118-117	078°29'S. 069°26'E.	1129-01401	29 Nov 72	22	●	0	
118-118	079°19'S. 063°11'E.	1490-01433	25 Nov 73	20	●	5	
118-119	080°01'S. 056°01'E.	1490-01435	25 Nov 73	19	●	5	
119-D6	065°20'S. 100°14'E.				☐	100	
119-107	066°40'S. 098°46'E.	1580-01364	23 Feb 74	20	☐	10	Shackleton Ice Shelf, Bunger Hills, Denman Glacier
119-108	067°59'S. 097°07'E.				☐	100	
119-109	069°17'S. 095°18'E.	1490-01394	25 Nov 73	31	☐	15	Surface features
119-110	070°35'S. 093°16'E.	1490-01401	25 Nov 73	29	☐	10	Surface features
119-111	071°50'S. 090°59'E.	1490-01403	25 Nov 73	28	●	0	
119-112	073°04'S. 088°23'E.	1472-01410	07 Nov 73	23	●	0	
119-113	074°16'S. 085°24'E.	1472-01413	07 Nov 73	22	●	0	
119-114	075°25'S. 081°58'E.	1472-01415	07 Nov 73	21	●	0	
119-115	076°31'S. 078°00'E.	1490-01421	25 Nov 73	24	●	0	
119-116	077°33'S. 073°23'E.	1490-01424	25 Nov 73	23	●	0	
119-117	078°29'S. 068°00'E.	1184-01453	23 Jan 73	19	●	0	
119-118	079°19'S. 061°45'E.	1526-01425	31 Dec 73	22	●	0	
119-119	080°01'S. 054°35'E.	1526-01431	31 Dec 73	20	●	0	
120-106	065°20'S. 098°48'E.				☐	100	
120-107	066°40'S. 097°20'E.	1527-01440	01 Jan 74	33	☐	30	Shackleton Ice Shelf, Queen Mary Coast, band 6
120-108	067°59'S. 095°41'E.	1527-01442	01 Jan 74	32	☐	50	Surface features, band 6
120-109	069°17'S. 093°52'E.	1491-01452	26 Nov 73	31	☐	25	Surface features
120-110	070°35'S. 091°50'E.	1491-01455	26 Nov 73	30	☐	10	Surface features, scan lines missing
120-111	071°50'S. 089°33'E.	1491-01461	26 Nov 73	28	☐	15	

TABLE 6.—*Optimum Landsat 1, 2, and 3 MSS and Landsat 2 RBV images of glaciers of Antarctica—Continued*

Path-Row	Nominal scene center (lat.—long.)	Landsat identification number	Date	Solar elev. angle (degrees)	Code	Cloud cover (percent)	Remarks
120-112	073°04'S. 086°57'E.	1491-01464	26 Nov 73	27	●	5	
120-113	074°16'S. 083°58'E.	1581-01450	24 Feb 74	13	●	5	
120-114	075°25'S. 080°32'E.	1581-01452	24 Feb 74	12	●	0	
120-115	076°31'S. 076°34'E.	1491-01475	26 Nov 73	24	◐	15	Surface features
120-116	077°33'S. 071°57'E.	1491-01482	26 Nov 73	23	●	0	Surface features
120-117	078°29'S. 066°34'E.	1581-01464	24 Feb 74	9	◐	10	
120-118	079°19'S. 060°19'E.	1527-01483	01 Jan 74	21	◐	15	Band 6
120-119	080°01'S. 053°09'E.	1509-01492	14 Dec 73	21	●	5	
121-105	063°59'S. 098°43'E.	1528-01485	02 Jan 74	35	◐	90	Tabular iceberg
121-106	065°20'S. 097°22'E.	1132-01524	02 Dec 72	35	◐	80	Shackleton Ice Shelf
121-107	066°40'S. 095°54'E.	1132-01531	02 Dec 72	34	◐	10	Helen Glacier Tongue, Blue ice'
121-108	067°59'S. 094°15'E.	1132-01533	02 Dec 72	33	●	0	
121-109	069°17'S. 092°26'E.	1132-01540	02 Dec 72	32	●	0	
121-110	070°35'S. 090°24'E.	1600-01490	15 Mar 74	10	●	0	Surface features
121-111	071°50'S. 088°07'E.	1186-01543	25 Jan 73	25	◐	40	
121-112	073°04'S. 085°31'E.	1186-01550	25 Jan 73	24	◐	70	
121-113	074°16'S. 082°32'E.	1186-01552	25 Jan 73	23	◐	70	
121-114	075°25'S. 079°06'E.	1582-01510	25 Feb 74	12	◐	15	
121-115	076°31'S. 075°08'E.	1150-01562	20 Dec 72	26	●	0	Surface features
121-116	077°33'S. 070°31'E.	1132-01565	02 Dec 72	24	●	0	Surface features, nunatak(?)
121-117	078°29'S. 065°08'E.	1186-01570	25 Jan 73	19	●	0	
121-118	079°19'S. 058°53'E.	1475-02004	10 Nov 73	17	◐	10	
121-119	080°01'S. 051°43'E.	1475-02011	10 Nov 73	16	◐	15	
122-105	063°59'S. 097°17'E.	1601-01524	16 Mar 74	15	◐	80	Tabular iceberg, band 6

TABLE 6.—Optimum Landsat 1, 2, and 3 MSS and Landsat 2 RBV images of glaciers of Antarctica—Continued

Path-Row	Nominal scene center (lat.—long.)	Landsat identification number	Date	Solar elev. angle (degrees)	Code	Cloud cover (percent)	Remarks
122-106	065°20'S. 095°56'E.	1133-01583	03 Dec 72	35		80	Shackleton Ice Shelf
122-107	066°40'S. 094°27'E.	1133-01585	03 Dec 72	34		20	Helen Glacier Tongue
122-108	067°59'S. 092°49'E.	1133-01592	03 Dec 72	33		0	
122-109	069°17'S. 091°00'E.	1133-01594	03 Dec 72	32		0	
122-110	070°35'S. 088°58'E.	1475-01572	10 Nov 73	26		0	
122-111	071°50'S. 086°41'E.	1475-01575	10 Nov 73	25		0	
122-112	073°04'S. 084°05'E.	1475-01581	10 Nov 73	24		0	Surface features
122-113	074°76'S. 081°06'E.	1475-01584	10 Nov 73	23		5	Surface features
122-114	075°25'S. 077°40'E.	1475-01590	10 Nov 73	22		0	Surface features
122-115	076°31'S. 073°42'E.	1475-01593	10 Nov 73	20		0	Surface features
122-116	077°33'S. 069°05'E.	1475-01595	10 Nov 73	19		0	Surface features, nunatak(?)
122-117	078°29'S. 063°42'E.	1565-01582	08 Feb 74	14		5	Surface features
122-118	079°19'S. 057°27'E.	1565-01584	08 Feb 74	13		10	
122-119	080°01'S. 050°17'E.	1476-02065	11 Nov 73	16		40	
123-105	063°59'S. 095°51'E.	1584-01584	27 Feb 74	21		90	Tabular iceberg
123-106	065°20'S. 094°30'E.	1584-01591	27 Feb 74	20		40	Shackleton Ice Shelf
123-107	066°40'S. 093°01'E.	1584-01593	27 Feb 74	19		0	Drygalski Island, Helen Glacier, excellent image
123-108	067°59'S. 091°23'E.	1584-02000	27 Feb 74	18		0	'Blue ice'
123-109	069°17'S. 089°34'E.	1584-02002	27 Feb 74	17		10	
123-110	070°35'S. 087°32'E.	1584-02005	27 Feb 74	16		40	
123-111	071°50'S. 085°15'E.	1476-02033	11 Nov 73	25		80	
123-112	073°04'S. 082°39'E.	1476-02040	11 Nov 73	24		0	Surface features
123-113	074°16'S. 079°40'E.	1476-02042	11 Nov 73	23		0	Surface features
123-114	075°25'S. 076°14'E.	1476-02045	11 Nov 73	22		0	Surface features

TABLE 6.—*Optimum Landsat 1, 2, and 3 MSS and Landsat 2 RBV images of glaciers of Antarctica—Continued*

Path-Row	Nominal scene center (lat.—long.)	Landsat identification number	Date	Solar elev. angle (degrees)	Code	Cloud cover (percent)	Remarks
123–115	076°31'S. 072°16'E.	1476–02051	11 Nov 73	21	●	0	Surface features
123–116	077°33'S. 067°39'E.	1133–02024	03 Dec 72	24	●	0	Surface features, nunatak(?)
123–117	078°29'S. 062°16'E.	1477–02115	12 Nov 73	19	◐	60	Surface features
123–118	079°19'S. 056°01'E.	1477–02121	12 Nov 73	17	●	5	
123–119	080°01'S. 048°51'E.	1567–02103	10 Feb 74	12	◐	30	
124–106	065°20'S. 093°04'E.	1207–02100	15 Feb 73	24	●	0	Drygalski Island
124–107	066°40'S. 091°35'E.	1207–02103	15 Feb 73	23	●	0	Philippi Glacier tongue, Leopold and Astrid Coast
124–108	067°59'S. 089°57'E.	1207–02105	15 Feb 73	22	●	0	Upper Philippi Glacier
124–109	069°17'S. 088°08'E.	1207–02112	15 Feb 73	21	●	0	
124–110	070°35'S. 086°06'E.	1207–02114	15 Feb 73	20	●	0	
124–111	071°50'S. 083°49'E.	1477–02092	12 Nov 73	26	◐	20	
124–111	071°50'S. 083°49'E.	1207–02121	15 Feb 73	19	●	5	
124–112	073°04'S. 081°13'E.	1477–02094	12 Nov 73	24	●	0	Surface features
124–113	074°16'S. 078°14'E.	1477–02101	12 Nov 73	23	●	0	Surface features
124–114	075°25'S. 074°48'E.	1477–02103	12 Nov 73	22	●	0	
124–115	076°31'S. 070°50'E.	1477–02110	12 Nov 73	21	●	0	Nunatak(?) and crevasses
124–116	077°33'S. 066°13'E.	1477–02112	12 Nov 73	20	●	5	Nunatak(?) and crevasses
124–117	078°29'S. 060°50'E.	1478–02173	13 Nov 73	19	◑	10	Surface features
124–118	079°19'S. 054°35'E.	1478–02180	13 Nov 73	18	◐	30	
124–119	080°01'S. 047°25'E.	1549–02111	23 Jan 74	17	◐	80	
125–106	065°20'S. 091°38'E.				◑	100	
125–107	066°40'S. 090°09'E.	1478–02132	13 Nov 73	30	◐	50	Leopold and Astrid Coast
125–108	067°59'S. 088°31'E.				◑	100	
125–109	069°17'S. 086°42'E.	1136–02170	06 Dec 72	32	◐	90	

TABLE 6.—Optimum Landsat 1, 2, and 3 MSS and Landsat 2 RBV images of glaciers of Antarctica—Continued

Path-Row	Nominal scene center (lat.—long.)	Landsat identification number	Date	Solar elev. angle (degrees)	Code	Cloud cover (percent)	Remarks
125-110	070°35'S. 084°40'E.	1136-02172	06 Dec 72	31		80	
125-111	071°50'S. 082°23'E.						
125-112	073°04'S. 079°47'E.					100	
125-113	074°16'S. 076°48'E.	1153-02125	23 Dec 72	28		60	
125-114	075°25'S. 073°22'E.	1586-02140	01 Mar 74	11		30	Surface features
125-115	076°31'S. 069°24'E.	1586-02142	01 Mar 74	10		30	
125-115	076°31'S. 069°24'E.	1153-02134	23 Dec 72	25		50	Nunatak(?), crevasses
125-116	077°33'S. 064°47'E.	1586-02145	01 Mar 74	8		60	Surface features
125-117	078°29'S. 059°24'E.	1514-02171	19 Dec 73	23		70	Band 6
125-118	079°19'S. 053°09'E.	1479-02234	14 Nov 73	18		30	
125-119	080°01'S. 045°59'E.	1479-02241	14 Nov 73	17		0	
126-107	066°40'S. 088°43'E.	1479-02191	14 Nov 73	31		0	Philippi Glacier, West Ice Shelf
126-108	067°59'S. 087°05'E.	1479-02193	14 Nov 73	30		0	Leopold and Astrid Coast
126-109	069°17'S. 085°16'E.	1479-02200	14 Nov 73	28		0	Nunatak(?)
126-110	070°35'S. 083°14'E.	1173-02224	12 Jan 73	29		0	
126-111	071°50'S. 080°56'E.	1173-02230	12 Jan 73	28		0	
126-112	073°04'S. 078°20'E.	1173-02233	12 Jan 73	27		0	Gale Escarpment, Grove Mountains
126-113	074°16'S. 075°22'E.	1173-02235	12 Jan 73	25		0	Crevasses
126-114	075°25'S. 071°56'E.	1479-02220	14 Nov 73	23		0	Surface features
126-115	076°31'S. 067°58	1479-02223	14 Nov 73	21		10	Crevasses, nunatak(?)
126-116	077°33'S. 063°20'E.	1136-02195	06 Dec 72	24		0	Surface features
126-117	078°29'S. 057°58'E.	1479-02232	14 Nov 73	19		80	
126-118	079°19'S. 051°43'E.						
126-119	080°01'S. 044°32'E.	1475-02013	10 Nov 73	14		40	

TABLE 6.—*Optimum Landsat 1, 2, and 3 MSS and Landsat 2 RBV images of glaciers of Antarctica—Continued*

Path-Row	Nominal scene center (lat.–long.)	Landsat identification number	Date	Solar elev. angle (degrees)	Code	Cloud cover (percent)	Remarks
127–107	066°40'S. 087°17'E.	1480–02245	15 Nov 73	31	●	0	West Ice Shelf (see Landsat 3 RBV 129/107B, D)
127–108	067°59'S. 085°39'E.	1480–02251	15 Nov 73	30	●	0	'Blue ice' (see Landsat 3 RBV 129/107 D)
127–109	069°17'S. 083°50'E.	1480–02254	15 Nov 73	29	●	0	Surface features, nunatak(?)
127–110	070°35'S. 081°48'E.	1480–02260	15 Nov 73	27	●	0	Surface features
127–111	071°50'S. 079°30'E.	1210–02292	18 Feb 73	18	●	0	Surface features
127–112	073°04'S. 076°54'E.	1210–02295	18 Feb 73	17	●	0	Grove Mountains, 'blue ice'
127–113	074°16'S.. 073°56'E.	1552–02254	26 Jan 74	22	●	0	Surface features
127–114	075°25'S. 070°30'E.	1552–02261	26 Jan 74	21	●	0	Surface features
127–115	076°31'S. 066°32'E.	1480–02281	15 Nov 73	22	●	5	Crevasses
127–116	077°33'S. 061°54'E.	1552–02270	26 Jan 74	19	◐	15	
127–117	078°29'S. 056°32'E.	1156–02313	26 Dec 72	23	◑	30	
127–118	079°19'S. 050°17'E.				⊙		
127–119	080°01'S. 043°06'E.				⊙		
128–106	065°20'S. 087°20'E.				◑	100	
128–107	066°40'S. 085°51'E.	1247–02334	27 Mar 73	10	◑	35	West Ice Shelf edge visible (see Landsat 3 RBV 129/107 B, C, D)
128–107	066°40'S. 085°51'E.	1193–02331'	01 Feb 73	27	◑	80	West Ice Shelf edge visible (see Landsat 3 RBV 129/107B, C, D)
128–108	067°59'S. 084°13'E.	1247–02340	27 Mar 73	8	◑	50	West Ice Shelf (see Landsat 3 RBV 129/107 C, D)
128–109	069°17'S. 082°24'E.	1535–02302	09 Jan 74	30	●	0	
128–110	070°35'S. 080°22'E.	1535–02305	09 Jan 74	29	●	0	
128–111	071°50'S. 078°04'E.	1481–02321	16 Nov 73	27	●	0	Surface features
128–112	073°04'S. 075°28'E.	1481–02324	16 Nov 73	25	●	0	Grove Mountains, Blue ice'
128–113	074°16'S. 072°30'E.	1481–02330	16 Nov 73	24	●	0	Nunatak(?)
128–114	075°25'S. 069°04'E.	1193–02361	01 Feb 73	20	●	5	Nunataks, crevasses
128–115	076°31'S. 065°06'E.	1553–02322	27 Jan 74	20	●	0	Crevasses, band 6

TABLE 6.—Optimum Landsat 1, 2, and 3 MSS and Landsat 2 RBV images of glaciers of Antarctica—Continued

Path-Row	Nominal scene center (lat.-long.)	Landsat identification number	Date	Solar elev. angle (degrees)	Code	Cloud cover (percent)	Remarks
128-116	077°33'S. 060°28'E.	1553-02324	27 Jan 74	19	●	0	Band 6
128-117	078°29'S. 055°06'E.	1571-02324	14 Feb 74	12	◐	10	
128-118	079°19'S. 048°51'E.	1571-02330	14 Feb 74	11	◑	15	
128-119	080°01'S. 041°40'E.	1571-02333	14 Feb 74	10	●	0	
129-106	065°20'S. 085°54'E.	1176-02381	15 Jan 73	32	●	0	West Ice Shelf
129-107	066°40'S. 084°25'E.	1176-02383	15 Jan 73	31	●	0	West Ice Shelf, Mikhaylov Island
129-108	067°59'S. 082°47'E.	1176-02390	15 Jan 73	30	●	0	Large outlet glacier, Barrier Bay
129-109	069°17'S. 080°57'E.	1176-02392	15 Jan 73	29	●	0	Band 5
129-110	070°35'S. 078°56'E.	1176-02395	15 Jan 73	28	●	0	Surface features
129-111	071°50'S. 076°38'E.	1176-02401	15 Jan 73	27	●	5	Nunataks
129-112	073°04'S. 074°02'E.	1176-02404	15 Jan 73	26	◐	25	Grove Mountains
129-113	074°16'S. 071°03'E.	1230-02415	10 Mar 73	9	●	0	Nunataks, upper Lambert Glacier
129-114	075°25'S. 067°38'E.	1176-02413	15 Jan 73	24	◐	10	Mount Twigg, Mount Borland
129-115	076°31'S. 063°39'E.	1139-02364	09 Dec 72	25	◐	10	Surface features
129-116	077°33'S. 059°02'E.	1139-02370	09 Dec 72	24	●	5	
129-117	078°29'S. 053°39'E.	1572-02382	15 Feb 74	12	●	5	
129-118	079°19'S. 047°24'E.	1518-02402	23 Dec 73	22	●	0	
129-119	080°01'S. 040°14'E.	1483-02470	18 Nov 73	18	◐	25	
130-106	065°20'S. 084°28'E.	1501-02412	06 Dec 73	35	●	0	Fast ice
130-107	066°40'S. 083°00'E.	1213-02445	21 Feb 73	21	◐	90	West Ice Shelf
130-108	067°59'S. 081°21'E.	1213-02452	21 Feb 73	20	◐	60	Barrier Bay
130-109	069°17'S. 079°31'E.	1213-02454	21 Feb 73	19	◐	20	Vestfold Hills
130-110	070°35'S. 077°30'E.	1213-02461	21 Feb 73	18	◐	70	
130-111	071°51'S. 075°12'E.	1591-02412	06 Mar 74	12	◐	40	

TABLE 6.—*Optimum Landsat 1, 2, and 3 MSS and Landsat 2 RBV images of glaciers of Antarctica—Continued*

Path-Row	Nominal scene center (lat.—long.)	Landsat identification number	Date	Solar elev. angle (degrees)	Code	Cloud cover (percent)	Remarks
130-112	073°04'S. 072°36'E.	1591-02414	06 Mar 74	11		50	Grove Mountains
130-113	074°16'S. 069°37'E.	1447-02445	13 Oct 73	14		80	Mawson Escarpment, Blake Nunataks
130-114	075°25'S. 066°12'E.	1447-02452	13 Oct 73	12		90	Wilson Bluff, Komsomol'skiy Peak
130-115	076°31'S. 062°13'E.	1159-02475	29 Dec 72	25		0	
130-116	077°33'S. 057°36'E.	1159-02482	29 Dec 72	24		0	
130-117	078°29'S. 052°13'E.	1573-02440	16 Feb 74	12		30	
130-118	079°19'S. 045°58'E.	1573-02443	16 Feb 74	11		40	
130-119	080°01'S. 038°48'E.	1573-02445	16 Feb 74	10		25	Mottled surface
130-119	080°01'S. 038°48'E.	1484-02525	19 Nov 73	18		10	
131-107	066°40'S. 081°33'E.	1196-02503	04 Feb 73	26		20	West Ice Shelf
131-108	067°59'S. 079°55'E.	1196-02505	04 Feb 73	25		0	Barrier Bay
131-109	069°17'S. 078°05'E.	1196-02512	04 Feb 73	24		0	Vestfold Hills, Sørsdal Glacier
131-110	070°35'S. 076°04'E.	1196-02514	04 Feb 73	23		0	Publications Ice Shelf
131-111	071°50'S. 073°46'E.	1196-02521	04 Feb 73	22		0	Ice front, melt ponds
131-112	073°04'S. 071°10'E.	1196-02523	04 Feb 73	21		0	Mawson Escarpment, melt ponds
131-113	074°16'S. 068°11'E.	1196-02530	04 Feb 73	20		5	Lambert Glacier, Mellor Glacier
131-114	075°25'S. 064°46'E.	1160-02531	30 Dec 72	26		10	Komsomol'skiy Peak, crevasses
131-115	076°31'S. 060°47'E.	1160-02534	30 Dec 72	25		5	
131-116	077°33'S. 056°10'E.	1160-02540	30 Dec 72	24		0	
131-117	078°29'S. 050°47'E.	1574-02495	17 Feb 74	11		75	
131-118	079°19'S. 044°32'E.	1484-02522	19 Nov 73	19		5	
131-119	080°01'S. 037°22'E.	1479-02243	14 Nov 73	15		0	Band 6
132-107	066°40'S. 080°07'S.	1179-02555	18 Jan 73	31		30	West Ice Shelf
132-108	067°59'S. 078°29'E.	1142-02510	12 Dec 72	33		0	Vestfold Hills

TABLE 6.—Optimum Landsat 1, 2, and 3 MSS and Landsat 2 RBV images of glaciers of Antarctica—Continued

Path-Row	Nominal scene center (lat.—long.)	Landsat identification number	Date	Solar elev. angle (degrees)	Code	Cloud cover (percent)	Remarks
132–108	067°59'S. 078°29'E.	1539–02525	13 Jan 74	30		5	Vestfold Hills, melt ponds
132–109	069°17'S. 076°39'E.	1179–02564	18 Jan 73	29		0	Ingrid Christensen Coast
132–110	070°35'S. 074°38'E.	1179–02571	18 Jan 73	28		20	Reinbolt Hills , Polar Times Glacier, melt ponds
132–110	070°35'S. 074°38'E.	1142–02515	12 Dec 72	31		0	Polar Times Glacier
132–111	071°50'S. 072°20'E.	1179–02573	18 Jan 73	27		80	
132–112	073°04'S. 069°44'E.	1179–02580	18 Jan 73	26		75	Lambert Glacier, melt ponds
132–113	074°16'S. 066°45'E.	1179–02582	18 Jan 73	24		70	Lambert, Mellor, Fisher Glaciers
132–114	075°25'S. 063°20'E.					100	
132–115	076°31'S. 059°21'E.	1179–02591	18 Jan 73	22		30	
132–116	077°33'S. 054°44'E.	1179–02594	18 Jan 73	21		40	
132–117	078°29'S. 049°21'E.	1179–03000	18 Jan 73	20		50	
132–118	079°19'S. 043°06'E.					100	
132–119	080°01'S. 035°56'E.					100	
133–108	067°59'S. 077°02'E.	1162–03021	01 Jan 73	32		50	West Ice Shelf
133–109	069°17'S. 075°13'E.					100	
133–110	070°35'S. 073°11'E.					100	
133–111	071°50'S. 070°54'E.					100	
133–112	073°04'S. 068°18'E.	1162–03035	01 Jan 73	28		80	Cumpston Massif
133–113	074°16'S. 065°19'E.	1162–03041	01 Jan 73	27		10	Mellor, Collins, Geysen Glaciers
133–114	075°25'S. 061°53'E.	1162–03044	01 Jan 73	26		0	Komsomol'skiy Peak, crevasses
133–115	076°31'S. 057°55'E.	1162–03050	01 Jan 73	25		0	
133–116	077°33'S. 053°18'E.	1162–03053	01 Jan 73	24		0	
133–117	078°29'S. 047°55'E.	1162–03055	01 Jan 73	23		30	
133–118	079°19'S. 041°40'E.	1577–03072	20 Feb 74	9		60	

TABLE 6.—Optimum Landsat 1, 2, and 3 MSS and Landsat 2 RBV images of glaciers of Antarctica—Continued

Path-Row	Nominal scene center (lat.—long.)	Landsat identification number	Date	Solar elev. angle (degrees)	Code	Cloud cover (percent)	Remarks
133-119	080°01'S. 034°30'E.	1469-03100	04 Nov 73	14		50	Band 6
134-109	069°17'S. 073°47'E.	1127-03083	27 Nov 72	31		70	Ice front
134-110	070°35'S. 071°45'E.	1127-03090	27 Nov 72	30		70	Gillock Island
134-111	071°50'S. 069°28'E.	1127-03092	27 Nov 72	29		60	Lambert Glacier, Fisher Massif
134-112	073°04'S. 066°52'E.	1577-03045	20 Feb 74	16		60	Lambert Glacier, melt ponds
134-113	074°16'S. 063°53'E.	1145-03101	15 Dec 72	28		0	Keyser Ridge, nunataks, crevasses
134-114	075°25'S. 060°27'E.	1145-03104	15 Dec 72	27		25	Komsomol'skiy Peak, crevasses
134-114	075°25'S. 060°27'E.	1199-03104	07 Feb 73	18		25	Komsomol'skiy Peak, crevasses
134-115	076°31'S. 056°29'E.	1199-03110	07 Feb 73	17		10	
134-116	077°33'S. 051°52'E.	1199-03113	07 Feb 73	16		10	Band 6
134-117	078°29'S. 046°29'E.	1577-03070	20 Feb 74	10		20	
134-118	079°19'S. 040°14'E.						
134-119	080°01'S. 033°04'E.	1487-03100	22 Nov 73	18		0	Snow dunes
135-109	069°17'S. 072°21'E.	1542-03102	16 Jan 74	29		5	Amery Ice Shelf, crevasse patterns
135-110	070°35'S. 070°19'E.	1236-03150	16 Mar 73	10		30	Gillock Island, Else Platform
135-111	071°50'S. 068°02'E.	1236-03153	16 Mar 73	9		20	Fisher Massif, melt ponds
135-112	073°04'S. 065°26'E.	1236-03155	16 Mar 73	8		50	Lambert Glacier, Mount Stinear
135-113	074°16'S. 062°27'E.	1182-03154	21 Jan 73	24		10	Mount Menzies, Fisher Glacier, crevasses
135-114	075°25'S. 059°01'E.	1182-03160	21 Jan 73	23		50	Crevasses
135-115	076°31'S. 055°03'E.	1182-03163	21 Jan 73	22		70	
135-116	077°33'S. 050°26'E.	1182-03165	21 Jan 73	21		40	
135-117	078°29'S. 045°03'E.	1127-03115	27 Nov 72	22		70	
135-118	079°19'S. 038°48'E.	1127-03122	27 Nov 72	20		70	
135-119	080°01'S. 031°38'E.	1471-03213	06 Nov 73	15		80	Band 5, scan lines missing

TABLE 6.—Optimum Landsat 1, 2, and 3 MSS and Landsat 2 RBV images of glaciers of Antarctica—Continued

Path-Row	Nominal scene center (lat.—long.)	Landsat identification number	Date	Solar elev. angle (degrees)	Code	Cloud cover (percent)	Remarks
136–109	069°17'S. 070°55'E.	1543–03160	17 Jan 74	29		60	Amery Ice Shelf
136–110	070°35'S. 068°53'E.	1219–03204	27 Feb 73	16		40	Loewe Massif, Beaver Lake
136–111	071°50'S. 066°36'E.	1219–03210	27 Feb 73	15		30	Fisher Massif, Lambert Glacier, melt ponds
136–112	073°04'S. 064°00'E.	1453–03184	19 Oct 73	17		40	Fisher and Geysen Glaciers, scan lines missing
136–113	074°16'S. 061°01'E.	1579–03164	22 Feb 74	14		60	Mount Menzies, crevasses
136–114	075°25'S. 057°35'E.	1579–03171	22 Feb 74	13		70	
136–115	076°31'S. 053°37'E.	1579–03173	22 Feb 74	12		30	
136–116	077°33'S. 049°00'E.	1165–03224	04 Jan 73	23		0	
136–117	078°29'S. 043°37'E.	1202–03291	10 Feb 73	14		0	
136–118	079°19'S. 037°22'E.	1580–03243	23 Feb 74	8		80	
136–119	080°01'S. 030°12'E.	1543–03201	17 Jan 74	18		90	
137–108	067°59'S. 071°18'E.	1526–03215	31 Dec 73	32		5	Bjerkø Peninsula
137–109	069°17'S. 069°29'E.	1580–03205	23 Feb 74	18		0	Foley and Landon Promontories, Amery Ice Shelf
137–110	070°35'S. 067°27'E.	1580–03211	23 Feb 74	17		0	Charybdis Glacier, melt ponds
137–111	071°50'S. 065°10'E.	1580–03214	23 Feb 74	16		10	Lambert Glacier, melt ponds
137–112	073°04'S. 062°34'E.	1130–03270	30 Nov 72	28		0	Mount Menzies, Fisher Glacier, 'blue ice'
137–113	074°16'S. 059°35'E.	1130–03273	30 Nov 72	27		0	Crevasses
137–114	075°25'S. 056°09'E.	1130–03275	30 Nov 72	26		10	
137–115	076°31'S. 052°11'E.	1202–03282	10 Feb 73	16		15	
137–116	077°33'S. 047°34'E.	1202–03284	10 Feb 73	15		0	Band 6
137–117	078°29'S. 042°11'E.	1130–03291	30 Nov 72	22		0	
137–118	079°19'S. 035°56'E.	1491–03323	26 Nov 73	20		0	
137–119	080°01'S. 028°46'E.	1130–03300	30 Nov 72	20		70	
138–108	067°59'S. 069°52'E.	1239–03313	19 Mar 73	11		60	Bjerkø Peninsula

TABLE 6.—*Optimum Landsat 1, 2, and 3 MSS and Landsat 2 RBV images of glaciers of Antarctica—Continued*

Path-Row	Nominal scene center (lat.–long.)	Landsat identification number	Date	Solar elev. angle (degrees)	Code	Cloud cover (percent)	Remarks
138–109	069°17'S. 068°03'E.	1239–03315	19 Mar 73	10		70	
138–110	070°35'S. 066°01'E.	1581–03270	24 Feb 74	17		0	Loewe Massif, Charybdis Glacier
138–111	071°50'S. 063°44'E.	1148–03263	18 Dec 72	30		0	Shaw Massif
138–112	073°04'S. 061°08'E.	1148–03270	18 Dec 72	29		0	Fisher Glacier, Goodspeed Nunataks
138–113	074°16'S. 058°09'E.	1148–03272	18 Dec 72	28		0	
138–114	075°25'S. 054°43'E.	1148–03275	18 Dec 72	27		0	
138–115	076°31'S. 050°45'E.	1148–03281	18 Dec 72	26		0	
138–116	077°33'S. 046°08'E.	1222–03402	02 Mar 73	8		10	
138–117	078°29'S. 040°45'E.	1148–03290	18 Dec 72	23		40	
138–118	079°19'S. 034°30'E.	1130–03293	30 Nov 72	21		40	
138–119	080°01'S. 027°20'E.	1564–03364	07 Feb 74	13		30	Snow dunes
139–108	067°59'S. 068°26'E.						
139–109	069°17'S. 066°37'E.	1600–03320	15 Mar 74	11		10	Single Island, nunataks
139–110	070°35'S. 064°35'E.	1600–03322	15 Mar 74	10		25	Athos, Porthos, Aramis Ranges
139–111	071°50'S. 062°18'E.	1456–03353	22 Oct 73	19		20	Nunataks
139–112	073°04'S. 059°42'E.	1168–03381	07 Jan 73	27		0	Goodspeed Nunataks
139–113	074°16'S. 056°43'E.	1168–03383	07 Jan 73	26		0	
139–114	075°25'S. 053°17'E.	1168–03390	07 Jan 73	25		10	
139–115	076°31'S. 049°19'E.	1169–03392	07 Jan 73	24		25	
139–116	077°33'S. 044°42'E.	1168–03395	07 Jan 73	23		5	
139–117	078°29'S. 039°19'E.	1168–03401	07 Jan 73	22		10	
139–118	079°19'S. 033°04'E.	1475–03440	10 Nov 73	17		5	Scan lines missing
139–119	080°01'S. 025°54'E.	1475–03443	10 Nov 73	16		0	Snow dunes, band 6
140–108	067°59'S. 067°00'E.	1151–03423	21 Dec 72	33		15	Lars Christensen Coast

TABLE 6.—Optimum Landsat 1, 2, and 3 MSS and Landsat 2 RBV images of glaciers of Antarctica— Continued

Path-Row	Nominal scene center (lat.—long.)	Landsat identification number	Date	Solar elev. angle (degrees)	Code	Cloud cover (percent)	Remarks
140-109	069°17'S. 065°11'E.	1205-03430	13 Feb 73	22		60	Nunataks
140-110	070°35'S. 063°09'E.	1169-03430	08 Jan 73	29		20	Porthos, Athos Ranges
140-111	071°50'S. 060°52'E.	1169-03433	08 Jan 73	28		10	Surface features
140-112	073°04'S. 058°16'E.	1169-03435	08 Jan 73	27		0	Goodspeed Nunataks
140-113	074°76's. 055°17'E.	1169-03442	08 Jan 73	26		10	
140-114	075°25'S. 051°51'E.	1151-03450	21 Dec 72	27		0	
140-115	076°31'S. 047°53'E.	1169-03451	08 Jan 73	24		0	
140-116	077°33'S. 043°16'E.	1169-03453	08 Jan 73	23		10	Band 6
140-117	078°29'S. 037°53'E.	1169-03460	08 Jan 73	22		5	
140-118	079°19'S. 031°38'E.	1476-03494	11 Nov 73	17		30	
140-119	080°01's. 024°28'E.	1547-03430	21 Jan 74	17		0	Snow dunes, line drop
141-108	067°59'S. 065°34'E.	1242-03484	22 Mar 73	10		60	
141-109	069°17'S. 063°45'E.	1242-03490	22 Mar 73	9		90	Mawson Coast, nunataks
141-110	070°35'S. 061°43'E.	1134-03491	04 Dec 72	31		50	Nunataks
141-111	071°50'S. 059°26'E.	1134-03493	04 Dec 72	29		60	
141-112	073°04'S. 056°50'E.	1134-03500	04 Dec 72	28		50	
141-113	074°16'S. 053°51'E.	1188-03501	27 Jan 73	22		15	
141-114	075°25'S. 050°25'E.	1188-03504	27 Jan 73	21		0	
141-115	076°31'S. 046°27'E.	1188-03510	27 Jan 73	20		10	
141-116	077°33'S. 041°50'E.	1188-03513	27 Jan 73	19		60	
241-117	078°29'S. 036°37'E.	1188-03515	27 Jan 73	18		80	
141-118	079°19'S. 030°12'E.						
141-119	080°01'S. 023°02'E.						
142-108	067°59'S. 064°08'E.	1171-03534	10 Jan 73	31		75	

TABLE 6.—*Optimum Landsat 1 ,2, and 3 MSS and Landsat 2 RBV images of glaciers of Antarctica — Continued*

Path-Row	Nominal scene center (lat.-long.)	Landsat identification number	Date	Solar elev. angle (degrees)	Code	Cloud cover (percent)	Remarks
142-109	069°17'S. 062°19'E.	1171-03540	10 Jan 73	30		60	
142-110	070°35'S. 060°17'E.	1459-03521	25 Oct 73	21		5	Surface features
142-111	071°50'S. 058°00'E.	1459-03523	25 Oct 73	20		0	Surface features
142-112	073°04'S. 055°24'E.	1459-03530	25 Oct 73	19		5	
142-113	074°16'S. 052°25'E.	1459-03532	25 Oct 73	18		5	Surface features
142-114	075°25'S. 048°59'E.	1459-03535	25 Oct 73	17		15	
142-115	076°31'S. 045°01'E.	1477-03541	12 Nov 73	21		30	
142-116	077°33'S. 040°24'E.	1171-03570	10 Jan 73	23		30	
142-117	078°29'S. 035°01'E.	1171-03572	10 Jan 73	21		15	
142-118	079°19'S. 028°46'E.	1478-04011	13 Nov 73	18		0	
142-119	080°01'S. 021°36'E.	1478-04014	13 Nov 73	16		0	Snow dunes, scan lines missing, bands 6 and 7
143-107	066°40'S. 064°20'E.	1478-03564	13 Nov 73	30		95	
143-108	067°59'S. 062°42'E.	1478-03570	13 Nov 73	29		95	Scan lines missing
143-109	069°17'S. 060°53'E.	1478-03573	13 Nov 73	28		80	Scan lines missing
143-110	070°35'S. 058°51'E.	1478-03575	13 Nov 73	27		65	Scan lines missing
143-111	071°50'S. 056°33'E.	1478-03582'	13 Nov 73	26		80	Scan lines missing, band 6
143-112	073°04'S. 053°57'E.	1478-03584	13 Nov 73	25		0	Band 6
143-113	074°16'S. 050°59'E.	1478-03591	13 Nov 73	24		60	Scan lines missing
143-114	075°25'S. 047°33'E.	1478-03593	13 Nov 73	22		10	
143-115	076°31'S. 043°35'E.	1478-04000	13 Nov 73	21		5	
143-116	077°33'S. 038°57'E.	1478-04002	13 Nov 73	20		20	
143-117	078°29'S. 033°35'E.	1550-03592	24 Jan 74	19		25	
143-118	079°19'S. 027°20'E.	1479-04070	14 Nov 73	18		10	
143-119	080°01'S. 020°09'E.	1479-04072	14 Nov 73	17		0	Snow dunes

TABLE 6.—Optimum Landsat 1, 2, and 3 MSS and Landsat 2 RBV images of glaciers of Antarctica—Continued

Path-Row	Nominal scene center (lat.—long.)	Landsat identification number	Date	Solar elev. angle (degrees)	Code	Cloud cover (percent)	Remarks
144-107	066°40'S. 062°54'E.	1137-04051	07 Dec 72	34	●	0	Holme Bay
144-108	067°59'S. 061°16'E.	1137-04053	07 Dec 72	33	●	0	Framnes Mountains, Mawson Coast
144-109	069°17'S. 059°27'E.	1137-04060	07 Dec 72	32	●	0	
144-110	070°35'S. 057°25'E.	1551-04020	25 Jan 74	26	◐	80	
144-111	071°50'S. 055°07'E.	1551-04023	25 Jan 74	25	◐	70	
144-112	073°04'S. 052°31'E.	1551-04025	25 Jan 74	24	◐	70	
144-113	074°16'S. 049°33'E.	1154-04014	21 Dec 72	28	●	0	
144-114	075°25'S. 046°05'E.	1551-04034	25 Jan 74	21	◐	90	
144-115	076°31'S. 042°09'E.	1587-04032	02 Mar 74	9	◑	10	
144-116	077°33'S. 037°31'E.	1587-04035	02 Mar 74	8	●	5	
144-117	078°29'S. 032°09'E.	1479-04063	14 Nov 73	19	◐	40	
144-118	079°19'S. 025°54'E.	1480-04124	15 Nov 73	18	●	0	Snow dunes
144-119	080°01'S. 018°43'E.	1480-04131	15 Nov 73	17	●	0	Snow dunes, scan lines missing
144-119	080°01's. 018°43'E.	1551-04055	25 Jan 74	16	●	0	Snow dunes, scan-line irregularities
145-107	066°40's. 061°28'E.				⊙		
145-108	067°59's. 059°50'E.				⊙		
145-109	069°17'S. 058°01'E.	1174-04111	13 Jan 73	30	●	0	Mawson Coast
145-110	070°35'S. 055°59'E.	1174-04114	13 Jan 73	28	●	0	
145-111	071°50'S. 053°41'E.	1137-04065	07 Dec 72	30	●	0	
145-112	073°04'S. 051°05'E.	1137-04071	07 Dec 72	29	●	0	
145-113	074°16'S. 048°07'E.	1570-04083	13 Feb 74	17	●	0	
145-114	075°25'S. 044°41'E.	1570-04090	13 Feb 74	16	●	5	
145-115	076°31'S. 040°43'E.	1570-04092	13 Feb 74	15	●	5	
145-116	077°33'S. 036°05'E.	1570-04095	13 Feb 74	14	◐	50	

TABLE 6. — *Optimum Landsat 1, 2, and 3 MSS and Landsat 2 RBV images of glaciers of Antarctica—Continued*

Path-Row	Nominal scene center (lat.—long.)	Landsat identification number	Date	Solar elev. angle (degrees)	Code	Cloud cover (percent)	Remarks
145-117	078°29'S. 030°43'E.	1480-04122	15 Nov 73	19	●	0	Surface features
145-118	079°19'S. 024°28'E.	1552-04110	26 Jan 74	17	◐	30	Snow dunes
145-119	080°01'S. 017°17'E.	1552-04113	26 Jan 74	16	◐	20	Snow dunes, band 6
146-107	066°40'S. 060°02'E.	1211-04164	19 Feb 73	22	●	0	Fast ice
146-108	067°59'S. 058°24'E.	1211-04171	19 Feb 73	21	●	0	Hoseason Glacier, Kemp Coast
146-109	069°17'S. 056°34'E.	1211-04173	19 Feb 73	20	●	0	Dismal Mountains, surface features
146-110	070°35'S. 054°33'E.	1211-04180	19 Feb 73	19	●	0	Surface features
146-111	071°50'S. 052°15'E.	1211-04182	19 Feb 73	18	◐	20	Surface features
146-112	073°04'S. 049°39'E.	1175-04181	14 Jan 73	26	◑	10	Surface features
146-113	074°16'S. 046°40'E.	1571-04141	14 Feb 74	17	●	5	Surface features
146-114	075°25'S. 043°15'E.	1571-04144	14 Feb 74	16	●	5	
146-115	076°31'S. 039°16'E.	1571-04150	14 Feb 74	15	◐	30	
146-116	077°33'S. 034°39'E.	1571-04153	14 Feb 74	14	◐	70	
146-117	078°29'S. 029°16'E.	1481-04180	16 Nov 73	20	◐	60	Surface features
146-118	079°19'S. 023°01'E.	1553-04165	27 Jan 74	17	◐	20	, Band 4
146-119	080°01'S. 015°51'E.	1476-03503	11 Nov 73	15	●	0	Snow dunes, band 6
147-107	066°40'S. 058°36'E.	1194-04221	02 Feb 73	27	●	0	Edward VII Bay
147-108	067°59'S. 056°58'E.	1194-04224	02 Feb 73	26	●	0	Robert Glacier, Wilma Glacier
147-109	069°17'S. 055°08'E.	1194-04230	02 Feb 73	25	●	0	Surface features
147-110	070°35'S. 053°07'E.	1194-04233	02 Feb 73	24	●	0	
147-111	071°50'S. 050°49'E.	1194-04235	02 Feb 73	23	●	0	Surface features
147-112	073°04'S. 048°13'E.	1194-04242	02 Feb 73	22	●	0	Surface features
147-113	074°76'S. 045°14'E.	1194-04244	02 Feb 73	21	●	0	Scan lines missing
147-114	075°25'S. 041°49'E.	1194-04251	02 Feb 73	20	●	0	

TABLE 6.—*Optimum Landsat 1, 2, and 3 MSS and Landsat 2 RBV images of glaciers of Antarctica — Continued*

Path-Row	Nominal scene center (lat.—long.)	Landsat identification number	Date	Solar elev. angle (degrees)	Code	Cloud cover (percent)	Remarks
147-115	076°31'S. 037°50'E.	1194-04253	02 Feb 73	19	●	5	
147-116	077°33'S. 033°13'E.	1194-04260	02 Feb 73	18	◐	70	
147-117	078°29'S. 027°50'E.	1500-04233	05 Dec 73	23	●	5	Surface features
147-118	079°19'S. 021°35'E.	1500-04240	05 Dec 73	22	◐	25	Surface features, snow dunes
147-119	080°01'S. 014°25'E.	1483-04302	18 Nov 73	18	●	0	Snow dunes, scan lines missing
148-107	066°40'S. 057°10'E.	1177-04273	16 Jan 73	31	●	0	King Edward Plateau
148-108	067°59'S. 055°32'E.	1177-04275	16 Jan 73	30	●	0	Robert Glacier, Wilma Glacier
148-109	069°17'S. 053°42'E.	1555-04243	29 Jan 74	26	●	0	Nunataks, band 6
148-110	070°35'S. 051°41'E.	1555-04245	29 Jan 74	25	●	0	
148-111	071°50'S. 049°23'E.	1555-04252	29 Jan 74	24	●	0	Surface features
148-112	073°04'S. 046°47'E.	1555-04254	29 Jan 74	23	●	0	Surface features
148-113	074°16'S. 043°48'E.	1177-04300	16 Jan 73	25	●	0	Surface features
148-114	075°25'S. 040°23'E.	1483-04281	18 Nov 73	23	●	0	Band 4
148-115	076°31'S. 036°24'E.	1483-04284	18 Nov 73	22	●	5	Band 6, scan lines missing
148-116	077°33'S. 031°47'E.	1483-04290	18 Nov 73	21	●	5	Surface features, band 6
148-117	078°29'S. 026°24'E.	1483-04293	18 Nov 73	20	●	5	Band 6
148-118	079°19'S. 020°09'E.	1483-04295	18 Nov 73	19	●	0	Snow dunes, surface features, scan lines missing
148-119	080°01'S. 012°59'E.	1484-04360	19 Nov 73	18	●	0	Snow dunes
149-107	066°40'S. 055°44'E.	1556-04292	30 Jan 74	27	●	5	King Edward Plateau, Mount Berrigan, scan lines missing
149-108	067°59'S. 054°06'E.	1556-04294	30 Jan 74	26	●	5	Nunataks, band 6
149-109	069°17'S. 052°16'E.	1556-04301	30 Jan 74	25	●	0	Nunataks
149-110	070°35'S. 050°15'E.	1556-04303	30 Jan 74	24	●	0	
149-111	071°50'S. 047°57'E.	1556-04310	30 Jan 74	23	●	0	Surface features
149-112	073°04'S. 045°21'E.	1556-04312	30 Jan 74	22	●	0	Surface features

TABLE 6.—Optimum Landsat 1, 2, and 3 MSS and Landsat 2 RBV images of glaciers of Antarctica—Continued

Path-Row	Nominal scene center (lat.—long.)	Landsat identification number	Date	Solar elev. angle (degrees)	Code	Cloud cover (percent)	Remarks
149-113	074°16'S. 042°22'E.	1556-04315	30 Jan 74	21	●	5	Surface features
149-114	075°25'S. 038°57'E.	1214-04365	22 Feb 73	13	◐	10	Surface features
149-115	076°31'S. 034°58'E.	1484-04342	19 Nov 73	23	◑	15	
149-116	077°33'S. 030°21'E.	1484-04345	19 Nov 73	21	●	0	Surface features
149-117	078°29'S. 024°58'E.	1484-04351	19 Nov 73	20	●	0	
149-118	079°19'S. 018°43'E.	1484-04354	19 Nov 73	19	●	0	Surface features
149-119	080°01'S. 011°33'E.	1467-04415	02 Nov 73	13	◑	40	Snow dunes
150-106	065°20'S. 055°47'E.	1575-04341	18 Feb 74	23	●	0	Enderby Land coast, unusual sea ice, band 6
150-107	066°40'S. 054°18'E.	1557-04350	31 Jan 74	27	◑	40	Enderby Land, Napier Mountains
150-108	067°59'S. 052°39'E.	1539-04361	13 Jan 74	30	●	0	Nunataks
150-109	069°17'S. 050°50'E.	1539-04363	13 Jan 74	29	●	0	Nunataks
150-110	070°35'S. 048°48'E.	1539-04370	13 Jan 74	28	●	0	
150-111	071°50'S. 046°31'E.	1539-04372	13 Jan 74	27	●	0	Surface features
150-112	073°04'S. 043°55'E.	1503-04384	08 Dec 73	29	◐	10	Surface features
150-113	074°16'S. 040°56'E.	1503-04390	08 Dec 73	28	◑	10	Surface features
150-114	075°25'S. 037°30'E.	1485-04394	20 Nov 73	24	◑	90	Band 5, scan lines missing
150-151	076°31'S. 033°32'E.	1485-04401	20 Nov 73	23	◑	50	Scan lines missing
150-116	077°33'S. 028°55'E.	1485-04403	20 Nov 73	22	●	0	Surface features
150-117	078°29'S. 023°32'E.	1485-04410	20 Nov 73	20	●	0	Surface features
150-118	079°19'S. 017°17'E.	1485-04412	20 Nov 73	19	●	0	Snow dunes
150-119	080°01'S. 010°07'E.	1485-04415	20 Nov 73	18	●	0	Snow dunes
151-106	065°20'S. 054°21'E.	1540-04410	14 Jan 74	32	●	0	Enderby Land coast, tabular iceberg
151-107	066°40'S. 052°52'E.	1540-04412	14 Jan 74	31	●	0	Tula Mountains, Beaver Glacier, 'blue ice'
151-108	067°59'S. 051°13'E.	1540-04415	14 Jan 74	30	●	0	Scott Mountains, upper Rayner and Thyer Glaciers

TABLE 6. —Optimum Landsat 1, 2, and 3 MSS and Landsat 2 RBV images of glaciers of Antarctica —Continued

Path-Row	Nominal scene center (lat.—long.)	Landsat identification number	Date	Solar elev. angle (degrees)	Code	Cloud cover (percent)	Remarks
151–109	069°17'S. 049°24'E.					100	
151–110	070°35'S. 047°22'E.	1576–04414	19 Feb 74	18		95	
151–111	071°50'S. 045°05'E.	1576–04420	19 Feb 74	17		50	Surface features
151–112	073°04'S. 042°29'E.	1576–04423	19 Feb 74	16		30	Surface features
151–113	074°16'S. 039°30'E.	1576–04425	19 Feb 74	15		90	
151–114	075°25'S. 036°04'E.	1180–04475	19 Jan 73	23		60	
151–115	076°31'S. 032°06'E.	1180–04481	19 Jan 73	22		85	
151–116	077°33'S. 027°29'E.	1143–04431	13 Dec 72	24		5	Surface features
151–117	078°29'S. 022°06'E.	1576–04443	19 Feb 74	11		60	
151–118	079°19'S. 015°51'E.	1469–04525	04 Nov 73	15		5	Band 6
151–119	080°01'S. 008°41'E.	1469–04532	04 Nov 73	14		20	Surface features, snow dunes
152–106	065°20'S. 052°55'E.						
152–107	066°40'S. 051°26'E.	2339–04365	27 Dec 75	33		0	Tula Mountains, Beaver Glacier, 'blue ice'
152–108	067°59'S. 049°47'E.	1559–04465	02 Feb 74	26		50	Nye Mountains, upper Rayner Glacier, 'blue ice'
152–109	069°17'S. 047°58'E.	1523–04483	28 Dec 73	32		70	
152–110	070°35'S. 045°56'E.	1577–04472	20 Feb 74	18		25	Surface features
152–111	071°50'S. 043°39'E.	1577–04474	20 Feb 74	17		0	Surface features
152–112	073°04'S. 041°03'E.	1577–04481	20 Feb 74	16		5	Surface features
152–113	074°16'S. 038°04'E.	1163–04531	02 Jan 73	27		0	Surface features
152–114	075°25'S. 034°38'E.	1163–04534	02 Jan 73	26		0	
152–115	076°31'S. 030°40'E.	1163–04540	02 Jan 73	25		0	
152–116	077°33'S. 026°03'E.	1163–04543	02 Jan 73	24		0	
152–117	078°29'S. 020°40'E.	1163–04545	02 Jan 73	23		0	
152–118	079°19'S. 014°25'E.	1487–04525	22 Nov 73	20		10	

TABLE 6.—*Optimum Landsat 1,2, and 3 MSS and Landsat 2 RBV images of glaciers of Antarctica—Continued*

Path-Row	Nominal scene center (lat.—long.)	Landsat identification number	Date	Solar elev. angle (degrees)	Code	Cloud cover (percent)	Remarks
152-119	080°01'S. 007°15'E.	1470-04590	05 Nov 73	14		50	Snow dunes
153-106	065°20'S. 051°28'E.					100	
153-107	066°40'S. 050°00'E.	1128-04564	28 Nov 72	33		90	
153-108	067°59'S. 048°21'E.	1506-04541	11 Dec 73	33		0	Rayner Glacier , Molle Glacier, 'blue ice'
153-109	069°17'S. 046°32'E.	1506-04543	11 Dec 73	32		0	Surface features
153-110	070°35'S. 044°30'E.	1488-04551	23 Nov 73	29		0	Surface features
153-111	071°50'S. 042°13'E.	1488-04554	23 Nov 73	28		0	Surface features
153-112	073°04'S. 039°37'E.	1488-04560	23 Nov 73	27		0	Surface features
153-113	074°16'S. 036°38'E.	1200-04591	08 Feb 73	19		15	Surface features
153-114	075°25'S. 033°12'E.	1506-04564	11 Dec 73	27		15	Surface features
153-115	076°31'S. 029°14'E.	1506-04570	11 Dec 73	25		0	
153-116	077°33'S. 024°37'E.	1524-14570	29 Dec 73	24		10	
153-117	078°29'S. 019°14'E.	1488-04581	23 Nov 73	21		5	Surface features
153-118	079°19'S. 012°59'E.	1524-04575	29 Dec 73	22		25	
153-119	080°01'S. 005°49'E.	1524-04582	29 Dec 73	21		30	Dunes
154-107	066°40'S. 048°34'E.	1525-04590	30 Dec 73	33		0	White Island, Sakellari Peninsula
154-108	067°59'S. 046°55'E.	1525-04593	30 Dec 73	32		0	Rayner Glacier , Molle Glacier, melt ponds
154-109	069°17'S. 045°06'E.	1525-04595	30 Dec 73	31		0	Surface features
154-110	070°35'S. 043°04'E.	1507-05004	12 Dec 73	31		5	Surface features
154-111	071°50'S. 040°47'E.	1507-05011	12 Dec 73	30		0	
154-112	073°04'S. 038°11'E.	1507-05013	12 Dec 73	29		0	Surface features, 'blue ice'
154-113	074°16'S. 035°12'E.	1507-05020	12 Dec 73	28		0	Surface features
154-114	075°25'S. 031°46'E.	1507-05022	12 Dec 73	27		15	
154-115	076°31'S. 027°48'E.	1183-05053	22 Jan 73	21		20	

TABLE 6.—*Optimum Landsat 1, 2, and 3 MSS and Landsat 2 RBV images of glaciers of Antarctica—Continued*

Path-Row	Nominal scene center (lat.—long.)	Landsat identification number	Date	Solar elev. angle (degrees)	Code	Cloud cover (percent)	Remarks
154-116	077°33'S. 023°11'E.	1183-05055	22 Jan 73	20		10	Scan lines missing
154-117	078°29'S. 017°48'E.	1183-05062	22 Jan 73	19		30	
154-118	079°19'S. 011°33'E.	1507-05040	12 Dec 73	22		50	
154-119	080°01'S. 004°23'E.	1472-05103	07 Nov 73	15		50	Surface features, band 4
155-107	066°40'S. 047°08'E.	1490-05052	25 Nov 73	33		0	White Island
155-108	067°59'S. 045°29'E.	1490-05055	25 Nov 73	32		5	Prince Olav Coast, Hays Glacier
155-108	067°59'S. 045°29'E.	1544-05043	18 Jan 74	29		0	Prince Olav Coast, Hays Glacier
155-109	069°17'S. 043°40'E.	1490-05061	25 Nov 73	31		0	Prince Olav Coast, surface features
155-110	070°35'S. 041°38'E.	1490-05064	25 Nov 73	29		0	Upper Shirase Glacier
155-111	071°50'S. 039°21'E.	1490-05070	25 Nov 73	28		0	'Blue ice'
155-112	073°04'S. 036°45'E.	1490-05073	25 Nov 73	27		0	Queen Fabiola Mountains area
155-113	074°16'S. 033°46'E.	1490-05075	25 Nov 73	26		0	Surface features
155-114	075°25'S. 030°20'E.	1526-05074	31 Dec 73	26		70	
155-115	076°31'S. 026°22'E.	1544-05073	18 Jan 74	22		50	
155-116	077°33'S. 021°45'E.	1544-05075	18 Jan 74	21		0	
155-117	078°29'S. 016°22'E.	1203-05181	11 Feb 73	14		0	
155-118	079°19'S. 010°07'E.	1526-05092	31 Dec 73	22		5	
155-119	080°01'S. 002°57'E.	1526-05095	31 Dec 73	20		5	Surface features
156-107	066°40'S. 045°42'E.						
156-108	067°59'S. 044°03'E.	1527-05105	01 Jan 74	32		10	Prince Olav Coast
156-109	069°17'S. 042°14'E.	1509-05114	14 Dec 73	32		0	Prince Olav Coast, Showa Station
156-110	070°35'S. 040°12'E.	1545-05111	19 Jan 74	27		0	Shirase Glacier
156-111	071°50'S. 037°55'E.	1527-05121	01 Jan 74	29		0	Queen Fabiola Mountains
156-112	073°04'S. 035°19'E.	1527-05123	01 Jan 74	28		0	'Blue ice'

TABLE 6.—*Optimum Landsat 1, 2, and 3 MSS and Landsat 2 RBV images of glaciers of Antarctica—Continued*

Path-Row	Nominal scene center (lat.-long.)	Landsat identification number	Date	Solar elev. angle (degrees)	Code	Cloud cover (percent)	Remarks
156-113	074°16'S. 032°20'E.	1527-05130	01 Jan 74	27	●	0	Surface features
156-114	075°25'S. 028°54'E.	1527-05132	01 Jan 74	26	●	0	
156-115	076°31'S. 024°56'E.	1203-05172	11 Feb 73	16	●	0	
156-116	077°33'S. 020°19'E.	1203-05174	11 Feb 73	15	●	0	
156-117	078°29'S. 014°56'E.	1527-05144	01 Jan 74	23	●	5	
156-118	079°19'S. 008°41'E.	1545-05143	19 Jan 74	19	●	5	Surface features
156-119	080°01'S. 001°31'E.	1564-05195	07 Feb 74	13	●	5	Surface features
157-108	067°59'S. 042°37'E.	1528-05164	02 Jan 74	32	●	0	Prince Olav Coast
157-109	069°17'S. 040°48'E.	1528-05170	02 Jan 74	31	●	0	Shirase 'Glacier Tongue,' Showa Station
157-110	070°35'S. 038°46'E.	1528-05173	02 Jan 74	30	●	0	Shirase Glacier
157-111	071°50'S. 036°29'E.	1528-05175	02 Jan 74	29	●	0	Queen Fabiola Mountains, excellent image
157-112	073°04'S. 033°53'E.	1528-05182	02 Jan 74	28	●	0	Belgica Mountains, 'blue ice'
157-113	074°16'S. 030°54'E.	1528-05184	02 Jan 74	27	●	0	Surface features
157-114	075°25'S. 027°28'E.	1582-05174	25 Feb 74	12	◐	50	
157-115	076°31'S. 023°30'E.	1131-05172	01 Dec 72	25	◐	15	
157-116	077°33'S. 018°53'E.	1131-05174	01 Dec 72	23	●	0	
157-117	078°29'S. 013°30'E.	1546-05194	20 Jan 74	19	●	5	Scan lines missing
157-118	079°19'S. 007°15'E.	1546-05201	20 Jan 74	18	●	0	Surface features
157-119	080°01'S. 000°05'E.	1546-05203	20 Jan 74	17	◐	10	Surface features
158-108	067°59'S. 041°11'E.	1547-05214	21 Jan 74	29	●	0	Prince Olav Coast
158-109	069°17'S. 039°22'E.	1511-05231	16 Dec 73	32	●	0	Showa Station, Shirase 'Glacier Tongue'
158-110	070°35'S. 037°20'E.	1547-05223	21 Jan 74	27	◐	10	Upper Shirase Glacier
158-111	071°50'S. 035°03'E.	1511-05240	16 Dec 73	30	◐	50	Queen Fabiola Mountains
158-111	071°50'S. 035°03'E.	1529-05233	03 Jan 74	29	◐	20	

TABLE 6.—*Optimum Landsat 1, 2, and 3 MSS and Landsat 2 RBV images of glaciers of Antarctica—Continued*

Path-Row	Nominal scene center (lat.—long.)	Landsat identification number	Date	Solar elev. angle (degrees)	Code	Cloud cover (percent)	Remarks
158-112	073°04'S. 032°27'E.	1547-05232	21 Jan 74	25		30	Belgica Mountains, 'blue ice'
158-113	074°16'S. 029°28'E.	1169-05273	08 Jan 73	26		20	Surface features
158-114	075°25'S. 026°02'E.	1528-05191	02 Jan 74	26		0	
158-115	076°31'S. 022°04'E.	1223-05290	03 Mar 73	9		0	
158-116	077°33'S. 017°27'E.	1223-05292	03 Mar 73	8		0	Surface features
158-117	078°29'S. 012°04'E.	1511-05263	16 Dec 73	23		5	
158-118	079°19'S. 005°49'E.	1476-05330	11 Nov 73	17		15	Surface features
158-119	080°01'S. 001°21'W.	1476-05333	11 Nov 73	16		10	Surface features, band 6, scan lines missing
159-108	067°59'S. 039°45'E.	1548-05272	22 Jan 74	28		90	
159-109	069°17'S. 037°56'E.	1548-05275	22 Jan 74	27		60	Djupvikneset Peninsula
159-110	070°35'S. 035°54'E.	1548-05281	22 Jan 74	26		30	'Blue ice'
159-111	071°50'S. 033°37'E.	1548-05284	22 Jan 74	25		20	Queen Fabiola Mountains
159-112	073°04'S. 031°01'S.	1548-05290	22 Jan 74	24		5	Belgica Mountains
159-113	074°16'S. 028°02'E.	1548-05293	22 Jan 74	23		50	Surface features
159-114	075°25'S. 024°36'E.	1152-05340	22 Dec 72	27		0	
159-115	076°31'S. 020°38'E.	1152-05342	82 Dec 72	26		15	
159-116	077°33'S. 016°01'E.	1189-05403	28 Jan 73	19		5	
159-117	078°29'S. 010°38'E.	1189-05405	28 Jan 73	18		20	
159-118	079°19'S. 004°23'E.	1477-05384	12 Nov 73	17		0	Surface features, scan lines missing
159-119	080°01'S. 002°47'W.	1477-05391	12 Nov 73	16		0	Surface features, band 4
160-108	067°59'S. 038°19'E.	1531-05334	05 Jan 74	32		40	Prince Harald Coast
160-109	069°17'S. 036°30'E.	1135-05374	05 Dec 72	32		90	
160-110	070°35'S. 034°28'E.	1135-05381	05 Dec 72	31		90	
160-111	071°50'S. 032°10'E.	2365-05240	22 Jan 76	25		0	'Blue ice,' nunataks

TABLE 6.—*Optimum Landsat 1, 2, and 3 MSS and Landsat 2 RBV images of glaciers of Antarctica—Continued*

Path-Row	Nominal scene center (lat.–long.)	Landsat identification number	Date	Solar elev. angle (degrees)	Code	Cloud cover (percent)	Remarks
160–112	073°04'S. 029°34'E.	1189–05385	28 Jan 73	23	●	5	Belgica Mountains, Vørterkaka Nunatak, band 6
160–113	074°16'S. 026°36'E.	1189–05391	28 Jan 73	22	◐	15	Surface features
160–114	075°25'S. 023°10'E.	1189–05394	28 Jan 73	21	◐	50	
160–115	076°31'S. 019°12'E.	1189–05400	28 Jan 73	20	◐	50	
160–116	077°33'S. 014°34'E.				⊙		
160–117	078°29'S. 009°12'E.				⊙		
160–118	079°19'S. 002°57'E.	1478–05443	13 Nov 73	18	●	0	Surface features
160–119	080°01'S. 004°14'W.	1478–05445	13 Nov 73	16	●	0	Surface features, band 4
161–109	069°17'S. 035°04'E.	1478–05404	13 Nov 73	28	◐	10	Riiser-Larsen Peninsula
161–110	070°35'S. 033°02'E.	1478–05411	13 Nov 73	27	●	0	Princess Ragnhild Coast, ice shelf
161–111	071°50'S. 030°44'E.	1478–05413	13 Nov 73	26	●	0	Eastern portion of Belgica Mountains
161–112	073°04'S. 028°08'E.	1478–05420	13 Nov 73	25	●	0	Vørterkaka Nunatak
161–113	074°76'S. 025°10'E.	1478–05422	13 Nov 73	24	●	0	Surface features
161–114	075°25'S. 021°44'E.	1478–05425	13 Nov 73	22	●	0	
161–115	076°31'S. 017°46'E.	1478–05431	13 Nov 73	21	●	0	Surface features
161–116	077°33'S. 013°08'E.	1478–05434	13 Nov 73	20	●	0	Surface features
161–117	078°29'S. 007°46'E.	1478–05440	13 Nov 73	19	●	0	Surface features
161–118	079°19'S. 001°31'E.	1479–05501	14 Nov 73	18	●	5	Surface features
161–119	080°01'S. 005°40'W.	1479–05504	14 Nov 73	17	●	0	Surface features
162–108	067°59'S. 035°27'E.	1209–05485	17 Feb 73	21	◐	40	Fast ice
162–109	069°17'S. 033°38'E.	1479–05463	14 Nov 73	28	◐	10	Riiser-Larsen Peninsula
162–110	070°35'S. 031°36'E.	1479–05465	14 Nov 73	27	●	5	Princess Ragnhild Coast
162–111	071°50'S. 029°18'E.	1479–05472	14 Nov 73	26	●	0	Sør Rondane Mountains
162–112	073°04'S. 026°42'E.	1479–05474	14 Nov 73	25	●	0	Sør Rondane Mountains

TABLE 6.—Optimum Landsat 1, 2, and 3 MSS and Landsat 2 RBV images of glaciers of Antarctica—Continued

Path-Row	Nominal scene center (lat.-long.)	Landsat identification number	Date	Solar elev. angle (degrees)	Code	Cloud cover (percent)	Remarks
162-113	074°16'S. 023°44'E.	1479-05481	14 Nov 73	24	●	0	Surface features
162-114	075°25'S. 020°18'E.	1479-05483	14 Nov 73	23	◐	10	
162-115	076°31'S. 016°20'E.	1209-05515	17 Feb 73	14	◐	15	
162-116	077°33'S. 011°42'E.	1551-05475	25 Jan 74	19	●	0	
162-117	078°29'S. 006°20'E.	1551-05481	25 Jan 74	18	●	0	
162-118	079°19'S. 000°05'E.	1480-05560	15 Nov 73	18	◐	10	Surface features
162-119	080°01'S. 007°06'W.	1480-05562	15 Nov 73	17	●	0	Surface features, band 4
163-108	067°59'S. 034°01'E.	1534-05505	08 Jan 74	31	●	5	Tip of Riiser-Larsen Peninsula
163-109	069°17'S. 032°12'E.	1480-05521	15 Nov 73	29	◐	20	Riiser-Larsen Peninsula, scan lines missing
163-110	070°35'S. 030°10'E.	1480-05524	15 Nov 73	27	◐	10	Princess Ragnhild Coast, melt ponds
163-110	070°35'S. 030°10'E.	2386-05403	12 Feb 76	20	◐	15	Small ice rises, melt ponds
163-111	071°50'S. 027°52'E.	2386-05405	12 Feb 76	19	●	5	Byrdreen
163-111	071°50'S. 027°52'E.	1480-05530	15 Nov 73	26	●	0	Byrdreen, band 6
163-112	073°04'S. 025°16'E.	1480-05533	15 Nov 73	25	●	0	Mjell, Gjell Glaciers, 'blue ice'
163-113	074°76'S. 022°18'E.	1480-05535	15 Nov 73	24	●	0	Surface features, scan lines missing
163-114	075°25'S. 018°52'E.	1552-05524	26 Jan 74	21	◐	40	
163-115	076°31'S. 014°54'E.	1192-05572	31 Jan 73	19	◐	40	
163-116	077°33'S. 010°16'E.	1192-05574	31 Jan 73	18	◐	30	
163-117	078°29'S. 004°54'E.	1534-05543	08 Jan 74	22	◐	20	Surface features
163-118	079°19'S. 001°22'W.	1534-05550	08 Jan 74	21	◐	75	Surface features
163-119	080°01'S. 008°32'W.	1481-06021	16 Nov 73	17	◐	10	Surface features, scan lines missing
164-109	069°17'S. 030°45'E.	1481-05580	16 Nov 73	29	◐	50	Riiser-Larsen Peninsula
164-110	070°35'S. 028°44'E.	1481-05582	16 Nov 73	28	◐	15	Princess Ragnhild Coast
164-111	071°50'S. 026°26'E.	1481-05585	16 Nov 73	27	●	0	Byrdreen

TABLE 6.—*Optimum Landsat 1, 2, and 3 MSS and Landsat 2 RBV images of glaciers of Antarctica—Continued*

Path-Row	Nominal scene center (lat.—long.)	Landsat identification number	Date	Solar elev. angle (degrees)	Code	Cloud cover (percent)	Remarks
164-112	073°04'S. 023°50'E.	1481-05591	16 Nov 73	25	●	0	Gunnestad Glacier, 'blue ice'
164-113	074°16'S. 20°51'E.	1481-05594	16 Nov 73	24	●	0	
164-114	075°25'S. 017°26'E.	1481-06000	16 Nov 73	23	●	0	
164-115	076°31'S. 13°27'E.	1481-06003	16 Nov 73	22	●	0	
164-116	077°33'S. 008°50'E.	1481-06005	16 Nov 73	21	●	0	
164-117	078°29'S. 003°27'E.	1481-06012	16 Nov 73	20	◐	15	
164-118	079°19'S. 002°48'W.	1535-06004	09 Jan 74	20	●	5	Surface features
164-119	080°01'S. 009°58'W.	1535-06011	09 Jan 74	19	●	0	Surface features
165-109	069°17'S. 029°19'E.	1554-06020	28 Jan 74	26	◐	50	Band 6
165-110	070°35'S. 027°18'E.	1482-06040	17 Nov 73	28	●	5	Large ice rise, Princess Ragnhild Coast
165-111	071°50'S. 025°00'E.	1212-06072	20 Feb 73	17	●	5	Byrdreen, Mount Romnaes
165-112	073°04'S. 022°24'E.	1212-06075	20 Feb 73	16	●	0	Hansenbreen, Sør Rondane Mountains
165-113	074°16'S. 019°25'E.	1212-06081	20 Feb 73	15	●	5	Surface features
165-114	075°25'S. 016°00'E.	1500-06053	05 Dec 73	26	●	0	
165-115	076°31'S. 012°01'E.	1500-06060	05 Dec 73	25	◐	15	
165-116	077°33'S. 007°24'E.	1482-06063	17 Nov 73	21	◐	25	Surface features
165-117	078°29'S. 002°01'E.	1482-06070	17 Nov 73	20	●	0	Surface features
165-118	079°19'S. 004°14'W.	1482-06072	17 Nov 73	19	●	5	Surface features
165-119	080°01'S. 011°24'W.	1477-05393	12 Nov 73	15	●	0	Surface features
166-109	069°17'S. 027°53'E.	1483-06092	18 Nov 73	29	◐	15	
166-110	070°35'S. 025°52'E.	1483-06095	18 Nov 73	28	●	0	Large ice rise
166-111	071°50'S. 023°34'E.	1483-06101	18 Nov 73	27	◐	25	Mount Romnaes
166-112	073°04'S. 020°58'E.	1555-06090	29 Jan 74	23	◐	60	Surface features
166-113	074°16'S. 017°59'E.	1178-06190	17 Jan 73	25	◐	30	Surface features

TABLE 6.—*Optimum Landsat 1, 2, and 3 MSS and Landsat 2 RBV images of glaciers of Antarctica—Continued*

Path-Row	Nominal scene center (lat.—long.)	Landsat identification number	Date	Solar elev. angle (degrees)	Code	Cloud cover (percent)	Remarks
166-114	075°25'S. 014°34'E.	1573-06092	16 Feb 74	15		20	
166-115	076°31'S. 010°35'E.	1573-06095	16 Feb 74	14		15	
166-116	077°33'S. 005°58'E.	1483-06122	18 Nov 73	21		30	
166-117	078°29'S. 000°35'E.	1466-06183	01 Nov 73	15		5	Band 6
166-118	079°19'S. 005°40'W.	1573-06110	16 Feb 74	11		15	Surface features
166-119	080°01'S. 012°50'W.	1466-06192	01 Nov 73	13		0	Surface features
167-109	069°17'S. 026°27'E.					100	
167-110	070°35'S. 024°25'E.	1484-06153	19 Nov 73	28		20	Scan lines missing
167-110	070°35'S. 024°25'E.	1556-06135	30 Jan 74	24		40	Princess Ragnhild Coast
167-111	071°50'S. 022°08'E.	1484-06160	19 Nov 73	27		0	Hansenbreen Sør Rondane Mountains
167-112	073°04'S. 019°32'E.	1484-06162	19 Nov 73	26		0	Sør Rondane Mountains
167-113	074°16'S. 016°33'E.	1484-06165	19 Nov 73	25		0	
167-114	075°25'S. 013°07'E.	1484-06171	19 Nov 73	24		0	
167-115	076°31'S. 009°09'E.	1484-06174	19 Nov 73	23		0	
167-116	077°33'S. 004°32'E.	1484-06180	19 Nov 73	21		0	Band 6, scan lines missing
167-117	078°29'S. 000°51'W.	1484-06183	19 Nov 73	20		0	Band 6, scan lines missing
167-118	² 079°19'S. ¹ 007°06'W.	1467-06244	02 Nov 73	15		0	Surface features
167-119	080°01'S. 014°16'W.	1520-06184	25 Dec 73	21		0	Surface features
167-119	080°01'S. 014°16'W.	1467-06250	02 Nov 73	13		5	Upper Slessor Glacier, crevasses
168-109	069°17'S. 025°01'E.	1485-06205	20 Nov 73	30		0	
168-110	070°35'S. 022°59'E.	1485-06212	20 Nov 73	29		0	Scan lines missing
168-111	071°50'S. 020°42'E.	1485-06214	20 Nov 73	27		0	Sør Rondane Mountains, band 6, scan lines missing
168-112	073°04'S. 018°06'E.	1485-06221	20 Nov 73	26		0	Nunataks, band 6
168-113	074°16'S. 015°07'E.	1575-06202	18 Feb 74	15		10	

TABLE 6.—*Optimum Landsat 1, 2, and 3 MSS and Landsat 2 RBV images of glaciers of Antarctica—Continued*

Path-Row	Nominal scene center (lat.—long.)	Landsat identification number	Date	Solar elev. angle (degrees)	Code	Cloud cover (percent)	Remarks
168-113	074°16'S. 015°07'E.	1521-06220	26 Dec 73	28	●	0	
168-114	075°25'S. 011°41'E.	1521-06222	26 Dec 73	26	●	0	Scan lines missing
168-115	076°31'S. 007°43'E.	1521-06225	26 Dec 73	25	●	0	Scan lines missing
168-116	077°33'S. 003°06'E.	1467-06235	02 Nov 73	17	●	5	Surface features
168-117	078°29'S. 002°17'W.	1198-06324	06 Feb 73	15	●	0	Surface features
168-118	079°19'S. 008°32'W.	1521-06240	26 Dec 73	22	●	0	Surface features
168-119	080°01'S. 015°42'W.	1485-06250	20 Nov 73	18	●	5	Surface features
169-109	069°17'S. 023°35'E.	2392-06142	18 Feb 76	19	◐	95	
169-110	070°35'S. 021°33'E.	2302-06160	20 Nov 75	27	◑	10	Princess Ragnhild Coast, 'blue ice'
169-111	071°50'S. 019°16'E.	2302-06162	20 Nov 75	26	●	0	Nunataks, scan lines missing
169-112	073°04'S. 016°40'E.	1126-06304	26 Nov 72	27	●	0	Surface features, partial image
169-113	074°16'S. 013°41'E.	1576-06261	19 Feb 74	15	◐	20	
169-114	075°25'S. 010°15'E.	1576-06263	19 Feb 74	14	◐	20	
169-115	076°31'S. 006°17'E.	1576-06270	19 Feb 74	13	◐	70	
169-116	077°33'S. 001°40'E.	1198-06321	06 Feb 73	16	◐	50	
169-117	078°29'S. 003°43'W.	1469-06356	04 Nov 73	16	◐	60	Surface features
169-118	079°19'S. 009°58'W.	1469-06361	04 Nov 73	15	◐	75	Surface features
169-119	080°01'S. 017°08'W.	1481-06023	16 Nov 73	16	◑	10	Upper Slessor Glacier, Shackleton Range, band 6
170-109	069°17'S. 022°09'E.	1541-06311	15 Jan 74	29	◐	50	Princess Ragnhild Coast
170-110	070°35'S. 020°07'E.	1487-06324	22 Nov 73	29	●	5	Princess Ragnhild Coast, 'blue ice'
170-111	071°50'S. 017°50'E.	2375-06212	01 Feb 76	22	●	0	Nunataks, 'blue ice'
170-112	073°04'S. 015°14'E.	1487-06333	22 Nov 73	27	◑	10	Nunataks, 'blue ice'
170-113	074°16'S. 012°15'E.	1487-06340	22 Nov 73	25	◐	15	
170-114	075°25'S. 008°49'E.	1469-06343	04 Nov 73	20	●	0	Surface features

TABLE 6. —Optimum Landsat 1, 2, and 3 MSS and Landsat 2 RBV images of glaciers of Antarctica —Continued

Path-Row	Nominal scene center (lat.—long.)	Landsat identification number	Date	Solar elev. angle (degrees)	Code	Cloud cover (percent)	Remarks
170-115	076°31'S. 004°51'E.	1469-06345	04 Nov 73	19	●	0	Surface features
170-116	077°33'S. 000°14'E.	1469-06352	04 Nov 73	18	●	0	Surface features
170-117	078°29'S. 005°09'W.	1487-06354	22 Nov 73	21	◐	70	Surface features
170-118	079°19'S. 011°24'W.	1487-06360	22 Nov 73	20	◐	60	Surface features
170-119	080°01'S. 018°34'W.	1487-06363	22 Nov 73	18	◑	10	Upper Slessor Glacier, Shackleton Range
171-109	069°17'S. 020°43'E.	2304-06270	22 Nov 75	29	◐	30	Princess Ragnhild Coast, Lazarev Ice Shelf
171-110	070°35'S. 018°41'E.	1164-06410	03 Jan 73	30	◑	10	Lazarev Ice Shelf
171-111	071°50'S. 016°24'E.	1164-06412	03 Jan 73	29	●	0	Nunataks, 'blue ice'
171-112	073°04'S. 013°48'E.	1164-06415	03 Jan 73	28	●	5	Surface features
171-113	074°16'S. 010°49'E.	1164-06421	03 Jan 73	27	◐	50	
171-114	075°25'S. 007°23'E.	1218-06431	26 Feb 73	12	◐	70	
171-115	076°31'S. 003°25'E.	1164-06430	03 Jan 73	25	◐	70	
171-116	077°33'S. 01°12'W.	1218-06440	26 Feb 73	10	◐	95	
171-117	078°29'S. 006°35'W.	1164-06435	03 Jan 73	22	◐	70	Surface features
171-118	079°19'S. 012°50'W.	1488-06415	23 Nov 73	20	◐	70	Surface features
171-119	080°01'S. 020°00'W.				⊙		
172-109	069°17'S. 019°17'E.				⊙		
172-110	070°35'S. 017°15'E.	1525-06433	30 Dec 73	30	◐	30	Lazarev Ice Shelf
172-111	071°50'S. 014°58'E.	2341-06331	29 Dec 75	29	◐	30	Entuziasty Glacier
172-112	073°04'S. 012°22'E.	1201-06475	09 Feb 73	20	◐	80	Nunataks
172-113	074°96'S. 009°23'E.	1579-06432	22 Feb 74	14	◐	80	
172-114	075°25'S. 005°57'E.	1201-06484	09 Feb 73	18	◐	60	
172-115	076°31'S. 001°59'E.	1579-06441	22 Feb 74	12	◐	40	
172-116	077°33'S. 002°38'W.	1579-06443	22 Feb 74	11	●	0	Surface features

TABLE 6.—*Optimum Landsat 1, 2, and 3 MSS and Landsat 2 RBV images of glaciers of Antarctica — Continued*

Path-Row	Nominal scene center (lat.—long.)	Landsat identification number	Date	Solar elev. angle (degrees)	Code	Cloud cover (percent)	Remarks
172-117	078°29'S. 008°01'W.	1579-06450	22 Feb 74	10		20	Surface features
172-118	079°19'S. 014°16'W.	1472-06532	07 Nov 73	16		25	Surface features
172-119	080°01'S. 021°26'W.	1508-06532	13 Dec 73	21		15	Upper Slessor Glacier, Shackleton Range
173-109	069°17'S. 017°51'E.	2270-06385	19 Oct 75	19		0	Lazarev Ice Shelf
173-110	070°35'S. 015°49'E.	2306-06385	24 Nov 75	28		5	Lazarev Ice Shelf
173-111	071°50'S. 013°32'E.	2306-06391	24 Nov 75	27		0	Entuziasty Glacier
173-112	073°04'S. 010°56'E.	1129-06475	29 Nov 72	28		15	Nunataks
173-113	074°16'S. 007°57'E.	1129-06481	29 Nov 72	27			
173-114	075°25'S. 004°31'E.	1129-06484	29 Nov 72	25		15	
173-115	076°31'S. 000°33'E.	1580-06495	23 Feb 74	12		40	
173-116	077°33'S. 004°04'W.	1129-06493	29 Nov 72	23		10	
173-117	078°29'S. 009°27'W.	1580-06504	23 Feb 74	9		5	Surface features
173-118	079°19'S. 015°42'W.	1580-06511	23 Feb 74	8		15	Upper Slessor Glacier
173-119	080°01'S. 022°52'W.						
174-109	069°17'S. 016°25'E.	1527-06543	01 Jan 74	31		60	Lazarev Ice Shelf
174-110	070°35'S. 014°23'E.	1167-06581	06 Jan 73	30		0	Schirmacher Hills, melt ponds
174-111	071°50'S. 012°06'E.	1167-06583	06 Jan 73	29		0	Wohlthat and Orvin Mountains, "Humboldt" Glacier
174-112	073°04'S. 009°30'E.	1167-06590	06 Jan 73	28		10	Nunataks
174-113	074°16'S. 006°31'E.	1167-06592	06 Jan 73	26		25	
174-114	075°25'S. 003°05'E.	1581-06551	24 Feb 74	12		90	
174-115	076°31'S. 000°53'W.	1581-06553	24 Feb 74	11		70	
174-116	077°33'S. 005°30'W.	1581-06560	24 Feb 74	10		95	
174-117	078°29'S. 010°53'W.	1581-06562	24 Feb 74	9		95	
174-118	079°19'S. 017°08'W.	1581-06565	24 Feb 74	8		90	Surface features

TABLE 6. — *Optimum Landsat 1, 2, and 3 MSS and Landsat 2 RBV images of glaciers of Antarctica—Continued*

Path-Row	Nominal scene center (lat.—long.)	Landsat identification number	Date	Solar elev. angle (degrees)	Code	Cloud cover (percent)	Remarks
174-119	080°01'S. 024°18'W.	1509-06591	14 Dec 73	21		50	Shackleton Range
175-109	069°17'S. 014°59'E.	2308-06495	26 Nov 75	30		0	Lazarev Ice Shelf
175-110	070°35'S. 012°57'E.	2308-06502	26 Nov 75	29		0	Schirmacher Hills, 'blue ice'
175-111	071°50'S. 010°40'E.	2308-06504	26 Nov 75	27		0	Wohlthat Mountains
175-112	073°04'S. 008°04'E.	1204-07051	12 Feb 73	19		0	Nunataks
175-113	074°16'S. 005°05'E.	1204-07053	12 Feb 73	18		0	Surface features
175-114	075°25'S. 001°39'E.	1204-07060	12 Feb 73	17		30	Surface features
175-115	076°31'S. 002°19'W.	1204-07062	12 Feb 73	15		80	
175-116	077°33'S. 006°56'W.	1150-07064	20 Dec 72	25		70	
175-117	078°29'S. 012°19'W.					100	
175-118	079°19'S. 018°34'W.	1475-07103	10 Nov 73	17		20	Upper Slessor Glacier
175-119	080°01'S. 025°44'W.	1470-06424	05 Nov 73	13		30	Upper Slessor Glacier
175-119	080°01'S. 025°44'W.	1510-07045	15 Dec 73	21		30	Shackleton Range
176-109	069°17'S. 013°33'E.	2309-06554	27 Nov 75	30		70	
176-110	070°35'S. 011°31'E.	1133-07100	03 Dec 72	30		5	Schirmacher Hills, 'blue ice'
176-111	071°50'S. 009°14'E.	1187-07101	26 Jan 73	25		90	
176-112	073°04'S. 006°38'E.	1187-07103	26 Jan 73	24		95	
176-113	074°16'S. 003°39'E.	1187-07110	26 Jan 73	23		65	
176-114	075°25'S. 000°13'E.						
176-115	076°31'S. 003°45'W.	1150-07061	20 Dec 72	26		85	
176-116	077°33'S. 008°22'W.					100	
176-117	078°29'S. 013°45'W.	1475-07101	10 Nov 73	18		10	Surface features
176-118	079°19'S. 020°00'W.	1476-07162	11 Nov 73	17		5	Upper Slessor Glacier, band 6, scan lines missing
176-119	080°01'S. 027°10'W.	1476-07164	11 Nov 73	16		15	Parry Point, band 6, scan lines missing

TABLE 6.—Optimum Landsat 1, 2, and 3 MSS and Landsat 2 RBV images of glaciers of Antarctica—Continued

Path-Row	Nominal scene center (lat.—long.)	Landsat identification number	Date	Solar elev. angle (degrees)	Code	Cloud cover (percent)	Remarks
177-109	069°17'S. 012°07'E.	2382-07003	08 Feb 76	22	●	0	
177-110	070°35'S. 010°05'E.	2382-07005	08 Feb 76	21	●	5	Schirmacher Hills, melt ponds
177-111	071°50'S. 007°47'E.	1133-07102	03 Dec 72	29	●	0	Wohlthat Mountains
177-112	073°04'S. 005°11'E.	1170-07161	09 Jan 73	27	●	0	Nunataks, surface features
177-113	074°16'S. 002°13'E.	1133-07111	03 Dec 72	27	●	5	
177-114	075°25'S. 001°13'W.	1476-07144	11 Nov 73	22	●	0	
177-115	076°31'S. 005°11'W.	1476-07150	11 Nov 73	21	●	0	
177-116	077°33'S. 009°49'W.	1133-07123	03 Dec 72	24	●	5	Surface features
177-117	078°29'S. 015°11'W.	1548-07142	22 Jan 74	19	◐	60	Surface features
177-118	079°19'S. 021°26'W.	1548-07145	22 Jan 74	18	◐	20	Upper Slessor Glacier
177-119	080°01'S. 028°37'W.	1548-07151	22 Jan 74	17	●	0	Parry Point, Slessor Glacier, Shackleton Range
178-109	069°17'S. 010°41'E.				◑	100	
178-110	070°35'S. 008°39'E.	2383-07064	09 Feb 76	21	●	0	Melt ponds
178-111	071°50'S. 006°21'E.	2383-07070	09 Feb 76	20	●	0	Muhlig-Hofmann Mountains
178-112	073°04'S. 003°45'E.	1477-07193	12 Nov 73	25	●	0	Muhlig-Hofmann Mountains
178-113	074°16'S. 000°47'E.	1477-07200	12 Nov 73	23	●	0	Nunatak
178-114	075°25'S. 002°39'W.	1477-07202	12 Nov 73	22	●	0	
178-115	076°31'S. 006°37'W.	1477-07205	12 Nov 73	21	●	0	Surface features
178-116	077°33'S. 011°15'W.	1477-07211	12 Nov 73	20	●	0	Surface features
178-117	078°29'S. 016°37'W.	1477-07214	12 Nov 73	19	●	5	Surface features
178-118	079°19'S. 022°52'W.	1478-07274	13 Nov 73	18	◐	40	Theron Mountains
178-118	079°19'S. 022°52'W.	1190-07302	29 Jan 73	16	◐	60	Slessor Glacier
178-119	080°01'S. 030°03'W.	1190-07304	29 Jan 73	15	◑	10	Parry Point
179-109	069°17'S. 009°15'E.	1478-07240	13 Nov 73	28	●	0	

TABLE 6.—*Optimum Landsat 1, 2, and 3 MSS and Landsat 2 RBV images of glaciers of Antarctica—Continued*

Path-Row	Nominal scene center (lat.—long.)	Landsat identification number	Date	Solar elev. angle (degrees)	Code	Cloud cover (percent)	Remarks
179-110	070°35'S. 007°13'E.	1478-07242	13 Nov 73	27	●	0	
179-111	071°50'S. 004°55'E.	1478-07245	13 Nov 73	26	●	0	Mühlig-Hofmann Mountains, band 6
179-112	073°04'S. 002°19'E.	1478-07251	13 Nov 73	25	●	5	Svea Glacier, Upper Jutulstraumen, band 6, scan lines missing
179-113	074°16'S. 000°39'W.	1478-07254	13 Nov 73	24	◐	20	Nunataks, scan lines missing, surface features
179-114	075°25'S. 004°05'W.	1190-07284	29 Jan 73	21	◐	20	
179-115	076°31'S. 008°03'W.	1478-07263	13 Nov 73	21	●	5	Surface features
179-116	077°33'S. 012°41'W.	1478-07265	13 Nov 73	20	●	0	Surface features
179-117	078°29'S. 018°03'W.	1478-07272	13 Nov 73	19	◐	15	Surface features
179-118	079°19'S. 024°18'W.	1479-07333	14 Nov 73	18	●	0	Theron Mountains, band 4
179-119	080°01'S. 031°29'W.	1479-07335	14 Nov 73	17	●	0	Parry Point, line drops
180-109	069°17'S. 007°49'E.				⊙		
180-110	070°35'S. 005°47'E.	2331-07184	19 Dec 75	30	◐	15	Scan lines missing
180-111	071°50'S. 003°29'E.	2331-07191	19 Dec 75	29	◐	35	Mühlig-Hofmann Mountains
180-112	073°04'S. 000°53'E.	1227-07340	07 Mar 73	11	◐	10	Mühlig-Hofmann Mountains, Jutulstraumen Glacier
180-113	074°16'S. 002°05'W.	1227-07342	07 Mar 73	10	●	5	Neumayer Cliffs
180-114	075°25'S. 005°31'W.	1227-07345	07 Mar 73	9	●	0	Nunataks
180-115	076°31'S. 009°29'W.	1479-07321	14 Nov 73	21	◐	60	Band 6, scan lines missing
180-116	077°33'S. 014°07'W.	1479-07324	14 Nov 73	20	●	0	Surface features
180-117	078°29'S. 019°29'W.	1479-07330	14 Nov 73	19	●	0	Surface features
180-118	079°19'S. 025°44'W.				⊙		
180-119	080°01'S. 032°55'W.	1480-07394	15 Nov 73	17	◐	10	Parry Point, Filchner Ice Shelf
181-109	069°17'S. 006°22'E.	2278-07244	27 Oct 75	22	●	0	
181-110	070°35'S. 004°21'E.	2278-07250	27 Oct 75	21	●	0	Fimbul Ice Shelf
181-111	071°50'S. 002°03'E.	2278-07253	27 Oct 75	20	●	0	Sverdrup Mountains

TABLE 6.—Optimum Landsat 1,2, and 3 MSS and Landsat 2 RBV images of glaciers of Antarctica—Continued

Path-Row	Nominal scene center (lat.—long.)	Landsat identification number	Date	Solar elev. angle (degrees)	Code	Cloud cover (percent)	Remarks
181-112	073°04'S. 000°33'W.	1210-07393	18 Feb 73	17	●	0	Jutulstraumen Glacier
181-113	074°16'S. 003°32'W.	1210-07400	18 Feb 73	16	◐	25	Kirwin Escarpment
181-114	075°25'S. 006°57'W.	1210-07402	18 Feb 73	15	◐	85	Nunataks
181-115	076°31'S. 010°56'W.	1193-07462	01 Feb 73	19	◐	15	Surface features
181-116	077°33'S. 015°33'W.	1480-07382	15 Nov 73	21	●	5	Surface features
181-117	078°29'S. 020°56'W.	1480-07385	15 Nov 73	19	●	0	Surface features
181-118	079°19'S. 027°11'W.	1480-07391	15 Nov 73	18	●	0	Theron Mountains, Slessor Glacier
181-118	079°19'S. 027°11'W.	1481-07450	16 Nov 73	18	●	0	Theron Mountains, Slessor Glacier
181-119	080°01'S. 034°21'W.	1481-07452	16 Nov 73	17	●	0	Filchner Ice Shelf, crevasses
182-109	069°17'S. 004°56'E.	1553-07393	27 Jan 74	26	●	5	Ice shelf
182-110	070°35'S. 002°55'E.	1499-07413	04 Dec 73	31	◐	10	Fimbul Ice Shelf
182-111	071°50'S. 000°37'E.	2279-07311	28 Oct 75	20	●	5	Jutulstraumen Glacier
182-112	073°04'S. 001°59'W.	1517-07420	22 Dec 73	29	●	0	Neumayer Cliffs
182-113	074°16'S. 004°58'W.	517-07422	22 Dec 73	28	●	0	Kirwin Escarpment
182-114	075°25'S. 008°23'W.	1517-07425	22 Dec 73	27	●	0	Nunataks
182-115	076°31'S. 012°22'W.	1517-07431	22 Dec 73	26	◐	20	Surface features
182-116	077°33'S. 016°59'W.	1176-07520	15 Jan 73	22	●	0	Surface features
182-117	078°29'S. 022°22'W.	1481-07443	16 Nov 73	20	◐	10	Surface features
182-118	079°19'S. 028°37'W.	1464-07504	30 Oct 73	14	◐	25	Theron Mountains
182-119	080°01'S. 035°47'W.	1464-07511	30 Oct 73	12	◐	75	
183-110	070°35'S. 001°29'E.	1230-07502	10 Mar 73	12	◐	50	Fimbul Ice Shelf
183-111	071°50'S. 000°49'W.	1230-07505	10 Mar 73	11	◐	15	Jutulstraumen Glacier
183-112	073°04'S. 003°25'W.	1139-07451	09 Dec 72	29	◐	10	Neumayer Cliffs, Kirwin Escarpment
183-113	074°16'S. 006°24'W.	1230-07514	10 Mar 73	9	◐	10	Nunataks

TABLE 6.—*Optimum Landsat 1, 2, and 3 MSS and Landsat 2 RBV images of glaciers of Antarctica—Continued*

Path-Row	Nominal scene center (lat.—long.)	Landsat identification number	Date	Solar elev. angle (degrees)	Code	Cloud cover (percent)	Remarks
183-113	074°16'S. 006°24'W.	1139-07454	09 Dec 72	28	●	0	Nunataks
183-114	075°25'S. 009°49'W.	1230-07520	10 Mar 73	8	●	5	Heimefront Range
183-115	076°31'S. 013°48'W.	1464-07493	30 Oct 73	17	●	0	Surface features, band 6
183-116	077°33'S. 018°25'W.	1518-07492	23 Dec 73	24	●	0	Surface features
183-117	078°29'S. 023°48'W.	1482-07502	17 Nov 73	20	●	0	Surface features
183-118	079°19'S. 030°03'W.	1518-07501	23 Dec 73	22	●	0	Parry Point
183-119	080°01'S. 037°13'W.	1518-07503	23 Dec 73	21	◐	40	Filchner Ice Shelf, crevasses
184-109	069°17'S. 002°04'E.	2281-07415	30 Oct 75	23	◐	70	Fimbul Ice Shelf
184-110	070°35'S. 000°02'E.	2281-07421	30 Oct 75	22	◐	20	Fimbul Ice Shelf
184-111	071°50'S. 002°15'W.	2281-07424	30 Oct 75	21	●	0	Jutulstraumen Glacier
184-112	073°04'S. 004°51'W.	1483-07535	18 Nov 73	26	●	5	Borg Massif
184-113	074°16'S. 007°50'W.	1483-07542	18 Nov 73	25	◐	20	Heimefront Range
184-114	075°25'S. 011°16'W.	1483-07544	18 Nov 73	24	◐	20	Heimefront Range
184-115	076°31'S. 015°14'W.	1519-07544	24 Dec 73	25	●	0	Surface features
184-116	077°33'S. 019°51'W.	1159-07581	29 Dec 72	24	◐	90	
184-117	078°29'S. 025°14'W.				⊙		
184-118	079°19'S. 031°29'W.	1501-07561	06 Dec 73	22	●	5	Parry Point
184-119	080°01'S. 038°39'W.	1501-07564	06 Dec 73	21	◐	40	Filchner Ice Shelf, crevasses
185-109	069°17'S. 000°38'E.	2336-07470	24 Dec 75	31	◐	20	Fimbul Ice Shelf
185-110	070°35'S. 001°24'W.	1142-08014	12 Dec 72	31	◐	95	
185-111	071°50'S. 003°41'W.				⊙		
185-112	073°04'S. 006°17'W.				⊙		
185-113	074°16'S. 009°16'W.				⊙		
185-114	075°25'S. 012°42'W.				⊙		

TABLE 6.—*Optimum Landsat 1, 2, and 3 MSS and Landsat 2 RBV images of glaciers of Antarctica—Continued*

Path-Row	Nominal scene center (lat.—long.)	Landsat identification number	Date	Solar elev. angle (degrees)	Code	Cloud cover (percent)	Remarks
185-115	076°31'S. 016°40'W.	1466-08010	01 Nov 73	18		35	Surface features, scan lines missing
185-116	077°33'S. 021°17'W.					—	
185-117	078°29'S. 026°40'W.						
185-118	079°19'S. 032°55'W.	1502-08020	07 Dec 73	22		45	Parry Point
185-119	080°01'S. 040°05'W.	1502-08022	07 Dec 73	21		40	Filchner Ice Shelf
186-109	069°17'S. 000°48'W.						
186-110	070°35'S. 002°50'W.	1467-08043	02 Nov 73	24		40	Fimbul Ice Shelf
186-111	071°50'S. 005°07'W.	1142-08020	12 Dec 72	30		40	Ahlmann Ridge
186-112	073°04'S. 007°43'W.	1142-08023	12 Dec 72	29		10	Nunataks
186-113	074°16'S. 010°42'W.	1467-08055	02 Nov 73	21		0	Heimefront Range
186-114	075°25'S. 014°08'W.	1467-08061	02 Nov 73	19		0	Heimefront Range
186-115	076°31'S. 018°06'W.	1467-08064	02 Nov 73	18		0	Stancomb-Wills Glacier, surface features
186-116	077°33'S. 022°43'W.	1142-08041	12 Dec 72	24		70	
186-117	078°29'S. 028°06'W.						
186-118	079°19'S. 034°21'W.						
186-119	080°01'S. 041°31'W.						
187-109	069°17'S. 002°14'W.	31333-07594	28 Oct 81	23		50	Partial image
187-110	070°35'S. 004°16'W.	1558-08083	01 Feb 74	24		80	Ice front
187-111	071°50'S. 006°33'W.	2320-07592	08 Dec 75	29		90	
187-112	073°04'S. 009°09'W.	1558-08092	01 Feb 74	22		50	Surface features
187-113	074°16'S. 012°08'W.	1179-08082	18 Jan 73	24		5	Heimefront Range
187-114	075°25'S. 015°34'W.	1216-08145	24 Feb 73	13		40	Heimefront Range
187-115	076°31'S. 019°32'W.	1216-08152	24 Feb 73	11		10	Stancomb-Wills Glacier, surface features
187-116	077°33'S. 024°09'W.	1216-08154	24 Feb 73	10		10	Surface features

TABLE 6.—*Optimum Landsat 1, 2, and 3 MSS and Landsat 2 RBV images of glaciers of Antarctica—Continued*

Path-Row	Nominal scene center (lat.—long.)	Landsat identification number	Date	Solar elev. angle (degrees)	Code	Cloud cover (percent)	Remarks
187-117	078°29'S. 029°32'W.	1216-08161	24 Feb 73	9		10	Theron Mountains
187-118	079°19'S. 035°47'W.	1504-08132	09 Dec 73	22		90	
187-119	080°01'S. 042°57'W.	1504-08135	09 Dec 73	21		25	Berkner Island
188-109	069°17'S. 003°40'W.	1163-08180	02 Jan 73	31		100	Ice front
188-110	070°35'S. 005°42'W.	1163-08183	02 Jan 73	30		100	Ice front
188-111	071°50'S. 007°59'W.	1127-08191	27 Nov 72	29		70	
188-112	073°04'S. 010°35'W.	1163-08192	02 Jan 73	28		90	Nunataks
188-113	074°16'S. 013°34'W.	1163-08194	02 Jan 73	27		80	Heimefront Range
188-114	075°25'S. 017°00'W.	1163-08201	02 Jan 73	26		85	Surface features
188-115	076°31'S. 020°58'W.	1127-08205	27 Nov 72	24		40	Surface features
188-116	077°33'S. 025°35'W.	1163-08210	02 Jan 73	24		5	Surface features
188-117	078°29'S. 030°58'W.	1163-08212	02 Jan 73	23		40	Luitpold Coast
188-118	079°19'S. 037°13'W.	1505-08191	10 Dec 73	22		10	Filchner Ice Shelf, crevasses
188-119	080°01'S. 044°23'W.	1505-08193	10 Dec 73	21		10	Berkner Island
189-110	070°35'S. 007°08'W.	2034-08125	25 Feb 75	16		50	Ekström and Jelbart Ice Shelves
189-111	071°50'S. 009°25'W.	2034-08131	25 Feb 75	15		60	Princess Martha Coast
189-112	073°04'S. 012°01'W.	1506-08222	11 Dec 73	29		95	
189-113	074°16'S. 015°00'W.					100	
189-114	075°25'S. 018°26'W.					100	
189-115	076°31'S. 022°24'W.					100	
189-116	077°33'S. 027°01'W.	1506-08240	11 Dec 73	24		70	
189-117	078°29'S. 032°24'W.	1506-08243	11 Dec 73	23		15	Luitpold Coast
189-118	079°19'S. 038°39'W.	1506-08245	11 Dec 73	22		5	Filchner Ice Shelf, Grand Chasms
189-119	080°01'S. 045°49'W.	1506-08252	11 Dec 73	21		10	Berkner Island

TABLE 6.—*Optimum Landsat 1, 2, and 3 MSS and Landsat 2 RBV images of glaciers of Antarctica—Continued*

Path-Row	Nominal scene center (lat.—long.)	Landsat identification number	Date	Solar elev. angle (degrees)	Code	Cloud cover (percent)	Remarks
190-109	069°17'S. 006°32'W.	2305-08160	23 Nov 75	29	●	0	Ice front
190-110	070°35'S. 008°34'W.	2305-08162	23 Nov 75	28	●	0	Ekström Ice Shelf, scan lines missing
190-111	071°50'S. 010°51'W.	2305-08165	23 Nov 75	27	●	0	Riiser-Larsen Ice Shelf
190-112	073°04'S. 013°27'W.				⊙		
190-113	074°16'S. 016°26'W.	2341-08171	29 Dec 75	27	◐	15	Kraul Mountains, Veststraumen Glacier
190-114	075°25'S. 019°52'W.	1579-08270	22 Feb 74	13	●	5	Stancomb-Wills Glacier and Glacier Tongue
190-115	076°31'S. 023°50'W.	1579-08272	22 Feb 74	12	●	0	Brunt Ice Shelf, Caird Coast
190-116	077°33'S. 028°27'W.	1579-08275	22 Feb 74	11	◐	20	Coats Land
190-117	078°29'S. 033°50'W.	1165-08325	04 Jan 73	22	◐	65	Filchner Ice Shelf, Luitpold Coast
190-118	079°19'S. 040°05'W.				⊙		
190-119	080°01'S. 047°15'W.				⊙		
191-110	070°35'S. 010°00'W.	1148-08360	18 Dec 72	31	◐	75	
191-111	071°50'S. 012°17'W.	1544-08322	18 Jan 74	26	◑	10	Riiser-Larsen Ice Shelf, melt ponds
191-112	073°04'S. 014°53'W.	1544-08325	18 Jan 74	25	◑	10	Kraul Mountains
191-113	074°16'S. 017°52'W.	1544-08331	18 Jan 74	24	◐	30	Caird Coast
191-114	075°25'S. 021°18'W.	1202-08374	10 Feb 73	17	◐	80	Caird Coast
191-115	076°31'S. 025°16'W.	1202-08381	10 Feb 73	16	◐	90	
191-116	077°33'S. 029°53'W.				◑	100	
191-117	078°29'S. 035°16'W.				⊙		
191-118	079°19'S. 041°31'W.				⊙		
191-119	080°01'S. 048°41'W.				⊙		
192-110	070°35'S. 011°26'W.	2397-08263	23 Feb 76	16	◐	100	Ice front
192-111	071°50'S. 013°43'W.				⊙		
192-112	073°04'S. 016°19'W.				⊙		

TABLE 6.—*Optimum Landsat 1, 2, and 3 MSS and Landsat 2 RBV images of glaciers of Antarctica—Continued*

Path-Row	Nominal scene center (lat.—long.)	Landsat identification number	Date	Solar elev. angle (degrees)	Code	Cloud cover (percent)	Remarks
192-113	074°16'S. 019°18'W.	1148-08371	18 Dec 72	28		80	
192-114	075°25'S. 022°44'W.	1148-08374	18 Dec 72	27		50	Stancomb-Wills Glacier, Caird Coast
192-115	076°31'S. 026°42'W.	1148-08380	18 Dec 72	26		20	Brunt Ice Shelf, Dawson-Lambton Glacier
192-116	077°33'S. 031°19'W.	1148-08383	18 Dec 72	24		50	Luitpold Coast
192-117	078°29'S. 036°42'W.	1148-08385	18 Dec 72	23		50	Schweitzer, Lerchenfeld, and Penck Glaciers
192-118	079°19'S. 042°57'W.						
192-119	080°01'S. 050°07'W.	1510-08481	15 Dec 73	21		80	
193-110	070°35'S. 012°52'W.						
193-111	071°50'S. 015°09'W.						
193-112	073°04'S. 017°45'W.						
193-113	074°16'S. 020°44'W.						
193-114	075°25'S. 024°10'W.						
193-115	076°31'S. 028°08'W.						
193-116	077°33'S. 032°45'W.						
193-117	078°29'S. 038°08'W.						
193-118	079°19'S. 044°23'W.	1475-08535	10 Nov 73	17		20	Berkner Island, McCarthy and Roberts Inlets, band 4
193-119	080°01'S. 051°33'W.	1475-08541	10 Nov 73	16		5	Berkner Island
194-111	071°50'S. 016°36'W.	2399-08382	25 Feb 76	15		60	Riiser-Larsen Ice Shelf
194-112	073°04'S. 019°12'W.	2291-08402	09 Nov 75	23		100	Ice front
194-113	074°16'S. 022°10'W.						
194-114	075°25'S. 025°36'W.						
194-115	076°31'S. 029°34'W.	1151-08551	21 Dec 72	26		80	
194-116	077°33'S. 034°12'W.					100	
194-117	078°29'S. 039°34'W.	1476-08591	11 Nov 73	18		15	Filchner Ice Shelf, Grand Chasms

TABLE 6.—*Optimum Landsat 1, 2, and 3 MSS and Landsat 2 RBV images of glaciers of Antarctica—Continued*

Path-Row	Nominal scene center (lat.-long.)	Landsat identification number	Date	Solar elev. angle (degrees)	Code	Cloud cover (percent)	Remarks
194-117	078°29'S. 039°34'W.	1475-08532	10 Nov 73	18		15	Grand Chasms, scan lines missing
194-118	079°19'S. 045°49'W.	1476-08593	11 Nov 73	17		5	Berkner Island, McCarthy and Roberts Inlets
194-119	080°01'S. 053°00'W.	1476-09000	11 Nov 73	16		10	
195-111	071°50'S. 018°02'W.					100	
195-112	073°04'S. 020°38'W.	1188-08593	27 Jan 73	23		60	Riiser-Larsen Ice Shelf
195-113	074°16'S. 023°36'W.	1188-09000	27 Jan 73	22		70	Riiser-Larsen Ice Shelf
195-114	075°25'S. 027°02'W.	1188-09002	27 Jan 73	21		5	Brunt Ice Shelf
195-115	076°31'S. 031°00'W.	1188-09005	27 Jan 73	20		0	Dawson-Lambton Glacier tongue
195-116	077°33'S. 035°38'W.	1188-09011	27 Jan 73	19		5	Luitpold Coast
195-117	078°29'S. 041°00'W.	1188-09014	27 Jan 73	18		70	Grand Chasms
195-118	079°19'S. 047°15'W.	1566-08573	09 Feb 74	13		80	Berkner Island
195-119	080°01'S. 054°26'W.	1567-09034	10 Feb 74	12		85	
196-112	073°04'S. 022°04'W.	1477-09025	12 Nov 73	25		100	Ice front
196-113	074°16'S. 025°02'W.	1477-09031	12 Nov 73	23		95	Ice front
196-113	074°16'S. 025°02'W.	1171-09053	10 Jan 73	26		75	Brunt Ice Shelf
196-114	075°25'S. 028°28'W.	1171-09060	10 Jan 73	25		40	Brunt Ice Shelf
196-115	076°31'S. 032°26'W.	1171-09062	10 Jan 73	24		60	Luitpold Coast
196-116	077°33'S. 037°04'W.	1171-09065	10 Jan 73	23		30	Filchner Ice Shelf
196-117	078°29'S. 042°26'W.						
196-118	079°19'S. 048°41'W.					100	
196-119	080°01'S. 055°52'W.					100	
197-114	075°25'S. 029°54'W.	1208-09121	16 Feb 73	15		0	Brunt Ice Shelf
197-115	076°31'S. 033°52'W.	1208-09124	16 Feb 73	14		20	Luitpold Coast
197-115	076°31'S. 033°52'W.	1154-09122	24 Dec 72	26		40	Luitpold Coast

TABLE 6.—*Optimum Landsat 1, 2, and 3 MSS and Landsat 2 RBV images of glaciers of Antarctica—Continued*

Path-Row	Nominal scene center (lat.—long.)	Landsat identification number	Date	Solar elev. angle (degrees)	Code	Cloud cover (percent)	Remarks
197-116	077°33'S. 038°30'W.	1154-09125	24 Dec 72	24		80	Ice front
197-117	078°29'S. 043°52'W.						
197-118	079°19'S. 050°07'W.					100	
197-119	080°01'S. 057°18'W.					100	
198-116	077°33'S. 039°56'W.	1479-09155	14 Nov 73	20		0	Filchner Ice Shelf
198-117	078°29'S. 045°19'W.	1479-09162	14 Nov 73	19		50	Berkner Island, Grand Chasms
198-117	078°29'S. 045°19'W.	1191-09185	30 Jan 73	17		50	Berkner Island, Grand Chasms
198-118	079°19'S. 051°34'W.						
198-119	080°01'S. 058°44'W.						
199-116	077°33'S. 041°22'W.						
199-117	078°29'S. 046°45'W.					100	
199-118	079°19'S. 053°00'W.	1570-09202	13 Feb 74	12		0	Berkner Island
199-119	08°01'S. 060°10'W.	1570-09205	13 Feb 74	11		10	Henry Ice Rise
200-116	077°33'S. 042°48'W.	1157-09295,	27 Dec 72	24		50	Filchner Ice Shelf
200-117	078°29'S. 048°11'W.					100	
200-118	079°19'S. 054°26'W.					100	
200-119	080°01'S. 061°36'W.	1535-09274	09 Jan 74	19		90	
201-116	077°33'S. 044°14'W.	1482-09331	17 Nov 73	21		90	Berkner Island
201-117	078°29'S. 049°37'W.	1482-09333	17 Nov 73	20		90	
201-118	079°19'S. 055°52'W.					100	
201-119	080°01'S. 063°02'W.					100	
202-116	077°33'S. 045°40'W.						
202-117	078°29'S. 051°03'W.						
202-118	079°19'S. 057°18'W.	1519-09391	24 Dec 73	22		50	

TABLE 6.—*Optimum Landsat 1, 2, and 3 MSS and Landsat 2 RBV images of glaciers of Antarctica—Continued*

Path-Row	Nominal scene center (lat.—long.)	Landsat identification number	Date	Solar elev. angle (degrees)	Code	Cloud cover (percent)	Remarks
202-119	080°01'S. 064°28'W.	1519-09393	24 Dec 73	21		30	Henry Ice Rise
203-116	077°33'S. 047°06'W.						
203-117	078°29'S. 052°29'W.						
203-118	079°19'S. 058°44'W.						
203-119	080°01'S. 065°54'W.					100	
204-116	077°33'S. 048°32'W.	1539-09491	13 Jan 74	22		50	Ronne Ice Shelf, giant icebergs
204-117	078°29'S. 053°55'W.	1539-09494	13 Jan 74	21		95	
204-118	079°19'S. 060°10'W.					100	
204-119	080°01'S. 067°20'W.					100	
205-116	077°33'S. 049°58'W.	1522-09553	27 Dec 73	24		95	Ice front
205-117	078°29'S. 055°21'W.	1522-09555	27 Dec 73	23		80	
205-118	079°19'S. 061°36'W.	1504-09564	09 Dec 73	22		10	Henry Ice Rise
205-119	080°01'S. 068°46'W.	1504-09570	09 Dec 73	21		30	Henry and Korff Ice Rises
206-116	077°33'S. 051°24'W.	1505-10013	10 Dec 73	24		40	Ronne Ice Shelf, giant icebergs
206-117	078°29'S. 056°47'W.	1505-10020	10 Dec 73	23		0	
206-118	079°19'S. 063°02'W.	1505-10022	10 Dec 73	22		0	Henry Ice Rise
206-119	080°01'S. 070°12'W.	1559-10011	02 Feb 74	14		5	Henry and Korff Ice Rises
207-115	076°31'S. 048°13'W.	1506-10065	11 Dec 73	25		0	Giant iceberg
207-116	077°33'S. 052°50'W.	1560-10054	03 Feb 74	17		70	Ronne Ice Shelf
207-117	078°29'S. 058°13'W.	1560-10060	03 Feb 74	16		60	Ronne Ice Shelf
207-118	079°19'S. 064°28'W.	1560-10063	03 Feb 74	15		50	
207-119	080°01'S. 071°38'W.	1560-10065	03 Feb 74	14		40	Skytrain Ice Rise
208-115	076°31'S. 049°39'W.	30274-10043	04 Dec 78	24		10	Ronne Ice Shelf
208-116	077°33'S. 054°16'W.	30274-10050	04 Dec 78	23		10	Crevasses

TABLE 6.—*Optimum Landsat 1, 2, and 3 MSS and Landsat 2 RBV images of glaciers of Antarctica—Continued*

Path-Row	Nominal scene center (lat.—long.)	Landsat identification number	Date	Solar elev. angle (degrees)	Code	Cloud cover (percent)	Remarks
208–117	078°29'S. 059°39'W.	1561–10114	04 Feb 74	15		95	
208–118	079°19'S. 065°54'W.	1561–10121	04 Feb 74	14		10	Ronne Ice Shelf, Korff Ice Rise
208–119	080°01'S. 073°04'W.	1561–10123	04 Feb 74	13		0	Korff and Skytrain Ice Rises
209–115	076°31'S. 051°05'W.	1544–10172	18 Jan 74	22		80	Ronne Ice Shelf, giant iceberg
209–116	077°33'S. 055°42'W.	1544–10174	18 Jan 74	21		95	
209–117	078°29'S. 061°05'W.	1203–10280	11 Feb 73	14		25	Crevasses
209–118	079°19'S. 067°20'W.	1544–10183	18 Jan 74	19		95	
209–119	080°01'S. 074°30'W.	1544–10190	18 Jan 74	18		80	
210–115	076°31'S. 052°31'W.	30294–10155	24 Dec 78	25		0	Ronne Ice Shelf
210–116	077°33'S. 057°08'W.	1563–10224	06 Feb 74	16		70	
210–117	078°29'S. 062°31'W.	1563–10231	06 Feb 74	15		70	crevasses
210–118	079°19'S. 068°46'W.	1545–10241	19 Jan 74	19		70	Korff Ice Rise
210–119	080°01'S. 075°56'W.	1545–10244	19 Jan 74	17		75	
211–115	076°31'S. 053°57'W.	1564–10280,	07 Feb 74	17		90	Ice front
211–116	077°33'S. 058°34'W.	1528–10294	02 Jan 74	24		10	Ronne Ice Shelf
211–117	078°29'S. 063°57'W.	1528–10301	02 Jan 74	22		10	Korff Ice Rise
211–118	079°19'S. 070°12'W.	1528–10303	02 Jan 74	21		0	Korff Ice Rise
211–119	080°01'S. 077°22'W.	1528–10310	02 Jan 74	20		10	Skytrain Ice Rise, Hercules Inlet
212–115	076°31'S. 055°23'W.	1169–10381	08 Jan 73	24		95	Ice front
212–116	077°33'S. 060°01'W.					100	
212–117	078°29'S. 065°23'W.					100	
212–118	079°19'S. 071°38'W.					100	
212–119	080°01'S. 078°49'W.					100	
213–115	0076°31'S. 056°49'W.	1566–10393	09 Feb 74	16		70	Ronne Ice Shelf, crevasses

TABLE 6.—*Optimum Landsat 1, 2, and 3 MSS and Landsat 2 RBV images of glaciers of Antarctica—Continued*

Path-Row	Nominal scene center (lat.—long.)	Landsat identification number	Date	Solar elev. angle (degrees)	Code	Cloud cover (percent)	Remarks
213-116	077°33'S. 061°27'W.	1566-10395	09 Feb 74	15		75	Crevasses
213-117	078°29'S. 066°49'W.	1530-10413	04 Jan 74	22		75	
213-118	079°19'S. 073°04'W.	1512-10422	17 Dec 73	22		10	Korff and Skytrain Ice Rises
213-119	080°01'S. 080°15'W.	1512-10425	17 Dec 73	21		10	Skytrain Ice Rise, Ellsworth Mountains
214-115	076°31'S. 058°15'W.					100	
214-116	077°33'S. 062°53'W.	1567-10454	10 Feb 74	15		60	
214-117	078°29'S. 068°15'W.	1567-10460	10 Feb 74	14		15	Korff Ice Rise, crevasses
214-118	079°19'S. 074°30'W.	1567-10463	10 Feb 74	13		15	Korff and Skytrain Ice Rises
214-119	080°01'S. 081°41'W.	1549-10473	23 Jan 74	17		30	Dott Ice Rise, Schmidt Glacier, Union Glacier
215-114	075°25'S. 055°43'W.	30353-10441	21 Feb 79	13		20	Ronne Ice Shelf
215-115	076°31'S. 059°42'W.	30335-10444	03 Feb 79	18		85	Crevasses
215-116	077°33'S. 064°19'W.	1209-11020	17 Feb 73	13		10	Crevasses
215-117	078°29'S. 069°42'W.	1209-11023	17 Feb 73	12		5	Korff Ice Rise, crevasses
215-118	079°19'S. 075°57'W.	1550-10524	24 Jan 74	17		90	
215-119	080°01'S. 083°07'W.	1550-10531	24 Jan 74	16		85	Ellsworth Mountains
216-114	075°25'S. 057°09'W.	1155-11005	25 Dec 72	27		100	Ice front
216-115	076°31'S. 061°08'W.	1569-10564	12 Feb 74	15		5	Crevasses
216-116	077°33'S. 065°45'W.	1569-10571	12 Feb 74	14		10	Crevasses
216-117	078°29'S. 071°08'W.	1569-10573	12 Feb 74	13		10	Korff Ice Rise
216-118	079°19'S. 077°23'W.	1569-10580	12 Feb 74	12		50	Kershaw Ice Rumples
216-119	080°01'S. 084°33'W.	1569-10582	12 Feb 74	11		70	Ellsworth Mountains
217-114	075°25'S. 058°35'W.						
217-115	076°31'S. 062°34'W.	1570-11022	13 Feb 74	15		10	Crevasses
217-116	077°33'S. 067°11'W.	1570-11025	13 Feb 74	14		5	Crevasses

TABLE 6.—*Optimum Landsat 1, 2, and 3 MSS and Landsat 2 RBV images of glaciers of Antarctica—Continued*

Path-Row	Nominal scene center (lat.—long.)	Landsat identification number	Date	Solar elev. angle (degrees)	Code	Cloud cover (percent)	Remarks
217-117	078°29'S. 072°34'W.	1570-11031	13 Feb 74	13	●	0	Korff Ice Rise
217-118	079°19'S. 078°49'W.	1570-11034	13 Feb 74	12	◐	25	Skytrain Ice Rise, Kershaw Ice Rumples
217-119	080°01'S. 085°59'W.	1516-11054	21 Dec 73	21	◐	60	Ellsworth Mountains
218-114	075°25'S. 060°01'W.				◑	100	
218-115	076°31'S. 064°00'W.	1571-11081	14 Feb 74	15	◐	25	Dodson Peninsula, crevasses
218-116	077°33'S. 068°37'W.	1571-11083	14 Feb 74	13	◐	70	Crevasses
218-117	078°29'S. 074°00'W.	1571-11090	14 Feb 74	12	◐	85	
218-118	079°19'S. 080°15'W.	1571-11092	14 Feb 74	11	◐	90	
218-119	080°01'S. 087°25'W.	1517-11112	22 Dec 73	21	◐	20	Ellsworth Mountains
219-113	074°16'S. 058°02'W.	1212-11180	20 Feb 73	15	◐	50	Lassiter Coast
219-114	075°25'S. 061°28'W.	1212-11183	20 Feb 73	14	◐	15	Wetmore Glacier, Bowman Peninsula
219-115	076°31'S. 065°26'W.	1212-11185	20 Feb 73	13	●	0	Orville Coast
219-116	077°33'S. 070°03'W.	1482-11162	17 Nov 73	21	◐	90	, Band 6
219-117	078°29'S. 075°26'W.	1482-11165,	17 Nov 73	20	◐	70	Band 6
219-118	079°19'S. 081°41'W.	1482-11171	17 Nov 73	19	◐	90	Band 6
219-119'	080°01'S. 088°51'W.				◉		
220-112	073°04'S. 056°29'W.				◉		
220-113	074°16'S. 059°28'W.				◑	100	
220-114	075°25'S. 062°54'W.				◉		
220-115	076°31'S. 066°52'W.				◉		
220-116	077°33'S. 071°29'W.				◑	100	
220-117	078°29'S. 076°52'W.				◑	100	
220-118	079°19'S. 083°07'W.	1555-11211	29 Jan 74	16	◐	75	Ellsworth Mountains
220-119	080°01'S. 090°17'W.	1555-11214	29 Jan 74	15	◐	75	

TABLE 6.—*Optimum Landsat 1, 2, and 3 MSS and Landsat 2 RBV images of glaciers of Antarctica—Continued*

Path-Row	Nominal scene center (lat.—long.)	Landsat identification number	Date	Solar elev. angle (degrees)	Code	Cloud cover (percent)	Remarks
221-112	073°04'S. 057°55'W.						
221-113	074°16'S. 060°54'W.	1538-11253	12 Jan 74	25		50	Lassiter Coast
221-114	075°25'S. 064°20'W.	1538-11260	12 Jan 74	24		50	Latady Mountains
221-115	076°31'S. 068°18'W.	1538-11262	12 Jan 74	23		75	Orville Coast
221-116	077°33'S. 072°55'W.	1538-11265	12 Jan 74	22		80	
221-117	078°29'S. 078°18'W.	1538-11271	12 Jan 74	21		75	
221-118	079°19'S. 084°33'W.	1538-11274	12 Jan 74	20		15	Ellsworth Mountains, Nimitz Glacier
221-119	080°01'S. 091°43'W.	1538-11280	12 Jan 74	19		10	Surface features
222-111	071°50'S. 056°45'W.					100	
222-112	073°04'S. 059°21'W.	30288-11233	18 Dec 78	28		0	Kemp Peninsula
222-113	074°16'S. 062°20'W.						
222-114	075°25'S. 065°46'W.						
222-115	076°31'S. 069°44'W.						
222-116	077°33'S. 074°21'W.						
222-117	078°29'S. 079°44'W.	1198-11423	06 Feb 73	15		10	Fowler Ice Rise, band 6
222-118	079°19'S. 085°59'W.						
222-119	080°01'S. 093°09'W.						
223-111	071°50'S. 058°11'W.						
223-112	073°04'S. 060°47'W.	1522-11370	27 Dec 73	29		70	Lassiter Coast
223-112	073°04'S. 060°46'W.	2284-11265	02 Nov 75	21		70	Lassiter Coast, scan lines missing
223-113	074°16'S. 063°46'W.	1522-11373	27 Dec 73	27		80	Lassiter Coast, Bowman Peninsula
223-114	075°25'S. 067°12'W.	1522-11375	27 Dec 73	26		80	Hauberg Mountains
223-115	076°31'S. 071°10'W.	1522-11382	27 Dec 73	25		75	Hauberg Mountains
223-116	077°33'S. 075°47'W.	1522-11384	27 Dec 73	24		95	

TABLE 6.—Optimum Landsat 1, 2, and 3 MSS and Landsat 2 RBV images of glaciers of Antarctica—Continued

Path-Row	Nominal scene center (lat.—long.)	Landsat identification number	Date	Solar elev. angle (degrees)	Code	Cloud cover (percent)	Remarks
223-117	078°29'S. 081°10'W.	1522-11391	27 Dec 73	23		90	Sentinel Range
223-118	079°19'S. 087°25'W.	1522-11393	27 Dec 73	22		95	
223-119	080°01'S. 094°35'W.	1558-11384	01 Feb 74	14		85	
224-110	070°35'S. 057°20'W.	1181-11450	20 Jan 73	27		50	
224-111	071°50'S. 059°37'W.	1181-11452	20 Jan 73	26		90	
224-112	073°04'S. 062°13'W.	1181-11455	20 Jan 73	25		90	
224-113	074°16'S. 065°12'W.	1181-11461	20 Jan 73	24		40	Lassiter Coast, nunataks
224-113	074°16'S. 065°12'W.	1505-11433	10 Dec 73	28		40	Lassiter Coast, Irvine Glacier
224-114	075°25'S. 068°38'W.	1505-11440	10 Dec 73	27		50	Hauberg Mountains, Sweeney Mountains
224-115	076°31'S. 072°36'W.	1505-11442	10 Dec 73	25		5	Evans Ice Stream
224-116	077°33'S. 077°13'W.	1559-11431	02 Feb 74	17		10	Fowler Ice Rise
224-117	078°29'S. 082°36'W.	1505-11451	10 Dec 73	23		75	Fletcher Ice Rise, Rutford Ice Stream
224-118	079°19'S. 088°51'W.	1505-11454	10 Dec 73	22		90	Nimitz Glacier, Ellsworth Mountains
224-119	080°01'S. 096°01'W.					100	
225-110	070°35'S. 058°46'W.						
225-111	071°50'S. 061°03'W.	30345-11402	13 Feb 79			30	Dyer Plateau
225-112	073°04'S. 063°39'W.	30345-11405	13 Feb 79			15	Carey Range, Meinardus Glacier
225-113	074°16'S. 066°38'W.					100	
225-114	075°25'S. 070°04'W.						
225-115	076°31'S. 074°02'W.						
225-116	077°33'S. 078°39'W.	1560-11485	03 Feb 74	17		5	Carlson Inlet
225-117	078°29'S. 084°02'W.	1560-11492	03 Feb 74	16		0	Fletcher Ice Rise, Ellsworth Mountains
225-118	079°19'S. 090°17'W.	1560-11494	03 Feb 74	15		20	Ellsworth Mountains
225-119	080°01'S. 097°27'W.	1560-11501	03 Feb 74	14		50	

TABLE 6.—*Optimum Landsat 1 ,2, and 3 MSS and Landsat 2 RBV images of glaciers of Antarctica — Continued*

Path-Row	Nominal scene center (lat.—long.)	Landsat identification number	Date	Solar elev. angle (degrees)	Code	Cloud cover (percent)	Remarks
226–109	069°17'S. 058°10'W.				☉		
226–110	070°35'S. 060°12'W..				☉		
226–111	071°50'S. 062°29'W.				☉		
226–112	073°04'S. 065°05'W.	1525–11541	30 Dec 73	28	☾	60	English Coast, nunataks
226–113	074°16'S. 068°04'W.	1164–11520	03 Jan 73	27	☾	95	Nunataks
226–114	075°25'S. 071°30'W.				☾	100	
226–115	076°31'S. 075°28'W.	1561–11541	04 Feb 74	18	●	0	Evans Ice Stream
226–116	077°33'S. 080°05'W.	1561–11543	04 Feb 74	17	●	0	Carlson Inlet, Fowler Ice Rise
226–117	078°29'S. 085°28'W.	1561–11550	04 Feb 74	15	●	0	Sentinel Range, Rutford Ice Stream
226–118	079°19'S. 091°43'W.	1561–11552	04 Feb 74	14	☾	20	Surface features
226–119	080°01'S. 098°53'W.	1561–11555	04 Feb 74	13	☾	80	Nunataks
227–108	067°59'S. 057°47'W.	1238–12020	18 Mar 73	11	☾	90	Ice front
227–109	069°17'S. 059°36'W.	2414–11462	11 Mar 76	11	☾	80	Larsen Ice Shelf, Gipps Ice Rise
227–110	070°35'S. 061°38'W.	30329–11513	28 Jan 79	24	☾	50	Hearst and Ewing Islands
227–111	071°50'S. 063°55'W.	30329–11515	28 Jan 79	23	☾	65	Dyer Plateau
227–112	073°04'S. 066°31'W.	30329–11522	28 Jan 79	22	☾	85	
227–113	074°16'S. 069°30'W.	1562–11590	05 Feb 74	19	☾	20	Nunatak, surface features
227–114	075°25'S. 072°56'W.	1562–11593	05 Feb 74	18	☾	15	Behrendt Mountains
227–114	075°25'S. 072°56'W.	1544–12001	18 Jan 74	23	☾	25	Behrendt Mountains
227–115	076°31'S. 076°54'W.	1562–11595	05 Feb 74	17	☾	10	Evans Ice Stream
227–116	077°33'S. 081°31'W.	1562–12002	05 Feb 74	16	●	0	Carlson Inlet, Fletcher Ice Rise
227–117	078°29'S. 086°54'W.	1562–12004	05 Feb 74	15	☾	15	Sentinel Range
227–118	079°19'S. 093°09'W.	1562–12011	05 Feb 74	14	☾	20	Surface features
227–119	080°01'S. 100°19'W.	1562–12013	05 Feb 74	13	☾	75	Mount Moore, Mount Woollard

TABLE 6.—*Optimum Landsat 1, 2, and 3 MSS and Landsat 2 RBV images of glaciers of Antarctica—Continued*

Path-Row	Nominal scene center (lat.—long.)	Landsat identification number	Date	Solar elev. angle (degrees)	Code	Cloud cover (percent)	Remarks
228-103	061°16'S. 052°24'W.				☉		
228-104	062°38'S. 053°32'W.	2055-11535	18 Mar 75	15	☾	90	
228-105	063°59'S. 054°45'W.	2055-11542	18 Mar 75	14	☾	60	
228-108	067°59'S. 059°13'W.	1473-12044	08 Nov 73	28	☾	60	Larsen Ice Shelf
228-109	069°17'S. 061°02'W.	1473-12051	08 Nov 73	27	☾	60	Larsen Ice Shelf, Gipps Ice Rise
228-110	070°35'S. 063°04'W.	1473-12053	08 Nov 73	26	☾	80	Ewing Island
228-111	071°50'S. 065°21'W.	1473-12060	08 Nov 73	25	☾	95	
228-112	073°04'S. 067°57'W.	1473-12062	08 Nov 73	23	☾	95	
228-113	074°16'S. 070°56'W.	1563-12045	06 Feb 74	19	☾	10	English Coast Nunataks, Sky-Hi Nunataks
228-114	075°25'S. 074°22'W.	1563-12051	06 Feb 74	18	☾	40	Behrendt Mountains
228-115	076°31'S. 078°20'W.	1563-12054	06 Feb 74	17	☾	80	Evans Ice Stream, Fowler Ice Rise
228-116	077°33'S. 082°57'W.	1221-12110	01 Mar 73	9	☾	90	
228-117	078°29'S. 088°20'W.				☉		
228-118	079°19'S. 094°35'W.	1492-12143,	27 Nov 73	21	☾	90	
228-119	080°01'S. 101°45'W.	1492-12145	27 Nov 73	19	☾	85	
229-103	061°16'S. 053°50'W.				☉		
229-104	062°38'S. 054°58'W.				☾	100	
229-105	063°59'S. 056°12'W.	2740-11454	31 Jan 77	27	☾	15	Joinville, Dundee, and Seymour Islands
229-106	065°20'S. 057°32'W.	2740-11461	31 Jan 77	26	●	0	James Ross and Snow Hill Islands, giant iceberg
229-107	066°40'S. 059°01'W.	1564-12080	07 Feb 74	25	☾	80	
229-108	067°59'S. 060°39'W.	1564-12082	07 Feb 74	24	☾	80	
229-109	069°17'S. 062°28'W.	1564-12085	07 Feb 74	23	☾	95	
229-110	070°35'S. 064°30'W.				☉		
229-111	071°50'S. 066°48'W.				☉		

TABLE 6.—Optimum Landsat 1, 2, and 3 MSS and Landsat 2 RBV images of glaciers of Antarctica—Continued

Path-Row	Nominal scene center Out.—long.)	Landsat identification number	Date	Solar elev. angle (degrees)	Code	Cloud cover (percent)	Remarks
229-112	073°04'S. 069°24'W.					100	
229-113	074°16'S. 072°22'W.					100	
229-114	075°25'S. 075°48'W.					100	
229-115	076°31'S. 079°46'W.	1204-12161	12 Feb 73	15		65	Evans Ice Stream, Fowler Ice Rise
229-116	077°33'S. 084°24'W.	1204-12163	12 Feb 73	14		70	Sentinel Range, Rutford Ice Stream
229-117	078°29'S. 089°46'W.					100	
229-118	079°19'S. 096°01'W.					100	
229-119	080°01'S. 103°12'W.						
230-103	061°16'S. 055°16'W.					100	
230-104	062°38'S. 056°24'W.					100	
230-105	063°59'S. 057°38'W.	2741-11513	01 Feb 77	27		75	Trinity Peninsula, James Ross Island
230-106	065°20'S. 058°58'W.	2741-11515	01 Feb 77	26		80	Larsen Ice Shelf
230-107	066°40'S. 060°27'W.						
230-108	067°59'S. 062°05'W.	2291-12051	09 Nov 75	27		90	Ice front
230-109	069°17'S. 063°54'W.	2291-12054	09 Nov 75	26		80	Wakefield Highland
230-110	070°35'S. 065°56'W.						
230-111	071°50'S. 068°14'W.						
230-112	073°04'S. 070°50'W.	1133-12203	03 Dec 72	28		80	Monteverdi Peninsula
230-113	074°16'S. 073°48'W.					100	
230-114	075°25'S. 077°14'W.					100	
230-115	076°31'S. 081°12'W.	1547-12174	21 Jan 74	21		5	Ellsworth Land
230-116	077°33'S. 085°50'W.	1547-12180	21 Jan 74	20		10	Sentinel Range, scan lines missing
230-117	078°29'S. 091°12'W.	1133-12224	03 Dec 72	23		5	Surface features
230-118	079°19'S. 097°27'W.						

TABLE 6.—*Optimum Landsat 1, 2, and 3 MSS and Landsat 2 RBV images of glaciers of Antarctica—Continued*

Path-Row	Nominal scene center (lat.—long.)	Landsat identification number	Date	Solar elev. angle (degrees)	Code	Cloud cover (percent)	Remarks
230-119	080°01'S. 104°38'W.						
231-103	061°16'S. 056°42'W.					100	
231-104	062°38'S. 057°50'W.					100	
231-105	063°59'S. 059°04'W.	30333-12122	01 Feb 79			75	James Ross Island, Detroit Plateau, partial image
231-106	065°20'S. 060°24'W.	30333-12124	01 Feb 79	27		75	Larsen Ice Shelf, melt ponds
231-107	066°40'S. 061°53'W.	2292-12103	10 Nov 75	29		90	Ice front
231-108	067°59'S. 063°31'W.					100	
231-109	069°17'S. 065°20'W.	30333-12140	01 Feb 79	24		90	Lurabee Glacier
231-110	070°35'S. 067°22'W.	1170-12251	09 Jan 73	29		30	George VI Ice Shelf, melt ponds
231-111	071°50'S. 069°40'W.	1170-12253	09 Jan 73	28		30	George VI Sound, melt ponds
231-112	073°04'S. 072°16'W.	1170-12260	09 Jan 73	27		10	Spaatz, DeAtley, and Eklund Islands
231-113	074°16'S. 075°14'W.	1170-12262	09 Jan 73	26		40	Stange Sound, FitzGerald Bluffs
231-114	075°25'S. 078°40'W.					100	
231-115	076°31'S. 082°38'W.					100	
231-116	077°33'S. 087°16'W.						
231-117	078°29'S. 092°38'W.						
231-118	079°19'S. 098°53'W.					100	
231-119	080°01'S. 106°04'W.	2310-12152	28 Nov 75	19		5	Marie Byrd Land
232-103	061°16'S. 058°08'W.	30352-12171	20 Feb 79	25		5	King George Island
232-104	062°38'S. 059°16'W.	30352-12173	20 Feb 79	24		50	Deception Island
232-105	063°59'S. 060°30'W.	30352-12180	20 Feb 79	23		30	Oscar II Coast, Larsen Ice Shelf
232-105	063°59'S. 060°30'W.	30244-12182	04 Nov 78	30		30	Bruce Plateau
232-106	065°20'S. 061°50'W.	30244-12184	04 Nov 78	28		50	Avery Plateau
232-107	066°40'S. 063°19'W.	1207-12300	15 Feb 73	23		95	

TABLE 6.—*Optimum Landsat 1, 2 and 3 MSS and Landsat 2 RBV images of glaciers of Antarctica—Continued*

Path-Row	Nominal scene center (lat.—long.)	Landsat identification number	Date	Solar elev. angle (degrees)	Code	Cloud cover (percent)	Remarks
232-108	067°59'S. 064°37'W.	1207-12303	15 Feb 73	22		95	
232-109	069°17'S. 066°47'W.					100	
232-110	070°35'S. 068°48'W.	1207-12312	15 Feb 73	20		90	George VI Sound, melt ponds
232-111	071°50'S. 071°06'W.						
232-112	073°04'S. 073°42'W.	1153-12315	23 Dec 72	29		75	Spaatz Island, band 6
232-113	074°16'S. 076°41'W.	1513-12292	18 Dec 73	28		70	Nunataks
232-114	075°25'S. 080°06'W.					100	
232-115	076°31'S. 084°05'W.	1153-12331	23 Dec 72	26		95	
232-116	077°33'S. 088°42'W.	1153-12333	23 Dec 72	24		60	Sentinel Range
232-116	077°33'S. 088°42'W.	1190-12392	29 Jan 73	18		45	Surface features
232-117	078°29'S. 094°05'W.	1190-12394	29 Jan 73	17		10	Surface features
232-118	079°19'S. 100°20'W.						
232-119	080°01'S. 107°30'W.					100	
233-104	062°38'S. 060°42'W.	1208-12343	16 Feb 73	26		70	South Shetland Islands
233-105	063°59'S. 061°56'W.	1208-12350	16 Feb 73	25		60	Trinity Island
233-105	063°59'S. 061°56'W.	1532-12311	06 Jan 74	34		50	Palmer Archipelago
233-105	063°59'S. 061°56'W.	30317-12235	16 Jan 79	32		70	Davis Coast
233-106	065°20'S. 063°16'W.	1208-12352	16 Feb 73	24		70	Anvers Island
233-106	065°20'S. 063°16'W.	1532-12314	06 Jan 74	33		70	Anvers Island
233-106	065°20'S. 063°16'W.	30299-12241	29 Dec 78	34		75	Graham Coast
233-107	066°40'S. 064°45'W.	1532-12320	06 Jan 74	32		65	Loubet Coast
233-108	067°59'S. 066°23'W.	1532-12323	06 Jan 74	31		50	Mercator Ice Piedmont
233-108	067°59'S. 066°23'W.	30299-12250	29 Dec 78	32		60	Pourquoi Pas Island
233-109	069°17'S. 068°13'W.	1532-12325	06 Jan 74	30		0	Wordie Ice Shelf

TABLE 6.—*Optimum Landsat 1, 2, and 3 MSS and Landsat 2 RBV images of glaciers of Antarctica—Continued*

Path-Row	Nominal scene center (lat.—long.)	Landsat identification number	Date	Solar elev. angle (degrees)	Code	Cloud cover (percent)	Remarks
233-109	069°17'S. 068°13'W.	30335-12253	03 Feb 79	24		20	Wordie Ice Shelf
233-110	070°35'S. 070°14'W.	30335-12255	03 Feb 79	23		60	Alexander Island'
233-111	071°50'S. 072°32'W.	1190-12371	29 Jan 73	24		25	Beethoven Peninsula, melt ponds
233-112	073°04'S. 075°08'W.	1190-12374	29 Jan 73	23		20	Spaatz and DeAtley Islands
233-113	074°16'S. 078°07'W.	1190-12380	29 Jan 73	22		70	Case Island
233-113	074°16'S. 078°07'W.	1136-12381	06 Dec 72	27		80	
233-114	075°25'S. 081°32'W.	1568-12335	11 Feb 74	17		25	Surface features
233-115	076°31'S. 085°31'W.	1568-12341	11 Feb 74	15		5	Upper Rutford Ice Stream
233-116	077°33'S. 090°08'W.	1568-12344	11 Feb 74	14		0	Sentinel Range
233-117	078°29'S. 095°31'W.	1568-12350	11 Feb 74	13		10	Surface features
233-118	079°19'S. 101°46'W.	1568-12353	11 Feb 74	12		60	
233-119	080°01'S. 108°56'W.						
234-104	062°38'S. 062°08'W.	1209-12402	17 Feb 73	26		50	Smith Island
234-105	063°59'S. 063°22'W.	1209-12404	17 Feb 73	25		30	Brabant Island
234-105	063°59'S. 063°22'W.	1173-12401	12 Jan 73	34		70	Anvers Island
234-105	063°59'S. 063°22'W.	30300-12293	30 Dec 78	35		50	Anvers Island
234-106	065°20'S. 064°42'W.	1173-12403	12 Jan 73	33		40	Bruce Plateau
234-107	066°40'S. 066°11'W.	1173-12410	12 Jan 73	32		60	Avery Plateau
234-107	066°40'S. 066°11'W.	1209-12413	17 Feb 73	22		50	Biscoe Islands
234-108	067°59'S. 067°49'W.	1173-12412	12 Jan 73	31		85	
234-109	069°17'S. 069°39'W.	1173-12415	12 Jan 73	30		80	Alexander Island
234-110	070°35'S. 071°40'W.	1173-12421	12 Jan 73	29		90	Colbert Mountains, Mount Alfred
234-111	071°50'S. 073°58'W.					100	
234-112	073°04'S. 076°34'W.						

TABLE 6.—*Optimum Landsat 1, 2, and 3 MSS and Landsat 2 RBV images of glaciers of Antarctica—Continued*

Path-Row	Nominal scene center Lat.—long.)	Landsat identification number	Date	Solar elev. angle (degrees)	Code	Cloud cover (percent)	Remarks
234-113	074°16'S. 079°33'W.				☉		
234-114	075°25'S. 082°58'W.				☉		
234-115	076°31'S. 086°57'W.				☾	100	
234-116	077°33'S. 091°34'W.	1173-12444	12 Jan 73	22	☾	15	Surface features
234-117	078°29'S. 096°57'W.				☉		
234-118	079°19'S. 103°12'W.				☉		
234-119	080°01'S. 110°22'W.				☉		
235-104	062°38'S. 063°34'W.				☉		
235-105	063°59'S. 064°48'W.	30283-12351	13 Dec 78	36	●	0	Anvers Island
235-106	065°20'S. 066°08'W.	30283-12354	13 Dec 78	35	☾	40	Renaud Island
235-107	066°40'S. 067°37'W.	30283-12360	13 Dec 78	34	☾	30	Loubet Coast
235-108	067°59'S. 069°15'W.	30283-12363	13 Dec 78	32	☾	60	Pourquoi Pas Island
235-109	069°17'S. 071°05'W.	30283-12365	13 Dec 78	31	☾	40	Alexander and Rothschild Islands
235-110	070°35'S. 073°06'W.				☉		
235-111	071°50'S. 075°24'W.				☉		
235-112	073°04'S. 078°00'W.	1173-12430	12 Jan 73	26	☾	50	Berg Ice Stream, Rydberg Peninsula
235-113	074°16'S. 080°59'W.	1173-12433	12 Jan 73	25	☾	15	Wirth Peninsula, Mount Tuve
235-114	075°25'S. 084°24'W.	1173-12435	12 Jan 73	24	☾	15	Surface features
235-115	076°31'S. 088°23'W.	1173-12442	12 Jan 73	23	☾	15	Sentinell Range
235-116	077°33'S. 093°00'W.	1570-12461	13 Feb 74	14	☾	80	Surface features
235-117	078°29'S. 098°23'W.	1570-12463	13 Feb 74	13	☾	85	
235-118	079°19'S. 104°38'W.	1570-12470	13 Feb 74	12	☾	90	
235-119	080°01'S. 111°48'W.	1570-12472	13 Feb 74	10	☾	70	
236-106	065°20'S. 067°34'W.	1535-12485	09 Jan 74	33	☾	80	

TABLE 6.—*Optimum Landsat 1, 2, and 3 MSS and Landsat 2 RBV images of glaciers of Antarctica—Continued*

Path-Row	Nominal scene center (lat.-long.)	Landsat identification number	Date	Solar elev. angle (degrees)	Code	Cloud cover (percent)	Remarks
236-107	066°40'S. 069°03'W.	30284-12414	14 Dec 78	34	●	5	Lavoisier Island, Adelaide Island
236-108	067°59'S. 070°42'W.	30284-12421	14 Dec 78	33	●	0	Adelaide Island
236-108	067°59'S. 070°42'W.	2027-12414	18 Feb 75	20	◐	15	Alexander Island
236-109	069°17'S. 072°31'W.	2027-12420	18 Feb 75	19	◐	40	Alexander and Rothschild Islands
236-109	069°17'S. 072°31'W.	1535-12500	09 Jan 74	30	●	0	Alexander and Rothschild Islands
236-110	070°35'S. 074°33'W.	2027-12423	18 Feb 75	18	◐	50	Latady and Charcot Islands
236-110	070°35'S. 074°33'W.	1121-12541	21 Nov 72	29	◐	30	Wilkins Ice Shelf
236-111	071°50'S. 076°50'W.	2027-12425	18 Feb 75	17	◐	30	Beethoven Peninsula and Smyley Islands, scan lines missing
236-111	071°50'S. 076°50'W.	1139-12543	09 Dec 72	30	◐	20	
236-112	073°04'S. 079°26'W.	2027-12432	18 Feb 75	16	◐	30	Berg Ice Stream, Rydberg and Wirth Peninsulas
236-113	074°16'S. 082°25'W.	2027-12434	18 Feb 75	15	◐	60	Eltanin Bay, Bryan Coast
236-114	075°25'S. 085°51'W.	1121-12555	21 Nov 72	24	◐	50	
236-115	076°31'S. 089°49'W.	1481-12533	16 Nov 73	22	◐	60	
236-115	076°31'S. 089°49'W.	1139-12561	09 Dec 72	25	◐	50	Surface features
236-116	077°33'S. 094°26'W.				⊙		
236-117	078°29'S. 099°49'W.				⊙		
236-118	079°19'S. 106°04'W.	1499-12543	04 Dec 73	21	◐	90	Scan lines missing
236-119	080°01'S. 113°14'W.	1499-12550	04 Dec 73	20	◐	20	Surface features
237-108	067°59'S. 072°08'W.	1536-12552	10 Jan 74	31	●	0	Northern tip of Alexander Island
237-109	069°17'S. 073°57'W.	1536-12554	10 Jan 74	30	◐	40	Bongrain Ice Piedmont, Alexander Island
237-110	070°35'S. 075°59'W.	1536-12561	10 Jan 74	29	◐	50	Charcot and Latady Island
237-111	071°50'S. 078°16'W.	1536-12563	10 Jan 74	28	●	5	Smyley Island
237-112	073°04'S. 080°52'W.	1482-12580	17 Nov 73	26	●	5	Rydberg and Wirth Peninsulas, scan lines missing
237-113	074°16'S. 083°51'W.	1176-13004	15 Jan 73	25	◐	40	Bryan Coast

TABLE 6.—*Optimum Landsat 1, 2, and 3 MSS and Landsat 2 RBV images of glaciers of Antarctica—Continued*

Path-Row	Nominal scene center (lat.—long.)	Landsat identification number	Date	Solar elev. angle (degrees)	Code	Cloud cover (percent)	Remarks
237-114	075°25'S. 087°17'W.	1176-13010	15 Jan 73	24		15	Surface features
237-115	076°31'S. 091°15'W.	1176-13013	15 Jan 73	23		5	Surface features
237-116	077°33'S. 095°52'W.	1176-13015	15 Jan 73	22		0	Surface features
237-117	078°29'S. 101°15'W.	1139-12570	09 Dec 72	23		20	
237-118	079°19'S. 107°30'W.	1518-13000	23 Dec 73	22		25	
237-119	080°01'S. 114°40'W.	1518-13002	23 Dec 73	21		90	
238-109	069°17'S. 075°23'W.	1537-13013	11 Jan 74	30		15	Charcot Island
238-110	070°35'S. 077°25'W.	1537-13015	11 Jan 74	29		40	Western end of Smyley Island
238-111	071°50'S. 079°42'W.	1537-13022	11 Jan 74	27		5	Smyley Island
238-112	073°04'S. 082°18'W.						
238-113	074°16'S. 085°17'W.						
238-114	075°25'S. 088°43'W.						
238-115	076°31'S. 092°41'W.						
238-116	077°33'S. 097°18'W.					100	
238-117	078°29'S. 102°41'W.	1519-13052	24 Dec 73	23		60	Scan lines missing
238-118	079°19'S. 108°56'W.						
238-119	080°01'S. 116°06'W.						
239-109	069°17'S. 076°49'W.	1124-13105	24 Nov 72	31		90	
239-111	0071°50'S. 081°08'W.					100	
239-112	073°04'S. 083°44'W.	1124-13121	24 Nov 72	27		90	
239-113	074°16'S. 086°43'W.	1538-13085	12 Jan 74	25		25	Surface features
239-114	075°25'S. 090°09'W.	1538-13091	12 Jan 74	24		40	Surface features
239-115	076°31'S. 094°07'W.	1538-13094	12 Jan 74	23		60	Surface features
239-116	077°33'S. 098°44'W.	1538-13100	12 Jan 74	22		20	

TABLE 6.—*Optimum Landsat 1, 2, and 3 MSS and Landsat 2 RBV images of glaciers of Antarctica— Continued*

Path-Row	Nominal scene center (lat.—long.)	Landsat identification number	Date	Solar elev. angle (degrees)	Code	Cloud cover (percent)	Remarks
239-117	078°29'S. 104°07'W.	1538-13103	12 Jan 74	21		75	
239-118	079°19'S. 110°22'W.					100	
239-119	080°01'S. 117°32'W.	1538-13112	12 Jan 74	19		95	
240-112	073°04'S. 085°10'W.	1557-13132	31 Jan 74	22		60	Bryan Coast, Allison Peninsula, Venable Ice Shelf
240-113	074°16'S. 088°09'W.	1179-13180	18 Jan 73	24		60	Surface features
240-114	075°25'S. 091°35'W.	1557-13141	31 Jan 74	20		20	Surface features
240-115	076°31'S. 095°33'W.	1557-13144	31 Jan 74	19		0	Surface features
240-116	077°33'S. 100°10'W.	1521-13162	26 Dec 73	24		60	
240-117	078°29'S. 105°33'W.	1521-13164	26 Dec 73	23		75	
240-118	079°19'S. 111°48'W.	2301-13064	19 Nov 75	18		50	Band 6
240-119	080°01'S. 118°58'W.	2301-13070	19 Nov 75	17		30	Surface features
241-112	073°04'S. 086°36'W.						
241-113	074°16'S. 089°35'W.						
241-114	075°25'S. 093°01'W.	1540-13204,	14 Jan 74	24		85	
241-115	076°31'S. 096°59'W.	1540-13210	14 Jan 74	23		70	
241-116	077°33'S. 101°36'W.	1540-13213	14 Jan 74	22		85	
241-117	078°29'S. 106°59'W.					100	
241-118	079°19'S. 113°14'W.					100	
241-119	080°01'S. 120°24'W.					100	
242-112	073°04'S. 088°02'W.					100	
242-113	074°16'S. 091°01'W.	1199-13295	07 Feb 73	19		5	Farwell Island
242-114	075°25'S. 094°27'W.	1199-13301	07 Feb 73	18		10	Surface features
242-115	076°31'S. 098°25'W.	1199-13304	07 Feb 73	17		10	Surface features
242-116	077°33'S. 103°02'W.	1199-13310	07 Feb 73	16		75	

TABLE 6.—*Optimum Landsat 1, 2, and 3 MSS and Landsat 2 RBV images of glaciers of Antarctica—Continued*

Path-Row	Nominal scene center (lat.-long.)	Landsat identification number	Date	Solar elev. angle (degrees)	Code	Cloud cover (percent)	Remarks
242-117	078°29'S. 108°25'W.	1199-13313	07 Feb 73	15		95	
242-118	079°19'S. 114°40'W.						
242-119	080°01'S. 121°50'W.						
243-112	073°04'S. 089°28'W.	1182-13345	21 Jan 73	25		30	Fletcher Peninsula, Farwell Island, Abbot and Venable Ice Shelves
243-113	074°16'S. 092°27'W.	1182-13351	21 Jan 73	24		10	Jones Mountains
243-114	075°25'S. 095°53'W.	1542-13320	16 Jan 74	23		0	Upper Pine Island Glacier
243-115	076°31'S. 099°51'W.	1182-13360	21 Jan 73	22		50	Upper Pine Island Glacier
243-116	077°33'S. 104°28'W.						
243-117	078°29'S. 109°51'W.						
243-118	079°19'S. 116°06'W.						
243-119	080°01'S. 123°16'W.						
244-111	071°50'S. 088°18'W.						
244-112	073°04'S. 090°54'W.						
244-113	074°16'S. 093°53'W.	1543-13372	17 Jan 74	24		20	Jones Mountains
244-114	075°25'S. 097°19'W.	1543-13374	17 Jan 74	23		35	Hudson Mountains
244-115	076°31'S. 101°17'W.						
244-116	077°33'S. 105°54'W.						
244-117	078°29'S. 111°17'W.						
244-118	079°19'S. 117°32'W.						
244-119	080°01'S. 124°42'W.						
245-111	071°50'S. 089°44'W.					100	
245-112	073°04'S. 092°20'W.					100	
245-113	074°16'S. 095°19'W.	1544-13430	18 Jan 74	24		70	Jones Mountains
245-114	075°25'S. 098°45'W.	31427-13365	30 Jan 82	20		20	Upper Pine Island Glacier, partial image

TABLE 6. —Optimum Landsat 1, 2, and 3 MSS and Landsat 2 RBV images of glaciers of Antarctica —Continued

Path-Row	Nominal scene center (lat.—long.)	Landsat identification number	Date	Solar elev. angle (degrees)	Code	Cloud cover (percent)	Remarks
245-115	076°31'S. 102°43'W.	1544-13435	18 Jan 74	22		10	Walgreen Coast
245-116	077°33'S. 107°20'W.	1544-13441	18 Jan 74	21		90	
245-117	078°29'S. 112°43'W.						
245-118	079°19'S. 118°58'W.						
245-119	080°01'S. 126°08'W.						
246-111	071°50'S. 091°11'W.					100	
246-112	073°04'S. 093°47'W.					100	
246-113	074°16'S. 096°45'W.	31428-13421	31 Jan 82			0	Hudson Mountains, partial image
246-114	075°25'S. 100°11'W.	1185-13530	24 Jan 73	22		10	Pine Island Glacier, Hudson Mountains
246-115	076°31'S. 104°09'W.	1185-13532	24 Jan 73	21		50	Surface features
246-116	077°33'S. 108°47'W.	1185-13535	24 Jan 73	20		80	
246-117	078°29'S. 114°09'W.	1185-13541	24 Jan 73	19		95	
246-118	079°19'S. 120°24'W.						
246-119	080°01'S. 127°35'W.						
247-109	069°17'S. 088°17'W.	1168-13563	07 Jan 73	30		0	Peter I Island
247-111	071°50'S. 092°37'W.	1168-13572	07 Jan 73	28		10	Abbot Ice Shelf, Lofgren Peninsula
247-112	073°04'S. 095°13'W.	1168-13574	07 Jan 73	27		25	Dustin Island, Abbot Ice Shelf
247-113	074°16'S. 098°11'W.	1168-13581	07 Jan 73	26		75	
247-114	075°25'S. 101°37'W.	31375-13471	09 Dec 81	26		40	Pine Island Glacier, partial image
247-115	076°31'S. 105°35'W.						
247-116	077°33'S. 110°13'W.	1205-14053	13 Feb 73	14		5	Surface features
247-117	078°29'S. 115°35'W.						
247-118	079°19'S. 121°50'W.						
247-119	080°01'S. 129°01'W.						

TABLE 6.—*Optimum Landsat 1, 2, and 3 MSS and Landsat 2 RBV images of glaciers of Antarctica—Continued*

Path-Row	Nominal scene center (lat.—long.)	Landsat identification number	Date	Solar elev. angle (degrees)	Code	Cloud cover (percent)	Remarks
248-109	069°17'S. 089°43'W.						
248-111	071°50'S. 094°03'W.					100	
248-112	073°04'S. 096°39'W.	1205-14035	13 Feb 73	18		95	
248-113	074°16'S. 099°37'W.	31412-13533	15 Jan 82	24		10	Hudson Mountains, partial image
248-114	075°25'S. 103°03'W.	31412-13535	15 Jan 82	23		0	Pine Island Glacier, partial image
248-115	076°31'S. 107°01'W.	1205-14044	13 Feb 73	16		30	Walgreen Coast
248-115	076°31'S. 107°01'W.	1205-14051	13 Feb 73	15		10	Thwaites Glacier
248-116	077°33'S. 111°39'W.						
248-117	078°29'S. 117°01'W.						
248-118	079°19'S. 123°16'W.						
248-119	080°01'S. 130°27'W.						
249-109	069°17'S. 091°09'W.	1134-14082	04 Dec 72	32		50	Peter I Island
249-II 1	071°50'S. 095°29'W.	1134-14091	04 Dec 72	30		0	Thurston Island
249-112	073°04'S. 098°05'W.	2022-13575	13 Feb 75	17		80	Eights Coast
249-113	074°16'S. 101°03'W.	2022-13582	13 Feb 75	16		50	Canisteo Peninsula
249-114	075°25'S. 104°29'W.	2022-13584	13 Feb 75	15		85	Walgreen Coast
249-115	076°31'S. 108°27'W.						
249-116	077°33'S. 113°05'W.						
249-117	078°29'S. 118°27'W.						
249-118	079°19'S. 124°42'W.						
249-119	080°01'S. 131°53'W.						
250-109	069°17'S. 092°36'W.						
250-111	071°50'S. 096°55'W.					100	
250-112	073°04'S. 099°31'W..					100	

TABLE 6.—*Optimum Landsat 1,2, and 3 MSS and Landsat 2 RBV images of glaciers of Antarctica—Continued*

Path-Row	Nominal scene center (lat.—long.)	Landsat identification number	Date	Solar elev. angle (degrees)	Code	Cloud cover (percent)	Remarks
250–113	074°16'S. 102°30'W.	31396–14044	30 Dec 81	26		70	Partial image
250–114	075°25'S. 105°55'W.	31378–14043	12 Dec 81	26		0	Partial image
250–115	076°31'S. 109°54'W.						
250–116	077°33'S. 114°31'W.						
250–117	078°29'S. 119°54'W.						
250–118	079°79'S. 126°09'W.						
250–119	080°01'S. 133°19'W.						
251–109	069°17'S. 094°02'W.					100	
251–111	071°50'S. 098°21'W.						
251–112	073°04'S. 100°57'W.	31379–14093	13 Dec 81	28		10	Cosgrove Ice Shelf, partial image
251–113	074°16'S. 103°56'W.	31379–14095	13 Dec 81	27		0	Cranton and Pine Island Bays, partial image
251–114	075°25'S. 107°21'W.	1154–14214	24 Dec 72	27		70	Thwaites Glacier
251–115	076°31'S. 111°20'W.	1154–14221	24 Dec 72	25		90	
251–116	077°33'S. 115°57'W.					100	
251–117	078°29'S. 121°20'W.						
251–118	079°19'S. 127°35'W.						
251–119	080°01'S. 134°45'W.						

TABLE 7.—*Usable or marginally usable Landsat 3 RBV images of glaciers of Antarctica*

[For explanation of code, see section entitled "Tables of Optimum Landsat 1, 2, and 3 Images of Antarctica"]

Path-Row	Nominal scene center (lat.-long.)	Landsat identification number	Subscene	Date	Solar elev. angle (degrees)	Code	Remarks
001-113	074°16'S. 105°22'W.	31848-14191	C	27 Mar 83	2	G 25	Thwaites Glacier Tongue, Marie Byrd Land
001-113	074°16'S. 105°22'W.	31848-14191	D	27 Mar 83	2	M 25	
001-114	075°25'S. 108°47'W.	31848-14194	C	27 Mar 83	1	M 25	
004-117	078°29'S. 127°04'W.	31671-14381	C	01 Oct 82	4	M 25	
007-115	076°31'S. 121°22'W.	31782-14541	D	20 Jan 83	22	M 25	
009-113	074°16'S. 116°50'W.	31748-15051	A	17 Dec 82	27	M 25	
009-113	074°16'S. 116°50'W.	31748-15051	B	17 Dec 82	27	M 50	
010-113	074°16'S. 118°16'W.	31677-15110	B	07 Oct 82	11	G 50	Martin Peninsula, Marie Byrd Land
010-113	074°16'S. 118°16'W.	31677-15110	C	07 Oct 82	11	M 25	
010-113	074°16'S. 118°16'W.	31677-15110	D	07 Oct 82	11	M 25	
010-115	076°31'S. 125°40'W.	31677-15115	D	07 Oct 82	9	G 50	Executive Committee Range, Marie Byrd Land
010-116	077°33'S. 130°17'W.	31677-15121	B	07 Oct 82	8	G 25	Executive Committee Range, Marie Byrd Land
027-118	079°19'S. 166°18'W.	31802-16502	B	09 Feb 83	13	M 25	
027-119	080°01'S. 173°28'W.	31802-16505	B	09 Feb 83	12	M 50	
032-116	077°33'S. 161°51'W.	31753-17181	D	22 Dec 82	24	M 25	
046-116	077°33'S. 178°05'E.	31677-18384	C	07 Oct 82	8	G 25	Ice front
046-116	077°33'S. 178°05'E.	31677-18384	D	07 Oct 82	8	G 25	Ice front
046-117	078°29'S. 172°42'E.	31677-18391	A	07 Oct 82	6	G 50, M 25	Ice front
046-117	078°29'S. 172°42'E.	31677-18391	B	07 Oct 82	6	M 25	
046-118	079°19'S. 166°27'E.	31677-18393	A	07 Oct 82	5	G 100	Minna Bluff, Victoria Land
046-118	079°19'S. 166°27'E.	31677-18393	C	07 Oct 82	5	G 25, M 25	Moore Embayment, Ross Ice Shelf
046-119	080°01'S. 159°17'E.	31677-18400	A	07 Oct 82	4	G 75, M 25	Mouth of Mulock Glacier, Victoria Land
046-119	080°01'S. 159°17'E.	31677-18400	B	07 Oct 82	4	G 25	Ross Ice Shelf
046-119	080°01'S. 159°17'E.	31677-18400	C	07 Oct 82	4	G 100	Brown Hills, Antarctic Mountains

TABLE 7.— Usable or marginally usable Landsat 3 RBV images of glaciers of Antarctica—Continued

Path-Row	Nominal scene center (lat.—long.)	Landsat identification number	Subscene	Date	Solar elev. angle (degrees)	Code	Remarks
046-119	080°01'S. 159°17'E.	31677-18400	D	07 Oct 82	4	G 100	Mouth of Byrd Glacier
057-115	076°31'S. 166°55'E.	30356-19381	D	24 Feb 79	11	M 25	
057-116	077°33'S. 162°18'E.	30356-19383	A	24 Feb 79	10	G 25, M 25	Scott Coast, Victoria Land
057-116	077°33'S. 162°18'E.	30356-19383	B	24 Feb 79	10	M 50	
057-116	077°33'S. 162°18'E.	30356-19383	C	24 Feb 79	10	G 75	'Dry valleys', Victoria Land
057-116	077°33'S. 162°18'E.	30356-19383	D	24 Feb 79	10	G 75	Ferrar Glacier, Victoria Land
057-117	078°29'S. 156°55'E.	30356-19390	A	24 Feb 79	9	M 25	
057-117	078°29'S. 156°55'E.	30356-19390	B	24 Feb 79	9	M 25	
057-117	078°29'S. 156°55'E.	30356-19390	C	24 Feb 79	9	M 25	
057-117	078°29'S. 156°55'E.	30356-19390	D	24 Feb 79	9	G 25	Boomerang Range, Transantarctic Mountains
058-116	077°33'S. 160°52'E.	31671-19473	C	01 Oct 82	5	G 25	Mount Bastion, Transantarctic Mountains
058-116	077°33'S. 160°52'E.	31671-19473	D	01 Oct 82	5	G 25	Taylor Glacier, Victoria Land
063-110	070°35'S. 173°35'E.	30992-19571	C	21 Nov 80	27	M 25	Cape Adare, Victoria Land
063-111	071°50'S. 171°18'E.	30992-19574	B	21 Nov 80	25	M 50	
063-111	071°50'S. 171°18'E.	30992-19574	D	21 Nov 80	25	M 50	
063-112	073°04'S. 168°42'E.	30992-19580	B	21 Nov 80	24	M 75	
063-112	073°04'S. 168°42'E.	30992-19580	D	21 Nov 80	24	M 75	
063-113	074°16'S. 165°43'E.	30992-19583	A	21 Nov 80	23	M 75	
063-113	074°16'S. 165°43'E.	30992-19583	B	21 Nov 80	23	M 50	
063-113	074°16'S. 165°43'E.	30992-19583	D	21 Nov 80	23	M 75	
070-110	070°35'S. 163°33'E.	30963-20365	B	23 Oct 80	19	M 50	
070-110	070°35'S. 163°33'E.	30963-20365	C	23 Oct 80	19	M 50	
070-110	070°35'S. 163°33'E.	30963-20365	D	23 Oct 80	19	M 100	
070-110	070°35'S. 163°33'E.	30945-20374	B	05 Oct 80	13	M 25	

TABLE 7.—Usable or marginally usable Landsat 3 RBV images of glaciers of Antarctica—Continued

Path-Row	Nominal scene center, Lat.—long.)	Landsat identification number	Subscene	Date	solar elev. angle (degrees)	Code	Remarks
070-110	070°35'S. 163°33'E.	30945-20374	D	05 Oct 80	13	G 50, M 25	Everett Range, Victoria Land
070-110	070°35'S. 163°33'E.	30927-20382	A	17 Sep 80	6	G 100	Sputnik Island, Victoria Land
070-110	070°35'S. 163°33'E.	30927-20382	B	17 Sep 80	6	G 100	Cape Williams, Victoria Land
070-110	070°35'S. 163°33'E.	30927-20382	C	17 Sep 80	6	G 100	Cape Cheetham, Victoria Land
070-110	070°35'S. 163°33'E.	30927-20382	D	17 Sep 80	6	G 100	Lillie Glacier, Victoria Land
071-110	070°35'S. 162°07'E.	30982-20422	D	11 Nov 80	25	M 50	
071-110	070°35'S. 162°07'E.	30964-20424	B	24 Oct 80	20	M 50	
071-110	070°35'S. 162°07'E.	30964-20424	C	24 Oct 80	20	M 25	
071-110	070°35'S. 162°07'E.	30964-20424	D	24 Oct 80	20	M 75	
071-110	070°35'S. 162°07'E.	30946-20432	A	06 Oct 80	13	M 25	
071-110	070°35'S. 162°07'E.	30946-20432	B	06 Oct 80	13	G 25	Victoria Land
071-110	070°35'S. 162°07'E.	30946-20432	C	06 Oct 80	13	M 25	
071-110	070°35'S. 162°07'E.	30946-20432	D	06 Oct 80	13	G 25, M 50	Bowers Mountains, Victoria Land
071-110	070°35'S. 162°07'E.	30928-20440	A	18 Sep 80	6	G 100	Cape Cheetham, Victoria Land
071-110	070°35'S. 162°07'E.	30928-20440	B	18 Sep 80	6	G 100	Sputnik Island, Victoria Land
071-110	070°35'S. 162°07'E.	30928-20440	C	18 Sep 80	6	G 100	Rennick Glacier, Victoria Land
071-110	070°35'S. 162°07'E.	30928-20440	D	18 Sep 80	6	G 100	Bowers Mountains, Victoria Land
073-107	066°40'S. 164°44'E.	30966-20524	C	26 Oct 80	24	M 25	Buckle Island
073-107	066°40'S. 164°44'E.	30966-20524	D	26 Oct 80	24	M 25	
073-107	066°40'S. 164°44'E.	30912-20544	C	02 Sep 80	3	G 25	Buckle Island
073-108	067°59'S. 163°05'E.	30912-20551	A	02 Sep 80	2	G 25	Buckle Island
073-108	067°59'S. 163°05'E.	30912-20551	B	02 Sep 80	2	G 25	Sturge Island
073-109	069°17'S. 161°16'E.	31848-21104	C	27 Mar 83	6	M 25	
073-109	069°17'S. 161°16'E.	30930-20550	C	20 Sep 80	8	M 25	

TABLE 7.—Usable or marginally usable Landsat 3 RBV images of glaciers of Antarctica—Continued

Path-Row	Nominal scene center (lat.—long.)	Landsat identification number	Subscene	Date	Solar elev. angle (degrees)	Code	Remarks
073-110	070°35'S. 159°14'E.	31848-21110	A	27 Mar 83	5	G 50	Wilson Hills, Victoria Land
073-110	070°35'S. 159°14'E.	31848-21110	C	27 Mar 83	5	M 25	
073-110	070°35'S. 159°14'E.	30966-20540	B	26 Oct 80	20	M 25	
073-110	070°35'S. 159°14'E.	30966-20540	D	26 Oct 80	20	M 25	
073-110	070°35'S. 159°14'E.	30930-20552	A	20 Sep 80	7	G 25	Wilson Hills, Victoria Land
073-110	070°35'S. 159°14'E.	30930-20552	B	20 Sep 80	7	G 25	Rennick Glacier, Victoria Land
073-110	070°35'S. 159°14'E.	30930-20552	C	20 Sep 80	7	G 75	Surface features, Victoria Land
073-110	070°35'S. 159°14'E.	30930-20552	D	20 Sep 80	7	G 75	Harlin Glacier, Lovejoy Glacier, Victoria Land
073-110	070°35'S. 159°14'E.	30912-20560	A	02 Sep 80	0	G 25, M 50	Wilson Hills, Victoria Land
073-110	070°35'S. 159°14'E.	30912-20560	B	02 Sep 80	0	M 50	
073-110	070°35'S. 159°14'E.	30912-20560	D	02 Sep 80	0	M 75	
075-107	066°40'S. 161°52'E.	30968-21040	B	28 Oct 80	24	M 25	
075-107	066°40'S. 161°52'E.	30968-21040	D	28 Oct 80	24	M 25	
075-107	066°40'S. 161°52'E.	30932-21053	B	22 Sep 80	11	M 25	
075-107,	066°40'S. 161°52'E.	30932-21053	D	22 Sep 80	11	M 25	
075-107'	066°40'S. 161°52'E.	30914-21061	D	04 Sep 80	4	, G 25	Buckle Island
075-109	069°17'S. 158°24'E.	30950-21054	C	10 Oct 80	16	M 25	
075-109	069°17'S. 158°24'E.	30950-21054	D	10 Oct 80	16	M 25	
075-109	069°17'S. 158°24'E.	30914-21070	C	04 Sep 80	2	G 50, M 25	Matusevich Glacier, Victoria Land
075-109	069°17'S. 158°24'E.	30914-21070	D	04 Sep 80	2	G 50, M 25	Tomilin Glacier, Victoria Land
075-110	070°35's. 156°22'E.	30914-21072	A	04 Sep 80	1	G 50	Upper Matusevich Glacier, Victoria Land
075-110	070°35'S. 156°22'E.	30914-21072	B	04 Sep 80	1	G 75	Wilson Hills, Victoria Land
076-109	069°17'S. 156°58'E.	31851-21275	C	30 Mar 83	5	G 50	Victoria Land
076-113	074°16'S. 147°04'E.	31671-21293	C	01 Oct 82	9	M 50	

TABLE 7.— Usable or marginally usable Landsat 3 RBV images of glaciers of Antarctica—Continued

Path-Row	Nominal scene center (lat.—long.)	Landsat identification number	Subscene	Date	Solar elev. angle (degrees)	Code	Remarks
076—113	074°16'S. 147°04'E.	31671—21293	D	01 Oct 82	9	M 25	
076—114	075°25'S. 143°38'E.	31671—21300	A	01 Oct 82	8	M 50	
076—114	075°25'S. 143°38'E.	31671—21300	B	01 Oct 82	8	M 50	
076—114	075°25'S. 143°38'E.	31671—21300	D	01 Oct 82	8	M 25	
077—116	077°33'S. 133°37'E.	31672—21363	A	02 Oct 82	6	M 50	
077—116	077°33'S. 133°37'E.	31672—21363	C	02 Oct 82	6	M 50	
084—116	077°33'S. 123°35'E.	31679—22165	B	09 Oct 82	8	M 25	
084—118	079°19'S. 111°57'E.	31679—22174	B	09 Oct 82	6	M 25	
085—108	067°59'S. 145°53'E.	31680—22191	B	10 Oct 82	18	G 25, M25	Ninnis Glacier Tongue, George V coast
085—108	067°59'S. 145°53'E.	31680—22191	D	10 Oct 82	18	G 50, M 50	Ninnis Glacier, George V Coast
085—109	069°17'S. 144°04'E.	31680—22194	B	10 Oct 82	17	M 50	
085—112	073°04'S. 137°09'E.	31680—22205	D	10 Oct 82	14	M 25	
085—113	074°16'S. 134°10'E.	31680—22212	D	10 Oct 82	12	M 25	
085—115	076°31'S. 126°46'E.	31680—22221	D	10 Oct 82	10	G 75, M 25	Surface features, Wilkes Land
086—108	067°59'S. 144°27'E.	31681—22250	B	11 Oct 82	19	M 25	
086—113	074°16'S. 132°44'E.	31681—22270	B	11 Oct 82	13	G 75, M 25	Surface features, Wilkes Land
086—113	074°16'S. 132°44'E.	31681—22270	D	11 Oct 82	13	M 50	
086—114	075°25'S. 129°18'E.	31681—22273	B	11 Oct 82	12	M 50	
086—114	075°25'S. 129°18'E.	31681—22273	D	11 Oct 82	12	G 75, M 25	Surface features, Wilkes Land
086—115	076°31'S. 125°20'E.	31681—22275	B	11 Oct 82	10	G 75, M 25	Surface features, Wilkes Land
086—115	076°31'S. 125°20'E.	31681—22275	D	11 Oct 82	10	G 75, M 25	Surface features, Wilkes Land
086—116	077°33'S. 120°43'E.	31681—22282	B	11 Oct 82	9	M 75	
086—116	077°33'S. 120°43'E.	31681—22282	D	11 Oct 82	9	M 75	
086—117	078°29'S. 115°20'E.	31681—22284	B	11 Oct 82	8	M 50	

TABLE 7.— Usable or marginally usable Landsat 3 RBV images of glaciers of Antarctica—Continued

Path-Row	Nominal scene center (lat.—long.)	Landsat identification number	Subscene	Date	Solar elev. angle (degrees)	Code	Remarks
086-117	078°29'S. 115°20'E.	31681-22284	D	11 Oct 82	8	G 50, M 25	Surface features, Wilkes Land
086-118	079°19'S. 109°05'E.	31681-22291	B	11 Oct 82	7	M 75	
086-118	079°19'S. 109°05'E.	31681-22291	D	11 Oct 82	7	M 25	
086-119	080°01'S. 101°55'E.	31681-22293	B	11 Oct 82	6	M 25	
087-108	067°59'S. 143°01'E.	31682-22304	A	12 Oct 82	19	M 25	
094-116	077°33'S. 109°14'E.	31671-23140	D	01 Oct 82	5	M 25	
095-106	065°20'S. 134°40'E.	31672-23154	D	02 Oct 82	18	M 25	
095-107	066°40'S. 133°11'E.	31672-23160	B	02 Oct 82	16	M 50	
095-108	067°59'S. 131°33'E.	31672-23163	D	02 Oct 82	15	M 25	
128-113	074°16'S. 072°30'E.	31472-02253	B	16 Mar 82	6	M 25	
128-114	075°25'S. 069°04'E.	31472-02255	A	16 Mar 82	5	M 25	
129-106	065°20'S. 085°54'E.	30951-02141	D	11 Oct 80	19	M 50	
129-106	065°20'S. 085°54'E.	30933-02145	D	23 Sep 80	12	G 50	West Ice Shelf
129-107	066°40'S. 084°25'E.	30951-02144	B	11 Oct 80	18	M 100	
129,107	066°40'S. 084°25'E.	30951-02144	D	11 Oct 80	18	M 25	
1291107	066°40'S. 084°25'E.	30933-02152	A	23 Sep 80	11	G 100	West Ice Shelf
129-107	066°40'S. 084°25'E.	30933-02152	B	23 Sep 80	11	G 100	West Ice Shelf
129-107	066°40'S. 084°25'E.	30933-02152	C	23 Sep 80	11	G 100	West Ice Shelf
129-107	066°40'S. 084°25'E.	30933-02152	D	23 Sep 80	11	G 25	West Ice Shelf
130-108	067°59'S. 081°21'E.	31492-02352	A	05 Apr 82	5	M 50	
130-108	067°59'S. 081°21'E.	31492-02352	B	05 Apr 82	5	G 25, M 50	West Ice Shelf
130-108	067°59'S. 081°21'E.	31492-02352	C	05 Apr 82	5	G 25	Ingrid Christensen Coast
130-109	069°17'S. 079°31'E.	31492-02354	A	05 Apr 82	3	M 50	
130-109	069°17'S. 079°31'E.	31492-02354	C	05 Apr 82	3	G 25	Ranvik Bay, Ingrid Christensen Coast

TABLE 7.—Usable or marginally usable Landsat 3 RBV images of glaciers of Antarctica—Continued

Path-Row	Nominal scene center (lat.–long.)	Landsat identification number	Subscene	Date	Solar elev. angle (degrees)	Code	Remarks
131–107	066°40'S. 081°33'E.	30989–02254	B	18 Nov 80	29	M 50	
131–107	066°40'S. 081°33'E.	30989–02254	D	18 Nov 80	29	M 50	
131–111	071°50'S. 073°46'E.	31475–02415	D	19 Mar 82	7	M 25	
131–112	073°04'S. 071°10'E.	31475–02422	A	19 Mar 82	6	G 50	Law Plateau, Mac. Robertson Land, partial image
131–112	073°04'S. 071°10'E.	31475–02422	C	19 Mar 82	6	G 50	Law Plateau, Mac. Robertson Land, partial image
132–108	067°59'S. 078°29'E.	31476–02462	D	20 Mar 82	10	M 25	
133–109	069°17'S. 075°13'E.	31495–02530	C	08 Apr 82	2	G 25	Publications Ice Shelf, Ingrid Christensen Coast
135–109	069°17'S. 072°21'E.	31497–03043	A	10 Apr 82	2	M 25	
135–111	071°50'S. 068°02'E.	31479–03050	B	23 Mar 82	6	G 50	Lambert Glacier, partial image
136–109	069°17'S. 070°55'E.	31498–03102	A	11 Apr 82	1	M 50	
136–109	069°17'S. 070°55'E.	31498–03102	D	11 Apr 82	1	M 25	
136–111	071°50'S. 066°36'E.	31480–03104	A	24 Mar 82	5	M 50	
136–112	073°04'S. 064°00'E.	31480–03111	B	24 Mar 82	4	G 50	Mount Stinear, Lambert Glacier, partial image
137–108	067°59'S. 071°18'E.	31481–03151	A	25 Mar 82	8	G 50	MacKenzie Bay, Amery Ice Shelf
137–108	067°59'S. 071°18'E.	31481–03151	C	25 Mar 82	8	G 50	Bjerkø Peninsula, Mac. Robertson Land
137–109	069°17'S. 069°29'E.	31481–03154	A	25 Mar 82	7	G 50	Amery Ice Shelf, partial image
137–109	069°17'S. 069°29'E.	31481–03154	C	25 Mar 82	7	G 50	Landon Promontory, Mac. Robertson Land, partial image
137–110	070°35'S. 067°27'E.	31481–03160	A	25 Mar 82	6	G 50	Amery Ice Shelf, partial image
137–112	073°04'S. 062°34'E.	31481–03165	B	25 Mar 82	4	G 25	Prince Charles Mountains, Mac. Robertson Land, partial image
137–112	073°04'S. 062°34'E.	31481–03165	D	25 Mar 82	4	G 25	Prince Charles Mountains, Mac. Robertson Land, partial image
141–109	069°17'S. 063°45'E.	31845–03405	B	24 Mar 83	8	G 50	Depot Peak, Mac. Robertson Land
154–113	074°16'S. 035°12'E.	31678–04571	A	08 Oct 82	11	M 25	
154–113	074°16'S. 035°12'E.	31678–04571	B	08 Oct 82	11	M 25	

TABLE 7.—Usable or marginally usable Landsat 3 RBV images of glaciers of Antarctica—Continued

Path-Raw	Nominal scene center (lat.—long.)	Landsat identification number	Subscene	Date	Solar elev. angle (degrees)	Code	Remarks
154-113	074°16'S. 035°12'E.	31678-04571	C	08 Oct 82	11	M 25	
164-111	071°50'S. 026°26'E.	31850-05533	A	29 Mar 83	4	M 25	
164-111	071°50'S. 026°26'E.	31850-05533	D	29 Mar 83	4	M 25	
164-112	073°04'S. 023°50'E.	31850-05535	A	29 Mar 83	2	M 25	
172-119	080°01'S. 021°26'W.	30346-06393	A	14 Feb 79	10	M 25	
172-119	080°01'S. 021°26'W.	30346-06393	B	14 Feb 79	10	G 50	Surface features northeast of Shackleton Range
172-119	080°01'S. 021°26'W.	30346-06393	C	14 Feb 79	10	G 25, M 50	Surface features northeast of Shackleton Range
172-119	080°01'S. 021°26'W.	30346-06393	D	14 Feb 79	10	G 50	Surface features northeast of Shackleton Range
172-119	080°01'S. 021°26'W.	30256-06395	D	16 Nov 78	17	M 25	
177-109	069°17'S. 012°07'E.	31791-07071	D	29 Jan 83	26	M 50	
177-110	070°35'S. 010°05'E.	31791-07073	B	29 Jan 83	25	G 25, M 75	Princess Astrid Coast, Queen Maud Land
177-111	071°50'S. 007°47'E.	31791-07080	B	29 Jan 83	24	G 50	Wohlthat Mountains, Queen Maud Land
177-112	073°04'S. 005°11'E.	31791-07082	B	29 Jan 83	22	G 50	Surface features, Queen Maud Land
178-111	071°50'S. 006°21'E.	31846-07135	A	25 Mar 83	5	M 25	
178-111	071°50'S. 006°21'E.	31846-07135	B	25 Mar 83	5	M 25	
178-111	071°50'S. 006°21'E.	31846-07135	C	25 Mar 83	5	G 25, M 25	Mühlig-Hofmann Mountains Queen Maud Land
178-112	073°04'S. 003°45'E.	31846-07142	A	25 Mar 83	4	G 25, M 25	Mühlig-Hofmann Mountains, Queen Maud Land
178-112	073°04'S. 003°45'E.	31846-07142	C	25 Mar 83	4	M 25	
184-110	070°35'S. 000°02'E.	31672-07475	A	02 Oct 82	13	G 100	Fimbul Ice Shelf, Queen Maud Land
184-110	070°35'S. 000°02'E.	31672-07475	C	02 Oct 82	13	G 50	Fimbul Ice Shelf, Queen Maud Land
184-111	071°50'S. 002°15'W.	31672-07482	A	02 Oct 82	11	G 75	Fimbul Ice Shelf, Queen Maud Land
184-111	071°50'S. 002°15'W.	31672-07482	B	02 Oct 82	11	G 50, M 50	Jutulstraumen Glacier, Queen Maud Land
184-111	071°50'S. 002°15'W.	31672-07482	C	02 Oct 82	11	G 75	Schytt Glacier, Queen Maud Land
184-111	071°50'S. 002°15'W.	31672-07482	D	02 Oct 82	11	G 50, M 50	Jutulstraumen Glacier, Queen Maud Land

TABLE 7.—Usable or marginally usable Landsat 3 RBV images of glaciers of Antarctica—Continued

Path-Row	Nominal scene center (lat.—long.)	Landsat identification number	Subscene	Date	Solar elev. angle (degrees)	Code	Remarks
184-112	073°04'S. 004°51'W.	31672-07484	A	02 Oct 82	10	G 50	Ahlmann Ridge, Queen Maud Land
184-112	073°04'S. 004°51'W.	31672-07484	B	02 Oct 82	10	G 50	Ahlmann Ridge, Queen Maud Land
184-112	073°04'S. 004°51'W.	31672-07484	C	02 Oct 82	10	G 25, M 25	Borg Massif, Queen Maud Land
184-113	074°16'S. 007°50'W.	31672-07491	B	02 Oct 82	9	G 50	Kirwin Escarpment, Queen Maud Land
184-113	074°16'S. 007°50'W.	31672-07491	C	02 Oct 82	9	G 50	Kirwin Escarpment, Queen Maud Land
184-113	074°16'S. 007°50'W.	31672-07491	D	02 Oct 82	9	G 50	Kirwin Escarpment, Queen Maud Land
184-114	075°25'S. 011°16'W.	31672-07493	A	02 Oct 82	8	G 25	Kirwin Escarpment, Queen Maud Land
184-114	075°25'S. 011°16'W.	31672-07493	B	02 Oct 82	8	M 25	
184-114	075°25'S. 011°16'W.	31672-07493	C	02 Oct 82	8	M 50	
188-113	074°16'S. 013°34'W.	31766-08114	D	04 Jan 83	26	M 50	
199-117	078°29'S. 046°45'W.	31795-09164	D	02 Feb 83	16	G 50	Berkner Island
205-116	077°33'S. 049°58'W.	30289-09473	A	19 Dec 78	24	M 50	
205-116	077°33'S. 049°58'W.	30289-09473	B	19 Dec 78	24	M 50	
205-116	077°33'S. 049°58'W.	30289-09473	C	19 Dec 78	24	M 25	
208-115	076°31'S. 049°39'W.	30310-10042	D	09 Jan 79	24	M 50	
208-115	076°31'S. 049°39'W.	30274-10043	D	04 Dec 78	25	M 50	
208-116	077°33'S. 054°16'W.	30310-10045	B	09 Jan 79	22	M 25	
208-116	077°33'S. 054°16'W.	30274-10050	A	04 Dec 78	23	M 50	
208-116	077°33'S. 054°16'W.	30274-10050	B	04 Dec 78	23	M 50	
210-115	076°31'S. 052°31'W.	30348-10155	C	16 Feb 79	14	M 25	
210-115	076°31'S. 052°31'W.	30348-10155	D	16 Feb 79	14	M 25	
210-115	076°31'S. 052°31'W.	30312-10155	C	11 Jan 79	23	M 25	
210-115	076°31'S. 052°31'W.	30294-10154	D	24 Dec 78	25	M 25	
210-116	077°33'S. 057°08'W.	30348-10162	A	16 Feb 79	13	G 25	Ice front

TABLE 7.—Usable or marginally usable Landsat 3 RBV images of glaciers of Antarctica—Continued

Path-Row	Nominal scene center (lat.—long.)	Landsat identification number	Subscene	Date	Solar elev. angle (degrees)	Code	Remarks
210-116	077°33'S. 057°08'W.	30348-10162	B	16 Feb 79	13	M 25	
210-116	077°33'S. 057°08'W.	30330-10162	A	29 Jan 79	18	M 25	
210-116	077°33'S. 057°08'W.	30330-10162	B	29 Jan 79	18	M 25	
210-116	077°33'S. 057°08'W.	30294-10161	A	24 Dec 78	24	M 25	
210-116	077°33'S. 057°08'W.	30294-10161	B	24 Dec 78	24	M 25	
215-114	075°25'W. 055°43'W.	30281-10441	B	11 Dec 78	26	M 25	
222-112	073°04'S. 059°21'W.	30360-11233	A	28 Feb 79	13	M 25	
222-112	073°04'S. 059°21'W.	30360-11233	C	28 Feb 79	13	M 50	
222-112	073°04'S. 059°21'W.	30360-11233	D	28 Feb 79	13	G 25	Cape Deacon, Palmer Land
222-112	073°04'S. 059°21'W.	30252-11235	D	12 Nov 78	24	M 25	
222-118	079°19'S. 085°59'W.	31782-11290	D	20 Jan 83	18	G 75	Ellsworth Mountains
223-113	074°16'S. 063°46'W.	30343-11294	B	11 Feb 79	18	M 50	
223-113	074°16'S. 063°46'W.	30343-11294	D	11 Feb 79	18	M 75	
225-111	071°50'S. 061°03'W.	30309-11402	D	08 Jan 79	28	M 25	
225-111	071°50'S. 061°03'W.	30291-11401	D	21 Dec 78	30	G 25, M 25	Hilton Inlet, Palmer Land
225-113	074°16'S. 066°38'W.	30291-11410	D	21 Dec 78	27	M 25	
225-117	078°29'S. 084°02'W.	31767-11454	C	05 Jan 83	22	M 50	
227-108	067°59'S. 057°47'W.	30959-11370	C	19 Oct 80	20	M 50	
227-111	071°50'S. 063°55'W.	30329-11515	A	28 Jan 79	24	M 25	
227-111	071°50'S. 063°55'W.	30329-11515	D	28 Jan 79	24	G 25	Dyer Plateau, Palmer Land
227-111	071°50'S. 063°55'W.	30311-11514	D	10 Jan 79	27	M 25	
227-112	073°04'S. 066°31'W.	30347-11521	A	15 Feb 79	17	M 25	
227-112	073°04'S. 066°31'W.	30347-11521	D	15 Feb 79	17	M 25	
227-112	073°04'S. 066°31'W.	30329-11521	D	28 Jan 79	23	G 25	Palmer Land

TABLE 7.—Usable or marginally usable Landsat 3 RBV images of glaciers of Antarctica—Continued

Path-Row	Nominal scene center (lat.—long.)	Landsat identification number	Subscene	Date	Solar elev. angle (degrees)	Code	Remarks
227—113	074°16'S. 069°30'W.	30347—11523	B	15 Feb 79	16	M 25	
227—113	074°16'S. 069°30'W.	30329—11524	B	28 Jan 79	22	M 25	
229—103	061°16'S. 053°50'W.	30907—11481	C	28 Aug 80	6	M 50	
229—103	061°16'S. 053°50'W.	30277—12000	C	07 Dec 78	37	M 50	
229—104	062°38'S. 054°58'W.	30925—11480	D	15 Sep 80	12	M 25	
229—104	062°38'S. 054°58'W.	30907—11483	A	28 Aug 80	5	G 25	Gibbs Island, South Shetland Islands
229—104	062°38'S. 054°58'W.	30907—11483	B	28 Aug 80	5	M 25	
229—105	063°59'S. 056°12'W.	30925—11483	A	15 Sep 80	10	M 75	
229—105	063°59'S. 056°12'W.	30925—11483	B	15 Sep 80	10	M 75	
229—105	063°59'S. 056°12'W.	30925—11483	C	15 Sep 80	10	M 50	
229—105	063°59'S. 056°12'W.	30925—11483	D	15 Sep 80	10	M 25	
229—105	063°59'S. 056°12'W.	30907—11490	A	28 Aug 80	4	M 25	
229—105	063°59'S. 056°12'W.	30907—11490	C	28 Aug 80	4	M 25	
229—106	065°02'S. 057°32'W.	30907—11492	A	28 Aug 80	3	M 25	
229—106	065°20'S. 057°32'W.	30277—12011	B	07 Dec 78	34	M 25	
229—108	067°59'S. 060°39'W.	30943—11490	D	03 Oct 80	14	M 25	
229—109	069°17'S. 062°28'W.	30349—12023	C	17 Feb 79	20	M 25	
229—109	069°17'S. 062°28'W.	30349—12023	D	17 Feb 79	20	M 25	
229—110	070°35'S. 064°30'W.	30349—12025	A	17 Feb 79	19	M 25	
229—110	070°35'S. 064°30'W.	30349—12025	B	17 Feb 79	19	M 25	
229—114	075°25'S. 075°48'W.	31843—12074	C	22 Mar 83	3	M 25	
229—114	075°25'S. 075°48'W.	31843—12074	D	22 Mar 83	3	M 25	
230—104	062°38'S. 056°24'W.	30350—12061	D	18 Feb 79	24	M 50	
230—104	062°38'S. 056°24'W.	30278—12061	D	08 Dec 78	37	M 25	

TABLE 7. — Usablør marginally usable Landsat 3 RBV images of glaciers of Antarctica—Continued

Path-Row	Nominal scene center (lat.-long.)	Landsat identification number	Subscene	Date	Solar elev. angle (degrees)	Code	Remarks
230-105	063°59'S. 057°38'W.	30350-12063	A	18 Feb 79	23	M 25	
230-105	063°59'S. 057°58'W.	30350-12063	B	18 Feb 79	23	M 100	
230-105	063°59'S. 057°38'W.	30350-12063	C	'18 Feb 79	23	M 50	
230-105	063°59'S. 057°38'W.	30350-12063	D	18 Feb 79	23	M 50	
230-105	063°59'S. 057°38'W.	30278-12063	B	08 Dec 78	36	M 50	
230-106	065°20'S. 058°58'W.	30278-12070	A	08 Dec 78	35	M 25	
231-103	061°16'S. 056°42'W.	30315-12112	D	14 Jan 79	34	M 25	
231-103	061°16'S. 056°42'W.	30279-12113	B	09 Dec 78	38	M 25	
231-103	061°16'S. 056°42'W.	30279-12113	D	09 Dec 78	38	M 25	
231-104	062°38'S. 057°50'W.	30279-12115	D	09 Dec 78	37	M 25	
231-105	063°59'S. 059°04'W.	30333-12121	A	01 Feb 79	28	M 25	
213-105	063°59'S. 059°04'W.	30333-12121	B	01 Feb 79	28	M 25	
213-105	063°59'S. 059°04'W.	30333-12121	C	01 Feb 79	28	M 25	
213-105	063°59'S. 059°04'W.	30333-12121	D	01 Feb 79	28	M 75	
231-105	063°59'S. 059°04'W.	30315-12121	B	14 Jan 79	33	M 25	
231-105	063°59'S. 059°04'W.	30315-15121	C	14 Jan 79	33	M 25	
231-105	063°59'S. 059°04'W.	30315-12121	D	14 Jan 79	33	M 50	
231-105	063°59'S. 059°04'W.	30297-12121	B	27 Dec 78	35	M 25	
231-105	063°59'S. 059°04'W.	30297-12121	D	27 Dec 78	35	M 25	
231-105	063°59'S. 059°04'W.	30279-12122	B	09 Dec 78	36	G 25	Trinity Peninsula
231-106	065°20'S. 060°24'W.	30315-12124	A	14 Jan 79	32	M 25	
231-106	065°20'S. 060°24'W.	30315-12124	B	14 Jan 79	32	M 25	
231-106	065°20'S. 060°24'W.	30297-12123	B	27 Dec 78	34	M 25	
231-106	065°20'S. 060°24'W.	30297-12123	D	27 Dec 78	34	M 25	

TABLE 7.—Usable or marginally usable Landsat 3 RBV images of glaciers of Antarctica—Continued

Path-Row	Nominal scene center (lat.—long.)	Landsat identification number	Subscene	Date	Solar elev. angle (degrees)	Code	Remarks
231-106	065°20'S. 060°24'W.	30279-12124	B	09 Dec 78	35	M 50	
231-106	065°20'S. 060°24'W.	36279-12124	D	09 Dec 78	35	M 50	
231-107	066°40'S. 061°53'W.	30279-12131	B	09 Dec 78	34	M 50	
231-110	070°35'S. 067°22'W.	30297-12141	C	27 Dec 78	30"	M 25	
231-110	070°35'S. 067°22'W.	30279-12142	B	09 Dec 78	30	M 25	
231-110	070°35'S. 067°22'W.	30279-12142	D	09 Dec 78	30	M 25	
231-111	071°50'S. 069°40'W.	30315-12144	D	14 Jan 79	27	G 25	Alexander Island
231-111	071°50'S. 069°40'W.	30297-12144	A	27 Dec 78	29	M 25	
231-111	071°50'S. 069°40'W.	30297-12144	B	27 Dec 78	29	G 25, M 75	George VI Sound
231-111	071°50'S. 069°40'W.	30297-12144	D	27 Dec 78	29	G 25	George VI Sound
231-111	071°50'S. 069°40'W.	30279-12145	B	09 Dec 78	29	M 25	
231-111	071°50'S. 069°40'W.	30279-12145	D	09 Dec 78	29	M 25	
232-104	062°38'S. 059°16'W.	30280-12173	B	10 Dec 78	37	M 25	
232-104	062°38'S. 059°16'W.	30244-12175	B	04 Nov 78	31	M 25	
232-104	062°38's. 059°16'W.	30244-12175	C	04 Nov 78	31	M 25	
232-104	062°38'S. 059°16'W.	30244-12175	D	04 Nov 78	31	M 25	
232-105	063°59'S. 060°30'W.	30316-12180	B	15 Jan 79	32	M 50	
232-105	063°59'S. 060°30'W.	30298-12175	B	28 Dec 78	35	M 25	
232-105	063°59'S. 060°30'W.	30244-12182	B	04 Nov 78	30	M 25	
232-105	063°59'S. 060°30'W.	30244-12182	C	04 Nov 78	30	M 25	
232-105	063°59'S. 060°30'W.	30244-12182	D	04 Nov 78	30	M 75	
232-106	065°20'S. 061°50'W.	30244-12184	B	04 Nov 78	28	M 50	
232-106	065°20'S. 061°50'W.	30244-12184	C	04 Nov 78	28	M 50	
232-106	065°20'S. 061°50'W.	30244-12184	D	04 Nov 78	28	M 25	

TABLE 7.—Usable or marginally usable Landsat 3 RBV images of glaciers of Antarctica—Continued

Path-Row	Nominal scene center (lat.—long.)	Landsat identification number	Subscene	Date	Solar elev. angle (degrees)	Code	Remarks
233—104	062°38'S. 060°42'W.	30317—12232	D	16 Jan 79	33	M 25	
233—104	062°38'S. 060°42'W.	30263—12233	B	23 Nov 78	35	M 25	
233—104	062°38'S. 060°42'W.	30263—12233	C	23 Nov 78	35	M 25	
233—104	062°38'S. 060°42'W.	30263—12233	D	23 Nov 78	35	M 25	
233—105	063°59'S. 061°56'W.	30317—12234	A	16 Jan 79	32	M 25	
233—105	063°59'S. 061°56'W.	30317—12234	B	16 Jan 79	32	M 25	
233—105	063°59'S. 061°56'W.	30317—12234	D	16 Jan 79	32	G 25, M 25	Cape Sterneck, Graham Land
233—105	063°59'S. 061°56'W.	30263—12235	A	23 Nov 78	34	M 25	
233—105	063°59'S. 061°56'W.	30263—12235	B	23 Nov 78	34	M 25	
233—105	063°59'S. 061°56'W.	30263—12235	C	23 Nov 78	34	M 25	
233—105	063°59'S. 061°56'W.	30263—12235	D	23 Nov 78	34	M 100	
233—106	065°20'S. 063°16'W.	31523—12255	B	06 May 82	0	M 25	
233—106	065°20'S. 063°16'W.	30317—12241	B	16 Jan 79	31	G 25	Danco Coast
233—106	065°20'S. 063°16'W.	30317—12241	D	16 Jan 79	31	M 50	
233—106	065°20'S. 063°16'W.	30299—12240	A	29 Dec 78	34	M 50	
233—106	065°20'S. 063°16'W.	30299—12240	B	29 Dec 78	34	G 25	Danco Coast
233—106	065°20'S. 063°16'W.	30299—12240	C	29 Dec 78	34	M 50	
233—106	065°20'S. 063°16'W.	30299—12240	D	29 Dec 78	34	M 50	
233—106	065°20'S. 063°16'W.	30281—12241	B	11 Dec 78	35	M 25	
233—106	065°20'S. 063°16'W.	30281—12241	D	11 Dec 78	35	M 25	
233—106	065°20'S. 063°16'W.	30263—12242	A	23 Nov 78	33	M 25	
233—106	065°20'S. 063°16'W.	30263—12242	B	23 Nov 78	33	G 50, M 25	Danco Coast
233—106	065°20'S. 063°16'W.	30263—12242	C	23 Nov 78	33	M 50	
233—106	065°20'S. 063°16'W.	30263—12242	D	23 Nov 78	33	M 75	

TABLE 7.—Usable or marginally usable Landsat 3 RBV images of glaciers of Antarctica—Continued

Path-Row	Nominal scene center (lat.—long.)	Landsat identification number	Subscene	Date	Solar elev. angle (degrees)	Code	Remarks
233-106	065°20'S. 063°16'W.	30245-12243	A	05 Nov 78	29	M 25	
233-106	065°20'S. 063°16'W.	30245-12243	B	05 Nov 78	29	M 25	
233-107	066°40'S. 064°45'W.	30317-12243	B	16 Jan 79	30	M 25	
233-107	066°40'S. 064°45'W.	30317-12243	C	16 Jan 79	30	M 25	
233-107	066°40'S. 064°45'W.	30299-12243	A	29 Dec 78	33'	M 25	
233-107	066°40'S. 064°45'W.	30299-12243	B	29 Dec 78	33	M 25	
233-107	066°40'S. 064°45'W.	30299-12243	C	29 Dec 78	33	M 25	
233-107	066°40'S. 064°45'W.	30263-12244	A	23 Nov 78	32	M 25	
233-107	066°40'S. 064°45'W.	30263-12244	B	23 Nov 78	32	M 100	
233-107	066°40'S. 064°45'W.	30263-12244	C	23 Nov 78	32	M 25	
233-107	066°40'S. 064°45'W.	30263-12244	D	23 Nov 78	32	M 50	
233-108	067°59'S. 066°23'W.	30353-12250	D	21 Feb 79	19	M 25	
233-108	067°59'S. 066°23'W.	30317-12250	A	16 Jan 79	29	M 50	
233-108	067°59'S. 066°23'W.	30317-12250	C	16 Jan 79	29	M 50	
233-108	067°59'S. 066°23'W.	30299-12245	A	29 Dec 78	32	M 50	
233-108	067°59'S. 066°23'W.	30299-12245	B	29 Dec 78	32	M 25	
233-108	067°59'S. 066°23'W.	30299-12245	C	29 Dec 78	32	M 50	
233-108	067°59'S. 066°23'W.	30299-12245	D	29 Dec 78	32	M 25	
233-108	067°59'S. 066°23'W.	30263-12251	A	23 Nov 78	31	M 50	
233-108	067°59'S. 066°23'W.	30263-12251	B	23 Nov 78	31	M 50	
233-108	067°59'S. 066°23'W.	30263-12251	C	23 Nov 78	31	M 50	
233-108	067°59'S. 066°23'W.	30263-12251	D	23 Nov 78	31	G 25, M 50	Bowman Coast
233-109	069°17'S. 068°13'W.	30353-12252	B	21 Feb 79	18	M 25	
233-109	069°17'S. 068°13'W.	30317-12252	B	16 Jan 79	28	M 25	

TABLE 7.—Usable or marginally usable Landsat 3 RBV images of glaciers of Antarctica—Continued

Path-Row	Nominal scene center (lat.—long.)	Landsat identification number	Subscene	Date	Solar elev. angle (degrees)	Code	Remarks
233–109	069°17'S. 068°13'W.	30299–12252	A	29 Dec 79	31	M 50	
233–109	069°17'S. 068°13'W.	30299–12252	C	29 Dec 79	31	M 50	
233–109	069°17'S. 068°13'W.	30299–12252	D	29 Dec 78	31	M 25	
233–109	069°17'S. 068°13'W.	30263–12253	B	23 Nov 78	30	M 50	
233–109	069°17'S. 068°13'W.	30263–12253	D	23 Nov 78	30	M 25	
233–110	070°35'S. 070°14'W.	30299–12254	A	29 Dec 78	30	M 25	
233–110	070°35'S. 070°14'W.	30299–12254	B	29 Dec 78	30	M 25	
233–110	070°35'S. 070°14'W.	30299–12254	D	29 Dec 78	30	M 50	
233–110	070°35'S. 070°14'W.	30281–12255	D	11 Dec 78	31	M 25	
233–110	070°35'S. 070°14'W.	30263–12260	A	23 Nov 78	29	M 25	
233–110	070°35'S. 070°14'W.	30263–12260	B	23 Nov 78	29	M 25	
233–110	070°35'S. 070°14'S.	30263–12260	D	23 Nov 78	29	M 50	
233–111	071°50'S. 072°32'W.	30299–12261	B	29 Dec 78	29	M 25	
233–111	071°50'S. 072°32'W.	30299–12261	C	29 Dec 78	29	M 25	
233–111	071°50'S. 072°32'W.	30281–12261	C	11 Dec 78	29	M 75	
233–111	071°50'S. 072°32'W.	30281–12261	D	11 Dec 78	29	M 25	
233–111	071°50'S. 072°32'W.	30263–12262	B	23 Nov 78	28	M 25	
234–104	062°38'S. 062°08'W.	30282–12290	D	12 Dec 78	37	M 25	
234–104	062°38'S. 062°08'W.	30264–12291	B	24 Nov 78	35	M 25	
234–104	062°38'S. 062°08'W.	30264–12291	D	24 Nov 78	35	M 25	
234–104	062°38'S. 062°08'W.	30246–12292	B	06 Nov 78	31	M 25	
234–104	062°38'S. 062°08'W.	30246–12292	D	06 Nov 78	31	M 50	
234–105	063°59'S. 063°22'W.	30336–12293	B	04 Feb 79	28	M 25	
234–105	063°59'S. 063°22'W.	30336–12293	D	04 Feb 79	28	M 25	

TABLE 7.—Usable or marginally usable Landsat 3 RBV images of glaciers of Antarctica—Continued

Path-Row	Nominal scene center (lat.—long.)	Landsat identification number	Subscene	Date	Solar elev. angle (degrees)	Code	Remarks
234-105	063°59'S. 063°22'W.	30300-12292	D	30 Dec 78	35	M 50	
234-105	063°59'S. 063°22'W.	30264-12294	A	24 Nov 78	34	M 25	
234-105	063°59'S. 063°22'W.	30264-12294	B	24 Nov 78	34	M 25	
234-105	063°59'S. 063°22'W.	30264-12294	C	24 Nov 78	34	M 25	
234-105	063°59'S. 063°22'W.	30264-12294	D	24 Nov 78	34	M 25	
234-105	063°59'S. 063°22'W.	30246-12294	B	06 Nov 78	30	M 25	
234-105	063°59'S. 063°22'W.	30246-12294	D	06 Nov 78	30	M 50	
234-106	065°20'S. 064°42'W.	30300-12295	B	30 Dec 78	34	M 50	
234-106	065°20'S. 064°42'W.	30264-12300	C	24 Nov 78	33	M 50	
234-106	065°20'S. 064°42'W.	30264-12300	D	24 Nov 78	33	G 50, M 25	Graham Coast
234-106	065°20'S. 064°42'W.	30246-12301	B	06 Nov 78	29	M 50	
235-109	069°17'S. 071°05'W.	30355-12365	D	23 Feb 79	18	M 25	
235-113	074°16'S. 080°59'W.	31795-12413	C	02 Feb 83	20	M 25	
236-106	065°20'S. 067°34'W.	30338-12412	D	06 Feb 79	26	M 25	
236-106	065°20'S. 067°34'W.	30320-12412	B	19 Jan 79	31	M 25	
236-106	065°20'S. 067°34'W.	30302-12411	D	01 Jan 79	34	M 25	
236-106	065°20'S. 067°34'W.	30284-12412	B	14 Dec 78	35	M 50	
236-106	065°20'S. 067°34'W.	30284-12412	C	14 Dec 78	35	M 25	
236-106	065°20'S. 067°34'W.	30284-12412	D	14 Dec 78	35	M 50	
236-107	066°40'S. 069°03'W.	30338-12414	B	06 Feb 79	25	M 25	
236-107	066°40'S. 069°03'W.	30338-12414	C	06 Feb 79	25	M 25	
236-107	066°40'S. 069°03'W.	30338-12414	D	06 Feb 79	25	M 25	
236-107	066°40'S. 069°03'W.	30284-12414	A	14 Dec 78	34	M 25	
236-107	066°40'S. 069°03'W.	30284-12414	D	14 Dec 78	34	M 50	

TABLE 7.—Usable or marginally usable Landsat 3 RBV images of glaciers of Antarctica—Continued

Path-Row	Nominal scene center (lat.—long.)	Landsat identification number	Subscene	Date	Solar elev. angle (degrees)	Code	Remarks
236–108	067°59'S. 070°42'W.	30338–12421	A	06 Feb 79	24	M 25	
236–108	067°59'S. 070°42'W.	30338–12421	B	06 Feb 79	24	M 50	
236–108	067°59'S. 070°42'W.	30338–12421	D	06 Feb 79	24	M 25	
236–108	067°59'S. 070°42'W.	30284–12421	B	14 Dec 78	33	M 50	
236–108	067°59'S. 070°42'W.	30284–12421	D	14 Dec 78	33	M 50	
236–109	069°17'S. 072°31'W.	30338–12423	C	06 Feb 79	23	M 50	
236–109	069°17'S. 072°31'W.	30338–12423	D	06 Feb 79	23	M 25	
236–109	069°17'S. 072°31'W.	30284–12423	B	14 Dec 78	32	M 50	
236–109	069°17'S. 072°31'W.	30284–12423	D	14 Dec 78	32	G 25, M 50	Alexander Island